Behavioral and Neurobiological Outcomes Following Genetic and Environmental Insults to the Developing Brain

By

ELIZABETH LAKEY BERG

DISSERTATION

Submitted in partial satisfaction of the requirements for the degree of

DOCTOR OF PHILOSOPHY

in

Psychology

in the

OFFICE OF GRADUATE STUDIES

of the

UNIVERSITY OF CALIFORNIA

DAVIS

Approved:

Jill L. Silverman, Chair

Brian C. Trainor

Karen L. Bales

Committee in Charge

2021

Abstract

Neurodevelopmental disorders (NDDs) are a broad group of conditions characterized by abnormal development of the nervous system that includes intellectual disability and autism spectrum disorders. NDDs are pervasive, lifelong, and increasing in prevalence, yet neither targeted pharmacological nor precision medicine therapies are currently available. This unmet need is in large part due to the complex and relatively unknown etiology of many NDDs. Multiple genetic loci, in combination with exposure to environmental risk factors during critical periods of development, contribute to both NDD susceptibility and symptom severity. In an effort to improve our understanding of NDD etiology, as well as help develop effective treatments, we used Sprague Dawley rats to examine the effects of two environmental risk factors and one causal genetic mutation on behaviors and neurobiological outcomes relevant to NDDs. While the mouse has predominated in recent decades as the species of choice for modeling NDDs, we sought to take advantage of the broader and more nuanced social communication repertoire of the rat. Therefore, we measured effects on a variety of behavioral domains including motor and cognition and gave particular focus to social and communication behaviors. Chapter 1 serves as an introduction to the study of social communication in rodent models of NDDs and provides detailed rationales behind many of the assays utilized in subsequent chapters. Chapters 2 and 3 investigate environmental factors that have been associated with increased risk for NDDs: air pollution and pesticides, respectively. Our findings support the hypothesis that developmental exposure to heavily trafficked roadways, or to the commonly used pesticide chlorpyrifos, increases NDD risk. Then, Chapters 4 and 5 characterize a novel genetic rat model of the NDD Angelman Syndrome, which is caused by dysfunction of the gene *UBE3A* (ubiquitin protein ligase E3A). We discovered that

the *Ube3a* deletion rat model of Angelman Syndrome recapitulated many of the core behavioral and neurobiological phenotypes of the disorder, including elevated expression of positive affect signals, and thereby utilized the rat model in Chapter 6 to test the efficacy of a candidate therapeutic, insulin-like growth factor 2. Although treatment with insulin-like growth factor 2 failed to rescue the model's deficits, the outcome measures used were robust and reproducible, indicating that the *Ube3a* deletion rat offers a strong preclinical model of Angelman Syndrome. Finally, Chapter 7 investigates a leading-edge "gene therapy-like" antisense oligonucleotide treatment in the rat model of Angelman Syndrome. Multiple clinical trials are currently evaluating antisense oligonucleotide therapies in humans with Angelman Syndrome and, while they have demonstrated remarkable efficacy, serious adverse reactions have been observed. By identifying an antisense oligonucleotide with molecular efficacy in the rat and delivering it via the brain, the cisterna magna, and lumbar puncture, we established a paradigm through which to elucidate the pathophysiology underlying the adverse clinical reactions. Taken together, this research advances our understanding of the complex etiology of NDDs, represents significant progress in modeling NDDs preclinically, and provides insights with direct implications to the ongoing pursuit of pharmacological treatments targeted to NDDs.

Table of Contents

Chapter 1

Introduction: Measuring Social Communication in Rodent Models of Neurodevelopmental Disorders

A version of this chapter has been accepted for publication: Elizabeth L. Berg and Jill L. Silverman (in press). *Encyclopedia of Behavioural Neuroscience, Second Edition.*

Abstract

Neurodevelopmental disorders (NDDs) are a group of complex conditions that affect the development of the nervous system and lead to abnormal behavior. NDDs include autism spectrum disorder, attention-deficit hyperactivity disorder, and intellectual disability. These disorders are characterized by abnormal social behavior and deficits in communication. A number of ethologically relevant tests that probe various forms of social communication have been developed for mice and rats. Mice are utilized due to the optimization of technically savvy genetic manipulations for the species. Rats are utilized for their sophisticated social behavioral repertoire. When test outcomes are interpreted in consideration of species differences and sensorimotor functioning, they can provide valuable information about NDD etiology, either genetic, environmental or both, and/or therapeutic efficacy.

Introduction

Mice and rats are the most commonly used laboratory animals in the study of neurodevelopmental disorders (NDDs), a class of complex conditions that includes autism spectrum disorder, attention-deficit hyperactivity disorder, intellectual disability, and communication disorders among others. In addition to advances in creating state of the art genetic models, both mice and rats are highly social and display a varied repertoire of behaviors that make them well suited for modeling a range of developmental delays, including learning and memory impairments, aberrant social behavior, and communication deficits that are characteristic of NDDs. The ability to closely study symptoms analogous to the human NDD phenotype in animals provides researchers the opportunity to experimentally gather information regarding NDD etiology and test potential interventions or therapeutics.

When analyzed appropriately, the behavior of an experimental mouse or rat study can help inform the nature of a social communication abnormality. This, in turn, can provide evidence that a given genotype or experimental group has strong face validity to (i.e., closely resembles) the human phenotype and could therefore be a suitable system in which to test a proposed therapy. The same assays used to detect a social communication deficit can then be performed in animals after receiving a treatment in order to test whether the deficit is normalized or improved by the intervention.

Communication deficits in NDDs vary widely and depend on the intellectual ability of the individual. Deficits can manifest as delays in the use or comprehension of language, stereotyped or absent speech, odd prosody or intonation, excessive use or interpretation of language literally, tendency to speak in monologues rather than interactively, and difficulties with language pragmatics such as those involved in initiating and maintaining appropriate and meaningful conversations (Lord et al., 2020; Tager-Flusberg et al., 2013). Appropriately modeling these types of social communication deficits in non-human species, such as mice and rats, is critically dependent on a comprehensive understanding of that which constitutes meaningful (i.e., ethologically relevant) communication in each model species.

It is beyond the scope of the present chapter to describe all of the intricacies of rodent behavior or all of the various models of NDD. Rather, this chapter seeks to provide the information necessary for understanding the rationales behind the most common tests of communication used in the behavioral phenotyping of rodent models of NDD. The focus will therefore be on the two most prevalent model species, namely mice and rats, and their three major categories of social communication: olfactory, vocal, and tactile. This chapter will outline the communication tests most utilized in mouse and rat models of NDD, point out important methodological considerations,

and highlight a few emerging approaches. In this way, the information provided herein can be considered alongside studies of specific NDD models to help to reveal the value, nuances, and limitations of the various tactics.

Why Mice and Rats

For most of the last century, rats have dominated as the animal model of choice in behavioral neuroscience, preferred for their size, behavioral repertoire, and physiological similarity to humans (Ellenbroek and Youn, 2016). When the manipulation of the mouse genome became possible in the 1990s however, gene-edited and transgenic mice were pushed to the forefront of the field. The ability to target a gene of choice allowed researchers to investigate the contribution of specific genes to NDD etiology, probe the biological mechanisms underlying NDD-relevant behaviors, and evaluate potential therapies. Expeditious discoveries were then generated to introduce cell-type specific, region specific, and temporal specific gene expression, all with the abilities of turning genes on and off.

Compared to mice, rats have an extra pair of chromosomes, making their genome approximately 6% larger than that of the mouse. It was not until the following decade that the generation of gene-edited and transgenic rats finally became achievable (Geurts et al., 2009), thanks to advances in gene-editing technologies (e.g., CRISPR-Cas9, zinc-finger nucleases) coupled with the 2004 publication of the rat genome (Gibbs et al., 2004; Shao et al., 2014). This has been a tremendous advancement for the field of NDD animal models and opened up new possible avenues of study into complexities of social behavior (e.g., play, cooperative behavior) that are not as easily evaluated in mice (Berg et al., 2020, 2018; Hamilton et al., 2014; Harony-Nicolas et al., 2017; Till et al., 2015; Wöhr and Schwarting, 2012).

Rats, in fact, display more nuanced and complex social behavior than mice (see next section), making them even more well-suited for modeling the communication deficits of NDD. Due to the lag in genetic technologies, along with the elevated cost and space associated with the maintenance of rat colonies, genetic rat models are still a relatively recent development and the field is still moving toward taking greatest advantage of the newly available tool. Both species therefore offer unique advantages to researchers aiming to model NDDs.

Studying Communication in Mice and Rats

While the field of animal behavior is not without its own debate as to what exactly constitutes animal communication, behavioral neuroscientists tend to utilize the transfer of information definition initially put forth by Shannon and Weaver (1998). By this characterization, communication involves the bi-directional transfer of information from a sender and a receiver (Shannon and Weaver, 1998). Evidence of communication can therefore be readily obtained by observing an animal send a signal that leads to an overt change in the behavior of a receiver animal. By documenting the nature of that behavioral change, researchers can work to elucidate the purpose of the signal and draw parallels to the various forms of human communication (Aubin, 2010; Portfors and Perkel, 2014). This type of investigation in mice and rats provides the foundation from which deficits in communication can be assayed.

Animal communication can be classified into four major categories based on sensory modalities used to send and receive social signals: visual, chemical, auditory, and tactile. The relative importance of each of these types varies by species. Unlike humans, mice and rats do not rely heavily on visual signals to communicate, but rather, primarily use chemical and acoustic signaling by way of olfactory pheromones and vocalizations, respectively, along with tactile

communication. While mice and rats differ in exactly how they use these types of signals (to be discussed more in a following section), the major social communication assays traditionally applied to mouse models are also feasible in rats.

Common Methodology

All of the presently described communication assays, which target shared features of mouse and rat communication systems, can and have been performed in both species. Sometimes, but not always, methodological adjustments are necessary to accommodate differences in the species. Even when carried out following identical protocols, however, the tests are not necessarily functionally equivalent, and results should be interpreted in a species-specific manner. This cannot be understated: rats are not large mice.

Most of the routinely used communication assays target a certain type of communication (e.g., olfactory) and will be herein categorized accordingly. That being said, mice and rats integrate information across sensory modalities when possible and often use multiple modes of communication concurrently. The categories used presently to group behavioral assays seek to provide a conceptual framework, rather than imply an ability to test for a pure deficit in a single communication type.

In fact, the detection of a communication deficit relies on data from tests of both communication and sensorimotor capabilities. This is because a sensorimotor deficit is a potential confound and can affect behavior such that it may appear that social communication is impaired. For instance, an inability to smell could lead an animal to ignore scent marks from a conspecific. Without information about the animal's olfactory deficit, the animal's behavior could be misinterpreted as evidence of reduced interest in conspecifics. Researchers must therefore collect

enough relevant information to be able to distinguish between an animal's motivation to communicate and its ability to do so by carrying out the appropriate assessments of sensory perception prior to interpreting social behavior data.

It is also recommended to conduct multiple assays with complementary readouts as to avoid basing conclusions on the outcome of a single test (Sukoff Rizzo and Silverman, 2016). In this way, the unique advantages of each assay (**Table 1**) can be exploited in order to garner a more wholistic view of the model's social communication phenotype. It is also recommended to evaluate whether impaired cognitive functioning may be contributing to altered behavior in social contexts. As mentioned previously, communication phenotypes in humans are highly dependent on the intellectual abilities of the individual. In rats, for instance, juveniles must learn how to appropriately engage in species-typical rough and tumble play through interactions with others over development (Panksepp, 1981). An impaired ability to learn could therefore contribute to reduced levels of play behavior, which could appear as a reduced interest in social engagement. Additional test- and species-specific considerations will be emphasized in the appropriate sections below.

Visual Communication

Mice and rats are nocturnal and have relatively poor vision (Prusky et al., 2000). Some strains that do not have eye pigmentation experience a high degree of light scattering and have severe visual impairment or even blindness, including the FVBN/J and C3H mice and Wistar and Sprague-Dawley rat strains that are common to laboratories (Hanson, 2004). While mice and rats are capable of detecting colors, if they have any visual abilities at all, they only have two types of cone receptors and are thus believed to perceive colors similarly to humans who have red-green

colorblindness. Unlike humans, mice and rats have cones in their retina that are ultraviolet-sensitive and are therefore potentially capable of detecting ultraviolet light. Their color saturation is quite faint, however, so they rely more on brightness cues than on colors.

With poor visual acuity, mouse and rat behavior is not as strongly driven by visual communication compared to other sensory modalities, making assays of visual communication not highly relevant to the study of social communication. That said, they do sometimes use visual signals such as fluffing up their hair and flicking their tail during territory defense (Horn, 1998) and tensing their facial muscles in a grimace-like fashion when in pain (Langford et al., 2010; Sotocinal et al., 2011). Importantly, since urine reflects ultraviolet light, mice and rats may be capable of seeing urine marks in their environment in addition to being able to smell them (Desjardins et al., 1973). This is, of course, conditional on their overall ability to see and would not be possible for blind animals. The idea of visual communication beyond signals of pain or tasting of bitter flavor may be overinterpreted in these species which are not highly reliant on sight.

Olfactory Communication

Mice and rats primarily rely on olfactory signals for social communication and habitually deposit urine throughout their environment in order to mark their territory. The urine of mice and rats have characteristic odors and contain hundreds, potentially thousands, of compounds. At least some of these urinary compounds are detectable, some are sex-specific (Achiraman and Archunan, 2002), and some have been identified as pheromones (Leinders-Zufall et al., 2004; Novotny et al., 1985; Vandenbergh et al., 1976).

Pheromones are excreted compounds that act as chemical messengers and play critical roles in the social communication systems of many animals, including mice and rats. They help to

convey identifying information about the donor animal, such as sex, strain, rank, and reproductive status. Therefore, in addition to their use in marking territory, pheromones are important for mating, maternal aggression, kin recognition, and avoidance of inbreeding, among others.

Urine is just one route by which pheromones are released. Mice and rats of both sexes also emit pheromones via specialized glands in the anogenital region called preputial glands. Therefore, urinary scent marks left in the environment and an animal's anogenital region itself elicit high levels of interest and investigation from conspecifics (Arakawa et al., 2008).

Animals receive pheromone signals through the main olfactory epithelium in the nose (Keller et al., 2009), but they are mainly detected with a part of the accessory olfactory system called the vomeronasal organ (VNO) (Spehr et al., 2006; Vaccarezza et al., 1981). Social signals and non-social chemicals, such as food odors, activate different neurological pathways. Upon the binding of a social chemical to a receptor in the VNO, a signal is sent from the VNO to the accessory bulb, which projects to the amygdala and bed nucleus of the stria terminalis (BNST), and then to the anterior hypothalamus (He et al., 2008; Leinders-Zufall et al., 2000; Pérez-Gómez et al., 2014). Upon the binding of a non-social chemical to a receptor in the main olfactory epithelium, a signal is sent to the main olfactory bulb, which connects to the olfactory cortex.

Therefore, depending on the types and relative quantities of chemical signals being detected, VNO and main olfactory epithelium activation will lead to an appropriate behavioral response. The pattern of sensory neuron activation caused by pheromones from a conspecific (e.g., hypothalamic and amygdala activation) will be unique from that caused by chemicals from a predator or odors from a food item (e.g., cortical activation), thereby being processed by distinct neural circuits, and resulting in different downstream behavioral effects (Papes et al., 2010; Rodriguez, 2003). Pheromone detection, for instance, has been shown to lead to hypothalamic

neuroendocrine signaling that promotes behaviors involved in mating or aggressive behaviors (Brennan and Kendrick, 2006; Halpern and Martínez-Marcos, 2003).

Testing Olfactory Communication

Urinary pheromones. An animal's propensity to send urinary pheromone signals can be quantified by counting the number of scent marks, or urinary deposits, that it makes in an enclosed arena. It can also be quantified by counting the number of countermarks it makes near urine previously deposited by a conspecific (Wöhr et al., 2011). An animal's inclination to receive pheromone signals can be assessed through its investigation of urine deposits, quantified by counting the number and duration of sniffing bouts it performs (Silverman et al., 2010; Wöhr and Scattoni, 2013).

Olfactory habituation/dishabituation. When presented with novel odors, mice and rats reliably approach, investigate, and then quickly habituate to its novelty (Yang and Crawley, 2009). Repeatedly presenting an animal to the same odor therefore results in the animal spending less and less time sniffing the odor. Introduction of a new odor, however, leads to dishabituation in which the animal once again displays a high level of interest and investigation. Deviations from this pattern can indicate that an animal's sense of smell is impaired, so this test is very commonly used to probe for olfactory deficits in laboratory animals.

This type of procedure can be carried out using both social (e.g., urine) and non-social (e.g., vanilla extract) scents in order to assess an animal's level of interest in each type of odor as well as their ability to discriminate between the two (Silverman et al., 2010). Interest in a particular scent is quantified by the amount of time that the animal spends sniffing that scent. Social odors typically elicit significantly more interest compared to non-social odors (Yang and Crawley, 2009)

so a lack of this preference, in the presence of an ability to discriminate between odors, can provide evidence for disrupted olfactory communication.

Social transmission of food preference. Mice and rats can become familiar with a new food odor by sniffing the breath, face, and whiskers of a cagemate who has just consumed a novel food item (Wrenn, 2004; Wrenn et al., 2003). When given a choice, this familiarity helps to reduce the animal's neophobia toward that food item and leads the subject to eat more of that food compared to a completely new one. The development of this novel food preference depends on the receiver animal's ability and motivation to gather meaningful information (e.g., worth remembering) from the interaction with their cagemate. Therefore, a lack of social transmission of food preference (i.e., equal consumption of both food options) may serve as an indication of an altered communication system (Silverman et al., 2010). The results of this test should be interpreted alongside information on the animal's learning and memory abilities.

Auditory Communication

The detection and emission of ultrasonic vocalizations (USV) is another central mode of communication for mice and rats. USV, in the frequency range of approximately 20 to 90 kilohertz (kHz), are emitted by male and female mice and rats in different contexts across the lifespan, making it possible to test various types of auditory communication at a range of developmental timepoints (Brudzynski, 2009; Takahashi, 1992; Thomas and Barfield, 1985).

As newborns, mouse and rat pups emit USV when separated from their nest and mother, called the dam (Ehret, 2005). Like humans, mice and rats are altricial, meaning that they are born in an undeveloped state and require significant caretaking. Since they are dependent on their mother for food and thermoregulation, it is critical to pup survival that they not be isolated for an

extended period of time. By vocalizing when separated, they can be easily located by their mother and subsequently carried back to the nest. Upon hearing pup USV, dams promptly respond by orienting towards the source of the sound, approaching it, and showing search behaviors (Branchi et al., 2001). This search-and-retrieval behavior elicited in dams by pup USV, clear demonstration of bi-directional social communication, is a highly motivated behavior and has been well-characterized, as has the typical developmental profile of pup calling.

Typically, the emission of USV by pups gradually increases over the first week of life and then steadily declines over the second week, with the highest rates of calling usually observed between postnatal day 7 and 10. By the time that mice are 14 days old, and rats are 17 days old, they are highly mobile, their eyes are open, they have gained the ability to hear, and they usually do not call if isolated.

As juveniles and adults, mice and rats emit USV while interacting with conspecifics, both of the same sex and of the opposite sex. When opposite sex conspecifics interact, only the males emit USV and they are therefore thought to serve as courtship calls (Sugimoto et al., 2011; Wang et al., 2008; Warburton et al., 1989; White et al., 1998; Whitney, 1973). When given the opportunity to interact with a sexually receptive female, males reliably approach and investigate the female, and sniff her anogenital region while simultaneously emitting USV (Maggio et al., 1983; Whitney and Nyby, 1979). Females do indeed show a preference for these calls over other sounds (Hammerschmidt et al., 2009; Shepard and Liu, 2011) and for vocal males over devocalized males (Pomerantz et al., 1983).

The phenomena of USV emission in the three aforementioned contexts (namely, pup USV, same-sex USV, and male-to-female USV) have been well established in both mice and rats. Extensive research has led to the consensus that mice do not hear or learn vocalizations from their

parents as birds do, but rather that call production is inherent (Hammerschmidt et al., 2012b; Portfors and Perkel, 2014). Although they are emitted by both species, USV do not play equivalent roles within the social communication systems of both species. This is due in large part to rats engaging in a broader range of more complex social behaviors than mice, particularly during same-sex interactions.

Rats Are Not Big Mice!

The communication systems of mice and rats share a high degree of similarity, but an estimated 12-24 million years of separate evolution has contributed to a number of important differences between the species (Gibbs et al., 2004). While both mice and rats are territorial and establish dominance hierarchies, rats are generally less aggressive than mice and establish hierarchies with less physical injury. Rats often groom each other, huddle while sleeping, and, unlike mice, frequently engage in play by chasing, pouncing, pinning, and wrestling in a manner similar to cats and dogs (Gordon et al., 2002; Panksepp, 1981). The variety of behaviors exhibited and their frequencies (i.e., the "social interaction signal") are therefore significantly greater in interactions between rats compared to mice.

In this type of fast-paced rough and tumble play, rats use USV to both facilitate the initiation of the interaction and maintain the level of play over time (Himmler et al., 2014). They may even use them in structuring play bouts, determining whose turn it is to do something, and keeping the interaction from escalating into aggression (Burke et al., 2018, 2017). If rats are devocalized and lose the ability to call to their playmate (Kisko et al., 2015), or are deafened and lose the ability to hear their playmate, they have significantly reduced levels of play (Siviy and Panksepp, 1987).

In an added level of complexity, the calls that rats use to elicit play are part of a category of high frequency pro-social calls, which are distinct from isolation-induced pup USV and from a category of low frequency alarm calls. Just like humans, rats are capable of modulating the pitch of their vocalizations, which translates into calls of different frequencies.

In affiliative or other situations of positive affect, including play and sugar consumption (Browning et al., 2011), rats often emit USV with a peak frequency around 50 kHz. The role of these high frequency USV as social contact calls is supported by the observations that rats will vocalize if they detect the odor of a conspecific (Brudzynski and Pniak, 2002) and spend more time with highly vocal conspecifics compared to those who are not as vocal (Panksepp et al., 2002; Panksepp and Burgdorf, 2003). The mesolimbic dopaminergic system, including nucleus accumbens, ventral tegmental area, and ventral striatum, have been identified as important for the production of 50-kHz calls (**Table 2**; Brudzynski, 2015; Burgdorf et al., 2007, 2001; Thompson et al., 2006).

Receiver rats who hear these USV will quickly approach and investigate the source of the sound (Browning et al., 2011; Portfors, 2007; Seffer et al., 2014; Willadsen et al., 2014; Wöhr and Schwarting, 2009, 2007). The reception of 50-kHz USV is associated with the release of dopamine in the nucleus accumbens and inhibition of activity in the amygdala (Parsana et al., 2012; Sadananda et al., 2008; Willuhn et al., 2014). The opioid system has also been implicated in the social approach behavior that occurs in response to hearing 50-kHz USV (Wöhr and Schwarting, 2009).

Alternatively, in situations of negative affect such as in the presence of a predator (Blanchard et al., 1991), while experiencing pain, or during aggressive encounters, rats often emit lower frequency USV with a peak around 22 kHz (Brudzynski, 2005). These are distinct from the

calls emitted by isolated pups, which typically fall around 40 kHz. Receiver rats who hear 22-kHz calls typically freeze, hide, or attempt to escape (Portfors, 2007), demonstrating the significance of these USV as alarm calls. The mesolimbic cholinergic system has shown to be important for the production of these calls, with the basal forebrain and lateral septum playing key roles (**Table 3**; Brudzynski, 2015).

Therefore, not only do rats show a more varied social behavioral repertoire than mice, they also exhibit a richer acoustic communication system (Ellenbroek and Youn, 2016; Siviy and Panksepp, 2011). Depending on the nature of their environment, rats differentially emit vocalizations (Schwarting et al., 2007; Simola and Brudzynski, 2018; Wöhr et al., 2008) that elicit distinct behavioral and neurological responses in receiver conspecifics. This phenomenon, to date, has only been observed in rats and not congenic inbred mouse lines.

While there is increasingly mounting evidence to support rats' use of distinct frequency ranges to communicate distinct types of information, it is not yet clear whether other call features are also used to send unique signals by rats or by mice. A number of research groups have suggested the categorization of mouse and rat USV based on such acoustic features as call frequency, frequency modulation, duration, amplitude, and bout structure (Brudzynski et al., 1999; Heckman et al., 2016; Holy and Guo, 2005; Scattoni et al., 2011; Wright et al., 2010). The number of proposed call subtypes, however, varies widely and there is currently no consensus regarding the existence, number, or meaning of distinct subtypes (Hammerschmidt et al., 2012a; Kas et al., 2014; Scattoni et al., 2018). Nevertheless, the quantification of USV remains a useful proxy for human communication and is consistently carried out in rodent models of NDDs.

Testing Auditory Communication

Pups in isolation. Since NDD symptoms onset early in life, collecting behavioral measures during the early developmental period is crucial (Bale et al., 2010; Branchi and Ricceri, 2002) and USV emitted by rodent pups is a useful tool for identifying early vocal communication deficits (Wöhr and Scattoni, 2013). Mouse and rat pup communication can be reliably assayed at multiple ages across the first two weeks of life or at a single timepoint during this period. When a single timepoint is used, it is usually when pups are around one week old, which is when pup call numbers are anticipated to be at their peak and therefore offer the greatest potential to reveal a deficit (Elwood and Keeling, 1982; Roy et al., 2012; Sungur et al., 2016).

To elicit pup USV in the laboratory, each pup is individually removed from the nest and placed into a container within a sound-attenuating chamber, as in **Chapters 2**, **3**, **4**, and **6** (Hofer et al., 2001; Scattoni et al., 2018). A microphone capable of detecting ultrasonic sounds hangs above the container and records the USV emitted during the session for later analysis. After the call collection session, which typically lasts a few minutes, the pup is retrieved by the experimenter and returned to the nest.

An experimental paradigm involving multiple isolation sessions has also been used to assay attachment in mouse and rat pups (Scattoni et al., 2018; Shair et al., 2015). In a phenomenon called maternal potentiation, isolated pups emit even higher numbers of USV if reunited with their mother for a few minutes before being isolated again (Hofer, 1996). Vocalization rates during the second isolation session can be three to four times that of the initial session, making it possible to quantify the modulation of calling rates as a function of external stimuli (Hofer et al., 2001; Shair et al., 1997).

Any deviation from the normative rise-and-fall developmental profile of isolation-induced USV, day-specific calling rate, or expected potentiation effect can be considered a hallmark of

altered communication (Chadman et al., 2008; Laviola et al., 2006; Moles et al., 2004; Shu et al., 2005). Additionally, call characteristics such as call duration, peak frequency, amplitude, and temporal clustering can also be compared (Ey et al., 2013; Mosienko et al., 2015; Schmeisser et al., 2012; Wöhr, 2014).

It is good practice to measure both the pup's body temperature and body weight before returning the pup to the nest (Hofer et al., 2001). Body temperature is a potentially confounding variable since vocalization rates tend to increase as body temperature deviates from the temperature of the nest (Ehret, 2005). Body weight is used to check the overall health status of the pup, which may affect its ability to produce USV. Altered USV emission that is discovered in conjunction with delayed growth, which may affect a pup's physical ability to produce calls, would not provide strong evidence for a communication deficit per se. Rather, it would suggest an overall atypical developmental trajectory (Scattoni et al., 2018).

Additionally, it should be determined whether olfactory deficits may be contributing to abnormal vocalization rates. For pups, it is common to use the homing test in which a pup is given the choice between bedding from its home nest that contains familiar scents and new, clean bedding. With intact olfactory abilities, pups will recognize and prefer the familiar odors and can therefore be expected to spend more time on or near the bedding from their own nest than the fresh bedding (Chadman et al., 2008; Ey et al., 2012).

Same-sex vocalizations. To elicit vocalizations between laboratory mice or rats of the same sex, a subject animal is given time to interact with a sex-matched conspecific partner in a designated, neutral setting (i.e., neither animal's home cage) while an ultrasonic microphone records the interaction. A brief period of isolation before the test is often used to promote USV emission, as mice and rats will emit much higher numbers of calls following social isolation.

There is currently no practical method for determining which calls were emitted by which individual when calls are collected from multiple interacting animals. One option is to surgically devocalize all partner animals and leave the subject intact, but this is likely to alter the nature of the subsequent behaviors and the associated vocalizations since mice and rats depend on reciprocal vocalization to mediate their interactions. Therefore, subjects are typically paired with an animal of the same genotype or treatment group (Ey et al., 2013; Kisko et al., 2020; Scattoni et al., 2011; Schmeisser et al., 2012; Wang et al., 2008). This allows for the group identity of the callers to be known without the need for surgical devocalization.

An alternative technique for collecting same-sex vocalizations while circumventing the issue of identity is to provide the subject with a social cue rather than another conspecific. The social stimulus could be a social odor (i.e., urine) (Scattoni et al., 2018), a social context (i.e., a previously played-in arena) (Knutson et al., 1998; Willey and Spear, 2012), or a pre-recorded USV. The subject can also be paired with a human partner for heterospecific play, as in **Chapter 5** (Cloutier et al., 2018; LaFollette et al., 2018; Panksepp and Burgdorf, 2000; Schwarting, 2018a, 2018b; Wöhr et al., 2009). With this approach, the experimenter can deliver a standardized sequence of physical manipulations, controlling for the level of play across subjects (Berg et al., 2019; Mällo et al., 2007).

Another commonly used paradigm in the study of same-sex USV is the resident-intruder test in which an aggressive encounter is used to elicit vocalizations. This assay is carried out by introducing a novel intruder animal into the home cage of a resident subject. Due to the territoriality of mice and rats, the resident animal will reliably attack the intruder. In mice, the resident animal can be expected to make most of the calls, likely using them to signal territory ownership, and the intruder animal is not expected to emit USV (Gourbal et al., 2004;

Hammerschmidt et al., 2012a; Maggio et al., 1983). In rats, the intruder who gets attacked produces the majority of the USV, which likely serve as alarm calls or signals of negative affect (Burgdorf et al., 2008). Therefore, the identity of the caller within this paradigm in both species can be determined with reasonable confidence.

For mice, it has been suggested that same-sex vocalization tests are more ethologically relevant in females than males. This is because of the structure of the mouse social system in which a single highly territorial male lives with multiple females. Therefore, although not typically the case in modern laboratories but true on an evolutionary timescale, females live in close proximity to each other whereas males rarely come into contact with other males. In this view, in order to assay male USV in the most ethologically relevant fashion, vocalizations should be measured when prompted by the presence of a female (Kas et al., 2014).

Male-to-female vocalizations. Recording male USV in the presence of a female conspecific, often called female-induced USV, is one the most well-represented assays of adult vocal communication in NDD rodent model research. This test is especially prevalent in studies of autism spectrum disorder, in which emphasis has been placed on the behavioral phenotypes of male rodents due to the significantly biased sex ratio of the disorder in humans (Ey et al., 2012; Wöhr et al., 2011; Yang et al., 2012).

To elicit these USV in a laboratory setting, a subject male is given time to interact with a sexually receptive female (i.e., in estrus) while an ultrasonic microphone records the interaction. Alternatively, the male can be presented with the odor or urine of a female (Byatt and Nyby, 1986; Hoffmann et al., 2009; Roullet et al., 2011; Whitney and Nyby, 1979). Maximal USV emission, however, is best achieved by allowing the male to have direct physical contact with the female (Wang et al., 2008).

In contrast to assays of same-sex vocalizations, the male subject does not need pretest isolation in order to vocalize at a high rate. Additionally, there is much greater certitude that the calls collected during male-female interaction sessions are subject initiated since males produce them for courtship (Hammerschmidt et al., 2009; Pomerantz et al., 1983) and the lack of female USV in this test is well-established (Sugimoto et al., 2011; Wang et al., 2008; White et al., 1998; Whitney, 1973). This also presents a limitation, as this test can only be performed in males and does not allow for female subjects.

A crucial component of this test is the sexual receptivity of the female, which can greatly influence the behavior of the male subject (Scattoni et al., 2011; Won et al., 2012; Yang et al., 2012). If male subjects, who may be sexually experienced or naïve, are allowed to interact with females in different phases of the estrus cycle, the high variability of the males' behavior can result in a high proportion of subjects not vocalizing (Scattoni et al., 2018). Therefore, in order to achieve maximal USV production and avoid obscuring results, males should be recorded while interacting with a female who has been confirmed to be in estrus.

As with pup USV, juvenile and adult USV collection should be carried out in conjunction with a test of olfaction. Commonly used tests involve observing an animal dig for buried food, which requires that they rely solely on olfactory cues to detect and locate it. Alternatively, the previously described method of habituating then dishabituating them to various scents and social odors presented on cotton swabs can be used (Silverman et al., 2010; Yang and Crawley, 2009). If there is reason to suspect an impaired ability to physically produce calls, this should also be evaluated and eliminated as a potentially confounding variable.

Tactile Communication

One of the primary ways by which mice and rats gather information about their environment is through their whiskers, or "vibrissae" (Diamond and Arabzadeh, 2013; Welker, 1964). Whiskers are in fact specialized sensory organs that can transduce information regarding an animal's immediate surroundings and allow them to navigate without the need acute vision (Hartmann, 2011; Mitchinson et al., 2007; Welker, 1964). For mice and rats who are most active at night and typically dwell in tunnels, whiskers play a key role in sensing their environment and collecting information about the features of any nearby bodies or objects.

By quickly sweeping their whiskers back and forth in an active process called whisking, mice and rats have the ability to distinguish subtle differences in the location of a surface (Petersen and Diamond, 2000) as well as its distance (O'Connor et al., 2010), size (Brecht et al., 1997), form, and texture (Carvell and Simons, 1995; Prigg et al., 2002). They can also monitor how the air or water around them is moving, both the direction and strength of the movements. Whiskers are therefore used for estimating hole size (Krupa et al., 2001), crossing gaps (Hutson and Masterton, 1986), swimming (Richter, 1957), and capturing prey (Anjum et al., 2006; Gregoire and Smith, 1975; Karli, 2018), but are also important for nursing (Sullivan et al., 2003), acts of aggression (Ahl, 1986), and social interaction (Lenschow and Brecht, 2015), including play (Waddell et al., 2016).

Tactile information from the whiskers, in combination with that from other body parts, is used to detect the presence and motion of those nearby and to mediate the nature of any subsequent interaction that takes place. When mice or rats interact with conspecifics, they engage in behaviors such as sniffing, following, chasing, pouncing, mounting, pinning, pushing by, crawling, wrestling, and grooming each other (Berg et al., 2018; Bolivar et al., 2007; McFarlane et al., 2008; Panksepp, 1981; Silverman et al., 2010; Terranova and Laviola, 2005). In these types of direct

physical contacts, the animal initiating contact uses tactile information to determine the location and motion of the target animal, and then incorporates tactile feedback in order to gauge the pressure of their contact and to sense the response of the receiver animal. The initiator sends tactile signals to the receiver animal, who senses the activity of the other animal and can incorporate the tactile information into their assessment of the actor's intent (i.e., the degree of affiliation or aggression). Therefore, in any situation involving multiple mice or rats physically interacting, tactile communication is bound to occur.

Testing Tactile Communication

Reciprocal social interactions. While tests of reciprocal social interactions between freely moving mice or rats do not solely evaluate tactile communication or even one type of communication, these types of tests are routinely carried out in studies of NDD rodent models (as in **Chapters 2** and **5**) and involve a high degree of physical contact between animals. Since other types of communication are used to mediate physical interactions, tests of olfactory, motor, and auditory abilities should be independently assessed.

To get a detailed examination of the varied and nuanced interactions that take place between freely moving animals, pairs or groups of mice or rats are placed together in an enclosed arena. Due to the speed and complexity of these interactions, these behaviors are typically scored by a highly trained investigator using event-recording software, although videotracking systems are also available (Ahern et al., 2009; Kazdoba et al., 2016; Pobbe et al., 2010; Reppucci et al., 2018; Silverman et al., 2010). Social behaviors scored may include sniffing another animal's face, body, or anogenital region; following, chasing, grooming, pouncing on, pinning down, pushing under, crawling over, pushing past, mounting, and biting another animal. In rats, rough and tumble

play, which encompasses a number of these behaviors, is another metric of social interaction. Other, non-social behaviors scored may include exploring the arena, digging, eating, and self-grooming.

The animals may be socially isolated for a brief period before the interaction session in order to encourage contact and boost the number of behaviors displayed (Berg et al., 2018; Ku et al., 2016; Panksepp, 1981; Panksepp and Beatty, 1980; Varlinskaya et al., 1999). The stronger "social signal" that results from a higher number of and extended durations of quantifiable behaviors facilitates detecting a deficit or reduction in social interactions. This can be particularly useful when studying females, who are typically outperformed by males in the level of non-motivated play that they exhibit (Meaney and Stewart, 1981; Pellis et al., 1997; Poole and Fish, 1976). Interestingly, the quality of the play and specific patterns of interactions also often differ between the sexes (Argue and McCarthy, 2015; Pellis et al., 1997).

Both the frequency, duration, and relative timing of the aforementioned behaviors are used to assess an animal's propensity to engage in social interactions and the manner in which they do so. Subject animals may be provided with one or more conspecifics with which to interact, who may be of the same or opposite sex, may be familiar or novel, and may be of the same or different genotype or experimental group. Pairing subjects with an untreated control conspecific will likely yield very different results than pairing the subject with another treated subject, so the nature of the experimental design used will depend on the goals of the particular experiment and should always be described in detail (Argue and McCarthy, 2015; Kas et al., 2014; Silverman et al., 2010; Thor and Holloway, 1984).

Regardless of the partner's other characteristics, it should be as close in size and weight to the subject as possible. Large disparities in weight can bias the dominance-submission dynamic,

creating noisy or otherwise affected results. It is also good practice to score the behaviors of all of the animals involved in the interaction, not just the subject, since the subject's behavior will be affected by that of the other animal(s) (e.g., if and how they initiate behaviors, if and how they reciprocate behaviors).

Tests of sensorimotor abilities should accompany the test of reciprocal social interactions. As examples, an olfactory deficiency may underlie a reduction in sniffing of a conspecific, a motor deficit may underlie a reduction in chasing, and/or an impairment of balance may underlie a reduction in pouncing behavior. Additionally, the examination of vocalizations emitted either during the interaction test or an independent assay can help to reveal if and how altered USV emission is contributing to aberrant reciprocal interactions.

Emerging Approaches

Quantifying Responses to Vocalizations

The three most commonly used assays of auditory communication (namely, pup USV, same-sex USV, and male-to-female USV) all target expressive vocal communication. Given the perceptual abnormalities in humans with NDD, receptive communication and the perception of auditory signals are also of great relevance to the human phenotype (O'Connor, 2012). Therefore, although not currently widely used in rodent models of NDDs, assays quantifying the behavioral responses to conspecific vocalizations have been developed (Seffer et al., 2014; Wöhr et al., 2016) and studied in three genetic rat models of NDDs (Berg et al., 2020, 2018; Kisko et al., 2018; Wohr et al., 2020).

The experimental approach employed to this end is called ultrasonic vocalization playback and involves the use of an ultrasonic speaker to present a subject animal with a pre-recorded

conspecific vocalization. Both the subject's movement in relation to the speaker (e.g., approach or avoidance; as in **Chapters 3**, **4**, and **6**) and the USV that they emit in response to the playback can be quantified (as in **Chapter 5**).

Importantly, in order to draw inferences regarding the subject's vocal signal perception based on their response to the playback, the subject's ultrasonic hearing abilities must be confirmed as intact. Additionally, when animals are presented with an acoustic stimulus, such as the call of a conspecific, their subsequent behavior should be compared against their reaction to another type of acoustic stimulus, such as white noise that is time- and amplitude-matched. The order of the two stimuli should be counterbalanced to control for any order effect and, in this way, the effect of a novel sound can be parsed out from the effect of a socially relevant signal (Wöhr et al., 2016).

USV playback experiments have been especially useful in elucidating the various functions of rodent USV, particularly male-to-female courtship calls, which are the most common type of USV used in mouse playback experiments (Chabout et al., 2017; Hammerschmidt et al., 2009). When presented with male USV, adult female mice show a sustained interest in the sound source (Hammerschmidt et al., 2009) but males presented with female USV do not demonstrate such a reliable or robust level of interest (Snoeren and Agmo, 2013; Wöhr et al., 2011). Vocalizations from any of the previously discussed social contexts can be used in the USV playback paradigm: pup isolation calls can be used to study the search-and-retrieval behavior of females (Cohen-Salmon et al., 1985; Crawley, 2007; Noirot, 1972; Smotherman et al., 1974) and same-sex or male-female social contact calls can be used to study the behavioral response of a juvenile or adult subject.

An essential prerequisite to the playback paradigm is that the subject animal must have intact hearing abilities. One likely factor that has contributed to these paradigms not yet being

widely used for studying rodent models of NDDs (Kas et al., 2014) is the rapid hearing loss that commonly afflicts laboratory mice which are inbred. The degree to which hearing degrades is strain-dependent, with some strains of mice experiencing hearing loss as early as three months of age, including the common C57BL/6J ("B6") strain (Erway et al., 1996; Henry and Chole, 1980; Johnson et al., 1997; Zheng et al., 1999). With this caveat in mind, USV playback assays should continue to be carried out, especially in rat models, as they can provide valuable insights into the receptive communication deficits underlying NDDs. When used in the phenotyping of rat models, calls of low or high frequency can be presented in order to gain a more nuanced assessment of affect-specific auditory perception.

Measuring Call Quantity and Quality

Following USV collection from any social context, investigators may score the number of vocalizations that a subject emitted as well as other acoustic properties about the calls, such as call frequency, frequency modulation, duration, amplitude, and bout structure. As mentioned prior, calls can then be categorized into discrete subtypes based on their various properties. Apart from the delineation between 22 and 50-kHz rat USV, which is based on the sole property of call frequency, there is currently no consensus regarding how to draw distinctions between call subtypes (Kazdoba et al., 2016).

Unlike low and high frequency rat calls, there has yet to be convincing evidence for functional differences between proposed subtypes. The number of subtypes therefore varies widely across research groups, ranging from three (Hammerschmidt et al., 2012a) to four (Kisko et al., 2018) to fifteen (Mahrt et al., 2013). Due in part to the lack of consensus regarding number and significance of possible subtypes, as well as the effortful and time-consuming process required if

carried out manually, call classification into subtypes is not routinely carried out in rodent models of NDDs. The exception to this is the frequency analysis of rat USV, which is typically performed via an automated or semi-automated process.

Categorizing calls into subtypes, however, is not a prerequisite for detecting abnormal call structure in a given context (Brudzynski et al., 1999; Wöhr and Schwarting, 2008). The acoustic features of USV can be quantified and compared without the need for defining subtypes or assigning significance to them. In addition to the quantification of frequency, which can provide insight into a rat's perception of its environment and accompanying affective experience, there is also evidence that mouse call characteristics differ across contexts (Barron and Gilbertson, 2005; Branchi et al., 1998; Brudzynski et al., 1999; Chabout et al., 2012). In fact, calls with different sets of features appear to elicit different neural responses within the auditory midbrain of the mouse (Mayko et al., 2012).

Thanks to various efforts over the last decade to develop more advanced, automatic systems for the detection and characterization of USV, multiple software programs for this purpose are now available (e.g., WAAVES (Reno et al., 2013); XBAT (Barker et al., 2014); VoICE (Burkett et al., 2015); DeepSqueak (Coffey et al., 2019); Mouse Syllable Classification Calculator, (Grimsley et al., 2012)) (Branchi et al., 2001; Lai et al., 2014; Scattoni et al., 2008; Wöhr, 2014). These computerized tools have significantly facilitated the speed at which USV can be counted and call features can be extracted, but there are a number of methodological caveats which must be considered.

As with any automatic program, its ability to accurately carry out the desired function must be verified and several iterations of calibration may be needed (Scattoni et al., 2008; Wöhr and Schwarting, 2013). Care must be taken to ensure that bedding noise is not misidentified as USV

and that call fragmentation does not artificially inflate call counts (Brudzynski, 2009). Even programs that involve machine learning (e.g., DeepSqueak), and are therefore capable of learning to avoid these pitfalls, must be appropriately trained and subsequently validated.

As USV analysis software continues to improve, get more reliable, user-friendly, and thereby make detailed acoustic analyses faster and easier, investigators should embrace the technology. There is much to be gained from collecting information on acoustic parameters above and beyond the metric of call quantity. By accumulating detailed information on the acoustic properties of calls and on the context in which they were emitted, the field can move toward a more comprehensive understanding of exactly how mice and rats use USV to exchange information. Additionally, carefully conducted playback experiments using calls of different acoustic characteristics can help to elucidate if and how proposed subtypes are meaningful to mice and rats.

Conclusions

Communication deficits or abnormalities in mouse and rat models of neurodevelopmental disorders can be measured in a wide array of social contexts. The three most commonly used types of communication assays examine the subject's use of olfactory, auditory, and tactile communication. Urine deposition and investigation are used to probe expressive and receptive olfactory communication. Since communication via pheromones is of primary importance to the sensory experience and thus behavior of mice and rats, it is crucial to include an assessment of olfactory abilities in conjunction with other behavioral phenotyping.

Additionally, auditory communication can be assessed across the lifespan, beginning from the neonatal period and extending throughout adulthood. Since different motivations underlie the

emission of vocalizations at various life stages (e.g., eliciting maternal care vs. courtship) and contexts (e.g., rat play vs. pain), the vocalization profile from each type of context contributes unique information regarding the communication phenotypes of the model under study. While not quite analogous to human language, mouse and rat vocalizations do have complexities and future studies of receptive auditory communication (potentially utilizing the playback of vocalizations) can help shed light on how exactly each species utilizes vocal signals to transfer information.

Finally, when evaluating an animal's propensity to communicate via tactile signals, it is of great importance to consider the reciprocal nature of the physical interactions and the ways in which the partner(s)' behavior may influence that of the subject. Sound interpretations of social communication data are only possible after confirming that the relevant sensorimotor systems are not significantly impaired, and the species-specific value of the communication is considered. Assays of olfaction, ultrasonic communication, and social interaction are and will continue to be central in the study of rodent models of NDDs and provide critical outcome measures in the pursuit of effective therapeutics.

References

Achiraman, S., Archunan, G., 2002. Urinary proteins and pheromonal communication in mammals. Indian J. Exp. Biol. 40, 1077–1078.

Ahern, T., Modi, M., Burkett, J., Young, L., 2009. Evaluation of two automated metrics for analyzing partner preference tests. J. Neurosci. Methods 182, 180–188.

Ahl, A.S., 1986. The role of vibrissae in behavior: A status review. Vet. Res. Commun. 10, 245–268. https://doi.org/10.1007/BF02213989

Anjum, F., Turni, H., Mulder, P.G.H., Van Der Burg, J., Brecht, M., 2006. Tactile guidance of prey capture in Etruscan shrews. Proc. Natl. Acad. Sci. U. S. A. 103, 16544–16549. https://doi.org/10.1073/pnas.0605573103

Arakawa, H., Blanchard, D.C., Arakawa, K., Dunlap, C., Blanchard, R.J., 2008. Scent marking behavior as an odorant communication in mice. Neurosci. Biobehav. Rev. 32, 1236–1248. https://doi.org/10.1016/j.neubiorev.2008.05.012

Argue, K.J., McCarthy, M.M., 2015. Characterization of juvenile play in rats: Importance of sex of self and sex of partner. Biol. Sex Differ. 6, 1–13. https://doi.org/10.1186/s13293-015-0034-x

Aubin, T., 2010. Social Communication. Encycl. Behav. Neurosci. 269–275. https://doi.org/10.1016/B978-0-08-045396-5.00113-5

Bale, T.L., Baram, T.Z., Brown, A.S., Goldstein, J.M., Insel, T.R., McCarthy, M.M., Nemeroff, C.B., Reyes, T.M., Simerly, R.B., Susser, E.S., Nestler, E.J., 2010. Early life programming and neurodevelopmental disorders. Biol. Psychiatry 68, 314–319. https://doi.org/10.1016/j.biopsych.2010.05.028

Barker, D.J., Herrera, C., West, M.O., 2014. Automated detection of 50-kHz ultrasonic vocalizations using template matching in XBAT. J. Neurosci. Methods 236, 68–75. https://doi.org/10.1016/j.jneumeth.2014.08.007

Barron, S., Gilbertson, R., 2005. Neonatal ethanol exposure but not neonatal cocaine selectively reduces specific isolation-induced vocalization waveforms in rats. Behav. Genet. 35, 93–102. https://doi.org/10.1007/s10519-004-0859-2

Berg, E.L., Copping, N.A., Rivera, J.K., Pride, M.C., Careaga, M., Bauman, M.D., Berman, R.F., Lein, P.J., Harony-Nicolas, H., Buxbaum, J.D., Ellegood, J., Lerch, J.P., Wöhr, M., Silverman, J.L., 2018. Developmental social communication deficits in the Shank3 rat model of phelan-mcdermid syndrome and autism spectrum disorder. Autism Res. 11, 587–601. https://doi.org/10.1002/aur.1925

Berg, E.L., Petkova, S.P., Shen, Y., Harris, S., Born, H.A., Anderson, A.E., Dindot, S. V., Weeber, E.J., Segal, D.J., Wohr, M., Silverman, J.L., 2019. Behavioral characterization of a full UBE3A deletion rat model, in: Neuroscience. Chicago, IL.

Berg, E.L., Pride, M.C., Petkova, S.P., Lee, R.D., Copping, N.A., Shen, Y., Adhikari, A., Fenton, T.A., Pedersen, L.R., Noakes, L.S., Nieman, B.J., Lerch, J.P., Harris, S., Born, H.A., Peters, M.M., Deng, P., Cameron, D.L., Fink, K.D., Beitnere, U., O'Geen, H., Anderson, A.E., Dindot, S. V., Nash, K.R., Weeber, E.J., Wöhr, M., Ellegood, J., Segal, D.J., Silverman, J.L., 2020. Translational outcomes in a full gene deletion of ubiquitin protein ligase E3A rat model of Angelman syndrome. Transl. Psychiatry 2020 101 10, 1–16. https://doi.org/10.1038/s41398-020-0720-2

Bihari, A., Hrycyshyn, A.W., Brudzynski, S.M., 2003. Role of the mesolimbic cholinergic projection to the septum in the production of 22 kHz alarm calls in rats. Brain Res. Bull. 60,

263–274. https://doi.org/10.1016/S0361-9230(03)00041-8.
Blanchard, D.C., Agullana, R., Squirrels, G., 1991. Twenty-two kHz alarm cries to presentation of a predator, by laboratory rats living in visible burrow systems. Physiol. Behav. 50, 967–972.
Bolivar, V.J., Walters, S.R., Phoenix, J.L., 2007. Assessing autism-like behavior in mice: Variations in social interactions among inbred strains. Behav. Brain Res. 176, 21–26. https://doi.org/10.1016/j.bbr.2006.09.007
Branchi, I., Ricceri, L., 2002. Transgenic and knock-out mouse pups: The growing need for behavioral analysis. Genes, Brain Behav. 1, 135–141. https://doi.org/10.1034/j.1601-183X.2002.10301.x
Branchi, I., Santucci, D., Alleva, E., 2001. Ultrasonic vocalisation emitted by infant rodents: A tool for assessment of neurobehavioural development. Behav. Brain Res. 125, 49–56. https://doi.org/10.1016/S0166-4328(01)00277-7
Branchi, I., Santucci, D., Vitale, A., Alleva, E., 1998. Ultrasonic vocalizations by infant laboratory mice: A preliminary spectrographic characterization under different conditions. Dev. Psychobiol. 33, 249–256. https://doi.org/10.1002/(SICI)1098-2302(199811)33:3<249::AID-DEV5>3.0.CO;2-R
Brecht, M., Preilowski, B., Merzenich, M.M., Keck, W.M., 1997. Functional architecture of the mystacial vibrissae. Behav. Brain Res. 84, 81–97.
Brennan, P.A., Kendrick, K.M., 2006. Mammalian social odours: Attraction and individual recognition. Philos. Trans. R. Soc. B Biol. Sci. 361, 2061–2078. https://doi.org/10.1098/rstb.2006.1931
Browning, J.R., Browning, D.A., Maxwell, A.O., Dong, Y., Jansen, H.T., Panksepp, J., Sorg, B.A., 2011. Positive affective vocalizations during cocaine and sucrose self-administration: A model for spontaneous drug desire in rats. Neuropharmacology 61, 268–275. https://doi.org/10.1016/j.neuropharm.2011.04.012
Brudzynski, S., 2015. Pharmacology of Ultrasonic Vocalizations in adult Rats: Significance, Call Classification and Neural Substrate. Curr. Neuropharmacol. 13, 180–192.
Brudzynski, S.M., Barnabi, F., 1996. Contribution of the ascending cholinergic pathways in the production of ultrasonic vocalization in the rat. Behav. Brain Res. 80, 145–152. https://doi.org/10.1016/0166-4328(96)00029-0.
Brudzynski, S.M., Bihari, F., 1990. Ultrasonic vocalization in rats produced by cholinergic stimulation of the brain. Neurosci. Lett. 109, 222–226. https://doi.org/10.1016/0304-3940(90)90567-S.
Brudzynski, S., Pniak, A., 2002. Social contacts and production of 50-kHz short ultrasonic calls in adult rats. J. Comp. Psychol. 116, 73–82.
Brudzynski, S.M., 2009. Communication of adult rats by ultrasonic vocalization: Biological, sociobiological, and neuroscience approaches. ILAR J. 50, 43–50. https://doi.org/10.1093/ilar.50.1.43
Brudzynski, S.M., 2005. Principles of rat communication: Quantitative parameters of ultrasonic calls in rats. Behav. Genet. 35, 85–92. https://doi.org/10.1007/s10519-004-0858-3
Brudzynski, S.M., Kehoe, P., Callahan, M., 1999. Sonographic structure of isolation-induced ultrasonic calls of rat pups. Dev. Psychobiol. 34, 195–204. https://doi.org/10.1002/(SICI)1098-2302(199904)34:3<195::AID-DEV4>3.0.CO;2-S
Burgdorf, J., Knutson, B., Panksepp, J., Ikemoto, S., 2001. Nucleus accumbens amphetamine microinjections unconditionally elicit 50-kHz ultrasonic vocalizations in rats. Behav. Neurosci. 115, 940–944. https://doi.org/10.1037/0735-7044.115.4.940

Burgdorf, J., Kroes, R.A., Moskal, J.R., Pfaus, J.G., Brudzynski, S.M., Panksepp, J., 2008. Ultrasonic Vocalizations of Rats (Rattus norvegicus) During Mating, Play, and Aggression: Behavioral Concomitants, Relationship to Reward, and Self-Administration of Playback. J. Comp. Psychol. 122, 357–367. https://doi.org/10.1037/a0012889

Burgdorf, J., Wood, P.L., Kroes, R.A., Moskal, J.R., Panksepp, J., 2007. Neurobiology of 50-kHz ultrasonic vocalizations in rats: Electrode mapping, lesion, and pharmacology studies. Behav. Brain Res. 182, 274–283. https://doi.org/10.1016/j.bbr.2007.03.010

Burke, C.J., Kisko, T.M., Euston, D.R., Pellis, S.M., 2018. Do juvenile rats use specific ultrasonic calls to coordinate their social play? Anim. Behav. 140, 81–92. https://doi.org/10.1016/j.anbehav.2018.03.019

Burke, C.J., Kisko, T.M., Pellis, S.M., Euston, D.R., 2017. Avoiding escalation from play to aggression in adult male rats: The role of ultrasonic calls. Behav. Processes 144, 72–81. https://doi.org/10.1016/j.beproc.2017.09.014

Burkett, Z.D., Day, N.F., Peñagarikano, O., Geschwind, D.H., White, S.A., 2015. VoICE: A semi-automated pipeline for standardizing vocal analysis across models. Sci. Rep. 5, 1–15. https://doi.org/10.1038/srep10237

Byatt, S., Nyby, J., 1986. Hormonal regulation of chemosignals of female mice that elicit ultrasonic vocalizations from males. Horm. Behav. 20, 60–72. https://doi.org/10.1016/0018-506X(86)90029-2

Carvell, G.E., Simons, D.J., 1995. Task- and subject-related differences in sensorimotor behavior during active touch. Somatosens. Mot. Res. 12, 1–9. https://doi.org/10.3109/08990229509063138

Chabout, J., Jones-Macopson, J., Jarvis, E.D., 2017. Eliciting and analyzing male mouse ultrasonic vocalization (USV) songs. J. Vis. Exp. 2017, 1–13. https://doi.org/10.3791/54137

Chabout, J., Serreau, P., Ey, E., Bellier, L., Aubin, T., Bourgeron, T., Granon, S., 2012. Adult male mice emit context-specific ultrasonic vocalizations that are modulated by prior isolation or group rearing environment. PLoS One 7, 1–9. https://doi.org/10.1371/journal.pone.0029401

Chadman, K.K., Gong, S., Scattoni, M.L., Boltuck, S.E., Gandhy, S.U., Heintz, N., Crawley, J.N., 2008. Minimal aberrant behavioral phenotypes of neuroligin-3 R451C knockin mice. Autism Res. 1, 147–158. https://doi.org/10.1002/aur.22

Choi, J.S., Brown, T.H., 2003. Central amygdala lesions block ultrasonic vocalization and freezing as conditional but not unconditional responses. J. Neurosci. 23, 8713–8721. https://doi.org/10.1523/jneurosci.23-25-08713.2003

Cloutier, S., LaFollette, M.R., Gaskill, B.N., Panksepp, J., Newberry, R.C., 2018. Tickling, a technique for inducing positive affect when handling rats. J. Vis. Exp. 2018. https://doi.org/10.3791/57190

Coffey, K.R., Marx, R.G., Neumaier, J.F., 2019. DeepSqueak: a deep learning-based system for detection and analysis of ultrasonic vocalizations. Neuropsychopharmacology 44, 859–868. https://doi.org/10.1038/s41386-018-0303-6

Cohen-Salmon, C., Carlier, M., Roubertoux, P., Jouhaneau, J., Semal, C., Paillette, M., 1985. Differences in patterns of pup care in mice V-Pup ultrasonic emissions and pup care behavior. Physiol. Behav. 35, 167–174. https://doi.org/10.1016/0031-9384(85)90331-2

Crawley, J.N., 2007. Mouse behavioral assays relevant to the symptoms of autism. Brain Pathol. 17, 448–459. https://doi.org/10.1111/j.1750-3639.2007.00096.x

Desjardins, C., Maruniak, J.A., Bronson, F.H., 1973. Social Rank in House Mice : Differentiation Revealed by Ultraviolet Visualization of Urinary Marking Patterns. Science (80-.). 182, 939–

941.
Diamond, M.E., Arabzadeh, E., 2013. Whisker sensory system - From receptor to decision. Prog. Neurobiol. 103, 28–40. https://doi.org/10.1016/j.pneurobio.2012.05.013
Ehret, G., 2005. Infant rodent ultrasounds - A gate to the understanding of sound communication. Behav. Genet. 35, 19–29. https://doi.org/10.1007/s10519-004-0853-8
Ellenbroek, B., Youn, J., 2016. Rodent models in neuroscience research: Is it a rat race? DMM Dis. Model. Mech. 9, 1079–1087. https://doi.org/10.1242/dmm.026120
Elwood, R.W., Keeling, F., 1982. Temporal organization of ultrasonic vocalizations in infant mice. Dev. Psychobiol. 15, 221–227. https://doi.org/10.1002/dev.420150306
Erway, L.C., Shiau, Y.W., Davis, R.R., Krieg, E.F., 1996. Genetics of age-related hearing loss in mice. III. Susceptibility of inbred and F1 hybrid strains to noise-induced hearing loss. Hear. Res. 93, 181–187. https://doi.org/10.1016/0378-5955(95)00226-X
Ey, E., Torquet, N., Le Sourd, A.M., Leblond, C.S., Boeckers, T.M., Faure, P., Bourgeron, T., 2013. The Autism ProSAP1/Shank2 mouse model displays quantitative and structural abnormalities in ultrasonic vocalisations. Behav. Brain Res. 256, 677–689. https://doi.org/10.1016/j.bbr.2013.08.031
Ey, E., Yang, M., Katz, A.M., Woldeyohannes, L., Silverman, J.L., Leblond, C.S., Faure, P., Torquet, N., Le Sourd, A.M., Bourgeron, T., Crawley, J.N., 2012. Absence of deficits in social behaviors and ultrasonic vocalizations in later generations of mice lacking neuroligin4. Genes, Brain Behav. 11, 928–941. https://doi.org/10.1111/j.1601-183X.2012.00849.x
Fendt, M., Schwienbacher, I., Schnitzler, H.U., 2006. Carbachol injections into the nucleus accumbens induce 50 kHz calls in rats. Neurosci. Lett. 401, 10–15. https://doi.org/10.1016/j.neulet.2006.02.069
Fu, X. wen, Brudzynski, S.M., 1994. High-frequency ultrasonic vocalization induced by intracerebral glutamate in rats. Pharmacol. Biochem. Behav. 49, 835–841. https://doi.org/10.1016/0091-3057(94)90231-3
Geurts, A.M., Cost, G.J., Freyvert, Y., Zeitler, B., Miller, J.C., Choi, V.M., Jenkins, S.S., Wood, A., Cui, X., Meng, X., Vincent, A., Lam, S., Michalkiewicz, M., Schilling, R., Foeckler, J., Kalloway, S., Weiler, H., Ménoret, S., Anegon, I., Davis, G.D., Zhang, L., Rebar, E.J., Gregory, P.D., Urnov, F.D., Jacob, H.J., Buelow, R., 2009. Knockout rats via embryo microinjection of zinc-finger nucleases. Science (80-.). 325, 433. https://doi.org/10.1126/science.1172447
Gibbs, R.A., Metzker, M.L., Muzny, D.M., Sodergren, E.J., Scherer, S., Scott, G., Steffen, D., Worley, K.C., Burch, P.E., 2004. Genome sequence of the Brown Norway rat yields insights into mammalian evolution. Nature 428, 493–521.
Gordon, N.S., Kollack-Walker, S., Akil, H., Panksepp, J., 2002. Expression of c-fos gene activation during rough and tumble play in juvenile rats. Brain Res. Bull. 57, 651–659. https://doi.org/10.1016/S0361-9230(01)00762-6
Gourbal, B.E.F., Barthelemy, M., Petit, G., Gabrion, C., 2004. Spectrographic analysis of the ultrasonic vocalisations of adult male and female BALB/c mice. Naturwissenschaften 91, 381–385. https://doi.org/10.1007/s00114-004-0543-7
Gregoire, S.E., Smith, D.E., 1975. Mouse-killing in the rat: Effects of sensory deficits on attack behaviour and stereotyped biting. Anim. Behav. 23, 186–191. https://doi.org/10.1016/0003-3472(75)90064-0
Grimsley, J., Gadziola, M., Wenstrup, J.J., 2012. Automated classification of mouse pup isolation syllables: From cluster analysis to an excel based “mouse pup syllable classification

calculator." Front. Behav. Neurosci. 6, 1–12. https://doi.org/10.3389/fnbeh.2012.00089
Halpern, M., Martínez-Marcos, A., 2003. Structure and function of the vomeronasal system: An update. Prog. Neurobiol. 70, 245–318. https://doi.org/10.1016/S0301-0082(03)00103-5
Hamilton, S.M., Green, J.R., Veeraragavan, S., Yuva, L., McCoy, A., Wu, Y., Warren, J., Little, L., Ji, D., Cui, X., Weinstein, E., Paylor, R., 2014. Fmr1 and Nlgn3 knockout rats: Novel tools for investigating autism spectrum disorders. Behav. Neurosci. 128, 103–109. https://doi.org/10.1037/a0035988
Hammerschmidt, K., Radyushkin, K., Ehrenreich, H., Fischer, J., 2012a. The structure and usage of female and male mouse ultrasonic vocalizations reveal only minor differences. PLoS One 7, 1–7. https://doi.org/10.1371/journal.pone.0041133
Hammerschmidt, K., Radyushkin, K., Ehrenreich, H., Fischer, J., 2009. Female mice respond to male ultrasonic "songs" with approach behaviour. Biol. Lett. 5, 589–592. https://doi.org/10.1098/rsbl.2009.0317
Hammerschmidt, K., Reisinger, E., Westekemper, K., Ehrenreich, L., Strenzke, N., Fischer, J., 2012b. Mice do not require auditory input for the normal development of their ultrasonic vocalizations. BMC Neurosci. 13. https://doi.org/10.1186/1471-2202-13-40
Hanson, A.E., 2004. What Do Rats See? [WWW Document]. URL http://www.ratbehavior.org/RatVision.htm
Harony-Nicolas, H., Kay, M., du Hoffmann, J., Klein, M.E., Bozdagi-Gunal, O., Riad, M., Daskalakis, N.P., Sonar, S., Castillo, P.E., Hof, P.R., Shapiro, M.L., Baxter, M.G., Wagner, S., Buxbaum, J.D., 2017. Oxytocin improves behavioral and electrophysiological deficits in a novel Shank3-deficient rat. Elife 6, 1–2. https://doi.org/10.7554/eLife.18904
Hartmann, M.J.Z., 2011. A night in the life of a rat: Vibrissal mechanics and tactile exploration. Ann. N. Y. Acad. Sci. 1225, 110–118. https://doi.org/10.1111/j.1749-6632.2011.06007.x
He, J., Ma, L., Kim, S., Nakai, J., Yu, C.R., 2008. Encoding Gender and Individual Information in the Mouse Vomeronasal Organ 320, 535–539.
Heckman, J., McGuinness, B., Celikel, T., Englitz, B., 2016. Determinants of the mouse ultrasonic vocal structure and repertoire. Neurosci. Biobehav. Rev. 65, 313–325. https://doi.org/10.1016/j.neubiorev.2016.03.029
Henry, K.R., Chole, R.A., 1980. Genotypic differences in behavioral, physiological and anatomical expressions of age-related hearing loss in the laboratory mouse: Original papers travaux originaux. Int. J. Audiol. 19, 369–383. https://doi.org/10.3109/00206098009070071
Himmler, B.T., Kisko, T.M., Euston, D.R., Kolb, B., Pellis, S.M., 2014. Are 50-kHz calls used as play signals in the playful interactions of rats? I. Evidence from the timing and context of their use. Behav. Processes 106, 60–66. https://doi.org/10.1016/j.beproc.2014.04.014
Hofer, M.A., 1996. Multiple regulators of ultrasonic vocalization in the infant rat. Psychoneuroendocrinology 21, 203–217. https://doi.org/10.1016/0306-4530(95)00042-9
Hofer, M.A., Shair, H.N., Brunelli, S.A., 2001. Ultrasonic Vocalizations in Rat and Mouse Pups. Curr. Protoc. Neurosci. 17, 1–16. https://doi.org/10.1002/0471142301.ns0814s17
Hoffmann, F., Musolf, K., Penn, D.J., 2009. Freezing urine reduces its efficacy for eliciting ultrasonic vocalizations from male mice. Physiol. Behav. 96, 602–605. https://doi.org/10.1016/j.physbeh.2008.12.014
Holy, T.E., Guo, Z., 2005. Ultrasonic songs of male mice. PLoS Biol. 3, 1–10. https://doi.org/10.1371/journal.pbio.0030386
Hori, M., Shimoju, R., Tokunaga, R., Ohkubo, M., Miyabe, S., Ohnishi, J., Murakami, K., Kurosawa, M., 2013. Tickling increases dopamine release in the nucleus accumbens and 50

kHz ultrasonic vocalizations in adolescent rats. Neuroreport 24, 241–245. https://doi.org/10.1097/WNR.0b013e32835edbfa
Horn, A., 1998. No Title [WWW Document]. Why Rats Need Co. URL https://www.nfrs.org/articles_company.html
Hutson, K.A., Masterton, R.B., 1986. The sensory contribution of a single vibrissa's cortical barrel. J. Neurophysiol. 56, 1196–1223. https://doi.org/10.1152/jn.1986.56.4.1196
Johnson, K.R., Erway, L.C., Cook, S.A., Willott, J.F., Zheng, Q.Y., 1997. A major gene affecting age-related hearing loss in C57BL/6J mice. Hear. Res. 114, 83–92. https://doi.org/10.1016/S0378-5955(97)00155-X
Karli, P., 2018. The Norway Rat's Killing Response to the White Mouse : An Experimental Analysis. Behaviour 10, 81–103.
Kas, M.J., Glennon, J.C., Buitelaar, J., Ey, E., Biemans, B., Crawley, J., Ring, R.H., Lajonchere, C., Esclassan, F., Talpos, J., Noldus, L.P.J.J., Burbach, J.P.H., Steckler, T., 2014. Assessing behavioural and cognitive domains of autism spectrum disorders in rodents: Current status and future perspectives. Psychopharmacology (Berl). 231, 1125–1146. https://doi.org/10.1007/s00213-013-3268-5
Kazdoba, T.M., Leach, P.T., Crawley, J.N., 2016. Behavioral phenotypes of genetic mouse models of autism. Genes, Brain Behav. 15, 7–26. https://doi.org/10.1111/gbb.12256
Keller, M., Baum, M.J., Brock, O., Brennan, P.A., Bakker, J., 2009. The main and the accessory olfactory systems interact in the control of mate recognition and sexual behavior. Behav. Brain Res. 200, 268–276. https://doi.org/10.1016/j.bbr.2009.01.020
Kisko, T.M., Braun, M.D., Michels, S., Witt, S.H., Rietschel, M., Culmsee, C., Schwarting, R.K.W., Wöhr, M., 2020. Sex-dependent effects of Cacna1c haploinsufficiency on juvenile social play behavior and pro-social 50-kHz ultrasonic communication in rats. Genes, Brain Behav. 19, 1–17. https://doi.org/10.1111/gbb.12552
Kisko, T.M., Braun, M.D., Michels, S., Witt, S.H., Rietschel, M., Culmsee, C., Schwarting, R.K.W., Wöhr, M., 2018. Cacna1c haploinsufficiency leads to pro-social 50-kHz ultrasonic communication deficits in rats. DMM Dis. Model. Mech. 11. https://doi.org/10.1242/dmm.034116
Kisko, T.M., Himmler, B.T., Himmler, S.M., Euston, D.R., Pellis, S.M., 2015. Are 50-kHz calls used as play signals in the playful interactions of rats? II. Evidence from the effects of devocalization. Behav. Processes 111, 25–33. https://doi.org/10.1016/j.beproc.2014.11.011
Knutson, B., Burgdorf, J., Panksepp, J., 1998. Anticipation of play elicits high-frequency ultrasonic vocalizations in young rats. J. Comp. Psychol. 112, 65–73.
Krupa, D.J., Matell, M.S., Brisben, A.J., Oliveira, L.M., Nicolelis, M.A.L., 2001. Behavioral properties of the trigeminal somatosensory system in rats performing whisker-dependent tactile discriminations. J. Neurosci. 21, 5752–5763. https://doi.org/10.1523/jneurosci.21-15-05752.2001
Ku, K.M., Weir, R.K., Silverman, J.L., Berman, R.F., Bauman, M.D., 2016. Behavioral phenotyping of juvenile long-evans and sprague-dawley rats: Implications for preclinical models of autism spectrum disorders. PLoS One 11, 1–25. https://doi.org/10.1371/journal.pone.0158150
LaFollette, M.R., O'Haire, M.E., Cloutier, S., Gaskill, B.N., 2018. Practical rat tickling: Determining an efficient and effective dosage of heterospecific play. Appl. Anim. Behav. Sci. 208, 82–91. https://doi.org/10.1016/j.applanim.2018.08.005
Lai, J.K.Y., Sobala-Drozdowski, M., Zhou, L., Doering, L.C., Faure, P.A., Foster, J.A., 2014.

Temporal and spectral differences in the ultrasonic vocalizations of fragile X knock out mice during postnatal development. Behav. Brain Res. 259, 119–130. https://doi.org/10.1016/j.bbr.2013.10.049

Langford, D.J., Bailey, A.L., Chanda, M.L., Clarke, S.E., Drummond, T.E., Echols, S., Glick, S., Ingrao, J., Klassen-Ross, T., Lacroix-Fralish, M.L., Matsumiya, L., Sorge, R.E., Sotocinal, S.G., Tabaka, J.M., Wong, D., Van Den Maagdenberg, A.M.J.M., Ferrari, M.D., Craig, K.D., Mogil, J.S., 2010. Coding of facial expressions of pain in the laboratory mouse. Nat. Methods 7, 447–449. https://doi.org/10.1038/nmeth.1455

Laviola, G., Adriani, W., Gaudino, C., 2006. Paradoxical effects of prenatal acetylcholinesterase blockade on neuro-behavioral development and drug-induced stereotypies in reeler mutant mice 331–344. https://doi.org/10.1007/s00213-006-0426-z

Leinders-Zufall, T., Brennan, P., Widmayer, P., Chandramani S., P., Maul-Pavicic, A., Jäger, M., Li, X.H., Breer, H., Zufall, F., Boehm, T., 2004. MHC class I peptides as chemosensory signals in the vomeronasal organ. Science (80-.). 306, 1033–1037. https://doi.org/10.1126/science.1102818

Leinders-Zufall, T., Lane, A.P., Puche, A.C., Ma, W., Novotny, M. V., Shipley, M.T., Zufall, F., 2000. Pheromone detection by mammalian vomeronasal neurons. Nature 405, 792–796. https://doi.org/10.1002/jemt.10152

Lenschow, C., Brecht, M., 2015. Barrel Cortex Membrane Potential Dynamics in Social Touch. Neuron 85, 718–725. https://doi.org/10.1016/j.neuron.2014.12.059

Lord, C., Brugha, T.S., Charman, T., Cusack, J., Dumas, G., Frazier, T., Jones, E.J.H., Jones, R.M., Pickles, A., State, M.W., Taylor, J.L., Veenstra-VanderWeele, J., 2020. Autism spectrum disorder. Nat. Rev. Dis. Prim. 6. https://doi.org/10.1038/s41572-019-0138-4

Maggio, J.C., Maggio, J.H., Whitney, G., 1983. Experience-based vocalization of male mice to female chemosignals. Physiol. Behav. 31, 269–272. https://doi.org/10.1016/0031-9384(83)90186-5

Mahrt, E.J., Perkel, D.J., Tong, L., Rubel, E.W., Portfors, C. V., 2013. Engineered deafness reveals that mouse courtship vocalizations do not require auditory experience. J. Neurosci. 33, 5573–5583. https://doi.org/10.1523/JNEUROSCI.5054-12.2013

Mällo, T., Matrov, D., Herm, L., Kõiv, K., Eller, M., Rinken, A., Harro, J., 2007. Tickling-induced 50-kHz ultrasonic vocalization is individually stable and predicts behaviour in tests of anxiety and depression in rats. Behav. Brain Res. 184, 57–71. https://doi.org/10.1016/j.bbr.2007.06.015

Mayko, Z.M., Roberts, P.D., Portfors, C. V., 2012. Inhibition shapes selectivity to vocalizations in the inferior colliculus of awake mice. Front. Neural Circuits 6, 1–15. https://doi.org/10.3389/fncir.2012.00073

McFarlane, H.G., Kusek, G.K., Yang, M., Phoenix, J.L., Bolivar, V.J., Crawley, J.N., 2008. Autism-like behavioral phenotypes in BTBR T+tf/J mice. Genes, Brain Behav. 7, 152–163. https://doi.org/10.1111/j.1601-183X.2007.00330.x

Meaney, M.J., Stewart, J., 1981. A descriptive study of social development in the rat (Rattus norvegicus). Anim. Behav. 29, 34–45. https://doi.org/10.1016/S0003-3472(81)80149-2

Mitchinson, B., Martin, C.J., Grant, R.A., Prescott, T.J., 2007. Feedback control in active sensing: Rat exploratory whisking is modulated by environmental contact. Proc. R. Soc. B Biol. Sci. 274, 1035–1041. https://doi.org/10.1098/rspb.2006.0347

Moles, A., Kieffer, B.L., D'Amato, F.R., 2004. Deficit in attachment behavior in mice lacking the μ-opioid receptor gene. Science (80-.). 304, 1983–1986.

https://doi.org/10.1126/science.1095943
Mosienko, V., Beis, D., Alenina, N., Wöhr, M., 2015. Reduced isolation-induced pup ultrasonic communication in mouse pups lacking brain serotonin. Mol. Autism 6, 1–13. https://doi.org/10.1186/s13229-015-0003-6
Noirot, E., 1972. Ultrasounds and maternal behavior in small rodents. Dev. Psychobiol. 5, 371–387. https://doi.org/10.1002/dev.420050410
Novotny, M., Harvey, S., Jemiolo, B., Alberts, J., 1985. Synthetic pheromones that promote inter-male aggression in mice. Proc. Natl. Acad. Sci. U. S. A. 82, 2059–2061. https://doi.org/10.1073/pnas.82.7.2059
O'Connor, D.H., Clack, N.G., Huber, D., Komiyama, T., Myers, E.W., Svoboda, K., 2010. Vibrissa-based object localization in head-fixed mice. J. Neurosci. 30, 1947–1967. https://doi.org/10.1523/JNEUROSCI.3762-09.2010
O'Connor, K., 2012. Auditory processing in autism spectrum disorder: A review. Neurosci. Biobehav. Rev. 36, 836–854. https://doi.org/10.1016/j.neubiorev.2011.11.008
Panksepp, J., 1981. The ontogeny of play in rats. Dev. Psychobiol. 14, 327–332. https://doi.org/10.1002/dev.420140405
Panksepp, J., Beatty, W.W., 1980. Social deprivation and play in rats. Behav. Neural Biol. 30, 197–206. https://doi.org/10.1016/S0163-1047(80)91077-8
Panksepp, J., Burgdorf, J., 2003. "Laughing" rats and the evolutionary antecedents of human joy? Physiol. Behav. 79, 533–547. https://doi.org/10.1016/S0031-9384(03)00159-8
Panksepp, J., Burgdorf, J., 2000. 50-kHz chirping (laughter?) in response to conditioned and unconditioned tickle-induced reward in rats: effects of social housing and genetic variables. Behav. Brain Res. 115, 25–38. https://doi.org/S0166-4328(00)00238-2 [pii]
Panksepp, J., Gordon, N., Burgdorf, J., 2002. Empathy and the action-perception resonances of basic socio-emotional systems of the brain. Behav. Brain Sci. 25, 43–44. https://doi.org/10.1017/S0140525X02000018
Papes, F., Logan, D.W., Stowers, L., 2010. The Vomeronasal Organ Mediates Interspecies Defensive Behaviors through Detection of Protein Pheromone Homologs. Cell 141, 692–703. https://doi.org/10.1016/j.cell.2010.03.037
Parsana, A.J., Li, N., Brown, T.H., 2012. Positive and negative ultrasonic social signals elicit opposing firing patterns in rat amygdala. Behav. Brain Res. 226, 77–86. https://doi.org/10.1016/j.bbr.2011.08.040
Pellis, S.M., Field, E.F., Smith, L.K., Pellis, V.C., 1997. Multiple differences in the play fighting of male and female rats. Implications for the causes and functions of play. Neurosci. Biobehav. Rev. 21, 105–120. https://doi.org/10.1016/0149-7634(95)00060-7
Pérez-Gómez, A., Stein, B., Leinders-Zufall, T., Chamero, P., 2014. Signaling mechanisms and behavioral function of the mouse Basal vomeronasal neuroepithelium. Front. Neuroanat. 8, 1–7. https://doi.org/10.3389/fnana.2014.00135
Pobbe, R.L.H., Pearson, B.L., Defensor, E.B., Bolivar, V.J., Blanchard, D.C., Blanchard, R.J., 2010. Expression of social behaviors of C57BL/6J versus BTBR inbred mouse strains in the visible burrow system. Behav. Brain Res. 214, 443–449. https://doi.org/10.1016/j.bbr.2010.06.025
Pomerantz, S.M., Nunez, A.A., Jay Bean, N., 1983. Female behavior is affected by male ultrasonic vocalizations in house mice. Physiol. Behav. 31, 91–96. https://doi.org/10.1016/0031-9384(83)90101-4
Poole, T.B., Fish, J., 1976. An investigation of individual, age and sexual differences in the play

of Rattus norvegicus (Mammalia: Rodentia). J. Zool. 179, 249–259. https://doi.org/10.1111/j.1469-7998.1976.tb02294.x
Portfors, C. V., 2007. Types and functions of ultrasonic vocalizations in laboratory rats and mice. J. Am. Assoc. Lab. Anim. Sci. 46, 28–34.
Portfors, C. V., Perkel, D.J., 2014. The role of ultrasonic vocalizations in mouse communication. Curr. Opin. Neurobiol. 28, 115–120. https://doi.org/10.1016/j.conb.2014.07.002
Prigg, T., Goldreich, D., Carvell, G.E., Simons, D.J., 2002. Texture discrimination and unit recordings in the rat whisker/barrel system. Physiol. Behav. 77, 671–675. https://doi.org/10.1016/S0031-9384(02)00917-4
Prusky, G.T., West, P.W.R., Douglas, R.M., 2000. Behavioral assessment of visual acuity in mice and rats. Vision Res. 40, 2201–2209. https://doi.org/10.1016/S0042-6989(00)00081-X
Reno, J.M., Marker, B., Cormack, L.K., Schallert, T., Duvauchelle, C.L., 2013. Automating ultrasonic vocalization analyses: The WAAVES program. J. Neurosci. Methods 219, 155–161. https://doi.org/10.1016/j.jneumeth.2013.06.006
Reppucci, C.J., Gergely, C.K., Veenema, A.H., 2018. Activation patterns of vasopressinergic and oxytocinergic brain regions following social play exposure in juvenile male and female rats. J. Neuroendocrinol. 30, 1–12. https://doi.org/10.1111/jne.12582
Richter, C.P., 1957. On the phenomenon of sudden death in animals and man. Psychosom. Med. 19, 191–198. https://doi.org/10.1097/00006842-195705000-00004
Rodriguez, I., 2003. Nosing into pheromone detectors. Nat. Neurosci. 6, 438–440. https://doi.org/10.1038/nn0503-438
Roullet, F.I., Wöhr, M., Crawley, J.N., 2011. Female urine-induced male mice ultrasonic vocalizations, but not scent-marking, is modulated by social experience. Behav. Brain Res. 216, 19–28. https://doi.org/10.1016/j.bbr.2010.06.004
Roy, S., Watkins, N., Heck, D., 2012. Comprehensive Analysis of Ultrasonic Vocalizations in a Mouse Model of Fragile X Syndrome Reveals Limited, Call Type Specific Deficits. PLoS One 7, 1–6. https://doi.org/10.1371/journal.pone.0044816
Sadananda, M., Wöhr, M., Schwarting, R.K.W., 2008. Playback of 22-kHz and 50-kHz ultrasonic vocalizations induces differential c-fos expression in rat brain. Neurosci. Lett. 435, 17–23. https://doi.org/10.1016/j.neulet.2008.02.002
Scardochio, T., Trujillo-Pisanty, I., Conover, K., Shizgal, P., Clarke, P.B.S., 2015. The effects of electrical and optical stimulation of midbrain dopaminergic neurons on rat 50-khz ultrasonic vocalizations. Front. Behav. Neurosci. 9, 1–15. https://doi.org/10.3389/fnbeh.2015.00331
Scattoni, M.L., Gandhy, S.U., Ricceri, L., Crawley, J.N., 2008. Unusual repertoire of vocalizations in the BTBR T+tf/J mouse model of autism. PLoS One 3, 48–52. https://doi.org/10.1371/journal.pone.0003067
Scattoni, M.L., Michetti, C., Ricceri, L., 2018. Rodent Vocalization Studies in Animal Models of the Autism Spectrum Disorder, 1st ed, Handbook of Behavioral Neuroscience. Elsevier B.V. https://doi.org/10.1016/B978-0-12-809600-0.00042-1
Scattoni, M.L., Ricceri, L., Crawley, J.N., 2011. Unusual repertoire of vocalizations in adult BTBR T+tf/J mice during three types of social encounters. Genes, Brain Behav. 10, 44–56. https://doi.org/10.1111/j.1601-183X.2010.00623.x
Schmeisser, M.J., Ey, E., Wegener, S., Bockmann, J., Stempel, A.V., Kuebler, A., Janssen, A.L., Udvardi, P.T., Shiban, E., Spilker, C., Balschun, D., Skryabin, B. V., Dieck, S.T., Smalla, K.H., Montag, D., Leblond, C.S., Faure, P., Torquet, N., Le Sourd, A.M., Toro, R., Grabrucker, A.M., Shoichet, S.A., Schmitz, D., Kreutz, M.R., Bourgeron, T., Gundelfinger,

E.D., Boeckers, T.M., 2012. Autistic-like behaviours and hyperactivity in mice lacking ProSAP1/Shank2. Nature 486, 256–260. https://doi.org/10.1038/nature11015
Schwarting, R.K.W., 2018a. Ultrasonic vocalization in juvenile and adult male rats: A comparison among stocks. Physiol. Behav. 191, 1–11. https://doi.org/10.1016/j.physbeh.2018.03.023
Schwarting, R.K.W., 2018b. Ultrasonic vocalization in female rats: A comparison among three outbred stocks from pups to adults. Physiol. Behav. 196, 59–66. https://doi.org/10.1016/j.physbeh.2018.08.009
Schwarting, R.K.W., Jegan, N., Wöhr, M., 2007. Situational factors, conditions and individual variables which can determine ultrasonic vocalizations in male adult Wistar rats. Behav. Brain Res. 182, 208–222. https://doi.org/10.1016/j.bbr.2007.01.029
Seffer, D., Schwarting, R.K.W., Wöhr, M., 2014. Pro-social ultrasonic communication in rats: Insights from playback studies. J. Neurosci. Methods 234, 73–81. https://doi.org/10.1016/j.jneumeth.2014.01.023
Shair, H.N., Masmela, J.R., Brunelli, S.A., Hofer, M.A., 1997. Potentiation and inhibition of ultrasonic vocalization of rat pups: Regulation by social cues. Dev. Psychobiol. 30, 195–200. https://doi.org/10.1002/(SICI)1098-2302(199704)30:3<195::AID-DEV2>3.0.CO;2-K
Shair, H.N., Rupert, D.D., Rosko, L.M., Hofer, M.A., Myers, M.M., Welch, M.G., 2015. Effects of maternal deprivation and the duration of reunion time on rat pup ultrasonic vocalization responses to isolation: Possible implications for human infant studies. Dev. Psychobiol. 57, 63–72. https://doi.org/10.1002/dev.21258
Shannon, C.E., Weaver, W., 1998. The Mathematical Theory of Communication. University of Illinois Press, Chicago, IL.
Shao, Y., Guan, Y., Wang, L., Qiu, Z., Liu, Meizhen, Chen, Y., Wu, L., Li, Y., Ma, X., Liu, Mingyao, Li, D., 2014. CRISPR/Cas-mediated genome editing in the rat via direct injection of one-cell embryos. Nat. Protoc. 9, 2493–2512. https://doi.org/10.1038/nprot.2014.171
Shepard, K.N., Liu, R.C., 2011. Experience restores innate female preference for male ultrasonic vocalizations. Genes, Brain Behav. 10, 28–34. https://doi.org/10.1111/j.1601-183X.2010.00580.x
Shu, W., Cho, J.Y., Jiang, Y., Zhang, M., Weisz, D., Elder, G.A., Schmeidler, J., De Gasperi, R., Gama Sosa, M.A., Rabidou, D., Santucci, A.C., Perl, D., Morrisey, E., Buxbaum, J.D., 2005. Altered ultrasonic vocalization in mice with a disruption in the Foxp2 gene. Proc. Natl. Acad. Sci. U. S. A. 102, 9643–9648. https://doi.org/10.1073/pnas.0503739102
Silverman, J.L., Yang, M., Lord, C., Crawley, J.N., 2010. Behavioural phenotyping assays for mouse models of autism. Nat. Rev. Neurosci. 11, 490–502. https://doi.org/10.1038/nrn2851
Simola, N., Brudzynski, S.M., 2018. Repertoire and Biological Function of Ultrasonic Vocalizations in Adolescent and Adult Rats, 1st ed, Handbook of Behavioral Neuroscience. Elsevier B.V. https://doi.org/10.1016/B978-0-12-809600-0.00017-2
Siviy, S.M., Panksepp, J., 2011. In search of the neurobiological substrates for social playfulness in mammalian brains. Neurosci. Biobehav. Rev. 35, 1821–1830. https://doi.org/10.1016/j.neubiorev.2011.03.006
Siviy, S.M., Panksepp, J., 1987. Sensory modulation of juvenile play in rats. Dev. Psychobiol. 20, 39–55. https://doi.org/10.1002/dev.420200108
Smotherman, W.P., Bell, R.W., Starzec, J., Elias, J., Zachman, T.A., 1974. Maternal responses to infant vocalizations and olfactory cues in rats and mice. Behav. Biol. 12, 55–66. https://doi.org/10.1016/S0091-6773(74)91026-8
Snoeren, E., Agmo, A., 2013. Female ultrasonic vocalizations have no incentive value for male

rats. Behav. Neurosci. 127, 439–450.
Sotocinal, S.G., Sorge, R.E., Zaloum, A., Tuttle, A.H., Martin, L.J., Wieskopf, J.S., 2011. The Rat Grimace Scale: a partially automated method for quantifying pain in the laboratory rat via facial expressions. Mol. Pain 7, 55.
Spehr, M., Spehr, J., Ukhanov, K., Kelliher, K.R., Leinders-Zufall, T., Zufall, F., 2006. Parallel processing of social signals by the mammalian main and accessory olfactory systems. Cell. Mol. Life Sci. 63, 1476–1484. https://doi.org/10.1007/s00018-006-6109-4
Sugimoto, H., Okabe, S., Kato, M., Koshida, N., Shiroishi, T., Mogi, K., Kikusui, T., Koide, T., 2011. A role for strain differences in waveforms of ultrasonic vocalizations during Male-Female interaction. PLoS One 6. https://doi.org/10.1371/journal.pone.0022093
Sukoff Rizzo, S.J., Silverman, J.L., 2016. Methodological Considerations for Optimizing and Validating Behavioral Assays. Curr. Protoc. Mouse Biol. 6, 364–379. https://doi.org/10.1002/cpmo.17
Sullivan, R.M., Landers, M.S., Flemming, J., Vaught, C., Young, T.A., Polan, H.J., 2003. Characterizing the functional significance of the neonatal rat vibrissae prior to the onset of whisking. Somatosens. Mot. Res. 20, 157–162. https://doi.org/10.1080/0899022031000105190
Sungur, A.Ö., Schwarting, R.K.W., Wöhr, M., 2016. Early communication deficits in the Shank1 knockout mouse model for autism spectrum disorder: Developmental aspects and effects of social context. Autism Res. 9, 696–709. https://doi.org/10.1002/aur.1564
Tager-Flusberg, H., Paul, R., Lord, C., 2013. Language and Communication in Autism. Handb. Autism Pervasive Dev. Disord. 335–364. https://doi.org/10.1002/9780470939345.ch12
Takahashi, L.K., 1992. Ontogeny of behavioral inhibition induced by unfamiliar adult male conspecifics in preweanling rats. Physiol. Behav. 52, 493–498. https://doi.org/10.1016/0031-9384(92)90336-Z
Terranova, M.L., Laviola, G., 2005. Scoring of Social Interactions and Play in Mice During Adolescence. Curr. Protoc. Toxicol. 26, 1–11. https://doi.org/10.1002/0471140856.tx1310s26
Thomas, D.A., Barfield, R.J., 1985. Ultrasonic vocalization of the female rat (Rattus norvegicus) during mating. Anim. Behav. 33, 720–725. https://doi.org/10.1016/S0003-3472(85)80002-6
Thompson, B., Leonard, K.C., Brudzynski, S.M., 2006. Amphetamine-induced 50 kHz calls from rat nucleus accumbens: A quantitative mapping study and acoustic analysis. Behav. Brain Res. 168, 64–73. https://doi.org/10.1016/j.bbr.2005.10.012
Thor, D.H., Holloway, W.R., 1984. Social play in juvenile rats: A decade of methodological and experimental research. Neurosci. Biobehav. Rev. 8, 455–464. https://doi.org/10.1016/0149-7634(84)90004-6
Till, S.M., Asiminas, A., Jackson, A.D., Katsanevaki, D., Barnes, S.A., Osterweil, E.K., Bear, M.F., Chattarji, S., Wood, E.R., Wyllie, D.J.A., Kind, P.C., 2015. Conserved hippocampal cellular pathophysiology but distinct behavioural deficits in a new rat model of FXS. Hum. Mol. Genet. 24, 5977–5984. https://doi.org/10.1093/hmg/ddv299
Vaccarezza, O.L., Sepich, L.N., Tramezzani, J.H., 1981. The vomeronasal organ of the rat. J. Anat. 132, 167–85.
Vandenbergh, J.G., Finlayson, J.S., Dobrogosz, W.J., Dills, S.S., Kost, T.A., 1976. Chromatographic Separation of Puberty Accelerating Pheromone from Male Mouse Urine. Biol. Reprod. 15, 260–265.
Varlinskaya, E.I., Spear, L.P., Spear, N.E., 1999. Social Behavior and Social Motivation in

Adolescent Rats. Physiol. Behav. 67, 475–482. https://doi.org/10.1016/s0031-9384(98)00285-6
Waddell, J., Yang, T., Ho, E., Wellmann, K.A., Mooney, S.M., 2016. Prenatal ethanol exposure and whisker clipping disrupt ultrasonic vocalizations and play behavior in adolescent rats. Brain Sci. 6. https://doi.org/10.3390/brainsci6040043
Wang, H., Liang, S., Burgdorf, J., Wess, J., Yeomans, J., 2008. Ultrasonic vocalizations induced by sex and amphetamine in M2, M4, M5 muscarinic and D2 dopamine receptor knockout mice. PLoS One 3, 30–33. https://doi.org/10.1371/journal.pone.0001893
Warburton, V.L., Sales, G.D., Milligan, S.R., 1989. The emission and elicitation of mouse ultrasonic vocalizations: The effects of age, sex and gonadal status. Physiol. Behav. 45, 41–47. https://doi.org/10.1016/0031-9384(89)90164-9
Welker, W.I., 1964. Analysis of sniffing of the albino rat Behaviour, 223–244.
White, N.R., Prasad, M., Barfield, R.J., Nyby, J.G., 1998. 40- and 70-kHz vocalizations of mice (Mus musculus) during copulation. Physiol. Behav. 63, 467–473. https://doi.org/10.1016/S0031-9384(97)00484-8
Whitney, G., 1973. Vocalization of mice influenced by a single gene in a heterogeneous population. Behav. Genet. 3, 57–64. https://doi.org/10.1007/BF01067689
Whitney, G., Nyby, J., 1979. Cues that elicit ultrasounds from adult male mice. Integr. Comp. Biol. 19, 457–463. https://doi.org/10.1093/icb/19.2.457
Willadsen, M., Seffer, D., Schwarting, R., Wohr, M., 2014. Rodent ultrasonic communication: Male prosocial 50-kHz ultrasonic vocalizations elicit social approach behavior in female rats (Rattus norvegicus). J. Comp. Psychol. 128, 56–64.
Willey, A.R., Spear, L.P., 2012. Development of anticipatory 50kHz USV production to a social stimuli in adolescent and adult male Sprague-Dawley rats. Behav. Brain Res. 226, 613–618. https://doi.org/10.1016/j.bbr.2011.10.001
Willuhn, I., Tose, A., Wanat, M.J., Hart, A.S., Hollon, N.G., Phillips, P.E.M., Schwarting, R.K.W., Wöhr, M., 2014. Phasic dopamine release in the nucleus accumbens in response to pro-social 50 kHz ultrasonic vocalizations in rats. J. Neurosci. 34, 10616–10623. https://doi.org/10.1523/JNEUROSCI.1060-14.2014
Wintink, A.J., Brudzynski, S.M., 2001. The related roles of dopamine and glutamate in the initiation of 50-kHz ultrasonic calls in adult rats. Pharmacol. Biochem. Behav. 70, 317–323. https://doi.org/10.1016/S0091-3057(01)00615-3
Wöhr, M., 2014. Ultrasonic vocalizations in Shank mouse models for autism spectrum disorders: Detailed spectrographic analyses and developmental profiles. Neurosci. Biobehav. Rev. 43, 199–212. https://doi.org/10.1016/j.neubiorev.2014.03.021
Wöhr, M., Houx, B., Schwarting, R.K.W., Spruijt, B., 2008. Effects of experience and context on 50-kHz vocalizations in rats. Physiol. Behav. 93, 766–776. https://doi.org/10.1016/j.physbeh.2007.11.031
Wöhr, M., Kehl, M., Borta, A., Schänzer, A., Schwarting, R.K.W., Höglinger, G.U., 2009. New insights into the relationship of neurogenesis and affect: Tickling induces hippocampal cell proliferation in rats emitting appetitive 50-khz ultrasonic vocalizations. Neuroscience 163, 1024–1030. https://doi.org/10.1016/j.neuroscience.2009.07.043
Wöhr, Markus, Moles, A., Schwarting, R.K.W., D'Amato, F.R., 2011. Lack of social exploratory activation in male μ-opioid receptor KO mice in response to playback of female ultrasonic vocalizations. Soc. Neurosci. 6, 76–87. https://doi.org/10.1080/17470911003765560
Wöhr, M., Roullet, F.I., Crawley, J.N., 2011. Reduced scent marking and ultrasonic vocalizations

in the BTBR T+tf/J mouse model of autism. Genes, Brain Behav. 10, 35–43. https://doi.org/10.1111/j.1601-183X.2010.00582.x
Wöhr, M., Scattoni, M.L., 2013. Behavioural methods used in rodent models of autism spectrum disorders: Current standards and new developments. Behav. Brain Res. 251, 5–17. https://doi.org/10.1016/j.bbr.2013.05.047
Wöhr, M., Schwarting, R.K.W., 2013. Affective communication in rodents: Ultrasonic vocalizations as a tool for research on emotion and motivation. Cell Tissue Res. 354, 81–97. https://doi.org/10.1007/s00441-013-1607-9
Wöhr, M., Schwarting, R.K.W., 2012. Testing social acoustic memory in rats: Effects of stimulus configuration and long-term memory on the induction of social approach behavior by appetitive 50-kHz ultrasonic vocalizations. Neurobiol. Learn. Mem. 98, 154–164. https://doi.org/10.1016/j.nlm.2012.05.004
Wöhr, M., Schwarting, R.K.W., 2009. Ultrasonic communication in rats: Effects of morphine and naloxone on vocal and behavioral responses to playback of 50-kHz vocalizations. Pharmacol. Biochem. Behav. 94, 285–295. https://doi.org/10.1016/j.pbb.2009.09.008
Wöhr, M., Schwarting, R.K.W., 2008. Ultrasonic calling during fear conditioning in the rat: no evidence for an audience effect. Anim. Behav. 76, 749–760. https://doi.org/10.1016/j.anbehav.2008.04.017
Wöhr, M., Schwarting, R.K.W., 2007. Ultrasonic communication in rats: Can playback of 50-kHz calls induce approach behavior? PLoS One 2. https://doi.org/10.1371/journal.pone.0001365
Wöhr, M., Seffer, D., Schwarting, R.K.W., 2016. Studying socio-affective communication in rats through playback of ultrasonic vocalizations. Curr. Protoc. Neurosci. 2016, 8.35.1-8.35.17. https://doi.org/10.1002/cpns.7
Wohr, M., Willadsen, M., Kisko, T., Schwarting, R., Fendt, M., 2020. Sex-dependent effects of Cacna1c haploinsufficiency on behavioral inhibition evoked by conspecific alarm signals in rats. Prog. Neuro-Psychopharmacology Biol. Psychiatry 99, 109849.
Won, H., Lee, H.R., Gee, H.Y., Mah, W., Kim, J.I., Lee, J., Ha, S., Chung, C., Jung, E.S., Cho, Y.S., Park, S.G., Lee, J.S., Lee, K., Kim, D., Bae, Y.C., Kaang, B.K., Lee, M.G., Kim, E., 2012. Autistic-like social behaviour in Shank2-mutant mice improved by restoring NMDA receptor function. Nature 486, 261–265. https://doi.org/10.1038/nature11208
Wrenn, C.C., 2004. Social Transmission of Food Preference in Mice. Curr. Protoc. Neurosci. 28, 1–7. https://doi.org/10.1002/0471142301.ns0805gs28
Wrenn, C.C., Harris, A.P., Saavedra, M.C., Crawley, J.N., 2003. Social transmission of food preference in mice: Methodology and application to galanin-overexpressing transgenic mice. Behav. Neurosci. 117, 21–31. https://doi.org/10.1037/0735-7044.117.1.21
Wright, J.M., Gourdon, J.C., Clarke, P.B.S., 2010. Identification of multiple call categories within the rich repertoire of adult rat 50-kHz ultrasonic vocalizations: Effects of amphetamine and social context. Psychopharmacology (Berl). 211, 1–13. https://doi.org/10.1007/s00213-010-1859-y
Yang, M., Bozdagi, O., Scattoni, M.L., Wöhr, M., Roullet, F.I., Katz, A.M., Abrams, D.N., Kalikhman, D., Simon, H., Woldeyohannes, L., Zhang, J.Y., Harris, M.J., Saxena, R., Silverman, J.L., Buxbaum, J.D., Crawley, J.N., 2012. Reduced excitatory neurotransmission and mild Autism-Relevant phenotypes in adolescent shank3 null mutant mice. J. Neurosci. 32, 6525–6541. https://doi.org/10.1523/JNEUROSCI.6107-11.2012
Yang, M., Crawley, J.N., 2009. Simple behavioral assessment of mouse olfaction. Curr. Protoc. Neurosci. 1–12. https://doi.org/10.1002/0471142301.ns0824s48

Zheng, Q.Y., Johnson, K.R., Erway, L.C., 1999. Assessment of hearing in 80 inbred strains of mice by ABR threshold analyses. Hear. Res. 130, 94–107. https://doi.org/10.1016/S0378-5955(99)00003-9

Table 1. Advantages of common rodent social communication assays.

Assay	*Advantages*
Urinary pheromone deposition/investigation	Expressive and receptive olfactory communication.
Olfactory habituation/ dishabituation (OHDH)	Olfactory abilities of neutral and social odors.
Social transmission of food preference	Expressive and receptive olfactory communication.
Isolation-induced pup ultrasonic vocalizations (USV)	Early life functional readout. Provides information on quality of maternal behavior.
Same-sex USV	USV can be linked to physical activity at time of emission. Can be carried out with partner animal or social cue.
Male-to-female USV	USV can be linked to physical activity at time of emission. Can be carried out with partner female or social cue.
Reciprocal social interactions	Expressive and receptive tactile communication.
USV playback	Expressive and receptive auditory communication.

Table 2. Key brain regions associated with the emission and reception of 50-kHz ultrasonic vocalizations in rats.

Region	*Evidence*	*References*
Ventral tegmental area (VTA)	50-kHz calling is induced by activation of the VTA via electrical stimulation	Burgdorf et al., 2007
	50-kHz calling is induced by agonism of μ-opiate receptors in the VTA using DAMGO	Burgdorf et al., 2007
	50-kHz calling is reduced by inactivation of the VTA via lesioning	Burgdorf et al., 2007
Nucleus accumbens (NAcc)	50-kHz calling is induced by agonism of dopamine receptors in the NAcc using amphetamine[1-3] and quinpirole[4]	[1]Burgdorf et al., 2001; [2]Thompson et al., 2006; [3]Brudzynski et al., 2011; [4]Brudzynski, 2012
	50-kHz calling is induced by agonism of acetylcholine receptors in the NAcc using carbachol	Fendt et al., 2006
	50-kHz calling is associated with dopamine release in the NAcc	Scardochio et al., 2015
	50-kHz calling is reduced by antagonism of dopamine receptors in the NAcc using haloperidol[1-2], raclopride[2,4-6], SKF-83566[2], flupenthixol[3], U-99194A[5], and SCH23390[6]	[1]Wintink & Brudzynski, 2001; [2]Thompson et al., 2006; [3]Burgdorf et al., 2007; [4]Brudzynski et al., 2011; [5]Brudzynski, 2012; [6]Hori et al., 2013
	Reception of 50-kHz calls is associated with the release of dopamine in the NAcc	Wöhr et al., 2013; Willuhn et al., 2014
Frontal cortex	50-kHz calling is induced by agonism of NMDA receptors in the frontal cortex using GLYX-13	Burgdorf et al., 2011
	Reception of 50-kHz calls is associated with frontal cortex activation measured via immediate early gene expression	Sadananda et al., 2008

Table 3. Key brain regions associated with the emission and reception of 22-kHz ultrasonic vocalizations in rats.

Region	*Evidence*	*References*
Laterodorsal tegmental nucleus (LDT)	22-kHz calling is induced by activation of cholinergic neurons in the LDT using L-glutamate	Brudzynski & Barnabi, 1996; Bihari et al., 2003
	22-kHz calling is associated with LDT activation measured via immediate early gene expression	Brudzynski et al., 2011
Anterior hypothalamic-preoptic area (AHPA)	22-kHz calling is induced by agonism of acetylcholine receptors in the AHPA using carbachol	Brudzynski & Bihari, 1990; Brudzynski et al., 1991; Brudzynski, 1994; Fu & Brudzynski, 1994
	22-kHz calling is induced by activation of cholinergic neurons in the AHPA using L-glutamate	Fu & Brudzynski, 1994
	22-kHz calling is reduced by antagonism of acetylcholine receptors in the AHPA using atropine[1,2] and scopolamine[3]	[1]Brudzynski & Bihari, 1990; [2]Brudzynski, 1994; [3]Brudzynski & Barnabi, 1996
Lateral septum	22-kHz calling is induced by agonism of acetylcholine receptors in the lateral septum using carbachol	Bihari et al., 2003
	22-kHz calling is reduced by antagonism of acetylcholine receptors in the lateral septum using scopolamine	Bihari et al., 2003
Amgydala	22-kHz calling is reduced by inactivation of the amygdala via lesioning	Choi & Brown, 2003
	Reception of 22-kHz calls is associated with amygdala activation measured via elevated immediate early gene expression[1] and single-unit responses[2]	[1]Sadananda et al., 2008; [2]Parsana et al., 2012

Chapter 2

Developmental Exposure to Near Roadway Pollution Produces Behavioral Phenotypes Relevant to Neurodevelopmental Disorders in Juvenile Rats

This chapter has been published as: Elizabeth L. Berg, Lauren R. Pedersen, Michael C. Pride, Stela P. Petkova, Kelley T. Patten, Anthony E. Valenzuela, Christopher Wallis, Keith J. Bein, Anthony Wexler, Pamela J. Lein, and Jill L. Silverman (2020). *Translational Psychiatry* 10(289): 1-16.

Abstract

Epidemiological studies consistently implicate traffic-related air pollution (TRAP) and/or proximity to heavily trafficked roads as risk factors for developmental delays and neurodevelopmental disorders (NDDs); however, there are limited preclinical data demonstrating a causal relationship. To test the effects of TRAP, pregnant rat dams were transported to a vivarium adjacent to a major freeway tunnel system in northern California where they were exposed to TRAP drawn directly from the face of the tunnel or filtered air (FA). Offspring remained housed under the exposure condition into which they were born and were tested in a variety of behavioral assays between postnatal day 4 and 50. To assess the effects of near roadway exposure, offspring of dams housed in a standard research vivarium were tested at the laboratory. An additional group of dams was transported halfway to the facility and then back to the laboratory to control for the effect of potential transport stress. Near roadway exposure delayed growth and development of psychomotor reflexes and elicited abnormal activity in open field locomotion. Near roadway exposure also reduced isolation-induced 40-kHz pup ultrasonic vocalizations, with the TRAP group having the lowest number of call emissions. TRAP affected some components of social communication, evidenced by reduced neonatal pup ultrasonic calling and altered juvenile reciprocal social interactions. These findings confirm that living in close proximity to highly trafficked roadways during early life alters neurodevelopment.

Introduction

Neurodevelopmental disorders (NDDs) result from abnormal brain development and include a wide range of conditions, such as intellectual disability, attention deficit hyperactivity disorder (ADHD), and autism spectrum disorder (ASD). Symptoms present in early childhood and

persist throughout life, significantly affecting social, cognitive, and behavioral functioning. ASD and ADHD, which affect ~1 and 5% of children respectively, are among the most common and well-studied NDDs[1]. The disorders often co-occur with 30–50% of ASD patients presenting symptoms of ADHD, and their prevalence is on the rise[2]. According to the U.S. Centers for Disease Control and Prevention, ASD is currently estimated to affect about 1 in 59 children, which represents a dramatic increase from their previously reported 1 in 68 estimate[3,4]. These increased prevalence rates highlight the crucial need to develop a better understanding of the etiology of these neurological disorders since these conditions already incur immense societal and economic costs.

While there is compelling evidence that susceptibility to NDDs, as well as symptom severity and treatment outcomes, are influenced by the interaction of genetic and environmental risk factors, the underlying mechanisms remain to be elucidated[4–7]. Environmental factors also contribute to these conditions—although researchers disagree on the relative contributions of genes and environment. Furthermore, studies suggest that more than 50% of new ASD cases are due to factors other than diagnostic drift[7–12].

Identifying and understanding the environmental risk factors contributing to the rising prevalence rates is crucial and important since they can be modified and/or avoided, unlike genetic risk factors, which are, for the most part, not currently modifiable risk variables. Mounting epidemiological data using independent samples, models, and methods from a variety of geographical locations have implicated exposure to traffic-related air pollution (TRAP) as one of these factors. Human exposure to TRAP and/or proximity to roadways, especially during the late gestational period and/or early life, has been significantly associated with an NDD diagnosis[13–33]. These studies of humans, however, fall short of establishing a causal relationship between TRAP

exposure and NDD development, due to an array of confounding factors and a lack of data quantifying individual exposures to complex environmental mixtures. Animal models, therefore, offer a unique benefit and can be used to fill this knowledge gap and directly test the hypothesis that exposure to TRAP impairs behaviors related to NDDs (e.g., developmental delays, social interaction, learning and memory). While there has been some concentrated research in preclinical models, many of the commonly employed exposure methods are limited in their translational relevance to the human condition due to reasons such as repeated anesthesia and failure to recapitulate the complexity and/or relative concentrations of trafficrelated emissions in the real world[34–39].

In order to fully understand the behavioral consequences of near roadway exposures during early life, we leveraged an innovative real-time rodent exposure facility to expose developing rats. Since composition, dose, duration, intensity, mixtures, and timing of air pollution exposures can influence biological outcomes[40–42], we designed our study to be translationally relevant by representing human TRAP exposure and combined realworld composition of pollutants and dosing in an animal model. The detailed components of the exposure can be found in our Supplementary Information and are reported in comprehensive detail in Bein et al. (under review)[43]. In brief, air from a traffic tunnel in northern California was diverted to a nearby exposure facility housing a large rat colony, with half the colony receiving polluted tunnel air and half the colony receiving filtered air. Using rats, which possess a larger and more sophisticated repertoire of social behaviors compared to mice, allowed for an extensive and nuanced examination of NDD-relevant outcomes. After delivering real-world polluted air to pregnant rats and their offspring, we sought to determine whether the gestational and early life near roadway exposure affected physical growth, neonatal

reflexes, communication, social interaction, and/or learning and memory, using a battery of validated behavioral assays.

Numerous epidemiological studies have associated near roadway exposure to a range of diseases, but it is difficult in such studies to disentangle confounders, such as socioeconomic status, smoking, and diet. The Childhood Autism Risks from Genetics and Environment (CHARGE) study examined the link between autism and living near freeways using a distribution of distances: closest 10% (<309 m), next 15% (309–647 m), the next 25% (647–1419 m), and farthest from freeways (>1419 m)[28,44]. In each trimester of pregnancy, living closest (<309 m) to the freeway was associated with autism, with the odds ratio reaching the highest significance during the third trimester, informing the timing of our exposure period. In order to generate toxicological data that complements the epidemiological data, the exposure facility that we employed in this study was designed to model near roadway exposures of air pollution, noise, and vibration, the same stressors experienced by people living in this environment. Epidemiological studies differ on the distance from the roadway that is "safe", as this distance is partially determined by how much the air pollution from vehicles dilutes and how much the noise and vibration dissipates before the near roadway population is exposed. We drew air from the eastern face of the tunnel, not from inside the tunnel itself, so that the air pollution was somewhat diluted already, we insulated the building to reduce noise, and we installed vibration isolators on the feet of the exposure chambers to reduce vibration. The goal of these measures was to expose the rodents to conditions that well model human exposures.

Our investigation led to the discovery that gestational and early life exposure to TRAP affects some components of social communication. Importantly, we also discovered that both roadside-reared groups, TRAP and filtered air (FA), with exposure to the same noise and

vibrational stress, had significantly delayed growth and development of psychomotor reflexes, displayed altered social interactions, and exhibited abnormal motor activity. Histological outcomes from these exposures are described in our companion manuscript[45]. Further, we found no evidence for an effect, due to stress or otherwise, of the pregnant dams' transport to the roadside facility on offspring behavior. This is the first report of functional outcomes of this exposure model, and the first report that illustrates behavioral deficits resulting from near roadway exposure alone.

Methods

Subjects. All animals were housed in a temperature-controlled vivarium maintained on a 12:12 light–dark cycle. All procedures were approved by the Institutional Animal Care and Use Committee (IACUC) of the University of California Davis (UC Davis) and were conducted in accordance with the National Institutes of Health Guide for the Care and Use of Laboratory Animals. To identify rats, pups were labeled with paw tattoos on postnatal day (PND) 2 using non-toxic animal tattoo ink (Ketchum Manufacturing Inc., Brockville, ON, Canada). Ink was delivered into the center of the paw with a 23-gauge hypodermic needle tip. Rats were also tail marked with non-toxic permanent marker at weaning to allow for additional identification. The tattoo and tail marks for each subject were coded to allow investigators to carry out testing and scoring blind to treatment group.

Order of behavioral testing and description of cohorts. Male and female Sprague-Dawley rat breeders (PND 80–90) were paired for two weeks before females were singly housed at approximately gestational day (GD) 14. A group of dams was transported to the roadside exposure facility adjacent to a major freeway tunnel system in the Bay Area of Northern California. Dams were randomly assigned to one of two exposure conditions within the same facility: traffic-related

air pollution (TRAP) or filtered air (FA). Two male and two female offspring from each of 20 dams were tested as follows: (1) developmental milestones at PND 4, 6, 7, 9, 10, and 12, (2) pup USV at PND 5, (3) reciprocal social interaction at PND 32–34, (4) open-field behavior at PND 39–41, (5) novel object recognition at PND 40–42, and (6) fear conditioning at PND 44–48.

A second group of dams remained housed at a UC Davis vivarium, constituting the laboratory control group. Two male and two female offspring from each of seven litters were tested as follows: (1) developmental milestones at PND 4, 6, 7, 9, 10, and 12, (2) pup USV at PND 5, (3) reciprocal social interaction at PND 34–36, and (5) open field behavior at PND 42–43.

At a later timepoint, a third group of dams was employed as a control for the approximately 1.5-h vehicular transport required to move the prior groups of dams to the roadside exposure facility. Two weeks after being paired with a male breeder, all dams were singlyhoused and half of the group was driven halfway to the roadside tunnel site (~45 min drive) and then back to UC Davis. The other half of the group of dams remained unmoved at the UC Davis vivarium, constituting the control group for the transported group. All of the dams and their offspring remained housed at the UC Davis vivarium for the duration of the study. Two male and two female offspring from each of 11 dams were tested as follows: (1) developmental milestones at PND 4, 6, 7, 9, 10, and 12, (2) pup USV at PND 5, and (3) open field behavior at PND 38–41.

All offspring remained in the location and exposure condition into which they were born. Behavioral testing was conducted in testing rooms adjacent to each vivarium. Two male and two female offspring from each litter were tested. To minimize carry-over effects from repeated testing, assays were performed in order from least to most stressful and at least 48 h elapsed between tests.

At separate timepoints, two additional cohorts of male and female Sprague-Dawley rats were used to collect laboratory control data for the learning and memory paradigms. These data

were collected at the UC Davis vivarium prior to the testing equipment being relocated to the roadside exposure facility. Both groups remained housed at the UC Davis vivarium for the duration of the study, were well-handled prior to testing, and were offspring of Sprague-Dawley breeders who remained housed at the UC Davis vivarium. One cohort of rats was sampled from five litters and tested in the novel object recognition test at PND 45–53 and a second cohort was sampled from seven litters and tested in the fear conditioning assay at PND 42–44.

Roadside exposure facility. Data from the CHARGE study found residential proximity to freeways to be a risk factor for NDDs when maternal residence was <309 m from a major roadway[28,44]. In order to generate toxicological data that complements the epidemiological data, the exposure facility that we employed in this study was designed to model near roadway exposures of air pollution, noise, and vibration, the same stressors experienced by people living in this environment. We drew air from the eastern face of the tunnel, not from within the tunnel itself, so that the air pollution was somewhat diluted already. Additionally, we installed vibration isolators on the feet of the exposure chambers to reduce vibration and insulated the building to reduce noise below the IACUC-mandated maximal tolerated limit of 85 decibels. Such measures were unnecessary for the UC Davis vivarium and adjacent laboratory testing rooms, which have ambient noise levels of only 64 and 43–47 decibels, respectively.

The dual housing and exposure facility, located adjacent to a major freeway tunnel system in the Bay Area of northern California, was composed of three rooms: one containing equipment for adjusting air temperature and flow, and measuring air pollutant concentrations; a second room for the two exposure chambers; and a third room for behavior testing. Each exposure chamber was 12.8 ft l × 3 ft w × 7.8 ft h and capable of accommodating 108 cages with filter tops removed. In

order to minimize noise stress, all pumps and blowers were housed outside the facility and plumbed through walls. The room containing the exposure chambers and the behavioral testing suite were also additionally insulated to block noise.

Air supplied to the TRAP-exposed animals was drawn directly from the face of the tunnel. Flexible ducting carried air from the exit of the tunnel's two eastbound bores to the exposure facility where rats were exposed to the tunnel air. Air supplied to the filtered air group was drawn from the outside of the exposure facility, where pollutant concentrations were expected to be much lower than at the tunnel face. This air was subjected to several emissions control technologies coupled together in series prior to being plumbed to the exposure chamber. These included (a) a pre-filter for removing large debris and coarse particulate matter (PM), (b) inline activated carbon filters for removing gas-phase volatile and semi-volatile organic compounds, (c) barium oxide-based catalytic converters for removing NO_x and (d) ultrahigh efficiency Teflon-bound glass microfiber filters for removing fine and ultrafine PM. Flow rate control and temperature conditioning were also included in compliance with IACUC specifications. Pressure within each exposure chamber was monitored constantly and blowers were programmed to maintain a small negative pressure in each chamber, with the TRAP chamber drawing in air from the tunnel and the filtered air chamber drawing in air from the outside via the filtration system.

Behavioral testing. Two males and two females from each litter were randomly selected as behavioral test subjects and were tested on all behavioral assays with the exception of 16 animals who were only tested as pups and not as juveniles. This was to carefully control for the effect of the litter, previously described as being the most influential factor in developmental toxicological exposure studies[46,47]. Rats at the roadside exposure facility were removed from the home exposure

chambers for testing and then immediately returned to the chamber following the completion of each test. For behavioral tests involving bedding, the same type of bedding as present in home cages was used.

Developmental milestones. Pup developmental milestones were assessed at PND 4, 6, 7, 9, 10, and 12 similarly to methods described previously[48–50]. Body length (cm; nose to tail base) and body weight (grams) were measured. Rooting reflex was measured as a turn of the head to whisker stimulation. Forelimb grasping was measured as grasping of a bar being moved upward along both front paws.

Isolation-induced pup ultrasonic vocalizations. During the first 2 weeks of life, rodent pups will emit ultrasonic vocalizations (USV) upon separation from their mothers and littermates[51–53]. On PND 5, isolationinduced USVs were collected from each pup for three min. A pup was randomly selected from the nest, placed in a small, open top container with bedding, and emitted USV were collected using Avisoft-RECORDER (Avisoft Bioacoustics, Glienicke, Germany) as described previously[48,54]. The container was cleaned with 70% ethanol and new clean bedding was added between each animal. USV were displayed as spectrograms and counted by a trained observer blinded to group using Avisoft-SASLab Pro (Avisoft Bioacoustics, Glienicke, Germany).

Juvenile reciprocal social interaction. Each rat was paired with an unfamiliar strain-, age-, and sex-matched stimulus rat and allowed to freely interact for 10 min in a clean, empty test arena (41.3 cm l × 41.3 cm w × 29 cm h) containing bedding. Behaviors were video recorded through the arena's transparent front wall and later scored by a trained observer blinded to group as described previously[54]. Both subject and stimulus animals were isolated for 30 min prior to the test session. Subject and stimulus animals were always from different litters and stimuli rats used at the roadside facility were housed in filtered air. All behaviors scored were those of the subject

animal. Behaviors scored for duration were: (1) exploring, (2) following or chasing, (3) social sniffing, (4) anogenital sniffing, and (6) self-grooming. The testing room was illuminated to ~30 lux.

Open field exploration. In order to control for the potentially confounding effects of hypo- or hyperactivity on the other behavioral assays, exploratory activity in a novel open arena was evaluated over a 30 min session. Rats were placed in the center of the arena at the start of the testing session. Using methods similar to those previously described[48,54], total distance traveled and time spent in the center of the arena were measured using one of two comparable automated systems: an opaque matte black arena (54.1 cm l × 54.1 cm w × 34.3 cm h) equipped with video tracking software (EthoVision XT 12; Noldus Information Technology, Wageningen, Netherlands) or the fully automated Digiscan Animal Activity Monitors with Integra software (Omnitech Electronics, Columbus, OH, USA). The testing room was illuminated to ~30 lux.

Novel object recognition. Novel object recognition was assayed using methods similar to those described previously[49,55]. Using an opaque matte black box (54.1 cm l × 54.1 cm w × 34.3 cm h), each animal was habituated to the empty arena for 30 min on the day prior to the test. On the day of the test, each subject was again habituated to the arena for 30 min before two identical objects were placed gently in the arena with the animal. After a 10 min familiarization session, the animal was isolated in a clean holding cage with bedding for 60 min. During this time, the arena and the objects were cleaned with 70% ethanol and one clean familiar object and one clean novel object were placed in the original positions of the two identical objects during familiarization. Both the identity and location of the novel object within the arena were counterbalanced to address potential inherent object preferences or side biases. Our protocol has been published as standard by the Intellectual and Developmental Disability's Behavior Cores[56]. Upon being returned to the

arena for the recognition test, the subject was allowed 5 min to interact with the familiar and novel objects. Time spent sniffing each object during each phase of testing was automatically measured via video tracking software (EthoVision XT 10 and 12; Noldus Information Technology, Wageningen, Netherlands). Objects used were orange plastic cones (8.5 cm l × 8.5 cm w × 9.5 cm h) and glass bell jars (7.5 cm d × 10.3 cm h). The testing room was illuminated to ~30 lux.

Contextual and cued fear conditioning. Contextual and cued fear conditioning was carried out using an automated fear conditioning chamber (Med Associates, Inc., Fairfax, VT, USA) similar to methods described previously[49,57]. During training on day one, rats were exposed to a series of three noise-shock (CS-US) pairings in a testing chamber with specific visual, odor, and tactile cues. The training environment was brightly lit (~100 lux), contained a metal wire floor, and included 0.3 mL of vanilla odor cue (1:100 dilution of McCormick Vanilla Extract). White noise (80 dB) was played for 30 s and a foot shock (0.7 mA) occurred during the final two sec of the noise cue. A two min period for exploration preceded the first noise-shock pairing and elapsed between each noise-shock pairing. A 30 s exploration period followed the final noise-shock pairing and the entire training session was eight min in duration. On day two of testing, the subject was placed back inside the training environment for five min. The chamber contained identical contextual cues as the training session, but no white noise or foot shock occurred. On day three of testing, the subject was placed back inside the training environment for 6 min, but the chamber context was altered. The overhead lighting was turned off and the chamber contained a novel smooth plastic floor, novel black angled walls, and a novel lemon scent (1:100 dilution of McCormick Lemon Extract). An initial three min exploration period was followed by a three min presentation of the white noise conditioned stimulus. Time spent freezing during each test phase was automatically measured by the VideoFreeze software (version 2.7; Med Associates).

Statistical analysis. Particulate matter concentrations were compared using paired t-test since measurements occurred on the same days in both groups. Vocalizations were analyzed via unpaired (Student's) t-test for two groups or via one-way ANOVA with Tukey's multiple comparisons *post hoc* test for three groups. Developmental metrics and open field parameters were analyzed via two-way repeated measures ANOVA with exposure as the between-group factor and time as the within-group factor. Significant ANOVAs were followed by Tukey's *post hoc* testing. Log-Rank (Mantel-Cox) test was used to compare the percentage of animals achieving developmental milestones. Social interaction parameters were compared with one-way ANOVA followed by Tukey's *post hoc* testing. Comparisons between sniff times of objects were made within each exposure group via paired t-test and comparisons between freezing times were compared within test day with repeated measures ANOVA (for training and cued freezing) or unpaired (Student's) t-test (for contextual freezing). Group sizes were chosen based on past experience and power analyses[58], and data were analyzed with GraphPad Prism. Behavioral data passed distribution normality tests, were collected using continuous variables, and thus were analyzed via parametric tests. Variances were similar between groups and data points within two standard deviations from the mean were included in analyses. All significance levels were set at $p < 0.05$ and all *t*-tests were two-tailed. Multiple comparisons were corrected for via *post hoc* testing via Tukey's multiple comparisons test. Data are presented as mean ± standard error of the mean.

Results

Reproductive success. Two of three groups of pregnant female rats were transported to the roadside exposure facility at approximately gestational day (GD) 14, while the third group

remained in the laboratory at UC Davis. Dams of the roadside cohort were randomly assigned to be housed in either the TRAP or filtered air (FA) exposure chamber. In the laboratory control setting, 10 of 11 dams gave birth. One litter was cannibalized and did not survive to PND 2. We assayed a final litter count of 9. In the FA-exposed group at the roadside facility, 17 of 18 dams gave birth. One litter was cannibalized and did not survive to PND 2, so we assayed a final litter count of 16. In the TRAP-exposed group at the roadside facility, 10 of 10 dams gave birth. The average number of days between arrival at the roadside vivarium and birth was 10 days for both exposure groups, and there was no effect of group on litter size nor male to female ratio (**Supplementary Table S1**). **Figure 1a** illustrates our experimental design described in the methods.

Particulate concentrations in TRAP and FA exposures. Twenty-four-hour $PM_{2.5}$ and total suspended particulate mass concentrations measured immediately upstream of the FA and TRAP exposure chambers at the roadside tunnel facility for the study duration are described with extensive detail in **Fig. S1** and Bein et al. (under review)[43]. A unique and defining characteristic of our design is that it captured significant diurnal and day-to-day variations in exposure concentrations that cannot be readily recreated in the laboratory. These variations were easily seen in the size distribution of particle number concentrations (**Fig. S1**) and described comprehensively in Bein et al. (under review)[43]. **Figure 1b, c** illustrate the clearly increased $PM_{2.5}$ and PM_{10}, respectively, in the tunnel-sampled air (TRAP) compared to filtered air (FA), thereby validating our exposure system (**Fig. 1b** $t_{(1, 18)} = 4.562$, $p < 0.001$ and **Fig. 1c** $t_{(1, 18)} = 4.923$, $p < 0.001$).

Reduced isolation-induced pup ultrasonic vocalizations (USV). Isolation-induced USV were collected for 3 min as social communication signals in rat pups on PND 5, as previously described[48,54]. In male offspring, a significant effect of exposure on USV was discovered (**Fig. 2a** $F_{(2, 50)} = 4.287$, $p < 0.02$). TRAP-exposed pups emitted the fewest USV calls (p = 0.014 versus laboratory controls) and, interestingly, the FA-exposed group also trended to emit lower calls compared to the laboratory control group (p = 0.154). Raw values show the phenomenon that TRAP had the lowest number of calls: non-significant but noteworthy effects on USV by exposure group using mean ± SD showed that in male laboratory controls USV were 412 ± 132.8, FA USV were 327 ± 99.90, and TRAP USV were 280 ± 145.3. Given that TRAP-exposed did not differ from FA-exposed by Tukey's multiple comparisons *post hoc* analysis (p = 0.475), we cannot conclude that the air quality alone caused the lower numbers of USV. Although, the SD of the raw values allows us to see the high variability in call numbers by group.

A similar pattern was illustrated in the female offspring (**Fig. 2b** $F_{(2, 52)} = 3.069$, $p = 0.055$) albeit statistical significance in the overall ANOVA was not <0.05. Nonsignificant but noteworthy effects on USV by exposure group using mean ± SD showed that in female laboratory controls USV were 407 ± 154.60, FA USV were 331 ± 155.7, and TRAP USV were 275 ± 162.20. However, as the overall ANOVA was not under $p = 0.05$, we did not run *post hoc* analyses. Given the effect of the roadside exposure (TRAP and FA) in males and trend in females, we were unable to extract a sound statistical finding on calls that resulted from our intermittent, intensity varying, mixture of real-world pollution in the TRAP group. Trends, raw values, and high SD allow us to see the high variability in call numbers by group.

Body weight and temperature were also collected since body temperature is known to alter pup USV emission[51,59–62]. Weights and temperature did not differ by roadside air exposure (weight

TRAP versus FA $t_{(1, 38)} = 0.753$, *ns* and temperature TRAP versus FA $t_{(1, 38)} = 1.375$, *ns*). On PND 5, males of both roadside exposed groups weighed less than laboratory controls (TRAP versus lab $t_{(1, 31)} = 2.603$, $p < 0.02$; FA versus lab $t_{(1, 31)} = 2.388$, $p < 0.03$).

Delayed growth and milestone achievement of both TRAP and FA-exposed pups. **Figure 3a–h** shows delayed early physical development and neurological reflexes in TRAP- and FA-exposed offspring compared to laboratory controls. All male and female subjects gained weight and grew in length over time (males **Fig. 3a** $_{\text{length}} F_{(5, 255)} = 390.8$, $p < 0.0001$; **Fig. 3b** $_{\text{weight}}$ $F_{(5, 255)} = 1186$, $p < 0.001$ and females **Fig. 3e** $_{\text{length}}$ $F_{(5, 270)} = 322.1$, $p < 0.0001$; **Fig. 3f** $_{\text{weight}}$ $F_{(5, 255)} = 1092$, $p < 0.001$). Significant effects of exposure on body length and weight were discovered in both sexes (males **Fig. 3a** $_{\text{length}}$ $F_{(2, 51)} = 12.66$, $p < 0.001$; **Fig. 3b** $_{\text{weight}}$ $F_{(2, 51)} = 10.04$, $p < 0.001$ and females **Fig. 3e** $_{\text{length}}$ $F_{(2, 54)} = 13.05$, $p < 0.001$; **Fig. 3f** $_{\text{weight}}$ $F_{(2, 54)} = 6.312$, $p < 0.004$). TRAP-exposed (males $p < 0.001$ and females $p < 0.006$) and FA-exposed (males $p < 0.001$ and females $p < 0.02$) offspring differed from laboratory controls in both length and weight. Interestingly, no differences were observed between TRAP- and FA-exposure for length (males *ns* and females *ns*) or weight (males *ns* and females *ns*). The rooting and grasping reflexes were delayed in both the TRAP- and FA-exposed offspring compared to laboratory controls in both males (TRAP **Fig. 3c** $_{\text{rooting}}$ Log-rank $\chi^2_{(1)} = 8.35$, $p < 0.005$; FA **Fig. 3c** $_{\text{rooting}}$ Log-rank $\chi^2_{(1)} = 7.18$, $p < 0.01$; TRAP **Fig. 3d** $_{\text{grasping}}$ Log-rank $\chi^2_{(1)} = 11.05$, $p < 0.001$; FA **Fig. 3d** $_{\text{grasping}}$ Log-rank $\chi^2_{(1)} = 14.30$, $p < 0.001$) and females (TRAP **Fig. 3g** $_{\text{rooting}}$ Log-rank $\chi^2_{(1)} = 13.98$, $p < 0.001$; FA **Fig. 3g** $_{\text{rooting}}$ Log-rank $\chi^2_{(1)} = 13.98$, $p < 0.001$; TRAP **Fig. 3h** $_{\text{grasping}}$ Log-rank $\chi^2_{(1)} = 5.92$, $p < 0.05$; FA **Fig. 3h** $_{\text{grasping}}$ Log-rank $\chi^2_{(1)} = 18.63$, $p < 0.001$). Additional developmental milestones are shown in **Supplementary Table S2**.

Juvenile reciprocal dyad social interactions (social play). Male and female subject exploration did not differ between exposure groups and neither exposure group differed from laboratory controls (males **Fig. 4a** $F_{(2, 42)} = 2.065$, *ns* and females **Fig. 4f** $F_{(2, 44)} = 0.2467$, *ns*). This key information suggests that any differences in social behavior are not confounded by motor abilities, or hypo-, or hyper-exploration of the arena. Levels of this parameter were comparable and consistent with earlier findings using Sprague-Dawley rats at this age[63–68] and with our transported laboratory-tested control group (**Fig. S2**).

Social deficits, by an unusually high amount of time on the play parameter of following/chasing, were observed in both sexes (males **Fig. 4b** $F_{(2, 42)} = 11.61$, $p < 0.001$ and females **Fig. 4f** $F_{(2, 44)} = 5.944$, $p < 0.006$). Specifically, TRAP-exposed males spent more time following/chasing compared to FA-exposed males ($p < 0.05$) and laboratory controls ($p < 0.001$). FA-exposed males also trended to spend more time following/chasing compared to laboratory controls ($p = 0.06$). TRAP-exposed females exhibited a strong trend to spend more time following/chasing compared to FA-exposed females ($p = 0.10$) and TRAP-exposed females spent more time following/chasing compared to laboratory controls ($p < 0.004$). FA-exposed females did not differ on time spent following/chasing compared to laboratory controls ($p = 0.356$).

In females, exposure had a significant effect on time engaged in the key interaction metric of social sniffing, which includes nose-to-nose sniffing, neck and body sniffing, and other bouts of contact sniffing with the partner stimulus rat (females **Fig. 4g** $F_{(2, 44)} = 3.264$, $p < 0.05$). The TRAP and FA-exposed groups did not differ from one another ($p = 0.650$). Interestingly, FA-exposed ($p = 0.040$) females spent less time engaged in social sniffing compared to laboratory controls but the TRAP-exposed female group did not differ from laboratory controls (*ns*). In

contrast, only a trending difference between groups was observed in the key metric of social sniffing in males (males **Fig. 4c** $F_{(2, 42)} = 2.622$, $p = 0.085$). Nose-to-anogenital sniffing time, when initiated by the subject rat, was significantly affected in both sexes (males **Fig. 4d** $F_{(2, 42)} = 3.492$, $p = 0.040$ and females **Fig. 4i** $F_{(2, 44)} = 5.944$, $p < 0.006$). TRAP and FA-exposed groups did not differ from one another (*ns*). Although neither the FA-exposed males ($p = 0.079$) nor the TRAP exposed males ($p = 0.056$) significantly differed compared to laboratory controls in anogenital sniffing upon *post hoc* analyses, trending differences were discovered. Whereas this parameter did not differ in the transport control group (**Fig. S2**) suggesting the cause was the roadside gestation.

Time spent engaged in self-grooming differed between exposure groups in males (**Fig. 4e** $F_{(2, 42)} = 6.870$, $p < 0.004$) but not females (**Fig. 4j** $F_{(2, 44)} = 0.6994$, *ns*). Tukey's multiple comparisons *post hoc* analysis revealed that both the TRAP ($p = 0.049$) and FA-exposed ($p = 0.002$) male groups exhibited higher self-grooming scores compared to laboratory controls. Social interaction metrics that did not differ between the transported group and laboratory control offspring are illustrated in **Fig. S2** and additional play metrics that did not differ between groups are summarized in **Supplementary Table S3**.

Normal exploratory locomotor behavior in an open field arena. Motor abilities were tested in an open field assay, assessing cm of distance traveled using beam breaks and time spent in the center of the arena. FA- and TRAP-exposed juvenile male rats, as well as a cohort of male laboratory controls, exhibited no group differences in total activity (**Fig. 5a** $F_{(2, 42)} = 3.042$, *ns*). As expected, all groups decreased activity over time (**Fig. 5a** $F_{(4, 151)} = 220.2$, $p < 0.0001$). No treatment group differences were detected in center time measures in males (**Fig. 5b** $F_{(2, 42)} = 1.367$, *ns*). Group effects were observed in FA- and TRAP-exposed juvenile female rats, as well as a

cohort of female laboratory controls, in total activity (**Fig. 5c** $F_{(2, 44)} = 4.690$, $p < 0.02$). There was not a significant difference in performance between TRAP- and FA-exposed rats, except at a single timepoint (20–25 min: $p = 0.019$). TRAP did not differ from the laboratory controls (*ns*) at any timepoint, while the FA-exposed group and lab controls differed at four timepoints upon *post hoc* analyses in females (5–10 min: $p = 0.009$; 10–15 min: $p = 0.011$; 15–20 min: $p = 0.049$; 20–25 min: $p = 0.009$). Group differences were detected in center time measures in females (**Fig. 5d** $F_{(2, 44)} = 10.39$, $p < 0.001$). As expected, all groups decreased center time across the 30-min testing session (**Fig. 5a** $F_{(3, 140)} = 8.70$, $p < 0.0001$). TRAP-exposed females exhibited lower time in the center compared to FA-exposed rats (p = 0.007). Both TRAP (0–5 min: $p = 0.001$; 10–15 min: $p = 0.007$) and FA-exposed (0–5 min: $p = 0.030$) females groups differed by lower center times compared to the laboratory controls upon *post hoc* analyses.

Intact object recognition and Pavlovian conditioning learning and memory behavior. Manual and automated scoring indicated both male TRAP- and FA-exposure groups spent more time investigating the novel object versus the familiar object, thereby exhibiting typical novel object preference (**Fig. 6a** TRAP-exposed, $t_{(1, 15)} = 3.269$, $p < 0.006$ and FA-exposed, $t_{(1, 15)} = 3.081$, $p < 0.008$). Times spent exploring the objects during the familiarization component were similar for both groups using mean ± SEM in that FA-exposed sniffing investigation times were 135.5 ± 15.2 s, and TRAP-exposed sniffing investigation times were 110.3 ± 12.1 s. Similarly, both female exposure groups spent more time investigating the novel object versus the familiar object, exhibiting typical novel object preference (**Fig. 6c** TRAP-exposed, $t_{(1, 12)} = 4.316$, $p < 0.001$ and FA-exposed, ($t_{(1, 12)} = 3.720$, $p < 0.003$). Thus, roadway exposure did not adversely affect object learning or short-term memory recall. This negative finding was not the result of a lack of

participation or object investigation as times spent exploring the objects during the familiar exposure component, in females, were similar for both groups using mean ± SEM in that FA-exposed sniffing investigation times were 138.6 ± 6.8 s, and TRAP exposed sniffing investigation times were 117.0 ± 9.4 s. Object sniff times observed 60 min following familiarization with one object type in laboratory control subjects (males **Fig. S3a** $t_{(1, 15)} = 3.997$, $p = 0.001$ and females **Fig. S3b** $t_{(1, 14)} = 2.788$, $p = 0.015$) illustrated typical novel object preference in groups run in our rat behavioral core when given the opportunity to investigate a novel and a familiar object.

Learning and memory were further evaluated using two measures of Pavlovian fear conditioning with a 24-h contextual component and a 48-h auditory cued fear conditioning. Significant main effects of time (males **Fig. 6b** $F_{(1, 30)} = 61.06$, $p < 0.0001$ and females **Fig. 6d** $F_{(1, 30)} = 31.27$, $p < 0.0001$) but not exposure group (males **Fig. 6b** $F_{(1, 30)} = 0.0213$, *ns* and females **Fig. 6d** $F_{(1, 30)} = 0.3597$, *ns*) or interaction (males **Fig. 6b** $F_{(1, 30)} = 0.0061$, *ns* and females **Fig. 6d** $F_{(1, 30)} = 0.3785$, *ns*) indicated that high levels of freezing were observed in both groups subsequent to the conditioned stimulus (CS)—unconditioned stimulus (UCS) pairings on the training day. Elevated post-training freezing in both exposure groups with no group difference in training freeze scores in males or females indicates no confounds and no deficits in the learning of the associations between the context stimuli and auditory cues. No difference in freezing scores was observed 24 h following CS-UCS training between TRAP and FA-exposed subjects freezing scores in males (**Fig. 6b** $t_{(1, 30)} = 1.510$, *ns*) or females (**Fig. 6d** $t_{(1, 30)} = 0.8535$, *ns*) when placed in the context chamber from conditioning training with identical stimulus cues. Levels of freezing, between the pre- and post-cue presentation 48 h after training, revealed significant main effects of cue presentation (males **Fig. 6b** $F_{(1, 30)} = 112.1$, $p < 0.0001$ and females **Fig. 6d** $F_{(1, 30)} = 47.86$, $p < 0.0001$) but not exposure group (males **Fig. 6b** $F_{(1, 30)} = 0.0006$, *ns* and females **Fig. 6d** $F_{(1, 30)} =$

0.0484, *ns*) or interaction (males **Fig. 6b** $F_{(1, 30)} = 0.0370$, *ns* and females **Fig. 6d** $F_{(1, 30)} = 0.0694$, *ns*). Therefore, no group difference was found in freezing in response to the auditory cue between TRAP- and FA-exposed subjects when placed in the novel chamber with unique contextual cues (olfactory, visual, and textural). Freezing scores in laboratory control subjects observed 24 h following CS-UCS training compared to pre-training scores (males **Fig. S4a** $t_{(1, 25)} = 5.722$, $p < 0.0001$ and females **Fig. S4b** $t_{(1, 22)} = 4.486$, $p < 0.001$) illustrated typical fear responses in groups run in our rat behavioral core when placed in the context chamber from conditioning training with identical stimulus cues.

Transport stress does not cause the observed behavioral phenotypes. The effect of potential stress on the pregnant dam during the transport to the roadside exposure facility was ruled out as a causal mechanism for these physical and behavioral changes. **Figure 7a–d** show no delay in early physical development and neurological reflexes. This figure combines sexes as no sex difference was observed throughout the developmental outcomes (**Fig. 2**). In transported and control offspring, all male and female subjects gained weight and grew in length over time (**Fig. 7a** $_{\text{length}}$ $F_{(5, 173)} = 846.2$, $p < 0.001$; **Fig. 7b** $_{\text{weight}}$ $F_{(5, 255)} = 1186$, $p < 0.001$). There was a trend but no statistically significant effect of transport on body length (**Fig. 7a** $F_{(1, 42)} = 3.278$, $p = 0.077$) or body weight (**Fig. 7b** $F_{(1, 42)} = 1.764$, *ns*). Neurological reflexes, including the rooting and grasping reflexes, were normal in transported and control offspring (**Fig. 7c** $_{\text{rooting}}$ Log-rank $\chi^2_{(1)} = 0.1716$, *ns*; **Fig. 7d** grasping Log-rank $\chi^2_{(1)} = 00.00$, *ns*). **Figure 7e** shows that there were no differences in PND 5 pup USV emissions across the transported and control offspring (**Fig. 7e** $t_{(1, 38)} = 0.4814$, *ns*). No differences in total activity (**Fig. 7f** $F_{(1, 42)} = 0.0049$, *ns*) or time spent in the center of the open field arena (**Fig. 7g** $F_{(1, 42)} = 0.4879$, *ns*) were observed between the transported offspring

compared to control group. Overall, no effect of transport alone was observed on offspring development. Pups born to dams that experienced a transport at approximately GD 14 exhibited no physical or behavioral abnormalities (**Fig. 7**) and exhibited no differences in social investigative events such as exploring, social sniffing, anogenital sniffing, following/chasing, or the repetitive behavior of self-grooming (**Fig. S2**). Pups born to dams that experienced a transport at approximately GD 14 also exhibited no differences in social play point events such as pouncing, pinning, and pushing under or crawling over (**Table S3**).

Discussion

Our goal was to corroborate human studies that have linked increased risk of NDDs to near roadway TRAP exposures. To do this, we developed an innovative exposure model that quantifies and delivers TRAP collected from a traffic tunnel to rats during both in utero and post-natal development. This design avoided limitations of single exposure paradigms, including requiring anesthesia and difficulties mimicking real-world mixtures of TRAP, while simultaneously leveraging earlier literature to yield consensus. Both roadside exposure groups had significantly delayed growth and development of psychomotor reflexes, displayed altered social interactions, and exhibited abnormal activity in an open field compared to lab controls. This is the first report that used carefully controlled subgroups to illustrate that developmental exposure to realistic near roadway exposures caused subtle but significant changes in developmental endpoints and functional outcomes (i.e., behavior). This confirms the theory suggested by epidemiological studies that in addition to TRAP, noise, vibration, and proximity to highways may be additional risk factors for NDDs in combination with genetic susceptibility or independently[19,20,28,69–73]. Our work presented herein is also a novel, important addition because, to our knowledge, this is the

first nonclinical study that did not use high levels of particulate matter (PM), concentrated ambient ultrafine particles (CAPS), and/or diesel exhaust and discovered subtle but reportable behavioral outcomes. These findings support the need for further research delineating causal link(s) between exposure to TRAP and behavioral outcomes relevant to NDDs and adding to our understanding of the risks posed by air pollution to the developing nervous system.

Recently, a few well recognized laboratories have used reductionist experimental designs to investigate the effects of diesel exhaust[69,70,74,75] and particulate matter (sizeable and ultrafine)[38,76–81], the components most implicated in mediating the neurotoxic effects of TRAP. We extended this published research with our innovative real-world exposure to a dynamic, complex mixture of components, noise, and vibration. Polluted tunnel air was delivered to subjects in the nearby exposure facility while control animals received thoroughly filtered air from a tunnel-adjacent area. Because behavioral outcomes vary by sex, time of year, vendor, and numerous additional variables, we ran, in parallel, a laboratory control group58,82.

An important finding was that we observed no significant difference in litter size between TRAP, FA, and laboratory groups, which eliminated litter size as a potential explanatory variable for effects of near roadway exposure on pup growth and development. Yet, both roadside groups had significantly delayed growth and development of psychomotor reflexes, altered social interactions, and abnormal activity in an open field compared to laboratory controls. A potential explanation was that transport stress confounded our observations.

However, we showed a complete absence of behavioral phenotypes resulting from the transport alone, strongly suggesting that adverse functional outcomes observed in the TRAP and FA groups were attributable to near roadway exposures. In both sexes of FA- and TRAPexposed

groups, we observed reduced isolation-induced 40-kHz pup ultrasonic vocalizations. Other atypical behaviors included juvenile social play behavior by the critical investigative parameter of anogenital sniffing and social play behavior of following/chasing. These data have direct translational implications as epidemiological studies directed at investigating ASD and NDDs have reported high levels of physical and developmental effects on health associated with the proximity of residence to heavily trafficked roads, using unique data sets from differing regional areas[21–24,28,75,83]. Follow-up studies will need to delineate the effects of noise and vibration during pregnancy from those of TRAP on offspring development and behavior. These findings add to our understanding of the risks posed to the developing nervous system by living in close proximity to roadways and support the need for further research delineating causal link(s) between exposure to TRAP and behavioral outcomes relevant to NDDs. We observed a strong trend toward reduced overall social sniffing in the TRAP- and FA-exposed groups. Social sniffing is a key investigative behavior that initiates numerous types of juvenile social play events such as following/chasing, pinning, pouncing, and rough and tumble play. The TRAP- and FA-exposed juveniles exhibited these deficits without confounding motor deficits. In addition, we observed a trend to elevated self-grooming in males, a well-reported, standardized restricted, repetitive behavior in rodents[84]. Less social sniffing in dyadic interactions and elevated self-grooming are likely indicators of stress in both exposure groups.

In addition, others observed elevated self-grooming, repetitive behavior in mice. Similar findings of reduced reciprocal interactions following diesel exhaust exposure from prenatal embryonic day 0 to postnatal day 21 were recently reported in male mice[70]. Chang et al. also reported their diesel exhaust exposure caused increased repeated entries in the T-maze test of spontaneous alternation, a learning and memory assay with the embedded ability to capture

restricted behavior. We observed high levels of repetitive motor behavior in the TRAP-exposed group, using a low-order motor stereotypy measure of grooming. Spontaneous alternation in T or Y maze, which may be mimicking higher order restricted, repetitive behaviors, are easily observable in mice[85–88].

Surprisingly, we did not observe deficits on our two standard assays of learning and memory, contextual and cued fear conditioning and novel object recognition, due to TRAP exposure. We hypothesized this behavioral domain to have a robust phenotype given earlier literature. Early postnatal life exposure to concentrated ambient ultrafine particles (CAPS) increased preference for immediate reward, a more complex type of cognition that assesses impulsivity using a fixed-ratio waiting-for-reward paradigm, in mice[80,89]. The discounting of delayed rewards in preclinical models is considered to be analogous to impulsivity and delay of gratification in humans and is relevant to ADHD. Follow-up investigations revealed that early postnatal exposures to CAPS caused sexually dimorphic impairments in fixed interval performance on an operant training task, with greater sensitivity in males, while adult exposures caused deficits in females, indicating dysfunctional learning and reduced behavioral flexibility in CAPS-exposed mice. CAPS exposure also impaired short-term memory on the novel object recognition memory task in both sexes[38,80]. Collectively, these observations indicate dysfunctional learning and reduced behavioral flexibility in CAPS-exposed mice. The different results observed in the CAPS study versus our study may be due to (a) our tasks being limited to fear conditioning and novel object recognition because of limitations on the type of equipment that could be housed at the exposure facility, (b) that there is >20 million years of evolution that separate mouse and rat and there is likely species differences[90,91], and/or (c) the variable intensities and concentrations of the exposures. Another limitation of our learning and memory data was that the laboratory control

data were collected from cohorts other than those under study herein, thereby precluding direct comparisons of performance scores. We were, however, able to make observational assessments with the knowledge that the cohorts were all Sprague-Dawley rats of similar ages tested by the same experimenter using the same equipment following the standard experimental protocol and the laboratory controls were within our standard validation scores. In future studies, we plan on employing operant touchscreen testing, as performed by our laboratories in mice and rats[48,92,93], which will allow for more direct comparisons of impulsivity via five choice serial reaction and continuous performance assays[94–98]. Other groups exposed rats in a highly trafficked location in Portugal to non-filtered air (NFA) during gestation and early life and found a significant decrease in object discrimination when compared to the group exposed to filtered air (FA), suggesting that the exposure to TRAP during the combined pre- and post-natal periods impaired short-term discriminative memory. Animals exposed during only pre- or post-natal period did not show impairment on this assay[99], similar to our findings. Another group found that ambient concentrated $PM_{2.5}$ exposure resulted in robust impairments in adult mice tested in the Barnes Maze, a hippocampal dependent spatial learning task. The $PM_{2.5}$exposed mice made more errors during training and took longer to reach the target during training trials and the memory retention test, indicating that chronic exposure to airborne fine particulate matter impaired hippocampal related learning and memory[100].

Multiple groups have reported strong associations between prenatal exposure to TRAP and developmental delays and/or NDDs. Since epidemiology studies are associative, rigorous experiments that test preclinical models in highly controlled environments are warranted. This is particularly pertinent for studies of TRAP, since for decades research has focused on the detrimental effects of tobacco and asthma/allergy-related illnesses. In conclusion, we developed

and functionally validated an innovative preclinical model that recapitulated human studies that have linked developmental exposure to TRAP, or proximity to TRAP, and increased risk of NDDs. This confirmation of TRAP as an environmental risk factor for NDDs provides a rationale for controlling and minimizing exposures during critical periods of neurodevelopment thereby reducing the incidence of NDDs and/or decreasing the severity of symptoms. This study sets the stage for future mechanistic investigations to determine the mechanisms by which this risk factor interacts with NDD genes of susceptibility. It will also inform our understanding of the molecular pathophysiology of NDDs, which will be useful for identifying developmental windows of vulnerability and possible novel intervention and/or therapeutic strategies.

References

1. Dall'Aglio, L. et al. The role of epigenetic modifications in neurodevelopmental disorders: a systematic review. Neurosci. Biobehav. Rev. 94, 17–30 (2018).
2. Dalley, J. W., Everitt, B. J. & Robbins, T. W. Impulsivity, compulsivity, and topdown cognitive control. Neuron 69, 680–694 (2011).
3. Baio, J. et al. Prevalence of autism spectrum disorder among children aged 8 years—autism and developmental disabilities monitoring network, 11 sites, United States, 2014. MMWR Surveill. Summ. 67, 1–23 (2018).
4. Sahin, M. & Sur, M. Genes, circuits, and precision therapies for autism and related neurodevelopmental disorders. Science 350, aab3897 (2015).
5. Hallmayer, J. et al. Genetic heritability and shared environmental factors among twin pairs with autism. Arch. Gen. Psychiatry 68, 1095–1102 (2011).
6. Zuk, O., Hechter, E., Sunyaev, S. R. & Lander, E. S. The mystery of missing heritability: genetic interactions create phantom heritability. Proc. Natl Acad. Sci. USA 109, 1193–1198 (2012).
7. Stamou, M., Streifel, K. M., Goines, P. E. & Lein, P. J. Neuronal connectivity as a convergent target of gene x environment interactions that confer risk for Autism Spectrum Disorders. Neurotoxicology Teratol. 36, 3–16 (2012).
8. Pessah, I. N. & Lein P. J. in: Autism: Current Theories and Evidence. (edsZimmerman A.), 409–428 (Humana Press, Totowa, NJ, 2008).
9. Hertz-Picciotto, I. & Delwiche, L. The rise in autism and the role of age at diagnosis. Epidemiology 20, 84–90 (2009).
10. Grether, J. K., Rosen, N. J., Smith, K. S. & Croen, L. A. Investigation of shifts in autism reporting in the California Department of Developmental Services. J. Autism Dev. Disord. 39, 1412–1419 (2009).
11. King, M. & Bearman, P. Diagnostic change and the increased prevalence of autism. Int. J. Epidemiol. 38, 1224–1234 (2009).
12. Keil, K. P. & Lein, P. J. DNA methylation: a mechanism linking environmental chemical exposures to risk of autism spectrum disorders? Environ. Epigenet 2, 1–15 (2016).
13. Kalkbrenner, A. E. et al. Perinatal exposure to hazardous air pollutants and autism spectrum disorders at age 8. Epidemiology 21, 631–641 (2010).
14. Kalkbrenner, A. E. et al. Particulate matter exposure, prenatal and postnatal windows of susceptibility, and autism spectrum disorders. Epidemiology 26, 30–42 (2015).
15. Kalkbrenner, A. E. et al. Air Toxics in relation to autism diagnosis, phenotype, and severity in a U.S. family-based study. Environ. Health Perspect. 126, 037004 (2018).
16. McGuinn, L. A. et al. Early life exposure to air pollution and autism spectrum disorder: findings from a multisite case-control study. Epidemiology 31, 103–114 (2020).
17. Thygesen, M. et al. Exposure to air pollution in early childhood and the association with attention-deficit hyperactivity disorder. Environ. Res. 183, 108930 (2020).
18. Ladd-Acosta, C. et al. Epigenetic marks of prenatal air pollution exposure found in multiple tissues relevant for child health. Environ. Int 126, 363–376 (2019).
19. Volk, H. E. et al. Autism spectrum disorder: interaction of air pollution with the MET receptor tyrosine kinase gene. Epidemiology 25, 44–47 (2014).
20. Volk, H. E., Lurmann, F., Penfold, B., Hertz-Picciotto, I. & McConnell, R. Trafficrelated air pollution, particulate matter, and autism. JAMA Psychiatry 70, 71–77 (2013).

21. Becerra, T. A., Wilhelm, M., Olsen, J., Cockburn, M. & Ritz, B. Ambient air pollution and autism in Los Angeles county, California. Environ. Health Perspect. 121, 380–386 (2013).
22. Jung, C. R., Lin, Y. T. & Hwang, B. F. Air pollution and newly diagnostic autism spectrum disorders: a population-based cohort study in Taiwan. PLoS ONE 8, e75510 (2013).
23. von Ehrenstein, O. S., Aralis, H., Cockburn, M. & Ritz, B. In utero exposure to toxic air pollutants and risk of childhood autism. Epidemiology 25, 851–858 (2014).
24. Windham, G. C., Zhang, L., Gunier, R., Croen, L. A. & Grether, J. K. Autism spectrum disorders in relation to distribution of hazardous air pollutants in the San Francisco bay area. Environ. Health Perspect. 114, 1438–1444 (2006).
25. Herr, C. E. et al. Exposure to air pollution in critical prenatal time windows and IgE levels in newborns. Pediatr. Allergy Immunol. 22(1 Pt 1), 75–84 (2011).
26. Kerin, T. et al. Association between air pollution exposure, cognitive and adaptive function, and ASD severity among children with autism spectrum disorder. J. Autism Dev. Disord. 48, 137–150 (2018).
27. Payne-Sturges, D. C. et al. Healthy air, healthy brains: advancing air pollution policy to protect children's health. Am. J. Public Health 109, 550–554 (2019).
28. Volk, H. E., Hertz-Picciotto, I., Delwiche, L., Lurmann, F. & McConnell, R. Residential proximity to freeways and autism in the CHARGE study. Environ. Health Perspect. 119, 873–877 (2011).
29. Chun, H., Leung, C., Wen, S. W., McDonald, J. & Shin, H. H. Maternal exposure to air pollution and risk of autism in children: a systematic review and metaanalysis. Environ. Pollut. 256, 113307 (2020).
30. Goodrich, A. J. et al. Joint effects of prenatal air pollutant exposure and maternal folic acid supplementation on risk of autism spectrum disorder. Autism Res. 11, 69–80 (2018).
31. Chandrakumar, A. & Willem't Jong, G. Maternal exposure to air pollution during pregnancy and autism spectrum disorder in offspring. JAMA Pediatr. 173, 697–698 (2019).
32. Pagalan, L. et al. Association of prenatal exposure to air pollution with autism spectrum disorder. JAMA Pediatr. 173, 86–92 (2019).
33. Pagalan, L., Brauer, M. & Lanphear, B. Maternal exposure to air pollution during pregnancy and autism spectrum disorder in offspring-reply. JAMA Pediatr. 173, 698 (2019).
34. Bein, K. J. & Wexler, A. S. A high-efficiency, low-biased method for extracting particulate matter from filter and impactor substrates. Atmos. Environ. 90, 87–95 (2014).
35. Plummer, L., Ham, W., Kleeman, M., Wexler, A. & Pinkerton, K. Influence of season and location on pulmonary response to California's San Joaquin Valley airborne particulate matter. J. Toxicol. Environ. Health Part A 75, 253–271 (2012).
36. Zhang, K. M. & Wexler, A. S. Evolution of particle number distribution near roadways. Part I: analysis of aerosol dynamics and its implications for engine emission measurement. Atmos. Environ. 38, 6643–6653 (2004).
37. Zhang, K. M. et al. Evolution of particle number distribution near roadways. Part III: Traffic analysis and on-road size resolved particulate emission factors. Atmos. Environ. 39, 4155–4166 (2005).
38. Cory-Slechta, D. A., Allen, J. L., Conrad, K., Marvin, E. & Sobolewski, M. Developmental exposure to low level ambient ultrafine particle air pollution and cognitive dysfunction. Neurotoxicology 69, 217–231 (2018).

39. Sobolewski, M. et al. Developmental exposures to ultrafine particle air pollution reduces early testosterone levels and adult male social novelty preference: Risk for children's sex-biased neurobehavioral disorders. Neurotoxicology 68, 203–211 (2018).
40. Carosino, C. M. et al. Allergic airway inflammation is differentially exacerbated by daytime and nighttime ultrafine and submicron fine ambient particles: heme oxygenase-1 as an indicator of PM-mediated allergic inflammation. J. Toxicol. Environ. Health, Part A 78, 254–266 (2015).
41. Plummer, L. E. et al. Pulmonary inflammatory effects of source-oriented particulate matter from California's San Joaquin Valley. Atmos. Environ. 119, 174–181 (2015).
42. Papapostolou, V. et al. Development and characterization of an exposure generation system to investigate the health effects of particles from fresh and aged traffic emissions. Air Qual., Atmosphere Health 6, 419–429 (2012).
43. Bein K. J. et al. Roadway tunnels as real-time exposure systems: a case study. Environ Sci. Technol. (2020).
44. Hertz-Picciotto, I. et al. The CHARGE study: an epidemiologic investigation of genetic and environmental factors contributing to autism. Environ. health Perspect. 114, 1119–1125 (2006).
45. Patten, K. T. et al. Effects of early life exposure to traffic-related air pollution on brain development in juvenile Sprague-Dawley rats. Transl. psychiatry 10, 1–12 (2020).
46. Hood R. D. Handbook of Developmental Toxicology (CRC Press, USA, 1996).
47. Lazic, S. E. & Essioux, L. Improving basic and translational science by accounting for litter-to-litter variation in animal models. BMC Neurosci. 14, 37 (2013).
48. Berg, E. L. et al. Translational outcomes in a full gene deletion of ubiquitin protein ligase E3A rat model of Angelman syndrome. Transl. Psychiatry 10, 1–6 (2020).
49. Adhikari, A. et al. Cognitive deficits in the Snord116 deletion mouse model for Prader-Willi syndrome. Neurobiol. Learn. Mem. 165, 106874 (2019).
50. Fox, W. M. Reflex-ontogeny and behavioural development of the mouse. Anim. Behav. 13, 234–241 (1965).
51. Hofer, M. A., Shair, H. N. & Brunelli S. A. Ultrasonic vocalizations in rat and mouse pups. Curr. Protoc. Neurosci. Chapter 8: Unit 8.14 (2002).
52. Wohr, M. & Schwarting, R. K. Maternal care, isolation-induced infant ultrasonic calling, and their relations to adult anxiety-related behavior in the rat. Behav. Neurosci. 122, 310–330 (2008).
53. Brudzynski, S. Handbook of Ultrasonic Vocalization: A Window Into the Emotional Brain, vol. 25 (Academic Press, 2018).
54. Berg, E. L. et al. Developmental social communication deficits in the Shank3 rat model of Phelan-Mcdermid syndrome and autism spectrum disorder. Autism Res. 11, 587–601 (2018).
55. Copping, N. A. et al. Neuronal overexpression of Ube3a isoform 2 causes behavioral impairments and neuroanatomical pathology relevant to 15q11.2-q13.3 duplication syndrome. Hum. Mol. Genet. 26, 3995–4010 (2017). 56. Gulinello, T. et al. Rigor and reproducibility in rodent behavioral research. Neurobiol. Learn. Mem. 165, 106780 (2019).
57. Gompers, A. L. et al. Germline Chd8 haploinsufficiency alters brain development in mouse. Nat. Neurosci. 20, 1062–1073 (2017).
58. Sukoff Rizzo, S. J. & Silverman, J. L. Methodological considerations for optimizing and validating behavioral assays. Curr. Protoc. Mouse Biol. 6, 364–379 (2016).

59. Hofer, M. A. & Shair, H. N. Ultrasonic vocalization by rat pups during recovery from deep hypothermia. Dev. Psychobiol. 25, 511–528 (1992).
60. Shair, H. N., Brunelli, S. A., Masmela, J. R., Boone, E. & Hofer, M. A. Social, thermal, and temporal influences on isolation-induced and maternally potentiated ultrasonic vocalizations of rat pups. Dev. Psychobiol. 42, 206–222 (2003).
61. Allin, J. T. & Banks, E. M. Effects of temperature on ultrasound production by infant albino rats. Dev. Psychobiol. 4, 149–156 (1971).
62. Oswalt, G. L. & Meier, G. W. Olfactory, thermal, and tactual influences on infantile ultrasonic vocalization in rats. Dev. Psychobiol. 8, 129–135 (1975).
63. Raza, S. et al. Effects of prenatal exposure to valproic acid on the development of juvenile-typical social play in rats. Behav. Pharm. 26, 707–719 (2015).
64. Thor, D. H. & Holloway, W. R. Jr. Social play in juvenile rats: a decade of methodological and experimental research. Neurosci. Biobehav. Rev. 8, 455–464 (1984).
65. Vanderschuren, L. J., Niesink, R. J. & Van Ree, J. M. The neurobiology of social play behavior in rats. Neurosci. Biobehav. Rev. 21, 309–326 (1997).
66. Ku, K. M., Weir, R. K., Silverman, J. L., Berman, R. F. & Bauman, M. D. Behavioral phenotyping of juvenile long-evans and Sprague-Dawley rats: implications for preclinical models of autism spectrum disorders. PLoS ONE 11, e0158150 (2016).
67. Panksepp, J. The ontogeny of play in rats. Dev. Psychobiol. 14, 327–332 (1981).
68. Panksepp, J. & Beatty, W. W. Social deprivation and play in rats. Behav. Neural Biol. 30, 197–206 (1980).
69. Costa, L. G., Chang, Y. C. & Cole, T. B. Developmental neurotoxicity of trafficrelated air pollution: focus on autism. Curr. Environ. Health Rep. 4, 156–165 (2017).
70. Chang, Y. C., Cole, T. B. & Costa, L. G. Prenatal and early-life diesel exhaust exposure causes autism-like behavioral changes in mice. Part Fibre Toxicol. 15, 18 (2018).
71. Lyall, K. et al. The changing epidemiology of autism spectrum disorders. Annu. Rev. Public Health 38, 81–102 (2017).
72. Costa, L. G. et al. Neurotoxicity of traffic-related air pollution. Neurotoxicology 59, 133–139 (2017).
73. Kim, D. et al. The joint effect of air pollution exposure and copy number variation on risk for autism. Autism Res. 10, 1470–1480 (2017).
74. Block, M. L. et al. The outdoor air pollution and brain health workshop. Neurotoxicology 33, 972–984 (2012).
75. Hansen, C. A., Barnett, A. G. & Pritchard, G. The effect of ambient air pollution during early pregnancy on fetal ultrasonic measurements during midpregnancy. Environ. Health Perspect. 116, 362–369 (2008).
76. Allen, J. L. et al. Early postnatal exposure to ultrafine particulate matter air pollution: persistent ventriculomegaly, neurochemical disruption, and glial activation preferentially in male mice. Environ. Health Perspect. 122, 939–945 (2014).
77. Allen, J. L. et al. Developmental exposure to concentrated ambient ultrafine particulate matter air pollution in mice results in persistent and sexdependent behavioral neurotoxicity and glial activation. Toxicol. Sci. 140, 160–178 (2014).
78. Zhao Y. et al. Field evaluation of the versatile aerosol concentration enrichment system (VACES) particle concentrator coupled to the rapid singleparticle mass spectrometer (RSMS-3). J. Geophys. Res. Atmos. https://doi.org/ 10.1029/2004JD004644 (2005).

79. Breysse, P. N. et al. US EPA particulate matter research centers: summary of research results for 2005–2011. Air Qual. Atmos. Health 6, 333–355 (2013).
80. Allen, J. L. et al. Developmental neurotoxicity of inhaled ambient ultrafine particle air pollution: Parallels with neuropathological and behavioral features of autism and other neurodevelopmental disorders. Neurotoxicology 59, 140–154 (2017).
81. Allen, J. L. et al. Consequences of developmental exposure to concentrated ambient ultrafine particle air pollution combined with the adult paraquat and maneb model of the Parkinson's disease phenotype in male mice. Neurotoxicology 41, 80–88 (2014).
82. Silverman, J. L., Yang, M., Lord, C. & Crawley, J. N. Behavioural phenotyping assays for mouse models of autism. Nat. Rev. Neurosci. 11, 490–502 (2010).
83. Currie, J., Neidell, M. & Schmieder, J. F. Air pollution and infant health: Lessons from New Jersey. J. Health Econ. 28, 688–703 (2009).
84. Kalueff, A. V. et al. Neurobiology of rodent self-grooming and its value for translational neuroscience. Nat. Rev. Neurosci. 17, 45–59 (2016).
85. Sukoff Rizzo, S. J. et al. Assessing healthspan and lifespan measures in aging mice: optimization of testing protocols, replicability, and rater reliability. Curr. Protoc. Mouse Biol. 8, e45 (2018).
86. Sukoff Rizzo, S. J. & Crawley, J. N. Behavioral phenotyping assays for genetic mouse models of neurodevelopmental, neurodegenerative, and psychiatric disorders. Annu Rev. Anim. Biosci. 5, 371–389 (2017).
87. Sukoff Rizzo, S. J. et al. Behavioral characterization of striatal-enriched protein tyrosine phosphatase (STEP) knockout mice. Genes Brain Behav. 13, 643–652 (2014).
88. Sukoff Rizzo, S. J., McTighe, S. & McKinzie, D. L. Genetic background and sex: impact on generalizability of research findings in pharmacology studies. Handb. Exp. Pharm. 257, 147–162 (2019).
89. Allen, J. L. et al. Developmental exposure to concentrated ambient particles and preference for immediate reward in mice. Environ. Health Perspect. 121, 32–38 (2013).
90. Iannaccone, P. M. & Jacob, H. J. Rats! . Dis. Model. Mech. 2, 206–210 (2009).
91. Parker, C. C. et al. Rats are the smart choice: rationale for a renewed focus on rats in behavioral genetics. Neuropharmacology 76 Pt B, 250–258 (2014).
92. Copping, N. A. et al. Touchscreen learning deficits and normal social approach behavior in the Shank3B model of Phelan-McDermid Syndrome and autism. Neuroscience 345, 155–165 (2017).
93. Petkova, S. P. et al. Cyclin D2-knock-out mice with attenuated dentate gyrus neurogenesis have robust deficits in long-term memory formation. Sci. Rep. 10, 1–16 (2020).
94. Bhakta, S. G. & Young, J. W. The 5 choice continuous performance test (5CCPT): a novel tool to assess cognitive control across species. J. Neurosci. methods 292, 53–60 (2017).
95. Cope, Z. A. & Young, J. W. The five-choice continuous performance task (5C-CPT): a cross-species relevant paradigm for assessment of vigilance and response inhibition in rodents. Curr. Protoc. Neurosci. 78, 9–56 (2017).
96. Lustig, C., Kozak, R., Sarter, M., Young, J. W. & Robbins, T. W. CNTRICS final animal model task selection: control of attention. Neurosci. Biobehav. Rev. 37 (9 Pt B), 2099–2110 (2013).
97. McKenna, B. S., Young, J. W., Dawes, S. E., Asgaard, G. L. & Eyler, L. T. Bridging the bench to bedside gap: validation of a reverse-translated rodent continuous performance test using functional magnetic resonance imaging. Psychiatry Res. 212, 183–191 (2013).

98. Cope, Z. A. et al. Premature responses in the five-choice serial reaction time task reflect rodents' temporal strategies: evidence from no-light and pharmacological challenges. Psychopharmacology 233, 3513–3525 (2016).
99. Zanchi, A. C. et al. Pre and post-natal exposure to ambient level of air pollution impairs memory of rats: the role of oxidative stress. Inhal. Toxicol. 22, 910–918 (2010).
100. Fonken, L. K. et al. Air pollution impairs cognition, provokes depressive-like behaviors and alters hippocampal cytokine expression and morphology. Mol. Psychiatry 16, 987–995 (2011).

Figures

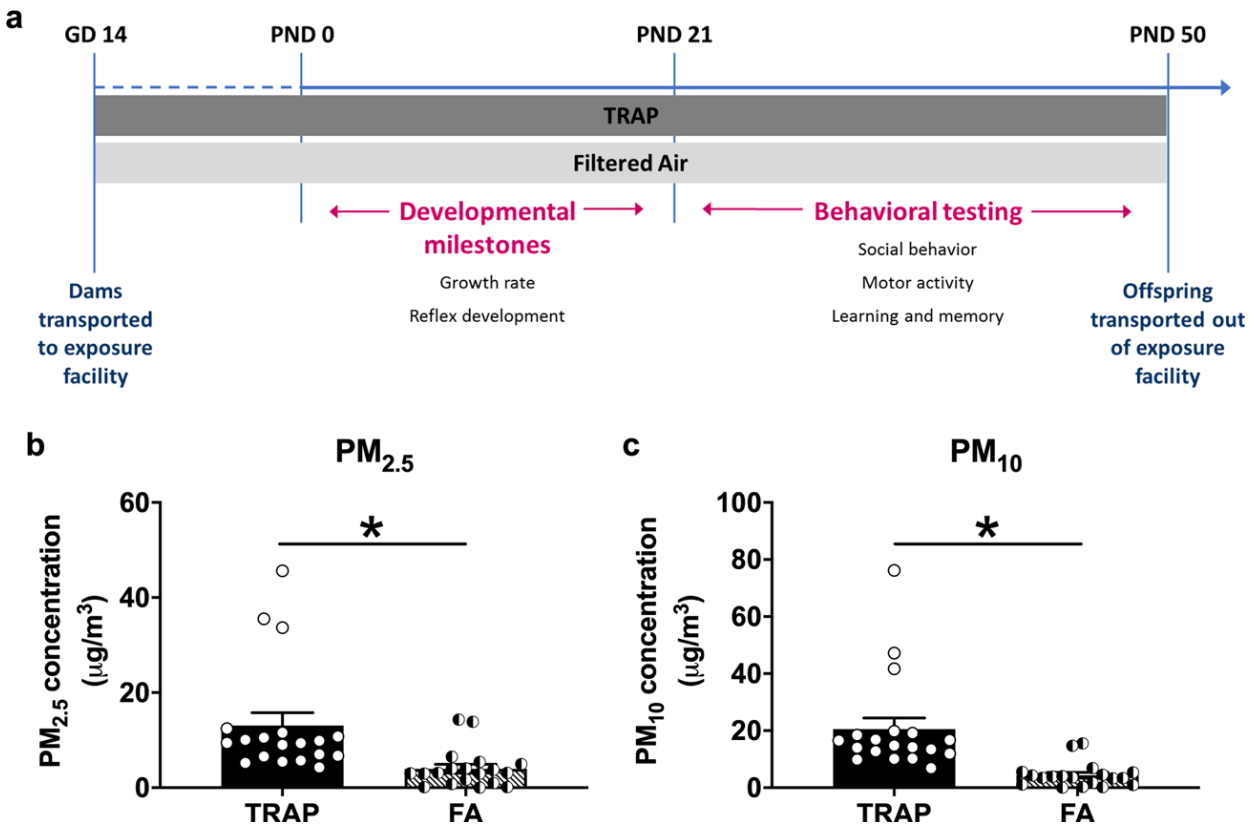

Fig. 1 Timeline and quantification of roadside TRAP exposure. a Pregnant female rats were transported to the roadside exposure facility at approximately gestational day (GD) 14 and were randomly assigned to be housed in either the TRAP or filtered air (FA) exposure chambers. Offspring, remained in the exposure condition into which they were born, were tested on a variety of developmental milestone assays between four days after birth (postnatal day (PND) 4) and weaning at PND 21 and then a battery of standardized behavioral assays between PND 21 and 50. **b**, **c** Particulate matter (PM) concentrations of the TRAP air and FA were quantified on 19 days. Both **b** $PM_{2.5}$ and **c** PM_{10} concentrations of the TRAP air were significantly higher than those of the FA. *$p < 0.05$, paired *t*-test.

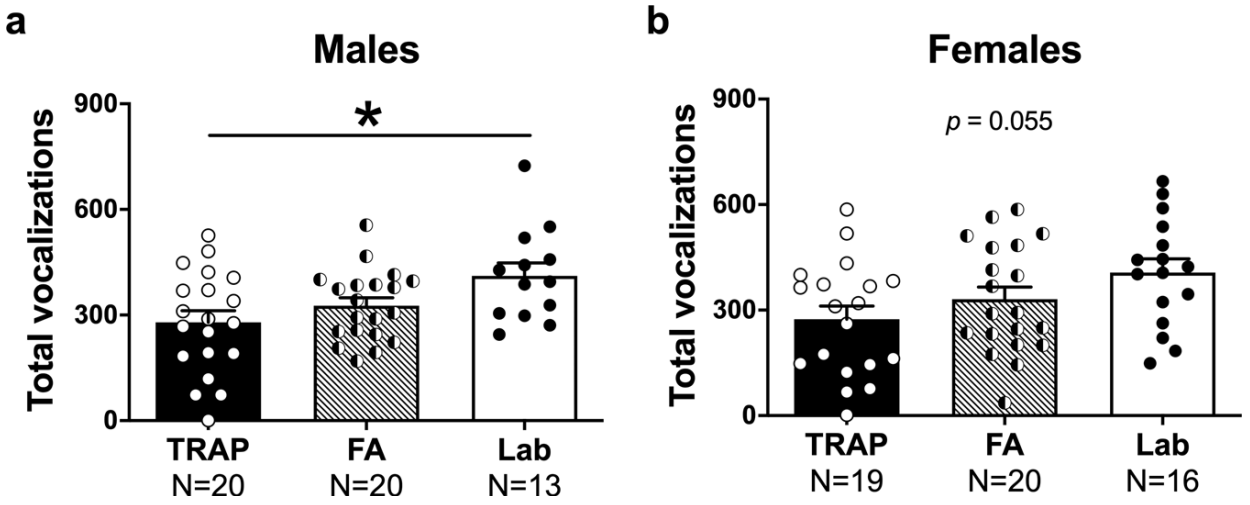

Fig. 2 Reduced isolation-induced ultrasonic vocalizations (USV) of TRAP-exposed pups at PND 5. a Male pups exposed to TRAP emitted significantly fewer USV during the three min isolation compared to lab controls. **b** Exposure did not affect USV emission in females, although the trend indicated reduced numbers of calls in the TRAP group compared to lab controls. *$p < 0.05$, one-way ANOVA followed by Tukey's multiple comparisons test.

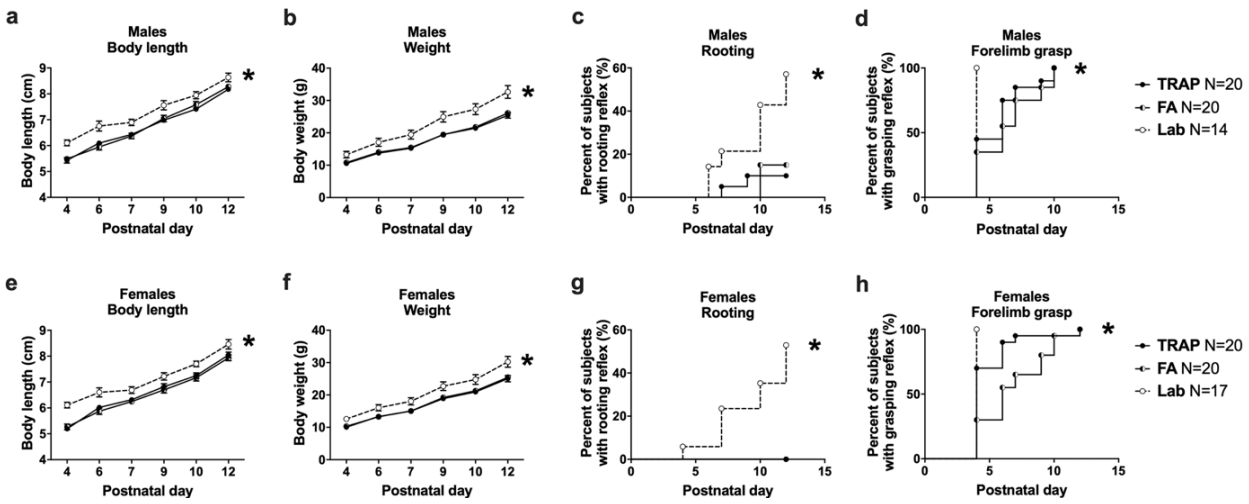

Fig. 3 Delayed growth and milestone achievement of roadside TRAP- and FA-exposed pups. **a** Male pups exposed to TRAP or FA had significantly reduced body length and **b** body weight throughout early development compared to lab controls. Males of both roadside groups exhibited a significant delay in the development of **c** rooting and **d** forelimb grasping reflexes. **e** Female pups exposed to TRAP or FA also had reduced body length and **f** body weight and developed **g** rooting and **h** forelimb grasping reflexes later than lab controls. **a**, **b**, **e**, **f** *$p < 0.05$, repeated measures ANOVA followed by Tukey's multiple comparisons test. **c**, **d**, **g**, **h** *$p < 0.05$, Log-Rank (Mantel-Cox) test.

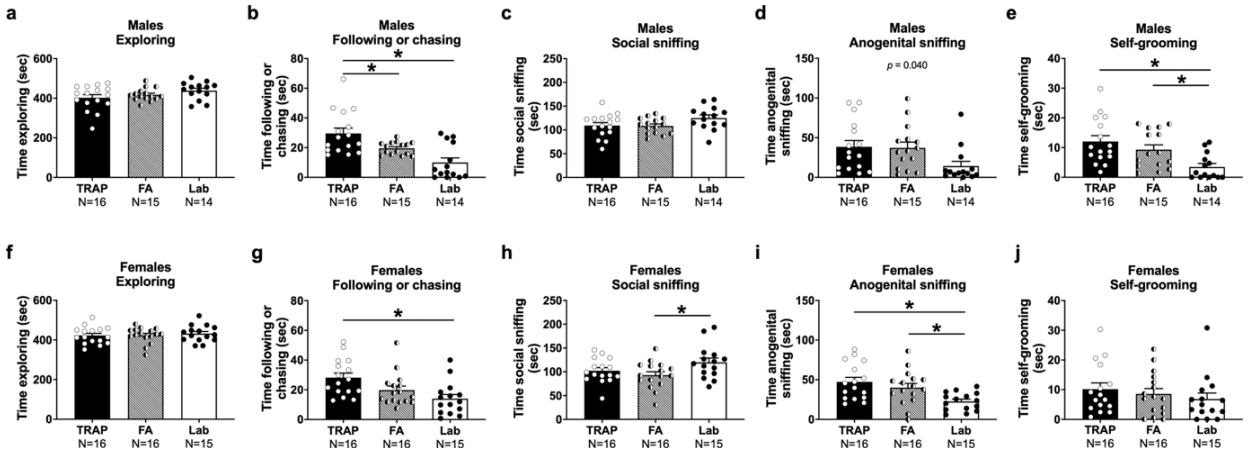

Fig. 4 Roadside TRAP- and FA-exposed rats differed from lab controls during juvenile reciprocal social interactions on several key parameters. a Roadside exposures did not affect levels of exploration during the social interaction assay for males, however **b** TRAP-exposed males spent significantly more time following or chasing the stimulus animal than did FA-exposed or lab controls. **c** Roadside-reared males showed typical levels of social sniffing but **d** there was a significant effect of group on anogenital sniffing, with *post hoc* trends suggesting that both roadside exposure groups spent more time anogenital sniffing compared to lab controls. **e** Both TRAP- and FA-exposed males spent more time self-grooming than lab controls. **f** Females of all groups exhibited comparable levels of exploration, but **g** TRAP-exposed females spent more time following or chasing than lab controls. **h** FA-exposed females spent significantly less time social sniffing relative to lab controls and **i** both roadside groups had elevated levels of anogenital sniffing. **j** Females of all groups displayed similar levels of self-grooming. $*p < 0.05$, one-way ANOVA followed by Tukey's multiple comparisons test.

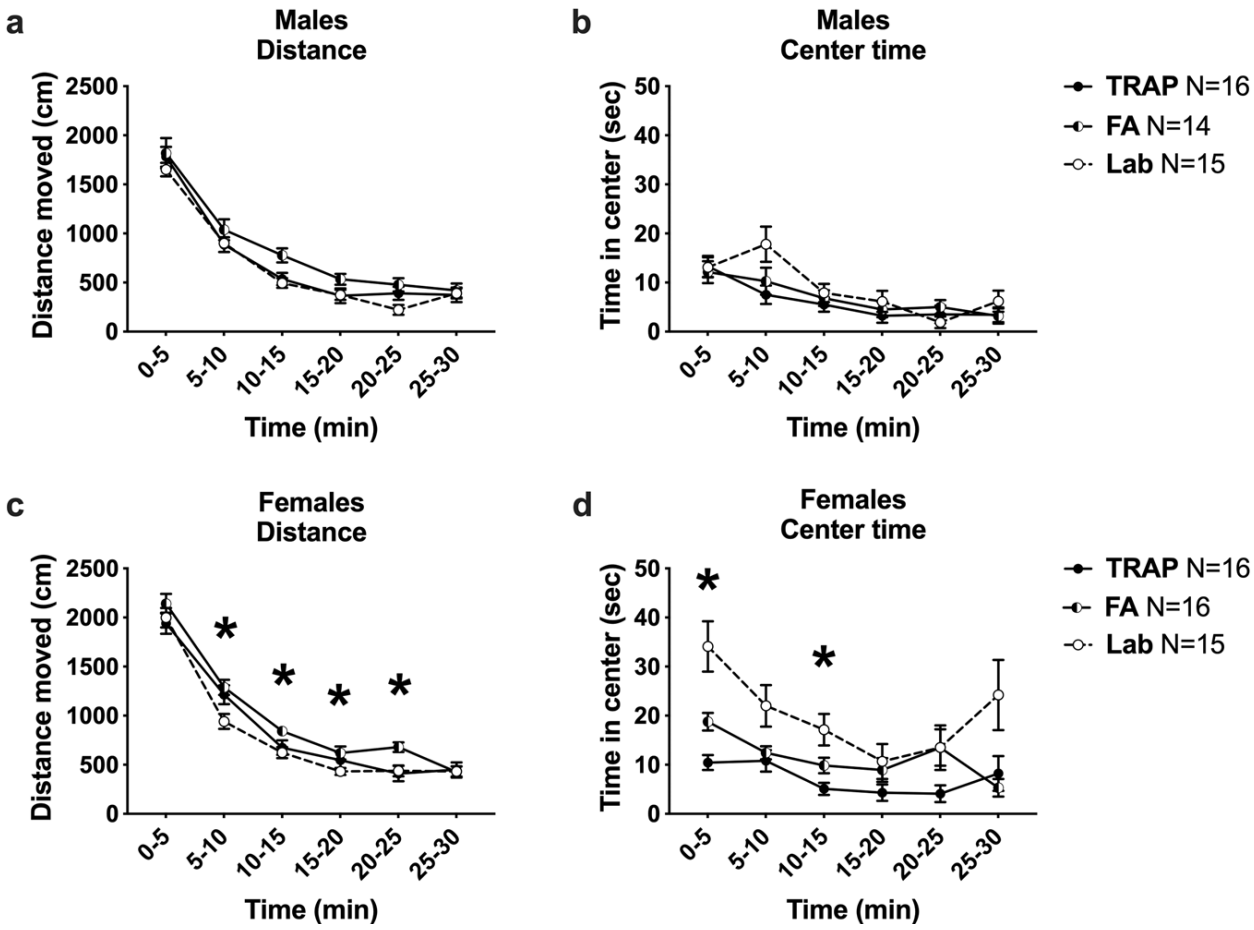

Fig. 5 Atypical exploratory activity in a novel open field in rats exposed to roadside TRAP and FA. a Roadside exposures did not affect males' gross locomotion or **b** time spent in the center during a 30-min exploration of a novel arena. **c** In females, there was a significant effect of group on distance moved, with trends suggesting that FA-exposed females covered more distance during the assay compared to lab controls. **d** TRAP-exposed females spent less time in the center than did FA-exposed females, and both TRAP- and FA-exposed females displayed significantly reduced center time relative to lab controls. $*p < 0.05$, repeated measures ANOVA followed by Tukey's multiple comparisons test.

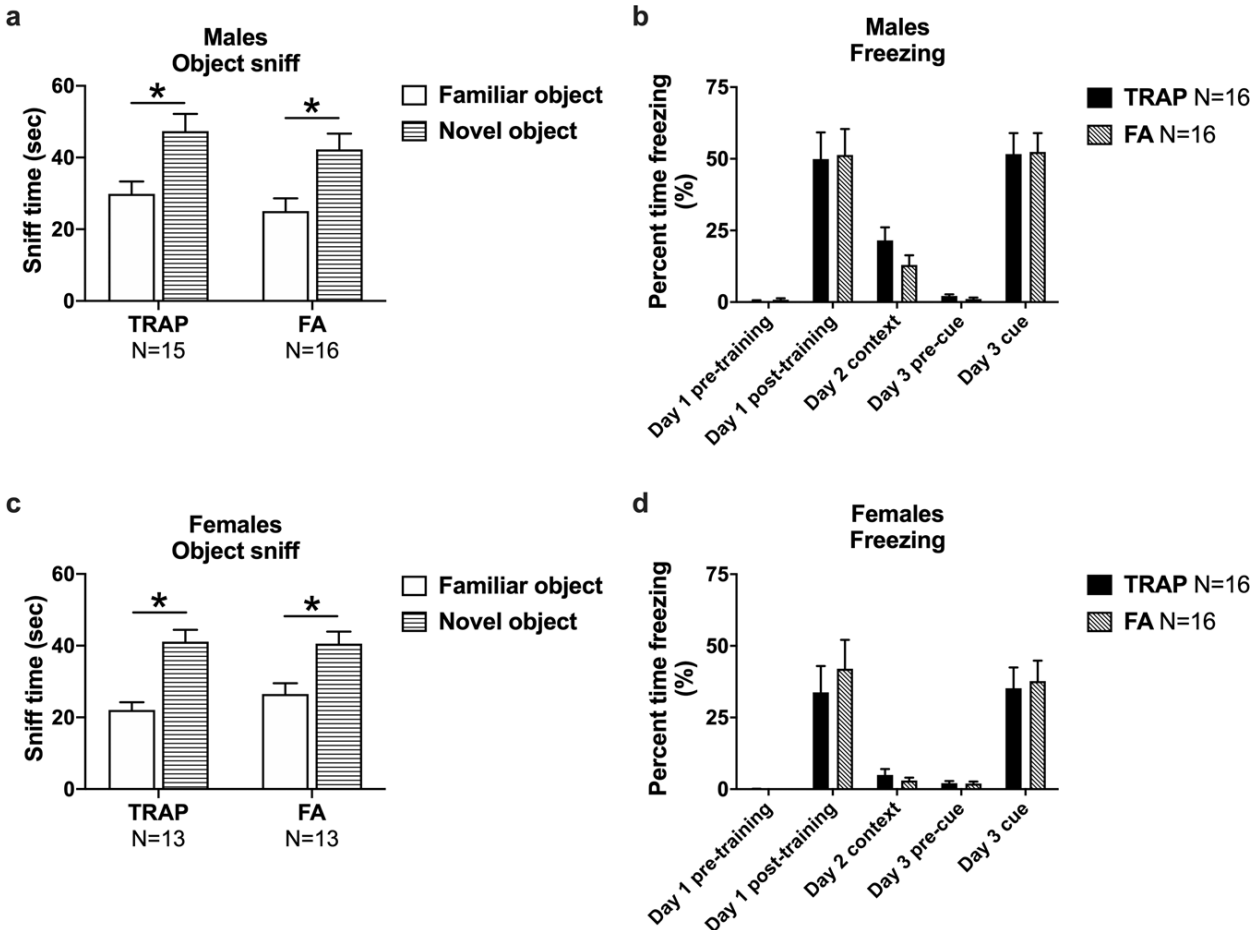

Fig. 6 Learning and memory in roadside exposed rats. a Males exposed to TRAP or FA displayed intact novel object recognition as evidenced by spending significantly more time sniffing the novel object than the familiar object. **b** Exposure to TRAP did not affect contextual or cued fear memory in males and both TRAP and FA groups displayed high levels freezing day 1 post-training and to the cue presentation on day 3. **c** Both groups of roadside exposed females spent significantly more time investigating the novel object compared to the familiar object and **d** no group differences were observed in percent time freezing during the test of contextual and cued memory. **a**, **c** $*p < 0.05$, paired *t*-test, familiar vs. novel. **b**, **d** $*p < 0.05$, Day 1, 3: repeated measures ANOVA; Day 2: Student's *t*-test, TRAP vs. FA.

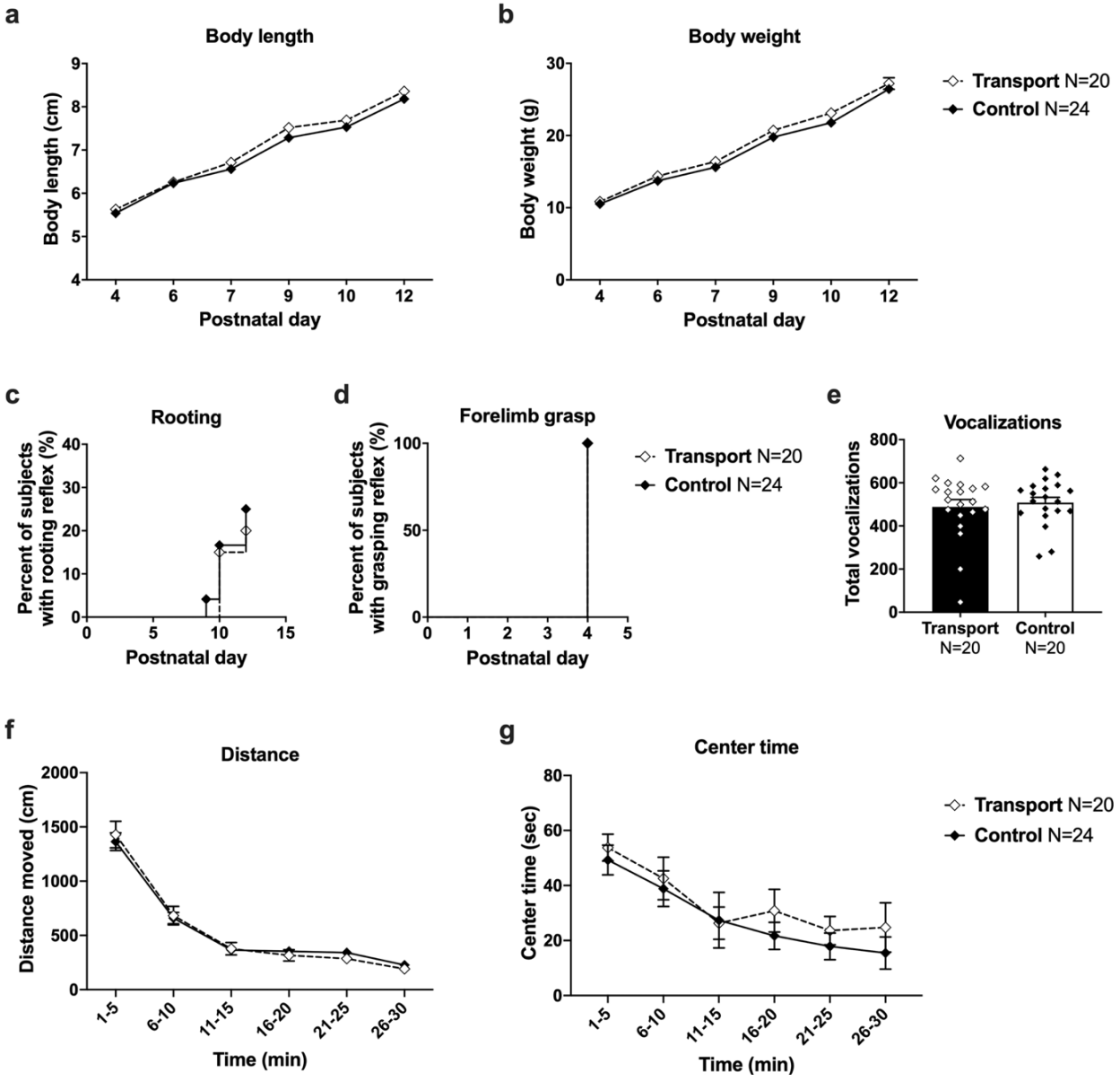

Fig. 7 No effect of gestational transport alone on offspring development and behavior. Pups born to dams that experienced a transport event at approximately GD 14 exhibited no physical or behavioral abnormalities. **a** Body length and **b** body weight were typical throughout early life, as was the timing of the development of **c** rooting and **d** forelimb grasping reflexes. **e** Gestational transport did not affect the number of isolation-induced pup ultrasonic vocalizations at PND 5 and **f** juveniles exhibited similar exploratory activity in a novel open field as indicated by total distance moved and **g** time spent in the center. **a**, **b**, **f**, **g** $*p < 0.05$, repeated measures ANOVA. **c**, **d** $*p < 0.05$, Log-Rank (Mantel-Cox) test. **e** $*p < 0.05$, Student's *t*-test.

Supplementary Information

Table S1. Comparison of litter size and offspring sex.

Parameter	**TRAP Mean ± SEM (N=10)**	**FA Mean ± SEM (N=16)**	**Lab Mean ± SEM (N=9)**	**Statistical Summary**			
Litter size	12 ± 1	12 ± 1	9 ± 1	**Litter Size: One-way ANOVA**			
				***F*(2, 32)**	***p***		**Sig?**
				2.242	0.123		No
Males	6 ± 1	6 ± 1	6 ± 1	**Offspring Sex: Two-way ANOVA**			
				Factor	***F*(1, 48)**	***p***	**Sig?**
				Group	0.1100	0.742	No
Females	6 ± 1	6 ± 1	3 ± 1	Sex	0.1100	0.742	No
				Interaction	0.2474	0.621	No

Table S2. Analysis summary of additional developmental milestones.

Males							
Milestone	**Repeated measures ANOVA**				**Tukey's multiple comparisons test for effect of group**		
	Factor	***F*(df)**	***p***	**Sig?**	**Comparison**	**Adjusted *p***	**Sig?**
Tail length (cm)	Time	$F(2.692, 137.3) = 1092$	<0.0001	Yes	TRAP vs. FA	0.480	No
	Group	$F(2, 51) = 6.329$	0.004	Yes	FA vs. Lab	0.032	Yes
	Int	$F(10, 255) = 3.116$	<0.001	Yes	TRAP vs. Lab	0.281	No
Righting reflex (sec)	Time	$F(2.573, 131.2) = 25.92$	<0.0001	Yes			
	Group	$F(2, 51) = 0.9020$	0.412	No			
	Int	$F(10, 255) = 1.508$	0.137	No			
Circle traverse (sec)	Time	$F(4.241, 216.3) = 46.95$	<0.0001	Yes			
	Group	$F(2, 51) = 1.173$	0.318	No			
	Int	$F(10, 255) = 0.4856$	0.899	No			
Negative geotaxis (sec)	Time	$F(3.852, 196.4) = 25.63$	<0.0001	Yes	TRAP vs. FA	0.999	No
	Group	$F(2, 51) = 0.0977$	0.907	No	FA vs. Lab	0.918	No
	Int	$F(10, 255) = 2.125$	0.023	Yes	TRAP vs. Lab	0.901	No
Cliff avoidance (sec)	Time	$F(4.196, 214) = 35.99$	<0.0001	Yes	TRAP vs. FA	0.400	No
	Group	$F(2, 51) = 6.422$	0.003	Yes	FA vs. Lab	<0.001	Yes
	Int	$F(10, 255) = 2.456$	0.008	Yes	TRAP vs. Lab	0.034	Yes
	TRAP % achieved	**FA % achieved**	**Lab % achieved**	**Chi square**	**df**	***p***	**Sig?**
Bar hold (day)	35.0	35.0	35.71	0.1516	2	0.927	No
Females							
Milestone	**Repeated measures ANOVA**				**Tukey's multiple comparisons test for effect of group**		
	Factor	***F*(df)**	***p***	**Sig?**	**Comparison**	**Adjusted *p***	**Sig?**
Tail length (cm)	Time	$F(4.597, 248.2) = 1815$	<0.0001	Yes	TRAP vs. FA	0.448	No
	Group	$F(2, 54) = 9.871$	<0.001	Yes	FA vs. Lab	0.005	Yes
	Int	$F(10, 270) = 5.179$	<0.0001	Yes	TRAP vs. Lab	0.111	No
Righting reflex (sec)	Time	$F(2.849, 153.8) = 12.16$	<0.0001	Yes			
	Group	$F(2, 54) = 0.6852$	0.508	No			
	Int	$F(10, 270) = 1.421$	0.171	No			
Circle traverse (sec)	Time	$F(3.956, 213.6) = 58.43$	<0.0001	Yes			
	Group	$F(2, 54) = 0.6107$	0.547	No			
	Int	$F(10, 270) = 1.656$	0.091	No			
Negative geotaxis (sec)	Time	$F(4.287, 231.5) = 26.01$	<0.0001	Yes			
	Group	$F(2, 54) = 0.0486$	0.953	No			
	Int	$F(10, 270) = 1.811$	0.059	No			
Cliff avoidance (sec)	Time	$F(3.866, 208.8) = 49.91$	<0.0001	Yes	TRAP vs. FA	0.172	No
	Group	$F(2, 54) = 7.517$	0.001	Yes	FA vs. Lab	0.001	Yes
	Int	$F(10, 270) = 3.708$	<0.001	Yes	TRAP vs. Lab	0.225	No
	TRAP % achieved	**FA % achieved**	**Lab % achieved**	**Chi square**	**df**	***p***	**Sig?**
Bar hold (day)	40.0	30.0	41.18	0.8043	2	0.669	No

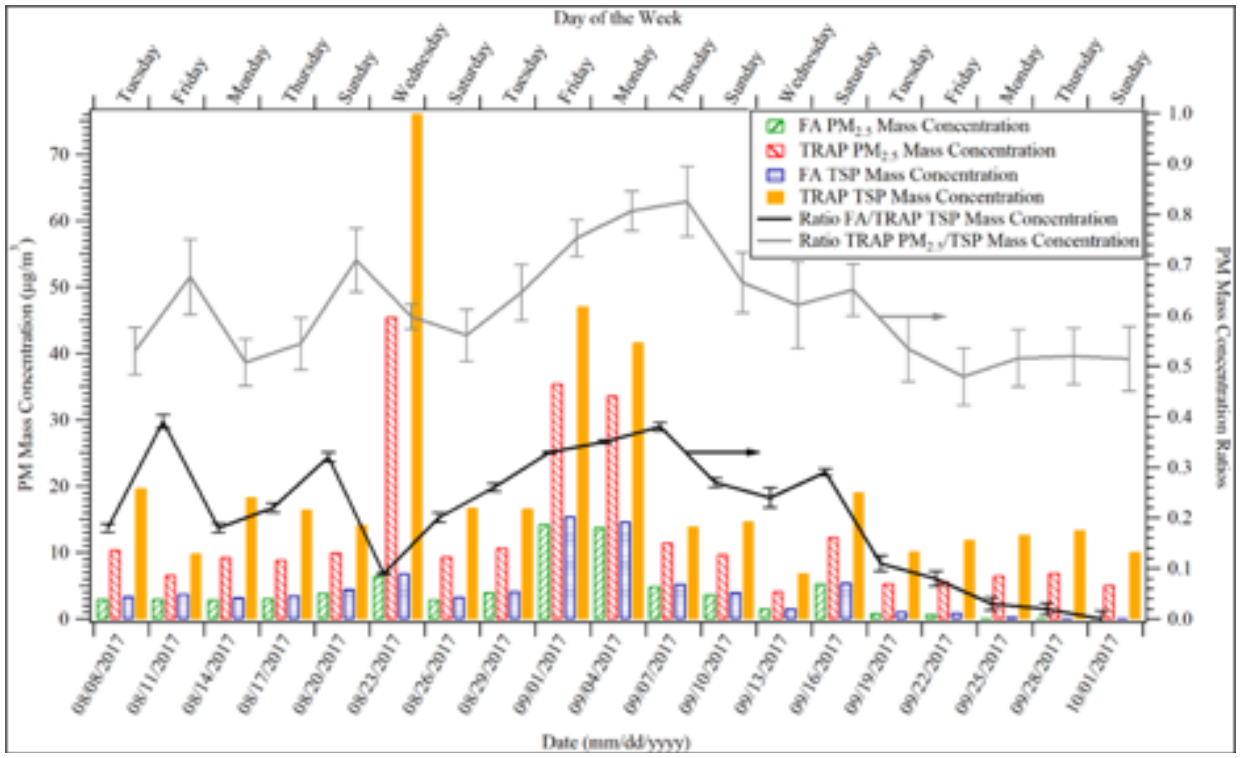

Figure S1. Bars/left axis: temporal trends in 24-hour PM2.5 and Total Suspended Particulate (TSP) mass concentrations measured immediately upstream of the Filtered Air (FA) and Traffic-Related Air Pollution (TRAP) exposure chambers at the Facility for Roadway Air Pollution Exposure for the study duration. Lines/markers/right axis: temporal trends in the ratio of FA to TRAP TSP mass concentrations (black line) and ratio of TRAP PM2.5 to TSP (gray line). Filter-based PM samplers (1) owned and maintained by the Interagency Monitoring of Protected Visual Environments (IMPROVE) were deployed in this study to collect 24-hour continuous PM samples every third day for the study duration. PM mass concentrations were determined from gravimetric analysis of the collected filter samples according to the handling, storage, measurement and QA/QC protocols of the IMPROVE Particle Monitoring Network (2). Random errors associated with gravimetric analysis of the filter samples are estimated to be ± 3 mg per measurement, which equates to ± 0.1 mg/m^3 for the concentration calculations. Propagation of these uncertainties in the calculation of mass concentration ratios are included in the lines of the plot.

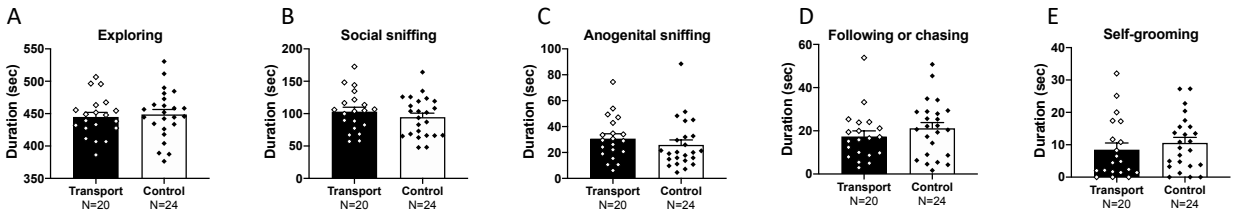

Fig. S2. Exposure to transportation at ~GD14 did not alter juvenile reciprocal social interactions on several key parameters. The transportation did not account for the findings observed in the roadside exposure groups in social play including A) levels of exploration during the social interaction assay, B) time social sniffing all body parts, C) time spent anogenital sniffing, and D) time spent following or chasing the stimulus animals. E) There was no effect of the transport on offspring measured by the time spent self-grooming compared to lab controls from dams that did not undergo the transport event.

Table S3. Analysis summary of reciprocal social interaction parameters following transport stress.

Parameter	Transport Mean ± SEM (N=20)	Control Mean ± SEM (N=24)	*t*	df	*p*	Significant?
Pounce (#)	1.90 ± 0.64	1.63 ± 0.48	0.3509	42	0.727	No
Pin (#)	0.25 ± 0.12	0.67 ± 0.21	1.654	42	0.106	No
Push under or crawl over (#)	6.10 ± 0.76	4.88 ± 0.75	1.147	42	0.258	No

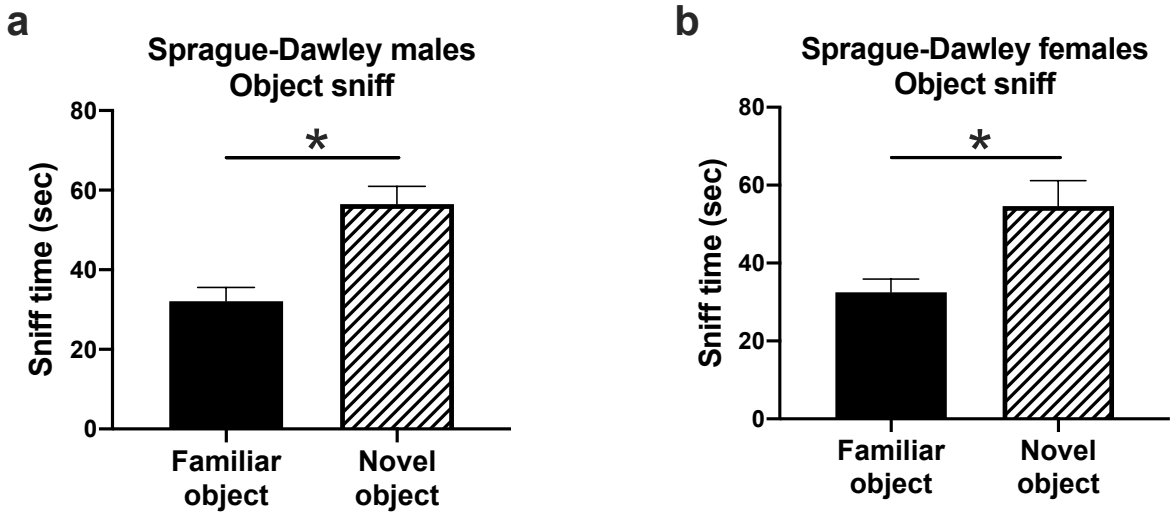

Fig. S3. Performance of laboratory-reared Sprague-Dawley rats in the test of novel object recognition. Following the same testing protocol employed at the tunnel-adjacent exposure facility, Sprague-Dawley rat A) males (N=16) and B) females (N=15) reared and tested under UC Davis laboratory conditions spent significantly more time sniffing the novel object compared to the familiar object. *$p < 0.05$, paired *t*-test.

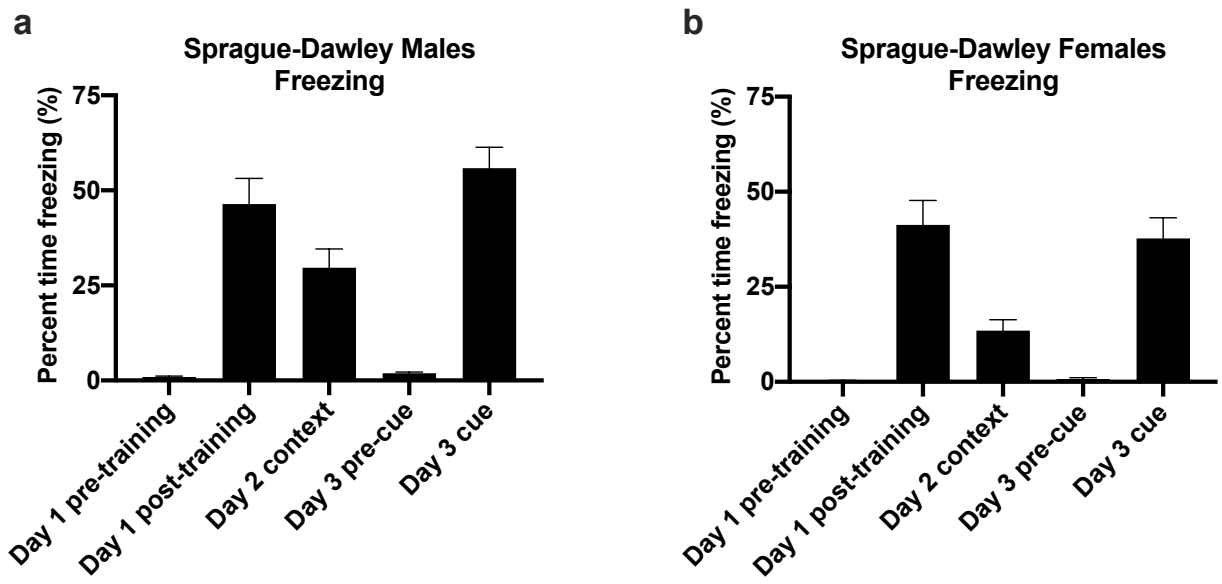

Fig. S4. Performance by laboratory-reared Sprague-Dawley rats within the contextual and cued fear conditioning paradigm. Following the same testing protocol employed at the tunnel-adjacent exposure facility, A) male Sprague-Dawley rats (N=26) reared and tested under UC Davis laboratory conditions exhibited little to no freezing pre-training and pre-cue, spent approximately 50% of the time freezing post-training and during the cue in a novel context, and 30% time freezing in the training context. B) Female Sprague-Dawley rats (N=23) reared and tested in a UC Davis laboratory exhibited little to no freezing pre-training and pre-cue, spent approximately 40% of the time freezing post-training and during the cue in a novel context, and 15% time freezing in the training context.

Chapter 3

Translational Outcomes Relevant to Neurodevelopmental Disorders Following Early Life Exposure of Rats to Chlorpyrifos

This chapter has been published as: Elizabeth L. Berg, Tianna M. Ching, Donald A. Bruun, Josef K. Rivera, Milo Careaga, Jacob Ellegood, Jason P. Lerch, Markus Wöhr, Pamela J. Lein, and Jill L. Silverman (2020). *Journal of Neurodevelopmental Disorders* 12(40): 1-15.

Abstract

Neurodevelopmental disorders (NDDs), including intellectual disability, attention deficit hyperactivity disorder (ADHD), and autism spectrum disorder (ASD), are pervasive, lifelong disorders for which pharmacological interventions are not readily available. Substantial increases in the prevalence of NDDs over a relatively short period may not be attributed solely to genetic factors and/or improved diagnostic criteria. There is now a consensus that multiple genetic loci combined with environmental risk factors during critical periods of neurodevelopment influence NDD susceptibility and symptom severity. Organophosphorus (OP) pesticides have been identified as potential environmental risk factors. Epidemiological studies suggest that children exposed prenatally to the OP pesticide chlorpyrifos (CPF) have significant mental and motor delays and strong positive associations for the development of a clinical diagnosis of intellectual delay or disability, ADHD, or ASD. We tested the hypothesis that developmental CPF exposure impairs behavior relevant to NDD phenotypes (i.e., deficits in social communication and repetitive, restricted behavior). Male and female rat pups were exposed to CPF at 0.1, 0.3, or 1.0 mg/kg (s.c.) from postnatal days 1-4. These CPF doses did not significantly inhibit acetylcholinesterase activity in the blood or brain but significantly impaired pup ultrasonic vocalizations (USV) in both sexes. Social communication in juveniles via positive affiliative 50-kHz USV playback was absent in females exposed to CPF at 0.3 mg/kg and 1.0 mg/kg. In contrast, this CPF exposure paradigm had no significant effect on gross locomotor abilities or contextual and cued fear memory. Ex vivo magnetic resonance imaging largely found no differences between the CPF-exposed rats and the corresponding vehicle controls using strict false discovery correction; however, there were interesting trends in females in the 0.3 mg/kg dose group. This work generated and characterized a rat model of developmental CPF exposure that exhibits adverse

behavioral phenotypes resulting from perinatal exposures at levels that did not significantly inhibit acetylcholinesterase activity in the brain or blood. These data suggest that current regulations regarding safe levels of CPF need to be reconsidered.

Background

The wide use of insecticides has raised a significant concern due to possible health effects associated with exposure to these compounds [1–5]. Insecticides are used globally to control crop pests in agriculture, to reduce household pests, to reduce insect damage to lawns and golf courses, and as mosquito control agents [6–8]. Among the most widely used insecticides are the organophosphorus pesticides (OPs), which include chlorpyrifos, parathion, and diazinon [9, 10]. Prenatal exposure to OPs has been associated with abnormal psychomotor ability, deficits in working memory and intelligence quotient, and disrupted behaviors in children [8, 11–18]. Experimental studies have also demonstrated an association between prenatal exposure to OPs and abnormal developmental reflexes [19].

The most extensively studied OP pesticide to date with respect to neurodevelopmental insults has been chlorpyrifos (CPF). Eaton and colleagues published a comprehensive review that examined the large body of toxicological data and epidemiological information describing effects of CPF in humans, with an emphasis on its controversial adverse effects on neurodevelopment [7]. Subsequently, the UC Davis Childhood Autism Risks from Genetics and Environment (CHARGE) study [8, 18] reported significant associations between prenatal OP exposures and mental and motor delays and an increased risk of autism spectrum disorder (ASD). Studies of a separate cohort of children in New York City provided corroborating behavioral data and brain structural neuroimaging of children prenatally exposed to CPF, illustrating enlargement of various cortical

regions and effects on underlying white matter [20]. A recent meta-analysis of the epidemiological data concluded that there is a positive association between CPF and neurodevelopmental disorders, which warranted further investigation of CPF developmental neurotoxicity [21].

Rodents exposed to relatively high, but subtoxic, doses of CPF during early life exhibit delayed development of psychomotor reflexes [22, 23], sexual-social behaviors [24, 25], and impaired cognitive performance [26–29] later in life. But whether developmental exposure to CPF at levels that do not significantly inhibit acetylcholinesterase (AChE) causes phenotypes of relevance to neurodevelopmental disorders remains unclear. The goal of this study was to generate and use a rat model of developmental exposure to CPF to study the effect of environmentally relevant levels of CPF on a range of behaviors in young animals, including social communication, Pavlovian learning and memory, anatomical phenotypes determined by magnetic resonance imaging, and sexually dimorphic effects on these outcomes. The exposure paradigm used in this study was based on the finding from the CHARGE study which showed that pesticides had the most significant effect on health outcomes when exposure occurred during the third trimester [8, 18].

Characterizing the developmental neurotoxicity of environmentally relevant CPF exposures is required for assessing the risk that CPF poses to the developing brain, and for developing policies to protect the developing brain from this risk. In 2017, the federal EPA administrator denied a widespread petition to ban CPF, which is currently being appealed and battled in litigation. Additionally, the California Department of Pesticide Regulation announced in early 2019 that it will cancel the registration that currently allows chlorpyrifos to be sold in California. Thus, we aimed to use our preclinical model system to further clarify links between CPF exposure and adverse neurodevelopmental outcomes. This knowledge of CPF developmental

neurotoxicity is crucial for implementing protective policies and mechanisms for estimating whether low dose exposures, via food and water consumption, pose real threats to human health.

Methods

Materials. Chlorpyrifos (CPF; o,o-diethyl [o-3,5,6-trichloro-2-pyridinol] phosphorothionate; 99.5% purity) was purchased from Chem Service (West Chester, PA, USA) and used within 6 months of purchase with interim storage as recommended by the manufacturer. Solutions were made weekly in NEOBEE® M-5 oil vehicle (Spectrum Chemical, Gardena, CA, USA) at their final concentrations and stored in a polypropylene container in the dark at room temperature.

Subjects. Male and female Sprague-Dawley rats were purchased from Envigo (Indianapolis, Indiana) to generate cohorts for testing. All procedures were approved by the Institutional Animal Care and Use Committee (IACUC) at the University of California Davis and were conducted in accordance with the National Institutes of Health Guide for the Care and Use of Laboratory Animals. All animals were housed in a temperature-controlled vivarium maintained on a 12:12 light-dark cycle. OP pesticides were not applied in the vivarium before or during the study. To identify individual subjects, pups were labeled on the back via permanent marker on postnatal day 1, which was reapplied daily. As fur developed, animals were identified via tail marks, which were coded to allow investigators to run and score behaviors blind to the experimental group.

Cohorts. One cohort of rats, which consisted of 58 rat pups from 9 litters, was tested for early life communication. Rat pups were exposed daily to CPF (1.0 or 3.0 mg/kg) or vehicle (Neobee Coconut Oil; Spectrum Chemical MFG Corp) via s.c. injection (2 mL/kg) with a 30 gauge Hamilton syringe on postnatal day (PND) 1-4. On PND 8, pups underwent isolation-induced ultrasonic vocalization (USV) collection. These data, summarized in **Supplementary Fig. S1**, were the basis for the decision to test doses lower than 1.0 mg/ kg in a second cohort. A second cohort of rats, which consisted of 2 males and 2 females from each of 25 litters, was analyzed for early life and juvenile behavioral effects as well as juvenile neuroanatomical effects of CPF exposure. Rat pups were exposed daily to CPF at 0.1, 0.3, or 1.0 mg/kg or to an equal volume of vehicle (Neobee Coconut Oil; Spectrum Chemical MFG Corp) via s.c. injection (2 mL/kg) with a 30 gauge Hamilton syringe on PND 1-4. Litters were reduced to 8 pups (4 m and 4 f when possible) on PND 4, at which time, the culled littermates of the behavioral subjects were analyzed for acetylcholinesterase (AChE) activity in brain and blood at 1 h postinjection. The behavioral battery consisted of pup ultrasonic vocalizations and developmental milestones on PND 8, 12, and 16, locomotion in an open field, response to USV playback, and cued and contextual fear conditioning. After behavioral testing, brains were harvested and fixed for MRI analysis.

Behavioral assays. *Isolation-induced pup 40-kHz ultrasonic vocalizations.* During the first few weeks of life, rodent pups emit ultrasonic vocalizations (USV) when separated from their mother and litter [30–32]. On PND 8, 12, and 16 pups were individually removed from the nest in a random order and placed into an open-top plastic isolation container containing corncob bedding. USV were collected for 3 min with an ultrasonic microphone (Avisoft Bioacoustics, Glienicke,

Germany) using methods outlined previously [33, 34]. Immediately following USV collection, body temperature and body weight were measured.

Open field locomotion. Sedation or hyperactivity may have confounding effects on assays of sociability. Therefore, on PND 19, exploratory activity in a novel open field was automatically measured for 30 min as described previously [33, 34].

USV playback. Behavioral responses to playback of 50-kHz ultrasonic vocalizations were measured on PND 24-27 as previously described [34]. Briefly, rats were placed individually on an 8-arm elevated radial maze and presented with pro-social 50-kHz USV and a time- and amplitude-matched white noise acoustic stimulus control using an ultrasonic speaker (Avisoft Bioacoustics, Glienicke, Germany). Social exploratory and approach behavior in response to the USV were assessed, as was the behavioral response to the white noise stimulus.

Cued and contextual fear conditioning. Learning and memory were assessed on PND 30-33 using a previously described 3-day cued and contextual fear conditioning assay [35]. On day one, rats were trained to associate a foot shock with a specific environmental context as well as with a white noise auditory cue using automated chambers (Med Associates, Inc., St. Albans, Vermont). Approximately 24 h later, rats were re-exposed to the same context without the auditory cue and time spent freezing was quantified to assess contextual fear memory. Approximately 48 h following the initial training, rats were re-exposed to the auditory cue in a novel environmental context and time spent freezing was quantified to assess cued fear memory.

Ex vivo neuroimaging via magnetic resonance imaging. On PND 35-36, brains were flushed via transcardial perfusion (flow rate of 2 mL/min) with 50 mL phosphate-buffered saline (PBS) containing 10 U/mL heparin and 2 mM ProHance (a gadolinium-based contrast agent;

Bracco Diagnostics Inc.), fixed with 50 mL 4% paraformaldehyde (PFA) in PBS containing 2 mM ProHance, and collected for neuroimaging following previously published protocols [36]. Following perfusion, brains were incubated in the 4% PFA solution for 24 h at 4 °C then transferred to a storage PBS solution containing 0.02% sodium azide. Brains were incubated in the storage solution at 4 °C for at least 1 month prior to scanning. Images were acquired and analyzed following a protocol previously described [33, 37]. Multiple comparisons were controlled for using the false discovery rate (FDR) with the significance level for the FDR-adjusted p value (q) set at $q < 0.05$ [38].

AChE activity assay. One hour following the final CPF dosing on PND 4, pups were euthanized by decapitation and blood was collected by cardiac puncture into tubes containing EDTA as an anti-coagulant (Becton-Dickinson, Franklin Lakes, NJ). Blood was diluted 1:25 with phosphate buffer with 0.03% Triton X-100 (Fisher Scientific, Pittsburg, PA), vortexed, and snap frozen for later analysis. Brains were collected and snap frozen for later analysis. For the AChE activity assay, brain tissue was thawed on ice, homogenized in phosphate buffer with 1% Triton X-100, and AChE activity quantified using the standard Ellman Assay [39] with 5,5′-dithio-bis-2-nitrobenzoic acid (DTMB) and acetylthiocholine iodide (ASChI) as the substrates (Sigma-Aldrich, St. Louis, MO). Tetraisopropyl pyrophosphoramide (Sigma) was included to inhibit pseudocholinesterase. Blood AChE activity was normalized to hemoglobin levels, which were determined using a StanBio Laboratory Stat-Site M hemoglobin meter and test strips (Boerne, TX, USA). Brain AChE activity was normalized to protein concentration as determined using the BCA assay kit (Pierce, Rockford, IL).

Statistical analyses. Developmental vocalizations, temperature, weight, and open field metrics were analyzed via repeated measures ANOVA with dose as the between-group factor and time as the within-group factor. Following detection of a significant main effect and/or time by dose interaction, *post hoc* testing was carried out using Holm-Sidak's multiple comparisons test. Paired t tests (one per dose group) were used to compare time spent on the proximal and distal arms during the USV playback paradigm and locomotion during the playback test was compared using repeated measures or one-way ANOVA. Comparisons between freezing times were carried out for each test phase with one-way ANOVA. Acetylcholinesterase activity was analyzed using one-way ANOVA. Data were analyzed via GraphPad Prism. All significance levels were set at $p < 0.05$ and all *t* tests were two tailed. Multiple comparisons were corrected for via *post hoc* testing using Holm-Sidak's multiple comparisons test.

Results

Developmental CPF exposure reduced isolation-induced pup ultrasonic vocalizations. Pup ultrasonic vocalizations (USV) of infant rats measure an early communicative behavior between pups and mother. Isolation-induced USV were collected for 3 min as social communication signals in rat pups, as previously described [33]. CPF-exposed pups emitted significantly fewer USV across early development (**Fig. 1a** (males) $F_{(2, 90)} = 286.5$, $p < 0.001$; **Fig. 1b** (females) $F_{(2, 90)} = 267.7$, $p < 0.001$). As pups grow, they learn to temperature regulate, open their eyes, and are less reliant on maternal care, which is why USV decrease in number over developmental days. There was a significant main effect of experimental group on USV emission ($F_{\text{males } (3, 45)} = 3.048$, $p < 0.05$). Holm-Sidak *post hoc* analysis corrected for multiple comparisons highlighted significant differences on PND 12, when fewer USV were emitted in the 1.0 mg/kg

CPF-exposed male pups, and on PND 16 in all CPF dose groups compared to vehicle. CPF-exposed female pups also emitted significantly fewer USV ($F_{(3, 37)} = 2.949$, $p < 0.05$). Holm-Sidak *post hoc* analysis highlighted strong trending differences on PND 8, as fewer USV were emitted in the 0.3 mg/kg CPF-exposed female pups (p = 0.061), and significant differences at PND 12 and 16 in the 0.3 mg/kg CPF-exposed female pups compared to vehicle.

Body weight and temperature were also collected to assure the reduced USV were not the result of being physically smaller as body weight is known to alter pup USV emission [30, 31]. Body temperature did not differ between CPF exposure groups and vehicle (**Fig. 1c** (males) $F_{(3, 46)} = 0.5381$, $p > 0.05$; **Fig. 1d** (females) $F_{(3,} 46) = 0.67$, $p > 0.05$). Weight did not differ between CPF exposure groups and vehicle (**Fig. 1e** (males) $F_{(3, 46)} = 0.2745$, $p > 0.05$; **Fig. 1f** (females) $F_{(3, 46)} = 0.5234$, $p > 0.05$), indicating typical growth and ability to thrive. In addition to being important control metrics for the pup USV assay, the observation that overall growth and health was not impacted by CPF exposure confirms the lack of systemic toxicity that has been reported with higher CPF doses using a functional observation battery [40, 41].

Analysis of typical early neurological reflexes did not reveal any significant differences between CPF-exposed pups and vehicle controls (**Supplementary Fig. S2**). Specifically, there were no significant differences between exposure groups in latencies to navigate upright in negative geotaxis and circle traverse, simple metrics for motoric, postural, and proprioceptive processes that underlie the ability of infant rodents to navigate on an inclined plane or to the outer rim from the center of circle (**Fig. S2A** (males) $F_{(3, 46)} = 0.4776$, $p > 0.05$; **Fig. S2B** (females) $F_{(3, 46)} = 1.098$, $p > 0.05$; **Fig. S2C** (males) $F_{(3,}46) = 1.224$, $p > 0.05$; **Fig. S2D** (females) $F_{(3, 46)} = 1.1319$, $p > 0.05$).

Normal locomotion and exploratory activity following developmental CPF exposure. Normal motor function following early life exposure to low doses of CPF was confirmed by lack of an effect of CPF on motor abilities in the open field exploratory locomotion task across a 30-min session. No CPF effect was observed in activity metrics of horizontal activity (**Fig. 2a** (males) $F_{(3, 46)} = 0.2303$, $p > 0.05$; **Fig. 2b** (females) $F_{(3, 46)} = 0.3341$, $p > 0.05$), vertical activity (**Fig. 2c** (males) $F_{(3, 46)} = 0.2278$, $p > 0.05$; **Fig. 2d** (females) $F_{(3, 46)} = 0.2562$, $p > 0.05$), or time spent in the center of the arena (**Fig. 2e** (males) $F_{(3, 46)} = 0.7749$, $p > 0.05$; **Fig. 2f** (females) $F_{(3, 46)} = 2.150$, $p > 0.05$).

Reduced social exploration to affiliative 50-kHz ultrasonic calls (USV) in female CPF-exposed juveniles. Social exploratory behavior displayed by the male (**Fig. 3c** $t_{(1, 13)} = 3.576$, $p < 0.005$) and female vehicle control groups (**Fig. 3d** $t_{(1, 13)} = 3.509$, $p < 0.005$) was directed toward playback of pro-social 50-kHz USV, as reflected in the parameter of time spent on the arms proximal to the sound source emitting 50-kHz USV as compared to the distal arms of the radial maze. All groups of male juvenile rats (vehicle and each dose of CPF) spent significantly longer on the arms proximal to the speaker emitting the 50-kHz USV upon playback (**Fig. 3c** (0.1 dose) $t_{(1, 13)} = 2.738$, $p < 0.02$; **Fig. 3c** (0.3 dose) $t_{(1, 13)} = 4.587$, $p < 0.001$; **Fig. 3c** (1.0 dose) $t_{(1, 13)} = 4.502$, $p < 0.001$). In contrast, the 0.3 mg/kg and 1.0 mg/kg CPF-exposed females rats did not spend significantly more time on the proximal arms (**Fig. 3d** (0.1 dose) $t_{(1,13)} = 3.001$, $p < 0.005$; **Fig. 3d** (0.3 dose) $t_{(1, 13)} = 1.373$, $p > 0.05$; **Fig. 3d** (1.0 dose) $t_{(1, 13)} = 0.7127$, $p > 0.05$).

All groups demonstrated a similar locomotor response to the 50-kHz USV, characterized by elevated movement during the USV as compared to baseline (**Fig. 3e** (males, time) $F_{(1, 46)} = 100.5$, $p < 0.0001$; **Fig. 3e** (males, group) $F_{(3, 46)} = 0.337$, $p > 0.05$; **Fig. 3e** (males, time x group)

$F_{(3, 46)} = 0.533$, $p > 0.05$; **Fig. 3f** (females, time) $F_{(1, 46)} = 45.90$, $p < 0.0001$; **Fig. 3f** (females, group) $F_{(3, 46)} = 0.379$, $p > 0.05$; **Fig. 3f** (females, time x group) $F_{(3, 46)} = 0.682$, $p > 0.05$). Distance traveled in response to the white noise control stimulus did not differ between exposure groups, and all groups exhibited comparable levels of locomotion before (**Fig. 3g** (males) $F_{(3, 46)} = 0.707$, $p > 0.05$; **Fig. 3h** (females) $F_{(3, 46)} = 0.448$, $p > 0.05$) and during the noise stimulus (**Fig. 3g** (males) $F_{(3, 46)} = 1.094$, $p > 0.05$; **Fig. 3h** (females) $F_{(3, 46)} = 1.596$, $p > 0.05$). These findings rule out the possibility of a confounding hearing deficit in the CPF-exposed groups.

CPF-exposed rats demonstrated intact contextual and cued fear memory. Learning and memory was evaluated using two measures of Pavlovian fear conditioning with a 24 h contextual component and a 48 h tone cued fear conditioning. High levels of freezing were observed subsequent to the conditioned stimulus (CS)—unconditioned stimulus (UCS) pairings on the training day, in both exposed groups (**Fig. 4a** (males) no group difference in post-training freeze scores, $F_{(3, 46)} = 0.3342$, $p > 0.05$; **Fig. 4b** (females) no group difference in post-training freeze scores, $F_{(3, 46)} = 0.2033$, $p > 0.05$), indicating no confounds and no deficits in the learning of the associations between the context stimuli and tone cues. No exposure group difference in freezing was observed 24 h following CSUCS training (**Fig. 4c** (males) $F_{(3, 46)} = 0.02571$, $p > 0.05$; **Fig. 4d** (females) $F_{(3, 46)} = 0.2045$, $p > 0.05$) when placed in the context chamber from conditioning training with identical stimulus cues. Levels of freezing, pre- and postcue presentation 48 h after training, showed no effect of exposure (**Fig. 4e** (males, pre-cue) $F_{(3, 46)} = 0.1365$, $p > 0.05$; Fig. 4e (males, cue) $F_{(3, 46)} = 0.6103$, $p > 0.05$; **Fig. 4f** (females, pre-cue) $F_{(3, 46)} = 0.3858$, $p > 0.05$; Fig. 4f (females, cue) $F_{(3, 46)} = 0.2999$, $p > 0.05$).

Neuroanatomical pathology at PND 35 following developmental CPF exposure. Overall, the total brain volumes were not observed to be different between groups (1683 ± 101 mm^3 for vehicle, 1649 ± 51 mm^3 for a CPF dosage of 0.1 mg/kg, 1675 ± 123 mm^3 for 0.3 mg/kg, and 1662 ± 68 mm^3 for 1.0 mg/ kg). A difference in total brain volume between vehicle and CPF exposure at 0.3 mg/kg of −2.27% observed in the females was a mere one hundredth from significance (p = 0.06, q = 0.22). There were no significant findings for any CPF exposure group nor for any sex when correcting for multiple comparisons. There was a trend toward a decrease in the hippocampal region (−3.29%, p = 0.03, q = 0.22), which appeared to be localized to Ammon's Horn (−3.52%, p = 0.02, q = 0.22). Additional trends toward a loss in volume were found in the fiber tracts (−2.61%, p = 0.03, q = 0.22), with the strongest trends found in the fimbria (−3.63%, p = 0.02, q = 0.22) and the cortical spinal tract (−5.11%, p = 0.01, q = 0.22). Voxelwise comparisons also revealed no significant differences, but again interesting trends were seen in the female rats exposed to CPF at 0.3 mg/kg (**Fig. 5**). Interestingly, at the 0.3 mg/kg dosage, opposite effects are seen in males versus females with males showing positive effect size differences and females showing negative effect size differences (**Fig. 5**).

Normal brain and blood AChE activity following CPF exposure. None of the three doses of CPF significantly altered the enzymatic activity of AChE in the brain (**Fig. 6a** $F_{(3,35)}$ = 0.1252, $p > 0.05$) or in the blood (**Fig. 6b** $F_{(3,34)} = 0.2137$, $p > 0.05$).

Discussion

There is an extensive literature describing the developmental neurotoxicity of the OP pesticide chlorpyrifos (CPF). Epidemiological studies [8, 11–17], which provide compelling links

between early life exposure to OPs and abnormal early cognitive development, may offer insights into the rising prevalence of neurodevelopmental disorders (NDDs). Epidemiological studies suggest that prenatal exposure to CPF, particularly during the second or third trimester, is associated with significant mental and motor delays and with a clinical diagnosis of NDD, including ADHD and ASD [8, 16, 18, 20, 42]. To date, there have been fewer reports in preclinical mouse and rat models testing the hypothesis that developmental CPF exposure impairs behaviors relevant to the broad NDD phenotype. Herein, we report the initial behavioral and anatomical characterization of a rat model of developmental CPF exposure at doses that do not significantly inhibit acetylcholinesterase (AChE) activity. The most significant effect, reduced ultrasonic vocalization emission in pups, was observed in both sexes. We also discovered reduced social communication via a 50-kHz USV playback assay, a USV call and behavioral response task that can only be performed/observed in rats, which supports our hypothesis because aberrant social communication aligns with the clinical profiles of many NDDs. Structural imaging illustrated a large number of changes in brain volume and a variety of neuroanatomical phenotypes. Collectively, this study identified unique NDD-relevant functional and anatomical phenotypes as preclinical outcomes in response to developmental CPF exposures that had no effects on AChE activity.

This is the first report of reduced ultrasonic vocalizations in rat pups following developmental CPF exposure. Ultrasonic vocalizations in pups are crucial signals that elicit maternal care, without which pups would not be able to thermoregulate or suckle [43]. Reduced USV communication has been discovered in many genetic rat models of NDD, including those with mutations in synaptic genes, such as Shank3, cellular housekeeping genes such as ubiquitin ligase Ube3a that causes Angelman syndrome, and the calcium channel gene Cacna1c [33, 34, 44],

as well as numerous genetic mouse models of NDD, including 16p11.2 deletion syndrome [45], the Ca(V)1.2 L-type calcium channel gene that causes Timothy Syndrome [46], synaptic genes such as neuroligins [47], and high confidence ASD candidate genes, such as Tbx1 [48]. Reduced USV communication has also been reported in models of environmentally induced NDD phenotypes, including maternal immune activation [49], prenatal exposure to valproic acid [50, 51], and developmental exposure to traffic-related air pollution [35].

While we exposed rats to CPF during the first days of postnatal life, our findings are consistent with earlier literature showing that exposure to CPF during the gestational period resulted in altered behavioral and physical development in rodent pups in a sex-dependent manner. Venerosi and colleagues reported delayed somatic growth, reduced ultrasonic vocalizations, and increased latency to emit calls in male and female CD-1 mouse pups prenatally exposed to CPF [52], corroborating clinical reports in epidemiological studies [53]. Among mice exposed to the subtoxic doses of 1 and 3 mg/kg/d CPF on PND 1-4 and PND 11-14, hyperactivity was observed only in those exposed to 3 mg/kg/d CPF on PND 11-14 [24], which is consistent with our observation that the lower CPF doses tested in this study caused neither hypoactivity nor hyperactivity in rats in the open field task. However, in contrast to our findings, in the CD-1 strain mouse studies, the PND 1-4 exposure reduced brain cholinesterase activity by 25%. Studies of rats injected with 1 mg/kg/d CPF on PND 1-4 have also reported significantly reduced AChE activity in the brain ranging from 20 to 60% depending on sex and the interval between the last injection of CPF and the collection of tissue for analyses [22, 54]. The key differences between our study and the two earlier rat studies was the vehicle used for CPF dosing: we used a coconut oil preparation whereas the previously published rat studies, and the mouse study, used DMSO. Pharmacokinetic studies in adult rats have shown that subcutaneous administration of CPF in corn

oil resulted in faster absorption and metabolism of CPF compared to a subcutaneous administration of CPF in DMSO [55]. Whether this is the reason why we did not see a significant inhibition of AChE whereas other studies have despite using the same doses over the same developmental ages in the same rat strain has yet to be determined.

Exposure to CPF at 1 mg/kg during early postnatal life elicited deficits in reflex righting and geotaxis behavior in female rat pups [22]. This was also observed recently in Harlan-derived B6 mice exposed to 2.5 mg/kg of CPF on gestational days 12-15 [23]. Exposure to CPF at 1.5 mg/kg in early postnatal life reduced body weight in male Sprague-Dawley rats [28]. In contrast, we observed no effect of the CPF doses on the neonatal reflexes of negative geotaxis and circle traverse.

We discovered impaired juvenile behavioral responses to the playback of 50-kHz USV, a positive affiliative social contact call associated with play and social interactions. Reductions in playback social approach have been observed in other genetic rat models of NDD such as Shank3, Ube3a, and Cacna1c [33, 34, 44]. Juvenile social approach during playback is a bidirectional social communication behavior commonly studied in rats rather than mice as most reports that use choice playback in mice use sexual mating calls to elicit behavior [56, 57] and because inbred or congenic B6J mice cannot hear in the frequency range of ultrasonic vocalizations [58, 59]. We observed that female rats exposed to CPF at 0.3 or 1.0 mg/kg have a deficit in the key social approach behavior following a playful 50-kHz USV. This effect is not a consequence of deficits in psychomotor activation, motor abilities, or hearing. This conclusion is based on no evidence of motor impairments in the open field, pre-training or pre-cue activity in fear conditioning, and the total distance traversed following presentation of 50kHz USV, a key control metric for the social playback assay. These observations suggest the arousal-evoking component of the playback is

intact but that the deficit is specific to the social approach parameter of the assay. This could be due to multiple reasons including the CPF-exposed rats not being able to localize the sound source, the CPF-exposed rats having less dopaminergic-mediated motivation for social reward, and/or the CPF-exposed rats not being able to understand the communicative function of the pro-social 50-kHz USV. Differentiating between the various possible explanations will require future experiments beyond the scope of this initial generation of the rat model [60–62].

Our observations of the effects of developmental CPF exposure are novel because they are among the first reports of NDD-relevant phenotypes in a socially sophisticated rodent species, the rat. Our findings extend earlier literature of unusual social behavior elicited by developmental CPF exposure in mouse models with a wide variety of doses and exposure windows. Mouse research showed that neonatal CPF exposure (3 mg/kg) increased sexual social soliciting behaviors, specifically aggressive behaviors in mice exposed to a subtoxic dose of CPF during a different early life period (PND 11-14) [24]. Adult male mice exposed to CPF prenatally (6 mg/kg) or postnatally (3 mg/kg) exhibited increased aggressive behaviors during a social dyadic interaction test [25]. The increase in aggressive behaviors in male mice at an age when affiliative behaviors should be prevalent suggests a deviation from the species-typical pattern of social behavior [63]. Moreover, gestational and neonatal exposure to CPF resulted in impaired nest building and maternal aggression in lactating female mice, indicating impaired maternal behavior [64, 65]. Mounting evidence suggests that CPF could disrupt the endocrine system and adversely affect social behavior in a sexually dimorphic manner, as extensively reviewed elsewhere [66]. A recent study reported reductions in social preference ratio in Harlan-derived B6 mice of both sexes exposed to 2.5 mg/kg or 5.0 mg/kg of CPF on gestational days 12-15 [67]. Our findings contrast with a report of increased social play in juvenile rats using CPF doses of less than 1.0 mg/kg [68];

however, the dosing in our study was across PND 1-4 while that exposure paradigm started at PND 10 and lasted for 7 days, emphasizing the critical effect of timing in behavioral toxicology. Detailed examination of reciprocal social play interactions is planned for subsequent studies.

This is also the first report to utilize ex vivo MRI to examine broad effects of developmental CPF exposure. Neuroanatomically, the CPF dosages had no significant effects on the mesoscopic brain structure of the rats. There were interesting trends at the 0.3 mg/kg dose, in particular, the divergent direction of the structural findings in males (increased volume) and females (volumetric reductions). Typically, in neuroimaging studies of genetic mouse models, significant differences in relative regional volumes are usually found in about 65% of cases [69]. These types of studies are powered at 80% which should typically find regional differences in the mouse at 3-5%, which is consistent with some of the differences at 0.3 mg/ kg dose. Powered at this level, our studies tend to be more sensitive to widespread changes rather than focal ones, which could explain our observation of "trends" in this work. Additionally, it is possible that there is increased variability in the rat versus mouse due to the substantially more variable genetic background than in the mouse, but this remains to be tested for CPF exposures specifically and is only beginning to be compared in genetic rat models of NDDs. It should also be noted that the findings here do not indicate that there are no structural differences due to CPF, only that no significant changes are detectable at the mesoscopic resolution of the MRI. Going forward, we will perform more regionally targeted neuroanatomy using the strongest trending areas observed in this study.

We did not observe effects of developmental CPF exposure on motor activity. While others have observed changes, those effects were found at higher dose exposures and/or in mice. For example, pre- and postnatal CPF exposure (6 or 3 mg/kg, respectively) markedly increased locomotor activity in adult male mice tested in the open field [25]. These results corroborated the

finding of decreased habituation rate in rats exposed to 1.0 mg/kg CPF during the later postnatal period [29]. However, habituation rate on a radial maze is not the same metric as assessing locomotion in a novel arena. Exposure to CPF at 1 mg/kg during early postnatal life reduced locomotor activity and rearing in adolescent Sprague Dawley male rats [22]. However, rats postnatally exposed to diazinon (0.5 and 2 mg/kg), another OP pesticide, exhibited normal locomotor activity and a normal habituation pattern in a 1 h figure-8 locomotor activity test [70]. Taken together, there is a lack of consistency and corroboration suggesting that locomotor activity is not a sensitive, reproducible, and rigorous endpoint for low level OP exposures in preclinical rodent models. Adverse effects on performance are often observed in a single laboratory, and follow-up literature is unable to reproduce or delineate cognitive impairments from motoric dysfunction [71, 72]. Future directions intended to comprehensively assess motor behavior with a specific behavioral battery that includes gait, balance, coordination, velocity, temporal and spatial dynamic metrics over rudimentary activity, and/or habituation will lead to improved translational value. This will allow for direct comparisons to humans using devices such as pressure sensitive mats, electromyographic recordings, and wrist or ankle monitors that measure activity/balance.

We also did not observe any deficits in cued and contextual fear conditioning, a classic yet simplistic assay of learning and memory. Earlier studies found that juvenile rats exposed to doses of CPF (0.3 or 7.0 mg/kg) early in life (PND 7, 11, and 15) exhibited spatial learning deficits in the Morris water maze [27]. A second cohort of juvenile rats exposed to CPF (0.3 and 7.0 mg/kg) at a later age (PND 22 and 26) exhibited similar impairments [27]. Neonatal CPF exposure (5 mg/kg) on PND 1-4, but not on PND 5-11, impaired radial-arm maze choice accuracy during the initial phase of training when the test situation is novel or cholinergic inputs are required [29]. As these assays measure substantially different components of learning and memory, we are cautious

to state there is a contrast between our findings and that of these earlier reports. As most literature points to a significant effect of CPF on learning and memory, we attribute differences between previous results and our lack of this finding in fear conditioning to the lack of task sensitivity as well as varying doses and timing of exposures. Future directions intend to comprehensively assess the adverse effects of developmental exposure to CPF on learning and memory with improved translational value by using computerized touchscreen technology, which will hopefully unify the current literature, as each earlier report measured a different parameter or form of learning and memory.

A key question is the relevance of the doses used in this study to human exposures. The estimated average daily combined intake of chlorpyrifos and chlorpyrifosmethyl for infants ranges from 0.003 μg/kg/day [73] to 0.018 ug/kg/day [7]. While these levels are many orders of magnitude lower than the doses administered to postnatal rats in this study, it is critical to remember that the human data reflect estimated average daily exposures and do not take into account exposures during periods of active pesticide exposure in the home, school, or nearby agricultural fields. A more relevant comparison is CPF levels in human cord blood at birth, which range from 3.7 pg/g [16] to > 6.17 pg/g [74]. The peak level of CPF in the blood of PND 5 rats dosed with CPF at 1 mg/kg in DMSO (s.c.) was approximately 9 ng/ml [75]. While these data imply that our dosing paradigm likely resulted in CPF levels in the postnatal rats that are 2-3 orders of magnitude higher than are detected in human neonates, direct comparison of these levels to determine relevance is complicated by the observation that rat blood contains high levels of circulating carboxyesterases, which metabolically inactivate organophosphorus (OP) insecticides, such as CPF, whereas humans have low levels of these enzymes [74]. Thus, the percentage of any CPF dose that reaches the brain is likely to be significantly lower in rats than in humans.

Biological mechanisms of OP toxicity are complex. The canonical mechanism of OP neurotoxicity is inhibition of AChE, which hydrolyzes acetylcholine. More importantly, and most relevant to the present work, it is widely posited that developmental OP neurotoxicity involves mechanisms other than or in addition to AChE inhibition, as recently reviewed [76, 77]. The robust behavioral findings reported in these animals exposed to CPF at doses that have no significant effect on blood or brain AChE clearly support non-cholinergic mechanisms as contributing to effects that are translationally relevant for NDDs. Further biochemical assays using this exposure paradigm must be evaluated in future follow-up studies.

Conclusions

Collectively, our results indicate that early life exposure to the OP pesticide CPF leads to behavioral and some possible neuroanatomical differences in rats that are highly relevant to NDDs. Interestingly, the effects of CPF we observed were strong, observed at multiple timepoints of development, in both sexes, and at doses that did not inhibit AChE activity. By developing and utilizing a novel rat model of developmental CPF exposure, which leverages the sophisticated vocal communication system of rats, we characterized the effect of environmentally relevant CPF exposures on a range of behaviors and were able to detect impaired social communication in pups and juveniles. Critically, these effects occurred in the absence of AChE inhibition, which is the endpoint used to regulate OP exposures to protect human health.

The public health implications of these results are significant, as pesticides continue to be widely used resulting in widespread human exposures. With the laws regarding pesticide application currently under debate, this work provides timely and much needed experimental evidence to inform future policy decisions.

References

1. Carvalho F. Agriculture, pesticides, food security and food safety. Environ Sci Policy. 2006;9(7-8):685–92.
2. Dich J, Zahm SH, Hanberg A, Adami HO. Pesticides and cancer. Cancer Causes Control. 1997;8:420–43. https://doi.org/10.1023/a:1018413522959.
3. Hertz-Picciotto I, et al. Organophosphate exposures during pregnancy and child neurodevelopment: recommendations for essential policy reforms. Plos Med. 2018a;15:e1002671. https://doi.org/10.1371/journal.pmed.1002671.
4. Hertz-Picciotto I, Schmidt RJ, Krakowiak P. Understanding environmental contributions to autism: causal concepts and the state of science. Autism Res. 2018b;11:554–86. https://doi.org/10.1002/aur.1938.
5. Hertz-Picciotto I, et al. A prospective study of environmental exposures and early biomarkers in autism spectrum disorder: design, protocols, and preliminary data from the MARBLES Study. Environ Health Perspect. 2018c; 126:117004. https://doi.org/10.1289/EHP535.
6. (EPA), E.P.A. (2000). Revised risk assessment for chlorpyrifos.
7. Eaton DL, et al. Review of the toxicology of chlorpyrifos with an emphasis on human exposure and neurodevelopment. Crit Rev Toxicol. 2008;38(Suppl 2):1–125. https://doi.org/10.1080/10408440802272158.
8. Shelton JF, Hertz-Picciotto I, Pessah IN. Tipping the balance of autism risk: potential mechanisms linking pesticides and autism. Environ Health Perspect. 2012;120:944–51. https://doi.org/10.1289/ehp.1104553.
9. (EPA), E.P.A, Grube A, Donaldson D, Kiely T, Wu L. In: (EPA), E.P.A, editor. Pesticides industry sales and usage: 2006 and 2007 Market Estimates; 2011.
10. Solomon KR, Williams WM, Mackay D, Purdy J, Giddings JM, Giesy JP. Properties and uses of chlorpyrifos in the United States. Revi Environ Contam Toxicol. 2014;231:13–34. https://doi.org/10.1007/978-3-319-03865-0_2.
11. Bouchard MF, Bellinger DC, Wright RO, Weisskopf MG. Attention-deficit/ hyperactivity disorder and urinary metabolites of organophosphate pesticides. Pediatrics. 2010;125:e1270–7. https://doi.org/10.1542/peds.20093058.
12. Bouchard MF, et al. Prenatal exposure to organophosphate pesticides and IQ in 7-year old children. Environ Health Perspect. 2011. https://doi.org/10.1289/ehp.1003185.
13. Engel SM, et al. Prenatal organophosphate metabolite and organochlorine levels and performance on the Brazelton Neonatal Behavioral Assessment Scale in a multiethnic pregnancy cohort. Am J Epidemiol. 2007;165:1397– 404. https://doi.org/10.1093/aje/kwm029.
14. Engel SM, et al. Prenatal exposure to organophosphates, paraoxonase 1, and cognitive development in childhood. Environ Health Perspect. 2011. https://doi.org/10.1289/ehp.1003183.
15. Furlong MA, Engel SM, Barr DB, Wolff MS. Prenatal exposure to organophosphate pesticides and reciprocal social behavior in childhood. Environ Int. 2014;70:125–31. https://doi.org/10.1016/j.envint.2014.05.011.
16. Rauh V, et al. 7-year neurodevelopmental scores and prenatal exposure to chlorpyrifos, a common agricultural pesticide. Environ Health Perspect. 2011. https://doi.org/10.1289/ehp.1003160.

17. Rauh VA, et al. Impact of prenatal chlorpyrifos exposure on neurodevelopment in the first 3 years of life among inner-city children. Pediatrics. 2006;118:e1845–59. https://doi.org/10.1542/peds.2006-0338.
18. Shelton JF, et al. Neurodevelopmental disorders and prenatal residential proximity to agricultural pesticides: the CHARGE Study. Environ Health Perspect. 2014;122:1103–9. https://doi.org/10.1289/ehp.1307044.
19. Young JG, et al. Association between in utero organophosphate pesticide exposure and abnormal reflexes in neonates. Neurotoxicology. 2005;26:199– 209. https://doi.org/10.1016/j.neuro.2004.10.004.
20. Rauh VA, et al. Brain anomalies in children exposed prenatally to a common organophosphate pesticide. Proc Natl Acad Sci U S A. 2012;109:7871–6. https://doi.org/10.1073/pnas.1203396109.
21. Pelch KE, Bolden AL, Kwiatkowski CF. Environmental chemicals and autism: a scoping review of the human and animal research. Environ Health Perspect. 2019;127:46001. https://doi.org/10.1289/EHP4386.
22. Dam K, Seidler FJ, Slotkin TA. Chlorpyrifos exposure during a critical neonatal period elicits gender-selective deficits in the development of coordination skills and locomotor activity. Brain Res Dev Brain Res. 2000;121: 179–87.
23. Lan A, Kalimian M, Amram B, Kofman O. Prenatal chlorpyrifos leads to autism-like deficits in C57Bl6/J mice. Environ Health. 2017;16:43. https://doi. org/10.1186/s12940-017-0251-3.
24. Ricceri L, et al. Developmental exposure to chlorpyrifos alters reactivity to environmental and social cues in adolescent mice. Toxicol Appl Pharmacol. 2003;191:189–201.
25. Ricceri L, et al. Developmental neurotoxicity of organophosphorous pesticides: fetal and neonatal exposure to chlorpyrifos alters sex-specific behaviors at adulthood in mice. Toxicol Sci. 2006;93:105–13. https://doi.org/ 10.1093/toxsci/kfl032.
26. Aldridge JE, Levin ED, Seidler FJ, Slotkin TA. Developmental exposure of rats to chlorpyrifos leads to behavioral alterations in adulthood, involving serotonergic mechanisms and resembling animal models of depression. Environ Health Perspect. 2005;113:527–31.
27. Jett DA, Navoa RV, Beckles RA, McLemore GL. Cognitive function and cholinergic neurochemistry in weanling rats exposed to chlorpyrifos. Toxicol Appl Pharmacol. 2001;174:89–98. https://doi.org/10.1006/taap.2001.9198.
28. Johnson FO, Chambers JE, Nail CA, Givaruangsawat S, Carr RL. Developmental chlorpyrifos and methyl parathion exposure alters radial-arm maze performance in juvenile and adult rats. Toxicol Sci. 2009;109:132–42. https://doi.org/10.1093/toxsci/kfp053.
29. Levin ED, Addy N, Nakajima A, Christopher NC, Seidler FJ, Slotkin TA. Persistent behavioral consequences of neonatal chlorpyrifos exposure in rats. Brain Res Dev Brain Res. 2001;130:83–9.
30. Hofer MA. Multiple regulators of ultrasonic vocalization in the infant rat. Psychoneuroendocrinology. 1996;21:203–17.
31. Hofer, M.A., H.N. Shair, S.A. Brunelli (2002). Ultrasonic vocalizations in rat and mouse pups. Current protocols in neuroscience/editorial board, Jacqueline N Crawley [et al] Chapter 8, Unit 8 14 doi:10.1002/0471142301.ns0814s17.
32. Wöhr M, Schwarting RK. Maternal care, isolation-induced infant ultrasonic calling, and their relations to adult anxiety-related behavior in the rat. Behav Neurosci. 2008;122:310–30. https://doi.org/10.1037/07357044.122.2.310.

33. Berg EL, et al. Developmental social communication deficits in the Shank3 rat model of Phelan-Mcdermid syndrome and autism spectrum disorder. Autism Res. 2018;11:587–601. https://doi.org/10.1002/aur.1925.
34. Berg EL, et al. Translational outcomes in a full gene deletion of ubiquitin protein ligase E3A rat model of Angelman syndrome. Transl Psychiatry. 2020;10. https://doi.org/10.1038/s41398-020-0720-2.
35. Berg EL, Pedersen LR, Pride MC, Petkova SP, Patten KT, Valenzuela AE, et al. Developmental exposure to near roadway pollution produces behavioral phenotypes relevant to neurodevelopmental disorders in juvenile rats. Transl Psychiatry. 2020;10(1):1–6. https://doi.org/10.1038/s41398-020-00978-0.
36. Cahill LS, et al. Preparation of fixed mouse brains for MRI. NeuroImage. 2012;60:933–9. https://doi.org/10.1016/j.neuroimage.2012.01.100.
37. Gompers AL, et al. Germline Chd8 haploinsufficiency alters brain development in mouse. Nat Neurosci. 2017;20:1062–73. https://doi.org/10. 1038/nn.4592.
38. Genovese CR, Lazar NA, Nichols T. Thresholding of statistical maps in functional neuroimaging using the false discovery rate. NeuroImage. 2002; 15:870–8. https://doi.org/10.1006/nimg.2001.1037.
39. Ellman GL, Courtney KD, Andres V Jr, Featherstone RM. A new and rapid colorimetric determination of acetylcholinesterase activity. Biochem Pharmacol. 1961;7(2):88–95. https://doi.org/10.1016/0006-2952(61)90145-9.
40. Bushnell PJ, Moser VC, Samsam TE. Comparing cognitive and screening tests for neurotoxicity. Effects of acute chlorpyrifos on visual signal detection and a neurobehavioral test battery in rats. Neurotoxicol Teratol. 2001;23:33–44.
41. Moser VC. Comparisons of the acute effects of cholinesterase inhibitors using a neurobehavioral screening battery in rats. Neurotoxicol Teratol. 1995;17:617–25.
42. Whyatt RM, et al. Biomarkers in assessing residential insecticide exposures during pregnancy and effects on fetal growth. Toxicol Appl Pharmacol. 2005;206:246–54. https://doi.org/10.1016/j.taap.2004.11.027.
43. Brudzynski S. Handbook of mammalian vocalization: an integrative neuroscience approach. Netherlands: Academic Press; 2009.
44. Kisko TM, et al. Cacna1c haploinsufficiency leads to pro-social 50-kHz ultrasonic communication deficits in rats. Dis Models Mech. 2018;11. https:// doi.org/10.1242/dmm.034116.
45. Yang M, Lewis FC, Sarvi MS, Foley GM, Crawley JN. 16p11.2 Deletion mice display cognitive deficits in touchscreen learning and novelty recognition tasks. Learn Memory. 2015;22:622–32. https://doi.org/10.1101/lm.039602.115.
46. Bader PL, et al. Mouse model of Timothy syndrome recapitulates triad of autistic traits. Proc Natl Acad Sci U S A. 2011;108:15432–7. https://doi.org/10. 1073/pnas.1112667108.
47. Wöhr M, et al. Developmental delays and reduced pup ultrasonic vocalizations but normal sociability in mice lacking the postsynaptic cell adhesion protein neuroligin2. Behav Brain Res. 2013;251:50–64. https://doi. org/10.1016/j.bbr.2012.07.024.
48. Hiramoto T, et al. Tbx1: identification of a 22q11.2 gene as a risk factor for autism spectrum disorder in a mouse model. Hum Mol Genet. 2011;20: 4775–85. https://doi.org/10.1093/hmg/ddr404.
49. Schwartzer JJ, Careaga M, Onore CE, Rushakoff JA, Berman RF, Ashwood P. Maternal immune activation and strain specific interactions in the development of autism-like

behaviors in mice. Translational psychiatry. 2013; 3:e240. https://doi.org/10.1038/tp.2013.16.
50. Moldrich RX, et al. Inhibition of histone deacetylase in utero causes sociability deficits in postnatal mice. Behav Brain Res. 2013;257:253–64. https://doi.org/10.1016/j.bbr.2013.09.049.
51. Tartaglione AM, et al. Early behavioral alterations and increased expression of endogenous retroviruses are inherited across generations in mice prenatally exposed to valproic acid. Mol Neurobiol. 2019;56:3736–50. https:// doi.org/10.1007/s12035-018-1328-x.
52. Venerosi A, Ricceri L, Scattoni ML, Calamandrei G. Prenatal chlorpyrifos exposure alters motor behavior and ultrasonic vocalization in CD-1 mouse pups. Environ Health. 2009;8:12. https://doi.org/10.1186/1476-069X-8-12.
53. Whyatt RM, et al. Prenatal insecticide exposures and birth weight and length among an urban minority cohort. Environ Health Perspect. 2004;112: 1125–32.
54. Song X, Seidler FJ, Saleh JL, Zhang J, Padilla S, Slotkin TA. Cellular mechanisms for developmental toxicity of chlorpyrifos: targeting the adenylyl cyclase signaling cascade. Toxicol Appl Pharmacol. 1997;145:158– 74. https://doi.org/10.1006/taap.1997.8171.
55. Smith JN, Campbell JA, Busby-Hjerpe AL, Lee S, Poet TS, Barr DB, Timchalk C. Comparative chlorpyrifos pharmacokinetics via multiple routes of exposure and vehicles of administration in the adult rat. Toxicology. 2009; 261:47–58. https://doi.org/10.1016/j.tox.2009.04.041.
56. Chabout J, Sarkar A, Dunson DB, Jarvis ED. Male mice song syntax depends on social contexts and influences female preferences. Front Behav Neurosci. 2015;9:76. https://doi.org/10.3389/fnbeh.2015.00076.
57. Hammerschmidt K, Radyushkin K, Ehrenreich H, Fischer J. Female mice respond to male ultrasonic 'songs' with approach behaviour. Biol Lett. 2009; 5:589–92. https://doi.org/10.1098/rsbl.2009.0317.
58. Hammerschmidt K, Reisinger E, Westekemper K, Ehrenreich L, Strenzke N, Fischer J. Mice do not require auditory input for the normal development of their ultrasonic vocalizations. BMC Neurosci. 2012;13:40. https://doi.org/ 10.1186/1471-2202-13-40.
59. Portfors CV, Perkel DJ. The role of ultrasonic vocalizations in mouse communication. Curr Opin Neurobiol. 2014;28:115–20. https://doi.org/10. 1016/j.conb.2014.07.002.
60. Seffer D, Schwarting RK, Wöhr M. Pro-social ultrasonic communication in rats: insights from playback studies. J Neurosci Methods. 2014. https://doi. org/10.1016/j.jneumeth.2014.01.023.
61. Wöhr M, Schwarting RK. Ultrasonic communication in rats: can playback of 50-kHz calls induce approach behavior? Plos One. 2007;2:e1365. https://doi. org/10.1371/journal.pone.0001365.
62. Wöhr M, Seffer D, Schwarting RK. Studying socio-affective communication in rats through playback of ultrasonic vocalizations. Curr Protoc Neurosci. 2016;75:8 35 1–17. https://doi.org/10.1002/cpns.7.
63. Terranova ML, Laviola G, Alleva E. Ontogeny of amicable social behavior in the mouse: gender differences and ongoing isolation outcomes. Dev Psychobiol. 1993;26:467–81. https://doi.org/10.1002/dev.420260805.
64. Venerosi A, Cutuli D, Colonnello V, Cardona D, Ricceri L, Calamandrei G. Neonatal exposure to chlorpyrifos affects maternal responses and maternal aggression of female mice

in adulthood. Neurotoxicol Teratol. 2008;30:468– 74. https://doi.org/10.1016/j.ntt.2008.07.002.
65. Venerosi A, Ricceri L, Rungi A, Sanghez V, Calamandrei G. Gestational exposure to the organophosphate chlorpyrifos alters social-emotional behaviour and impairs responsiveness to the serotonin transporter inhibitor fluvoxamine in mice. Psychopharmacology. 2010;208:99–107. https://doi. org/10.1007/s00213-009-1713-2.
66. Venerosi A, Ricceri L, Tait S, Calamandrei G. Sex dimorphic behaviors as markers of neuroendocrine disruption by environmental chemicals: the case of chlorpyrifos. Neurotoxicology. 2012;33:1420–6. https://doi.org/10.1016/j. neuro.2012.08.009.
67. Lan A, Stein D, Portillo M, Toiber D, Kofman O. Impaired innate and conditioned social behavior in adult C57Bl6/J mice prenatally exposed to chlorpyrifos. Behav Brain Functions. 2019;15:2. https://doi.org/10.1186/ s12993-019-0153-3.
68. Carr RL, et al. Inhibition of fatty acid amide hydrolase by chlorpyrifos in juvenile rats results in altered exploratory and social behavior as adolescents. Neurotoxicology. 2020;77:127–36. https://doi.org/10.1016/j. neuro.2020.01.002.
69. Ellegood J, et al. Clustering autism: using neuroanatomical differences in 26 mouse models to gain insight into the heterogeneity. Mol Psychiatry. 2015; 20:118–25. https://doi.org/10.1038/mp.2014.98.
70. Timofeeva OA, Roegge CS, Seidler FJ, Slotkin TA, Levin ED. Persistent cognitive alterations in rats after early postnatal exposure to low doses of the organophosphate pesticide, diazinon. Neurotoxicol Teratol. 2008;30:38– 45. https://doi.org/10.1016/j.ntt.2007.10.002.
71. Sukoff Rizzo SJ, Anderson LC, Green TL, McGarr T, Wells G, Winter SS. Assessing healthspan and lifespan measures in aging mice: optimization of testing protocols, replicability, and rater reliability. Curr Protoc Mouse Biol. 2018;8:e45. https://doi.org/10.1002/cpmo.45.
72. Sukoff Rizzo SJ, Silverman JL. Methodological considerations for optimizing and validating behavioral assays. Curr Protoc Mouse Biol. 2016;6:364–79. https://doi.org/10.1002/cpmo.17.
73. Morgan MK, Sheldon LS, Croghan CW, Jones PA, Robertson GL, Chuang JC, Wilson NK, Lyu CW. Exposures of preschool children to chlorpyrifos and its degradation product 3, 5, 6-trichloro-2-pyridinol in their everyday environments. J Exposure Sci Environ Epidemiol. 2005;15:297– 309.
74. Burke RD, et al. Developmental neurotoxicity of the organophosphorus insecticide chlorpyrifos: from clinical findings to preclinical models and potential mechanisms. J Neurochem. 2017;142(Suppl 2):162–77. https://doi.org/10.1111/jnc.14077.
75. Marty MS, Domoradzki JY, Hansen SC, Timchalk C, Bartels MJ, Mattsson JL. The effect of route, vehicle, and divided doses on the pharmacokinetics of chlorpyrifos and its metabolite trichloropyridinol in neonatal Sprague Dawley rats. Toxicol Sci. 2007;100:360–73. https://doi.org/10.1093/toxsci/ kfm239.
76. Guignet M, Lein PJ. Organophosphates. In: Advances in neurotoxicology: role of inflammation in environmental neurotoxicity. In: Aschner M, Costa LG, editors. Advances in Neurotoxicology: Role of Inflammation in Environmental Neurotoxicity. Cambridge, MA: Academic Press; 2019. p. 35–79.
77. Voorhees JR, Rohlman DS, Lein PJ, Pieper AA. Neurotoxicity in preclinical models of occupational exposure to organophosphorus compounds. Front Neurosci. 2016;10:590. https://doi.org/10.3389/fnins.2016.00590.

Figures

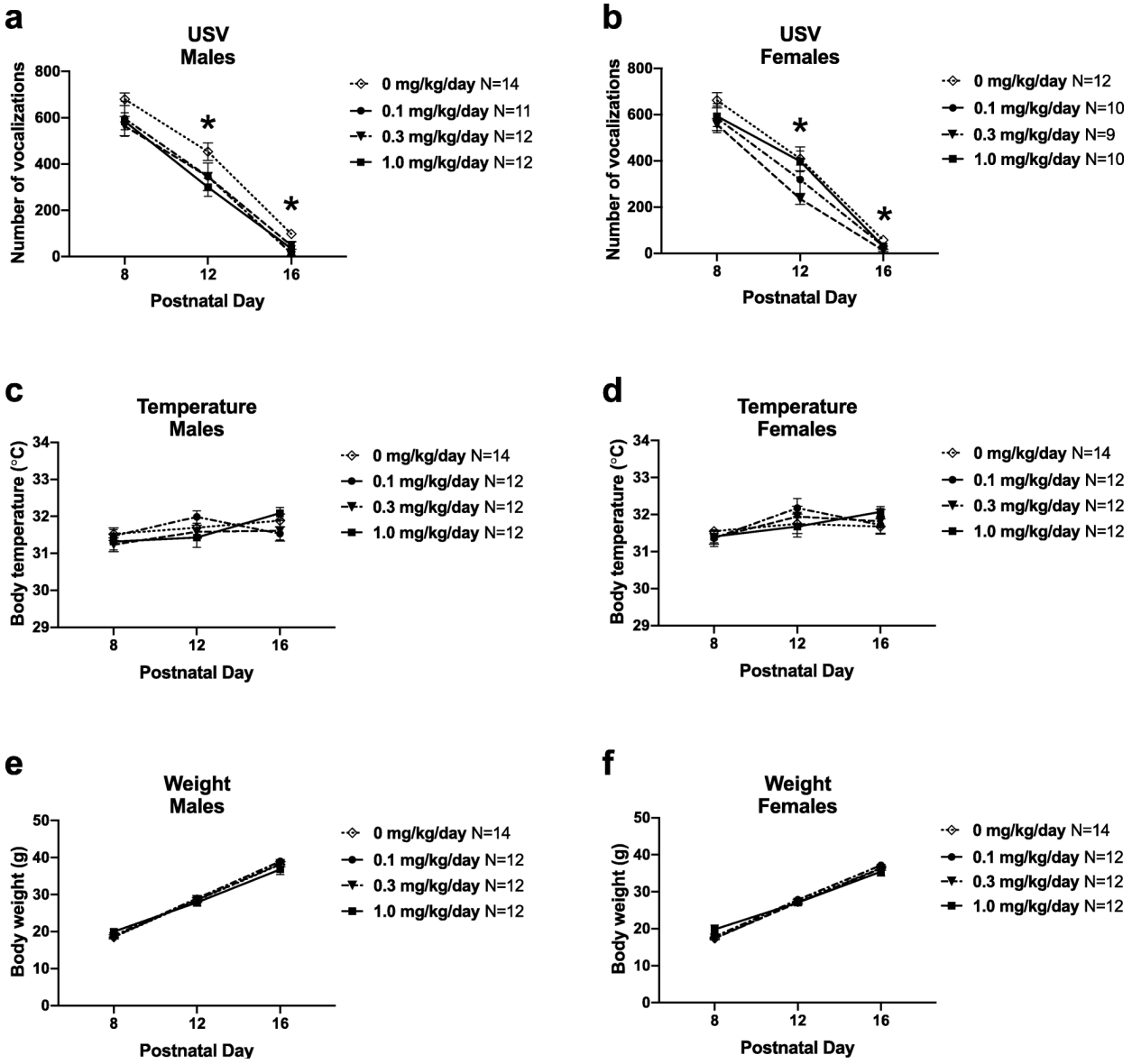

Fig. 1 Early life CPF exposure reduces USV emission in male and female rat pups in a dose- and time-dependent manner. **a** Male pups exposed to 1.0 mg/kg/day CPF emitted fewer USV compared to vehicle controls on PND 12. By PND 16, all three male CPF exposure groups had significantly lower USV emission than controls. **b** In females, exposure to 0.3 mg/kg/day CPF led to reduced pup USV emission on PND 12 and 16. **c**, **d** Body temperature and **e**, **f** body weight immediately following USV collection were similar across exposure groups, eliminating these two variables as potential confounds on call quantity. Data are mean ± S.E.M. *$p < 0.05$, repeated measures ANOVA, Holm-Sidak's multiple comparisons test *post hoc.*

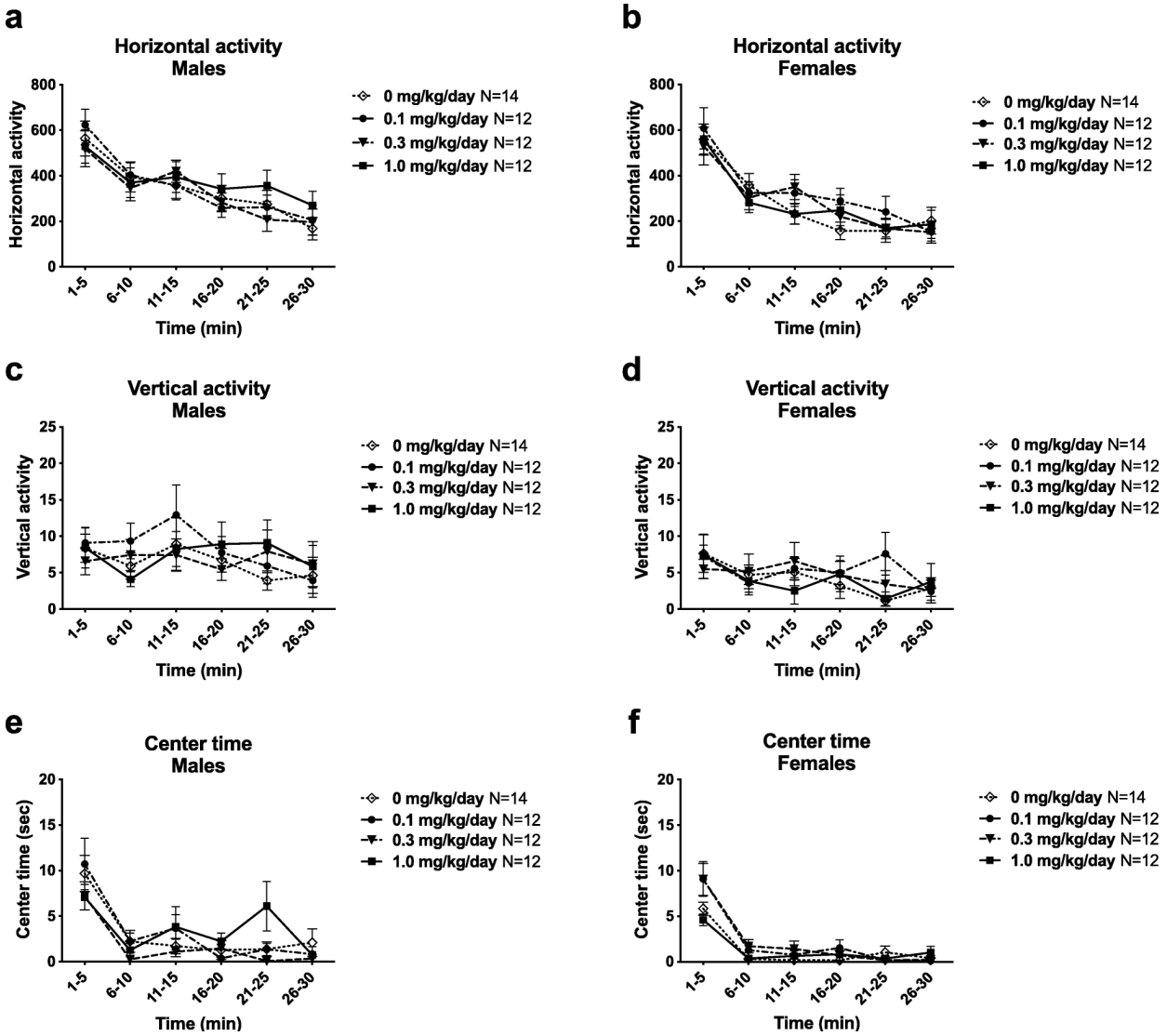

Fig. 2 Early life exposure to CPF did not affect gross locomotor abilities. Both male and female rats of all exposure groups exhibited normal levels of (**a**, **b**) horizontal activity, (**c**, **d**) vertical activity, and (**e**, **f**) center time on PND 19. Data are mean ± S.E.M.

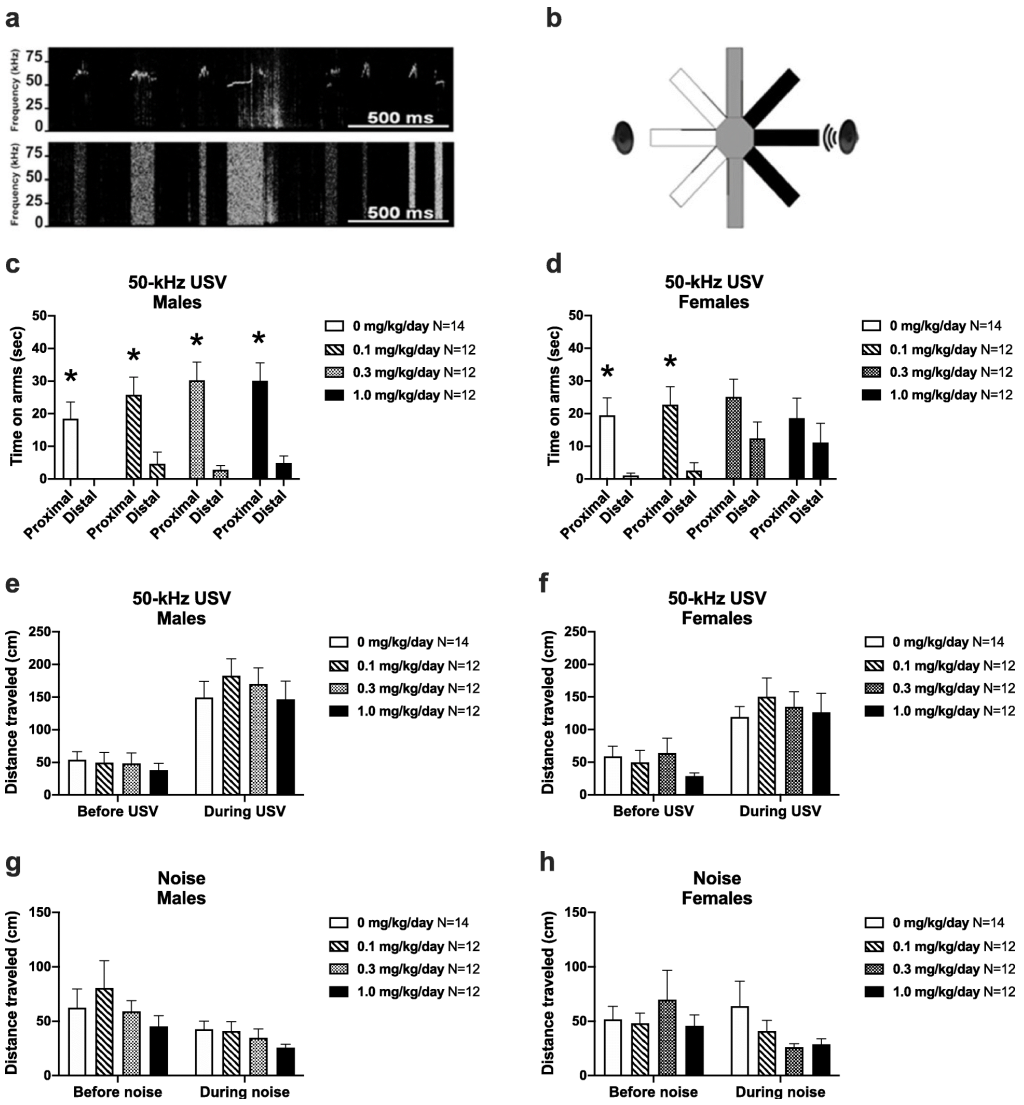

Fig. 3 Lack of social approach to pro-social 50-kHz USV in female CPF-exposed rats. **a** Exemplary spectrograms showing 2 s of the pro-social 50-kHz USV (upper panel) and time- and amplitude-matched white noise (lower panel) stimuli used in the playback assay. **b** Illustration of the radial maze used, with arms proximal to the active ultrasonic speaker shown in black, arms distal shown in white, and neutral arms shown in gray. **c** During the minute of USV playback, males of all exposure groups spent significantly more time on the arms proximal to the speaker compared to the distal arms. **d** In females, only the vehicle and 0.1 mg/kg/day CPF groups showed a significant preference for the proximal arms. Female rats exposed to 0.3 mg/kg/day or 1.0 mg/kg/day did not spend significantly more time on the proximal arms compared to the distal arms. Regardless of exposure, (**e**) all males and (**f**) females displayed similar patterns of locomotion in response to playback of 50-kHz USV. **g** All males and (**h**) females exhibited comparable levels of movement during the minute before and the minute of white noise. Data are mean + S.E.M. **c**, **d**: $*p < 0.05$, paired *t* test, proximal vs. distal.

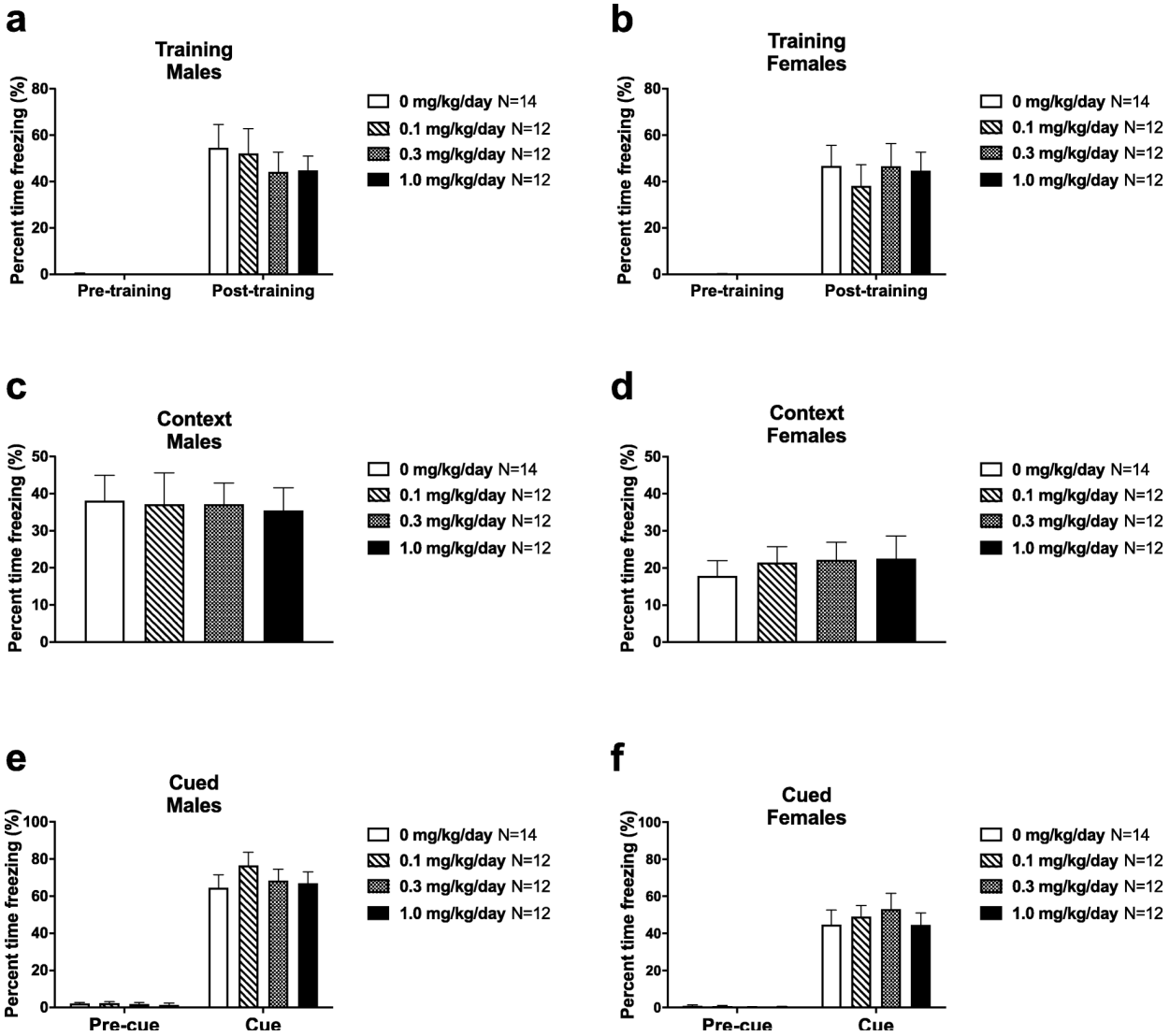

Fig. 4 Intact contextual and cued fear memory in rat pups exposed to CPF during early life. (**a**) Male and (**b**) female rats of all exposure groups exhibited typical levels of freezing following foot-shock training, (**c**, **d**) in the same context 24 h later, and (**e**, **f**) upon hearing the auditory cue in a new context 48 h after training. Data are mean + S.E.M.

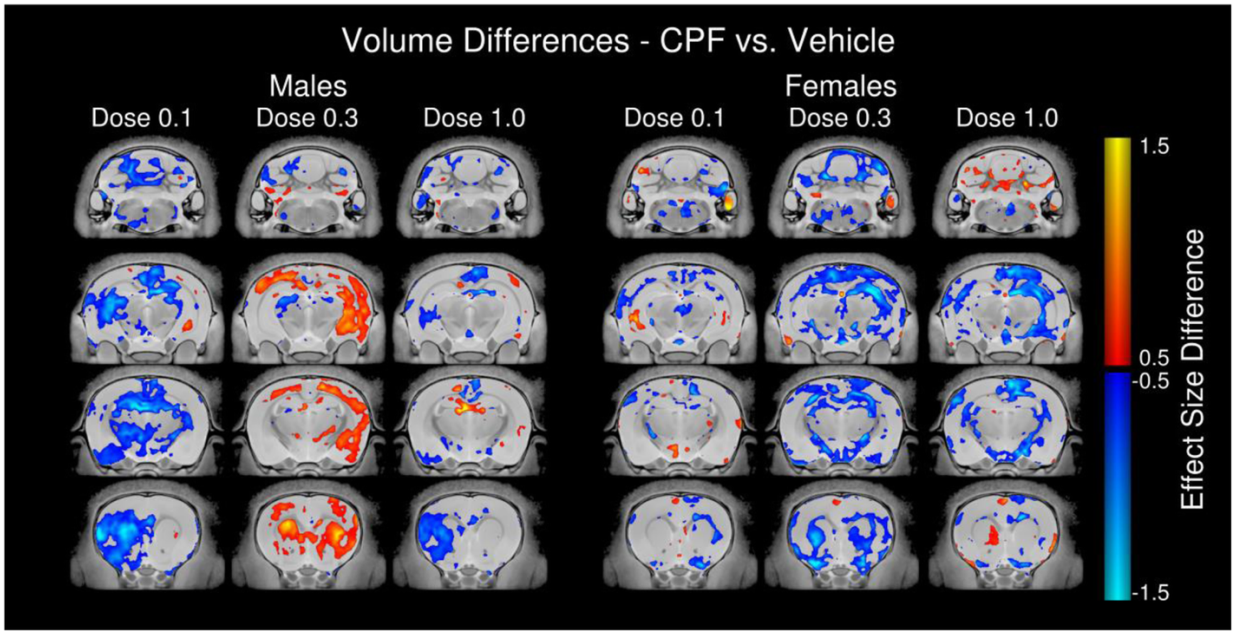

Fig. 5 Neuroanatomical pathology at PND 35 in rats exposed to CPF during early life. **a** Representative coronal slice series for males and females highlighting effect size differences in absolute brain volume (mm^3) between vehicle and 0.1 mg/kg/day, 0.3 mg/kg/day, and 1.0 mg/kg/day CPF exposure groups. Red-to-yellow coloration indicates areas that trended larger in CPF-exposed groups compared to vehicle and dark-to-light blue coloration indicates areas that were smaller in CPF-exposed groups compared to vehicle.

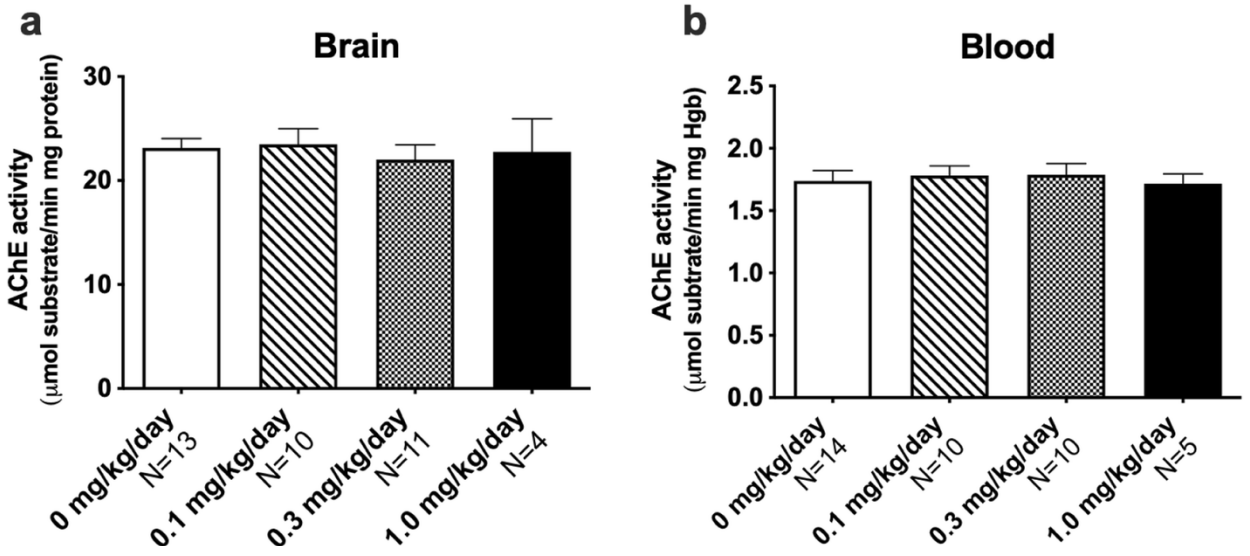

Fig. 6 Developmental CPF exposure did not significantly inhibit acetylcholinesterase (AChE). **a** Regardless of exposure group, all pups exposed to CPF on PND 1-4 showed normal AChE activity in the (**a**) brain and (**b**) blood at 1 h following the final dose on PND 4. Data include males and females and are mean + S.E.M.

Supplementary Information

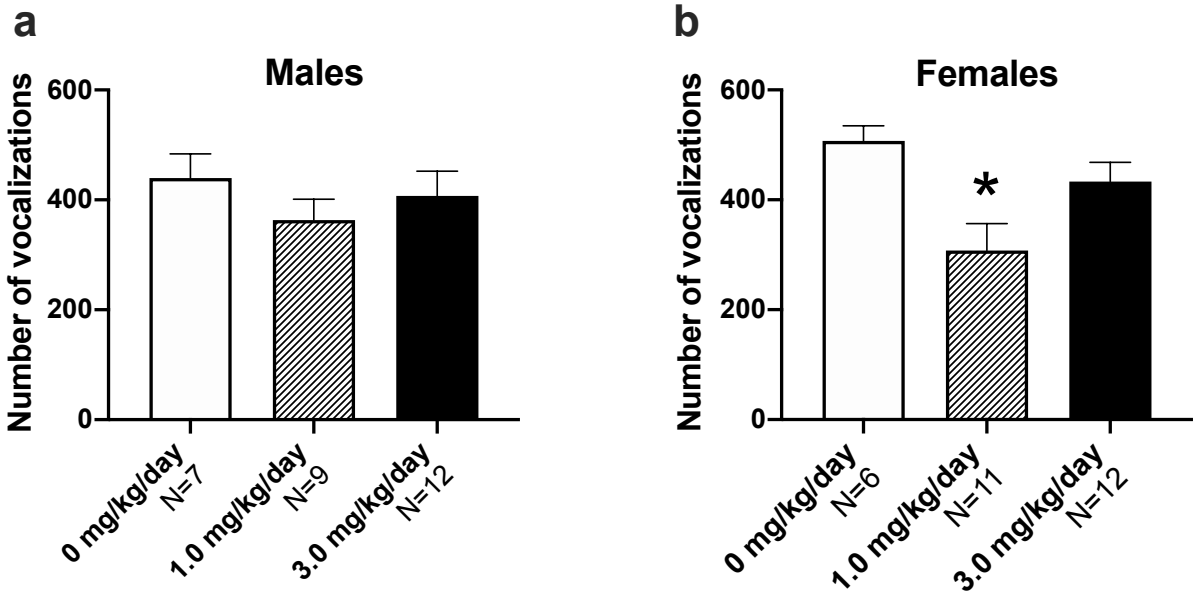

Supplementary Fig S1. Reduced USV emission in rat pups exposed to CPF during early life. **a** Male pups exposed to CPF emitted normal numbers of USV on PND 8 compared to vehicle controls while **b** exposure to 1.0 mg/kg/day CPF in females resulted in reduced USV emission relative to controls. Data are mean + S.E.M. *$p < 0.05$, one-way ANOVA, Holm-Sidak's multiple comparisons *post hoc*.

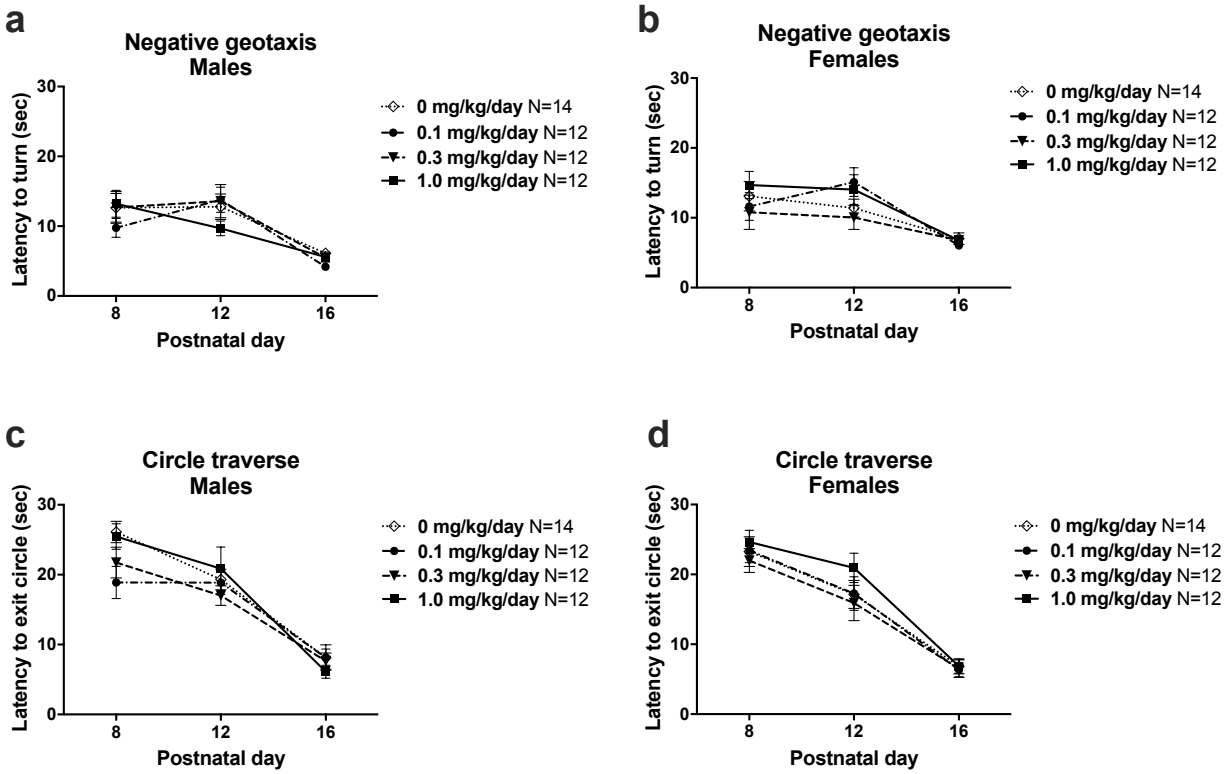

Supplementary Fig S2. No effect of early life CPF exposure on developmental milestone achievement. a,b Performance on the negative geotaxis and **c,d** circle traverse tasks did not differ between exposure groups for males or females, respectively. Data are mean ± S.E.M.

Chapter 4

Translational Outcomes in a Full Gene Deletion of *Ubiquitin Protein Ligase E3A* Rat Model of Angelman Syndrome

This chapter has been published as: Elizabeth L. Berg, Michael C. Pride, Stela P. Petkova, Ruth D. Lee, Nycole A. Copping, Yutian Shen, Anna Adhikari, Timothy A. Fenton, Lauren R. Pedersen, Leigh S. Noakes, Brian J. Nieman, Jason P. Lerch, Sarah Harris, Heather A. Born, Melinda M. Peters, Peter Deng, David L. Cameron, Kyle D. Fink, Ulrika Beitnere, Henriette O'Geen, Anne E. Anderson, Scott V. Dindot, Kevin R. Nash, Edwin J. Weeber, Markus Wöhr, Jacob Ellegood, David J. Segal, and Jill L. Silverman (2020). *Translational Psychiatry* 10(39): 1-16.

Abstract

Angelman syndrome (AS) is a rare neurodevelopmental disorder characterized by developmental delay, impaired communication, motor deficits and ataxia, intellectual disabilities, microcephaly, and seizures. The genetic cause of AS is the loss of expression of *UBE3A* (ubiquitin protein ligase E6-AP) in the brain, typically due to a deletion of the maternal 15q11-q13 region. Previous studies have been performed using a mouse model with a deletion of a single exon of *Ube3a*. Since three splice variants of Ube3a exist, this has led to a lack of consistent reports and the theory that perhaps not all mouse studies were assessing the effects of an absence of all functional UBE3A. Herein, we report the generation and functional characterization of a novel model of Angelman syndrome by deleting the entire *Ube3a* gene in the rat. We validated that this resulted in the first comprehensive gene deletion rodent model. Ultrasonic vocalizations from newborn *Ube3a*$^{m-/p+}$ were reduced in the maternal inherited deletion group with no observable change in the *Ube3a*$^{m+/p-}$ paternal transmission cohort. We also discovered *Ube3a*$^{m-/p+}$ exhibited delayed reflex development, motor deficits in rearing and fine motor skills, aberrant social communication, and impaired touchscreen learning and memory in young adults. These behavioral deficits were large in effect size and easily apparent in the larger rodent species. Low social communication was detected using a playback task that is unique to rats. Structural imaging illustrated decreased brain volume in *Ube3a*$^{m-/p+}$ and a variety of intriguing neuroanatomical phenotypes while *Ube3a*$^{m+/p-}$ did not exhibit altered neuroanatomy. Our report identifies, for the first time, unique AS relevant functional phenotypes and anatomical markers as preclinical outcomes to test various strategies for gene and molecular therapies in AS.

Introduction

Angelman syndrome (AS) is a rare neurodevelopmental disorder characterized by developmental delay, impaired communication skills, ataxia, motor and balance deficits, poor attention, intellectual disabilities, microcephaly, and seizures[1,2,3]. AS is caused by loss-of-expression or loss-of-function of the maternally inherited allele of the Ubiquitin protein ligase E3A (*UBE3A* E6-AP*)*, which typically arises through a de novo deletion in the maternal 15q11-q13 region[4,5,6]. Owing to genomic imprinting, the paternal allele is silenced in neurons of the central nervous system (CNS). Angelman syndrome is thus caused by loss of UBE3A in neurons of the CNS[7].

The Foundation for Angelman Syndrome Therapeutics (FAST) funded the generation of a genetic rat model of AS via a 90-kb deletion on chromosome 1, which includes the entire *Ube3a* gene. This has opened new possible avenues of research into the neurobiological and behavioral effects of loss of all isoforms of UBE3A and, crucially, the development of novel therapeutics in the near future, including gene replacement therapies. This unique rat model of AS also provides opportunities to investigate complex AS relevant behaviors that have been difficult to capture with high signal sensitivity, rigor, and reproducibility in mice, such as behaviors across developmental time points, juvenile acoustic social communication, and cognitive dysfunction.

Well-validated tools for behavioral and functional outcomes for neurodevelopmental disorders have been well standardized[8], but sophisticated social communication, translationally relevant learning and memory, and other AS-symptom domains are less developed in mice[9]. One prominent example is the less complex acoustic communication system in the mouse. Rats emit uniquely detectable ultrasonic vocalizations (USV) that serve as situation-dependent evolved signals and that accomplish important communicative functions as alarm or social contact calls[10,11,12]. Another advantage of a rat model is the ability to utilize advanced cognitive tests for

measuring learning and memory. Examining cognitive functions in an evolutionarily advanced species[13,14] through the use of behavioral tests highly relevant to clinical diagnostic assays may improve translational predictability.

The present experiments aimed to take advantage of the first generated rat model of a complete *Ube3a* deletion and define behavioral and anatomical phenotypes by utilizing our comprehensive battery of standardized and innovative outcome measures to identify functional outcomes relevant to AS. Using sophisticated and nuanced behavioral readouts of isolation-induced USV, juvenile social communication via USV playback, computerized touchscreen learning and memory, and magnetic resonance imaging (MRI), we evaluated various aspects of social communication, cognition, and behavior during development in the AS rat model.

Results

Model generation. The *Ube3a*$^{m-/p+}$ rat line (background Sprague-Dawley) was originally designed by the Segal laboratory using the CRISPR-Cas9 system, generated by Transposagen (**Fig. S1**). Two genomic RNAs (gRNAs) were designed to target the 5′-end of the *Ube3a* gene (upstream of the *Ube3a* coding sequence) and two gRNAs target sequences downstream of *Ube3a*. gRNA pairs were used on each end of the deletion to maximize the probability of a complete deletion of the 90-kb region encompassing the *Ube3a* gene. 5′ CRISPR-1 Target site GGCCCTGCAGAGATGCAATC, 5′CRISPR-2 Target site GGAGCCCTCCGCCGGCA, 3′CRISPR-1 Target site TACCCTTCCCAGGCCCC, and 3′CRISPR-2 Target site GCATTTCTAGTACATCATCC. In addition, a bridging DNA fragment was constructed with 600-bp homology to the sequence upstream and homology to 1-kb downstream of the deletion. The Rnor_6.0 genome build coordinates of homology arms are 116587209–116587779 and

116678173–116679214, respectively. CRISPR/gRNA complexes were co-injected with the "bridging construct" into fertilized Sprague-Dawley rat embryos and inserted into a surrogate. Founders were screened for deletion of the entire 90-kb region and germline transmission was confirmed using genotyping primers (Ube3aDel-F: 5′-ACCTAGCCCAAAGCCATCTC-3′ and Ube3aDel-R: GGGAACAGCAAAAGACATGG-3′). Junction of deletion of the entire Ube3a gene (~90 kb) was confirmed by Sanger sequencing (**Fig. S1**). Deletion was further validated by Western blotting (**Fig. S2**). For transparency, we do have knowledge via foundation collaboration and conference presentations that another laboratory has access to these novel AS rats and is working on adult characterization and long-term potentiation (personal communication).

Reduced isolation-induced pup ultrasonic vocalizations (USV) and delayed neonatal reflex development in *Ube3a* $^{m-/p+}$ pups. Pup ultrasonic vocalizations (USV) of infant rats and mice measure an early communicative behavior between pups and mother. Isolation-induced USV were collected for 3 min as social communication signals in rat pups on postnatal day (PND) 4, 6, 8, 10, 12, 14, 16, and 18, as previously described15. *Ube3a*$^{m-/p+}$ pups emitted significantly fewer USV across early development compared to wildtype *Ube3a*$^{m+/p+}$ littermate controls (**Fig. 1a** $F_{(1, 67)} = 10.80$, $p < 0.002$). Holm-Sidak corrected posthoc analysis for multiple comparisons highlights PND 10 and PND 12 as reduced in the *Ube3a*$^{m-/p+}$ compared to *Ube3a*$^{m+/p+}$ littermates (PND 10: $p = 0.0023$; PND 12: $p = 0.022$) with a trend on PND 14 ($p = 0.091$). *Ube3a*$^{m-/p+}$ pups also emitted significantly fewer USV on PND 8 in the Baylor laboratory compared to wildtype *Ube3a*$^{m+/p+}$ littermate controls, independently reproducing our results (**Fig. S3** $t_{(1, 23)} = 2.991$, $p < 0.007$). Body weight and temperature were also collected to assure that the reduced USV were not the result of being physically smaller as body weight is known to alter pup USV

emission[16,17]. Weight did not differ between genotypes (**Fig. 1b** $F_{(1, 67)} = 0.154$, $p > 0.05$) indicating typical growth and ability to thrive. As expected, pups with paternal inheritance of the deletion (*Ube3a*$^{m+/p-}$) did not have reductions in USV emissions (**Fig. 1c** $F_{(1, 58)} = 3.555$, $p > 0.05$) or body weight across early development (**Fig. 1d** $F_{(1, 58)} = 0.140$, $p > 0.05$), compared to wildtype *Ube3a*$^{m+/p+}$ littermate controls. Body temperature did not differ between genotypes (*Ube3a*$^{m-/p+}$ versus *Ube3a*$^{m+/p+}$: $F_{(1, 67)} = 3.859$, $p > 0.05$ and *Ube3a*$^{m+/p-}$ versus *Ube3a*$^{m+/p+}$: $F_{(1, 58)} = 0.038$, $p > 0.05$). **Supplementary Tables S1 and S2** show mostly typical early physical development and neurological reflexes in various parameters in *Ube3a*$^{m-/p+}$ versus *Ube3a*$^{m+/p+}$ littermates. Interestingly, longer latencies to navigate upright in negative geotaxis, a simple metric for motoric, postural, and proprioceptive processes that underlie the ability of infant rodents to navigate on an inclined plane, was robustly delayed in the *Ube3a*$^{m-/p+}$ versus *Ube3a*$^{m+/p+}$ (**Fig. 1e** $F_{(1, 88)} = 37.22$, $p < 0.0001$). Longer latencies were observed for 6 of the 8 days tested (Bonferroni-corrected $p < 0.05$): PND 4, 6, 8, 10, 12, and 18. Yet, similar latencies to flip over 180 degrees from supine to prone in the test of righting reflex were observed (**Fig. 1f** $F_{(1, 71)} = 0.651$, $p = 0.422$).

Reduced vertical activity, poor rotarod performance, and long latencies to remove adhesive illustrate poor gross and fine motor abilities in *Ube3a*$^{m-/p+}$ rats. Motor abilities were tested in an open field assay, assessing cm^2 of horizontal and vertical movements using beam breaks and time spent in the center of the arena. At PND 19, *Ube3a*$^{m-/p+}$ juvenile rats exhibited normal horizontal activity (**Fig. 2a** $F_{(1, 71)} = 0.1866$, $p > 0.05$) yet significantly reduced vertical activity (**Fig. 2b** $F_{(1, 71)} = 18.55$, $p < 0.0001$) compared to wildtype *Ube3a*$^{m+/p+}$ littermate controls for every 5-min time bin across the 30-min task. No genotype differences were detected in center

time measures at either the early or later developmental time points (**Fig. 2c** PND 19 $F_{(1, 71)} = 0.1866, p > 0.05$ and **Fig. 2f** PND 40 $F_{(1, 71)} = 1.397, p > 0.05$). Young-adult (PND 40) *Ube3a*$^{m-/p+}$ rats exhibited normal horizontal activity (**Fig. 2d** $F_{(1, 71)} = 1.266, p > 0.05$) yet significantly reduced vertical activity (**Fig. 2e** $F_{(1, 71)} = 5.882, p < 0.02$) compared to wildtype *Ube3a*$^{m+/p+}$ littermate controls. In the adhesive removal task, *Ube3a*$^{m-/p+}$ rats were significantly slower to initiate removal of the sticker (**Fig. 2g** $t = 2.986$, df = 16, $p < 0.009$), and trended slower to complete adhesive removal (**Fig. 2h** $t = 2.032$, df = 16, $p = 0.059$), suggesting fine motor skill deficits of the fore paws; the *Ube3a*$^{m-/p+}$ rats were 48.63 +/− 23.93 sec slower to finish removing the adhesive. *Ube3a*$^{m-/p+}$ rats had normal rotarod performance on the first 2 days of testing but were significantly faster to fall off the rotarod on the third day compared to wildtypes (**Fig. 2i** time × genotype interaction: $F_{(2, 96)} = 7.339, p = 0.001$; day 3 Holm-Sidak $p = 0.0197$), highlighting a motor learning deficit.

Reduced exploration of pro-social 50-kHz USV in *Ube3a* $^{m-/p+}$ juvenile rats. Distance traveled in response to the white noise control stimulus did not differ between groups and both genotypes exhibited behavioral inhibition (i.e., a reduction in motion following the noise control) (**Fig. 3a** genotype $F_{(1, 68)} = 2.548, p > 0.05$). As shown by our laboratory and others previously[15,18,19,20,21,22], a striking increase in social exploratory behavior (i.e., distance traveled) was observed in response to playback of pro-social 50-kHz USV. Distance traveled increased in response to playback of 50-kHz USV (i.e., higher during playback compared to the minute prior) in *Ube3a*$^{m+/p+}$ and *Ube3a*$^{m-/p+}$ rats (**Fig. 3b** paired *t*-test *Ube3a*$^{m-/p+}$: $t_{(1, 38)} = 5.271, p < 0.0001$ and paired *t*-test *Ube3a*$^{m+/p+}$: $t_{(1, 14)} = 4.94, p < 0.0001$, respectively), as expected. Interestingly, however, the magnitude of the distance increase in the *Ube3a*$^{m-/p+}$ juvenile rats was significantly

lower than in the wildtype *Ube3a*$^{m+/p+}$ littermates (**Fig. 3b** genotype $F_{(1,\ 68)} = 4.908$, $p < 0.04$, Bonferroni correction $p < 0.05$, for minutes 1 and 2 post call play).

Social exploratory behavior displayed by *Ube3a*$^{m+/p+}$ rats was clearly directed towards playback of pro-social 50-kHz USV, as reflected in the more sensitive parameter of time spent on the arms proximal to the sound source emitting 50-kHz USV. *Ube3a*$^{m+/p+}$ rats spent significantly longer on the arms proximal to the speaker emitting the 50-kHz USV upon playback and for minutes afterwards (**Fig. 3c** $F_{(1, 60)} = 7.471$, $p < 0.01$, Bonferroni-corrected $p < 0.05$ for minutes 1, 2, and 5). In contrast, the *Ube3a*$^{m-/p+}$ rats failed to show a sustained preference and only spent significantly more time on the proximal arms during the minute of the USV playback (**Fig. 3d** $F_{(1, 60)} = 3.380$, $p > 0.05$). **Fig. 3e, f** show representative heat maps of the distance and direction traveled in response to the 50-kHz stimuli by *Ube3a*$^{m+/p+}$ and *Ube3a*$^{m-/p+}$ respectively. These figures illustrate the striking increase in directed social exploratory behavior quantified in **Fig. 3c** and the lower, atypical pattern of social exploration quantified in **Fig. 3d**.

***Ube3a*$^{m-/p+}$ but not *Ube3a* $^{m+/p-}$ illustrate neuroanatomical pathology at PND 21.** Total brain volumes were not observed to be different between groups, but there was a trend found in the difference between the *Ube3a*$^{m-/p+}$ and *Ube3a*$^{m+/p+}$ littermates (−3.5% in *Ube3a*$^{m-/p+}$, $p = 0.06$, $q = 0.10$). Structural differences were further examined on a regional and voxelwise level. In the *Ube3a*$^{m-/p+}$ rats, several regional differences were observed voxelwise in both absolute and relative volume at a false discovery rate (FDR) of $q < 0.15$ (**Fig. 4**). Regionally, when the 98 different regions were examined, there were no differences found in absolute volume for the full group, males, or females. However, there were several trends in the combined group. The majority of the 98 different regions were decreased in size in comparison to their wildtype

counterparts by −3 to −5%. This led to trends in several different areas of interest. For example, the primary motor cortex appears to be smaller in the *Ube3a*$^{m-/p+}$ rats (−3.6%, $p = 0.046$, $q = 0.10$), however, this effect is not observed upon controlling for multiple comparisons. Similar findings were seen in the cerebellum, with the cerebellar lobules decreased in size by −3.8 to −4.6% and *p*-values ranging from 0.03 to 0.05; however, again these trends were not considered significant based on FDR thresholds (**Supplementary Table S3**). Dividing the groups into different sexes revealed that the females seemed to be driving these volume differences; however, no sex by genotype interaction was found to be statistically significant. In contrast to these results, when examined on a regional or voxelwise basis, no differences were present between *Ube3a*$^{m+/p-}$ rats and their *Ube3a*$^{m+/p+}$ littermates, highlighting a distinct phenotype based on parental allele inheritance, as expected given the genetic paternal imprinting of *Ube3a*.

***Ube3a*$^{m-/p+}$ rats exhibit deficits in touchscreen discrimination learning and memory.** Given a limited number of testing chambers, for feasibility our initial touchscreen experiments were selectively performed in males. *Ube3a*$^{m-/p+}$ required significantly more training days to learn to discriminate two images displayed on the touchscreen. Representative task images are shown in **Fig. 5a**. Analysis of survival curves (i.e., percentage of rats that reached the 80% accuracy criterion on each training day) indicated that *Ube3a*$^{m+/p+}$ wildtype control male rats took about 10–15 sessions to reach criterion while *Ube3a*$^{m-/p+}$ rats took about 20–40 sessions (**Fig. 5b** Log-rank (Mantel-Cox) test: Chi square = 15.70, df = 1, $p < 0.001$). Analysis of additional parameters indicated that *Ube3a*$^{m-/p+}$ rats illustrate robust learning and memory impairments. *Ube3a*$^{m-/p+}$ rats took more sessions (**Fig. 5c** $t_{(1, 12)} = 5.281, p < 0.001$), required more trials (**Fig. 5d** $t_{(1, 12)} = 4.055, p < 0.002$), required a greater number of incorrect responses (**Fig. 5e** $t_{(1,}$

$_{12)} = 4.003$, $p < 0.002$), and needed more correction trials (**Fig. 5f** $t_{(1, 12)} = 4.255$, $p < 0.002$) to reach the learning criterion. Motivational control parameters such as numbers of trials completed per session did not differ between genotypes, also showing no motor impairments (**Fig. 5g** $t_{(1, 12)} = 0.018$, $p > 0.05$). Panel h is the latency or time it takes for the rat to collect its pellet after responding correctly. *Ube3a*$^{m-/p+}$ rats took approximately twice as long as wildtypes to collect rewards (**Fig. 5h** $t_{(1, 12)} = 6.918$, $p < 0.0001$). Learning and memory as assessed in the novel object recognition test was not affected (Fig. S4). Both *Ube3a*$^{m-/p+}$ and *Ube3a*$^{m+/p+}$ rats spent significantly more time investigating the novel object than the familiar object as determined by automated tracking (**Fig. S3a** *Ube3a*$^{m-/p+}$ $t = 4.428$, $df = 80$, $p < 0.001$; *Ube3a*$^{m+/p+}$ $t = 5.162$, $df = 60$, $p < 0.001$) and hand-scoring (**Fig. S3b** *Ube3a*$^{m-/p+}$ $t_{(1, 80)} = 5.005$, $p < 0.001$; *Ube3a*$^{m+/p+}$ $t_{(1,60)} = 4.832$, $p < 0.001$).

Discussion

Genetically engineered rat models are becoming a widely feasible investigative approach for preclinical research that retains a high degree of genetic conservation relative to humans for targeted therapeutic development while providing enhanced behavioral capabilities relative to mice. In addition to the species advantages, this is the first model to be null for the entire *Ube3a* gene. Since the gene that is causal in AS is known to be *UBE3A*, several innovative gene correction strategies are being pursued for AS and *UBE3A*/UBE3A replacement. In order to measure whether therapeutic methods have efficacy, clear and robust functional phenotypes are required. The results presented here address this unmet need in AS research by providing a novel rat model system with a complete gene deletion and quantifying behavioral and anatomical characteristics that can be used to test the efficacy of therapeutics.

Gene targeted therapeutic approaches, including antisense oligonucleotides[23], viral vector delivery[24], and artificial transcription factors (ATFs)[25,26], are being tested for application to AS. Other innovative methodologies that are currently being pursued include gene-modifying CRISPR-dCas9 and cross correction of UBE3A by hematopoietic stem cells[27]. In addition to UBE3A targeted therapies, numerous dietary and traditional pharmaceutical treatments have shown alleviation of one or more symptom domains found in the mouse model, including but not limited to ketone esters[28], dietary methylation, ErbB inhibitors[29], and topoisomerase inhibitor drugs[30]. Behavioral rescues have been reported utilizing the original exon-2 deletion mouse from Jiang and Beaudet backcrossed onto the C57BL6/J[23,31,32] and maintained by the Jackson Laboratory, or a genetic-based tamoxifen-induced conditional hypomorphic line on a 129-based mixed background backcrossed to a sub-strain of C57BL6 in the Elgersma group[33,34,35]. Reports of rescue have relied heavily on outcomes of the rotarod, marble-burying, elevated plus and zero maze tasks of conflict anxiety, and contextual fear conditioning. These tasks are well standardized, but may lack translational predictive value and may underlie some of the large gap between basic scientific research and translation to therapeutics, given the lack of compound approval for the AS community to date.

Our results illustrate a robust phenotype and impairment in developmental ultrasonic vocalizations (USV), a clear social communication readout in models of neurodevelopmental disorders (NDD). Some Angelman syndrome mouse models have demonstrated USV dysregulation. One study reported increased USV emission. The reported results were highly dependent on the mouse's inbred background strain, and conclusions varied across publications[36,37]. Our results, which highlight reduced USV emission, were reproduced by two independent laboratories (UC Davis MIND and Baylor College of Medicine) and align with the

AS clinical profile of reduced communication. Moreover, given the outbred nature of the rat over the mouse, phenotypes are likely more generalizable by inherent natural genetic variation, which is proving to be a successful approach in neurodegenerative disorder research[38]. Signal to noise ratio and assay sensitivity have plagued bench-to-bedside drug development efforts across neurodevelopmental and neurodegenerative disorders, an issue that may be alleviated by this novel rodent species approach.

We discovered impairments in juvenile behavioral responses to the playback of 50-kHz USV, a positive affiliative social contact call associated with play and social interactions, in the *Ube3a*$^{m-/p+}$ rats. Social exploratory and approach behaviors, typically evoked by the social contact calls, were weak in rats with the *Ube3a*$^{m-/p+}$ deletion. They did not exhibit as highly elevated distance traveled nor extended durations of the behavioral response compared to that of wildtype littermate controls. Wildtype rats spent significantly longer on the arms proximal to the speaker upon initial playback of the 50-kHz USV (i.e., hearing it) and for minutes after the 50-kHz USV stopped being played (i.e., after hearing it), suggesting that they kept searching for the conspecific even after 50-kHz USV emission ended. In contrast to the wildtype, *Ube3a*$^{m-/p+}$ subjects failed to show a strong, sustained response to hearing the cue and only spent significantly more time on the proximal arms during the time period the audio cue was "on". This was an unusual display of social behavior as there should be (1) a clear behavioral preference for the proximal versus distal arms and (2) sustained attempts to locate the source of the emission, as previously reported across genetic models and groups[12,15,18,20,39]. The behavioral alterations displayed by *Ube3a*$^{m-/p+}$ rats in response to pro-social 50-kHz USV were clear and substantially more prominent than the social communication deficits seen in other recently developed rat models relevant to autism, including *Shank3*[15] and *Cacna1c*[18,19]. While individuals

with AS are typically thought of as being highly social, and/or uninhibited socially, with excessive smiling being a hallmark behavioral feature in AS, aberrant social behavior is considered a core phenotypic trait. Thus, the absence of typical social approach to the acoustic call is an interesting, discovered abnormality. Of additional potential will be the in-depth investigation of whether the social communication deficit shall be attributed to a lack of understanding of the 50-kHz USV call (i.e., resulting from cognitive circuit disruption) or a requirement for longer bouts of stimulation than tested on this initial series of experiments (i.e., resulting from impairments in motivation circuits). Other testable hypotheses include impaired sustained attention. Future directions will be focused on the detailed nuance of this social behavior and deciphering the response calls during the playback assay. These functional findings of reduced USV and response to USV are critical to the AS community in positioning for an FDA approved clinical trial with a communication outcome, now that two preclinical developmental time points, postnatal life and juveniles, illustrate preclinical deficient USV. This lower signal in communication will open new opportunities to test therapeutics as most individuals with AS do not ever develop speech or more than a few vocalizations[40,41,42].

Movement disorders affect nearly every individual with AS[40,41,43,44]. The most common motor problems include spasticity, ataxia of gait (observed in the majority of ambulatory individuals), tremor, and muscle weakness[45]. We observed motor deficits in vertical rearing at two different time points across development, however gross overall motor ability to navigate an open field was unaltered. Low counts in vertical rearing may indicate hindlimb weaknesses. We also observed motor coordination dysfunction in young subjects on the rotarod. Motor deficits have been key in the study of mouse models of AS, as dysfunction on the rotarod and fewer rearing movements have been one of the most consistently reported motor behavioral phenotypes when

using the C57BL6/J[46,47,48] but not in the 129/SvEv background strain AS mice. Observation of these motor deficits in the genetically heterogenous rat model extends the theory that preclinical data can generalize to genetically diverse clinical populations[49]. A secondary advantage of this unique motor phenotype in rat models is the added value of a larger species. While *Ube3a*$^{m-/p+}$ rats show motor phenotypes that support its use for future pharmacological/gene therapy rescue studies, these hindlimb coordination motor deficits do not confound other behavioral measures such as social communication and learning and memory. Motor confounds have plagued the interpretation of complex behaviors for numerous neurodevelopmental disorder mouse models, such as those of Phelan-McDermid and Timothy syndromes[50,51,52], yet by using a larger species, motor deficits can be delineated and detected without affecting other measures.

Our imaging data highlighted a wide variety of volumetric abnormalities. The majority of regions decreased in size from 3 to 5%. Several differences were seen at $q < 0.10$, including, but not limited to, the cortex, several white matter structures, and the cerebellum. This does highlight the expected microcephaly although merely by a trend. Our full group showed 3.5% reduction but only was $p = 0.06$, $q = 0.10$, leading to our conclusion of no differences in total brain volume at PND 21. This could be the result of the juvenile age at image acquisition as clinically microcephaly develops over the first 3 years of life in AS individuals and is not 100% penetrant[43,53]. Fiber tracts throughout the brain show an insignificant loss in size in the *Ube3a*$^{m-/p+}$ rats (−3.2% in the corpus callosum, −4.0% in the fimbria, and −4.3% in the arbor vita of the cerebellum). However, when the total brain volume is accounted for, there is a slight increase in the volume of the fiber tracts, particularly in the fimbria, fornix, and cerebral peduncle. Interestingly, the effect on the white matter at postnatal day 21 appeared minimal in the *Ube3a*$^{m-/p+}$ rats, in contrast to what has been shown in adult exon-2 deletion mice[54]. While the overall cortical losses seem to be consistent

between our work and the earlier mouse study, Judson et al. report volume losses of 11–13% in several white matter regions throughout the brain of *Ube3a*$^{m-/p+}$ mice, whereas we discovered modest 2–5% differences here for the same white matter tracts. While the white matter findings were not as drastic as those shown in the previous work with mice, it will be interesting to examine the rats using diffusion tensor imaging (DTI) to see if that technique is more sensitive to the white matter differences seen with the mouse model. In comparison to other rodent mouse models related to intellectual disability and autism, the *Ube3a*$^{m-/p+}$ seems to closely resemble the Magel2 mouse[55,56], which also displayed a 3.4% decrease in total brain volume and similar volume differences in structures throughout the brain ranging from −4 to 5%, including the parietotemporal lobe, the amygdala, and the dentate gyrus of the hippocampus. All of these regions had similar differences on the order of −3 to 5% in the *Ube3a*$^{m-/p+}$ rat but did not reach significance at current thresholds. This is likely due to the increased variability for regions in the outbred rat versus a congenic wildtype C57Bl/6J mouse. In an average region in a wildtype C57Bl/6J mouse one standard deviation for a combined sex group of 20 mice is ~6%, but in the wildtype rat here it is ~8.4%. A recent clustering analysis by Ellegood et al. examined 26 different mouse models related to autism and clustered them into three different groups[57]. Group 2 in that study was characterized by smaller cortical and white matter structures throughout the brain consistent with what has been shown here in the *Ube3a*$^{m-/p+}$ rat model. Other models in Group 2 were the 15q11-13 duplication[58], Itgb3[59], Slc6a4 Ala56 KI[60], and the humanized Androgen Receptor mouse[61].

Learning and memory impairments have been observed in some but not all studies of *Ube3a* mutant mouse models depending on the background strain and age at time of testing[46,47]. The preponderance of these findings used standard assessments such as the electrophysiological correlate of learning and memory, long-term potentiation, and behavioral assays, including Morris

water maze and contextual fear conditioning[29,62,63,64,65,66,67]. Cognitive dysfunction was also postulated by enhanced operant extinction[68] and touchscreen visual discrimination in the exon-2 deletion mouse model[67], albeit this exon-2 line has prominent motor deficits that complicate delineation of cognitive versus motor. Moreover, frequently, learning and memory deficits in the mouse model were not observed or reproduced. We expanded and improved the translational value by using computerized-based touchscreen technology and illustrating robust deficits in visual discrimination of two novel equi-luminescent stimuli in *Ube3a*$^{m-/p+}$ rats. The discrimination deficit in the *Ube3a*$^{m-/p+}$ rats has translational value via the touchscreen methodology, which is utilized by clinicians using Cogmed™ or the NIH Toolbox® computerized-based testing batteries for many domains of learning and memory and executive function in several genetic NDD[69,70,71], and will allow for testing of cognitive enhancing agents, as well as the cognitive domain by gene therapies. Our data make an interesting observation in the *Ube3a*$^{m-/p+}$ rat beyond the obvious learning deficit: we also saw longer timings to collect food rewards upon correct responses, which has been suggested as evidence of impaired motivational circuity. While one metric of impaired motivation may be a fluke, this elevated latency to collect reward was supported by the lack of social approach in the playback assay. Combined, these data make a stronger statement about reduced motivation in the AS rat model. Of course, this is our first characterization and we will have to perform more assays specific to the motivational domain in order to more definitively make this conclusion. We have also been trying differing flavors of pellet rewards (chocolate, banana, sucrose) to gather more data on motivational components of the behavioral deficits, as motivation is clearly not a problem in the AS clinical population for neither learning nor social assessments.

The pipeline of translation from preclinical studies to clinical trial is highly unique and varies greatly depending on the type of therapy (pharmaceutical, biological, genetic therapy) and prior research performed. For example, some traditional medicines may be re-purposed when safety data is already published and known, however, for precision medicine genetic therapies, more work on the safety and tolerability end is required. In our experience, to date, the first steps are to show functional efficacy of the compound in a preclinical model and to illustrate a lack of toxicity and sufficient safety in a secondary species. Then, our ability to manufacture said novel therapeutic at levels of human doses, generated in a good manufacturing process facility, needs to be demonstrated. This, combined with therapeutic profile, pharmacokinetics, pharmacodynamics, and therapeutic kinetics would be put together for an innovative drug discovery (IND) application for the Food and Drug Administration (FDA) for clinical trial approval. Currently for AS, preclinical testing is ongoing for viral vectors, antisense oligonucleotides, artificial transcription factors, and stem cell delivered viral vectors and proteins, as well as simpler therapeutics from pharmaceutical companies. Each has a unique pathway to clinical trial.

Going forward, for successful translation to clinical trials, targeted treatments need to improve functional behavioral outcomes relevant to Angelman syndrome to improve the likelihood of translational success and receive FDA approval to conduct a clinical trial. Our report describes, for the first time, a novel model for Angelman syndrome that exhibits translationally relevant functional behavioral and anatomical outcomes resulting from a full deletion of *Ube3a*. The data presented are therefore highly relevant and important for the advancement of testing genetic and pharmacological therapeutics for Angelman syndrome.

Methods

Subjects. All animals were housed in a temperature-controlled vivarium maintained on a 12:12 light–dark cycle. All procedures were conducted in compliance with the NIH Guidelines for the Care and Use of Laboratory Animals and approved by the Institutional Animal Care and Use Committee of UC Davis. *Ube3a*$^{m+/p-}$ males were bred with wildtype (*Ube3a*$^{m+/p+}$) Sprague-Dawley females purchased from Envigo (East Millstone, New Jersey, USA) in a conventional rat vivarium at UC Davis. The resulting female paternally inherited rats (*Ube3a*$^{m+/p-}$) and male wildtype (*Ube3a*$^{m+/p+}$) rats were paired for breeding to generate maternally inherited mutants (*Ube3a*$^{m-/p+}$) and wildtype (*Ube3a*$^{m+/p+}$) offspring for behavioral and anatomical testing. Male paternally inherited mutant (*Ube3a*$^{m+/p-}$) and female wildtype (*Ube3a*$^{m+/p+}$) rats were also paired for breeding to generate paternally inherited rats (*Ube3a*$^{m+/p-}$) and wildtype (*Ube3a*$^{m+/p+}$) for colony maintenance and control testing. To identify rats, pups were labeled via paw tattoo on postnatal day (PND) 2 with non-toxic animal tattoo ink (Ketchum Manufacturing Inc., Brockville, ON, Canada). A 23-gauge needle was used to subcutaneously insert the ink into the center of the paw. Rats were additionally identified at weaning via tail-marks made with permanent marker. Tattoos and tail-marks were coded to allow investigators to run and score behaviors blind to genotype. At PND 2, tissue samples were collected for genotyping via a small tail snip. Genotyping was performed with REDExtract-N-Amp (Sigma Aldrich, St. Louis, MO, USA) using primers Rube1123 TAGTGCTGAGGCACTGGTTCAGAGC, Rube1606r TGCAAGGGGTAGCTTACTCATAGC, Ub3aDelSpcfcF6 ACCTAGCCCAAAGCCATCTC, and Ub3aDelR2 GGGAACAGCAAAAGACATGG.

Western blots. Rats were cervically dislocated and discrete brain structures were rapidly removed using a 4×4 mm matrix. Protein was extracted using RIPA buffer + 1% protease

inhibitor. Extracted protein was quantitated using BCA assay (ThermoFisher, Waltham, MA). Forty micrograms of protein was denatured with 5x loading dye (National Diagnostics) for 5 min at 95 °C and separated on a 10% Bis-Tris Gel (BioRad, Hercules, CA). Overnight transfer was performed at 30 V to polyvinylidene difluoride (PVDF) membranes (Invitrogen, Carlsbad, CA). PVDF membranes were blocked for 45 min with Tris-buffered saline with Tween (TBST) (1x TBS + 0.1% Tween-20) with 5% seablock. Following blocking, PVDF membranes were incubated with ms-UBE3a (1:1000, Sigma 8655) and rb-beta Tubulin (1:2000) in 5% seablock TBST for 2 h at room temperature (RT). Following incubation, membranes were washed with TBST 3x for 5 min. PVDF were then incubated with Donkey anti-mouse LICOR 680 (1:2000) and donkey anti-rabbit LICOR 800 (1:2000) in 5% seablock TBST for 2 h at RT. Following incubation, gels were washed 2x with TBST before being stored in 1x TBS. PVDF membranes were imaged on a LICOR Odyssey. Densitometry analysis were performed using ImageJ (NIH, Bethesda, MD).

Cohort 1 behavioral assays. *Pup ultrasonic vocalizations (USV).* On PND 4, 6, 8, 10, 12, 14, 16, and 18, isolation-induced USV were collected for 3 min as previously described[15]. Each pup, randomly selected from the nest, was placed in a small container with clean bedding and calls were recorded within a sound-attenuating chamber using an ultrasonic microphone and Avisoft-RECORDER software (Avisoft Bioacoustics, Glienicke, Germany). Immediately following, body temperature and weight were measured. Call spectrograms were displayed using Avisoft-SASLab Pro and counted manually by a trained investigator blind to genotype. Pup calls were also collected at Baylor College of Medicine on PND 8 for 2 min over the 3 min protocol used at the UC Davis facility. Calls were recorded within a sound-attenuating chamber using an ultrasonic microphone and Noldus Ultravox XT 3.2 (Noldus, Wageningen, The Netherlands).

Developmental milestones. In a separate group of animals, on PND 4, 6, 8, 10, 12, 14, 16, and 18, developmental milestones were assessed as described previously[1]. Body weight, body length, tail length, and head width were measured with a scale and sliding ruler. Righting reflex was tested by placing each pup on its back and measuring the time taken to flip over onto all four paws. The average of two trials was recorded. Circle traverse was tested by placing each pup in the center of a circle (12.5 cm *d*) and measuring the time taken to fully exit the circle. Cliff avoidance was tested by placing each pup near the edge of a table, with its nose just beyond the edge, and measuring the time taken to make a 90 degree turn away from the cliff, thereby becoming parallel with the table edge. Each pup was allotted 30 sec to complete each task and failure to complete a task was recorded as the maximum score of 30 sec. The first day in which rooting reflex, forelimb grasping, and bar hold were demonstrated was recorded. Rooting reflex was measured as a turn of the head to whisker stimulation. Forelimb grasping was measured as grasping of a bar being moved upward along both front paws. Bar hold was measured as a pup's ability to hold onto a bar with their front paws and support their body weight for at least ten seconds. Day of eye opening was also recorded.

Open field locomotion. At PND 19 and again at PND 39–44, exploratory activity in a novel open arena was evaluated as described previously[15,72]. Each animal was placed in an Accuscan Animal Activity Monitor (Omnitech Electronics, Columbus, OH, USA), which automatically measured beam breaks for cm^2 of movement via horizontal activity, vertical activity, time in center, and total distance moved over a 30-min session.

Novel object recognition. At PND 45–53, novel object recognition was assessed using methods similar to those described previously[51,73,74]. Rats were given 30 min to freely explore an empty arena (54.1 cm *l* × 54.1 cm *w* × 34.3 cm *h*) on 2 consecutive days. After the second

exploration session, two identical objects were placed in the arena with the subject and the rat was allowed 10 min to investigate and become familiar with the objects. Following a 60-min isolation, the rat was placed back in the arena (clean) with one familiar and one novel object (both clean) and allowed 5 min to investigate.

Touchscreen pairwise discrimination. Starting at PND 65–72, pairwise visual discrimination was tested in an automated Bussey-Saksida touchscreen system (Lafayette Instrument, Lafayette, IN, USA) using a procedure modified for rats from those described previously in mice[50,75,76,77]. Rats were food restricted to 85% of their free-feeding weight. An efficient pre-training procedure based on previously published work was utilized. The pre-training consisted of five stages to train rats to touch the screen, collect the reward, and initiate trials. Stage 1 consisted of a 20-min habituation to the chamber and the sucrose pellet reinforcer with no light or images on the screen. All following sessions lasted 30 min. During Stage 2, three sucrose pellets were dispensed upon the screen being touched, and one pellet was dispensed if the screen was not touched. Stage 2 lasted 5 days, until rats completed an average of 30 trials in the 30 min session. During Stage 3, one sucrose pellet was dispensed upon the screen being touched, and no pellets were dispensed if the screen was not touched. Stage 3 lasted 2 days, until rats completed an average of 30 trials during the 30 min session. During Stage 4, rats were required to initiate each trial by entering and exiting the food magazine. One sucrose pellet was dispensed upon the screen being touched, and no pellets were dispensed if the screen was not touched. Stage 4 lasted 1 day, until rats completed an average of 30 trials in the 30 min session. During Stage 5, a random image from a set of 40 images was presented in one of the windows until the screen was touched. One pellet was dispensed if the image was touched, while touching the blank side was discouraged by no reward and by a 5-sec timeout during which an overhead light was turned on. Stage 5 lasted 3

days, until every rat completed at least 30 trials with an average accuracy of at least 80% over two consecutive sessions. Images used in Stages 4 and 5 were not used in the subsequent pairwise visual discrimination task and successful completion of all five stages of pre-training was required for participation in the discrimination task. Rats were trained to discriminate between two novel images (spider and plane) displayed in two side-by-side windows in a pseudo-randomized order. Each 30 min session consisted of an unlimited number of trials separated by a 20-sec intertrial interval. The image designated as correct was counterbalanced across rats within each genotype. Touching the correct image was rewarded with a sucrose pellet while touching the incorrect image was discouraged with no pellet and a 5-sec timeout with the light on. Incorrect responses were immediately followed by correction trials in which the images were presented in the identical manner to the previous trial until the rat selected the correct image. Successful acquisition was defined as achieving at least 80% correct responses over two consecutive sessions with a minimum of 30 trials completed during each 30 min session.

Cohort 2 behavioral assays. *Developmental milestones.* On PND 4, 6, 8, 10, 12, 14, 16, and 18, developmental milestones were assessed as described previously[73]. Negative geotaxis was tested by placing each pup on an angled screen (45 degrees) facing downwards and measuring the time taken to make a complete 180 degree turn up the screen. The maximum time allowed was 30 sec.

Playback of pro-social 50-kHz USV. On PND 26–33, behavioral response to playback of pro-social 50-kHz USV was used to identify if *Ube3a*$^{m-/p+}$ would exhibit similar social exploratory behaviors as *Ube3a*$^{m+/p+}$ in response to social contact calls. The procedure was performed as previously described[15]. All rats were handled for 2 days prior to testing in a

standardized manner (5 min per rat per day). Social exploratory and approach behavior in response to playback of pro-social 50-kHz USV was assessed on an elevated radial eight-arm maze (48.0 cm above floor; arms: 40.0 cm *l* x 10.0 cm *w*) surrounded by a black curtain under indirect dim white light (8 lux) according to a modified protocol previously established[12,15,19]. Acoustic stimuli were presented through Ultra-SoundGate 116 Player (Avisoft Bioacoustics) connected to an ultrasonic loudspeaker (ScanSpeak, Avisoft Bioacoustics) placed 20 cm away from the end of one arm. An additional, but inactive loudspeaker was arranged symmetrically at the opposite arm as a visual control. Two acoustic stimuli were used: (1) pro-social 50-kHz USV and (2) White Noise; the latter serving as a time- and amplitude-matched acoustic stimulus control[20]. Pro-social 50-kHz USV used for playback were recorded from a naive male rat during exploration of a cage containing scents from a recently separated cage mate. The 50-kHz USV stimulus consisted of 221 natural 50-kHz USV (total calling time: 15.3 sec), composed of a sequence of 3.5 sec, which was repeated for 1 min, that is, 17 times, to assure the presentation of a high number of frequency-modulated calls within a relatively short period of time. After an initial 15-min habituation period, each rat was exposed to 1-min playback presentations of 50-kHz USV and White Noise, separated by a 10-min inter-stimulus interval. Stimulus order was counterbalanced to account for possible sequence effects. The session ended after an additional 10-min post-stimulus phase (total test duration: 37-min period). Behavior was monitored by a video camera mounted 1.7 m centrally above the arena and analyzed using EthoVision XT 10 (Noldus, Wageningen, The Netherlands). Distance traveled served as a measure for locomotor activity. Time spent on arms proximal and distal to the active ultrasonic loudspeaker served as measures for stimulus-directed locomotor activity[20].

Accelerating rotarod. To corroborate and reproduce the Nash laboratory report, at PND 43–45, motor coordination, balance, and motor learning were tested with an accelerating rotarod (Ugo Basile, Gemonio, Italy) as described previously[2,3]. Rats were placed on a rotating cylinder that slowly accelerated from 5 to 40 revolutions per min over 5 min. Rats were given three trials per day with a 45–60-min intertrial rest interval and tested for 3 consecutive days for a total of nine trials. Performance was scored as latency to fall off the cylinder with a maximum latency of 5 min.

Adhesive removal. At PND 52, a task of adhesive removal was used to assess sensory and find motor ability using a previously described mouse protocol modified for rats[78]. Rats individually habituated to an observation arena for 10 min and then a small round adhesive sticker (0.64 cm *d*; Avery Products Corporation, Strongsville, OH) was placed on the forehead. The latency to initiate removal of the sticker and the total elapsed time until complete removal of the sticker were recorded.

Magnetic resonance imaging. A multi-channel 7.0 Tesla MRI scanner (Agilent Inc., Palo Alto, CA) was used to image the rat brains within their skulls. Seven brains were scanned in one session, using an array of millipede coils and a T2 weighted 3D Fast Spin Echo Sequence (FSE) with an echo train length of 12 and a cylindrical sampling of k-space to reduce acquisition time[79]. Other sequence parameters included: TR of 350 ms, echo spacing of 10.5 ms, with the center of k-space acquired in successive averages on the 5^{th} and the 6^{th} echo, FOV of $3.6 \times 3.6 \times 4.0$ and a matrix size of $456 \times 456 \times 504$, yielding an image resolution of 79 μm isotropic. Total imaging time for this protocol is ~3 h and 20 min.

To visualize and compare any changes in the rat brains, the images are linearly (6 followed by 12 parameters) and non-linearly registered together. Registrations were performed with a combination of mni_autoreg tools and ANTS (advanced normalization tools)[80,81]. All scans are then resampled with the appropriate transform and averaged to create a population atlas representing the average anatomy of the study sample. The result of the registration was to deform all images into alignment with each other in an unbiased fashion. For the volume measurements, this allowed us to analyze the deformations needed to take each individual rat brain's[82] anatomy into this final atlas space, the goal being to model how the deformation fields relate to genotype. The Jacobian determinants of the deformation fields were then calculated as measures of volume at each voxel. Significant volume changes could then be calculated by warping a pre-existing rat MRI atlas onto the population atlas. An open-source classified atlas for the Fischer-344 rat brain has been created and maintained by the Near Lab at the Douglas Institute in Montreal, QC (https://www.nearlab.xyz/fischer344atlas). This segmented atlas allowed us to assess the volume of 98 different segmented structures[83], encompassing the cortex, large white matter structures (i.e., corpus callosum), ventricles, cerebellum, brain stem and olfactory bulbs in all brains. Further, these measurements could be examined on a voxelwise basis to localize the differences found within regions or across the brain. Multiple comparisons in this study were controlled for using the false discovery rate[84]. We reported combined sex results in the main text.

Statistical analysis. Developmental assays were analyzed with two-way repeated measures ANOVA, with genotype as the between-group factor and time as the within-group factor. Touchscreen parameters (sessions to reach criterion, trials to criterion, errors to criterion, and correction trials to criterion) were analyzed with unpaired (Student's) *t*-test. Log-rank (Mantel-

Cox) test was used to analyze the percentage of animals that reached criteria in the survival/completion analysis for the touchscreen test. Open field parameters (horizontal activity, vertical activity, and center time) were analyzed with two-way repeated measures ANOVA, with genotype as the between-group factor and time as the within-group factor. Comparisons between time sniffing the novel object were compared within each genotype, as previously described[73,85]. Data were analyzed with Graphpad Prism. All significance levels were set at $p < 0.05$ and all *t*-tests were two-tailed. Groups sizes were chosen based on past experience and power analyses[86]. Significant ANOVAs were followed by Bonferroni-Dunn or Holm-Sidak posthoc testing. Behavioral data passed distribution normality tests, were collected using continuous variables, and thus were analyzed via parametric analysis in all assays. For all behavioral analyses, variances were similar between groups and data points within 2 standard deviations of the mean were included in analysis. For the MRI analysis, separate linear models were measured for both absolute and relative regional and voxelwise volumes. Additionally, a final linear model was used to determine if there were any sex by genotype interactions. In all cases, multiple comparisons were controlled for using the false discovery rate[84]. Anatomical results reported combined both sexes.

References

1. Buiting, K., Williams, C. & Horsthemke, B. Angelman syndrome-insights into a rare neurogenetic disorder. Nat. Rev. Neurol. 12, 584–593 (2016).
2. Williams, C. A. Neurological aspects of the Angelman syndrome. Brain Dev. 27, 88–94 (2005).
3. Williams, C. A. The behavioral phenotype of the Angelman syndrome. Am. J. Med Genet C. Semin Med Genet 154C, 432–437 (2010).
4. Chamberlain, S. J. & Lalande, M. Neurodevelopmental disorders involving genomic imprinting at human chromosome 15q11-q13. Neurobiol. Dis. 39, 13–20 (2010).
5. Matsuura, T. et al. De novo truncating mutations in E6-AP ubiquitin-protein ligase gene (UBE3A) in Angelman syndrome. Nat. Genet. 15, 74–77 (1997).
6. Kishino, T., Lalande, M. & Wagstaff, J. UBE3A/E6-AP mutations cause Angelman syndrome. Nat. Genet. 15, 70–73 (1997).
7. Albrecht, U. et al. Imprinted expression of the murine Angelman syndrome gene, Ube3a, in hippocampal and Purkinje neurons. Nat. Genet. 17, 75–78 (1997).
8. Silverman, J. L., Yang, M., Lord, C. & Crawley, J. N. Behavioural phenotyping assays for mouse models of autism. Nat. Rev. Neurosci. 11, 490–502 (2010).
9. Silverman, J. L. & Ellegood, J. Behavioral and neuroanatomical approaches in models of neurodevelopmental disorders: opportunities for translation. Curr. Opin. Neurol. 31, 126–133 (2018).
10. Brudzynski, S. M. Ethotransmission: communication of emotional states through ultrasonic vocalization in rats. Curr. Opin. Neurobiol. 23, 310–317 (2013).
11. Wohr, M. & Schwarting, R. K. Affective communication in rodents: ultrasonic vocalizations as a tool for research on emotion and motivation. Cell Tissue Res. 354, 81–97 (2013).
12. Wohr, M., Seffer, D. & Schwarting, R. K. Studying socio-affective communication in rats through playback of ultrasonic vocalizations. Curr. Protoc. Neurosci 75, 8.35.1–8.35.17 (2016).
13. Gibbs, R. A. et al. Genome sequence of the Brown Norway rat yields insights into mammalian evolution. Nature 428, 493–521 (2004).
14. Tuzun, E., Bailey, J. A. & Eichler, E. E. Recent segmental duplications in the working draft assembly of the brown Norway rat. Genome Res. 14, 493–506 (2004).
15. Berg, E. L. et al. Developmental social communication deficits in the Shank3 rat model of phelan-mcdermid syndrome and autism spectrum disorder. Autism Res. 11, 587–601 (2018).
16. Hofer, M. A. Multiple regulators of ultrasonic vocalization in the infant rat. Psychoneuroendocrinology 21, 203–217 (1996).
17. Hofer, M. A., Shair, H. N. & Brunelli, S. A. Ultrasonic vocalizations in rat and mouse pups. Curr. Protoc. Neurosci 17, 8.14.1–8.14.16 (2002).
18. Kisko, T. M. et al. Sex-dependent effects of Cacna1c haploinsufficiency on juvenile social play behavior and pro-social 50-kHz ultrasonic communication in rats. Genes Brain Behav. 27, e12552 (2018).
19. Kisko, T. M. et al. Cacna1c haploinsufficiency leads to pro-social 50-kHz ultrasonic communication deficits in rats. Dis. Model Mech. 11, dmm034116 (2018).
20. Seffer, D., Schwarting, R. K. & Wohr, M. Pro-social ultrasonic communication in rats: insights from playback studies. J. Neurosci. Methods. 234, 73–81 (2014).

21. Willuhn, I. et al. Phasic dopamine release in the nucleus accumbens in response to pro-social 50 kHz ultrasonic vocalizations in rats. J. Neurosci. 34, 10616–10623 (2014).
22. Wohr, M., Engelhardt, K. A., Seffer, D., Sungur, A. O. & Schwarting, R. K. Acoustic communication in rats: effects of social experiences on ultrasonic vocalizations as socio-affective signals. Curr. Top. Behav. Neurosci. 30, 67–89 (2017).
23. Meng, L. et al. Truncation of Ube3a-ATS unsilences paternal Ube3a and ameliorates behavioral defects in the Angelman syndrome mouse model. PLoS Genet. 9, e1004039 (2013).
24. Daily, J. L. et al. Adeno-associated virus-mediated rescue of the cognitive defects in a mouse model for Angelman syndrome. PLoS ONE 6, e27221 (2011).
25. Bailus, B. J. et al. Protein delivery of an artificial transcription factor restores widespread Ube3a expression in an Angelman syndrome mouse brain. Mol. Ther. 24, 548–555 (2016).
26. Bailus, B. J. & Segal, D. J. The prospect of molecular therapy for Angelman syndrome and other monogenic neurologic disorders. BMC Neurosci. 15, 76 (2014).
27. Biffi, A. Genetically-modified hematopoietic stem cells and their progeny for widespread and efficient protein delivery to diseased sites: the case of lysosomal storage disorders. Curr. Gene Ther. 12, 381–388 (2012).
28. Ciarlone, S. L., Grieco, J. C., D'Agostino, D. P. & Weeber, E. J. Ketone ester supplementation attenuates seizure activity, and improves behavior and hippocampal synaptic plasticity in an Angelman syndrome mouse model. Neurobiol. Dis. 96, 38–46 (2016).
29. Kaphzan, H. et al. Reversal of impaired hippocampal long-term potentiation and contextual fear memory deficits in Angelman syndrome model mice by ErbB inhibitors. Biol. Psychiatry 72, 182–190 (2012).
30. Huang, H. S. et al. Topoisomerase inhibitors unsilence the dormant allele of Ube3a in neurons. Nature 481, 185–189 (2012).
31. Beaudet, A. L. Angelman syndrome: drugs to awaken a paternal gene. Nature 481, 150–152 (2012).
32. Jiang, Y. H. et al. Mutation of the Angelman ubiquitin ligase in mice causes increased cytoplasmic p53 and deficits of contextual learning and long-term potentiation. Neuron 21, 799–811 (1998).
33. Elgersma, Y. Genetic engineering cures mice of neurological deficits: prospects for treating Angelman syndrome. Pharmacogenomics 8, 539–541 (2007).
34. Rotaru, D. C., van Woerden, G. M., Wallaard, I. & Elgersma, Y. Adult Ube3a gene reinstatement restores the electrophysiological deficits of prefrontal cortex layer 5 neurons in a mouse model of Angelman syndrome. J. Neurosci. 38, 8011–8030 (2018).
35. Silva-Santos, S. et al. Ube3a reinstatement identifies distinct developmental windows in a murine Angelman syndrome model. J. Clin. Invest 125, 2069–2076 (2015).
36. Jiang, Y. H. et al. Altered ultrasonic vocalization and impaired learning and memory in Angelman syndrome mouse model with a large maternal deletion from Ube3a to Gabrb3. PLoS ONE 5, e12278 (2010).
37. Mandel-Brehm, C., Salogiannis, J., Dhamne, S. C., Rotenberg, A. & Greenberg, M. E. Seizure-like activity in a juvenile Angelman syndrome mouse model is attenuated by reducing Arc expression. Proc. Natl Acad. Sci. USA 112, 5129–5134 (2015).
38. Onos, K. D. et al. Enhancing face validity of mouse models of Alzheimer's disease with natural genetic variation. PLoS Genet. 15, e1008155 (2019).

39. Sadananda, M., Wohr, M. & Schwarting, R. K. Playback of 22-kHz and 50-kHz ultrasonic vocalizations induces differential c-fos expression in rat brain. Neurosci. Lett. 435, 17–23 (2008).
40. Wheeler, A. C., Sacco, P. & Cabo, R. Unmet clinical needs and burden in Angelman syndrome: a review of the literature. Orphanet. J. Rare Dis. 12, 164 (2017).
41. Gentile, J. K. et al. A neurodevelopmental survey of Angelman syndrome with genotype-phenotype correlations. J. Dev. Behav. Pediatr. 31, 592–601 (2010).
42. Grieco, J. C. et al. Quantitative measurement of communication ability in children with Angelman syndrome. J. Appl Res Intellect. Disabil. 31, e49–e58 (2018).
43. Tan, W. H. et al. Angelman syndrome: Mutations influence features in early childhood. Am. J. Med. Genet. A 155A, 81–90 (2011).
44. Tan, W. H. et al. A randomized controlled trial of levodopa in patients with Angelman syndrome. Am. J. Med. Genet. A 176, 1099–1107 (2018).
45. Grieco, J. C., Gouelle, A. & Weeber, E. J. Identification of spatiotemporal gait parameters and pressure-related characteristics in children with Angelman syndrome: A pilot study. J. Appl. Res. Intellect. Disabil. 31, 1219–1224 (2018).
46. Born, H. A. et al. Strain-dependence of the Angelman Syndrome phenotypes in Ube3a maternal deficiency mice. Sci. Rep. 7, 8451 (2017).
47. Huang, H. S. et al. Behavioral deficits in an Angelman syndrome model: effects of genetic background and age. Behavioural. Brain Res. 243, 79–90 (2013).
48. Sonzogni, M. et al. A behavioral test battery for mouse models of Angelman syndrome: a powerful tool for testing drugs and novel Ube3a mutants. Mol. Autism 9, 47 (2018).
49. Homberg, J. R., Wohr, M. & Alenina, N. Comeback of the rat in biomedical research. ACS Chem. Neurosci. 8, 900–903 (2017).
50. Copping, N. A. et al. Touchscreen learning deficits and normal social approach behavior in the Shank3B model of Phelan-McDermid Syndrome and autism. Neuroscience 345, 155–165 (2017).
51. Dhamne, S. C. et al. Replicable in vivo physiological and behavioral phenotypes of the Shank3B null mutant mouse model of autism. Mol. Autism 8, 26 (2017).
52. Kabitzke, P. et al. Comprehensive analysis of two shank3 and the Cacna1c mouse models of Autism spectrum disorder. Genes Brain Behav. 17, 4–22 (2017).
53. Bird, L. M. et al. A therapeutic trial of pro-methylation dietary supplements in Angelman syndrome. Am. J. Med. Genet. A 155A, 2956–2963 (2011).
54. Judson, M. C. et al. GABAergic neuron-specific loss of Ube3a causes Angelman syndrome-like EEG abnormalities and enhances seizure susceptibility. Neuron 90, 56–69 (2016).
55. Mercer, R. E. et al. Regionally reduced brain volume, altered serotonin neurochemistry, and abnormal behavior in mice null for the circadian rhythm output gene Magel2. Am. J. Med. Genet. Part B, Neuropsychiatr. Genet.: Off. Publ. Int. Soc. Psychiatr. Genet. 150B, 1085–1099 (2009).
56. Mercer, R. E. & Wevrick, R. Loss of magel2, a candidate gene for features of Prader-Willi syndrome, impairs reproductive function in mice. PLoS ONE 4, e4291 (2009).
57. Ellegood, J. et al. Clustering autism: using neuroanatomical differences in 26 mouse models to gain insight into the heterogeneity. Mol. Psychiatry 20, 118–125 (2015).
58. Ellegood, J. et al. Neuroanatomical phenotypes are consistent with autism-like behavioral phenotypes in the 15q11-13 duplication mouse model. Autism Res.: Off. J. Int. Soc. Autism Res. 8, 545–555 (2015).

59. Ellegood, J., Henkelman, R. M. & Lerch, J. P. Neuroanatomical assessment of the integrin beta3 mouse model related to autism and the serotonin system using high resolution MRI. Front. Psychiatry 3, 1–9 (2012).
60. Ellegood, J. et al. Analysis of neuroanatomical differences in mice with genetically modified serotonin transporters assessed by structural magnetic resonance imaging. Mol. Autism 9, 24 (2018).
61. Albertelli, M. A. et al. Glutamine tract length of human androgen receptors affects hormone-dependent and -independent prostate cancer in mice. Hum. Mol. Genet. 17, 98–110 (2008).
62. Kaphzan, H. et al. Genetic reduction of the alpha1 subunit of Na/K-ATPase corrects multiple hippocampal phenotypes in Angelman syndrome. Cell Rep. 4, 405–412 (2013).
63. Santini, E. et al. Mitochondrial superoxide contributes to hippocampal synaptic dysfunction and memory deficits in Angelman syndrome model mice. J. Neurosci. 35, 16213–16220 (2015).
64. Hethorn, W. R. et al. Reelin supplementation recovers synaptic plasticity and cognitive deficits in a mouse model for Angelman syndrome. Eur. J. Neurosci. 41, 1372–1380 (2015).
65. van Woerden, G. M. et al. Rescue of neurological deficits in a mouse model for Angelman syndrome by reduction of alphaCaMKII inhibitory phosphorylation. Nat. Neurosci. 10, 280–282 (2007).
66. Weeber, E. J. et al. Derangements of hippocampal calcium/calmodulindependent protein kinase II in a mouse model for Angelman mental retardation syndrome. J. Neurosci. 23, 2634–2644 (2003).
67. Leach, P. T. & Crawley, J. N. Touchscreen learning deficits in Ube3a, Ts65Dn and Mecp2 mouse models of neurodevelopmental disorders with intellectual disabilities. Genes Brain Behav. 17, e12452 (2018).
68. Sidorov, M. S. et al. Enhanced operant extinction and prefrontal excitability in a mouse model of Angelman syndrome. J. Neurosci. 38, 2671–2682 (2018).
69. Benyakorn, S. et al. Computerized cognitive training in children with autism and intellectual disabilities: feasibility and satisfaction study. JMIR Ment. Health 5, e40 (2018).
70. Hessl, D. et al. The NIH toolbox cognitive battery for intellectual disabilities: three preliminary studies and future directions. J. Neurodevelopmental Disord. 8, 35 (2016).
71. Hessl, D. et al. Cognitive training for children and adolescents with fragile X syndrome: a randomized controlled trial of Cogmed. J. Neurodevelopmental Disord. 11, 4 (2019).
72. Ku, K. M., Weir, R. K., Silverman, J. L., Berman, R. F. & Bauman, M. D. Behavioral phenotyping of juvenile long-evans and Sprague-Dawley rats: implications for preclinical models of autism spectrum disorders. PLoS ONE 11, e0158150 (2016).
73. Adhikari, A. et al. Cognitive deficits in the snord116 deletion mouse model for Prader-Willi syndrome. Neurobiol. Learn. Mem. 165, 106874 (2018).
74. Yang, M. et al. Reduced excitatory neurotransmission and mild autism-relevant phenotypes in adolescent Shank3 null mutant mice. J. Neurosci. 32, 6525–6541 (2012).
75. Brigman, J. L. et al. GluN2B in corticostriatal circuits governs choice learning and choice shifting. Nat. Neurosci. 16, 1101–1110 (2013).
76. Horner, A. E. et al. The touchscreen operant platform for testing learning and memory in rats and mice. Nat. Protoc. 8, 1961–1984 (2013).
77. Morton, A. J., Skillings, E., Bussey, T. J. & Saksida, L. M. Measuring cognitive deficits in disabled mice using an automated interactive touchscreen system. Nat. Methods 3, 767 (2006).

78. Sukoff Rizzo, S. J. et al. Assessing healthspan and lifespan measures in aging mice: optimization of testing protocols, replicability, and rater reliability. Curr. Protoc. Mouse Biol. 8, e45 (2018).
79. Spencer Noakes, T. L., Henkelman, R. M. & Nieman, B. J. Partitioning k-space for cylindrical three-dimensional rapid acquisition with relaxation enhancement imaging in the mouse brain. NMR Biomed. 30, 1–13 (2017).
80. Avants, B. B., Epstein, C. L., Grossman, M. & Gee, J. C. Symmetric diffeomorphic image registration with cross-correlation: evaluating automated labeling of elderly and neurodegenerative brain. Med. Image Anal. 12, 26–41 (2008).
81. Avants, B. B. et al. A reproducible evaluation of ANTs similarity metric performance in brain image registration. NeuroImage 54, 2033–2044 (2011).
82. Collins, D. L., Neelin, P., Peters, T. M. & Evans, A. C. Automatic 3D intersubject registration of MR volumetric data in standardized Talairach space. J. Comput. Assist. Tomogr. 18, 192–205 (1994).
83. Goerzen, et al. An MRI-derived neuroanatomical atlas of the fischer 344 rat brain. https://doi.org/10.1101/743583v1.
84. Genovese, C. R., Lazar, N. A. & Nichols, T. Thresholding of statistical maps in functional neuroimaging using the false discovery rate. NeuroImage 15, 870–878 (2002).
85. Gompers, A. L. et al. Germline Chd8 haploinsufficiency alters brain development in mouse. Nat. Neurosci. 20, 1062–1073 (2017).
86. Sukoff Rizzo, S. J. & Silverman, J. L. Methodological considerations for optimizing and validating behavioral assays. Curr. Protoc. Mouse Biol. 6, 364–379 (2016).

Figures

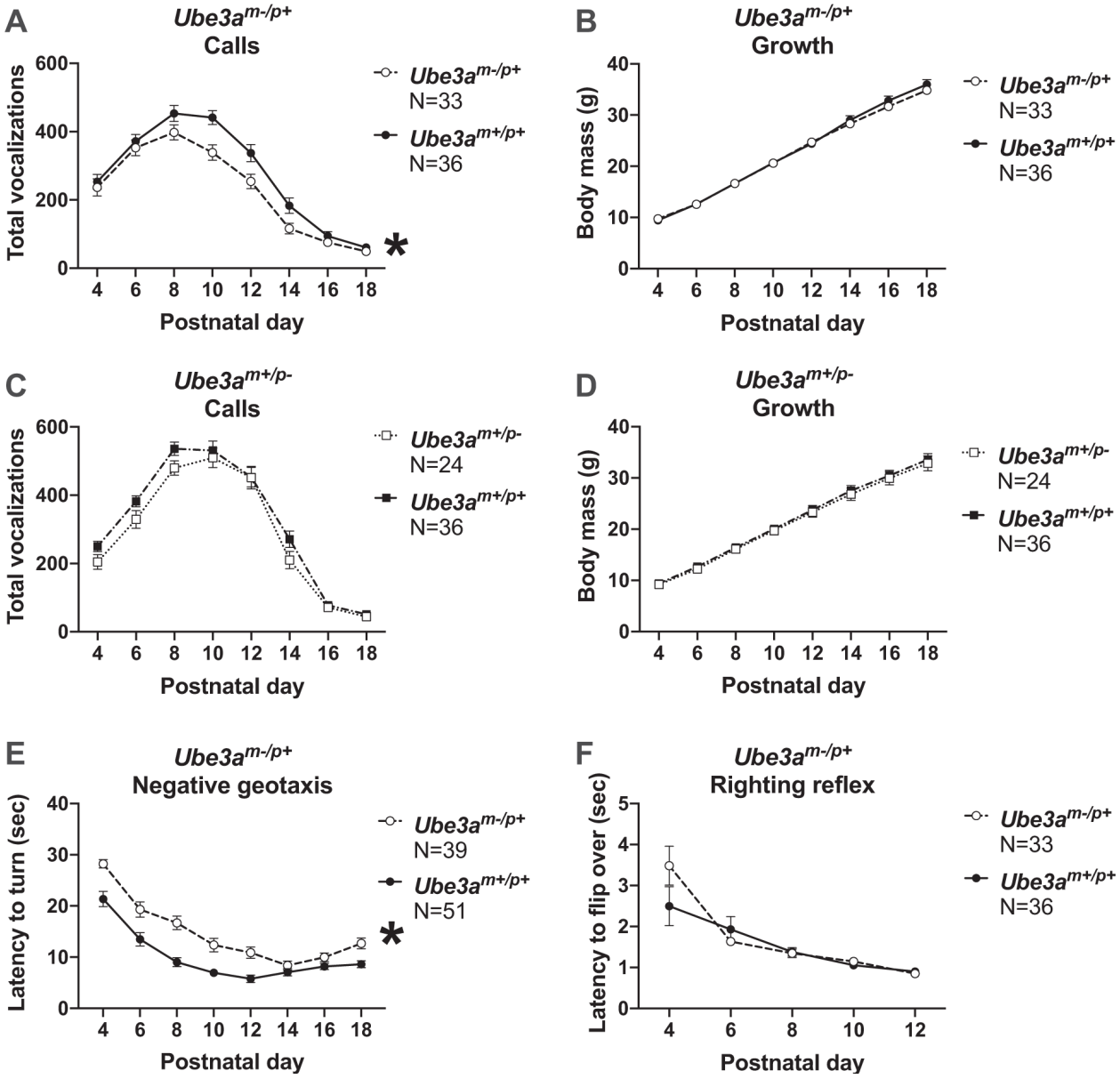

Fig. 1 Reduced isolation-induced pup ultrasonic vocalizations and delayed neonatal reflex development in *Ube3a*$^{m-/p+}$ pups. **a** *Ube3a*$^{m-/p+}$ pups emitted significantly fewer USV across early development compared to wildtypes, and **b** demonstrated normal weight gain. **c** *Ube3a*$^{m+/p-}$ pups emitted normal numbers of USV across early development, and **d** also demonstrated normal weight gain. **e** Compared to wildtype littermates, *Ube3a*$^{m-/p+}$ pups were significantly slower in the negative geotaxis test but **f** had normal latencies to flip over in the test of righting reflex. All analyses include males and females. Mean +/− S.E.M. is depicted. **a**–**f**: *$p < 0.05$, repeated measures ANOVA, main effect of genotype.

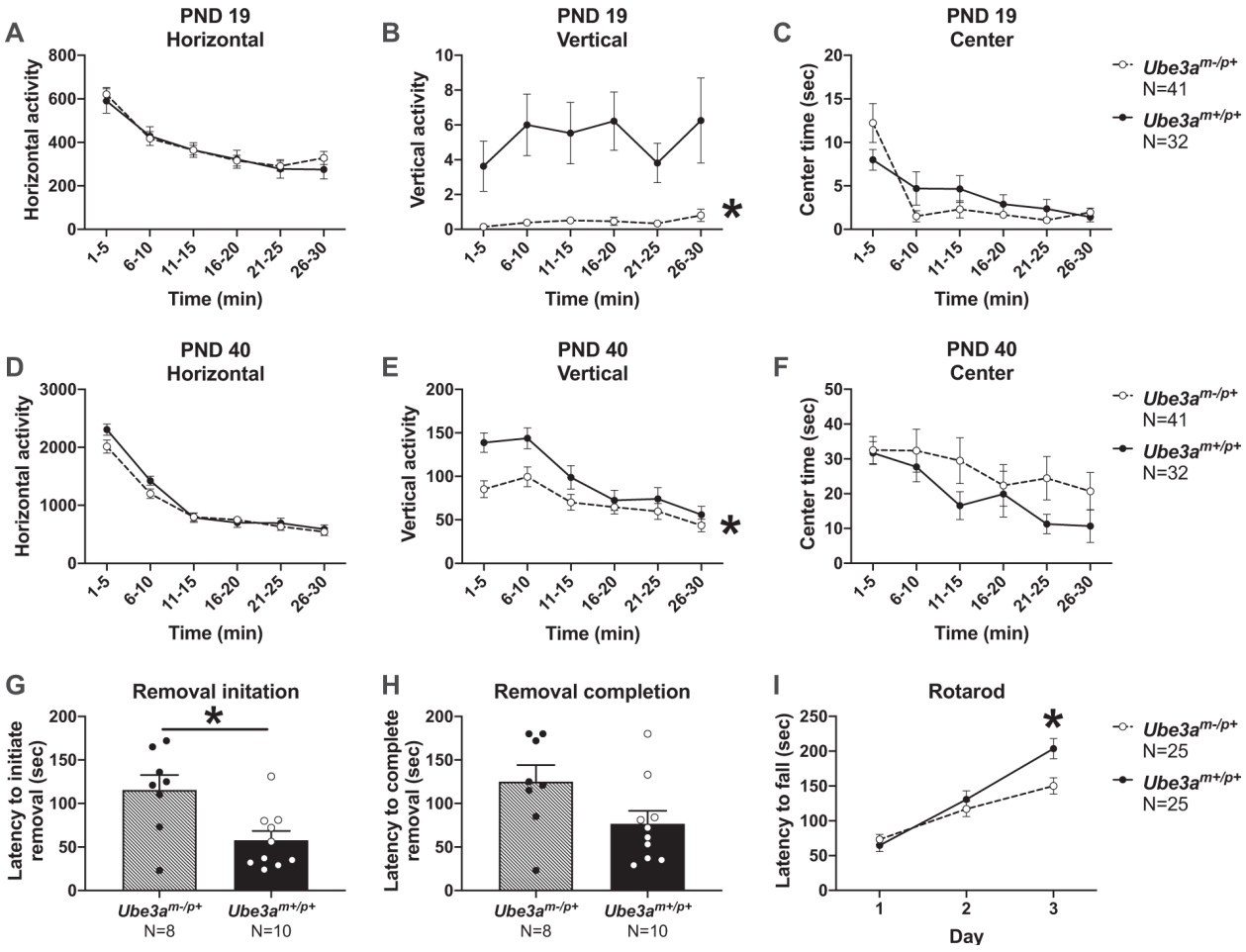

Fig. 2 Reduced vertical activity and motor learning deficit in *Ube3a*$^{m-/p+}$ rats. **a** At PND 19, *Ube3a*$^{m-/p+}$ juvenile rats exhibited normal horizontal activity but **b** had significantly reduced vertical activity compared to wildtypes. **c** Center time did not differ between groups. **d** At PND 40, *Ube3a*$^{m-/p+}$ rats again exhibited normal horizontal activity, **e** significantly lower vertical activity, and **f** normal center time. Note: the difference in axis labels shows how much more active PND 40 rats are over PND 19. **g** In the adhesive removal task, *Ube3a*$^{m-/p+}$ rats had significantly higher latencies to initiate removal of the adhesive. **h** Latency to completely remove the adhesive did not differ between groups but trended longer ($p = 0.059$) in the *Ube3a*$^{m-/p+}$ rats, suggesting fine motor skill deficits of the fore paws. **i** *Ube3a*$^{m-/p+}$ rats had significantly lower latencies to fall of the rotarod on day 3 compared to wildtypes. Analyses include both males and females. Mean +/− S.E.M. is depicted. **a**–**f**: $*p < 0.05$, repeated measures ANOVA, main effect of genotype. **g**–**h**: $*p < 0.05$, Student's *t*-test. **i**: $*p < 0.05$, repeated measures ANOVA, Holm-Sidak's multiple comparisons test.

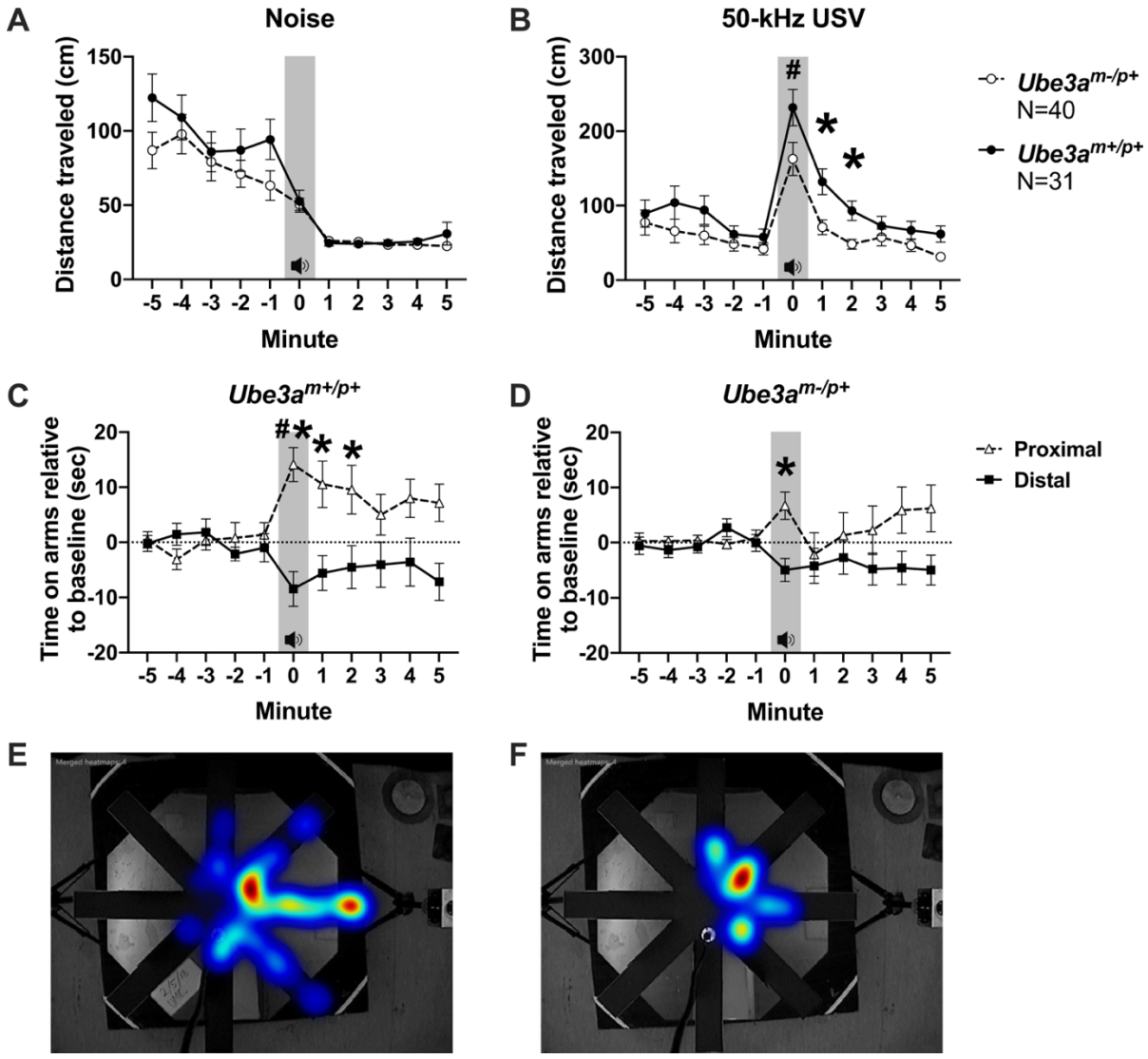

Fig. 3 Atypical social communication in *Ube3a*$^{m-/p+}$ juveniles using 50-kHz pro-social ultrasonic vocalizations. a Distance traveled in response to the white noise control stimulus (gray zone) did not differ between groups: both exhibited behavioral inhibition (i.e., a reduction in motion following the noise control). **b** Distance traveled increased in response to playback of 50-kHz USV (gray zone) in *Ube3a*$^{m-/p+}$ and *Ube3a*$^{m+/p+}$ rats. Interestingly, the duration of the response was shorter in *Ube3a*$^{m-/p+}$ compared to that of wildtypes. **c** In the radial maze used, time spent in the arms proximal to the active ultrasonic speaker versus time spent in the distal arms indicate social interest, preference and social engagement. *Ube3a*$^{m+/p+}$ rats spent significantly longer time on the arms proximal to the speaker emitting the 50-kHz USV upon playback and for several minutes afterwards showing a strong, sustained social response. **d** *Ube3a*$^{m-/p+}$ subjects failed to show a strong, sustained response to hearing the USV and only spent significantly more time on the proximal arms during the initial time period the audio cue was "on" (gray zone). **e**, **f** Representative heat maps of the distance and direction traveled in response to the 50-kHz USV. Analyses include both males and females. Mean +/− S.E.M. is depicted. *$p < 0.05$, repeated measures ANOVA, Bonferroni multiple comparisons test. $^{\#}p < 0.05$, paired *t*-test, min −1 versus min 0.

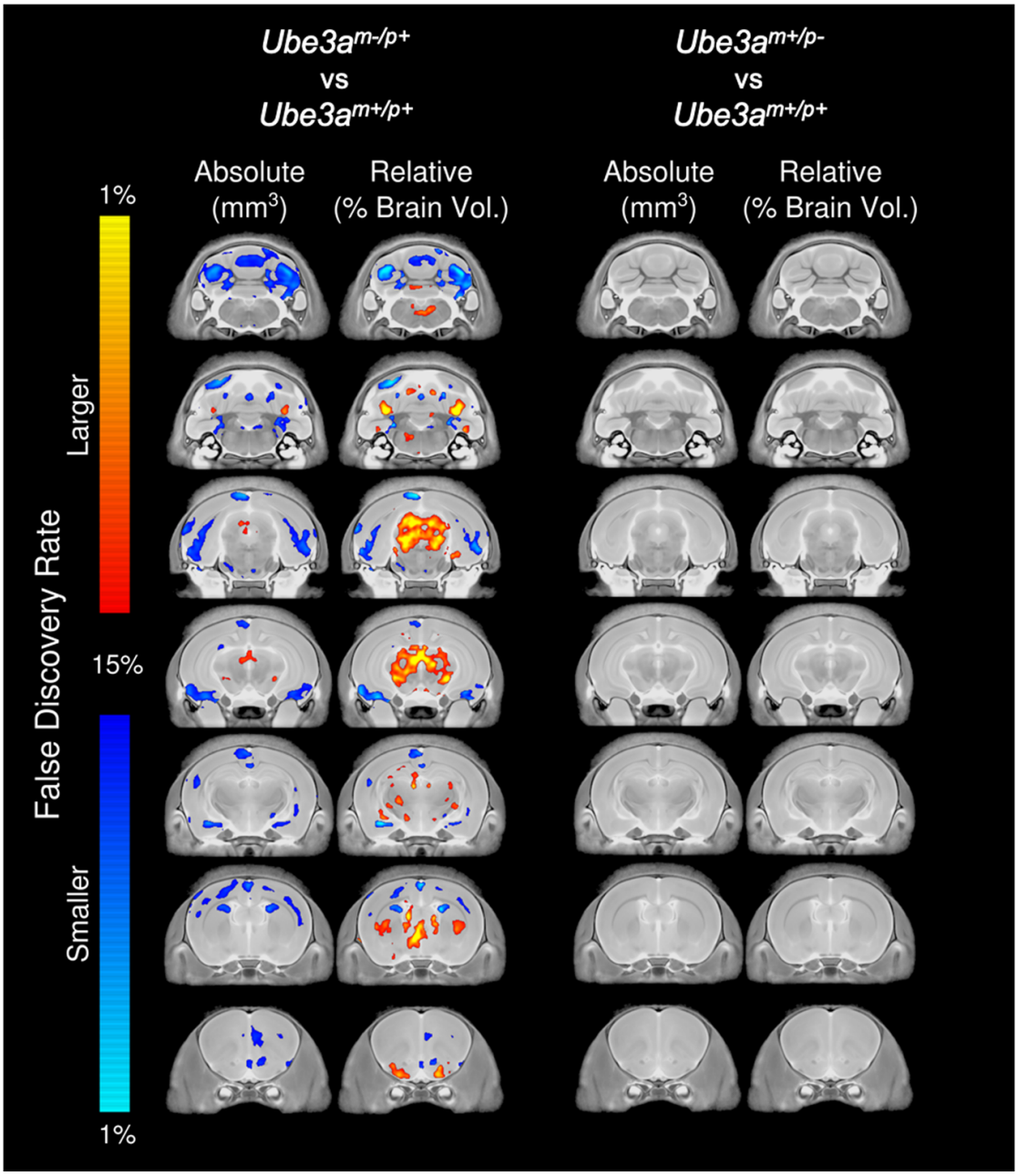

Fig. 4 Neuroanatomical pathology in *Ube3a*$^{m-/p+}$ rats at PND 21. Representative coronal slice series highlighting regional brain differences in absolute (mm^3) and relative (%) brain volume between *Ube3a*$^{m-/p+}$ and *Ube3a*$^{m+/p+}$ (left) and between *Ube3a*$^{m+/p-}$ and *Ube3a*$^{m+/p+}$ (right). Regions with decreased volume in *Ube3a*$^{m-/p+}$ include the cerebral cortex, cerebellum, and amygdala. Regions with increased volume in *Ube3a*$^{m-/p+}$ include the periacqueductal gray, thalamus, and hypothalamus. *Ube3a*$^{m+/p-}$ did not exhibit altered neuroanatomy compared to wildtype. Analyses include both males and females.

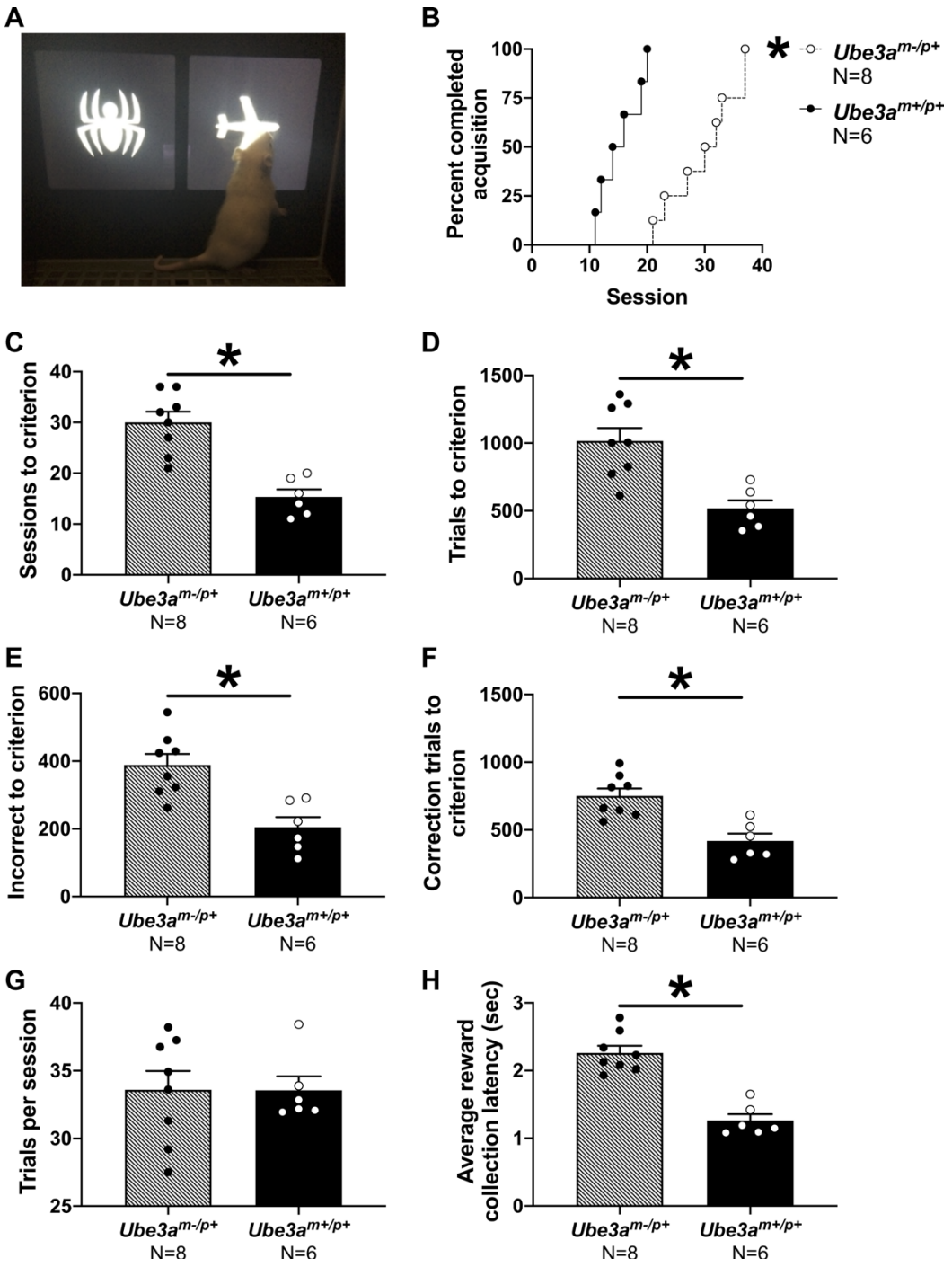

Fig. 5 Delayed touchscreen learning in *Ube3a*$^{m-/p+}$ rats.
a Representative image of a subject rat performing the touchscreen pairwise discrimination. **b** *Ube3a*$^{m-/p+}$ adult rats took significantly longer to learn the correct response compared to wildtype littermates, requiring **c** more sessions, **d** more trials, **e** more incorrect responses, and **f** more correction trials to reach criterion. **g** The average number of trials completed per session did not differ between genotypes. **h** *Ube3a*$^{m-/p+}$ adult rats took longer to collect the pellet after responding correctly. Mean + S.E.M. is depicted. **b**: *$p < 0.0001$, Log-rank (Mantel-Cox test). **c**–**h**: *$p < 0.05$, Student's *t*-test.

Supplementary Information

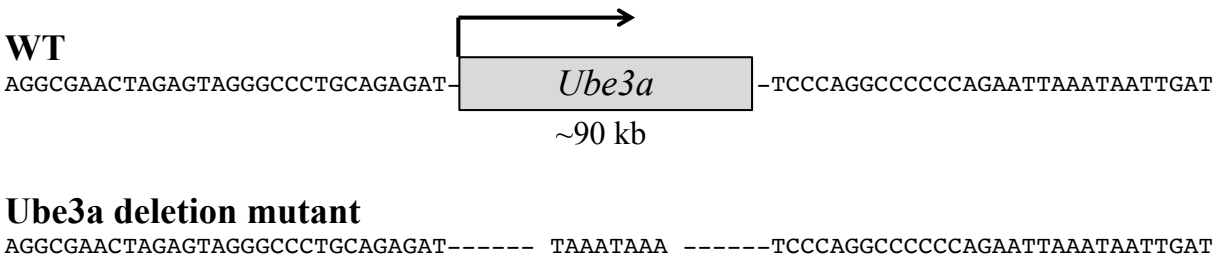

Supplementary Figure S1. Schematic of the Angelman syndrome rat model. The rat wildtype (WT) locus encompassing the Ube3a coding region is shown on top. Using the CRISPR/Cas9 system the ~90 kb *Ube3a* gene region was deleted and the genomic junction of the *Ube3a* knock-out allele was determined by Sanger sequencing. Genomic sequence of the *Ube3a* knockout allele is shown in the lower panel.

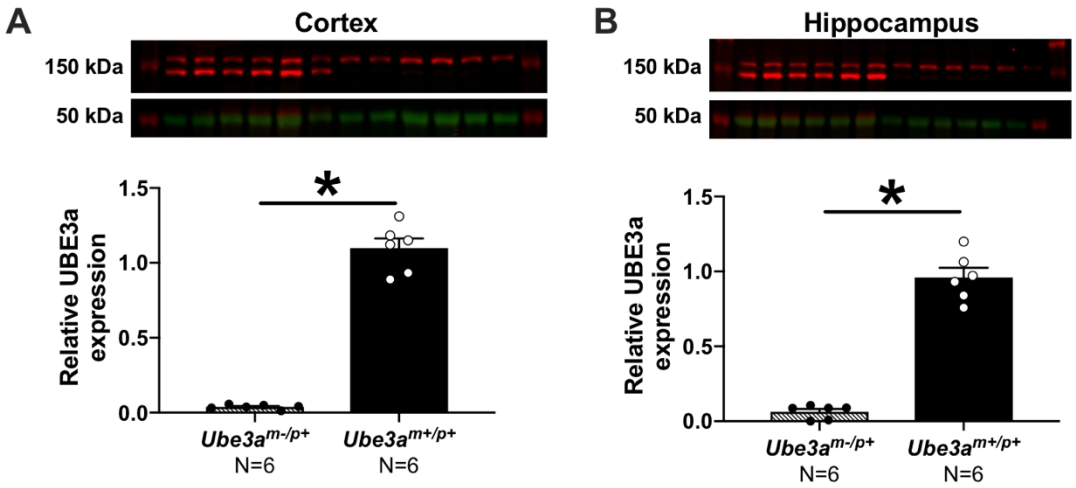

Supplementary Figure S2. Reduced UBE3a protein in *Ube3a*$^{m-/p+}$ rats. Western blots of brain samples from *Ube3a*$^{m-/p+}$ and *Ube3a*$^{m+/p+}$ rats show a lack of UBE3a expression (around 95 kDa; red) compared to beta-Tubulin expression (around 50 kDa; green). The upper band was approximately >100 kDa and the lower band was <100 kDa. Quantification confirmed that *Ube3a*$^{m-/p+}$ rats had significantly lower relative expression of UBE3a in both the A) cortex and B) hippocampus compared to wildtypes. Analyses include both males and females. *$p < 0.05$, Student's *t*-test. Quantitation was assessed on the lower band.

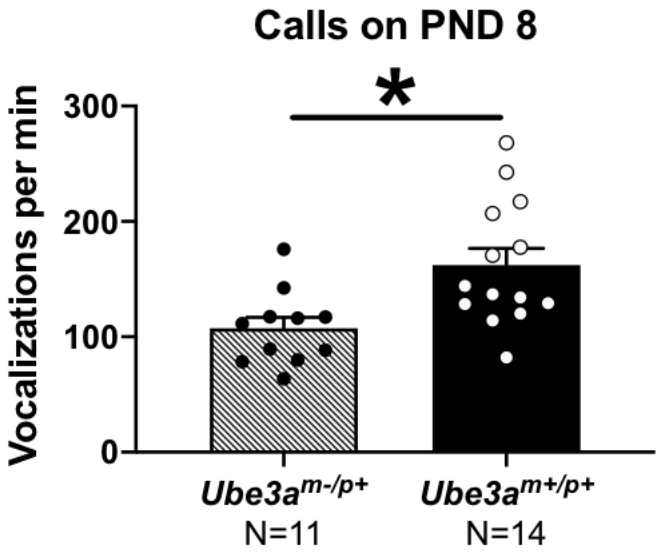

Supplementary Figure S3. Reduced rate of isolation-induced pup ultrasonic vocalizations corroborated in an independent lab. A research team at Baylor College of Medicine also discovered *Ube3a*$^{m-/p+}$ pups to make significantly fewer calls than wildtype littermates in an independent cohort, illustrating replication. Analyses include both males and females. *$p < 0.05$, Student's *t*-test.

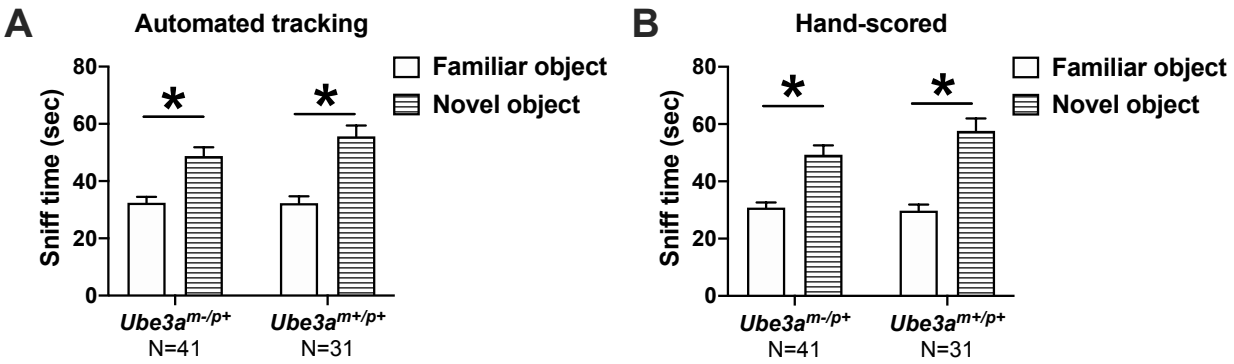

Supplementary Figure S4. Intact novel object recognition in *Ube3a*$^{m-/p+}$ rats. A) Utilizing automated tracking software, both *Ube3a*$^{m-/p+}$ and *Ube3a*$^{m+/p+}$ rats were found to spend significantly more time investigating the novel object than the familiar object. B) The same result was found when sniff time was hand-scored by a trained observer blind to genotype. Analyses include both males and females. *$p < 0.05$, paired *t*-test.

Supplementary Table 1. Cohort 1 developmental milestone analysis via repeated measures ANOVA results summary.

Milestone		F(df)	p	Significant?
Body temperature (°C)	Time	$F(3.935, 279.4) = 26.20$	$p < 0.0001$	Yes
	Genotype	$F(1, 71) = 0.4083$	$p = 0.525$	No
	Interaction	$F(7, 497) = 1.098$	$p = 0.363$	No
Body weight (g)	Time	$F(1.325, 94.06) = 1586$	$p < 0.0001$	Yes
	Genotype	$F(1, 71) = 0.0010$	$p = 0.975$	No
	Interaction	$F(7, 497) = 0.5124$	$p = 0.825$	No
Body length (cm)	Time	$F(5.356, 380.3) = 1068$	$p < 0.0001$	Yes
	Genotype	$F(1, 71) = 0.9787$	$p = 0.326$	No
	Interaction	$F(7, 497) = 1.706$	$p = 0.105$	No
Tail length (cm)	Time	$F(3.472, 246.5) = 2250$	$p < 0.0001$	Yes
	Genotype	$F(1, 71) = 0.1091$	$p = 0.742$	No
	Interaction	$F(7, 497) = 0.9624$	$p = 0.458$	No
Head width (cm)	Time	$F(1.554, 110.4) = 1.249$	$p = 0.284$	No
	Genotype	$F(1, 71) = 0.05429$	$p = 0.816$	No
	Interaction	$F(2, 142) = 1.253$	$p = 0.289$	No
Righting reflex (sec)	Time	$F(1.467, 104.2) = 25.59$	$p < 0.0001$	Yes
	Genotype	$F(1, 71) = 0.6512$	$p = 0.422$	No
	Interaction	$F(4, 284) = 2.240$	$p = 0.065$	No
Circle traverse (sec)	Time	$F(3.971, 282.0) = 217.2$	$p < 0.0001$	Yes
	Genotype	$F(1, 71) = 1.248$	$p = 0.267$	No
	Interaction	$F(7, 497) = 0.3435$	$p = 0.934$	No
Cliff avoidance (sec)	Time	$F(5.258, 373.3) = 52.43$	$p < 0.0001$	Yes
	Genotype	$F(1, 71) = 1.778$	$p = 0.186$	No
	Interaction	$F(7, 497) = 0.8706$	$p = 0.530$	No

Supplementary Table 2. Cohort 1 developmental milestone survival curve analysis via Log-Rank (Mantel-Cox) test results summary.

Milestone	*Ube3a*$^{m+/p+}$ Median (N=32)	*Ube3a*$^{m-/p+}$ Median (N=41)	Chi square	df	*p*	Significant?
Eye opening (days)	16	16	3.642	1	$p = 0.056$	No
Rooting reflex (days)	14	14	0.0798	1	$p = 0.777$	No
Forelimb grasp (days)	4	4	1.281	1	$p = 0.258$	No
Bar hold >10 sec (days)	18	16	2.165	1	$p = 0.141$	No

Supplementary Table 3. Absolute (mm^3) and relative (%) brain volumes of *Ube3a*$^{m-/p+}$ (Het) and *Ube3a*$^{m+/p+}$ (WT) rats determined by high resolution magnetic resonance imaging at postnatal day 21.

	2	9	10	11	12	13	57	62	64	65	70	72	105	107	108	109	6	7	61
	Het	Het	Het	Het	Het	Het	Het	Het	Het	Het	Het	Het	Het	Het	Het	Het	Het	Het	Het
Absolute Volume	F	F	F	F	F	F	F	F	F	F	F	F	F	F	F	F	M	M	M
	Mat	Mat	Mat	Mat	Mat	Mat	Mat	Mat	Mat	Mat	Mat	Mat	Mat	Mat	Mat	Mat	Mat	Mat	Mat
amygdaloid_area	29.35902	29.73343	30.64752	28.9679	30.6432	30.20506	29.94069	29.83561	28.02939	29.23587	29.09009	30.15226	29.87882	30.01451	30.41895	29.35155	32.28531	30.99425	29.20554
Anterior_part_of_anterior_commissure	1.318282	1.322994	1.373379	1.322096	1.390281	1.361746	1.312196	1.34831	1.256617	1.311338	1.271225	1.349252	1.327204	1.369352	1.356006	1.309768	1.469568	1.426043	1.297184
Aqueduct	1.591558	1.628993	1.684259	1.53172	1.654535	1.701931	1.685484	1.619027	1.588172	1.590756	1.634114	1.684666	1.633032	1.657479	1.650703	1.619428	1.713932	1.661843	1.588753
auditory_cortex	20.4056	20.72686	21.26804	20.17811	21.21355	21.1869	21.00374	20.66918	19.79766	20.38305	20.43662	21.08283	20.82883	20.85071	21.07441	20.41635	22.27274	21.49934	20.40214
basal_forebrain	16.73997	17.00031	17.57312	16.50322	17.44263	17.50569	17.23892	16.98488	16.20985	16.72646	16.76692	17.39813	17.05451	17.27289	17.34688	16.93636	18.38801	17.66257	16.7133
Bed_nucleus_of_stria_terminalis	2.914299	2.873025	2.966278	2.852277	2.928658	2.94713	2.908591	2.882257	2.774189	3.017429	2.78902	2.799643	2.960213	2.935681	2.983034	2.90197	3.154018	3.021073	2.934641
caudaputamen	45.21301	45.86107	47.40092	44.66798	47.01791	47.13072	46.41952	45.88079	43.60961	45.13018	45.14044	46.74522	46.15766	46.51547	46.93182	45.678	49.68182	47.77829	45.11418
cerebellar_lobule_1_2	8.031842	7.924643	8.324682	7.79038	8.226434	8.088503	7.995342	8.175982	7.750496	7.860519	7.770128	8.038095	8.090144	8.181508	8.184991	7.977784	8.638629	8.340141	7.831719
cerebellar_lobule_10	3.342766	3.318748	3.408154	3.189873	3.339759	3.464392	3.430556	3.408451	3.235053	3.314682	3.286389	3.427812	3.371743	3.473804	3.441284	3.335588	3.595635	3.502978	3.261738
cerebellar_lobule_3	6.938516	6.819842	7.144827	6.683538	7.023798	6.966703	6.916837	7.051119	6.591784	6.739113	6.650668	6.899064	6.989203	7.116779	7.102245	6.894466	7.475379	7.281465	6.713479
cerebellar_lobule_4_5	21.34411	21.13093	21.95194	20.67293	21.5994	21.94821	21.67872	21.72414	20.79083	21.21807	20.9361	21.7517	21.55345	21.87628	21.75065	21.3116	22.80381	22.10892	20.9419
cerebellar_lobule_6	8.487425	8.352786	8.775461	8.29352	8.476111	8.796327	8.613773	8.718529	8.323384	8.491289	8.37454	8.586692	8.517017	8.64268	8.642926	8.376715	9.048947	8.81068	8.306688
cerebellar_lobule_7	3.290491	3.180381	3.359843	3.238873	3.238111	3.44151	3.332871	3.348199	3.29935	3.336067	3.267613	3.291451	3.241103	3.28582	3.30676	3.202142	3.442315	3.368366	3.194787
cerebellar_lobule_8	3.651194	3.604753	3.806313	3.566347	3.66707	3.801767	3.733685	3.780579	3.548191	3.60057	3.611413	3.706304	3.666596	3.739351	3.736467	3.597923	3.909298	3.815444	3.566958
cerebellar_lobule_9	8.513123	8.399781	8.857899	8.366426	8.530721	8.869043	8.66325	8.799066	8.364684	8.4842	8.433592	8.639118	8.535583	8.669805	8.676286	8.38342	9.092241	8.843766	8.338444
Cerebellar_White_Matter_Arbor_vita_of_cerebellum	26.79418	26.55153	27.80911	26.03751	27.22858	27.49497	26.89071	27.50547	25.9985	26.55395	26.05776	26.96606	26.91493	27.39089	27.33494	26.60505	28.79535	27.91265	26.15293
cerebral_peduncle	2.883088	2.930074	2.983501	2.826809	2.965652	2.97063	2.959156	2.897853	2.772323	2.896523	2.867285	2.920947	2.953172	2.915633	2.995598	2.882788	3.14209	3.02314	2.893633
Cingulate_Cortex_area_1	14.97705	15.22119	15.55677	14.78298	15.59967	15.71206	15.38709	15.17145	14.49532	15.00348	14.949	15.50504	15.31008	15.34594	15.53918	15.03863	16.36873	15.94327	14.88491
Cingulate_Cortex_area_2	9.272366	9.413257	9.644694	9.165091	9.587122	9.767371	9.620252	9.361127	9.052195	9.321255	9.324098	9.682711	9.473113	9.560316	9.586232	9.37302	10.124578	9.800582	9.276963
cingulum	3.263429	3.282323	3.390705	3.223539	3.378099	3.35643	3.30608	3.302563	3.113462	3.250157	3.20576	3.30727	3.322498	3.352855	3.374446	3.261295	3.594386	3.474498	3.232455
Cochlear_nucleus	1.0464036	1.0509427	1.1139757	1.0034019	1.0933098	1.0452108	1.0240929	1.0946282	0.966971	0.9970065	0.978581	1.0263843	1.0574541	1.0869509	1.0924927	1.043237	1.1695514	1.1296123	1.0115681
Commisure_inferior_Colliculus	0.3030857	0.3159274	0.3102741	0.3014947	0.3134708	0.3480332	0.3407029	0.299497	0.335388	0.3266278	0.3378302	0.3488137	0.3131333	0.3144695	0.3041821	0.3174235	0.3096368	0.3029453	0.3171635
commisure_superior_colliculus	0.1862444	0.1873825	0.1967696	0.1836911	0.1937331	0.1943192	0.1890854	0.1899483	0.1803519	0.1866147	0.1808886	0.1835	0.1884106	0.187848	0.1881994	0.182223	0.2022124	0.1957408	0.1846853
copula	2.787467	2.688312	2.887057	2.774919	2.782277	2.829166	2.730725	2.870778	2.720262	2.791594	2.693173	2.699752	2.763349	2.750224	2.80714	2.713607	2.936826	2.861548	2.710508
Corpus_Callosum_associated_White_Matter	41.15899	41.60527	42.85151	40.36179	42.43935	42.81767	42.45498	41.50544	39.87778	41.22777	41.26816	42.30904	42.06587	42.04585	42.60976	41.38123	44.85723	43.26012	41.16107
Crus_1_ansiform_lobule	16.6405	16.34911	17.2074	16.30563	16.81379	17.05211	16.6378	17.08808	16.27075	16.6955	16.18163	16.60644	16.70108	16.83412	16.88905	16.46929	17.74175	17.23224	16.29689
Crus_2_ansiform_lobule	9.694494	9.600109	10.173922	9.591237	9.822725	10.014537	9.644205	10.082837	9.498405	9.660349	9.476612	9.606074	9.662728	9.84351	9.86719	9.512823	10.441554	10.115503	9.424523
dentate_gyrus	16.02061	16.33404	16.81806	15.88962	16.80686	16.55463	16.3291	16.3504	15.44972	15.8944	15.94162	16.48366	16.38147	16.3871	16.61384	16.02683	17.58385	16.99403	15.99531
Dentate_nucleus	0.838649	0.8220156	0.8735524	0.7998492	0.84537	0.8238843	0.8139655	0.8549595	0.7680826	0.8024965	0.7749065	0.7994055	0.8435141	0.8601025	0.8676405	0.8279778	0.9185377	0.8927691	0.801477
Dorsal_Peduncular_Cortex	1.480887	1.497574	1.549254	1.447532	1.513857	1.491409	1.490866	1.510184	1.365497	1.454655	1.447881	1.481171	1.533977	1.496186	1.554328	1.481701	1.63509	1.582985	1.470492
Dorsal_Tenia_Tecta	1.0377331	1.0320214	1.0588158	1.0221891	1.0549976	1.0669557	1.0436293	1.0361941	0.9786659	1.0311485	0.9930462	1.0449408	1.0435136	1.074914	1.0608898	1.0255619	1.1402587	1.1214806	1.0187857
Endopiriform_Nucleus	8.673728	8.832468	9.076942	8.609129	9.034075	9.221248	9.085433	8.777409	8.564168	8.782996	8.838738	9.183577	8.862797	8.948856	8.957865	8.81042	9.451472	9.084898	8.730793
entopeduncular_nucleus	0.2154504	0.2172485	0.2167775	0.2060597	0.2114391	0.2320715	0.2383541	0.2103624	0.2081538	0.2083803	0.227219	0.23893	0.2219058	0.2277593	0.2249681	0.2194463	0.2339902	0.2304305	0.212124
external_medullary_lamina	0.6439862	0.6544266	0.6708551	0.627033	0.6636246	0.6632701	0.6588597	0.648321	0.6248193	0.6571396	0.6392764	0.6374744	0.6551395	0.6455636	0.6643081	0.6416591	0.7005516	0.6694245	0.6458237
Fasciculus_retroflexus	0.2211476	0.2322048	0.2290362	0.2217508	0.2324407	0.2491902	0.2572399	0.2244067	0.2348317	0.2233296	0.2509527	0.2690047	0.2291707	0.235074	0.2285367	0.2304869	0.239825	0.2320258	0.2276625
fastigial_nucleus	1.0013969	1.0275492	1.0553906	0.962222	1.0415442	1.0580294	1.0424425	1.0352667	0.9733527	0.9949445	1.0038046	1.0746897	1.0242477	1.0460346	1.0399132	1.017724	1.0931479	1.0463253	1.0015872
Fimbria	4.616601	4.669561	4.829013	4.545612	4.832	4.808116	4.77375	4.694389	4.426344	4.558062	4.625127	4.855677	4.689443	4.772024	4.786159	4.640408	5.094818	4.894675	4.57439
flocculus	10.439282	10.356838	10.775883	10.053223	10.599999	10.733492	10.653422	10.575909	10.103813	10.243748	10.258696	10.68983	10.557668	10.738566	10.662365	10.448099	11.188585	10.834569	10.208737
Fornix	0.5553031	0.5875055	0.6176685	0.5513375	0.6169056	0.5798585	0.5547519	0.5857455	0.5274679	0.5510341	0.5473384	0.5709504	0.5775548	0.5622475	0.5885766	0.5641864	0.6269016	0.5836235	0.5596473
Fourth_ventricle	2.822457	2.740441	2.93282	2.766883	2.858546	2.796903	2.729103	2.901709	2.671004	2.753061	2.651672	2.718246	2.821269	2.82746	2.86547	2.767168	3.020087	2.938802	2.726779
Frontal_Association_Cortex	111.4225	110.9428	114.8713	108.037	116.0403	115.6756	113.1459	112.2616	106.3886	111.6176	110.0376	113.4876	113.0983	112.1547	116.2247	110.1556	120.8636	117.8011	108.5748
Globus_pallidus	4.35037	4.410823	4.569828	4.26402	4.516755	4.484646	4.442501	4.410445	4.124417	4.3224	4.310956	4.438013	4.442219	4.464716	4.526123	4.381191	4.801943	4.594784	4.327863
hindbrain_medulla_pons	92.90638	91.61116	96.09669	90.33969	94.02236	95.3427	93.67661	95.06929	90.34909	91.90447	90.8838	93.59253	93.16726	94.86467	94.62752	91.88126	99.43498	96.66811	90.54342
Hippocampal_layer_CA1	20.18726	20.51396	21.04266	19.96298	21.01812	20.96186	20.76477	20.48723	19.63804	20.15533	20.24921	20.86195	20.63707	20.69535	20.91907	20.21244	22.04666	21.32129	20.20757
Hippocampal_layer_CA2	2.220997	2.249563	2.291754	2.190341	2.288668	2.358391	2.352433	2.221288	2.212966	2.259299	2.284787	2.344529	2.252384	2.279084	2.267518	2.232295	2.391394	2.296332	2.230082
Hippocampal_layer_CA3	20.17381	20.40245	20.98742	19.92705	21.00977	20.66047	20.47656	20.47802	19.23735	20.04075	19.85513	20.52723	20.53839	20.57169	20.82966	20.05413	22.14535	21.34344	20.01714
hypothalamus	27.04676	27.47099	28.3388	26.71759	28.25327	27.98533	27.68579	27.49331	25.89704	26.9903	26.91091	27.87235	27.57454	27.67695	28.0559	27.13848	29.75504	28.50388	26.97302
Inferior_Colliculus	15.12084	15.04545	15.71164	14.5913	15.49698	15.398	15.3046	15.35895	14.53275	14.70572	14.85336	15.39739	15.31876	15.57096	15.4972	15.0737	16.32351	15.89561	14.77986
Infralimbic_Cortex	1.459198	1.490689	1.524371	1.481083	1.563078	1.503933	1.442832	1.503328	1.376775	1.430789	1.412556	1.505305	1.490449	1.49957	1.510976	1.44624	1.627885	1.598462	1.429705
Insular_Cortex	23.49319	23.89463	24.78275	23.15889	24.61111	24.21478	23.82583	24.02827	22.39337	23.41774	23.20171	23.97457	24.03725	24.04094	24.48883	23.66539	25.91764	24.91322	23.45757
Internal_capsule	7.700469	7.801755	8.016107	7.565981	7.971508	8.036359	8.013207	7.772633	7.479118	7.770861	7.794224	8.035131	7.846692	7.896841	7.979795	7.766745	8.435912	8.067837	7.734423
intersposed_nucleus	1.242144	1.229498	1.278847	1.209136	1.270716	1.247598	1.210551	1.270387	1.203304	1.251018	1.174275	1.208251	1.244384	1.26192	1.269684	1.234302	1.350187	1.306642	1.209314
intrabulbar_part_of_anterior_commisure	2.602815	2.639043	2.788145	2.497951	2.754437	2.7174	2.660475	2.649564	2.544888	2.616404	2.66091	2.674187	2.666698	2.571018	2.744975	2.600438	2.794293	2.677959	2.560221
Lateral_olfactory_tract	2.337425	2.31616	2.358189	2.306626	2.394551	2.457888	2.398008	2.315439	2.297147	2.396312	2.319462	2.408896	2.357276	2.411124	2.387199	2.324787	2.522575	2.481057	2.311257
lateral_septum	9.410612	9.515392	9.884662	9.230847	9.73733	9.672392	9.563088	9.550991	8.906894	9.324112	9.292031	9.529134	9.665094	9.631764	9.837162	9.502555	10.388002	9.963109	9.365024
Lateral_ventricle	13.4922	13.59665	13.98094	13.33916	13.94963	13.98652	13.80289	13.59495	13.07655	13.66646	13.42855	13.77094	13.7421	13.74285	13.91552	13.52082	14.71071	14.10467	13.53806
mamillary_bodies	1.594474	1.626419	1.639809	1.565132	1.637897	1.709836	1.722178	1.595672	1.604887	1.617966	1.676881	1.741499	1.629938	1.645717	1.633721	1.611434	1.718812	1.656497	1.605782
mammilothalamic_tract	0.3455684	0.345036	0.3506806	0.3386096	0.3607681	0.3521259	0.349763	0.3457721	0.3245889	0.333958	0.3369049	0.3495746	0.3463089	0.3531386	0.3500971	0.3359009	0.3798199	0.3693286	0.3333123
medial_septum	1.283508	1.316773	1.376984	1.266823	1.361244	1.318469	1.293176	1.337807	1.202119	1.247221	1.26512	1.319754	1.329452	1.309701	1.361396	1.297836	1.430843	1.370482	1.265605
median_preoptic_area	0.04914168	0.04970824	0.05284945	0.05085417	0.056158	0.0527614	0.0498904	0.05302217	0.05018445	0.05146038	0.04926724	0.05335433	0.04912542	0.05143134	0.04975178	0.04949082	0.05531695	0.05232517	0.0490857
midbrain	33.33902	33.61968	34.97695	32.76893	34.66524	34.11289	33.64122	33.92998	32.16327	32.94514	32.92362	33.8263	33.92841	34.04917	34.36575	33.24614	36.28761	35.17472	33.11701
Navicular_nuclear_basin_forebrain	1.685841	1.74425	1.78161	1.683564	1.773869	1.757065	1.701177	1.731967	1.608458	1.66787	1.652763	1.731468	1.73119	1.736675	1.75253	1.701302	1.86967	1.819067	1.683613
Nucleus_accumbens	6.858811	6.969522	7.198423	6.715265	7.083397	7.110935	7.053824	6.958774	6.547023	6.796668	6.834179	6.99443	7.066272	7.015157	7.18044	6.927245	7.548941	7.286391	6.83487
Occipital_Cortex	13.2457	13.00753	13.65504	12.78545	13.46396	13.33163	13.2203	13.40053	12.72851	12.90819	12.86322	13.23787	13.34901	13.52151	13.48715	13.13063	14.18543	13.7861	12.86487
Olfactory_Bulb	136.2583	134.8943	135.1205	149.2488	131.8703	129.9357	127.9758	142.6922	137.8467	132.8195	134.93	129.386	135.7023	142.8428	132.8774	137.7363	144.5507	149.7976	139.9193
Olfactory_tubercle	11.65999	11.89327	12.23369	11.50164	12.11582	12.21322	12.02607	11.86052	11.217	11.56179	11.67093	12.08514	11.98755	11.99863	12.15822	11.78846	12.84307	12.42869	11.60815
Optic_Chiasm	0.2501834	0.2511075	0.260295	0.2605157	0.2730917	0.2596135	0.2435766	0.2582574	0.2414117	0.2478838	0.2382338	0.2594118	0.2499568	0.2615934	0.2528486	0.2473683	0.2784253	0.2703801	0.2432265
Optic_tract	2.892751	2.938537	3.033631	2.89854	3.062844	3.010026	2.949978	2.953317	2.825819	2.910125	2.878027	2.99959	2.920624	2.954628	2.958213	2.887824	3.164391	3.040591	2.888759
Orbitofrontal_Cortex	0.437924	0.4376046	0.4379765	0.4373722	0.4454842	0.4671736	0.4566461	0.4318133	0.4431988	0.4619708	0.4448516	0.4530907	0.4454223	0.4500274	0.4448756	0.4397455	0.4662334	0.4591753	0.4461372
parafloccullus	11.89474	11.64374	12.2026	11.47587	11.93088	12.04716	11.91706	12.09543	11.37462	11.68078	11.47935	11.8961	11.99358	12.13141	12.13381	11.80094	12.73428	12.38694	11.56962
paramedian_lobe	7.709275	7.661239	7.986939	7.487161	7.747837	7.941251	7.78593	7.953999	7.443788	7.624917	7.528608	7.805043	7.758156	7.95019	7.932073	7.631854	8.342866	8.1318	7.518852
Parietal_Association_Cortex	10.671253	10.761835	11.065377	10.571063	11.090235	10.9337	10.848489	10.823044	10.163095	10.637596	10.530955	10.914805	10.827414	10.897877	11.020067	10.622622	11.717974	11.286897	10.599419
Periaqueductal_grey	10.006058	9.874388	10.357374	9.753577	10.199067	10.002549	9.979392	10.12974	9.430574	9.707144	9.705526	9.966233	10.142809	10.220132	10.262304	9.871981	10.856891	10.627044	9.789934
Piriform_Cortex	26.54258	26.93078	27.69116	26.17962	27.59629	27.74587	27.44745	26.88647	25.66641	26.49469	26.68788	27.70273	27.11306	27.29985	27.51272	26.77487	29.1209	27.98926	26.48674
pons	21.63988	21.58122	22.59057	21.03028	22.20809	22.07434	21.83188	21.92315	20.91259	21.26833	21.34264	21.86162	21.96139	22.20207	22.19218	21.57569	23.38342	22.76223	21.34081
posterior_commisure	0.2057705	0.1987808	0.2059928	0.1969255	0.2046156	0.1956674	0.197647	0.2058603	0.1823876	0.1916385	0.1912711	0.1946686	0.2104243	0.2109394	0.2173794	0.201192	0.2264569	0.2244006	0.1969205
Posterior_part_of_anterior_commissure	0.3121295	0.3051848	0.3162388	0.3048391	0.3112211	0.3129388	0.3118496	0.3091804	0.2916338	0.3081153	0.3012234	0.3101185	0.3139508	0.3169204	0.3188139	0.3091576	0.341285	0.3310472	0.3046036
Prelimbic_Cortex	3.871732	3.908966	3.98346	3.776622	3.981824	4.039982	4.002502	3.896107	3.70406	3.851125	3.880417	3.97905	3.974823	3.926623	4.033262	3.86868	4.20943	4.108736	3.844474
Primary_Motor_Cortex	18.97391	19.19388	19.75354	18.64971	19.69683	19.50363	19.18666	19.29335	17.90786	18.75729	18.61624	19.23508	19.43462	19.34827	19.76422	18.96074	20.89783	20.28391	18.77074
Primary_Somatosensory_Cortex	79.10645	80.28032	82.88657	78.00961	82.47723	82.16793	81.0199	80.38896	75.9875	78.971	78.73858	81.54659	80.79795	81.13659	82.13224	79.65119	86.96949	83.62224	78.92066
Primary_Visual_Cortex	25.35986	25.38021	26.40254	24.73778	26.10383	25.97903	25.75415	25.66104	24.53566	25.00662	25.09807	25.74337	25.72333	25.9417	26.03572	25.26908	27.42908	26.65588	25.05545
Retrosplenial_Cortex	30.50373	30.48205	31.62455	29.83096	31.27351	31.31878	31.07208	30.73949	29.48107	30.33406	30.25314	30.9104	30.95892	31.15159	31.32874	30.40781	33.0489	32.0257	30.25213
rhinal_cortex	45.90086	46.1246	47.90503	44.90182	47.39046	47.14838	46.72902	46.51755	44.31042	45.35313	45.49957	46.78585	46.6888	47.01534	47.25398	45.79788	49.89855	48.42374	45.50061
Secondary_Motor_Cortex	11.5809	11.83816	12.22304	11.38389	12.0944	12.02377	11.89124	11.82306	11.12073	11.63053	11.60834	11.84407	11.96362	11.71003	12.13709	11.71333	12.68234	12.16858	11.68057
Secondary_Somatosensory_Cortex	21.00892	21.24523	21.97968	20.64733	21.85396	21.60561	21.34509	21.32268	19.99133	20.97188	20.72893	21.42543	21.39325	21.50103	21.78641	21.07403	23.15671	22.1884	20.93697
Secondary_Visual_Cortex	30.54767	30.61199	31.83425	29.99958	31.54091	31.27078	30.90404	30.94724	29.52897	30.31777	30.15531	30.92762	31.03742	31.14991	31.34762	30.41193	33.12863	32.12142	30.30462
Simple_Lobule	16.32013	16.20842	16.92691	15.76295	16.61005	16.73578	16.53114	16.69563	15.71717	16.02557	15.93	16.60319	16.47206	16.78631	16.69542	16.27037	17.55672	17.02939	15.94051
stria_medullaris_thalamus	0.6059552	0.6457276	0.6717402	0.5950143	0.6616081	0.6255136	0.6123197	0.6379466	0.5714898	0.5930775	0.6063082	0.6341639	0.6196368	0.6185454	0.6402978	0.6181019	0.6842723	0.646819	0.6095015
Stria_terminalis	2.466181	2.52138	2.577602	2.433101	2.589201	2.591538	2.583887	2.513283	2.39762	2.429505	2.520019	2.666756	2.518167	2.548967	2.561134	2.484702	2.707098	2.603237	2.446387
Subfornical_organ	0.07372005	0.0731142	0.07496086	0.0717602	0.0718322	0.07446445	0.07746064	0.07400943	0.06703136	0.07100843	0.07371129	0.07866028	0.0774361	0.07779653	0.08010773	0.07460347	0.08255866	0.08188724	0.07209447
subicular_region	24.80958	24.84603	25.92921	24.29105	25.57677	25.41245	25.12131	25.15006	24.04595	24.57243	24.52852	25.09871	25.16679	25.32439	25.43371	24.71529	26.83959	26.12058	24.59572
substantia_nigra	2.245061	2.258854	2.334366	2.189983	2.309597	2.235107	2.214709	2.279857	2.075824	2.178218	2.144624	2.17835	2.298999	2.282455	2.351443	2.216351	2.485919	2.435781	2.209833
Superior_Colliculus	15.7962	15.88727	16.53206	15.38953	16.28196	16.26215	16.07257	15.97921	15.38207	15.72922	15.71423	16.03371	16.04263	16.14873	16.22656	15.7913	17.13093	16.59129	15.70398
Temporal_Association	11.042659	11.080613	11.608687	10.854418	11.4886	11.196396	10.964588	11.257025	10.617506	10.911752	10.762212	10.999549	11.188654	11.193386	11.30266	10.952713	11.955692	11.597679	10.917862
Thalamus	47.4872	48.10342	49.37019	46.88505	49.34181	49.23949	48.90593	48.08824	45.81068	47.57734	47.54331	49.13936	48.43383	48.54528	49.15957	47.56613	52.02242	49.98499	47.44927
Third_ventricle	4.431963	4.449441	4.583024	4.368647	4.543478	4.67676	4.668151	4.436827	4.336073	4.45968	4.515762	4.647899	4.527639	4.559037	4.575393	4.475072	4.859308	4.661498	4.446592
trochlear_nerve	0.07804491	0.08210972	0.08575314	0.07410948	0.08589348	0.08123347	0.07977976	0.08237389	0.07363419	0.07657761	0.07486922	0.07635777	0.08014134	0.08327822	0.08400918	0.08013138	0.08927818	0.08556139	0.07538303
ventral_pallidum	2.46496	2.52445	2.608312	2.436	2.572177	2.572383	2.53514	2.518342	2.351524	2.39768	2.464929	2.575156	2.518168	2.549323	2.571648	2.496353	2.728306	2.624363	2.429371
brainvolumes	1407.441	1411.006	1458.327	1394.715	1443.824	1441.647	1421.771	1433.645	1363.288	1397.074	1392.838	1426.608	1427.025	1441.405	1444.352	1407.05	1527.159	1487.323	1397.221

	69	75	85	111	112	115	3	5	58	66	67	76	78	79	83	84	104	106	110
	Het	Het	Het	Het	Het	Het	WT	WT	WT	WT	WT	WT	WT	WT	WT	WT	WT	WT	WT
Absolute Volume	M	M	M	M	M	M	F	F	F	F	F	F	F	F	F	F	F	F	F
	Mat	Mat	Mat	Mat	Mat	Mat	Mat	Mat	Mat	Mat	Mat	Mat	Mat	Mat	Mat	Mat	Mat	Mat	Mat
amygdaloid_area	29.36504	31.99945	30.86809	33.3316	29.27442	31.11734	29.3747	29.83585	31.49435	35.3881	29.59433	30.69104	28.64941	28.25286	30.68501	30.51821	30.23532	31.44342	40.672
Anterior_part_of_anterior_commissure	1.310151	1.439037	1.389704	1.501569	1.306293	1.388557	1.343863	1.337771	1.434894	1.557645	1.2933	1.403232	1.238829	1.226027	1.395343	1.374945	1.358035	1.408683	1.863452
Aqueduct	1.639193	1.729727	1.664805	1.782026	1.62616	1.688633	1.602239	1.605215	1.687477	1.96486	1.65467	1.678715	1.636553	1.65403	1.664701	1.681757	1.686709	1.736412	2.207933
auditory_cortex	20.51212	22.11815	21.39338	23.12971	20.42638	21.65961	20.42196	20.75052	21.74344	24.92343	20.747	21.32649	20.319	20.01018	21.25498	21.16941	21.01075	21.86046	28.31949
basal_forebrain	16.76486	18.18561	17.4846	18.9412	16.77716	17.69084	16.99411	17.05546	18.03106	19.85537	17.0494	17.57068	16.62796	16.48363	17.33758	17.42889	17.40258	18.07363	22.95897
Bed_nucleus_of_stria_terminalis	2.861262	3.103496	2.998735	3.233081	2.834552	3.040088	2.895179	2.968876	3.159481	3.500791	2.86145	3.043061	2.643213	2.542583	2.98817	3.000478	2.940598	3.068223	3.931343
caudaputamen	45.28208	49.25691	47.26521	51.29494	45.24008	47.89473	45.88682	46.13758	48.65316	53.74956	45.97155	47.51251	44.78804	44.3558	46.95639	47.134	47.01017	48.80467	62.25121
cerebellar_lobule_1_2	8.035818	8.630971	8.406809	9.070658	8.074534	8.500879	7.920155	8.122082	8.507312	9.645301	8.082261	8.424351	7.763547	7.755429	8.35111	8.356537	8.336066	8.642341	11.222019
cerebellar_lobule_10	3.494792	3.633889	3.517992	3.838034	3.384537	3.540553	3.310679	3.410398	3.635044	4.058582	3.412976	3.560567	3.238229	3.286353	3.502779	3.488538	3.524534	3.657204	4.643854
cerebellar_lobule_3	7.01655	7.530006	7.285458	7.962887	6.976151	7.366691	6.837206	7.073204	7.41355	8.400004	6.963775	7.364159	6.597162	6.631554	7.259725	7.251045	7.262428	7.51651	9.779512
cerebellar_lobule_4_5	21.7702	22.94136	22.18646	24.22487	21.53592	22.45093	21.10936	21.66697	22.79922	25.5506	21.72428	22.4857	21.04497	21.02315	22.14973	22.18574	22.30686	23.16016	29.64958
cerebellar_lobule_6	8.79255	9.131588	8.827501	9.677406	8.437576	9.022252	8.437701	8.731064	9.25964	10.179186	8.623188	8.917691	8.386834	8.377501	8.758109	8.784396	8.902728	9.163693	11.699655
cerebellar_lobule_7	3.366507	3.469532	3.357668	3.658903	3.192635	3.446352	3.289128	3.382251	3.556777	3.925932	3.344241	3.376116	3.257732	3.258575	3.326424	3.347103	3.419625	3.469499	4.400536
cerebellar_lobule_8	3.815621	3.944205	3.824629	4.209739	3.626244	3.910923	3.640984	3.772268	4.020051	4.392777	3.728806	3.859097	3.637959	3.651709	3.773449	3.78389	3.847125	3.976863	5.110373
cerebellar_lobule_9	8.840977	9.163294	8.865039	9.731697	8.443229	9.084332	8.505257	8.805097	9.3237	10.177274	8.672377	8.970541	8.504631	8.505785	8.781317	8.818492	8.963158	9.20491	11.807365
Cerebellar_White_Matter_Arbor_vita_of_cerebellum	27.38794	28.92025	28.00128	30.53822	26.87718	28.34388	26.64828	27.32056	28.9461	32.13313	27.05857	28.23961	25.94534	25.98526	27.90388	27.96138	28.07008	28.96104	37.24394
cerebral_peduncle	2.900587	3.133857	3.008964	3.252918	2.862044	3.064851	2.881566	2.93098	3.061595	3.544539	2.911877	3.006087	2.804446	2.765855	2.996371	2.985813	2.96485	3.068935	3.945662
Cingulate_Cortex_area_1	15.04204	16.42793	15.62057	17.0537	14.91114	15.86055	15.32144	15.15064	16.01557	17.81726	15.30111	15.75853	15.10399	15.00473	15.53312	15.63122	15.59509	16.23496	20.80841
Cingulate_Cortex_area_2	9.343253	10.096342	9.665646	10.504642	9.26253	9.782749	9.468973	9.458668	9.958737	10.996335	9.527175	9.76089	9.392109	9.310844	9.575878	9.665692	9.640447	10.031972	12.768912
cingulum	3.2646	3.556385	3.442398	3.723059	3.249264	3.465954	3.287165	3.343433	3.504564	3.941647	3.278511	3.447629	3.15458	3.114522	3.42241	3.401238	3.364098	3.507676	4.570593
Cochlear_nucleus	1.0763526	1.1806758	1.13582	1.2316517	1.0589946	1.1323082	1.0516194	1.084478	1.1504727	1.2668602	1.0357436	1.146638	0.9512157	0.9733474	1.1308448	1.1237281	1.1160492	1.1413151	1.5163771
Commisure_inferior_Colliculus	0.3115525	0.3120584	0.3017305	0.3207674	0.3162072	0.3066517	0.3104962	0.2993993	0.3114903	0.3645883	0.3288767	0.3066685	0.3529961	0.3487003	0.3057334	0.312194	0.3168967	0.3292861	0.4055134
commisure_superior_collicuus	0.1853142	0.1977118	0.1945874	0.2055431	0.1802526	0.1947908	0.1883514	0.1888405	0.197984	0.2270596	0.1859516	0.1936985	0.1769223	0.1744768	0.191019	0.1911627	0.1882742	0.1946178	0.2537798
copula	2.811155	2.959113	2.867792	3.150819	2.714898	2.957627	2.770687	2.863064	3.014415	3.301169	2.784049	2.868119	2.700441	2.661091	2.835253	2.852315	2.884765	2.942173	3.795467
Corpus_Callosum_associated_White_Matter	41.39135	44.75515	42.97245	46.56999	41.15365	43.63132	41.47561	41.91694	43.86862	49.60926	41.95871	43.07249	40.88853	40.41077	42.69973	42.76212	42.6179	44.2771	56.6401
Crus_1_ansiform_lobule	16.95395	17.86238	17.2569	18.92133	16.61513	17.57244	16.54072	16.96397	17.97405	19.86895	16.77952	17.39752	16.17132	16.04635	17.18168	17.24752	17.33455	17.88971	22.9655
Crus_2_ansiform_lobule	9.97868	10.475708	10.121612	11.105501	9.558154	10.381444	9.734957	10.008943	10.651658	11.559209	9.710766	10.234412	9.351444	9.414832	10.059158	10.106854	10.19975	10.397398	13.533201
dentate_gyrus	16.12758	17.48236	16.90675	18.31775	16.0975	17.15095	16.05997	16.33839	17.15822	19.58041	16.24112	16.87033	15.8548	15.59837	16.81379	16.73701	16.55796	17.21746	22.58475
Dentate_nucleus	0.8539686	0.9315065	0.8994843	0.9785406	0.8387715	0.8969226	0.829765	0.8614068	0.9062789	1.0260057	0.8242011	0.9044271	0.7480106	0.7600565	0.896989	0.884263	0.8848307	0.9026483	1.1945528
Dorsal_Peduncular_Cortex	1.511416	1.655785	1.5628	1.717802	1.467817	1.605701	1.507558	1.532865	1.596336	1.781912	1.500383	1.583197	1.449116	1.425913	1.551528	1.561356	1.549402	1.612422	2.077324
Dorsal_Tenia_Tecta	1.0505394	1.1384094	1.0979858	1.1864609	1.0209057	1.0915718	1.0567956	1.070349	1.1274131	1.249508	1.0344623	1.1147333	0.9801948	0.9738083	1.084407	1.0867219	1.0674409	1.1145822	1.4512287
Endopiriform_Nucleus	8.692999	9.36298	8.98872	9.745975	8.705521	9.100781	8.826176	8.816598	9.286748	10.265777	8.942306	9.035019	8.88239	8.805555	8.938531	9.0023	9.02181	9.380074	11.879814
entopeduncular_nucleus	0.2262403	0.2319209	0.2257807	0.244226	0.2166935	0.2269197	0.2141168	0.2251997	0.2281053	0.2653869	0.2309506	0.2290217	0.2346241	0.2353124	0.2244712	0.2185408	0.2247601	0.2388658	0.3054677
external_medullary_lamina	0.6462481	0.6993864	0.6641851	0.7203818	0.6374693	0.6791344	0.6461388	0.6504998	0.6825246	0.79868	0.6476235	0.666827	0.6116977	0.6088832	0.6626131	0.6692573	0.6623941	0.6815169	0.8642994
Fasciculus_retroflexus	0.2315547	0.2408813	0.2309469	0.2509697	0.2304995	0.2320684	0.2246458	0.2234492	0.2339317	0.2660521	0.2463203	0.2290143	0.2660924	0.2686563	0.2286386	0.2258755	0.2337073	0.2464347	0.3014939
fastigial_nucleus	1.0519836	1.0942527	1.0646398	1.1417597	1.0275944	1.0536229	1.0074088	1.0250754	1.0865648	1.1828164	1.0367373	1.0668159	1.016699	1.0232897	1.0587516	1.053716	1.0621055	1.098398	1.3924753
Fimbria	4.645194	5.035123	4.868362	5.25695	4.635136	4.868165	4.623845	4.698198	4.963275	5.518831	4.691058	4.834464	4.581013	4.561729	4.830919	4.787959	4.780752	4.977778	6.380076
flocculus	10.625978	11.214977	10.896967	11.837117	10.549196	10.983225	10.292133	10.585477	11.074114	12.55525	10.672058	10.99783	10.338255	10.408054	10.857223	10.852634	10.918125	11.353607	14.519011
Fornix	0.5574505	0.6188716	0.5837049	0.630896	0.5601448	0.6068788	0.5788017	0.555778	0.5996299	0.6502581	0.5636	0.5860716	0.5466513	0.5465837	0.5880326	0.5987476	0.5898877	0.6055148	0.7878758
Fourth_ventricle	2.823775	3.041795	2.955867	3.239324	2.79145	2.993886	2.78307	2.876779	3.041046	3.362911	2.792746	2.957071	2.646048	2.613245	2.929227	2.935071	2.921871	3.014795	3.968985
Frontal_Association_Cortex	110.8704	122.4139	114.056	127.3763	109.4	118.2922	112.2217	111.419	118.373	133.7568	113.8063	116.6273	111.7594	111.7753	114.8687	115.7108	115.8958	121.8495	153.6205
Globus_pallidus	4.354002	4.739624	4.556849	4.929414	4.344127	4.637095	4.396498	4.454139	4.677433	5.219872	4.406527	4.592334	4.236801	4.182633	4.533769	4.533276	4.515706	4.690493	6.002336
hindbrain_medulla_pons	95.0362	99.98035	96.85861	105.43863	92.62714	98.37119	92.31071	94.84897	100.10867	111.8304	93.9276	97.90702	90.97916	91.19901	96.33991	96.54006	97.07592	99.95813	129.11214
Hippocampal_layer_CA1	20.33884	21.92177	21.25278	22.97844	20.29659	21.51699	20.19504	20.5438	21.52025	24.73009	20.55377	21.17979	20.14891	19.84432	21.07456	20.99697	20.82538	21.67082	28.25359
Hippocampal_layer_CA2	2.220178	2.374463	2.299936	2.47129	2.214683	2.313081	2.225687	2.239664	2.336782	2.686286	2.292047	2.280699	2.28044	2.265422	2.28347	2.281046	2.282714	2.378171	2.988682
Hippocampal_layer_CA3	20.17901	21.95826	21.25349	22.99286	20.087	21.43468	20.09931	20.48476	21.57503	24.53638	20.26418	21.0967	19.54639	19.29104	21.09919	20.9351	20.69492	21.5281	28.04142
hypothalamus	27.04513	29.4379	28.38995	30.6372	27.0154	28.67281	27.16132	27.46135	28.97664	32.43626	27.38316	28.26898	26.58229	26.24858	28.23098	28.13307	27.92223	29.02533	37.4455
Inferior_Colliculus	15.31023	16.4303	15.9393	17.15208	15.24643	16.07728	14.94284	15.35455	16.0787	18.46207	15.32585	16.02621	14.9244	14.88875	15.80715	15.8087	15.75265	16.33606	21.24468
Inframimbic_Cortex	1.447004	1.619713	1.53378	1.676869	1.450386	1.557104	1.510511	1.476767	1.569629	1.724122	1.443339	1.550729	1.423902	1.407936	1.544327	1.53793	1.515589	1.570941	2.102529
Insular_Cortex	23.57387	25.7989	24.6575	26.84482	23.46111	25.07331	23.86603	23.97519	25.38624	27.96432	23.73342	24.74769	22.92155	22.63982	24.47266	24.62718	24.46825	25.3596	32.51772
Internal_capsule	7.732718	8.373266	8.051582	8.699975	7.70472	8.134112	7.721437	7.822704	8.23589	9.259369	7.851622	8.010229	7.667835	7.570106	8.002888	7.962207	7.966407	8.270085	10.499015
intersposed_nucleus	1.250849	1.352542	1.303185	1.406374	1.242759	1.298062	1.240189	1.26342	1.334848	1.498196	1.230087	1.309815	1.117674	1.121571	1.314321	1.301895	1.287295	1.307593	1.710796
intrabulbar_part_of_anterior_commisure	2.543245	2.83457	2.591386	2.979277	2.559075	2.856125	2.618302	2.51603	2.712454	3.085933	2.725153	2.670345	2.792304	2.780077	2.647323	2.713363	2.740395	2.897664	3.493332
Lateral_olfactory_tract	2.323489	2.518559	2.404566	2.624325	2.303649	2.415711	2.369259	2.368933	2.510725	2.787069	2.366858	2.452681	2.304541	2.295159	2.401752	2.407985	2.394035	2.511161	3.192409
lateral_septum	9.421201	10.27837	9.873141	10.734443	9.391104	10.052496	9.538135	9.642917	10.150632	11.240084	9.513486	9.931373	9.114855	8.995411	9.809203	9.829134	9.804162	10.155515	13.044872
Lateral_ventricle	13.41308	14.54674	14.01996	15.16999	13.42606	14.18432	13.53985	13.71636	14.42465	16.17085	13.64092	14.03381	13.22416	12.99946	13.97075	13.96951	13.83994	14.40534	18.58171
mamillary_bodies	1.618556	1.712189	1.641562	1.781153	1.608346	1.663494	1.59858	1.618383	1.673655	1.940566	1.672311	1.641266	1.691289	1.685733	1.633584	1.626968	1.643611	1.722578	2.134109
mammilothalamic_tract	0.3408453	0.3707686	0.3623458	0.3877991	0.3362781	0.3598498	0.3404431	0.3466165	0.365518	0.4225736	0.3455877	0.3590857	0.3299758	0.3291494	0.3629582	0.3527038	0.3491675	0.3663104	0.4911062
medial_septum	1.292999	1.424587	1.348116	1.480455	1.293052	1.407484	1.316833	1.305419	1.372867	1.514979	1.298254	1.363024	1.26987	1.257296	1.354114	1.360759	1.365653	1.399511	1.817288
median_preoptic_area	0.04702285	0.05316941	0.05280411	0.05710409	0.04935533	0.05079755	0.04979956	0.04822823	0.05385474	0.05294886	0.04783107	0.05001697	0.04783629	0.04757918	0.05202883	0.05200521	0.05051473	0.05199439	0.07090475
midbrain	33.42666	36.33417	35.19187	38.01682	33.49687	35.64035	33.30315	33.88937	35.5839	40.86227	33.54624	35.14291	32.70418	32.06202	34.8407	34.88976	34.41497	35.71435	46.90024
Navicular_nuclear_basin_forebrain	1.714744	1.8785	1.789427	1.946354	1.687098	1.81518	1.750401	1.736767	1.824468	2.005508	1.720882	1.803212	1.686353	1.669076	1.766689	1.806579	1.764586	1.83341	2.36087
Nucleus_accumbens	6.951977	7.591947	7.190057	7.888995	6.852038	7.3579	7.013176	7.025421	7.342246	8.186391	7.038136	7.266539	6.8254	6.808265	7.13238	7.20583	7.19884	7.462948	9.504874
Occipital_Cortex	13.26457	14.22465	13.88316	14.92099	13.27355	14.02448	12.98552	13.36846	13.9736	16.05328	13.31429	13.89455	12.87146	12.80898	13.73122	13.76603	13.69941	14.22554	18.53184
Olfactory_Bulb	138.6629	144.1643	144.8952	142.1175	140.0448	137.2112	142.0169	149.3399	137.5954	168.848	129.8301	136.9194	128.1504	126.927	142.1974	133.5835	134.9553	132.6176	216.0959
Olfactory_tubercle	11.79524	12.8378	12.20801	13.34828	11.67344	12.4345	11.97837	11.91494	12.49848	13.8735	11.97117	12.33693	11.76255	11.72437	12.12415	12.239	12.2213	12.70564	16.26415
Optic_Chiasm	0.240362	0.2672785	0.2638636	0.2810918	0.248958	0.2598016	0.2540421	0.2495577	0.2756774	0.2925345	0.2421059	0.2644662	0.2353523	0.2312718	0.2672195	0.2613656	0.2551304	0.2651001	0.370514
Optic_tract	2.868347	3.121831	3.022146	3.262121	2.886529	3.036443	2.906335	2.921045	3.100568	3.455203	2.918573	3.000855	2.867586	2.823225	3.003482	3.000533	2.976674	3.08833	3.984702
Orbitofrontal_Cortex	0.4378208	0.4674878	0.4479625	0.4885776	0.4308809	0.4529186	0.446537	0.4432742	0.472548	0.5222444	0.4530668	0.4545915	0.448893	0.4384641	0.4472931	0.452278	0.4447371	0.4654259	0.6013274
paraflocculus	12.12598	12.83291	12.44524	13.61121	11.93286	12.55627	11.71279	12.10168	12.74153	14.33555	12.00148	12.54847	11.45935	11.45196	12.38062	12.34309	12.38935	12.85185	16.63944
paramedian_lobe	8.051588	8.42823	8.1393	8.914035	7.742458	8.26384	7.6961	7.972766	8.506301	9.340695	7.793238	8.246467	7.437248	7.493651	8.077522	8.071228	8.144069	8.385112	10.79347
Parietal_Association_Cortex	10.652564	11.61254	11.234831	12.119627	10.605415	11.292497	10.637265	10.843513	11.436633	12.90297	10.718931	11.149096	10.371074	10.204555	11.152376	11.035767	10.940307	11.388647	14.762641
Periaqueductal_grey	10.04044	10.896684	10.584973	11.46155	9.994128	10.704983	9.859903	10.224035	10.687296	12.329233	9.978056	10.605481	9.651268	9.411661	10.426409	10.391655	10.277269	10.684817	14.12034
Piriform_Cortex	26.65726	28.88294	27.76369	30.093	26.59141	28.09288	26.82664	27.02638	28.4325	31.66955	27.12899	27.81273	26.61541	26.36367	27.5786	27.58588	27.55594	28.67934	36.6412
pons	21.70568	23.57525	22.82724	24.524	21.76831	23.0295	21.54586	21.96456	23.02292	26.55233	21.77422	22.87373	21.17945	20.84296	22.58504	22.61156	22.41772	23.20717	30.45146
posterior_commisure	0.2079943	0.2283591	0.2247831	0.2462272	0.2069417	0.2288734	0.1958911	0.2113715	0.2242236	0.261472	0.2020913	0.2248939	0.1845932	0.1796878	0.2211822	0.2168113	0.2133321	0.2206676	0.3078151
Posterior_part_of_anterior_commissure	0.3089842	0.3357685	0.3267708	0.3516561	0.3056879	0.326776	0.308605	0.3212555	0.337964	0.3737679	0.3073493	0.3281697	0.2871724	0.2801523	0.325289	0.3180749	0.3151718	0.3312403	0.4292245
Prelimbic_Cortex	3.919694	4.297657	4.028904	4.44751	3.842836	4.107316	3.96406	3.919499	4.099376	4.616015	3.964044	4.05461	3.925798	3.921547	3.991681	4.021508	4.037544	4.216761	5.327171
Primary_Motor_Cortex	19.07823	20.9814	19.9416	21.78309	18.8503	20.26252	19.3074	19.33177	20.36718	22.58975	19.12629	20.09378	18.57798	18.37	19.8	19.86994	19.73681	20.51826	26.52145
Primary_Somatosensory_Cortex	79.31316	86.37452	82.79527	89.89906	79.02687	83.93417	80.15796	80.57259	84.98409	94.279	80.24526	83.05872	78.06912	77.29053	82.25647	82.50209	82.1411	85.33051	109.26959
Primary_Visual_Cortex	25.46822	27.539	26.64138	28.71589	25.43177	26.96877	25.28138	25.72596	26.96863	31.08391	25.62718	26.69856	24.9348	24.60738	26.38434	26.40566	26.18935	27.1644	35.3708
Retrosplenial_Cortex	30.5576	33.04432	31.95066	34.45868	30.48543	32.30779	30.38082	31.00935	32.42072	37.27228	30.79155	31.98684	29.84906	29.40963	31.67762	31.62694	31.40689	32.61445	42.26962
rhinal_cortex	46.15538	49.96274	48.35357	52.13486	46.08105	48.87995	45.84719	46.66821	48.93894	56.28999	46.44077	48.37971	45.2222	44.57837	47.91326	47.87845	47.45036	49.23972	64.32109
Secondary_Motor_Cortex	11.69085	12.77944	12.06402	13.27047	11.57975	12.40721	11.85276	11.80414	12.40232	13.82703	11.87556	12.11692	11.71089	11.50474	11.9643	12.14477	12.10879	12.59063	15.96262
Secondary_Somatosensory_Cortex	21.02413	22.91479	22.03662	23.8218	20.93015	22.25658	21.13799	21.40592	22.65578	25.08206	21.14752	22.05805	20.27779	20.04082	21.91078	21.87839	21.69261	22.54561	28.93917
Secondary_Visual_Cortex	30.57037	33.12203	32.08156	34.62676	30.54881	32.46793	30.44619	31.04005	32.53453	37.43089	30.76175	32.08328	29.9217	29.37263	31.80594	31.789	31.43629	32.64188	42.71821
Simple_Lobule	16.72725	17.66275	17.11508	18.66915	16.47082	17.25344	16.17015	16.61296	17.54481	19.61367	16.59853	17.26475	15.98717	16.07294	17.03408	17.02994	17.11728	17.76182	22.88531
stria_medullaris_thalamus	0.6172151	0.682454	0.6415357	0.6993518	0.6127504	0.6592005	0.623601	0.6235104	0.6614666	0.723751	0.6200375	0.6363427	0.5985243	0.6045453	0.6377931	0.6436616	0.6393226	0.6591691	0.837857
Stria_terminalis	2.493827	2.691811	2.590326	2.798437	2.495956	2.612277	2.474563	2.503333	2.626509	2.967084	2.549756	2.576905	2.561129	2.543355	2.578659	2.565218	2.561647	2.672227	3.422452
Subfornical_organ	0.07470985	0.08434903	0.07967764	0.08869246	0.07559434	0.07853654	0.07240461	0.07824039	0.08183857	0.0917341	0.07490167	0.08047927	0.07310949	0.07177738	0.08025606	0.07790802	0.07968636	0.08105549	0.09845568
subicular_region	24.85635	26.90547	26.04717	28.08497	24.85733	26.38167	24.79473	25.21481	26.39701	30.43549	24.98077	26.10806	24.35582	23.86217	25.76	25.84498	25.54682	26.49698	34.53337
substantia_nigra	2.274087	2.477323	2.406894	2.623033	2.23297	2.443116	2.214622	2.310905	2.416151	2.808202	2.225285	2.409086	2.064949	2.029911	2.385086	2.359918	2.306678	2.390769	3.245227
Superior_Colliculus	15.82067	17.18353	16.57397	17.83465	15.86194	16.78974	15.84516	16.0451	16.78718	19.41151	15.92198	16.62377	15.43988	15.20984	16.43263	16.4848	16.33008	16.88652	21.86506
Temporal_Association	10.982389	11.9937	11.591699	12.513295	11.020489	11.768246	11.024857	11.185256	11.755289	13.454506	11.001601	11.608409	10.664275	10.429212	11.487551	11.545651	11.374646	11.747771	15.495447
Thalamus	47.60155	51.60754	49.77464	53.79772	47.43012	50.25548	47.4952	48.26087	50.68953	57.43265	48.20018	49.49716	47.0002	46.3691	49.48946	49.16156	48.86726	50.90635	65.57421
Third_ventricle	4.43419	4.774519	4.613577	5.003445	4.441808	4.659479	4.448633	4.553659	4.713575	5.377335	4.546968	4.630761	4.491916	4.442844	4.600253	4.549462	4.572153	4.779176	6.107715
trochlear_nerve	0.08221831	0.09001292	0.08417616	0.09149263	0.08091456	0.08552138	0.0817867	0.07940367	0.08551076	0.09947601	0.07764158	0.08791886	0.07077685	0.07449278	0.08566161	0.08796327	0.08750501	0.08684254	0.10907855
ventral_pallidum	2.484669	2.709252	2.599673	2.821428	2.478207	2.628369	2.522107	2.521945	2.655251	2.914777	2.529854	2.599059	2.478456	2.482553	2.562702	2.581865	2.584249	2.681791	3.405658
brainvolumes	1418.258	1526.602	1473.769	1587.029	1409.329	1486.291	1416.743	1441.574	1498.638	1701.388	1418.083	1472.316	1380.86	1368.889	1463.585	1456.687	1453.816	1502.202	1980.076

	113	114	1	4	59	60	63	68	71	73	74	77	80	81	82	15	20	25	26
	WT	WT	WT	WT	WT	WT	WT	WT	WT	WT	WT	WT	WT	WT	WT	Het	Het	Het	Het
Absolute Volume	F	F	M	M	M	M	M	M	M	M	M	M	M	M	M	F	F	F	F
	Mat	Mat	Mat	Mat	Mat	Mat	Mat	Mat	Mat	Mat	Mat	Mat	Mat	Mat	Mat	Pat	Pat	Pat	Pat
amygdaloid_area	32.66211	29.90887	32.68524	32.30904	30.8699	29.29585	29.95299	30.04039	30.82854	31.20427	30.66683	29.15662	29.93522	34.2369	30.82439	29.75405	29.59462	29.98781	30.58363
Anterior_part_of_anterior_commissure	1.462977	1.359874	1.48861	1.466246	1.390974	1.325452	1.32864	1.34048	1.345226	1.409974	1.398321	1.346687	1.336017	1.560494	1.413533	1.343131	1.325743	1.332273	1.373625
Aqueduct	1.762667	1.640885	1.761519	1.770368	1.655036	1.572746	1.672201	1.606534	1.676625	1.690246	1.659581	1.562274	1.663705	1.938459	1.661358	1.635251	1.607936	1.658872	1.668385
auditory_cortex	22.70194	20.75002	22.49792	22.43132	21.43899	20.30754	20.95147	20.80491	21.5136	21.68208	21.26272	20.23086	20.92639	23.90051	21.34609	20.78547	20.63383	20.96155	21.33774
basal_forebrain	18.52326	17.21292	18.61918	18.34437	17.62833	16.93681	17.27488	17.05937	17.62064	17.75235	17.42406	16.62781	17.15727	19.35513	17.56281	17.03291	17.0117	17.26312	17.47976
Bed_nucleus_of_stria_terminalis	3.234672	2.96437	3.181425	3.13865	3.112459	2.880199	2.895561	2.997035	3.013176	3.043297	2.97785	2.874753	2.928997	3.350758	3.02354	3.00525	2.907121	3.092036	2.996848
caudaputamen	50.17562	46.52156	50.3057	49.51442	47.67191	45.68104	46.61096	46.15365	47.67358	48.07356	47.13615	44.977	46.34486	52.43512	47.47851	46.11285	45.96543	46.6229	47.18918
cerebellar_lobule_1_2	9.02027	8.178727	8.823475	8.916243	8.200244	7.747122	8.079545	8.143974	8.097717	8.542117	8.371524	7.806507	8.005547	10.166285	8.334068	8.14672	7.96031	8.124336	8.220357
cerebellar_lobule_10	3.828857	3.469541	3.668426	3.732105	3.440142	3.285067	3.480719	3.385136	3.458343	3.609023	3.53349	3.229744	3.401441	4.669976	3.485399	3.469448	3.302574	3.420469	3.448822
cerebellar_lobule_3	7.911877	7.111885	7.646437	7.742929	7.071803	6.69032	7.007817	7.050996	6.99384	7.447568	7.279958	6.753808	6.892202	9.059414	7.233453	7.098329	6.857843	7.002847	7.075275
cerebellar_lobule_4_5	24.06143	21.81776	23.34814	23.58612	21.86914	20.88345	21.85912	21.64036	21.85723	22.7576	22.36404	20.65644	21.5614	28.34949	22.07614	21.86438	21.19971	21.81217	21.97892
cerebellar_lobule_6	9.656189	8.666178	9.233334	9.407434	8.740163	8.31711	8.792984	8.660648	8.824891	9.016047	8.917951	8.100585	8.607315	11.913923	8.711604	8.684359	8.385595	8.6928	8.753351
cerebellar_lobule_7	3.691022	3.320532	3.514348	3.586777	3.390924	3.19344	3.408723	3.335351	3.459954	3.423485	3.38909	3.080799	3.357068	4.559262	3.299389	3.362805	3.22904	3.415195	3.392342
cerebellar_lobule_8	4.18211	3.748338	3.995318	4.065406	3.732743	3.589304	3.782084	3.723052	3.805581	3.89226	3.849415	3.482669	3.698131	5.174994	3.761524	3.714144	3.579114	3.716234	3.747313
cerebellar_lobule_9	9.707335	8.694118	9.283227	9.465686	8.763457	8.343609	8.832318	8.705225	8.890747	9.037461	8.962055	8.105018	8.646055	12.010681	8.739873	8.678986	8.393509	8.71868	8.777691
Cerebellar_White_Matter_Arbor_vita_of_cerebellum	30.34915	27.38032	29.46109	29.85171	27.51716	26.0963	27.36828	27.20827	27.42297	28.60115	28.28269	25.91258	26.98973	36.41195	27.75422	27.4227	26.45194	27.36825	27.55452
cerebral_peduncle	3.211827	2.933156	3.16934	3.15266	3.051963	2.849462	2.953209	2.946491	3.048782	3.057785	2.974249	2.838802	2.960039	3.34077	2.983944	2.959508	2.906175	2.996747	3.005853
Cingulate_Cortex_area_1	16.62001	15.39933	16.71726	16.33867	15.75198	15.13582	15.50371	15.129	15.83126	15.95861	15.64851	14.90331	15.54505	17.62612	15.7509	15.31393	15.25524	15.43059	15.67928
Cingulate_Cortex_area_2	10.253713	9.573134	10.267586	10.096297	9.782349	9.391339	9.651893	9.425616	9.849513	9.865806	9.643749	9.208524	9.638765	10.777527	9.717454	9.51687	9.494681	9.653106	9.742495
cingulum	3.651753	3.345403	3.628575	3.600243	3.432002	3.272128	3.335442	3.343585	3.406268	3.496652	3.419579	3.270461	3.320269	3.829624	3.449066	3.329255	3.307499	3.324019	3.393044
Cochlear_nucleus	1.2249317	1.0858383	1.1921054	1.2009154	1.0740921	1.0093303	1.0523721	1.0748929	1.0510014	1.160155	1.1392375	1.0422912	1.0418581	1.4270428	1.1286172	1.0742445	1.0283079	1.0477062	1.0740465
Commisure_inferior_Colliculus	0.3206621	0.3099154	0.3264244	0.3245759	0.3232282	0.3090587	0.330665	0.2986297	0.332787	0.3057393	0.3065864	0.2902988	0.3377265	0.352742	0.3035709	0.3159486	0.3188496	0.3393792	0.3338117
commisure_superior_collicuus	0.204822	0.1832525	0.2047505	0.2047043	0.1933844	0.1831405	0.1879437	0.1875259	0.1922989	0.1964774	0.1933547	0.18822	0.1874702	0.218862	0.1938007	0.1864384	0.1865453	0.1871933	0.1943357
copula	3.140579	2.790582	3.004153	3.052693	2.864156	2.697305	2.823075	2.847262	2.88607	2.921476	2.899585	2.638851	2.769447	3.875576	2.810658	2.814548	2.733244	2.844491	2.835851
Corpus_Callosum_associated_White_Matter	45.71108	42.12993	45.39769	44.96657	43.27111	41.12291	42.44828	41.98277	43.51603	43.73507	42.71274	40.70676	42.32489	48.08333	42.92575	42.12259	41.72203	42.56218	42.93843
Crus_1_ansiform_lobule	18.79384	16.90997	18.15711	18.39857	17.12886	16.21862	16.97723	16.8925	17.0992	17.65097	17.49674	16.02142	16.77511	22.87796	17.05757	17.04418	16.44579	17.09547	17.06989
Crus_2_ansiform_lobule	11.04884	9.881286	10.667049	10.858315	10.025384	9.428786	10.006968	9.945005	10.023944	10.318718	10.278826	9.246282	9.772068	13.780264	10.006626	9.863366	9.522478	9.930268	9.99024
dentate_gyrus	17.95024	16.35087	17.78363	17.77524	16.81753	15.90759	16.3733	16.38235	16.82639	17.14754	16.82775	16.01216	16.3688	18.93653	16.89848	16.29191	16.19994	16.3467	16.71977
Dentate_nucleus	0.9728545	0.8606624	0.9353797	0.9509193	0.8558942	0.8003058	0.8410608	0.8575046	0.8404187	0.9187098	0.8931801	0.8277699	0.8224432	1.1391627	0.8884608	0.8612979	0.8226342	0.8324057	0.8486965
Dorsal_Peduncular_Cortex	1.684898	1.53085	1.651732	1.624214	1.576784	1.484506	1.517777	1.523154	1.571658	1.619845	1.556166	1.476703	1.508728	1.754056	1.565518	1.531311	1.502723	1.518389	1.534927
Dorsal_Tenia_Tecta	1.1714638	1.071857	1.1494309	1.1500136	1.087957	1.0371252	1.0581494	1.0571407	1.0759595	1.1264865	1.088173	1.0446261	1.0593201	1.2437194	1.1061773	1.0687798	1.0472992	1.0599992	1.0839714
Endopiriform_Nucleus	9.517804	8.910442	9.591859	9.41024	9.151932	8.809838	9.051553	8.796186	9.224393	9.149985	8.992956	8.586306	9.039116	9.957261	9.038814	8.849081	8.883266	9.038853	9.129516
entopeduncular_nucleus	0.247351	0.2252293	0.2348067	0.2334473	0.2234678	0.2222629	0.234604	0.2206952	0.2392637	0.2356769	0.2210392	0.2108825	0.2234655	0.2518612	0.2253667	0.2247956	0.225918	0.2149862	0.2304732
external_medullary_lamina	0.7145875	0.6506605	0.7054594	0.7021584	0.6839522	0.6281476	0.6560108	0.6558578	0.6800878	0.6717709	0.6595275	0.6243988	0.6644597	0.7450758	0.6579745	0.6647292	0.6391878	0.6831952	0.6687962
Fasciculus_retroflexus	0.2400943	0.2296784	0.2449607	0.2424964	0.2327053	0.2336219	0.2467339	0.2240882	0.2492763	0.2323882	0.2296055	0.2166078	0.2441454	0.2601195	0.229563	0.2260986	0.2343008	0.2295841	0.2431059
fastigial_nucleus	1.1362547	1.0430367	1.1203151	1.120512	1.0411054	1.0017353	1.0372986	1.0108108	1.0371019	1.0916831	1.0710215	0.9827121	1.0368024	1.3628694	1.0566729	1.0278728	1.0048993	1.0245542	1.0554489
Fimbria	5.124467	4.725139	5.159603	5.097509	4.82198	4.651117	4.763022	4.710291	4.855948	4.924861	4.835214	4.593392	4.725692	5.38854	4.864682	4.651886	4.683205	4.654047	4.83158
flocculus	11.754604	10.67577	11.454722	11.579784	10.614252	10.181939	10.676666	10.535707	10.635532	11.136458	10.910308	10.126939	10.513857	13.488206	10.825586	10.6739	10.377523	10.580713	10.770897
Fornix	0.6126989	0.56515	0.6506964	0.6198326	0.5880285	0.5584668	0.5698344	0.5671256	0.5939884	0.590119	0.5961603	0.5604953	0.5788104	0.6457361	0.5916714	0.5599006	0.5647214	0.5691833	0.5810652
Fourth_ventricle	3.203018	2.842642	3.088847	3.128286	2.871897	2.705312	2.796652	2.873188	2.839471	3.010725	2.974	2.733506	2.765127	3.796731	2.915595	2.853604	2.758441	2.833336	2.850959
Frontal_Association_Cortex	125.9249	114.0275	124.5792	121.9798	115.5237	112.0346	113.2064	112.0078	118.4226	117.7786	115.9103	108.691	115.5738	138.5003	116.0457	113.9671	112.3528	112.4136	116.023
Globus_pallidus	4.890591	4.462815	4.858711	4.789878	4.587005	4.364769	4.456173	4.464297	4.594599	4.63663	4.532577	4.307742	4.416902	5.072157	4.56371	4.427665	4.400444	4.459486	4.530077
hindbrain_medulla_pons	105.08233	94.78064	101.68872	103.29109	95.38066	90.31248	95.16774	94.43721	95.6152	98.82407	97.37158	89.45408	93.73537	124.293	95.98541	94.8295	91.72375	94.84433	95.54889
Hippocampal_layer_CA1	22.51113	20.60025	22.24686	22.26123	21.16898	20.09657	20.73348	20.62257	21.24799	21.52113	21.08929	20.08595	20.67968	23.73183	21.17671	20.58599	20.41769	20.71777	21.08363
Hippocampal_layer_CA2	2.418184	2.254607	2.4227	2.408489	2.327124	2.228056	2.313643	2.248861	2.368296	2.324425	2.280993	2.180699	2.321339	2.552449	2.291596	2.259131	2.257067	2.313892	2.334294
Hippocampal_layer_CA3	22.49761	20.46737	22.31245	22.24242	21.16292	19.97825	20.48794	20.62545	21.09192	21.47921	21.09281	20.06173	20.48653	23.66008	21.18925	20.45885	20.27328	20.532	20.96983
hypothalamus	29.99531	27.56654	30.13132	29.71091	28.44763	27.05669	27.70152	27.64813	28.48595	28.72017	28.25798	26.87151	27.68199	31.43244	28.38659	27.39702	27.372	27.67239	28.24216
Inferior_Colliculus	17.05242	15.46956	16.65736	16.88328	15.48306	14.71836	15.40292	15.32645	15.44421	16.17681	15.81639	14.79683	15.18383	18.8693	15.8335	15.35485	15.05124	15.27246	15.54734
Infralimbic_Cortex	1.622369	1.503269	1.666148	1.620423	1.545661	1.476016	1.483211	1.476795	1.510187	1.585011	1.57054	1.495056	1.489763	1.740388	1.573886	1.477789	1.483121	1.455702	1.527651
Insular_Cortex	26.21939	24.13651	26.27558	25.84061	24.8337	23.58886	24.01805	24.03373	24.68578	25.07504	24.60265	23.39512	24.01071	27.43742	24.73906	23.92534	23.76235	24.23291	24.44502
Internal_capsule	8.508796	7.863292	8.530879	8.41209	8.128433	7.729183	7.969812	7.881243	8.164411	8.146683	7.981673	7.584146	7.961689	8.892099	8.011056	7.850047	7.808902	7.979011	8.06841
intersposed_nucleus	1.418139	1.270629	1.375824	1.383799	1.303661	1.189873	1.247534	1.260262	1.260966	1.340119	1.318551	1.212707	1.245001	1.684429	1.30305	1.296363	1.229703	1.294774	1.282446
intrabulbar_part_of_anterior_commisure	2.901153	2.616139	2.881182	2.837551	2.680724	2.575659	2.640956	2.597554	2.838897	2.694022	2.671237	2.450337	2.728955	3.316644	2.658667	2.62985	2.616958	2.654194	2.692739
Lateral_olfactory_tract	2.608898	2.414537	2.573135	2.536366	2.454438	2.370631	2.402912	2.353385	2.449057	2.469386	2.421716	2.317477	2.423245	2.787525	2.453656	2.41198	2.372059	2.427318	2.453952
lateral_septum	10.539573	9.691205	10.493197	10.320709	9.944679	9.463929	9.647633	9.663504	9.913248	10.044334	9.805853	9.355331	9.534093	10.942637	9.889954	9.627877	9.540503	9.656369	9.76389
Lateral_ventricle	14.89842	13.7406	14.86961	14.67863	14.25827	13.49462	13.78478	13.74744	14.17594	14.1965	13.99037	13.34661	13.85455	15.57245	14.06381	13.75471	13.66066	14.01723	14.0684
mamillary_bodies	1.743095	1.6212	1.734053	1.725629	1.668952	1.610894	1.683257	1.60791	1.721152	1.665898	1.628432	1.547828	1.681669	1.83477	1.636706	1.628725	1.625086	1.659279	1.701224
mammilothalamic_tract	0.3830972	0.3491842	0.3857024	0.3814207	0.3525128	0.3443181	0.3497234	0.3535659	0.3593848	0.3657955	0.3613472	0.3459539	0.3467082	0.4036623	0.3651199	0.3465335	0.3460206	0.3357699	0.3575051
medial_septum	1.428676	1.324457	1.45879	1.420744	1.356662	1.296245	1.319514	1.319956	1.35541	1.385722	1.360198	1.295888	1.310955	1.487008	1.359751	1.304841	1.306123	1.296208	1.339977
median_preoptic_area	0.05113255	0.0501065	0.05683186	0.05442966	0.05211739	0.05078731	0.04901591	0.04837669	0.0482371	0.05129179	0.05375143	0.05199945	0.05119876	0.05719763	0.05355386	0.04852472	0.04873081	0.04883791	0.05197835
midbrain	37.39712	33.93933	36.7358	36.92266	34.72581	32.77944	33.82721	34.03349	34.55237	35.60275	34.97348	33.18145	33.70889	39.82545	35.04075	33.85558	33.43915	34.03735	34.43491
Navicular_nuclear_basin_forebrain	1.890676	1.738002	1.898785	1.868047	1.78469	1.69572	1.740421	1.714464	1.788468	1.825573	1.790866	1.698233	1.751713	2.007022	1.799702	1.717487	1.726655	1.743569	1.769794
Nucleus_accumbens	7.682563	7.094947	7.639854	7.497911	7.218556	6.916864	7.12977	7.015392	7.294727	7.378553	7.167479	6.836251	7.083493	8.014653	7.19795	7.077091	6.967772	7.090907	7.139863
Occipital_Cortex	14.87099	13.46411	14.49331	14.69753	13.48455	12.77753	13.34067	13.41209	13.37241	14.03719	13.76578	12.86094	13.15839	16.60293	13.71206	13.41477	13.13917	13.35823	13.52638
Olfactory_Bulb	145.8843	133.9785	146.5423	141.3392	137.9682	135.8424	137.8191	138.7036	130.7415	139.6195	144.8209	142.5287	130.0537	159.1486	138.4326	144.8685	137.0118	131.9933	129.1477
Olfactory_tubercle	12.9808	12.0763	13.01985	12.75819	12.29554	11.80907	12.15327	11.87595	12.39332	12.52631	12.22516	11.63228	12.08327	13.65182	12.28022	11.95853	11.93159	12.00949	12.21196
Optic_Chiasm	0.2764692	0.255922	0.2878715	0.2815872	0.2612982	0.2548352	0.2482989	0.2548383	0.2505976	0.2668404	0.2699051	0.2606534	0.2492206	0.295073	0.2739184	0.2467117	0.2561342	0.2470518	0.2609996
Optic_tract	3.190389	2.929436	3.206607	3.187391	3.027721	2.883434	2.937649	2.931435	3.022361	3.042285	3.028009	2.879018	2.972837	3.367733	3.035523	2.89694	2.920497	2.957393	3.025401
Orbitofrontal_Cortex	0.48286	0.4491169	0.4776045	0.4677676	0.4702115	0.4420584	0.4512937	0.4412437	0.4649658	0.4573741	0.4471875	0.4311755	0.4659753	0.5073299	0.4535275	0.4567178	0.4495717	0.4718478	0.4640941
paraflocculus	13.51372	12.14117	13.00437	13.16961	12.12585	11.56965	12.05602	12.062	12.11629	12.74193	12.50078	11.52535	11.84036	16.04565	12.30725	12.19341	11.72649	12.02037	12.14127
paramedian_lobe	8.897495	7.97851	8.509391	8.682981	7.970789	7.554687	7.999214	7.889932	7.990664	8.32345	8.190332	7.442032	7.814403	10.968857	8.039067	7.936742	7.613778	7.86527	7.953644
Parietal_Association_Cortex	11.887848	10.833257	11.826652	11.742959	11.209633	10.594692	10.844972	10.92289	11.18859	11.341578	11.143333	10.592491	10.848154	12.487658	11.194822	10.796387	10.750708	10.863997	11.109863
Periaqueductal_grey	11.363451	10.172568	10.942162	11.099401	10.310995	9.795641	10.064733	10.260019	10.249509	10.732602	10.463245	9.923272	9.873503	12.131553	10.518654	10.1323	9.960135	10.031951	10.216466
Piriform_Cortex	29.4107	27.28229	29.48422	29.03557	27.91248	26.80178	27.46932	27.08124	28.10719	28.23958	27.65005	26.36603	27.34363	30.78512	27.84206	27.05162	27.04272	27.26398	27.78922
pons	24.38241	22.08848	23.74615	23.93597	22.37726	21.16328	21.98791	22.04784	22.21394	23.04584	22.66068	21.37024	21.69976	26.34215	22.68844	21.99044	21.63167	22.09489	22.22897
posterior_commisure	0.2455528	0.2131375	0.2242369	0.2314525	0.2109231	0.2003742	0.2051261	0.214985	0.2086786	0.2290166	0.2166305	0.2083548	0.1974304	0.2513466	0.2211343	0.2113409	0.2045792	0.1980406	0.2027443
Posterior_part_of_anterior_commissure	0.3514386	0.3212334	0.341375	0.3397031	0.3267507	0.3120318	0.3133324	0.32213	0.3197089	0.3336089	0.3228357	0.3116462	0.3050135	0.3625562	0.3293273	0.3192447	0.3139578	0.3174167	0.3195888
Prelimbic_Cortex	4.319356	3.9796	4.302613	4.189077	4.053519	3.919195	4.036914	3.912849	4.124268	4.131542	4.017153	3.828132	4.02905	4.575956	4.035206	3.974083	3.941589	3.967156	4.04074
Primary_Motor_Cortex	21.25249	19.53416	21.27199	20.84893	19.98148	19.07245	19.45575	19.32896	19.94032	20.3937	19.89901	18.96069	19.39515	22.41837	20.03142	19.38683	19.21761	19.35005	19.72124
Primary_Somatosensory_Cortex	87.85533	81.20371	88.1238	86.68361	83.3841	79.59986	81.33554	80.71424	83.36606	84.1951	82.59377	78.65614	81.16959	92.00858	83.09165	80.58618	80.22551	81.4437	82.55225
Primary_Visual_Cortex	28.38333	25.82136	27.80726	28.01023	26.2949	24.88799	25.85954	25.82935	26.26649	26.98666	26.43976	25.04408	25.62431	30.47503	26.52553	25.80595	25.38424	25.90221	26.15413
Retrosplenial_Cortex	34.06211	31.03327	33.42598	33.53312	31.77841	30.03852	31.13659	31.09286	31.74492	32.37025	31.67997	30.08546	30.91292	36.25484	31.80267	31.08066	30.61513	31.2875	31.53212
rhinal_cortex	51.44843	46.79224	50.527	50.75094	47.77548	45.2341	46.87659	46.81071	47.70903	48.95253	47.99944	45.51361	46.51503	55.00423	48.14738	46.70127	46.09971	46.91531	47.46996
Secondary_Motor_Cortex	12.92288	11.85632	12.92507	12.58113	12.26359	11.6752	11.95133	11.81982	12.38401	12.30213	12.04664	11.4305	12.01037	13.53787	12.05717	11.86769	11.77563	12.06893	12.09829
Secondary_Somatosensory_Cortex	23.3862	21.49359	23.42668	23.10832	22.12196	21.03726	21.39948	21.51537	22.02322	22.31733	21.92371	20.88138	21.3719	24.45319	22.07876	21.3489	21.18203	21.54877	21.84384
Secondary_Visual_Cortex	34.16987	31.04043	33.52274	33.69829	31.82969	30.00868	31.02604	31.15101	31.65768	32.47674	31.86571	30.25532	30.89324	36.53436	31.95727	31.05997	30.62477	31.27292	31.56607
Simple_Lobule	18.5196	16.72556	17.98893	18.16052	16.65561	15.94785	16.64867	16.52712	16.66987	17.49384	17.22144	15.84261	16.41213	21.86389	16.97035	16.69636	16.12343	16.55246	16.77902
stria_medullaris_thalamus	0.6841784	0.619561	0.6948731	0.6824247	0.6442664	0.6013045	0.6160441	0.61829	0.6457669	0.6445386	0.6474945	0.5939336	0.6258345	0.7170221	0.6370186	0.6055013	0.6104097	0.6286864	0.6376449
Stria_terminalis	2.72861	2.534217	2.744723	2.712526	2.572655	2.498211	2.572977	2.508281	2.623931	2.628116	2.587184	2.445194	2.549735	2.870805	2.595323	2.481832	2.510348	2.491364	2.594676
Subfornical_organ	0.08638948	0.0790057	0.08303478	0.08442106	0.07828075	0.07323895	0.07707336	0.07981605	0.07832668	0.08233919	0.0782654	0.07322347	0.07452937	0.08918869	0.07921453	0.07503201	0.07619495	0.07303957	0.0762201
subicular_region	27.77261	25.17796	27.20655	27.41712	25.81199	24.35496	25.22778	25.27575	25.69204	26.37606	25.90036	24.56793	25.01911	29.7322	25.94464	25.23436	24.86657	25.41985	25.61169
substantia_nigra	2.586913	2.295239	2.494338	2.524433	2.362802	2.188477	2.256251	2.313546	2.330792	2.452464	2.365354	2.262491	2.214109	2.701777	2.385945	2.305518	2.247809	2.255833	2.299167
Superior_Colliculus	17.6598	16.0996	17.33309	17.42332	16.50133	15.5029	16.13976	16.08055	16.40498	16.78681	16.47143	15.613	16.04356	18.91447	16.49303	16.13775	15.84558	16.33406	16.34288
Temporal_Association	12.354274	11.16451	12.170305	12.236469	11.48342	10.748726	11.103532	11.245346	11.326835	11.73189	11.554767	10.930835	11.056864	13.317808	11.555461	11.182454	10.997442	11.272459	11.341365
Thalamus	52.66253	48.35987	52.62334	52.08794	49.97429	47.44196	48.76075	48.5107	50.19617	50.36646	49.41531	47.04136	48.74654	55.26971	49.65491	48.29414	48.05539	48.76527	49.66928
Third_ventricle	4.92311	4.543649	4.89621	4.838722	4.691488	4.483416	4.638435	4.532844	4.728655	4.706733	4.582002	4.378868	4.594419	5.118455	4.607419	4.557633	4.540466	4.569158	4.664846
trochlear_nerve	0.09110421	0.08186461	0.09198474	0.09401608	0.08253682	0.07452062	0.08172816	0.0793458	0.07999165	0.08606523	0.08484685	0.07909787	0.08304567	0.09828771	0.08468635	0.08147014	0.07837034	0.08128452	0.08106112
ventral_pallidum	2.742512	2.55091	2.75305	2.720487	2.576566	2.504106	2.566005	2.520455	2.60671	2.652472	2.581828	2.451254	2.515277	2.878447	2.597105	2.504377	2.51052	2.505835	2.565267
brainvolumes	1569.459	1433.123	1552.009	1541.581	1463.22	1397.252	1438.813	1432.718	1459.018	1492.065	1472.754	1394.087	1425.699	1710.151	1466.178	1440.811	1414.535	1432.741	1448.001

	38	40	43	45	53	56	87	88	90	91	103	21	30	31	42	46	49	52	93
	Het	Het	Het	Het	Het	Het	Het	Het	Het	Het	Het	Het	Het	Het	Het	Het	Het	Het	Het
Absolute Volume	F	F	F	F	F	F	F	F	F	F	F	M	M	M	M	M	M	M	M
	Pat	Pat	Pat	Pat	Pat	Pat	Pat	Pat	Pat	Pat	Pat	Pat	Pat	Pat	Pat	Pat	Pat	Pat	Pat
amygdaloid_area	28.63957	29.05513	29.16501	30.59519	32.44435	40.08194	30.00493	30.01602	29.6882	29.82179	30.94147	29.30455	30.17296	29.1625	29.2636	28.08464	32.7909	31.10084	30.83383
Anterior_part_of_anterior_commissure	1.286987	1.307254	1.30173	1.32995	1.470496	1.84581	1.35142	1.342698	1.335632	1.319067	1.405239	1.318641	1.348498	1.302794	1.33439	1.245479	1.48139	1.393793	1.369277
Aqueduct	1.608424	1.580126	1.661202	1.699509	1.754958	2.192896	1.663001	1.6407	1.639346	1.685152	1.660255	1.584678	1.663796	1.565574	1.597101	1.604783	1.74291	1.66562	1.698
auditory_cortex	20.21494	20.13354	20.57059	21.31932	22.45958	27.66286	20.91681	20.89656	20.73677	21.00516	21.52875	20.54029	21.21262	20.34866	20.39663	19.79962	22.65503	21.44961	21.60822
basal_forebrain	16.57883	16.51254	16.95125	17.49916	18.45661	22.93347	17.16366	17.11961	17.02068	17.19782	17.53419	16.77366	17.40628	16.83077	16.80721	16.4266	18.69046	17.73186	17.43511
Bed_nucleus_of_stria_terminalis	2.920878	2.850792	2.706803	2.947128	3.20578	3.945612	2.885074	2.92553	2.944776	2.812442	3.083676	3.018059	2.965577	3.387831	2.922331	2.783555	3.259968	3.085433	2.944255
caudaputamen	44.56421	44.62553	45.5258	47.17665	49.97852	62.22221	46.28851	46.19858	45.87559	46.43588	47.48993	45.36327	46.96877	45.53374	45.35246	44.28267	50.57972	47.97481	47.10052
cerebellar_lobule_1_2	7.776408	7.84269	7.769265	8.103338	8.843868	11.370808	8.030685	8.046712	7.977456	8.09637	8.36678	7.866465	8.078814	7.8059	7.883677	7.594543	8.795361	8.354904	8.465943
cerebellar_lobule_10	3.233477	3.24075	3.273628	3.407479	3.71824	5.20482	3.412115	3.403019	3.351947	3.397051	3.521181	3.314362	3.462197	3.186241	3.319011	3.12017	3.73851	3.516035	3.614015
cerebellar_lobule_3	6.623009	6.781878	6.59377	6.932253	7.743223	10.202672	6.944353	6.93498	6.831076	6.995663	7.251652	6.80521	7.024345	6.575731	6.834105	6.438276	7.685613	7.286631	7.375593
cerebellar_lobule_4_5	20.83564	20.64645	21.06721	21.73368	23.57147	31.71047	21.62117	21.65663	21.41626	21.83967	22.3319	21.17482	21.81198	20.65414	21.11698	20.27419	23.49311	22.28655	22.62833
cerebellar_lobule_6	8.36848	8.155904	8.301197	8.63783	9.353981	13.532053	8.592254	8.751725	8.534864	8.652202	8.964639	8.431445	8.7505	8.240032	8.474953	7.928422	9.381762	8.866718	9.17289
cerebellar_lobule_7	3.335551	3.116043	3.268712	3.373431	3.534755	5.235283	3.292745	3.400693	3.339586	3.348225	3.491339	3.275624	3.448847	3.359997	3.295348	3.125892	3.575917	3.376458	3.513674
cerebellar_lobule_8	3.601351	3.514635	3.592314	3.720708	4.039506	5.896008	3.741947	3.773569	3.678662	3.73939	3.855751	3.626218	3.781835	3.41188	3.654083	3.380781	4.04218	3.841028	3.989906
cerebellar_lobule_9	8.45532	8.182475	8.39176	8.701104	9.400893	13.707739	8.662563	8.832152	8.590891	8.730629	8.99957	8.457304	8.809168	8.189219	8.536536	7.945382	9.40096	8.909043	9.234756
Cerebellar_White_Matter_Arbor_vita_of_cerebellum	26.02208	26.0181	26.02361	27.19152	29.61454	40.82821	26.96358	27.25026	26.77414	27.0333	28.12681	26.42916	27.3044	25.93844	26.5642	25.14983	29.55603	28.06894	28.69209
cerebral_peduncle	2.843848	2.865675	2.846754	3.032167	3.179907	3.895386	2.912315	2.93284	2.922776	2.909182	3.048509	2.902433	2.99499	2.998779	2.870607	2.799782	3.211668	3.034504	3.022193
Cingulate_Cortex_area_1	14.86175	14.82107	15.22947	15.60184	16.56856	21.21861	15.40704	15.43685	15.30817	15.44697	15.83164	15.04221	15.73546	15.24835	15.15602	14.79151	16.74434	15.79646	15.61887
Cingulate_Cortex_area_2	9.298729	9.132463	9.508819	9.706207	10.191371	12.810685	9.549231	9.513524	9.489022	9.641247	9.751375	9.379881	9.754495	9.554528	9.382445	9.227635	10.341309	9.784831	9.656428
cingulum	3.179863	3.21716	3.199745	3.338152	3.623701	4.528145	3.334234	3.327508	3.293137	3.320877	3.456921	3.28677	3.365895	3.259941	3.266818	3.117361	3.66747	3.459868	3.434916
Cochlear_nucleus	0.9683717	1.0510719	0.9569851	1.0462138	1.2019117	1.6042645	1.0502676	1.0511064	1.0218885	1.0250847	1.1061292	1.0125489	1.0519437	0.9496165	1.0323317	0.9460982	1.1849063	1.1290446	1.143484
Commisure_inferior_Colliculus	0.3398908	0.2887708	0.3626288	0.344501	0.3158904	0.3893623	0.3244562	0.32593	0.3324138	0.3460049	0.3126745	0.3162016	0.3309131	0.3475896	0.3133079	0.3444723	0.3145068	0.3040496	0.3121853
commisure_superior_collicuus	0.1840102	0.1823995	0.1848735	0.1900425	0.2014072	0.2488133	0.1897474	0.1886763	0.187621	0.1855279	0.1980886	0.1854342	0.1920907	0.1827437	0.1885264	0.1765865	0.2061985	0.1937843	0.1977191
copula	2.734455	2.653129	2.645077	2.792983	3.026594	4.400184	2.743109	2.859995	2.767573	2.783066	2.953455	2.738923	2.832724	2.781665	2.763061	2.570181	3.051619	2.894044	2.979365
Corpus_Callosum_associated_White_Matter	40.82883	40.6061	41.35209	43.02605	45.35044	56.31557	42.07207	42.087	41.83818	42.34394	43.31984	41.4502	42.88726	41.82671	41.23226	40.31366	45.76747	43.40631	43.14544
Crus_1_ansiform_lobule	16.25131	16.07264	16.11579	16.86683	18.26296	25.57996	16.63797	16.98846	16.67435	16.75405	17.54713	16.4865	16.93123	16.50138	16.49039	15.63916	18.32807	17.37002	17.74247
Crus_2_ansiform_lobule	9.536124	9.382978	9.331847	9.852921	10.724692	15.721494	9.709693	10.035722	9.733487	9.693563	10.286175	9.539883	9.917185	9.508233	9.703037	8.993048	10.711766	10.140577	10.530987
dentate_gyrus	15.70447	15.86163	15.9385	16.58206	17.74252	21.84201	16.41579	16.42131	16.21744	16.44875	16.91296	16.06354	16.49354	15.68547	15.97108	15.36662	17.8649	16.91929	17.04275
Dentate_nucleus	0.7692504	0.8338851	0.7460017	0.8191852	0.9526973	1.2823789	0.825182	0.8290407	0.8098075	0.8169422	0.8832327	0.8132115	0.8436799	0.7775412	0.82005	0.745036	0.9503246	0.8965739	0.9095234
Dorsal_Peduncular_Cortex	1.422367	1.483538	1.40739	1.518232	1.674787	2.146885	1.499861	1.510119	1.471165	1.507501	1.567096	1.482506	1.541571	1.463479	1.489711	1.423238	1.69165	1.593876	1.561388
Dorsal_Tenia_Tecta	1.0218043	1.0164751	1.0003333	1.029048	1.1542859	1.4907223	1.0567203	1.0485286	1.0448115	1.0409153	1.0985569	1.0578857	1.0830231	1.0648516	1.0578503	0.979042	1.1774563	1.0991939	1.09062
Endopiriform_Nucleus	8.754644	8.529206	9.06525	9.211967	9.471479	11.778592	8.965762	8.945578	8.926088	9.085279	9.099075	8.774197	9.117851	8.928938	8.75981	8.722952	9.599576	9.117747	9.005051
entopeduncular_nucleus	0.209591	0.2070409	0.2316193	0.2305413	0.2407793	0.3077142	0.2294574	0.2203564	0.2166197	0.24049	0.2252484	0.2188204	0.241687	0.1856721	0.217695	0.2074824	0.2411423	0.2292882	0.2380838
external_medullary_lamina	0.6490212	0.6485255	0.6326978	0.6852159	0.7009507	0.8701755	0.6424864	0.6506379	0.6555933	0.6330714	0.6784778	0.6495007	0.6694453	0.7170269	0.6413094	0.638125	0.7129591	0.67126	0.6680514
Fasciculus_retroflexus	0.2382924	0.2159891	0.2705669	0.2525969	0.2391335	0.3008873	0.2471696	0.2382373	0.2384263	0.2651347	0.2304631	0.2274053	0.2475786	0.2015521	0.2291311	0.235903	0.2421749	0.2294702	0.2394458
fastigial_nucleus	0.9861316	0.982519	1.0290268	1.0537324	1.1097033	1.5112569	1.0494704	1.0378044	1.0241728	1.0450134	1.0478873	0.9942872	1.0351456	0.9266234	0.9980607	0.9633806	1.1037926	1.0640353	1.0919841
Fimbria	4.497549	4.559749	4.697848	4.82931	5.104121	6.318043	4.77777	4.73602	4.678834	4.788969	4.852172	4.572116	4.779528	4.361233	4.623488	4.420996	5.144856	4.88957	4.888656
flocculus	10.174221	10.120355	10.382226	10.625409	11.533859	15.159339	10.631916	10.522202	10.428346	10.737014	10.840714	10.323571	10.689254	9.896943	10.305893	9.941937	11.452684	10.879833	11.09097
Fornix	0.5231957	0.5710969	0.5491816	0.5969121	0.6241176	0.7578868	0.569984	0.5763607	0.5692522	0.5538996	0.589816	0.5433741	0.5585822	0.5441824	0.5481542	0.5470608	0.6279699	0.5964157	0.5824179
Fourth_ventricle	2.678926	2.724651	2.610089	2.786728	3.113003	4.24451	2.774478	2.828177	2.759773	2.788157	2.965971	2.756261	2.815655	2.711407	2.765416	2.568786	3.11527	2.96267	3.010848
Frontal_Association_Cortex	108.99	109.141	111.2084	114.5643	124.7257	170.9176	114.5743	115.9388	113.9084	114.0032	118.9656	111.3233	118.8567	111.2471	112.0565	106.8971	123.6789	116.883	117.8187
Globus_pallidus	4.199991	4.301815	4.271955	4.527108	4.840171	6.015769	4.415419	4.444912	4.3684	4.40097	4.55998	4.331645	4.493319	4.324468	4.32857	4.176997	4.889147	4.641857	4.574723
hindbrain_medulla_pons	90.99351	90.06782	90.66172	94.31746	102.55447	140.43458	93.70582	94.8134	93.21412	94.53803	97.5012	91.81343	95.13121	90.23308	92.36912	87.33119	102.20236	97.00689	99.32176
Hippocampal_layer_CA1	20.01782	19.9475	20.32947	21.00506	22.28483	27.36824	20.73115	20.68936	20.55295	20.87172	21.31399	20.35441	20.93621	20.01006	20.13473	19.58852	22.42398	21.25248	21.41672
Hippocampal_layer_CA2	2.266354	2.168213	2.352759	2.367971	2.399576	2.928563	2.295605	2.282966	2.299535	2.326122	2.330946	2.260085	2.348601	2.292892	2.229093	2.224301	2.430749	2.29908	2.308236
Hippocampal_layer_CA3	19.70256	19.94435	19.88014	20.82467	22.27381	27.5087	20.57584	20.56014	20.36318	20.40213	21.31486	20.20559	20.70149	20.01262	20.05905	19.15319	22.51081	21.27579	21.30175
hypothalamus	26.42904	26.74301	27.02881	28.32401	29.87183	36.88484	27.6897	27.71227	27.42072	27.54155	28.47828	27.02932	27.84577	26.94266	26.98496	26.05901	30.17154	28.63215	28.37513
Inferior_Colliculus	14.64246	14.85298	14.83525	15.37432	16.78424	21.38389	15.36819	15.23057	15.05376	15.58619	15.73182	14.87603	15.39811	14.30424	14.93325	14.35545	16.68055	15.84818	16.08822
Infralimbic_Cortex	1.391226	1.45311	1.44841	1.480719	1.629872	2.107365	1.504839	1.50888	1.47226	1.487082	1.560722	1.446622	1.49069	1.376929	1.47381	1.390668	1.645563	1.544214	1.522089
Insular_Cortex	22.98007	23.42685	23.15908	24.435	26.11585	32.66628	23.95154	24.03162	23.73534	23.77626	24.74046	23.44752	24.17257	23.73733	23.56097	22.78244	26.3867	25.05101	24.52263
Internal_capsule	7.664494	7.630696	7.829472	8.178686	8.472428	10.442378	7.895478	7.904579	7.867837	7.934401	8.112168	7.736183	8.035407	7.893694	7.712179	7.56551	8.570522	8.126681	8.061195
intersposed_nucleus	1.194225	1.23322	1.155128	1.252713	1.379463	1.867064	1.210166	1.253644	1.239148	1.203278	1.319506	1.220329	1.257603	1.306089	1.225326	1.169954	1.379748	1.309396	1.324592
intrabulbar_part_of_anterior_commisure	2.555988	2.546107	2.682304	2.821298	2.86674	4.158888	2.660923	2.722643	2.687344	2.701445	2.758193	2.551796	2.772345	2.603512	2.555831	2.591828	2.812313	2.701764	2.774314
Lateral_olfactory_tract	2.361124	2.264261	2.387205	2.377791	2.574422	3.32964	2.409251	2.410958	2.413645	2.405309	2.479713	2.392706	2.480846	2.508455	2.380456	2.29525	2.588084	2.448637	2.413687
lateral_septum	9.106144	9.326358	9.171747	9.725025	10.504396	13.078749	9.567028	9.558004	9.431074	9.533686	9.904877	9.427244	9.713413	9.421033	9.389362	9.079212	10.615217	10.05945	9.825418
Lateral_ventricle	13.42675	13.26684	13.49458	14.08414	14.80208	18.20583	13.74946	13.81785	13.77208	13.71137	14.23218	13.6556	13.89968	14.17758	13.48888	13.16852	14.95312	14.22518	13.96776
mamillary_bodies	1.651336	1.549289	1.738435	1.729649	1.720739	2.129283	1.674584	1.650739	1.656829	1.717675	1.66306	1.616779	1.714117	1.605223	1.614326	1.616137	1.745209	1.648693	1.686917
mammilothalamic_tract	0.3244996	0.3358506	0.3430167	0.3474025	0.3811334	0.4728843	0.3569452	0.3466348	0.3443216	0.3479109	0.3661136	0.3448808	0.3567193	0.313564	0.3412749	0.3149473	0.3861134	0.3615479	0.3654249
medial_septum	1.213343	1.293317	1.249396	1.333507	1.444779	1.795716	1.31718	1.316088	1.295285	1.313466	1.360018	1.269598	1.313012	1.192285	1.277771	1.244188	1.449249	1.373102	1.371286
median_preoptic_area	0.04944848	0.04887809	0.05264483	0.05094141	0.05260465	0.0617493	0.05112299	0.05167151	0.0532524	0.05023993	0.05306408	0.04895288	0.04854132	0.0482626	0.05000256	0.04868106	0.05361416	0.05017184	0.04915091
midbrain	32.61118	32.98	32.72079	34.14704	36.85616	45.47933	33.81676	33.92412	33.52557	34.07885	35.08247	33.2917	34.04052	32.68072	33.03024	31.90486	36.9271	35.11754	35.3401
Navicular_nuclear_basin_forebrain	1.658993	1.681915	1.679791	1.754999	1.86784	2.414615	1.730359	1.734216	1.714496	1.707295	1.77253	1.69111	1.75262	1.71578	1.70932	1.654779	1.90867	1.802303	1.772911
Nucleus_accumbens	6.715799	6.851844	6.827943	7.158755	7.652093	9.660253	7.02645	6.992084	6.930152	7.070896	7.230499	6.884505	7.174461	6.900942	6.888697	6.765725	7.741553	7.295914	7.174579
Occipital_Cortex	12.80935	12.95747	12.79731	13.29444	14.56428	18.64497	13.29284	13.22233	13.11439	13.46166	13.76756	12.97198	13.34821	12.74467	13.01367	12.49428	14.49562	13.74213	13.98166
Olfactory_Bulb	130.0588	150.7763	126.1823	134.362	135.3291	200.3507	130.3868	130.7922	125.569	136.4732	135.9128	126.7865	134.8206	121.6694	134.7687	134.9683	139.9391	139.7374	140.4003
Olfactory_tubercle	11.48071	11.59854	11.83095	12.1978	12.94094	16.44231	12.01398	11.96806	11.83752	12.08606	12.29958	11.70359	12.24317	11.59101	11.77299	11.54578	13.08383	12.38354	12.2259
Optic_Chiasm	0.2360877	0.2414096	0.250426	0.2455968	0.2786792	0.3422201	0.2588945	0.258063	0.2546664	0.2511507	0.2679863	0.2522879	0.2486912	0.2303924	0.2489712	0.2302397	0.2789503	0.2639117	0.2596332
Optic_tract	2.876081	2.846822	2.945429	3.009289	3.158473	3.88868	2.966239	2.974235	2.951402	2.956421	3.036578	2.890739	2.95976	2.90779	2.892646	2.796264	3.1822	3.023429	3.020102
Orbitofrontal_Cortex	0.4592526	0.425001	0.456637	0.4585608	0.4763176	0.6054763	0.4523922	0.4558578	0.4623789	0.4569731	0.4661711	0.4587727	0.4666494	0.5185828	0.4501473	0.4494338	0.4831657	0.457753	0.4463885
paraflocculus	11.39327	11.50318	11.40276	11.90945	13.22015	17.96555	11.94155	11.98398	11.77513	12.03689	12.48069	11.74595	12.09958	11.31974	11.70795	11.03448	13.19477	12.5004	12.69002
paramedian_lobe	7.456781	7.494732	7.397469	7.818993	8.624883	12.416357	7.824518	7.91658	7.708601	7.794765	8.159575	7.612932	7.935585	7.32632	7.697816	7.100797	8.632882	8.141167	8.415063
Parietal_Association_Cortex	10.423027	10.517437	10.549682	11.060516	11.767987	14.596082	10.897393	10.894167	10.769736	10.813573	11.257073	10.672126	10.961483	10.634123	10.644621	10.122406	11.908004	11.275818	11.232425
Periaqueductal_grey	9.574312	9.820835	9.534505	9.982769	11.124407	13.95827	10.096639	10.051329	9.873402	10.209326	10.535176	9.939227	10.170144	9.388872	9.882356	9.250871	11.138727	10.586592	10.677189
Piriform_Cortex	26.18806	26.16355	27.02751	27.86372	29.299	36.43915	27.35299	27.23193	27.01749	27.52138	27.9312	26.64286	27.68046	26.35693	26.61222	25.99291	29.61293	28.07728	27.80689
pons	21.10179	21.35	21.16078	22.09173	23.9154	29.89065	21.90879	21.90099	21.62779	22.16013	22.69802	21.51674	22.06173	20.9662	21.40887	20.69636	23.86184	22.76929	22.93539
posterior_commisure	0.1829893	0.2032943	0.174019	0.1926887	0.237813	0.2990992	0.2031049	0.2018852	0.1970684	0.2068476	0.2188129	0.2054797	0.204308	0.181456	0.1968579	0.1757236	0.2357456	0.2205515	0.2231268
Posterior_part_of_anterior_commissure	0.3015575	0.3014671	0.2948888	0.3104936	0.3460426	0.434014	0.3121297	0.312539	0.3086136	0.316565	0.3313505	0.3166624	0.3177423	0.3146561	0.309891	0.2875354	0.3522339	0.3321987	0.3193055
Prelimbic_Cortex	3.828538	3.853907	3.929841	4.037339	4.302584	5.556157	3.978331	3.996738	3.942356	4.041248	4.108285	3.856694	4.113883	3.87862	3.922764	3.824554	4.342854	4.08692	4.058027
Primary_Motor_Cortex	18.38803	18.87129	18.58253	19.51203	21.18693	26.98969	19.33513	19.3794	19.10287	19.25825	20.07868	18.93051	19.69152	18.88172	19.07868	18.2461	21.42211	20.20248	19.86418
Primary_Somatosensory_Cortex	77.73617	78.34448	79.26226	82.56724	87.5063	109.08363	80.97764	80.99265	80.23613	80.89825	83.26106	79.20559	81.92829	79.55269	79.30634	77.13308	88.46515	83.86862	82.60305
Primary_Visual_Cortex	24.82465	24.97942	25.00791	26.00822	27.94135	34.77973	25.72779	25.71462	25.45718	26.03618	26.62878	25.28367	26.02889	24.75642	25.14066	24.33635	27.99773	26.60817	26.83917
Retrosplenial_Cortex	29.98893	30.00663	30.11229	31.43983	33.568	41.66127	30.90768	30.95622	30.70996	31.20136	32.0815	30.55369	31.38615	30.52943	30.32076	29.36862	33.73573	32.01344	32.11776
rhinal_cortex	44.95357	45.34036	45.39018	47.26522	50.74476	63.08374	46.77314	46.68474	46.20915	47.15634	48.30876	45.89746	47.19366	44.82838	45.61913	44.03385	50.86838	48.33415	48.67984
Secondary_Motor_Cortex	11.47535	11.5999	11.58888	12.21639	12.8671	16.28672	11.8438	11.95656	11.78455	11.8882	12.23866	11.6061	12.08948	12.00983	11.66247	11.54023	13.00109	12.32724	12.11515
Secondary_Somatosensory_Cortex	20.51823	20.78444	20.65885	21.78974	23.27992	28.8539	21.40261	21.4191	21.21414	21.20076	22.10433	21.00881	21.55612	21.19326	20.98562	20.16207	23.54216	22.33601	21.92711
Secondary_Visual_Cortex	30.0282	30.10795	30.04633	31.30908	33.6641	41.75154	30.96142	31.03774	30.73209	31.19281	32.16443	30.57289	31.29488	30.32044	30.33217	29.28052	33.7729	32.09114	32.27788
Simple_Lobule	15.79528	15.86768	16.02446	16.57219	18.10261	24.48449	16.59235	16.53443	16.30304	16.63393	17.07123	16.11611	16.68487	15.35744	16.13432	15.34071	18.02578	17.15219	17.46483
stria_medullaris_thalamus	0.584863	0.6179219	0.5978674	0.6529821	0.6749031	0.8546199	0.615423	0.6288097	0.6077295	0.6076578	0.6254047	0.5796644	0.614606	0.590885	0.6031663	0.5924244	0.6793349	0.6513497	0.6412193
Stria_terminalis	2.419196	2.427165	2.590835	2.622086	2.717016	3.364672	2.581469	2.55028	2.514949	2.622936	2.579952	2.450271	2.577992	2.280476	2.463042	2.408897	2.73688	2.600445	2.616941
Subfornical_organ	0.06987539	0.07370176	0.0707503	0.07596741	0.08488712	0.11254052	0.07490777	0.07463708	0.0712357	0.07850014	0.07708365	0.07280063	0.07761216	0.0651667	0.07402628	0.06529137	0.08433044	0.08246907	0.07968747
subicular_region	24.36206	24.46413	24.4378	25.44199	27.3133	33.90004	25.10344	25.19713	24.91486	25.39128	26.09016	24.76714	25.48213	24.4784	24.67885	23.83635	27.39192	26.05696	26.2655
substantia_nigra	2.105676	2.241757	2.036762	2.236333	2.542075	3.160212	2.246663	2.249099	2.210277	2.225682	2.392195	2.234637	2.277684	2.172175	2.211825	2.056037	2.550483	2.399495	2.422618
Superior_Colliculus	15.59773	15.64512	15.59843	16.3576	17.36856	21.48054	15.95645	16.043	15.92575	16.1096	16.61591	15.80659	16.26494	15.85886	15.71837	15.36546	17.44138	16.56806	16.67524
Temporal_Association	10.72593	10.90987	10.640779	11.250016	12.157913	15.153518	11.05586	11.167908	11.010066	11.115596	11.577744	10.923443	11.158954	10.926412	10.920865	10.516117	12.169481	11.580072	11.641257
Thalamus	46.84841	46.88244	47.84523	49.83831	52.2967	64.50084	48.69727	48.68948	48.27905	48.70631	50.07465	47.67063	49.21769	47.69724	47.45736	45.96496	52.84887	50.09333	49.96011
Third_ventricle	4.406923	4.342247	4.585589	4.683809	4.868466	6.003452	4.56747	4.553678	4.530025	4.651384	4.674322	4.487426	4.695405	4.486061	4.452064	4.378228	4.94282	4.677576	4.660384
trochlear_nerve	0.07436673	0.08507615	0.07349945	0.08311064	0.09060803	0.11331316	0.07940479	0.0797582	0.07873999	0.07649439	0.08213597	0.07415838	0.07860692	0.07854401	0.0801158	0.07585331	0.08952766	0.08381926	0.08344066
ventral_pallidum	2.392168	2.42959	2.490778	2.566779	2.733241	3.438434	2.535631	2.509157	2.466742	2.557841	2.570349	2.438224	2.574974	2.303901	2.465952	2.407662	2.764571	2.62418	2.597303
brainvolumes	1376.534	1400.712	1386.544	1445.894	1541.25	2005.495	1425.351	1429.977	1409.433	1435.615	1474.957	1395.573	1448.762	1381.363	1403.209	1356.322	1551.748	1478.476	1482.482

	96	18	22	27	28	29	32	33	35	36	37	39	44	47	50	51	94	95	98
	Het	WT	WT	WT	WT	WT	WT	WT	WT	WT	WT	WT	WT	WT	WT	WT	WT	WT	WT
Absolute Volume	M	F	F	F	F	F	F	F	F	F	F	F	F	F	F	F	F	F	F
	Pat	Pat	Pat	Pat	Pat	Pat	Pat	Pat	Pat	Pat	Pat	Pat	Pat	Pat	Pat	Pat	Pat	Pat	Pat
amygdaloid_area	31.33838	30.60431	34.58584	31.55728	31.40155	30.20401	40.3895	28.83276	29.77102	29.38304	32.38616	30.06278	29.13217	36.57243	35.05733	32.58853	28.80175	31.43042	29.5574
Anterior_part_of_anterior_commissure	1.397107	1.367294	1.564537	1.436425	1.409223	1.391092	1.807626	1.272334	1.303286	1.301148	1.471762	1.325151	1.304831	1.657907	1.579512	1.447187	1.293153	1.435251	1.301426
Aqueduct	1.660365	1.673976	1.890825	1.720302	1.720396	1.612098	2.248127	1.655637	1.684578	1.610061	1.743126	1.731308	1.664463	1.978913	1.833512	1.775346	1.627413	1.683236	1.660895
auditory_cortex	21.69453	21.23731	24.1216	21.84865	21.85951	20.94757	28.32423	20.31738	20.958	20.6022	22.48272	21.05435	20.40123	25.44021	24.08758	22.64954	20.15292	21.69147	20.70503
basal_forebrain	17.70068	17.44021	19.62006	18.10365	17.91179	17.15805	22.73172	16.8176	17.21664	16.81635	18.37314	17.49027	16.82218	20.69359	19.84693	18.34221	16.69749	17.8316	16.90717
Bed_nucleus_of_stria_terminalis	3.082029	2.997988	3.469714	3.127196	3.114992	2.907173	3.885697	2.786333	2.922208	2.971854	3.135584	2.922572	2.87229	3.564508	3.423959	3.149895	2.79284	3.033599	2.857501
caudaputamen	47.89454	47.21256	53.25413	48.94945	48.41115	46.27269	61.55483	45.2318	46.40221	45.44119	49.57025	47.14045	45.37082	56.13726	53.77686	49.6352	44.87219	48.1977	45.59007
cerebellar_lobule_1_2	8.315839	8.336288	9.698805	8.616543	8.488789	8.066528	11.266883	7.710393	8.093271	7.962245	8.81037	8.090646	8.069229	10.155617	9.220405	8.954376	7.79181	8.390598	7.881681
cerebellar_lobule_10	3.517803	3.505462	4.106877	3.64263	3.583132	3.328406	4.678514	3.21095	3.405152	3.38205	3.699706	3.413255	3.337381	4.369234	3.887773	3.843555	3.269171	3.522767	3.399306
cerebellar_lobule_3	7.272443	7.239549	8.492686	7.513249	7.322791	6.941282	9.686105	6.524172	6.913363	6.912843	7.670736	6.923926	6.915682	8.926807	8.064139	7.853307	6.650632	7.275696	6.836303
cerebellar_lobule_4_5	22.19756	22.12232	25.80296	22.97774	22.6512	21.33661	29.43564	20.70278	21.83536	21.40546	23.34235	21.68907	21.43364	27.21276	24.55627	24.08045	20.84644	22.33258	21.36487
cerebellar_lobule_6	8.811345	8.841942	10.473369	9.169019	9.079472	8.479875	11.799697	8.184901	8.62974	8.665461	9.408461	8.636987	8.515158	11.086795	9.743319	9.749541	8.206047	8.873593	8.500957
cerebellar_lobule_7	3.350663	3.396536	4.051699	3.5018	3.544287	3.243553	4.579243	3.229678	3.395868	3.424742	3.62359	3.382166	3.323707	4.270063	3.680269	3.71338	3.182965	3.362549	3.306754
cerebellar_lobule_8	3.802934	3.806979	4.533616	3.972636	3.900309	3.679435	5.15522	3.51908	3.702741	3.725876	4.095911	3.721752	3.652594	4.826754	4.200468	4.232493	3.517184	3.837178	3.646539
cerebellar_lobule_9	8.841508	8.891062	10.54006	9.206145	9.117261	8.544202	11.852479	8.262602	8.68334	8.72444	9.492862	8.705836	8.568288	11.166346	9.750649	9.816028	8.220446	8.9172	8.51099
Cerebellar_White_Matter_Arbor_vita_of_cerebellum	27.8756	27.91458	32.66842	28.93602	28.6201	26.94705	37.56931	25.74511	27.12239	26.86142	29.60222	27.17742	26.79117	34.57833	30.80167	30.51363	25.95585	28.1929	26.65299
cerebral_peduncle	3.076287	3.026274	3.445335	3.076514	3.106046	2.917723	3.964679	2.867624	2.958945	2.932167	3.15495	2.995319	2.874694	3.572651	3.404969	3.195684	2.81738	3.042964	2.930226
Cingulate_Cortex_area_1	15.71987	15.56989	17.53493	16.17499	16.15114	15.36791	20.53138	15.18544	15.58021	15.04944	16.45303	15.80453	15.08176	18.57596	17.85751	16.44992	14.93863	16.05568	15.08544
Cingulate_Cortex_area_2	9.761163	9.652436	10.877995	10.035159	9.96854	9.437798	12.622218	9.450102	9.646339	9.423961	10.133535	9.800815	9.379722	11.408993	10.976317	10.115021	9.296097	9.835673	9.404961
cingulum	3.492723	3.406237	3.883481	3.529629	3.492639	3.344971	4.527074	3.162262	3.290414	3.274935	3.603864	3.318342	3.237416	4.089861	3.904214	3.625677	3.195758	3.494679	3.266153
Cochlear_nucleus	1.1237555	1.1184248	1.3083613	1.1559026	1.1214901	1.0783878	1.5029931	0.9637111	1.0127128	1.0328736	1.1911297	1.0455809	1.0323793	1.3903549	1.2481869	1.2244269	0.9870825	1.1373499	1.0234722
Commisure_inferior_Colliculus	0.3012437	0.3130952	0.3444716	0.3171572	0.3339917	0.3020288	0.4206232	0.3590978	0.3538928	0.322445	0.3168173	0.3548342	0.3377414	0.3529069	0.3289218	0.3193215	0.338373	0.3099645	0.3334774
commisure_superior_collicuus	0.1958601	0.1894262	0.2155751	0.197298	0.1973437	0.1935097	0.2507915	0.1806477	0.1853779	0.1854522	0.2024334	0.1875587	0.1842145	0.2285598	0.2172096	0.2073325	0.1821538	0.1980644	0.1836112
copula	2.85993	2.886745	3.427517	2.958887	2.964503	2.784321	3.878512	2.629115	2.794193	2.833058	3.079774	2.762813	2.762086	3.604385	3.157195	3.174727	2.620889	2.885505	2.722649
Corpus_Callosum_associated_White_Matter	43.52195	42.88166	48.60539	44.21626	44.15879	41.90292	56.57667	41.2087	42.41068	41.68024	45.04544	42.99986	41.42828	51.17436	48.5961	45.361	40.76597	43.65281	41.7218
Crus_1_ansiform_lobule	17.26136	17.26335	20.31912	17.86547	17.76198	16.69123	23.21294	15.95804	16.87951	16.75749	18.31787	16.78543	16.60894	21.43545	19.05113	18.91724	16.07272	17.45694	16.53103
Crus_2_ansiform_lobule	10.049958	10.17566	12.017464	10.4762	10.455384	9.805295	13.607185	9.333219	9.756846	9.853602	10.839256	9.924281	9.71284	12.723698	11.112195	11.231767	9.288596	10.247999	9.623117
dentate_gyrus	17.13062	16.74099	19.02731	17.21987	17.1371	16.59295	22.64488	15.77509	16.29277	16.04052	17.79035	16.39768	15.98517	20.20342	18.98362	17.93154	15.70777	17.16569	16.13702
Dentate_nucleus	0.8951269	0.8845175	1.0486442	0.916988	0.8912195	0.8425239	1.1956979	0.7491213	0.8046015	0.8302557	0.9428315	0.8191788	0.8181896	1.1119967	0.9933015	0.973441	0.7764409	0.894254	0.8143977
Dorsal_Peduncular_Cortex	1.590165	1.57126	1.785786	1.614149	1.586196	1.519398	2.049223	1.445573	1.491992	1.497889	1.651358	1.532973	1.474025	1.880346	1.797838	1.654315	1.413616	1.587607	1.45829
Dorsal_Tenia_Tecta	1.106841	1.0776133	1.2485536	1.1363299	1.1044085	1.0549094	1.4323676	0.9918259	1.0311679	1.0541868	1.1501781	1.0433483	1.0194509	1.2968907	1.2484716	1.1453834	1.0066765	1.1038922	1.0264087
Endopiriform_Nucleus	9.108361	9.003971	10.080648	9.336114	9.330929	8.856274	11.732209	8.964835	9.131734	8.799408	9.419328	9.254243	8.823828	10.597814	10.216031	9.418432	8.796058	9.189984	8.875955
entopeduncular_nucleus	0.2349824	0.2249816	0.2589657	0.2333189	0.2273893	0.2118524	0.2968681	0.2114096	0.2227217	0.2266248	0.2376994	0.2219897	0.2173123	0.271797	0.2610155	0.2423823	0.2181945	0.2226814	0.2308942
external_medullary_lamina	0.6810377	0.6724361	0.7702685	0.6852246	0.7051075	0.6492624	0.8677359	0.6570255	0.6673772	0.6575864	0.7004201	0.6874402	0.6451374	0.7960628	0.7550042	0.7051786	0.6280937	0.6758744	0.6524718
Fasciculus_retroflexus	0.232242	0.2294467	0.2561916	0.238036	0.2377317	0.2307956	0.2956307	0.2497667	0.2495449	0.2327233	0.2463872	0.2468371	0.2372144	0.2716311	0.2566156	0.2447518	0.2448108	0.2369202	0.2476392
fastigial_nucleus	1.0509508	1.0473376	1.2083246	1.0896315	1.07077	1.0287137	1.4525361	1.0040648	1.0398909	1.00543	1.1173297	1.0455671	1.0096381	1.2955659	1.1594144	1.1521134	1.000534	1.0707559	1.0194919
Fimbria	4.927669	4.802117	5.400602	4.971249	4.903959	4.772481	6.33935	4.549875	4.687553	4.617905	5.106776	4.741878	4.608514	5.76345	5.522515	5.125032	4.595369	4.967673	4.689451
flocculus	10.823471	10.805768	12.600547	11.255806	11.046609	10.427603	14.529911	10.159326	10.689838	10.43234	11.428497	10.631284	10.522596	13.276687	12.00524	11.720409	10.229778	10.885886	10.413682
Fornix	0.5872317	0.6013976	0.6504514	0.6067784	0.6143775	0.5873424	0.815633	0.5662026	0.5773483	0.5332161	0.6098096	0.6062818	0.563523	0.6841552	0.6744148	0.6186043	0.5529779	0.6192225	0.5592171
Fourth_ventricle	2.943771	2.917545	3.459414	3.024968	2.966677	2.839833	4.011963	2.591248	2.76329	2.80067	3.138257	2.747067	2.7677	3.662688	3.251172	3.217024	2.637331	2.958903	2.709603
Frontal_Association_Cortex	116.6423	115.7522	132.313	119.0517	121.0856	112.9816	152.8749	110.4519	115.0054	109.3432	123.4739	116.716	110.793	139.9533	133.4777	123.5274	108.5254	120.7767	111.6869
Globus_pallidus	4.652653	4.564301	5.169289	4.711261	4.65896	4.427496	5.968336	4.264402	4.408715	4.366017	4.78001	4.489585	4.321666	5.412164	5.215601	4.836501	4.259149	4.642081	4.366514
hindbrain_medulla_pons	96.4649	96.85273	113.53162	100.16914	99.01224	93.24926	129.52708	89.66453	94.27069	93.7356	102.66471	94.388	93.45429	119.55074	106.72601	105.33809	90.04756	97.2943	92.5335
Hippocampal_layer_CA1	21.52764	21.06858	23.94734	21.61748	21.60603	20.7753	28.25396	20.05467	20.71024	20.36857	22.2826	20.81797	20.23394	25.37418	23.80802	22.46936	19.96619	21.52207	20.47709
Hippocampal_layer_CA2	2.332114	2.281843	2.567483	2.357619	2.389031	2.250216	2.991233	2.297256	2.350229	2.274137	2.398517	2.35667	2.25476	2.702333	2.588526	2.412172	2.253759	2.329407	2.303278
Hippocampal_layer_CA3	21.56261	20.99272	23.81768	21.62126	21.55282	20.77196	27.99223	19.65837	20.36097	20.18526	22.3445	20.45643	19.90638	25.22072	24.00986	22.46005	19.6624	21.56776	20.25727
hypothalamus	28.80927	28.21428	31.76902	29.09205	29.01418	27.77763	37.31429	26.76384	27.57395	27.05366	29.74669	27.91746	26.96598	33.58073	32.26681	29.96625	26.65928	28.94647	27.31093
Inferior_Colliculus	15.81359	15.7948	18.28671	16.30468	15.98423	15.25962	21.27398	14.6501	15.27113	15.04383	16.69679	15.36509	15.25615	19.22836	17.59351	16.9806	14.77393	15.91357	15.07007
Infralimbic_Cortex	1.538727	1.53174	1.707601	1.588654	1.575058	1.55777	2.05892	1.425436	1.470062	1.420033	1.636743	1.485513	1.445026	1.845633	1.766254	1.617422	1.434477	1.613351	1.428911
Insular_Cortex	24.96768	24.65437	27.79039	25.46475	25.22495	24.21943	32.21668	23.33685	23.9098	23.47697	25.91327	24.44744	23.49423	29.29183	28.08859	25.92275	23.05201	25.22473	23.40776
Internal_capsule	8.169375	8.010203	9.026419	8.260337	8.27784	7.859529	10.440161	7.77142	7.952818	7.823368	8.434839	8.069769	7.752775	9.521046	9.159936	8.469293	7.694541	8.187439	7.868244
intersposed_nucleus	1.303341	1.303858	1.523956	1.331932	1.340081	1.253116	1.763318	1.170665	1.238992	1.249987	1.376593	1.247478	1.230062	1.608782	1.437382	1.417662	1.18967	1.315963	1.231013
intrabulbar_part_of_anterior_commisure	2.655288	2.690045	3.060407	2.722555	2.867589	2.612157	3.582572	2.71655	2.771961	2.473222	2.84551	2.880938	2.622467	3.22101	3.042857	2.887566	2.527518	2.78667	2.626237
Lateral_olfactory_tract	2.443513	2.390878	2.735772	2.511242	2.521716	2.364864	3.146687	2.344429	2.42347	2.364804	2.546019	2.424447	2.338479	2.879381	2.759497	2.533448	2.342392	2.487047	2.363245
lateral_septum	10.058152	9.899018	11.229794	10.220483	10.076726	9.5953	12.876409	9.227091	9.514122	9.403953	10.343981	9.710877	9.382966	11.785321	11.292911	10.400249	9.182103	10.043135	9.395871
Lateral_ventricle	14.28297	13.98729	15.82142	14.43606	14.47237	13.74365	18.46025	13.47367	13.89083	13.61984	14.69963	13.9728	13.49901	16.61503	15.94403	14.76076	13.33768	14.30328	13.6241
mamillary_bodies	1.667479	1.637219	1.84855	1.698616	1.711426	1.614737	2.099384	1.68785	1.707196	1.647427	1.73579	1.711541	1.627568	1.941805	1.852867	1.736194	1.638189	1.669656	1.686807
mammilothalamic_tract	0.3683317	0.3534673	0.4093858	0.3692763	0.3655091	0.3554854	0.4855759	0.3215432	0.3396057	0.3363149	0.3836436	0.3390029	0.3339703	0.4288255	0.4165608	0.3821795	0.3336395	0.3719578	0.3445904
medial_septum	1.369284	1.373162	1.530451	1.403559	1.379667	1.333011	1.807999	1.262128	1.298246	1.246708	1.428987	1.346258	1.287771	1.620885	1.543936	1.422757	1.253629	1.40612	1.276418
median_preoptic_area	0.04972172	0.05061253	0.05367381	0.05316631	0.05456922	0.05469188	0.06449356	0.0502946	0.05018834	0.04767475	0.05479094	0.05120335	0.05007258	0.05929339	0.05808583	0.05288311	0.0508109	0.05493008	0.04883377
midbrain	35.35695	34.74345	39.77865	35.72033	35.49465	34.32683	47.17226	32.50538	33.75497	33.30081	36.86398	33.99789	33.2991	42.20566	39.16301	37.24103	32.53189	35.53406	33.27213
Navicular_nuclear_basin_forebrain	1.788407	1.775971	2.012887	1.845345	1.818899	1.742584	2.352247	1.703768	1.740239	1.690191	1.861648	1.778715	1.684257	2.08385	2.024166	1.864167	1.660295	1.812451	1.671225
Nucleus_accumbens	7.274398	7.21222	8.157575	7.447221	7.383289	6.97562	9.398964	6.897491	7.051086	6.931688	7.543724	7.266063	6.924919	8.606096	8.23052	7.551675	6.751714	7.329883	6.900516
Occipital_Cortex	13.75456	13.73759	15.98813	14.16309	13.92756	13.2423	18.73907	12.65948	13.28344	13.12919	14.57337	13.32106	13.34155	16.7255	15.27197	14.75781	12.82631	13.79766	13.03623
Olfactory_Bulb	142.7445	136.6313	150.0538	134.8669	133.381	143.7381	182.3665	133.5911	132.037	146.076	151.2187	130.7062	138.4851	164.4805	149.1762	147.1515	133.5896	138.2288	137.802
Olfactory_tubercle	12.31158	12.24247	13.76588	12.6665	12.56922	11.97308	16.07918	11.81205	12.06543	11.74331	12.84898	12.36425	11.78439	14.5196	13.93117	12.82216	11.60709	12.50496	11.763
Optic_Chiasm	0.2638767	0.2582514	0.2936025	0.2746559	0.2667389	0.2690144	0.3621287	0.2334994	0.2452566	0.2382837	0.2781556	0.2408689	0.2422982	0.3143941	0.301364	0.2777593	0.2477446	0.2781952	0.2435166
Optic_tract	3.055785	2.98228	3.36904	3.091663	3.090366	3.002061	3.978971	2.895966	2.971392	2.882698	3.17758	2.971627	2.882552	3.557312	3.406019	3.177341	2.873209	3.097934	2.907637
Orbitofrontal_Cortex	0.4554036	0.4495068	0.5167644	0.4692945	0.4749447	0.4442922	0.5920481	0.4565171	0.4700636	0.4553017	0.4698037	0.4676219	0.4489488	0.5273785	0.5131117	0.4661335	0.4462323	0.4610357	0.4474233
paraflocculus	12.44086	12.30452	14.50863	12.81364	12.53147	11.87985	16.63079	11.16469	11.94473	11.88987	13.13082	11.80545	11.78368	15.38186	13.77124	13.56968	11.40419	12.46537	11.7676
paramedian_lobe	8.119592	8.130054	9.612089	8.424839	8.27982	7.764032	10.831386	7.327911	7.73077	7.831098	8.637673	7.820229	7.68203	10.208568	8.973369	8.964018	7.415107	8.162103	7.727689
Parietal_Association_Cortex	11.417751	11.086801	12.614222	11.440523	11.391967	10.962819	14.684922	10.397778	10.763423	10.690582	11.792089	10.808384	10.525828	13.283247	12.743634	11.846719	10.419048	11.403246	10.731931
Periaqueductal_grey	10.650049	10.416105	12.073827	10.735011	10.482436	10.226805	14.03885	9.357515	9.856778	9.987288	11.124066	9.848965	9.849028	12.795725	11.840133	11.241339	9.55008	10.600978	9.852195
Piriform_Cortex	28.14398	27.68092	31.18055	28.63841	28.44351	27.15995	36.27197	26.64072	27.34706	26.73696	29.09877	27.72102	26.67001	32.91475	31.60664	29.19764	26.44754	28.31832	26.96894
pons	22.7681	22.53564	25.97225	23.19398	22.98944	22.05337	30.65545	20.99207	21.84532	21.60876	23.89939	22.09449	21.70309	27.43225	25.31164	24.20403	21.12324	22.93469	21.62313
posterior_commisure	0.2289653	0.2177066	0.2563695	0.2220423	0.2113412	0.2078063	0.3074865	0.1718075	0.191627	0.2035007	0.2338993	0.1874856	0.1956262	0.2789768	0.2556784	0.2376531	0.1854197	0.2184589	0.2004185
Posterior_part_of_anterior_commissure	0.3354101	0.3233524	0.3736464	0.3363043	0.3264713	0.3163346	0.4139482	0.2874529	0.3052957	0.3165359	0.3413478	0.3030524	0.3035793	0.4002791	0.3774252	0.3439089	0.2983257	0.3273974	0.3075096
Prelimbic_Cortex	4.065178	4.034513	4.525655	4.161517	4.168774	3.960225	5.277927	3.920874	4.037634	3.924848	4.263008	4.115464	3.915097	4.830756	4.62865	4.261708	3.843393	4.147157	3.909531
Primary_Motor_Cortex	20.136	19.88224	22.47681	20.56891	20.35958	19.50739	26.18848	18.62583	19.27295	18.98056	20.97294	19.60234	18.89477	23.82593	22.84652	21.04607	18.50821	20.43767	18.86209
Primary_Somatosensory_Cortex	83.87027	82.618	93.08747	85.47978	84.85299	81.19196	108.26418	78.99526	81.05865	79.40025	86.91991	82.41653	79.23388	98.23158	94.29432	87.0663	78.24003	84.56897	79.57521
Primary_Visual_Cortex	26.71059	26.40755	30.26248	27.17242	26.97597	25.8578	35.47357	24.78629	25.74188	25.40926	27.89542	25.96131	25.4311	31.95292	29.62808	28.24958	24.83034	26.83424	25.45543
Retrosplenial_Cortex	32.18757	31.67696	36.3112	32.64281	32.48223	30.99902	42.28726	29.87509	31.02878	30.72928	33.4344	31.26513	30.54326	38.24005	35.79999	33.84459	29.88412	32.23488	30.69999
rhinal_cortex	48.57585	47.86995	54.75987	49.24743	48.88042	46.98616	64.44833	44.91267	46.59373	46.06988	50.67222	47.00894	45.96353	57.95285	54.00805	51.28463	44.99588	48.79745	46.16729
Secondary_Motor_Cortex	12.25848	12.16773	13.65321	12.4948	12.52196	11.83273	15.89195	11.80444	12.06303	11.66532	12.72001	12.33895	11.70826	14.35164	13.85443	12.75537	11.43202	12.37444	11.61673
Secondary_Somatosensory_Cortex	22.3802	21.92873	24.79145	22.71759	22.47209	21.54652	28.72383	20.61122	21.25676	21.02257	23.11398	21.58921	20.88636	26.1379	25.10229	23.20129	20.58484	22.46776	21.04347
Secondary_Visual_Cortex	32.24716	31.73537	36.41782	32.70798	32.5237	31.2674	42.76257	29.81968	30.96805	30.65314	33.6501	31.12141	30.52202	38.43629	35.77422	34.00829	29.80993	32.39351	30.55532
Simple_Lobule	17.04838	16.95067	19.8713	17.66353	17.32596	16.43166	22.93338	15.72037	16.5698	16.28953	18.04102	16.54272	16.30606	21.06241	18.87027	18.58442	15.86382	17.17563	16.25003
stria_medullaris_thalamus	0.6506818	0.6494957	0.7174121	0.6597446	0.6588059	0.6402585	0.841408	0.6232303	0.6184561	0.5944774	0.6850906	0.651142	0.6045124	0.7575141	0.7286491	0.6841485	0.5931874	0.659359	0.600691
Stria_terminalis	2.622929	2.570605	2.880961	2.652587	2.632745	2.548864	3.388533	2.502926	2.561796	2.466486	2.722002	2.574972	2.475332	3.070871	2.933788	2.73954	2.481762	2.645398	2.542994
Subfornical_organ	0.08420515	0.07839046	0.09305906	0.08077392	0.07709272	0.07615344	0.09566542	0.0681598	0.07185733	0.07497053	0.08290002	0.07296567	0.07305918	0.09877164	0.09151498	0.08534645	0.07032213	0.07945576	0.07530239
subicular_region	26.10939	25.80489	29.61033	26.57106	26.40984	25.43115	34.6719	24.24586	25.17354	24.90074	27.30146	25.38133	24.86552	31.25217	28.99997	27.63512	24.27466	26.30783	24.81406
substantia_nigra	2.453058	2.37722	2.743297	2.423219	2.375288	2.309495	3.262132	2.052217	2.166218	2.252016	2.528167	2.188814	2.179967	2.919359	2.716978	2.571984	2.112109	2.408862	2.206289
Superior_Colliculus	16.58361	16.46581	18.83715	16.93383	16.93119	16.14762	22.05143	15.62142	16.12771	15.90713	17.33394	16.42319	15.88902	19.8543	18.42606	17.53786	15.54097	16.7435	15.91097
Temporal_Association	11.587018	11.48957	13.186735	11.804261	11.758456	11.348807	15.523184	10.678929	11.081438	10.939858	12.159525	11.208065	11.008501	13.887501	12.878681	12.300564	10.675546	11.725611	10.888102
Thalamus	50.59174	49.44348	55.81308	50.8947	50.89623	48.66157	65.28905	47.21957	48.64905	47.88398	52.20682	49.02394	47.40295	58.97769	56.46007	52.59882	46.93302	50.64272	48.26727
Third_ventricle	4.705066	4.607384	5.226634	4.746355	4.742286	4.497078	6.060723	4.484242	4.610628	4.549089	4.845943	4.633914	4.47242	5.486884	5.286082	4.88769	4.457529	4.70548	4.579123
trochlear_nerve	0.08337088	0.08741775	0.09691615	0.08753149	0.08740665	0.08114642	0.11140264	0.07952646	0.07955035	0.07680096	0.08902971	0.08779529	0.08275119	0.10132964	0.094347	0.08949802	0.07865103	0.08792166	0.08041348
ventral_pallidum	2.618633	2.596614	2.902644	2.689851	2.628002	2.53321	3.360865	2.463194	2.521872	2.449245	2.730866	2.577592	2.461865	3.067542	2.939745	2.727809	2.434802	2.637145	2.482022
brainvolumes	1482.788	1461.225	1665.584	1502.347	1493.665	1438.698	1942.706	1384.016	1428.934	1420.697	1552.037	1440.107	1410.484	1764.361	1646.794	1562.984	1379.396	1489.912	1413.453

	100	101	102	14	16	17	19	23	24	34	41	48	54	55	86	89	92	97	99
	WT	WT	WT	WT	WT	WT	WT	WT	WT	WT	WT	WT	WT	WT	WT	WT	WT	WT	WT
Absolute Volume	F	F	F	M	M	M	M	M	M	M	M	M	M	M	M	M	M	M	M
	Pat	Pat	Pat	Pat	Pat	Pat	Pat	Pat	Pat	Pat	Pat	Pat	Pat	Pat	Pat	Pat	Pat	Pat	Pat
amygdaloid_area	29.74046	29.12352	27.21824	30.54346	29.22214	30.46414	32.09189	30.9695	30.56559	28.38346	31.65174	32.71297	33.35946	35.10222	30.24294	30.64456	31.42934	30.69019	31.67874
Anterior_part_of_anterior_commissure	1.338523	1.285915	1.196055	1.364688	1.30787	1.372404	1.44864	1.39516	1.385217	1.251354	1.433288	1.466441	1.522125	1.588885	1.35619	1.393353	1.385158	1.366285	1.422174
Aqueduct	1.617315	1.661876	1.509739	1.639199	1.589037	1.649159	1.709649	1.662757	1.701882	1.567555	1.684179	1.782821	1.787701	1.849783	1.609484	1.657834	1.694386	1.738195	1.693781
auditory_cortex	20.68581	20.61687	19.04325	21.25971	20.34057	21.16235	22.05205	21.42773	21.30931	19.66796	21.87666	22.65053	23.05344	24.16893	20.9613	21.28517	21.79544	21.53956	21.96593
basal_forebrain	16.81968	16.8397	15.94176	17.55768	16.90552	17.38227	18.18446	17.59919	17.74421	16.28388	18.01447	18.57729	19.08478	19.94309	17.13243	17.38429	17.68091	17.71771	17.86766
Bed_nucleus_of_stria_terminalis	2.882779	2.758481	2.618898	3.054613	2.941163	3.052429	3.097106	3.094309	3.048792	2.839798	3.066659	3.200449	3.271164	3.451168	3.041483	3.001786	3.098591	2.891322	3.054958
caudaputamen	45.41901	45.34946	42.9468	47.4842	45.57004	46.96563	49.14153	47.62697	47.80417	43.9652	48.71009	50.29138	51.60906	53.98846	46.40101	47.13653	47.955	47.76112	48.41325
cerebellar_lobule_1_2	7.990418	7.861474	7.038944	8.043979	7.76398	8.250775	8.547083	8.290057	8.29623	7.749425	8.449806	8.997638	8.970694	9.408366	8.016873	8.350254	8.456215	8.476774	8.613033
cerebellar_lobule_10	3.337896	3.306948	2.959336	3.424096	3.241885	3.478256	3.561858	3.482605	3.491446	3.208333	3.492817	3.855778	3.763394	3.97849	3.384717	3.547816	3.520898	3.581209	3.645862
cerebellar_lobule_3	6.886033	6.72391	5.972106	7.007517	6.670836	7.173589	7.359238	7.235753	7.144573	6.668215	7.329572	7.92006	7.82032	8.263484	6.960858	7.318566	7.299963	7.277112	7.512958
cerebellar_lobule_4_5	21.24215	21.30445	19.06804	21.67572	20.7344	22.00302	22.63365	22.02819	22.24342	20.61618	22.33271	24.25812	23.93381	25.09739	21.34192	22.28943	22.3583	22.80809	22.93034
cerebellar_lobule_6	8.384771	8.475621	7.665782	8.650102	8.168169	8.799691	9.014009	8.690589	8.771677	8.16103	8.865343	9.737121	9.472245	10.020669	8.496974	8.902895	8.97275	9.17319	9.21241
cerebellar_lobule_7	3.229948	3.315245	3.063323	3.355374	3.1495	3.400937	3.435852	3.303972	3.353645	3.13837	3.382399	3.688583	3.595581	3.809423	3.270511	3.406222	3.519889	3.568457	3.546525
cerebellar_lobule_8	3.600925	3.63607	3.267099	3.710287	3.484439	3.769681	3.891006	3.740301	3.773516	3.503575	3.838185	4.214856	4.102086	4.331298	3.640227	3.87066	3.848882	3.979705	3.996895
cerebellar_lobule_9	8.390129	8.546178	7.712417	8.659155	8.162139	8.820979	9.064394	8.698453	8.78923	8.190276	8.926496	9.771949	9.518905	10.064599	8.48535	8.960916	9.004845	9.282266	9.276256
Cerebellar_White_Matter_Arbor_vita_of_cerebellum	26.68803	26.43437	23.64937	27.14919	25.82102	27.72364	28.63886	27.68765	27.65885	25.86664	28.14571	30.58157	30.03913	31.60243	26.82191	28.09767	28.24509	28.45091	28.95985
cerebral_peduncle	2.925561	2.873738	2.6815	3.018897	2.878357	3.001642	3.099112	3.042703	2.991297	2.806713	3.07864	3.18859	3.228246	3.41346	2.980756	2.997859	3.132501	2.986264	3.092398
Cingulate_Cortex_area_1	15.0106	15.19544	14.35796	15.72735	15.03714	15.44746	16.22986	15.69135	15.78568	14.53979	16.06528	16.72221	17.04607	17.89415	15.32146	15.56107	15.8845	15.96222	16.04502
Cingulate_Cortex_area_2	9.279741	9.437281	8.94631	9.813548	9.416565	9.615085	10.011238	9.74694	9.871177	9.002594	9.9537	10.280935	10.547576	10.987248	9.487988	9.609313	9.799843	9.905501	9.905867
cingulum	3.288714	3.211839	3.008845	3.41581	3.255951	3.402094	3.527994	3.451521	3.416375	3.132076	3.511507	3.660062	3.744915	3.920079	3.374859	3.426029	3.474456	3.392143	3.525121
Cochlear_nucleus	1.0540852	0.9804926	0.8626996	1.0613426	0.9987931	1.0984788	1.1531303	1.1163245	1.066866	1.0172716	1.1354517	1.225282	1.2150485	1.2821021	1.0684754	1.1418203	1.1184695	1.0793556	1.1687382
Commisure_inferior_Colliculus	0.3105684	0.3616273	0.3258604	0.3203187	0.3218759	0.3112234	0.3158099	0.3055401	0.3432719	0.3033678	0.3093265	0.3217518	0.3256046	0.330102	0.3015669	0.3019495	0.3175261	0.3589122	0.3069938
commisure_superior_collicuus	0.1879325	0.1844269	0.1685104	0.1930973	0.183772	0.1922549	0.199971	0.1933879	0.1899261	0.177283	0.1978901	0.2061851	0.2075933	0.2144498	0.1920038	0.1918671	0.196538	0.1895485	0.1980273
copula	2.728656	2.731724	2.505586	2.816265	2.644878	2.87878	2.940207	2.812801	2.811646	2.658127	2.900006	3.147024	3.081499	3.252885	2.771813	2.900921	2.967189	2.957593	3.018858
Corpus_Callosum_associated_White_Matter	41.42683	41.45827	38.84734	43.00855	41.29527	42.68089	44.34137	43.2567	43.26897	39.95009	44.05617	45.66325	46.49536	48.80203	42.20727	42.90019	43.87973	43.42081	44.06036
Crus_1_ansiform_lobule	16.56301	16.4532	14.84504	16.90622	16.0393	17.21813	17.71044	17.11448	17.14294	16.05781	17.39998	18.94532	18.54901	19.56069	16.6609	17.39484	17.579	17.63626	17.96674
Crus_2_ansiform_lobule	9.59872	9.57659	8.624462	9.828406	9.24292	10.096688	10.440531	9.95737	9.904793	9.349484	10.218973	11.079376	10.853402	11.46174	9.667492	10.210471	10.319542	10.35952	10.561229
dentate_gyrus	16.2667	16.0814	14.71202	16.62774	15.89308	16.66695	17.39063	16.87941	16.68587	15.40896	17.29859	17.89424	18.22652	19.05786	16.44291	16.85026	17.10459	16.8609	17.35095
Dentate_nucleus	0.8344675	0.7711669	0.6901829	0.8488725	0.7924111	0.8777141	0.8985388	0.8894529	0.848421	0.8001886	0.8922429	0.9753168	0.9615499	1.0201208	0.8569485	0.9038909	0.8939107	0.8486935	0.9265827
Dorsal_Peduncular_Cortex	1.468455	1.443933	1.36196	1.562824	1.479359	1.54871	1.603903	1.573591	1.544615	1.446033	1.617209	1.682129	1.715735	1.80157	1.536189	1.575367	1.596638	1.555458	1.617183
Dorsal_Tenia_Tecta	1.0323679	0.9944719	0.9324236	1.0924593	1.0371238	1.0783465	1.1120229	1.1028549	1.0904192	0.9725247	1.114235	1.1712004	1.1925024	1.2445585	1.071946	1.086784	1.0871627	1.0695041	1.1259652
Endopiriform_Nucleus	8.742715	8.966304	8.500074	9.129454	8.835422	8.979886	9.39557	9.084571	9.251545	8.488721	9.295011	9.545558	9.806692	10.230106	8.847571	8.943849	9.15906	9.334301	9.213748
entopeduncular_nucleus	0.2160957	0.22846	0.2173389	0.234617	0.2229996	0.2242202	0.2275679	0.2254685	0.2321051	0.1982095	0.2274687	0.2446765	0.2449501	0.2590531	0.2239191	0.2246641	0.226717	0.2410034	0.2362813
external_medullary_lamina	0.6525642	0.6302894	0.5984805	0.6683363	0.642861	0.67041	0.6957052	0.6823829	0.6606815	0.6412946	0.6858932	0.7023353	0.7108012	0.7567832	0.6640266	0.6615005	0.7038386	0.6548795	0.6849174
Fasciculus_retroflexus	0.2264911	0.2592364	0.2437046	0.2379519	0.2311541	0.2261617	0.239906	0.2288185	0.246936	0.2144541	0.2382646	0.2422259	0.2478501	0.26153	0.2218108	0.2291141	0.2310045	0.2680558	0.2392996
fastigial_nucleus	1.0137786	1.0235216	0.9036687	1.0147822	0.9795345	1.0318276	1.0906215	1.0362648	1.0576209	0.9797591	1.0595357	1.1592019	1.1433208	1.1789943	1.0051599	1.0579253	1.0474695	1.1071284	1.0923831
Fimbria	4.689034	4.647564	4.361673	4.803124	4.608983	4.774086	5.059444	4.859939	4.845456	4.428045	4.98536	5.1579	5.260641	5.533808	4.734719	4.828107	4.886201	4.916782	5.002617
flocculus	10.360133	10.412525	9.309746	10.550911	10.13948	10.712881	11.05292	10.763494	10.91795	10.063135	10.94877	11.834405	11.707911	12.268365	10.383275	10.892148	10.895577	11.193106	11.187942
Fornix	0.5738281	0.5537004	0.5187113	0.5789961	0.558625	0.5825652	0.6355899	0.5933476	0.5809651	0.5637475	0.6131057	0.6290216	0.6439158	0.6676922	0.5693503	0.5839889	0.6074535	0.5829244	0.6020997
Fourth_ventricle	2.784184	2.694346	2.411912	2.832525	2.673197	2.906986	3.000876	2.90585	2.852906	2.692051	2.967786	3.207155	3.173277	3.342451	2.83109	2.969695	2.977104	2.926982	3.065808
Frontal_Association_Cortex	110.5174	111.1983	104.539	115.4667	109.0616	114.4419	121.1412	115.7087	116.0483	107.2888	118.6856	127.1873	126.4734	136.1005	113.4745	115.3213	118.1794	118.6002	120.2889
Globus_pallidus	4.372891	4.300244	4.057139	4.567297	4.372834	4.540047	4.748382	4.607657	4.558293	4.240737	4.67659	4.896636	4.984965	5.228702	4.483875	4.534561	4.64223	4.539938	4.687292
hindbrain_medulla_pons	92.16292	92.15782	82.85675	94.2271	89.63707	96.11214	98.95145	95.81127	96.09367	89.32599	97.56398	105.42541	103.96234	109.34656	92.90094	97.52617	97.99147	99.51982	100.34763
Hippocampal_layer_CA1	20.47527	20.42273	18.76024	20.97895	20.10195	20.94605	21.77614	21.21008	21.14035	19.45322	21.69049	22.4144	22.82208	23.96883	20.7287	21.16874	21.52818	21.33246	21.77065
Hippocampal_layer_CA2	2.248061	2.306546	2.175922	2.325337	2.245035	2.283284	2.381822	2.310535	2.353758	2.150641	2.354937	2.411515	2.459249	2.593032	2.26171	2.276752	2.352909	2.376165	2.34477
Hippocampal_layer_CA3	20.4273	19.90967	18.43994	20.93592	19.95443	20.91555	21.91717	21.25934	20.86776	19.36775	21.72642	22.44768	22.86844	24.05961	20.7828	21.07103	21.60354	20.95094	21.81919
hypothalamus	27.39924	26.99853	25.32182	28.20752	27.02253	28.06606	29.59423	28.50164	28.24831	26.24806	29.11319	30.12216	30.75433	32.2676	27.82074	28.16333	28.9064	28.34905	29.1285
Inferior_Colliculus	15.08668	15.00389	13.4423	15.30321	14.75217	15.5788	16.14296	15.7512	15.78669	14.50374	16.04068	17.03407	17.06475	17.84794	15.23511	15.89589	15.92203	16.16381	16.31487
Infralimbic_Cortex	1.473641	1.451869	1.345516	1.521443	1.442993	1.512261	1.611828	1.540247	1.519208	1.392465	1.599792	1.643587	1.703927	1.77251	1.504957	1.551214	1.551391	1.548071	1.598364
Insular_Cortex	23.60879	23.21911	21.91331	24.56684	23.55005	24.44223	25.74078	24.86871	24.67334	23.00884	25.48521	26.27131	26.91382	28.16532	24.16114	24.57286	25.08949	24.59963	25.28774
Internal_capsule	7.806263	7.780115	7.386262	8.051965	7.771455	7.996125	8.396962	8.120797	8.083787	7.524872	8.264171	8.513382	8.683282	9.174513	7.913792	8.022363	8.256275	8.133432	8.265117
intersposed_nucleus	1.256274	1.193973	1.067836	1.267648	1.20482	1.305609	1.339555	1.304483	1.262244	1.202201	1.30696	1.405452	1.396567	1.469992	1.270516	1.307512	1.347646	1.270927	1.349704
intrabulbar_part_of_anterior_commisure	2.577303	2.680271	2.510187	2.671497	2.501592	2.653812	2.83895	2.643318	2.717341	2.607302	2.768806	2.982901	2.919203	3.112304	2.564555	2.604407	2.814723	2.836966	2.756217
Lateral_olfactory_tract	2.330223	2.360659	2.220294	2.4585	2.349635	2.412231	2.501569	2.441426	2.481461	2.224604	2.473364	2.593193	2.635864	2.793661	2.402083	2.409611	2.436163	2.467973	2.491314
lateral_septum	9.401988	9.247493	8.772644	9.889749	9.447127	9.829937	10.231527	9.983976	9.900945	9.168595	10.165109	10.555593	10.792424	11.342118	9.738303	9.873664	10.04161	9.784909	10.12837
Lateral_ventricle	13.61089	13.48854	12.68963	14.12281	13.57569	14.01481	14.57586	14.18076	14.17036	13.12383	14.4007	14.87889	15.22132	15.99364	13.87679	13.97442	14.40325	14.07582	14.38194
mamillary_bodies	1.606285	1.695355	1.589167	1.679164	1.619077	1.633244	1.700992	1.654554	1.697063	1.540199	1.684054	1.737339	1.766301	1.853989	1.61268	1.62454	1.683268	1.754986	1.688079
mammilothalamic_tract	0.349567	0.3342644	0.3125508	0.3623836	0.3386155	0.3572813	0.3750196	0.3628492	0.35731	0.3183128	0.3707245	0.3848122	0.3928838	0.4130312	0.3555715	0.3612463	0.3639951	0.3538042	0.3754595
medial_septum	1.294985	1.272079	1.202687	1.338363	1.273058	1.339332	1.420796	1.361866	1.350967	1.258686	1.407488	1.449252	1.488526	1.558596	1.321542	1.368563	1.387656	1.36259	1.400284
median_preoptic_area	0.05340634	0.05094274	0.0464845	0.04858525	0.04849583	0.05044801	0.05602061	0.05082829	0.05200731	0.04804702	0.05553417	0.05348827	0.05597867	0.0588457	0.049747	0.05307425	0.05243525	0.05145127	0.05186985
midbrain	33.69299	33.14798	30.13303	34.17943	32.88265	34.564	35.88359	35.011	34.64707	32.07839	35.81281	37.18775	37.75273	39.52046	34.07227	35.09501	35.48071	34.91279	35.9874
Navicular_nuclear_basin_forebrain	1.691473	1.679579	1.578544	1.773602	1.701975	1.747386	1.849961	1.787573	1.770911	1.651294	1.830237	1.910364	1.955208	2.012656	1.733731	1.761503	1.809794	1.786692	1.82235
Nucleus_accumbens	6.852054	6.835094	6.541441	7.253951	6.903617	7.126093	7.426206	7.257668	7.253474	6.703274	7.420085	7.692368	7.858525	8.25528	7.067681	7.219058	7.341278	7.245387	7.388943
Occipital_Cortex	13.12879	12.97036	11.64552	13.28246	12.80883	13.60295	14.01037	13.7091	13.73408	12.68912	13.91963	14.8051	14.77422	15.51879	13.25955	13.76374	13.91688	13.98835	14.19011
Olfactory_Bulb	139.9928	136.5481	151.9883	128.8717	139.9966	136.1064	134.4214	140.525	128.8662	143.5689	136.5177	140.7861	137.8497	146.1017	143.1788	149.3792	141.5941	128.3598	141.8416
Olfactory_tubercle	11.68797	11.77997	11.17833	12.3076	11.75352	12.0854	12.66842	12.30103	12.35748	11.36657	12.61587	13.051	13.36623	13.95131	11.94891	12.21302	12.40298	12.43619	12.55286
Optic_Chiasm	0.2580918	0.2463282	0.2231514	0.2578033	0.246812	0.2608531	0.2798844	0.2624827	0.2645251	0.229303	0.2741427	0.2811877	0.2939952	0.3036113	0.2563621	0.262678	0.2581542	0.2596756	0.2722923
Optic_tract	2.935112	2.917083	2.702187	2.984456	2.874194	2.980253	3.162375	3.031294	3.025104	2.791703	3.106606	3.178986	3.271368	3.406707	2.941146	2.986846	3.047705	3.050937	3.099721
Orbitofrontal_Cortex	0.4379773	0.4512415	0.4271965	0.4634589	0.4511071	0.4530987	0.4645946	0.4601797	0.4762388	0.4280843	0.4596224	0.4764921	0.489433	0.5119348	0.45166	0.4471156	0.4598606	0.4707157	0.4591523
paraflocculus	11.78101	11.61829	10.4243	12.0622	11.44597	12.24348	12.58567	12.2708	12.26109	11.3612	12.45351	13.61707	13.39213	14.12008	11.95735	12.53073	12.48068	12.54164	12.88501
paramedian_lobe	7.668268	7.592289	6.775542	7.886381	7.41559	8.059188	8.267055	8.021513	7.960171	7.399508	8.144828	8.950035	8.712533	9.23671	7.788081	8.221236	8.176109	8.259557	8.472267
Parietal_Association_Cortex	10.77862	10.543686	9.830594	11.089843	10.583101	11.070746	11.625253	11.23924	11.065439	10.22971	11.497533	11.872331	12.116815	12.740805	11.002194	11.140926	11.404105	11.116452	11.540258
Periaqueductal_grey	9.993838	9.704591	8.791736	10.214553	9.750659	10.333664	10.665613	10.502942	10.314621	9.445468	10.727625	11.283081	11.375603	11.952543	10.263119	10.610645	10.588689	10.425526	10.916259
Piriform_Cortex	26.77814	26.85394	25.36045	27.87687	26.73479	27.52175	28.83115	27.91608	28.04577	25.72368	28.55666	29.52666	30.2053	31.67518	27.22584	27.65761	28.18862	28.22984	28.4894
pons	21.76872	21.4028	19.40202	22.03632	21.27141	22.36294	23.16752	22.70301	22.53765	20.77217	23.07442	24.21325	24.44566	25.56444	22.06038	22.71962	22.99028	22.73484	23.35829
posterior_commisure	0.2049032	0.1856991	0.1672099	0.2105699	0.197053	0.2165679	0.2164386	0.2211415	0.208799	0.1895568	0.2243599	0.2401133	0.2394925	0.2574891	0.2157194	0.2247402	0.2208948	0.2028557	0.2312221
Posterior_part_of_anterior_commissure	0.310321	0.2976882	0.281793	0.3269881	0.3091108	0.322869	0.3329978	0.327708	0.3257864	0.2914862	0.3330415	0.3472256	0.3552989	0.3766751	0.3222475	0.328444	0.3285304	0.3178165	0.336317
Prelimbic_Cortex	3.854873	3.931983	3.744629	4.073787	3.865103	3.966731	4.164534	4.038143	4.074378	3.748379	4.152404	4.330283	4.389543	4.640146	3.958833	4.042398	4.125308	4.158575	4.162819
Primary_Motor_Cortex	18.9643	18.72304	17.70213	19.89275	18.9185	19.642	20.65675	20.01991	19.8283	18.34955	20.49762	21.40122	21.78454	22.88786	19.55168	19.95745	20.2441	19.89941	20.49852
Primary_Somatosensory_Cortex	79.64208	79.08463	74.61738	82.8497	79.44921	82.11156	86.1771	83.40936	83.24965	77.012	85.29969	88.11314	90.19413	94.52435	81.21875	82.50092	84.21103	83.34501	84.95298
Primary_Visual_Cortex	25.52641	25.25318	22.99113	26.02042	25.00651	26.2405	27.13742	26.56802	26.41543	24.34553	27.05874	28.2781	28.55693	29.91175	25.84652	26.57259	26.94632	26.70787	27.30003
Retrosplenial_Cortex	30.69435	30.36801	27.94952	31.47362	30.24312	31.59936	32.67722	31.99351	31.78864	29.33995	32.50386	33.90635	34.3231	36.04729	31.21012	31.87715	32.49017	31.95119	32.75443
rhinal_cortex	46.3366	45.74971	41.77412	47.25549	45.39835	47.56965	49.38738	48.2036	47.87158	44.10915	49.16678	51.3365	51.94745	54.39594	46.968	48.1927	48.91147	48.32759	49.56086
Secondary_Motor_Cortex	11.57211	11.6911	11.08731	12.17279	11.6405	11.99187	12.60387	12.18048	12.21208	11.47048	12.5028	12.95791	13.18259	13.86677	11.8973	12.06762	12.45843	12.31603	12.42832
Secondary_Somatosensory_Cortex	21.13759	20.66063	19.46672	21.9234	21.01112	21.84641	22.93021	22.21806	21.99448	20.39318	22.62624	23.44915	23.96024	25.14869	21.63293	21.93556	22.37211	21.85346	22.56429
Secondary_Visual_Cortex	30.78289	30.36182	27.68235	31.38865	30.16592	31.64669	32.78902	32.02778	31.75577	29.32952	32.66493	34.02159	34.46838	36.08553	31.19501	31.98357	32.4988	31.99398	32.89066
Simple_Lobule	16.24758	16.14868	14.39147	16.53599	15.73568	16.8174	17.42268	16.87998	16.96329	15.73353	17.16952	18.65862	18.40862	19.32	16.32268	17.1912	17.09217	17.44156	17.68259
stria_medullaris_thalamus	0.6128027	0.6027451	0.5586211	0.6265032	0.6049156	0.6335931	0.6870731	0.645042	0.627259	0.6125461	0.6717503	0.6819052	0.7002637	0.7251559	0.6148148	0.6293827	0.6551947	0.6436966	0.6617741
Stria_terminalis	2.511099	2.558143	2.377264	2.578313	2.470134	2.53865	2.696809	2.577702	2.600966	2.369488	2.659153	2.749778	2.808022	2.942215	2.511611	2.574375	2.608608	2.690467	2.663575
Subfornical_organ	0.07242666	0.07188405	0.06858384	0.0765078	0.07530424	0.07753236	0.08218321	0.08021267	0.07605276	0.06916526	0.08162418	0.08546329	0.0867217	0.09420797	0.07768852	0.08132498	0.07825942	0.07860755	0.08300787
subicular_region	24.98641	24.74012	22.48838	25.44774	24.51333	25.70641	26.58403	25.99171	25.807	23.8337	26.51592	27.64105	27.98052	29.24961	25.32681	26.03681	26.37202	26.04171	26.69176
substantia_nigra	2.257512	2.134995	1.934782	2.329555	2.192012	2.364442	2.41875	2.390241	2.284102	2.13069	2.435785	2.555516	2.572933	2.717884	2.351586	2.405646	2.435386	2.258983	2.470801
Superior_Colliculus	15.95578	15.75095	14.38485	16.23673	15.66597	16.41371	16.97024	16.61573	16.4409	15.29694	16.87588	17.54813	17.75925	18.59944	16.13864	16.53246	16.90836	16.55016	16.95142
Temporal_Association	11.101512	10.843777	9.805722	11.232704	10.812087	11.44592	11.891888	11.573042	11.382342	10.640267	11.817521	12.292447	12.465755	12.983329	11.231239	11.556538	11.739982	11.4866	11.880233
Thalamus	48.1093	47.72709	44.64924	49.58493	47.48466	49.25245	51.65178	49.96557	49.61182	45.90613	51.0104	52.73281	53.70818	56.51589	48.87806	49.45043	50.82871	50.01201	51.1242
Third_ventricle	4.485772	4.559968	4.321551	4.699174	4.509357	4.630977	4.774501	4.667126	4.70176	4.277474	4.738971	4.928933	5.026129	5.301312	4.574814	4.630005	4.725828	4.737852	4.758896
trochlear_nerve	0.08171088	0.07501481	0.06717205	0.0799742	0.07756468	0.08557577	0.0900113	0.08743975	0.08171331	0.08126914	0.08748207	0.09145131	0.09035091	0.09488285	0.08070799	0.08582192	0.0864016	0.08059924	0.08661996
ventral_pallidum	2.453283	2.477989	2.33993	2.595859	2.475839	2.556721	2.691425	2.596961	2.60467	2.381653	2.679194	2.770392	2.841004	2.95067	2.511074	2.579925	2.602596	2.634191	2.659575
brainvolumes	1414.896	1403.774	1323.311	1443.015	1396.394	1452.319	1506.031	1470.399	1455.54	1371.3	1493.989	1566.951	1576.302	1659.041	1438.892	1477.819	1491.986	1471.731	1511.133

	Mat – Full Group							
Absolute Volume	Het		WT					
	Mean	SD	Mean	SD	%Diff	Effect	P-Value	FDR
amygdaloid_area	30.1577964	1.1660264	31.1218486	2.44609931	-3.09767	-0.3941182	0.07849588	0.09526268
Anterior_part_of_anterior_commissure	1.35312608	0.05962013	1.40034014	0.11957828	-3.3716139	-0.3948381	0.08024763	0.09526268
Aqueduct	1.65003716	0.05330138	1.70555268	0.13368128	-3.254987	-0.4152827	0.0577221	0.09526268
auditory_cortex	20.9974404	0.73832125	21.6644096	1.69855327	-3.0786403	-0.392669	0.07543771	0.09526268
basal_forebrain	17.2523556	0.616181	17.7845896	1.28045893	-2.9926698	-0.4156588	0.06436178	0.09526268
Bed_nucleus_of_stria_terminalis	2.9445856	0.11049786	3.04143529	0.2557963	-3.1843415	-0.3786204	0.08588366	0.09674232
caudaputamen	46.5723424	1.70963647	48.0701821	3.51622526	-3.1159436	-0.4259795	0.05865489	0.09526268
cerebellar_lobule_1_2	8.15766524	0.31331438	8.48435271	0.76695114	-3.8504702	-0.425956	0.05249237	0.09526268
cerebellar_lobule_10	3.42236808	0.13965875	3.5859695	0.35211839	-4.5622647	-0.4646205	0.03439744	0.09526268
cerebellar_lobule_3	7.04546272	0.31166974	7.36586218	0.70979797	-4.3497889	-0.4513953	0.04226868	0.09526268
cerebellar_lobule_4_5	21.7681372	0.76608411	22.6980064	2.07073291	-4.0967	-0.4490532	0.03908885	0.09526268
cerebellar_lobule_6	8.66097452	0.31900304	9.06384793	0.88408029	-4.4448386	-0.4556978	0.0359208	0.09526268
cerebellar_lobule_7	3.326306	0.10832731	3.47728939	0.32506023	-4.3419853	-0.4644782	0.03137858	0.09526268
cerebellar_lobule_8	3.73766336	0.15173863	3.91708143	0.3933218	-4.5804018	-0.4561606	0.03706072	0.09526268
cerebellar_lobule_9	8.70356064	0.32511487	9.11524175	0.89381836	-4.5164036	-0.460587	0.0342034	0.09526268
Cerebellar_White_Matter_Arbor_vita_of_cerebellum	27.3225528	1.04605617	28.5365979	2.7294102	-4.2543441	-0.4448012	0.04167406	0.09526268
cerebral_peduncle	2.95612464	0.10634936	3.04789482	0.23869273	-3.0109366	-0.3844699	0.08262565	0.09526268
Cingulate_Cortex_area_1	15.4283108	0.57933073	15.9691289	1.18555095	-3.3866476	-0.4561745	0.04359152	0.09526268
Cingulate_Cortex_area_2	9.5624602	0.33014692	9.88213918	0.69919938	-3.2349168	-0.4572072	0.04197571	0.09526268
cingulum	3.3477564	0.13580338	3.46925414	0.28098387	-3.5021286	-0.4324011	0.0548348	0.09526268
Cochlear_nucleus	1.07390231	0.06528172	1.12833467	0.1217366	-4.8241322	-0.4471322	0.05161746	0.09526268
Commisure_inferior_Colliculus	0.31716269	0.01450149	0.32376606	0.02432041	-2.0395495	-0.2715156	0.24262527	0.24768044
commisure_superior_collicous	0.18960193	0.00679804	0.19543378	0.01591006	-2.9840563	-0.3665514	0.0955608	0.10405502
copula	2.81040352	0.10879088	2.93908843	0.29006663	-4.3783953	-0.4436391	0.04170661	0.09526268
Corpus_Callosum_associated_White_Matter	42.3093116	1.49039161	43.6868854	3.27764552	-3.153289	-0.4202937	0.05924958	0.09526268
Crus_1_ansiform_lobule	16.9278116	0.61446888	17.6720368	1.70550623	-4.2113153	-0.4363661	0.04414934	0.09526268
Crus_2_ansiform_lobule	9.89417744	0.40150204	10.3661051	1.06261909	-4.5526035	-0.4441174	0.04165774	0.09526268
dentate_gyrus	16.5175216	0.63738795	17.0703921	1.40142106	-3.2387688	-0.3945071	0.07603383	0.09526268
Dentate_nucleus	0.84913398	0.05038812	0.89386293	0.09763201	-5.0040058	-0.4581382	0.04475514	0.09526268
Dorsal_Peduncular_Cortex	1.52027388	0.07566279	1.58485361	0.12631198	-4.0748071	-0.5112716	0.03063353	0.09526268
Dorsal_Tenia_Tecta	1.05886459	0.04810653	1.10497302	0.09236914	-4.1728104	-0.4991757	0.02961442	0.09526268
Endopiriform_Nucleus	8.96495952	0.28050374	9.22542082	0.63494833	-2.8232999	-0.4102087	0.06425778	0.09526268
entopeduncular_nucleus	0.22291406	0.01054914	0.23300868	0.01822439	-4.3322912	-0.5539067	0.01872577	0.09526268
external_medullary_lamina	0.65833445	0.02288187	0.67689588	0.05342974	-2.7421397	-0.3473989	0.11379682	0.12121835
Fasciculus_retroflexus	0.23540951	0.01172117	0.2410856	0.0181617	-2.3543901	-0.312531	0.18827621	0.19422112
fastigial_nucleus	1.03893864	0.03913339	1.08074234	0.09498327	-3.8680545	-0.4401165	0.04561243	0.09526268
Fimbria	4.75980396	0.18603046	4.90969121	0.36892622	-3.0528856	-0.4062798	0.07268785	0.09526268
flocculus	10.6492074	0.38851815	11.0905036	0.98236805	-3.9790461	-0.4492168	0.04048063	0.09526268
Fornix	0.57866205	0.02787921	0.59593739	0.04705375	-2.8988517	-0.3671406	0.11556964	0.12178316
Fourth_ventricle	2.84623908	0.13374509	2.97813793	0.30441493	-4.4289033	-0.4332864	0.05090463	0.09526268
Frontal_Association_Cortex	113.8084	4.81196348	118.638939	9.57135222	-4.0716305	-0.5046872	0.02695753	0.09526268
Globus_pallidus	4.46980496	0.1768661	4.62287046	0.35603351	-3.311049	-0.4299188	0.05734525	0.09526268
hindbrain_medulla_pons	94.6117644	3.52232488	98.8413314	9.20958651	-4.2791482	-0.459257	0.03567003	0.09526268
Hippocampal_layer_CA1	20.8075292	0.74229545	21.4753907	1.71620383	-3.1098923	-0.3891505	0.0778058	0.09526268
Hippocampal_layer_CA2	2.28470944	0.06747445	2.34866325	0.16243995	-2.7229876	-0.3937074	0.07293577	0.09526268
Hippocampal_layer_CA3	20.6872444	0.82500905	21.3581593	1.73889823	-3.141258	-0.3858276	0.08455126	0.09634974
hypothalamus	27.8215456	1.04370525	28.6917989	2.2041418	-3.0331083	-0.3948264	0.07765567	0.09526268
Inferior_Colliculus	15.445288	0.6125071	16.0738175	1.41579226	-3.910269	-0.4439419	0.04520334	0.09526268
Infralimbic_Cortex	1.5032832	0.07266797	1.56203479	0.13277673	-3.7612213	-0.442484	0.05498602	0.09526268
Insular_Cortex	24.1970876	0.98257344	24.98471	1.90980251	-3.1524176	-0.4124104	0.06961987	0.09526268
Internal_capsule	7.93527884	0.27363437	8.16447425	0.59268374	-2.807228	-0.3867078	0.08253534	0.09526268
intersposed_nucleus	1.26103716	0.05317903	1.31615157	0.13379551	-4.1875429	-0.4119302	0.05960332	0.09526268
intrabulbar_part_of_anterior_commisure	2.67141996	0.11497331	2.76722686	0.22334912	-3.4621989	-0.4289558	0.05949391	0.09526268
Lateral_olfactory_tract	2.38766708	0.08224086	2.47853325	0.18481006	-3.6661267	-0.4916733	0.02782028	0.09526268
lateral_septum	9.668838	0.39828884	10.0007021	0.77401603	-3.3184077	-0.4287561	0.05959073	0.09526268
Lateral_ventricle	13.8288128	0.46316687	14.2567825	1.08480337	-3.0018674	-0.3945136	0.07340833	0.09526268
mamillary_bodies	1.65039404	0.05320446	1.69264564	0.11552156	-2.4961871	-0.3657465	0.09992566	0.10761224
mammilothalamic_tract	0.35036572	0.01517878	0.36459616	0.03217258	-3.9030672	-0.4423156	0.048805	0.09526268
medial_septum	1.32804024	0.06374516	1.37413725	0.106587	-3.3546147	-0.4324825	0.06559811	0.09526268
median_preoptic_area	0.0514173	0.00244981	0.05198467	0.00449731	-1.0914192	-0.1261577	0.57757463	0.57757489
midbrain	34.2075116	1.33256855	35.3964307	2.99804425	-3.3588672	-0.3965649	0.07358113	0.09526268
Navicular_nuclear_basin_forebrain	1.74581008	0.07678632	1.81147082	0.13674495	-3.6247198	-0.4801694	0.03892681	0.09526268
Nucleus_accumbens	7.07253924	0.29509195	7.32783604	0.53778415	-3.4839316	-0.4747198	0.04014839	0.09526268
Occipital_Cortex	13.4305612	0.51827143	13.974095	1.26542804	-3.8895814	-0.4295256	0.05068869	0.09526268
Olfactory_Bulb	138.140016	5.88490565	142.232139	17.0591937	-2.8770736	-0.2398779	0.25986665	0.2625462
Olfactory_tubercle	12.0459648	0.47413252	12.4777107	0.91494777	-3.4601372	-0.4718804	0.03909674	0.09526268
Optic_Chiasm	0.25634946	0.01175525	0.26613095	0.0258075	-3.6754427	-0.3790173	0.08798294	0.09798127
Optic_tract	2.97462528	0.10245855	3.06031925	0.23260014	-2.8001644	-0.3684175	0.095331	0.10405502
Orbitofrontal_Cortex	0.44929485	0.01345136	0.46429901	0.03350295	-3.2315732	-0.4478461	0.04143432	0.09526268
parafloccului	12.0757352	0.49476307	12.6313271	1.23105482	-4.3985239	-0.4513137	0.03996993	0.09526268
paramedian_lobe	7.89924916	0.34024112	8.29320254	0.8486487	-4.7503166	-0.4642125	0.03478038	0.09526268
Parietal_Association_Cortex	10.9400476	0.42701429	11.2929751	0.90130228	-3.1251951	-0.3915751	0.08008302	0.09526268
Periaqueductal_grey	10.182619	0.45789027	10.5910261	0.95691021	-3.8561618	-0.4267977	0.05752646	0.09526268
Piriform_Cortex	27.3580204	0.9840605	28.2402889	2.06245695	-3.1241484	-0.4277755	0.05686034	0.09526268
pons	22.1244944	0.85107662	22.9564046	1.99707118	-3.6238699	-0.4165651	0.05909713	0.09526268
posterior_commisure	0.2080847	0.01492841	0.21937188	0.02493441	-5.1452258	-0.4526747	0.05440108	0.09526268
Posterior_part_of_anterior_commissure	0.3154438	0.01347661	0.32771887	0.02792799	-3.7456079	-0.4395256	0.05103561	0.09526268
Prelimbic_Cortex	3.97943168	0.16306386	4.12550157	0.2998035	-3.5406578	-0.4872188	0.0350562	0.09526268
Primary_Motor_Cortex	19.485018	0.85491703	20.2141243	1.58762822	-3.606915	-0.4592425	0.04599975	0.09526268
Primary_Somatosensory_Cortex	81.446162	3.07441355	84.0763611	6.28249704	-3.1283455	-0.418655	0.063264	0.09526268
Primary_Visual_Cortex	25.9454972	0.96505846	26.8820775	2.24263193	-3.4840324	-0.4176255	0.05880853	0.09526268
Retrosplenial_Cortex	31.1920836	1.12590483	32.273845	2.63201048	-3.3518206	-0.4110019	0.06257966	0.09526268
rhinal_cortex	47.0685256	1.78132234	48.7580357	4.06568254	-3.4650906	-0.4155539	0.06067118	0.09526268
Secondary_Motor_Cortex	11.9563772	0.46411633	12.3439107	0.9006344	-3.1394711	-0.4302895	0.05878339	0.09526268
Secondary_Somatosensory_Cortex	21.5658776	0.84449444	22.2611014	1.72104622	-3.1230433	-0.4039542	0.07291672	0.09526268
Secondary_Visual_Cortex	31.2602056	1.15861238	32.3596218	2.71919702	-3.3974939	-0.4043165	0.06667705	0.09526268
Simple_Lobule	16.6686484	0.65674419	17.40505	1.64147187	-4.2309652	-0.4486227	0.04101189	0.09526268
stria_medullaris_thalamus	0.63242188	0.03132359	0.6493619	0.04966547	-2.6087185	-0.3410825	0.1492469	0.1555981
Stria_terminalis	2.55369596	0.09509261	2.63483304	0.19198946	-3.079401	-0.4226121	0.06142478	0.09526268
Subfornical_organ	0.0763911	0.00475169	0.07993552	0.00605326	-4.434101	-0.5855389	0.02263524	0.09526268
subicular_region	25.388444	0.93360267	26.2788596	2.19203418	-3.3883344	-0.4062052	0.0654408	0.09526268
substantia_nigra	2.29531016	0.1254006	2.38934714	0.23640141	-3.9356769	-0.3977852	0.08153239	0.09526268
Superior_Colliculus	16.190404	0.58100691	16.7411121	1.37357191	-3.2895553	-0.4009314	0.06864357	0.09526268
Temporal_Association	11.2704988	0.44668713	11.6698398	1.01991044	-3.4219921	-0.3915452	0.07656312	0.09526268
Thalamus	48.8448224	1.75575871	50.3591275	3.86222217	-3.0070122	-0.3920813	0.07777837	0.09526268
Third_ventricle	4.56597048	0.15572528	4.71710268	0.34605301	-3.2039201	-0.4367313	0.04994243	0.09526268
trochlear_nerve	0.08171421	0.00494799	0.08525645	0.00816709	-4.154801	-0.4337208	0.06567443	0.09526268
ventral_pallidum	2.54640732	0.10605394	2.63348039	0.18875847	-3.3063877	-0.4612936	0.04695679	0.09526268
brainvolumes	1440.99988	50.6370149	1492.96371	125.112419	-3.4805825	-0.4153371	0.05814462	

	Mat – Males							
Absolute Vol	Het		WT					
	Mean	SD	Mean	SD	%Diff	Effect	P-Value	FDR
amygdaloid_	30.9378933	1.45578908	30.9235523	1.43288964	0.04637574	0.01000846	0.98193066	0.9978163
Anterior_par	1.39201178	0.07453666	1.39620415	0.07205713	-0.3002696	-0.0581813	0.89604329	0.9978163
Aqueduct	1.67723022	0.05861898	1.68389631	0.09747046	-0.3958727	-0.0683908	0.85682129	0.9978163
auditory_cor	21.4903967	0.93575292	21.4841846	0.99520472	0.02891453	0.00624198	0.98838525	0.9978163
basal_forebr	17.6231278	0.7861415	17.6433085	0.74636106	-0.1143815	-0.0270388	0.9519387	0.9978163
Bed_nucleus	3.02010511	0.13137141	3.03213077	0.13646912	-0.3966075	-0.08812	0.8386715	0.9978163
caudaputam	47.64536	2.18132423	47.6966508	2.03951723	-0.1075354	-0.0251485	0.95558666	0.9978163
cerebellar_lc	8.39223978	0.37663602	8.40264369	0.63406492	-0.1238172	-0.0164083	0.96537716	0.9978163
cerebellar_lc	3.53001644	0.16020891	3.56761623	0.3597107	-1.053919	-0.1045279	0.77294662	0.9978163
cerebellar_lc	7.28978511	0.36338208	7.29773423	0.61696829	-0.1089259	-0.0128842	0.97276614	0.9978163
cerebellar_lc	22.3293744	0.94496366	22.5237438	1.94135832	-0.8629533	-0.1001203	0.78462138	0.9978163
cerebellar_lc	8.89502089	0.40086399	9.01876838	0.93464157	-1.3721108	-0.132401	0.71378312	0.9978163
cerebellar_lc	3.38856278	0.14302725	3.46143154	0.35448492	-2.1051626	-0.2055624	0.56755419	0.9978163
cerebellar_lc	3.84700678	0.1866257	3.88865238	0.4159054	-1.0709522	-0.1001324	0.78241579	0.9978163
cerebellar_lc	8.93366878	0.41134374	9.06041631	0.95412944	-1.3989151	-0.132841	0.7130323	0.9978163
Cerebellar_W	28.1032978	1.27469915	28.3752385	2.67067118	-0.9583732	-0.1018248	0.78049314	0.9978163
cerebral_ped	3.03134267	0.1314742	3.025192	0.13677562	0.20331492	0.04496903	0.91717303	0.9978163
Cingulate_Cc	15.7903156	0.75390835	15.8338615	0.72763064	-0.2750181	-0.0598463	0.8931601	0.9978163
Cingulate_Cc	9.76192056	0.42808408	9.79357062	0.40872927	-0.3231718	-0.0774353	0.86267639	0.9978163
cingulum	3.44477767	0.16933224	3.44645338	0.16044275	-0.0486215	-0.0104443	0.98144073	0.9978163
Cochlear_nuc	1.1251683	0.06730435	1.12260857	0.11024941	0.22801632	0.02321764	0.9512852	0.9978163
Commisure_	0.31096814	0.00645649	0.31861791	0.01784911	-2.4009207	-0.4285796	0.23528532	0.9978163
commisure_s	0.19342649	0.00841652	0.19476409	0.00967436	-0.6867813	-0.1382627	0.74067799	0.9978163
copula	2.88558733	0.13683536	2.93002362	0.30538804	-1.5165844	-0.1455076	0.68845245	0.9978163
Corpus_Callo	43.3058144	1.88010619	43.3226077	1.95040729	-0.0387632	-0.0086101	0.98412875	0.9978163
Crus_1_ansif	17.3836678	0.77078064	17.5962969	1.72128831	-1.2083744	-0.1235291	0.73339545	0.9978163
Crus_2_ansif	10.1780754	0.50725842	10.3352488	1.12327462	-1.520751	-0.1399243	0.70003496	0.9978163
dentate_gyru	16.9617867	0.78369451	16.9274838	0.83485953	0.20264571	0.04108813	0.92362182	0.9978163
Dentate_nuc	0.89021977	0.0527739	0.89009305	0.08767517	0.01423677	0.00144534	0.99695696	0.9978163
Dorsal_Pedu	1.57887644	0.08514868	1.57160315	0.07686397	0.46279435	0.09462548	0.83661558	0.9978163
Dorsal_Tenia	1.09626644	0.05731558	1.09879067	0.05733406	-0.2297275	-0.0440266	0.92013002	0.9978163
Endopiriform	9.09601544	0.36742705	9.13849531	0.35778364	-0.4648453	-0.1187306	0.78927201	0.9978163
entopeduncu	0.22759176	0.00940757	0.22898766	0.01055885	-0.6095988	-0.1322025	0.753571	0.9978163
external_me	0.67362277	0.02859554	0.67191394	0.0325213	0.25432248	0.05254488	0.90014806	0.9978163
Fasciculus_re	0.23515931	0.00735276	0.23740862	0.01178313	-0.9474432	-0.1908926	0.61812354	0.9978163
fastigial_nuc	1.06387928	0.04122632	1.07466465	0.0962171	-1.0036039	-0.1120942	0.75602121	0.9978163
Fimbria	4.874757	0.22941077	4.87629623	0.22228883	-0.0315656	-0.0069245	0.98757833	0.9978163
flocculus	10.9265946	0.46657361	10.9753812	0.86856409	-0.4445101	-0.0561693	0.87981954	0.9978163
Fornix	0.59201322	0.02972493	0.59315117	0.02962541	-0.1918477	-0.0384112	0.9303895	0.9978163
Fourth_ventr	2.94797389	0.154108	2.96148746	0.2829019	-0.4563103	-0.0477677	0.89791185	0.9978163
Frontal_Assc	116.627589	6.40265354	117.711831	7.52699715	-0.9210985	-0.1440471	0.72834724	0.9978163
Globus_palli	4.58730011	0.21524627	4.58808846	0.21308256	-0.0171825	-0.0036997	0.99330431	0.9978163
hindbrain_m	97.2176256	4.36279707	98.1197392	8.7628548	-0.9194008	-0.1029475	0.77938245	0.9978163
Hippocampal	21.3201033	0.93082314	21.2817131	0.99771155	0.18039082	0.03847831	0.92829677	0.9978163
Hippocampal	2.31238211	0.0870213	2.32835923	0.09539144	-0.6861965	-0.1674901	0.69346535	0.9978163
Hippocampal	21.2679144	1.02471574	21.2208431	1.02500644	0.22181667	0.045923	0.91670423	0.9978163
hypothalamu	28.4922589	1.30939907	28.5025254	1.27857331	-0.0360196	-0.0080296	0.98554998	0.9978163
Inferior_Colli	15.9060667	0.71507341	15.8917154	1.10030711	0.09030669	0.01304298	0.97297683	0.9978163
Infralimbic_(	1.54898978	0.08991431	1.55639115	0.0816135	-0.4755473	-0.0906881	0.84293554	0.9978163
Insular_Corte	24.8553267	1.20450315	24.8104854	1.1405186	0.18073521	0.03931657	0.93024439	0.9978163
Internal_cap	8.10383833	0.34904662	8.10718438	0.34477041	-0.0412727	-0.0097052	0.98246034	0.9978163
intersposed_	1.30221267	0.06177083	1.31736738	0.12491357	-1.150379	-0.1213216	0.7411678	0.9978163
intrabulbar_p	2.71068344	0.15992055	2.73633731	0.21009508	-0.9375256	-0.122106	0.76069802	0.9978163
Lateral_olfac	2.43390978	0.11118926	2.462533	0.11966674	-1.1623488	-0.2391911	0.57680471	0.9978163
lateral_septu	9.94076556	0.48283416	9.92454623	0.44538711	0.16342636	0.03641624	0.93610312	0.9978163
Lateral_vent	14.1237322	0.60906915	14.1564292	0.60036601	-0.2309693	-0.0544618	0.9018745	0.9978163
mamillary_b	1.66737678	0.0592248	1.67285769	0.07205195	-0.3276378	-0.0760689	0.85273502	0.9978163
mammiloth	0.36003861	0.01941642	0.36270885	0.01783117	-0.7361945	-0.1497514	0.74245799	0.9978163
medial_septu	1.36818033	0.0737265	1.36360331	0.06050384	0.33565668	0.07564852	0.87475178	0.9978163
median_prec	0.0518868	0.00317734	0.05221453	0.00288631	-0.6276617	-0.1135464	0.80405709	0.9978163
midbrain	35.1873422	1.61945659	35.0699654	1.88826931	0.33469334	0.06216107	0.88102695	0.9978163
Navicular_nu	1.80040589	0.09131082	1.797208	0.08788205	0.17793649	0.03638842	0.93498138	0.9978163
Nucleus_acc	7.278124	0.36117408	7.260881	0.316889	0.23747807	0.05441337	0.90678204	0.9978163
Occipital_Cor	13.8253111	0.62003424	13.82426	1.00759243	0.00760338	0.00104319	0.99781323	0.9978163
Olfactory_Bu	142.373722	3.89475235	140.273869	7.38819682	1.49696661	0.28421725	0.44612036	0.9978163
Olfactory_tul	12.35302	0.59444036	12.3618654	0.54059407	-0.0715538	-0.0163623	0.97144411	0.9978163
Optic_Chiasm	0.26148749	0.01470144	0.26576445	0.01521112	-1.6093038	-0.281173	0.51858486	0.9978163
Optic_tract	3.03235089	0.13564858	3.04015408	0.13985786	-0.2566708	-0.0557937	0.89769303	0.9978163
Orbitofrontal	0.45524379	0.01744904	0.45982423	0.01951049	-0.9961289	-0.2347682	0.57871024	0.9978163
parafloccului	12.4661456	0.58483779	12.54347	1.16448562	-0.6164518	-0.0664022	0.85670982	0.9978163
paramedian_	8.17032989	0.40033852	8.25967685	0.88331496	-1.0817246	-0.1011496	0.78052066	0.9978163
Parietal_Ass	11.2357516	0.53664835	11.2260326	0.53403737	0.08657502	0.01819899	0.96700414	0.9978163
Periaqueduct	10.5507363	0.5271165	10.4896376	0.63494834	0.58246739	0.09622628	0.81496069	0.9978163
Piriform_Cor	27.9642311	1.25233536	28.0090977	1.18733741	-0.1601857	-0.0377876	0.93291345	0.9978163
pons	22.7684933	1.02167927	22.7138046	1.36653962	0.24077304	0.04001986	0.92001088	0.9978163
posterior_co	0.22121741	0.01480875	0.2168992	0.01468498	1.99088384	0.29405641	0.50687967	0.9978163
Posterior_pa	0.32584214	0.01648356	0.32615536	0.01553584	-0.0960331	-0.0201609	0.96426491	0.9978163
Prelimbic_Co	4.08961744	0.2061425	4.08888262	0.19134659	0.01797139	0.0038403	0.99323554	0.9978163
Primary_Mot	20.0944022	1.04306825	20.0767862	0.97183057	0.08774347	0.01812669	0.96802773	0.9978163
Primary_Som	83.4283822	3.87961015	83.4555415	3.67353038	-0.0325435	-0.0073932	0.98686546	0.9978163
Primary_Visu	26.65616	1.18267958	26.6193177	1.48009836	0.1384044	0.0248918	0.95112629	0.9978163
Retrosplenia	32.0145789	1.40362518	31.9889623	1.66186534	0.08007944	0.01541435	0.97023843	0.9978163
rhinal_cortex	48.3767167	2.17046914	48.2935438	2.60880713	0.17222348	0.03188155	0.9381987	0.9978163
Secondary_M	12.2581367	0.57663407	12.2296023	0.55163567	0.23332205	0.05172682	0.90792021	0.9978163
Secondary_S	22.1406833	1.03954622	22.1275815	1.01516184	0.05921024	0.01290611	0.97677571	0.9978163
Secondary_V	32.1080144	1.44014244	32.0674438	1.73207743	0.12651647	0.02342309	0.95456359	0.9978163
Simple_Lobu	17.1583456	0.77981237	17.2617562	1.54790442	-0.5990735	-0.0668068	0.85591063	0.9978163
stria_medull	0.65034448	0.03341277	0.64375474	0.03601213	1.02364129	0.18298666	0.6687578	0.9978163
Stria_termin	2.60437289	0.11459384	2.60843546	0.11339801	-0.1557475	-0.0358258	0.93524952	0.9978163
Subfornical_(	0.07978891	0.00519999	0.07930402	0.0045817	0.61143546	0.10583245	0.81957832	0.9978163
subicular_reg	26.0765389	1.14930589	26.0404992	1.42876915	0.13839849	0.02522427	0.95057326	0.9978163
substantia_n	2.39877289	0.1351825	2.37329069	0.14225757	1.07370735	0.17912718	0.67799841	0.9978163
Superior_Col	16.6100778	0.71916052	16.5929408	0.89680506	0.10327891	0.01910896	0.96251027	0.9978163
Temporal_As	11.5934501	0.53923647	11.5740198	0.68445665	0.16787828	0.02838787	0.94404012	0.9978163
Thalamus	49.9915256	2.23818425	50.06888	2.24103876	-0.0307047	-0.0068515	0.9875439	0.9978163
Third_ventric	4.65493511	0.19901644	4.67674354	0.19195536	-0.4663165	-0.113612	0.79891929	0.9978163
trochlear_ne	0.08495095	0.0050466	0.0846272	0.00663568	0.38256609	0.04879002	0.90302137	0.9978163
ventral_palli	2.61151533	0.12984744	2.60952015	0.11689172	0.07645772	0.01706861	0.97034758	0.9978163
brainvolume	1479.22011	62.88512	1480.42654	83.7478321	-0.0814919	-0.0144055	0.97119591	

	Mat – Females							
Absolute Volume	Het		WT					
	Mean	SD	Mean	SD	%Diff	Effect	P-Value	FDR
amygdaloid_area	29.7189919	0.68888777	31.2937053	3.11631167	-5.0320454	-0.5053132	0.05814292	0.07172646
Anterior_part_of_anterior_commissure	1.33125288	0.03614771	1.40392467	0.15197514	-5.1763313	-0.4781821	0.07314283	0.08334788
Aqueduct	1.63474106	0.04494197	1.72432153	0.15971439	-5.1951141	-0.5608792	0.03947318	0.07054758
auditory_cortex	20.7201525	0.42114922	21.8206047	2.15843612	-5.0431791	-0.5098377	0.05479686	0.07160182
basal_forebrain	17.0437963	0.38600077	17.9070333	1.62787103	-4.8206594	-0.5302859	0.04823123	0.07054758
Bed_nucleus_of_stria_terminalis	2.90210588	0.07060023	3.0494992	0.33177772	-4.8333617	-0.4442532	0.09292567	0.10007386
caudaputamen	45.96877	1.02930612	48.3939093	4.47630502	-5.0112491	-0.5417726	0.04354666	0.07054758
cerebellar_lobule_1_2	8.02571706	0.17269473	8.5551672	0.88217694	-6.1886591	-0.6001632	0.02547115	0.07054758
cerebellar_lobule_10	3.36181588	0.08157443	3.60187567	0.35724974	-6.664855	-0.6719663	0.01388551	0.07054758
cerebellar_lobule_3	6.90803138	0.170392	7.4249064	0.79832527	-6.9613676	-0.6474492	0.01702632	0.07054758
cerebellar_lobule_4_5	21.4524413	0.40923326	22.849034	2.23304495	-6.1122617	-0.6254208	0.02006154	0.07054758
cerebellar_lobule_6	8.52932344	0.16051243	9.10291687	0.86895555	-6.3012047	-0.6600952	0.01463826	0.07054758
cerebellar_lobule_7	3.29128656	0.06505182	3.49103287	0.30925199	-5.7216965	-0.6459014	0.0171998	0.07054758
cerebellar_lobule_8	3.67615769	0.08399462	3.94171993	0.38559998	-6.7372175	-0.6886988	0.01171494	0.07054758
cerebellar_lobule_9	8.57412481	0.17098868	9.16275713	0.86904326	-6.4241834	-0.6773337	0.01265847	0.07054758
Cerebellar_White_Matter_Arbor_vita_of_cerebellum	26.8833838	0.55921166	28.6764427	2.86505694	-6.2527244	-0.6258371	0.02025039	0.07054758
cerebral_peduncle	2.9138145	0.05977659	3.0675706	0.30487768	-5.0123084	-0.5043206	0.05735109	0.07172646
Cingulate_Cortex_area_1	15.2246831	0.33317676	16.0863607	1.49169053	-5.3565723	-0.5776517	0.03193734	0.07054758
Cingulate_Cortex_area_2	9.45026375	0.19839545	9.9588986	0.88659385	-5.1073404	-0.5736954	0.03305408	0.07054758
cingulum	3.29318194	0.07342208	3.4890148	0.35958151	-5.6128413	-0.5446133	0.04144171	0.07054758
Cochlear_nucleus	1.04506519	0.0440324	1.13329729	0.13455741	-7.7854323	-0.6557208	0.01887917	0.07054758
Commisure_inferior_Colliculus	0.32064712	0.0166812	0.32822779	0.02866529	-2.3095753	-0.2644546	0.37179246	0.37562554
commisure_superior_collicous	0.18745061	0.00473794	0.19601418	0.02017868	-4.368851	-0.424387	0.10944047	0.11532415
copula	2.76811263	0.06042618	2.9469446	0.28668142	-6.068386	-0.6238004	0.02100253	0.07054758
Corpus_Callosum_associated_White_Matter	41.7487788	0.85898014	44.0025927	4.15065156	-5.1220025	-0.5430024	0.04211657	0.07054758
Crus_1_ansiform_lobule	16.6713925	0.30404494	17.737678	1.74934851	-6.0114154	-0.6095329	0.02291564	0.07054758
Crus_2_ansiform_lobule	9.73448481	0.21244513	10.3928472	1.04619197	-6.3347644	-0.6292941	0.01980981	0.07054758
dentate_gyrus	16.2676225	0.37070823	17.194246	1.77619192	-5.3891488	-0.5216911	0.05033343	0.07079605
Dentate_nucleus	0.82602322	0.03153446	0.89713016	0.10848837	-7.9260451	-0.6554338	0.01776378	0.07054758
Dorsal_Peduncular_Cortex	1.48730994	0.04553381	1.59633733	0.15937824	-6.8298469	-0.6840796	0.01361926	0.07054758
Dorsal_Tenia_Tecta	1.03782605	0.02528386	1.11033106	0.11649394	-6.5300353	-0.622393	0.02143054	0.07054758
Endopiriform_Nucleus	8.89124056	0.19439181	9.30075627	0.80913683	-4.4030366	-0.5061143	0.05883039	0.07172646
entopeduncular_nucleus	0.22028286	0.01050431	0.23649356	0.02273644	-6.8546042	-0.712983	0.0153616	0.07054758
external_medullary_lamina	0.64973477	0.01350903	0.68121356	0.06749814	-4.6209872	-0.4663653	0.07773482	0.08656832
Fasciculus_retroflexus	0.23555024	0.01381755	0.24427232	0.02221918	-3.5706363	-0.3925472	0.19656029	0.20065565
fastigial_nucleus	1.02490953	0.0309945	1.08600967	0.09695362	-5.626114	-0.6301997	0.02325251	0.07054758
Fimbria	4.69514288	0.12212476	4.93863353	0.46712389	-4.9303245	-0.521255	0.05326473	0.07134981
flocculus	10.4931771	0.23081953	11.1902763	1.0915852	-6.229509	-0.6386119	0.01839968	0.07054758
Fornix	0.57115201	0.02460181	0.59835211	0.05919649	-4.5458352	-0.4594884	0.10169299	0.10832524
Fourth_ventricle	2.78901325	0.07906339	2.99256833	0.33111486	-6.8020196	-0.6147567	0.02357011	0.07054758
Frontal_Association_Cortex	112.222606	2.78090799	119.442433	11.252825	-6.0446082	-0.6416013	0.01878754	0.07054758
Globus_pallidus	4.40371394	0.11134833	4.65301487	0.451055	-5.3578365	-0.5527063	0.04050653	0.07054758
hindbrain_medulla_pons	93.1459675	1.82572315	99.4667113	9.84145036	-6.3546324	-0.6422574	0.01726078	0.07054758
Hippocampal_layer_CA1	20.5192063	0.41616782	21.6432447	2.18222025	-5.1934839	-0.5150894	0.05230455	0.07134981
Hippocampal_layer_CA2	2.26914356	0.05027712	2.36626007	0.20585078	-4.1042194	-0.4717811	0.07729119	0.08656832
Hippocampal_layer_CA3	20.3606175	0.46140786	21.4771667	2.23121495	-5.1987731	-0.504492	0.05787612	0.07172646
hypothalamus	27.4442694	0.63777653	28.855836	2.8117886	-4.891789	-0.5020173	0.06001601	0.07172646
Inferior_Colliculus	15.1861	0.35847932	16.2316393	1.66449925	-6.4413662	-0.6281405	0.02031585	0.07054758
Infralimbic_Cortex	1.47757325	0.04667668	1.56692593	0.1680346	-5.7024191	-0.5317517	0.04986298	0.07079605
Insular_Cortex	23.8268281	0.60394313	25.1357047	2.4221057	-5.2072403	-0.5403879	0.0449816	0.07054758
Internal_capsule	7.84046413	0.16748942	8.21412547	0.7549055	-4.5490094	-0.4949776	0.06319517	0.07372777
intersposed_nucleus	1.23787594	0.03000586	1.31509787	0.14541977	-5.871953	-0.5310277	0.04650481	0.07054758
intrabulbar_part_of_anterior_commisure	2.64933425	0.07787896	2.7939978	0.23815611	-5.1776544	-0.6074316	0.02857506	0.07054758
Lateral_olfactory_tract	2.36165556	0.04715219	2.49240013	0.23054663	-5.2457296	-0.5671068	0.03425994	0.07054758
lateral_septum	9.51587875	0.24526715	10.0667038	0.9875853	-5.4717518	-0.5577493	0.03890374	0.07054758
Lateral_ventricle	13.6629206	0.25268198	14.3437553	1.393964	-4.7465583	-0.4884163	0.06443204	0.07428664
mamillary_bodies	1.64084125	0.04886766	1.7097952	0.14355723	-4.0328777	-0.4803238	0.08000867	0.08809945
mammilothalamic_tract	0.34492473	0.0089359	0.36623182	0.04144288	-5.8179257	-0.5141316	0.05387614	0.07134981
medial_septum	1.30546144	0.04573841	1.38326667	0.13630848	-5.6247455	-0.5708026	0.03923475	0.07054758
median_preoptic_area	0.0511532	0.0020029	0.05178546	0.0056369	-1.2209083	-0.1121632	0.67645378	0.67645376
midbrain	33.6563569	0.73646273	35.6793673	3.75414255	-5.6699729	-0.5388742	0.04315911	0.07054758
Navicular_nuclear_basin_forebrain	1.71509994	0.04682583	1.82383193	0.17055839	-5.9617333	-0.637506	0.02029086	0.07054758
Nucleus_accumbens	6.95689781	0.17358489	7.38586373	0.68111819	-5.8079317	-0.6297966	0.02109869	0.07054758
Occipital_Cortex	13.2085144	0.28043572	14.103952	1.47618257	-6.348842	-0.60659	0.02391552	0.07054758
Olfactory_Bulb	135.758556	5.52423725	143.929307	22.5346569	-5.6769192	-0.362586	0.16993439	0.175301
Olfactory_tubercle	11.8732463	0.28780913	12.57811	1.15788997	-5.6038924	-0.6087485	0.02516589	0.07054758
Optic_Chiasm	0.25345931	0.0090043	0.26644858	0.03295336	-4.8749622	-0.3941713	0.13961164	0.14555266
Optic_tract	2.94215463	0.0621193	3.07779573	0.2947379	-4.4070861	-0.4602093	0.0821747	0.08947913
Orbitofrontal_Cortex	0.44594858	0.00969231	0.46817716	0.04247038	-4.7479003	-0.5233903	0.05056865	0.07079605
paraflocculus	11.8561294	0.25758886	12.70747	1.32176177	-6.6995289	-0.6440954	0.01715781	0.07054758
paramedian_lobe	7.74676625	0.1756492	8.32225813	0.84748812	-6.9150929	-0.679056	0.01262962	0.07054758
Parietal_Association_Cortex	10.7737142	0.23701208	11.350992	1.14649277	-5.0857036	-0.5035163	0.05824489	0.07172646
Periaqueductal_grey	9.975553	0.24542411	10.6788961	1.18429961	-6.5862906	-0.5938895	0.02725106	0.07054758
Piriform_Cortex	27.0170269	0.60698174	28.4406547	2.62727988	-5.0056084	-0.5418638	0.04356334	0.07054758
pons	21.762245	0.46196103	23.166658	2.44725127	-6.0622167	-0.5738736	0.03182029	0.07054758
posterior_commisure	0.20069755	0.00882742	0.22151487	0.03167967	-9.3977063	-0.6571191	0.01715716	0.07054758
Posterior_part_of_anterior_commissure	0.30959474	0.00665672	0.32907391	0.03595988	-5.9193904	-0.5416916	0.04173725	0.07054758
Prelimbic_Cortex	3.91745219	0.09218332	4.157238	0.37368008	-5.7679116	-0.6416874	0.01876131	0.07054758
Primary_Motor_Cortex	19.1422394	0.49092884	20.3331507	2.0047095	-5.8569934	-0.5940568	0.02845316	0.07054758
Primary_Somatosensory_Cortex	80.3311631	1.8472162	84.6144047	7.99282302	-5.0620714	-0.5358859	0.04577536	0.07054758
Primary_Visual_Cortex	25.5457494	0.52026355	27.1098027	2.77527367	-5.7693275	-0.5635672	0.03473122	0.07054758
Retrosplenial_Cortex	30.72943	0.58590735	32.5207433	3.2942693	-5.5082177	-0.5437665	0.04075822	0.07054758
rhinal_cortex	46.3326681	0.97983257	49.1605953	5.06668262	-5.7524267	-0.5581418	0.0365836	0.07054758
Secondary_Motor_Cortex	11.7866375	0.2862547	12.442978	1.13175406	-5.2747863	-0.5799321	0.03244251	0.07054758
Secondary_Somatosensory_Cortex	21.2425494	0.50494733	22.3768187	2.19047849	-5.068948	-0.517818	0.05303374	0.07134981
Secondary_Visual_Cortex	30.7833131	0.60647945	32.6128427	3.39712246	-5.6098438	-0.5385527	0.04261331	0.07054758
Simple_Lobule	16.3931938	0.37544796	17.529238	1.76269355	-6.4808536	-0.6444933	0.01747957	0.07054758
stria_medullaris_thalamus	0.62234041	0.02594809	0.65422144	0.05992516	-4.8731248	-0.532014	0.06163472	0.07277359
Stria_terminalis	2.52519019	0.07111206	2.65771093	0.24260486	-4.9862739	-0.5462411	0.04518448	0.07054758
Subfornical_organ	0.07447983	0.00329861	0.08048282	0.00720988	-7.4587246	-0.8326066	0.00531781	0.07054758
subicular_region	25.0013906	0.49620333	26.4854387	2.72370639	-5.6032602	-0.5448634	0.04053216	0.07054758
substantia_nigra	2.23711238	0.07333958	2.40326273	0.29997727	-6.9135328	-0.5538765	0.04000459	0.07054758
Superior_Colliculus	15.9543375	0.31489139	16.8695273	1.70622838	-5.4251066	-0.5363818	0.04361894	0.07054758
Temporal_Association	11.0888386	0.25765778	11.7528837	1.26042208	-5.6500605	-0.5268434	0.04805643	0.07054758
Thalamus	48.1998019	1.01382448	50.6644087	4.92424395	-4.8645723	-0.5005046	0.05963069	0.07172646
Third_ventricle	4.51592788	0.10127448	4.7520806	0.44333422	-4.9694596	-0.5326742	0.04687435	0.07054758
trochlear_nerve	0.07989355	0.00397082	0.0858018	0.00949789	-6.8859314	-0.6220593	0.02973293	0.07054758
ventral_pallidum	2.50978406	0.07091967	2.65424593	0.2366595	-5.4426709	-0.6104207	0.02668695	0.07054758
brainvolumes	1419.501	24.9799441	1503.82927	154.609074	-5.6075692	-0.545429	0.03965875	

	Pat – Full Group							
Absolute Vol	Het		WT					
	Mean	SD	Mean	SD	%Diff	Effect	P-Value	FDR
amygdaloid_	30.5177463	2.31701165	31.3014281	2.52573554	-2.5036617	-0.3102787	0.22649652	0.4736692
Anterior_par	1.36926767	0.11456895	1.40402351	0.12102392	-2.4754462	-0.2871816	0.26784968	0.4736692
Aqueduct	1.67245167	0.12062718	1.71136605	0.12855251	-2.2738787	-0.302712	0.24161275	0.4736692
auditory_cor	21.286195	1.52020048	21.7768668	1.71927241	-2.2531789	-0.2853195	0.25964448	0.4736692
basal_forebr	17.4815808	1.28163113	17.8778819	1.32263833	-2.2167115	-0.2996292	0.25191106	0.4736692
Bed_nucleus	3.02828267	0.24718009	3.06491489	0.24644507	-1.1952118	-0.1486426	0.57322057	0.6040396
caudaputame	47.2217613	3.53671463	48.3124249	3.64984716	-2.257522	-0.2988245	0.25317415	0.4736692
cerebellar_lc	8.24323121	0.73256149	8.46422959	0.76370224	-2.6109687	-0.2893777	0.26653442	0.4736692
cerebellar_lc	3.48305683	0.39705295	3.56348543	0.32997688	-2.2570206	-0.2437401	0.39432412	0.48304735
cerebellar_lc	7.13194875	0.72875177	7.32994408	0.70125576	-2.7011847	-0.282344	0.29308037	0.4736692
cerebellar_lc	22.1218079	2.1968277	22.5953468	1.95135388	-2.0957361	-0.2426719	0.3818361	0.4736692
cerebellar_lc	8.85080421	1.05657735	9.01836141	0.82400083	-1.8579561	-0.2033459	0.49063617	0.54025161
cerebellar_lc	3.43575688	0.39934417	3.47963797	0.30636168	-1.2610823	-0.143233	0.62986036	0.64298167
cerebellar_lc	3.81006213	0.47478311	3.88990427	0.37478024	-2.0525478	-0.2130372	0.46756334	0.52668075
cerebellar_lc	8.89782658	1.08434106	9.06203157	0.83268847	-1.8120107	-0.1971986	0.50717066	0.54519168
Cerebellar_W	27.7592604	2.99203594	28.4030397	2.61026812	-2.266586	-0.2466334	0.37802377	0.4736692
cerebral_ped	3.00703688	0.21445309	3.07303724	0.23970824	-2.1477243	-0.2753362	0.27842452	0.4736692
Cingulate_Co	15.7193375	1.26117012	16.0262811	1.20668767	-1.9152515	-0.2543687	0.34422116	0.4736692
Cingulate_Co	9.74343917	0.70571335	9.92119276	0.71217168	-1.7916554	-0.2495937	0.34313731	0.4736692
cingulum	3.39687592	0.2730173	3.48075665	0.29366774	-2.4098419	-0.2856314	0.26732761	0.4736692
Cochlear_nuc	1.07838873	0.13083298	1.11943373	0.12378097	-3.6665856	-0.3315938	0.22090629	0.4736692
Commisure_	0.32812427	0.02166071	0.32844212	0.02371886	-0.0967753	-0.0134008	0.95801501	0.95801703
commisure_s	0.19227765	0.01376724	0.19597905	0.01521608	-1.8886719	-0.243256	0.3395867	0.4736692
copula	2.87746942	0.34418833	2.93117114	0.27617206	-1.8320909	-0.1944502	0.50364484	0.54519168
Corpus_Callo	43.001525	3.12365256	43.9299022	3.34851616	-2.1133149	-0.2772503	0.28205108	0.4736692
Crus_1_ansif	17.2565567	1.8872597	17.6115997	1.59510084	-2.0159615	-0.2225835	0.4327433	0.5109514
Crus_2_ansif	10.1004051	1.26903035	10.3117922	0.97808892	-2.0499556	-0.2161226	0.4666134	0.52668075
dentate_gyru	16.6743154	1.25689074	17.1209005	1.45469825	-2.6084208	-0.306995	0.22214913	0.4736692
Dentate_nuc	0.85765297	0.1057204	0.88752092	0.10037015	-3.3653239	-0.297578	0.27068736	0.4736692
Dorsal_Pedur	1.54724479	0.14528722	1.58764041	0.1389834	-2.5443806	-0.2906506	0.28039509	0.4736692
Dorsal_Tenia	1.08245896	0.0975337	1.10218747	0.09806724	-1.7899413	-0.2011733	0.44485026	0.51899196
Endopiriform	9.11950496	0.6115559	9.28589062	0.62560089	-1.7918116	-0.2659614	0.31017982	0.4736692
entopeduncu	0.22793685	0.0216436	0.23226795	0.01846181	-1.8646974	-0.2345974	0.40644635	0.49175061
external_me	0.67297822	0.04832464	0.68501861	0.05082557	-1.7576726	-0.2368962	0.36066753	0.4736692
Fasciculus_re	0.23978706	0.01923342	0.24288228	0.01536277	-1.2743699	-0.2014753	0.48939666	0.54025161
fastigial_nuc	1.05073974	0.10694236	1.07566508	0.09766432	-2.3172026	-0.2552144	0.35204867	0.4736692
Fimbria	4.80288396	0.37346797	4.93376303	0.38895488	-2.652723	-0.3364891	0.19735491	0.4736692
flocculus	10.7901329	1.0138999	11.0447698	0.96580234	-2.305497	-0.2636532	0.32791214	0.4736692
Fornix	0.57883178	0.045527	0.60217789	0.05218203	-3.876946	-0.4473976	0.07818359	0.4736692
Fourth_ventr	2.88420363	0.32071239	2.96436578	0.30617199	-2.7041926	-0.2618207	0.33082211	0.4736692
Frontal_Assc	116.962392	12.2564108	118.851697	9.97586246	-1.5896329	-0.1893877	0.51181188	0.54519168
Globus_pallic	4.52406421	0.36316013	4.64600968	0.37532886	-2.6247355	-0.324903	0.21430234	0.4736692
hindbrain_m	96.3176058	10.0805002	98.4846105	8.85797992	-2.2003486	-0.2446387	0.3803156	0.4736692
Hippocampal	21.06508	1.50927325	21.5687324	1.74615915	-2.3351045	-0.2884344	0.25107672	0.4736692
Hippocampal	2.32950604	0.13984575	2.36676889	0.1555197	-1.5744186	-0.2396021	0.34582444	0.4736692
Hippocampal	20.9319683	1.60150846	21.4638681	1.80110924	-2.478117	-0.2953179	0.24441319	0.4736692
hypothalamu	28.1523933	2.10230682	28.8693714	2.28345827	-2.4835249	-0.3139878	0.22163733	0.4736692
Inferior_Colli	15.5986325	1.37831683	16.0437281	1.43340285	-2.7742655	-0.3105168	0.23395406	0.4736692
Infralimbic_(	1.51741917	0.1413636	1.56469968	0.13944883	-3.0216987	-0.3390527	0.20322114	0.4736692
Insular_Corte	24.5005342	1.94387917	25.1155492	1.99850039	-2.4487421	-0.3077383	0.24010811	0.4736692
Internal_caps	8.06290554	0.56142852	8.23570019	0.59482968	-2.0981173	-0.2904943	0.26191552	0.4736692
intersposed_	1.28738413	0.1368982	1.31784943	0.12750357	-2.3117442	-0.2389369	0.37940242	0.4736692
intrabulbar_p	2.74060854	0.31517541	2.77566178	0.22408374	-1.2628787	-0.1564292	0.61347555	0.63284879
Lateral_olfac	2.45959425	0.19900789	2.48544986	0.18335088	-1.0402791	-0.1410171	0.6048137	0.63055052
lateral_septu	9.79517617	0.79616124	10.0507133	0.81975312	-2.5424773	-0.3117245	0.23388482	0.4736692
Lateral_venti	14.0784771	0.97649934	14.3627473	1.08115939	-1.9792189	-0.2629309	0.30199409	0.4736692
mamillary_b	1.68378383	0.10656539	1.70467995	0.10494113	-1.2258086	-0.1991222	0.4531596	0.52246512
mammilotha	0.35438944	0.030837	0.36514098	0.03393498	-2.9444918	-0.3168279	0.21547326	0.4736692
medial_septu	1.33495913	0.11580363	1.38051373	0.11894865	-3.2998299	-0.3829771	0.1451788	0.4736692
median_preo	0.05086619	0.00288377	0.05264755	0.00367327	-3.3835577	-0.4849516	0.04940313	0.4736692
midbrain	34.5282913	2.64458334	35.4850849	3.09300417	-2.6963261	-0.3093412	0.2171551	0.4736692
Navicular_nu	1.76960225	0.14975213	1.81020914	0.14620397	-2.2432151	-0.2777413	0.29813948	0.4736692
Nucleus_acc	7.18721563	0.5816472	7.35680381	0.57358407	-2.3051884	-0.295664	0.26644758	0.4736692
Occipital_Co	13.5796638	1.19283238	13.9524124	1.27800218	-2.6715716	-0.2916651	0.2581216	0.4736692
Olfactory_Bu	137.293721	14.9679522	141.353362	10.3012594	-2.8719807	-0.3940917	0.21407243	0.4736692
Olfactory_tul	12.2362254	0.97795183	12.5158751	0.95565852	-2.2343601	-0.2926252	0.2730641	0.4736692
Optic_Chiasn	0.25720966	0.02200322	0.26640708	0.02661301	-3.4523937	-0.3455986	0.16428434	0.4736692
Optic_tract	3.00577479	0.2080039	3.07593057	0.23565945	-2.2807984	-0.2976998	0.23952871	0.4736692
Orbitofrontal	0.46681444	0.03387515	0.46798882	0.03090744	-0.2509419	-0.0379967	0.8894514	0.89862178
parafloccului	12.2678288	1.32954994	12.5616295	1.19770606	-2.3388742	-0.2453028	0.37376996	0.4736692
paramedian_	8.04020175	1.00608054	8.23053097	0.80301357	-2.3124781	-0.2370187	0.4166282	0.49792159
Parietal_Ass	11.0806827	0.85250919	11.3533734	0.93539392	-2.4018469	-0.2915249	0.25440353	0.4736692
Periaqueduct	10.2827437	0.91775065	10.5875108	1.00649917	-2.8785527	-0.3027991	0.23677381	0.4736692
Piriform_Cor	27.7545825	2.05314469	28.3903084	2.12763864	-2.2392356	-0.2987941	0.252493	0.4736692
pons	22.3640233	1.79900585	22.9934586	2.0343743	-2.7374538	-0.3094	0.22206157	0.4736692
posterior_co	0.20860591	0.0256658	0.2177873	0.02861255	-4.2157577	-0.3208866	0.20773597	0.4736692
Posterior_pa	0.32189603	0.02801723	0.32904087	0.02953259	-2.1714124	-0.2419305	0.35023779	0.4736692
Prelimbic_Co	4.06868275	0.34254685	4.14458324	0.31101384	-1.8313179	-0.2440422	0.37457897	0.4736692
Primary_Mot	19.7839108	1.71255211	20.2778086	1.68612943	-2.4356568	-0.2929181	0.27116703	0.4736692
Primary_Son	82.5669388	6.26627697	84.5258903	6.50593784	-2.3175757	-0.3011021	0.24855789	0.4736692
Primary_Visu	26.2522504	2.03412524	26.9461903	2.27381612	-2.57528	-0.3051873	0.23012562	0.4736692
Retrosplenia	31.6400929	2.37837413	32.41	2.65485058	-2.3755232	-0.2900002	0.2540991	0.4736692
rhinal_cortex	47.6302879	3.70161251	48.8941135	4.15395217	-2.5848216	-0.3042465	0.23094172	0.4736692
Secondary_M	12.1736133	0.95457595	12.4201995	0.99539124	-1.9853637	-0.2636182	0.32245834	0.4736692
Secondary_S	21.8433717	1.69015491	22.3870922	1.7961548	-2.4287232	-0.3027136	0.242081	0.4736692
Secondary_V	31.6545583	2.40799662	32.4556665	2.75172536	-2.4683152	-0.2911294	0.24860721	0.4736692
Simple_Lobu	16.8940663	1.76098646	17.3139411	1.60055462	-2.4250679	-0.2623308	0.3398777	0.4736692
stria_medull	0.63140651	0.05450053	0.65304383	0.05362784	-3.3133031	-0.4034718	0.13144521	0.4736692
Stria_termin	2.57611038	0.19698673	2.64536578	0.1981868	-2.6179899	-0.3494451	0.18654126	0.4736692
Subfornical_(	0.07709011	0.00918391	0.07952755	0.00769898	-3.064891	-0.3165914	0.26759842	0.4736692
subicular_reg	25.7006375	1.95263871	26.3677424	2.21917634	-2.530004	-0.3006092	0.23454211	0.4736692
substantia_n	2.31387792	0.22264854	2.39014141	0.2539907	-3.1907522	-0.3002609	0.23450596	0.4736692
Superior_Col	16.4017279	1.19948938	16.8183416	1.37697396	-2.477139	-0.3025574	0.2300397	0.4736692
Temporal_As	11.3742728	0.90517538	11.6953038	1.029197	-2.7449566	-0.3119238	0.21753901	0.4736692
Thalamus	49.5393625	3.57358782	50.6883154	3.92466399	-2.2667017	-0.2927519	0.25228124	0.4736692
Third_ventric	4.65352075	0.31997044	4.75486173	0.34481696	-2.1313129	-0.2938979	0.2535614	0.4736692
trochlear_ne	0.0819221	0.00794948	0.0857081	0.00788057	-4.4173118	-0.4804213	0.07279535	0.4736692
ventral_palli	2.56550454	0.21212434	2.63804962	0.20509394	-2.7499513	-0.3537163	0.1881148	0.4736692
brainvolume	1460.35721	125.673551	1495.19522	118.880913	-2.3299973	-0.2930496	0.27868987	

	Pat – Males							
Absolute Volume	Het		WT					
	Mean	SD	Mean	SD	%Diff	Effect	P-Value	FDR
amygdaloid_area	30.2280222	1.43376335	31.2345213	1.5958128	-3.222393	-0.6307125	0.13073265	0.25481962
Anterior_part_of_anterior_commissure	1.35459656	0.06704852	1.403702	0.07954341	-3.4982813	-0.6173415	0.13185772	0.25481962
Aqueduct	1.64253633	0.05832479	1.68858763	0.07495423	-2.7272077	-0.6143922	0.12605935	0.25481962
auditory_cortex	21.0783567	0.88204811	21.65729	1.04776407	-2.6731569	-0.5525417	0.17519535	0.25481962
basal_forebrain	17.3114033	0.69026141	17.81624	0.85855019	-2.8335758	-0.5880107	0.14543964	0.25481962
Bed_nucleus_of_stria_terminalis	3.04989311	0.1827291	3.07536188	0.14437749	-0.828155	-0.176404	0.70378371	0.7184468
caudaputamen	46.7833889	1.90659126	48.1764775	2.3477138	-2.8916365	-0.5933809	0.14295307	0.25481962
cerebellar_lobule_1_2	8.12904956	0.38163685	8.41757388	0.44137511	-3.4276423	-0.6536941	0.11406535	0.25481962
cerebellar_lobule_10	3.42092711	0.2017272	3.54121625	0.20063092	-3.3968312	-0.5995544	0.16440962	0.25481962
cerebellar_lobule_3	7.03310522	0.40608638	7.31016338	0.42208116	-3.7900405	-0.6564097	0.12410332	0.25481962
cerebellar_lobule_4_5	21.7375178	1.0253659	22.4552931	1.19648838	-3.1964639	-0.5999016	0.14434122	0.25481962
cerebellar_lobule_6	8.67311856	0.45474372	8.944304	0.50473598	-3.0319346	-0.5372818	0.1952977	0.25481962
cerebellar_lobule_7	3.36915778	0.13408889	3.4328275	0.18241015	-1.8547312	-0.349047	0.37022504	0.39012954
cerebellar_lobule_8	3.72564944	0.23045035	3.85597494	0.2323645	-3.3798325	-0.5608666	0.1901728	0.25481962
cerebellar_lobule_9	8.70265289	0.47021991	8.979763	0.52058846	-3.0859401	-0.5323017	0.19965389	0.25481962
Cerebellar_White_Matter_Arbor_vita_of_cerebellum	27.2865211	1.40202509	28.2181325	1.55699786	-3.3014637	-0.5983383	0.15093254	0.25481962
cerebral_peduncle	2.99013811	0.12134996	3.05858969	0.14160237	-2.2380111	-0.483407	0.23565065	0.26853179
Cingulate_Cortex_area_1	15.5392322	0.57374996	15.9350381	0.79344186	-2.4838717	-0.4988468	0.20281754	0.25481962
Cingulate_Cortex_area_2	9.64919056	0.32623926	9.87219488	0.45940298	-2.2589133	-0.485422	0.213086	0.2610303
cingulum	3.372418	0.16175487	3.476937	0.18429483	-3.0060654	-0.5671293	0.16932056	0.25481962
Cochlear_nucleus	1.06374771	0.08625316	1.12168439	0.07608418	-5.1651496	-0.7614812	0.0946634	0.25481962
Commisure_inferior_Colliculus	0.32049666	0.01670938	0.31844632	0.01568944	0.64385634	0.13068259	0.76193431	0.76978672
commisure_superior_collicous	0.19099372	0.00881558	0.1952372	0.00906883	-2.1734986	-0.4679188	0.26850992	0.30245722
copula	2.830168	0.14099979	2.91003075	0.16398177	-2.7443954	-0.4870221	0.23270061	0.26828911
Corpus_Callosum_associated_White_Matter	42.6168067	1.6174268	43.7054381	2.05082792	-2.4908375	-0.5308254	0.18483503	0.25481962
Crus_1_ansiform_lobule	16.9722867	0.80171414	17.4926288	0.94405987	-2.9746363	-0.5511749	0.17722483	0.25481962
Crus_2_ansiform_lobule	9.89940822	0.53412165	10.2219961	0.59052222	-3.1558204	-0.5462755	0.18869909	0.25481962
dentate_gyrus	16.5042011	0.80227498	17.0399663	0.87027275	-3.1441678	-0.615629	0.14272252	0.25481962
Dentate_nucleus	0.8501186	0.06742733	0.88967848	0.06050479	-4.4465368	-0.6538306	0.14540636	0.25481962
Dorsal_Peduncular_Cortex	1.53750933	0.0822681	1.59103206	0.0867186	-3.3640258	-0.6172001	0.14523612	0.25481962
Dorsal_Tenia_Tecta	1.07964043	0.05257017	1.1031006	0.06233054	-2.1267477	-0.3763832	0.35079858	0.37778324
Endopiriform_Nucleus	9.01494256	0.27099039	9.22131656	0.40878456	-2.2380102	-0.5048479	0.19002322	0.25481962
entopeduncular_nucleus	0.22387262	0.01858062	0.23087007	0.01331487	-3.0309024	-0.5255364	0.28533488	0.31639116
external_medullary_lamina	0.6720795	0.02829533	0.68041544	0.02935648	-1.2251247	-0.2839556	0.49705739	0.51275434
Fasciculus_retroflexus	0.23165589	0.01312776	0.23778361	0.01383739	-2.5770142	-0.4428378	0.29056309	0.31639116
fastigial_nucleus	1.02536226	0.05930641	1.06509559	0.06012466	-3.730495	-0.6608493	0.12468855	0.25481962
Fimbria	4.73423467	0.25783939	4.91782575	0.25905622	-3.7331759	-0.708692	0.10192446	0.25481962
flocculus	10.6005062	0.52375797	10.9695169	0.59088472	-3.3639645	-0.6245053	0.13288706	0.25481962
Fornix	0.57059877	0.02961314	0.59958678	0.03110617	-4.8346654	-0.9319057	0.03261976	0.25481962
Fourth_ventricle	2.85000933	0.17071107	2.95785869	0.17725758	-3.646197	-0.608433	0.15270507	0.25481962
Frontal_Association_Cortex	115.044844	5.07802632	118.341769	7.06328594	-2.7859346	-0.4667692	0.23179773	0.26828911
Globus_pallidus	4.49037544	0.22150911	4.64437725	0.23745108	-3.3158763	-0.6485623	0.12483099	0.25481962
hindbrain_medulla_pons	94.65266	4.66725937	97.7964381	5.32484552	-3.2146141	-0.590398	0.15303523	0.25481962
Hippocampal_layer_CA1	20.8494167	0.9000869	21.4394544	1.04802645	-2.7521116	-0.5629989	0.16976344	0.25481962
Hippocampal_layer_CA2	2.30279456	0.06411799	2.34259069	0.09873061	-1.6988086	-0.4030779	0.2903205	0.31639116
Hippocampal_layer_CA3	20.7536556	1.01311578	21.4092231	1.11298184	-3.0620801	-0.5890191	0.15842424	0.25481962
hypothalamus	27.8722011	1.25725742	28.7821031	1.4366	-3.1613465	-0.6333719	0.12638593	0.25481962
Inferior_Colliculus	15.3664022	0.81087119	15.95862	0.85271038	-3.7109586	-0.6945122	0.10351097	0.25481962
Infralimbic_Cortex	1.49214578	0.08313974	1.56339113	0.09285164	-4.5571032	-0.7673031	0.06888352	0.25481962
Insular_Cortex	24.2920944	1.07945837	25.0873319	1.25929415	-3.1698765	-0.6314946	0.12532169	0.25481962
Internal_capsule	7.98563844	0.30122591	8.19826813	0.38055435	-2.5935927	-0.5587367	0.16401904	0.25481962
intersposed_nucleus	1.27737533	0.06434992	1.31323975	0.07109158	-2.7309877	-0.504482	0.22362126	0.26828911
intrabulbar_part_of_anterior_commisure	2.66877678	0.10022418	2.74961838	0.16324009	-2.9401025	-0.4952313	0.19239332	0.25481962
Lateral_olfactory_tract	2.43907044	0.08350873	2.47329075	0.12576847	-1.3835941	-0.2720897	0.47420926	0.49438574
lateral_septum	9.73205567	0.46581286	10.0546223	0.51432785	-3.2081422	-0.6271614	0.13370197	0.25481962
Lateral_ventricle	13.9799211	0.51834346	14.3106806	0.66036708	-2.3112773	-0.5008722	0.20939423	0.25975616
mamillary_bodies	1.65720889	0.04988245	1.68309556	0.07348452	-1.5380394	-0.3522738	0.35800088	0.38134906
mammilothalamic_tract	0.35031158	0.02427548	0.36520627	0.0215318	-4.0784324	-0.6917533	0.12615065	0.25481962
medial_septum	1.31775278	0.07982004	1.38047281	0.07568393	-4.5433734	-0.8287101	0.06332191	0.25481962
median_preoptic_area	0.04967767	0.00161777	0.05230355	0.00307869	-5.0204524	-0.8529203	0.02675642	0.25481962
midbrain	34.1877478	1.60898356	35.3167538	1.80231036	-3.1968	-0.6264215	0.13253713	0.25481962
Navicular_nuclear_basin_forebrain	1.7551	0.07503791	1.80657731	0.09203069	-2.8494387	-0.5593494	0.1666513	0.25481962
Nucleus_accumbens	7.12230822	0.30196558	7.3383055	0.36587588	-2.9434217	-0.5903567	0.14654238	0.25481962
Occipital_Cortex	13.3940867	0.64866044	13.87333	0.7264792	-3.4544218	-0.6596794	0.11415296	0.25481962
Olfactory_Bulb	135.092756	6.90248074	138.622806	6.16899509	-2.5465151	-0.5722246	0.20085873	0.25481962
Olfactory_tubercle	12.09571	0.49492075	12.4611494	0.61595139	-2.9326298	-0.5932926	0.14196336	0.25481962
Optic_Chiasm	0.25299492	0.0158872	0.26648517	0.01779975	-5.0622879	-0.7578897	0.07186143	0.25481962
Optic_tract	2.96985722	0.1141149	3.05871256	0.14912418	-2.9049915	-0.595848	0.13580838	0.25481962
Orbitofrontal_Cortex	0.46514409	0.02290286	0.46392179	0.01894347	0.26347143	0.06452362	0.88695461	0.88695424
paraflocculus	12.0815278	0.69311552	12.5130381	0.72552791	-3.4484858	-0.5947536	0.1606696	0.25481962
paramedian_lobe	7.886906	0.49995398	8.18567263	0.49100499	-3.6498726	-0.6084798	0.16025605	0.25481962
Parietal_Association_Cortex	10.9854174	0.53226951	11.3334219	0.59040937	-3.0706039	-0.5894291	0.15697872	0.25481962
Periaqueductal_grey	10.1871141	0.63126727	10.5856631	0.60683428	-3.7649886	-0.6567675	0.13379156	0.25481962
Piriform_Cortex	27.4362733	1.14036204	28.275325	1.38006491	-2.9674342	-0.6079799	0.13551647	0.25481962
pons	22.1093911	1.04704912	22.8757625	1.17396544	-3.3501458	-0.6528058	0.11765496	0.25481962
posterior_commisure	0.20802382	0.02087521	0.21981336	0.0170555	-5.3634293	-0.6912453	0.13925762	0.25481962
Posterior_part_of_anterior_commissure	0.32062616	0.01810799	0.33015893	0.01895394	-2.8873275	-0.5029438	0.23267257	0.26828911
Prelimbic_Cortex	4.01661044	0.16402052	4.11821025	0.21027544	-2.4670864	-0.4831748	0.22469813	0.26828911
Primary_Motor_Cortex	19.6059222	0.94321108	20.251885	1.08737431	-3.1896427	-0.5940574	0.14944586	0.25481962
Primary_Somatosensory_Cortex	81.7703422	3.4172853	84.2886613	4.14608476	-2.9877317	-0.6073969	0.13562233	0.25481962
Primary_Visual_Cortex	25.96685	1.1793378	26.8070425	1.3351371	-3.134223	-0.6292931	0.1297085	0.25481962
Retrosplenial_Cortex	31.3570167	1.30940584	32.2611925	1.57327876	-2.8026733	-0.574708	0.15794973	0.25481962
rhinal_cortex	47.1145222	2.19673984	48.6626556	2.46393064	-3.1813582	-0.6283186	0.13128122	0.25481962
Secondary_Motor_Cortex	12.0677856	0.45229418	12.371865	0.59056958	-2.4578303	-0.5148918	0.19478126	0.25481962
Secondary_Somatosensory_Cortex	21.6768178	0.99613468	22.3662256	1.132026	-3.0823611	-0.6090035	0.14149348	0.25481962
Secondary_Visual_Cortex	31.3544422	1.37254645	32.3066125	1.61609586	-2.9472922	-0.5891793	0.1503371	0.25481962
Simple_Lobule	16.5916256	0.92696303	17.2109694	0.97449023	-3.5985412	-0.6355567	0.13450003	0.25481962
stria_medullaris_thalamus	0.62259242	0.03424563	0.65130438	0.03433161	-4.408378	-0.8363125	0.05642718	0.25481962
Stria_terminalis	2.52865256	0.13874955	2.62749163	0.13640596	-3.7617273	-0.7245949	0.09727671	0.25481962
Subfornical_organ	0.07617659	0.00742169	0.08024149	0.00564407	-5.0658343	-0.7202071	0.13628721	0.25481962
subicular_region	25.4518489	1.10956826	26.2337581	1.29905622	-2.980546	-0.6019056	0.14271053	0.25481962
substantia_nigra	2.308668	0.15765034	2.3946445	0.14614659	-3.5903659	-0.5882895	0.18288272	0.25481962
Superior_Colliculus	16.2536122	0.63515976	16.7189975	0.7928127	-2.7835717	-0.5870053	0.14574993	0.25481962
Temporal_Association	11.269291	0.51042371	11.6519934	0.59044483	-3.2844369	-0.6481594	0.11697562	0.25481962
Thalamus	49.05577	2.07784831	50.4823769	2.46553787	-2.8259503	-0.5786189	0.15660866	0.25481962
Third_ventricle	4.60944778	0.174374	4.73019431	0.22504661	-2.552676	-0.5365401	0.17851105	0.25481962
trochlear_nerve	0.08082632	0.0047145	0.08549163	0.00482997	-5.4570316	-0.9659071	0.02848225	0.25481962
ventral_pallidum	2.53282222	0.14001885	2.63323431	0.13786277	-3.8132607	-0.7283481	0.09548847	0.25481962
brainvolumes	1442.30256	62.6500694	1486.42763	70.0517367	-2.9685313	-0.6298926	0.13070491	

	Pat – Females							
Absolute Vol	Het		WT					
	Mean	SD	Mean	SD	%Diff	Effect	P-Value	FDR
amygdaloid_	30.6915807	2.74931594	31.3524048	3.09298212	-2.1077302	-0.2136527	0.51293391	0.80227648
Anterior_par	1.37807033	0.13701811	1.40426848	0.14703302	-1.8656078	-0.1781786	0.59138999	0.80227648
Aqueduct	1.69040087	0.14505414	1.72872105	0.15748462	-2.2166781	-0.2433265	0.46237596	0.80227648
auditory_cor	21.410898	1.81869486	21.8679729	2.11658236	-2.0901565	-0.2159495	0.50345167	0.80227648
basal_forebr	17.5836873	1.54805376	17.9248471	1.60955981	-1.9032788	-0.2119585	0.52846276	0.80227648
Bed_nucleus	3.0153164	0.28427974	3.05695529	0.30583629	-1.3621032	-0.1361476	0.68110913	0.80227648
caudaputame	47.4847847	4.27487748	48.4160038	4.45181101	-1.9233705	-0.2091776	0.53360058	0.80227648
cerebellar_lc	8.3117402	0.88600036	8.49977681	0.9490294	-2.2122535	-0.1981357	0.55101529	0.80227648
cerebellar_lc	3.52033467	0.48142925	3.58045243	0.40632986	-1.6790549	-0.1479531	0.6878292	0.80227648
cerebellar_lc	7.19125487	0.87647356	7.3450151	0.8666034	-2.0933957	-0.1774286	0.6047911	0.80227648
cerebellar_lc	22.352382	2.67877393	22.7020543	2.39847272	-1.5402672	-0.1457896	0.68377246	0.80227648
cerebellar_lc	8.9574156	1.29744823	9.0747861	1.01161254	-1.2933693	-0.1160232	0.762169	0.8117298
cerebellar_lc	3.47571633	0.49715143	3.5153031	0.37536621	-1.1261266	-0.1054617	0.78688177	0.8117298
cerebellar_lc	3.86070973	0.57676257	3.91575519	0.45903249	-1.4057431	-0.1199163	0.75185558	0.80969109
cerebellar_lc	9.0149308	1.32896058	9.12471238	1.01748076	-1.2031237	-0.1078955	0.78046786	0.8117298
Cerebellar_W	28.042904	3.65434064	28.5439214	3.22458138	-1.7552509	-0.1553744	0.66641635	0.80227648
cerebral_ped	3.01717613	0.25854736	3.0840449	0.29680876	-2.1682165	-0.2252924	0.48733011	0.80227648
Cingulate_Cc	15.8274007	1.54647142	16.0957995	1.46187348	-1.6675087	-0.1835992	0.59938573	0.80227648
Cingulate_Cc	9.79998833	0.86500834	9.95852448	0.8667566	-1.5919642	-0.1829073	0.59169625	0.80227648
cingulum	3.41155067	0.32693962	3.48366686	0.36019346	-2.070123	-0.2002152	0.54267359	0.80227648
Cochlear_nuc	1.08717335	0.15378406	1.11771894	0.15241512	-2.7328513	-0.2004105	0.55867277	0.80227648
Commisure_	0.33270084	0.02348231	0.33605797	0.02621447	-0.9989739	-0.1280641	0.69513651	0.80227648
commisure_s	0.19304801	0.01628737	0.19654427	0.01882269	-1.7788688	-0.1857473	0.5655495	0.80227648
copula	2.90585027	0.42539415	2.9472781	0.34130683	-1.4056301	-0.12138	0.7479075	0.80969109
Corpus_Callo	43.232356	3.79243466	44.1009224	4.11790844	-1.9694971	-0.2109242	0.52364639	0.80227648
Crus_1_ansif	17.4271187	2.32401454	17.7022443	1.97267249	-1.554185	-0.1394685	0.70403804	0.80227648
Crus_2_ansif	10.2210032	1.56241641	10.3802084	1.20377798	-1.5337378	-0.1322546	0.73182361	0.80669257
dentate_gyru	16.776384	1.48249136	17.1825648	1.79772098	-2.3639123	-0.225942	0.47811197	0.80227648
Dentate_nuc	0.86217359	0.12532172	0.88587707	0.12402145	-2.6757074	-0.191124	0.57718628	0.80227648
Dorsal_Pedu	1.55308607	0.17525155	1.58505629	0.17062588	-2.0169769	-0.1873703	0.58721614	0.80227648
Dorsal_Tenia	1.08415007	0.11849398	1.10149175	0.11998306	-1.5743808	-0.1445344	0.67010598	0.80227648
Endopiriform	9.1822424	0.74914658	9.3350899	0.75714701	-1.6373437	-0.201873	0.55264945	0.80227648
entopeduncu	0.23037539	0.02356521	0.233333	0.02185843	-1.2675475	-0.1353074	0.70079526	0.80227648
external_me	0.67351745	0.05812216	0.68852578	0.06303658	-2.1797771	-0.2380892	0.47216321	0.80227648
Fasciculus_re	0.24466577	0.02100593	0.24676699	0.01563901	-0.8514993	-0.1343575	0.73260979	0.80669257
fastigial_nuc	1.06596623	0.12695092	1.08371802	0.11958378	-1.6380451	-0.1484465	0.67130691	0.80227648
Fimbria	4.84407353	0.43163221	4.94590571	0.47076959	-2.0589188	-0.21631	0.51247164	0.80227648
flocculus	10.9039089	1.22274459	11.1021053	1.18707741	-1.7852141	-0.1669616	0.62882839	0.80227648
Fornix	0.58377158	0.05323849	0.60415206	0.06454592	-3.3734027	-0.3157517	0.32327889	0.80227648
Fourth_ventr	2.9047202	0.38874549	2.96932357	0.38093234	-2.1756932	-0.1695928	0.62208354	0.80227648
Frontal_Assc	118.11292	15.1086813	119.240214	11.8889897	-0.9453977	-0.0948183	0.8036752	0.81196134
Globus_palli	4.54427747	0.43297048	4.64725343	0.45965002	-2.2158456	-0.2240312	0.5019663	0.80227648
hindbrain_m	97.3165733	12.3143215	99.0089324	10.9225384	-1.7092994	-0.1549419	0.66652348	0.80227648
Hippocampal	21.194478	1.7976339	21.66723	2.15429861	-2.1818756	-0.2194459	0.49241479	0.80227648
Hippocampal	2.34553293	0.17042883	2.38519038	0.18815071	-1.6626533	-0.2107749	0.52141112	0.80227648
Hippocampal	21.038956	1.89589767	21.5055024	2.21493448	-2.169428	-0.2106367	0.5133941	0.80227648
hypothalamu	28.3205087	2.50537823	28.9358614	2.7976647	-2.1266094	-0.2199523	0.50179916	0.80227648
Inferior_Colli	15.7379707	1.64008746	16.1085724	1.7727982	-2.300649	-0.209049	0.52801636	0.80227648
Infralimbic_C	1.5325832	0.16799844	1.56569667	0.16892091	-2.114935	-0.1960294	0.56496065	0.80227648
Insular_Corte	24.625598	2.34462672	25.1370481	2.44922809	-2.0346466	-0.2088209	0.53380246	0.80227648
Internal_caps	8.1092658	0.678116	8.26421986	0.72545782	-1.8749992	-0.2135949	0.52075266	0.80227648
intersposed_	1.2933894	0.1682846	1.32136157	0.15950683	-2.1169203	-0.1753666	0.61537921	0.80227648
intrabulbar_p	2.7837076	0.39006018	2.79550438	0.26352006	-0.4219911	-0.0447662	0.91426187	0.91426203
Lateral_olfac	2.47190853	0.24626349	2.49471395	0.22009069	-0.9141497	-0.1036183	0.77225404	0.8117298
lateral_septu	9.83304847	0.95565412	10.047735	1.00556946	-2.136666	-0.2134975	0.52356891	0.80227648
Lateral_venti	14.1376107	1.18449391	14.4024171	1.33159509	-1.8386252	-0.1988641	0.54246404	0.80227648
mamillary_b	1.6997288	0.1284847	1.72112519	0.12294753	-1.2431629	-0.1740286	0.61661421	0.80227648
mammilotha	0.35683615	0.03476177	0.36509124	0.04153468	-2.2611031	-0.1987518	0.53425592	0.80227648
medial_septu	1.34528293	0.13448524	1.3805449	0.1455052	-2.5542068	-0.2423417	0.46474821	0.80227648
median_preo	0.0515793	0.00327319	0.05290964	0.00412453	-2.5143752	-0.3225449	0.30735061	0.80227648
midbrain	34.7326173	3.14503343	35.6133371	3.83976995	-2.4730056	-0.2293679	0.47055557	0.80227648
Navicular_nu	1.7783036	0.18277955	1.81297624	0.17917939	-1.9124706	-0.193508	0.57398201	0.80227648
Nucleus_acc	7.22616007	0.70665597	7.37089776	0.70093969	-1.9636373	-0.2064909	0.54673006	0.80227648
Occipital_Co	13.69101	1.43585531	14.0126657	1.59225531	-2.2954641	-0.2020126	0.53811671	0.80227648
Olfactory_Bu	138.6143	18.3264048	143.433786	12.3270843	-3.360077	-0.3909672	0.35142516	0.80227648
Olfactory_tul	12.3205347	1.18782727	12.557571	1.16410536	-1.8875966	-0.203621	0.55427929	0.80227648
Optic_Chiasn	0.25973851	0.02515699	0.26634759	0.03220594	-2.4813755	-0.2052132	0.51209911	0.80227648
Optic_tract	3.02732533	0.24962179	3.08904905	0.28786679	-1.9981461	-0.2144176	0.50778491	0.80227648
Orbitofrontal	0.46781665	0.03978207	0.47108751	0.03777605	-0.6943213	-0.0865856	0.80366144	0.81196134
paraflocculus	12.3796093	1.61054785	12.5986514	1.477829	-1.7386154	-0.1482188	0.67537884	0.80227648
paramedian_	8.1321792	1.22306785	8.26470876	0.98845569	-1.60356	-0.1340774	0.72161687	0.80669257
Parietal_Ass	11.1378419	1.01131388	11.3685744	1.14583276	-2.0295646	-0.2013667	0.53630104	0.80227648
Periaqueduct	10.3401215	1.07079572	10.5889185	1.24389804	-2.3495984	-0.200014	0.53551918	0.80227648
Piriform_Cor	27.945568	2.46535782	28.4779148	2.58867789	-1.869332	-0.2056443	0.53919758	0.80227648
pons	22.5168027	2.15030814	23.0831319	2.52912048	-2.4534333	-0.2239234	0.48638508	0.80227648
posterior_co	0.20895517	0.02885901	0.21624363	0.03535063	-3.3704884	-0.2061764	0.51583568	0.80227648
Posterior_pa	0.32265796	0.03317463	0.32818901	0.03603765	-1.6853258	-0.1534799	0.64208405	0.80227648
Prelimbic_Co	4.09992613	0.4178614	4.16467695	0.37412712	-1.5547621	-0.1730717	0.62888677	0.80227648
Primary_Mot	19.890704	2.06815705	20.29756	2.05662928	-2.0044577	-0.1978266	0.56318872	0.80227648
Primary_Som	83.0448967	7.56194779	84.7066362	7.9509226	-1.9617584	-0.2089996	0.53242219	0.80227648
Primary_Visu	26.4234907	2.43290943	27.0522076	2.81819035	-2.3240874	-0.2230924	0.49022594	0.80227648
Retrosplenia	31.8099387	2.86895959	32.5233771	3.28621368	-2.1936174	-0.2171005	0.50351859	0.80227648
rhinal_cortex	47.9397473	4.41352286	49.0704624	5.14109384	-2.3042682	-0.2199367	0.49552523	0.80227648
Secondary_M	12.23711	1.16986316	12.4570257	1.14457411	-1.765395	-0.1921376	0.57699848	0.80227648
Secondary_S	21.943304	2.02422137	22.4029905	2.20122326	-2.0518978	-0.2088323	0.52752029	0.80227648
Secondary_V	31.834628	2.89082569	32.5692314	3.4116633	-2.2555136	-0.2153212	0.50268646	0.80227648
Simple_Lobu	17.0755307	2.12356555	17.3923957	1.97079332	-1.8218597	-0.1607805	0.64804002	0.80227648
stria_medull	0.63669496	0.064263	0.65436912	0.0654862	-2.7009471	-0.2698914	0.42669643	0.80227648
Stria_termin	2.60458507	0.22456989	2.65898419	0.23726599	-2.0458611	-0.2292749	0.49287227	0.80227648
Subfornical_(	0.07763823	0.01030689	0.07898359	0.00906001	-1.703343	-0.1484945	0.68086201	0.80227648
subicular_reg	25.8499107	2.34450603	26.4698257	2.75201286	-2.3419688	-0.2252588	0.48410051	0.80227648
substantia_n	2.31700387	0.25924955	2.38671048	0.31634253	-2.9206144	-0.2203517	0.48812415	0.80227648
Superior_Col	16.4905973	1.45279252	16.8940324	1.71101671	-2.3880329	-0.2357867	0.46356553	0.80227648
Temporal_As	11.4372618	1.08896783	11.7283021	1.2816126	-2.4815215	-0.2270892	0.48019654	0.80227648
Thalamus	49.829518	4.27463408	50.845221	4.80691593	-1.997637	-0.2113003	0.51761926	0.80227648
Third_ventric	4.67996453	0.38577784	4.77365595	0.41853981	-1.9626764	-0.2238531	0.49881153	0.80227648
trochlear_ne	0.08257957	0.00948067	0.08587303	0.00970688	-3.8352616	-0.3392907	0.31807788	0.80227648
ventral_palli	2.58511393	0.24823686	2.64171843	0.24784482	-2.1427149	-0.2283868	0.50415426	0.80227648
brainvolumes	1471.19	152.868788	1501.87529	147.139469	-2.0431314	-0.2085456	0.54785481	

	2	9	10	11	12	13	57	62	64	65	70	72	105	107	108	109	6	7	61
	Het	Het	Het	Het	Het	Het	Het	Het	Het	Het	Het	Het	Het	Het	Het	Het	Het	Het	Het
Relative Volumes	F	F	F	F	F	F	F	F	F	F	F	F	F	F	F	F	M	M	M
	Mat	Mat	Mat	Mat	Mat	Mat	Mat	Mat	Mat	Mat	Mat	Mat	Mat	Mat	Mat	Mat	Mat	Mat	Mat
amygdaloid_area	2.08598584	2.10725043	2.10155336	2.0769763	2.12236394	2.09517725	2.10587289	2.08110167	2.05601384	2.09265007	2.08854799	2.11356308	2.09378392	2.08230927	2.1060621	2.08603461	2.11407653	2.08389502	2.09025916
Anterior_part_of_anterior_commissure	0.09366517	0.09376246	0.09417497	0.09479327	0.09629158	0.09445766	0.09229306	0.09404769	0.09217546	0.09386317	0.09126869	0.09457763	0.09300496	0.0950012	0.09388335	0.0930861	0.09622888	0.09587985	0.09284029
Aqueduct	0.11308169	0.11544905	0.11549255	0.10982315	0.11459395	0.11805463	0.11854821	0.11293082	0.11649571	0.1138634	0.11732262	0.11808892	0.11443612	0.11499051	0.11428675	0.11509385	0.1122301	0.11173383	0.11370807
auditory_cortex	1.44983697	1.46894202	1.45838622	1.44675507	1.46926149	1.46963161	1.47729416	1.44172232	1.45219939	1.45898141	1.46726468	1.47782923	1.45959811	1.44655458	1.459091	1.45100387	1.45844277	1.44550578	1.4601942
basal_forebrain	1.18939053	1.20483612	1.20501918	1.18326827	1.20808561	1.21428408	1.21249625	1.18473402	1.18902609	1.19724939	1.20379542	1.21954524	1.19510941	1.19833704	1.20101471	1.20367862	1.20406651	1.18754097	1.19618156
Bed_nucleus_of_stria_terminalis	0.20706367	0.20361536	0.2034028	0.20450608	0.20284037	0.20442799	0.20457521	0.20104398	0.20349251	0.21598205	0.20024009	0.19624473	0.20743946	0.20366802	0.20653096	0.20624498	0.20652846	0.20312151	0.21003413
caudaputamen	3.21242667	3.25023919	3.25036292	3.20266004	3.25648486	3.26922749	3.26490834	3.20028947	3.19885527	3.23033569	3.24089664	3.27666885	3.23453759	3.22709232	3.24933396	3.24636651	3.25321856	3.21236813	3.2288507
cerebellar_lobule_1_2	0.57066989	0.56163071	0.57083782	0.55856429	0.56976709	0.56105988	0.5623509	0.57029334	0.56851494	0.56264156	0.55786301	0.56344104	0.56692377	0.56760647	0.56668949	0.56698653	0.56566664	0.56074847	0.56052113
cerebellar_lobule_10	0.23750665	0.23520439	0.233703	0.22871146	0.23131344	0.24030793	0.24128752	0.23774721	0.23729784	0.23725887	0.23594912	0.24027708	0.23627778	0.24100125	0.23825799	0.23706251	0.23544601	0.23552234	0.23344467
cerebellar_lobule_3	0.49298805	0.48333189	0.48993312	0.47920457	0.4864719	0.48324611	0.48649445	0.49183159	0.48352102	0.48237337	0.47749042	0.48359914	0.48977439	0.49373903	0.49172536	0.48999439	0.48949579	0.48956851	0.48048798
cerebellar_lobule_4_5	1.51651899	1.49757903	1.50528242	1.48223329	1.49598566	1.52243996	1.52476876	1.51530818	1.52505047	1.51875062	1.50312527	1.52471457	1.51037648	1.51770529	1.50591061	1.5146299	1.4932178	1.48649083	1.49882517
cerebellar_lobule_6	0.60303949	0.59197381	0.60174851	0.59463905	0.58705985	0.61015817	0.60584813	0.60813723	0.61053747	0.60779093	0.60125729	0.60189569	0.59683727	0.59960108	0.59839471	0.59533883	0.5925347	0.59238511	0.59451497
cerebellar_lobule_7	0.23379246	0.22539812	0.23039023	0.23222472	0.22427325	0.23872071	0.23441686	0.2335445	0.24201416	0.23878957	0.23460108	0.23071867	0.22712307	0.22795953	0.22894419	0.22757841	0.22540646	0.22647172	0.22865295
cerebellar_lobule_8	0.25942075	0.25547397	0.26100545	0.25570436	0.25398317	0.26370998	0.26260804	0.26370399	0.26026716	0.25772221	0.2592845	0.25979835	0.25693986	0.25942403	0.25869504	0.25570683	0.255985	0.25653096	0.25528946
cerebellar_lobule_9	0.60486535	0.59530441	0.60740143	0.59986635	0.59084217	0.61520213	0.60932808	0.61375487	0.61356691	0.60728351	0.60549698	0.60557056	0.59813829	0.60148293	0.6007044	0.59581536	0.59536964	0.59460964	0.59678777
Cerebellar_White_Matter_Arbor_vita_of_cerebellum	1.90375156	1.88174466	1.90691868	1.86686958	1.88586559	1.90719157	1.89135311	1.9185691	1.90704385	1.90068314	1.87083925	1.89022212	1.88608679	1.90029104	1.89254005	1.89083899	1.88555023	1.87670398	1.87178192
cerebral_peduncle	0.2048461	0.20765851	0.20458381	0.20268005	0.2054026	0.20605807	0.20813169	0.20213184	0.20335564	0.20732782	0.20585919	0.2047477	0.20694606	0.20227715	0.20740083	0.2048817	0.2057474	0.20326049	0.20709916
Cingulate_Cortex_area_1	1.06413342	1.07874736	1.06675458	1.05992837	1.08044124	1.08986874	1.08224813	1.05824315	1.06326176	1.07392164	1.07327629	1.08684656	1.07286698	1.0646515	1.07585824	1.06880566	1.0718419	1.07194402	1.06532252
Cingulate_Cortex_area_2	0.65881028	0.6671309	0.66135332	0.65713002	0.66400905	0.67751475	0.67663864	0.6529599	0.66399726	0.66719837	0.66943162	0.67872261	0.66383651	0.66326369	0.66370469	0.6661469	0.66296817	0.65894106	0.66395817
cingulum	0.23186968	0.23262289	0.2325065	0.23112528	0.23396889	0.23281913	0.23253252	0.23036128	0.22837889	0.23264029	0.23016029	0.23182752	0.2328269	0.2326102	0.23363044	0.23178245	0.23536423	0.23360749	0.23134887
Cochlear_nucleus	0.07434795	0.0744818	0.07638724	0.07194315	0.0757232	0.07250116	0.07202938	0.07635281	0.07092933	0.0713639	0.07025806	0.07194578	0.074102	0.07540913	0.07563895	0.07414356	0.07658216	0.07594936	0.07239858
Commisure_inferior_Colliculus	0.02153452	0.02239022	0.02127603	0.02161694	0.02171115	0.02414136	0.02396328	0.0208906	0.0246014	0.02337942	0.02425481	0.02445056	0.02194308	0.02181687	0.02106011	0.0225595	0.02027535	0.02036849	0.02269959
commisure_superior_collicuus	0.01323284	0.01328006	0.01349283	0.01317051	0.01341806	0.01347897	0.01329929	0.01324933	0.01322919	0.01335754	0.01298705	0.01286268	0.01320303	0.01303228	0.01303002	0.01295071	0.01324108	0.01316061	0.01321804
copula	0.19805214	0.19052449	0.19797048	0.19895957	0.19270195	0.19624541	0.19206504	0.2002433	0.19953686	0.19981719	0.19335867	0.18924274	0.19364405	0.19080161	0.1943529	0.19285789	0.1923065	0.19239587	0.19399279
Corpus_Callosum_associated_White_Matter	2.92438475	2.9486246	2.93840202	2.89390951	2.93937142	2.97005231	2.98606316	2.89509886	2.9251178	2.95100832	2.96288298	2.96570887	2.9478019	2.91700459	2.95009527	2.94099215	2.93729926	2.90858946	2.94592409
Crus_1_ansiform_lobule	1.1823231	1.15868465	1.17994112	1.16910121	1.16453183	1.18282145	1.17021658	1.19193245	1.19349323	1.19503333	1.16177402	1.16405067	1.1703425	1.1678966	1.16931676	1.17048364	1.16174871	1.15860778	1.16637883
Crus_2_ansiform_lobule	0.68880287	0.68037336	0.6976434	0.68768437	0.68032703	0.69465944	0.67832337	0.70330082	0.69672769	0.6914701	0.68038149	0.67335063	0.67712395	0.68291077	0.68315688	0.6760828	0.68372409	0.68011474	0.67451913
dentate_gyrus	1.13827933	1.15761662	1.15324341	1.13927362	1.16405185	1.1483137	1.14850422	1.14047759	1.13326898	1.13769206	1.14454229	1.15544424	1.14794555	1.1368838	1.15026254	1.1390377	1.15140925	1.14259176	1.14479456
Dentate_nucleus	0.0595868	0.05825741	0.059901	0.05734858	0.05855077	0.05714882	0.05725011	0.05963537	0.05634045	0.05744123	0.05563508	0.0560354	0.05910997	0.05967112	0.06007126	0.05884495	0.06014683	0.06002523	0.05736222
Dorsal_Peduncular_Cortex	0.10521841	0.1061352	0.10623502	0.10378694	0.10485052	0.10345175	0.10485978	0.10533877	0.10016203	0.10412154	0.10395186	0.10382467	0.10749475	0.10380053	0.10761421	0.1053055	0.10706744	0.10643182	0.10524405
Dorsal_Tenia_Tecta	0.07373191	0.07314082	0.07260483	0.07329018	0.07306968	0.0740095	0.07340347	0.0722769	0.07178717	0.07380772	0.0712966	0.07324653	0.07312511	0.07457404	0.07345092	0.07288738	0.07466536	0.07540263	0.07291514
Endopiriform_Nucleus	0.61627649	0.62596956	0.62242158	0.61726797	0.62570473	0.63963286	0.63902225	0.61224424	0.62819947	0.62867078	0.63458478	0.64373514	0.6210681	0.62084258	0.62019958	0.62616254	0.61889247	0.61082213	0.62486844
entopeduncular_nucleus	0.01530795	0.01539671	0.01486481	0.01477432	0.01464438	0.01609766	0.01676459	0.01467326	0.01526851	0.01491548	0.01631338	0.01674812	0.01555024	0.0158012	0.01557571	0.0155962	0.01532193	0.01549297	0.01518185
external_medullary_lamina	0.04575582	0.04638014	0.04600169	0.04495779	0.04596298	0.0460078	0.04634077	0.04522186	0.04583179	0.04703685	0.0458974	0.04468462	0.04590946	0.04478711	0.0459935	0.04560315	0.04587287	0.04500868	0.04622201
Fasciculus_retroflexus	0.01571274	0.01645668	0.01570541	0.01589936	0.01609896	0.01728511	0.01809292	0.01565288	0.01722539	0.01598552	0.01801736	0.01885625	0.01605933	0.01630867	0.01582278	0.01638086	0.015704	0.01560023	0.01629395
fastigial_nucleus	0.07115019	0.07282387	0.07236996	0.06899058	0.07213789	0.07339032	0.07332	0.07221221	0.07139744	0.07121631	0.07206901	0.07533182	0.07177504	0.07257049	0.0719986	0.07233034	0.07158049	0.07034957	0.07168424
Fimbria	0.32801382	0.33093842	0.33113376	0.32591691	0.33466683	0.33351549	0.33576082	0.32744431	0.32468151	0.32625774	0.33206496	0.34036519	0.32861674	0.33106753	0.33137068	0.32979695	0.33361412	0.32909294	0.32739202
flocculus	0.74172075	0.73400382	0.7389209	0.72080841	0.73416144	0.74452983	0.74930646	0.73769371	0.74113562	0.73322873	0.73653189	0.74931796	0.73983763	0.74500685	0.73821098	0.7425535	0.73264048	0.72846107	0.73064583
Fornix	0.0394548	0.04163735	0.0423546	0.03953048	0.0427272	0.04022195	0.03901837	0.04085708	0.03869086	0.03944201	0.03929663	0.04002153	0.04047265	0.03900691	0.04075022	0.04009711	0.04105019	0.03923986	0.04005431
Fourth_ventricle	0.20053821	0.19421895	0.20110853	0.1983834	0.19798438	0.19400748	0.19195095	0.2024008	0.19592368	0.19705907	0.19037907	0.1905391	0.19770284	0.19616	0.19839139	0.19666451	0.19775852	0.19759003	0.19515732
Frontal_Association_Cortex	7.91667288	7.86267387	7.87692335	7.74617036	8.03701144	8.0238505	7.95809592	7.83050197	7.80382428	7.98938353	7.90024396	7.95506544	7.92546031	7.78092902	8.04684038	7.82883337	7.91427743	7.92034414	7.77076783
Globus_pallidus	0.30909786	0.31260129	0.313361	0.30572698	0.3128328	0.31107795	0.31246249	0.30763857	0.30253453	0.30938948	0.30950879	0.31108847	0.3112923	0.3097475	0.31336703	0.31137422	0.31443635	0.3089298	0.30974792
hindbrain_medulla_pons	6.60108523	6.49261307	6.58951593	6.47728676	6.51203748	6.61345669	6.58872702	6.63129924	6.62729299	6.57835376	6.52508045	6.56049384	6.5287756	6.58140287	6.5515553	6.53006361	6.51110854	6.49946985	6.48025044
Hippocampal_layer_CA1	1.43432371	1.45385349	1.44293152	1.43133042	1.45572591	1.45402168	1.46048625	1.4290309	1.44049093	1.44268163	1.45380942	1.46234635	1.44616037	1.4357762	1.448336	1.43651185	1.44363881	1.43353461	1.4462687
Hippocampal_layer_CA2	0.15780392	0.15942973	0.15714953	0.15704578	0.15851433	0.16359005	0.16545794	0.15493989	0.16232564	0.16171649	0.16403824	0.1643429	0.15783774	0.15811545	0.15699206	0.15865072	0.15659103	0.15439363	0.15960839
Hippocampal_layer_CA3	1.43336808	1.44595062	1.43914362	1.42875426	1.45514758	1.43311573	1.44021506	1.42838848	1.41109949	1.43448021	1.4255161	1.4388837	1.43924528	1.42719708	1.44214568	1.42526065	1.45010114	1.43502387	1.4326395
hypothalamus	1.92169761	1.94690809	1.94324044	1.91563079	1.95683615	1.94120544	1.94727491	1.91772091	1.89960155	1.93191628	1.93209189	1.95374973	1.93230953	1.92013695	1.94245586	1.92875022	1.94839175	1.91645527	1.93047628
Inferior_Colliculus	1.07434983	1.06629242	1.07737428	1.04618506	1.07332888	1.06808393	1.07644621	1.0713217	1.06600733	1.05260852	1.06640973	1.07930069	1.07347524	1.08026266	1.07295175	1.07129811	1.06888084	1.06873961	1.05780403
Infralimbic_Cortex	0.10367738	0.10564725	0.10452875	0.10619252	0.10825959	0.10432048	0.10148132	0.10486055	0.1009893	0.10241326	0.10141567	0.10551637	0.10444449	0.1040353	0.10461273	0.10278526	0.10659565	0.10747242	0.1023249
Insular_Cortex	1.66921313	1.69344638	1.69939595	1.66047472	1.70457826	1.67966083	1.67578534	1.67602649	1.6426001	1.67619897	1.66578669	1.68052962	1.6844309	1.66788238	1.69548905	1.68191535	1.69711471	1.67503763	1.67887328
Internal_capsule	0.54712553	0.55292146	0.5496783	0.54247506	0.55211078	0.55744291	0.56360743	0.54215883	0.5486088	0.55622401	0.559593	0.56323328	0.54986367	0.54785719	0.55248271	0.55198785	0.55239251	0.54244014	0.5535576
interposed_nucleus	0.08825549	0.08713627	0.08769275	0.08669413	0.08801045	0.08653977	0.08514388	0.08861238	0.08826484	0.08954558	0.08430808	0.08469397	0.08720128	0.08754791	0.08790683	0.08772268	0.08841168	0.08785193	0.08655138
intrabulbar_part_of_anterior_commisure	0.18493244	0.18703273	0.19118792	0.17910118	0.19077374	0.18849274	0.18712402	0.18481312	0.18667281	0.18727741	0.19104232	0.18745072	0.18687115	0.17836888	0.19004889	0.1848149	0.18297329	0.18005228	0.18323665
Lateral_olfactory_tract	0.16607623	0.16414955	0.16170509	0.16538332	0.16584785	0.17049167	0.16866345	0.16150714	0.16850049	0.17152363	0.16652777	0.16885479	0.16518814	0.16727596	0.1652782	0.16522419	0.1651809	0.1668136	0.16541814
lateral_septum	0.66863279	0.67436935	0.67780834	0.66184468	0.67441253	0.67092652	0.67261802	0.66620335	0.65333913	0.66740287	0.66712934	0.66795742	0.67728975	0.66822052	0.68107788	0.67535304	0.68021745	0.66986855	0.67026075
Lateral_ventricle	0.95863343	0.9636139	0.95869719	0.95640758	0.96615862	0.97017647	0.97082371	0.94827869	0.95919204	0.97822019	0.96411428	0.9652925	0.96298944	0.95343432	0.96344381	0.96093387	0.96327298	0.94832595	0.96892761
mamillary_bodies	0.11328887	0.11526663	0.11244453	0.11221877	0.1134416	0.11860296	0.12112907	0.11130175	0.11772179	0.11581105	0.12039311	0.12207271	0.1142193	0.1141745	0.113111	0.11452571	0.11254964	0.1113744	0.11492684
mammilothalamic_tract	0.02455296	0.02445319	0.02404677	0.02427805	0.02498699	0.02442525	0.02460052	0.02411839	0.02380927	0.0239041	0.02418838	0.0245039	0.02426789	0.02449961	0.02423904	0.02387271	0.02487101	0.02483177	0.02385537
medial_septum	0.09119444	0.09332157	0.09442217	0.09083024	0.09428047	0.09145574	0.09095529	0.09331508	0.08817792	0.0892738	0.09083038	0.09250993	0.09316249	0.0908628	0.09425652	0.09223809	0.09369313	0.09214421	0.09058016
median_preoptic_area	0.00349156	0.00352289	0.00362398	0.00364621	0.00388953	0.0036598	0.00350903	0.00369842	0.00368113	0.00368344	0.00353718	0.00373994	0.00344251	0.00356814	0.00344457	0.00351735	0.00362221	0.00351808	0.00351309
midbrain	2.36876857	2.38267449	2.39842984	2.34950725	2.40093252	2.3662443	2.36614898	2.36669329	2.35924251	2.35815283	2.36377956	2.37109984	2.37756241	2.36222089	2.37931958	2.36282577	2.3761514	2.36496847	2.37020557
Navicular_nuclear_basin_forebrain	0.11978058	0.12361748	0.12216807	0.12071025	0.12285909	0.121879	0.11965197	0.12080864	0.11798373	0.11938308	0.11866154	0.12136957	0.12131462	0.12048487	0.12133677	0.12091269	0.12242799	0.12230477	0.12049726
Nucleus_accumbens	0.48732494	0.49393993	0.49360829	0.48147937	0.49059975	0.49325077	0.4961294	0.48539032	0.4802377	0.48649306	0.49066575	0.49028395	0.49517507	0.48668882	0.4971392	0.49232401	0.49431271	0.48989971	0.48917601
Occipital_Cortex	0.94111938	0.92186213	0.93634967	0.916707	0.93252086	0.92474996	0.92984735	0.93471745	0.93366259	0.92394462	0.92352592	0.92792624	0.93544332	0.93807847	0.93378553	0.9332028	0.92887708	0.92690693	0.92074697
Olfactory_Bulb	9.68127971	9.5601507	9.26544595	10.7010249	9.13340546	9.01300388	9.00115419	9.95310555	10.1113411	9.50697672	9.68741519	9.0694851	9.50945499	9.90996979	9.1997934	9.78901247	9.465334	10.0716253	10.0141137
Olfactory_tubercle	0.8284532	0.84289294	0.83888524	0.8246588	0.83914798	0.84717133	0.84585141	0.82729825	0.8227902	0.82757177	0.83792444	0.84712409	0.84003784	0.832426	0.8417768	0.83781387	0.84097792	0.83564162	0.83080271
Optic_Chiasm	0.01777576	0.01779635	0.01784888	0.01867878	0.01891447	0.01800812	0.01713192	0.01801404	0.01770805	0.01774307	0.0171042	0.01818382	0.01751594	0.0181485	0.01750602	0.01758063	0.01823159	0.01817898	0.01740788
Optic_tract	0.20553267	0.20825829	0.20802131	0.2078231	0.21213417	0.20879078	0.20748616	0.20600058	0.20727968	0.20830142	0.20663042	0.21026028	0.20466523	0.2049825	0.20481247	0.20523961	0.2072077	0.2044338	0.20675033
Orbitofrontal_Cortex	0.03111491	0.03101366	0.0300328	0.03135925	0.03085447	0.03240555	0.03211812	0.03011996	0.03250955	0.03306702	0.0319385	0.03176	0.03121335	0.03122144	0.03080105	0.03125301	0.03052946	0.0308726	0.03193032
paraflocculus	0.84513241	0.8252084	0.83675335	0.82281111	0.82633894	0.83565256	0.83818421	0.84368376	0.83435195	0.83608885	0.82416979	0.83387308	0.8404604	0.84163785	0.84008677	0.83870083	0.83385424	0.83283456	0.8280451
paramedian_lobe	0.5477512	0.54296289	0.5476782	0.53682372	0.53661921	0.55084573	0.54762194	0.55480952	0.54601728	0.5457776	0.54052287	0.54710495	0.54365943	0.55155838	0.54917866	0.54240105	0.54629976	0.54674069	0.53812904
Parietal_Association_Cortex	0.75820251	0.76270654	0.758772	0.75793714	0.76811544	0.75841728	0.76302646	0.75493194	0.74548408	0.76141965	0.75607896	0.76508789	0.75874032	0.75605933	0.76297655	0.75495697	0.76730543	0.75887329	0.75860719
Periaqueductal_grey	0.71093978	0.69981191	0.71022302	0.69932402	0.70639268	0.69382789	0.70189869	0.70657241	0.69175215	0.6948196	0.69681657	0.69859646	0.71076603	0.70903958	0.71051267	0.7016084	0.7109208	0.71450815	0.70067183
Piriform_Cortex	1.88587515	1.90862264	1.89883065	1.87705875	1.91133338	1.92459527	1.93051131	1.87539244	1.88268436	1.89644142	1.91607926	1.94185999	1.89997092	1.89397498	1.90484868	1.90290821	1.90686759	1.88185485	1.89567291
pons	1.53753372	1.52949172	1.54907438	1.50785501	1.53814385	1.53118898	1.53554124	1.52918958	1.53398181	1.52234814	1.53231316	1.53241956	1.53896323	1.54030755	1.53648003	1.53339896	1.53117128	1.53041606	1.52737541
posterior_commisure	0.01462019	0.01408788	0.01412528	0.01411941	0.01417178	0.01357249	0.01390147	0.01435922	0.01337851	0.01371713	0.01373247	0.01364556	0.01474566	0.01463429	0.01505031	0.01429885	0.01482864	0.01508755	0.01409373
Posterior_part_of_anterior_commissure	0.02217709	0.02162888	0.02168504	0.02185673	0.02155533	0.02170703	0.02193388	0.02156604	0.02139194	0.02205433	0.02162659	0.02173817	0.02200037	0.02198691	0.02207314	0.02197204	0.02234771	0.02225792	0.02180067
Prelimbic_Cortex	0.27509018	0.27703397	0.27315273	0.27078091	0.2757832	0.28023379	0.28151524	0.27176233	0.27170048	0.27565648	0.27859787	0.27891684	0.27853913	0.27241636	0.2792437	0.27494972	0.27563797	0.27625042	0.27515146
Primary_Motor_Cortex	1.34811406	1.36029755	1.35453434	1.33716996	1.36421267	1.3528714	1.34949018	1.34575505	1.31357864	1.34261249	1.33656893	1.34830872	1.36189765	1.34232017	1.36837973	1.34755268	1.3684122	1.36378648	1.34343386
Primary_Somatosensory_Cortex	5.62058729	5.68958034	5.6836752	5.59322944	5.71241578	5.69958735	5.69851966	5.60731283	5.5738406	5.65259965	5.65310395	5.71611753	5.6619856	5.62899324	5.68644209	5.66086422	5.69485496	5.6223322	5.64840208
Primary_Visual_Cortex	1.80184178	1.79873154	1.81046775	1.77367993	1.80796482	1.80203822	1.81141337	1.78991591	1.79974151	1.78992809	1.80193748	1.80451603	1.8025844	1.79975094	1.80258829	1.79589069	1.79608541	1.79220519	1.79323457
Retrosplenial_Cortex	2.16731856	2.16030619	2.16854999	2.13885704	2.16601954	2.17243056	2.18544899	2.14414935	2.16249758	2.1712565	2.17205016	2.16670592	2.16947285	2.16119619	2.16905159	2.16110373	2.16407722	2.15324445	2.16516428
rhinal_cortex	3.26129905	3.26891594	3.28493061	3.21942619	3.28228787	3.27045248	3.28667697	3.24470493	3.25026113	3.24629404	3.26668069	3.27951687	3.27175768	3.26177167	3.27163877	3.25488646	3.26741027	3.25576489	3.25650774
Secondary_Motor_Cortex	0.82283378	0.83898722	0.83815495	0.81621622	0.83766442	0.83403011	0.83636816	0.82468533	0.81572859	0.83249205	0.83343074	0.83022596	0.83836093	0.81240387	0.84031386	0.83247433	0.83045315	0.81815315	0.83598586
Secondary_Somatosensory_Cortex	1.49270342	1.50567964	1.5071846	1.48039779	1.51361662	1.49867547	1.50130295	1.48730543	1.46640548	1.50112879	1.48825133	1.50184423	1.49915033	1.49167167	1.50838646	1.49774564	1.51632607	1.49183466	1.49847232
Secondary_Visual_Cortex	2.17044054	2.16951523	2.18292948	2.15094697	2.18453981	2.16910104	2.17362993	2.15864039	2.16601114	2.17009049	2.16502637	2.16791298	2.17497381	2.16107964	2.17035875	2.16139654	2.16929802	2.15968018	2.16892102
Simple_Lobule	1.15956051	1.14871375	1.16070744	1.13019147	1.15042069	1.16087919	1.16271467	1.16455817	1.15288699	1.14708097	1.14370803	1.16382286	1.15429372	1.1645797	1.15591075	1.15634626	1.14963275	1.14496918	1.14087249
stria_medullaris_thalamus	0.04305368	0.04576363	0.04606239	0.04266207	0.04582332	0.04338882	0.04306739	0.04449823	0.04191996	0.0424514	0.04353042	0.04445257	0.04342158	0.04291267	0.04433115	0.04392892	0.04480688	0.04348881	0.04362241
Stria_terminalis	0.17522447	0.17869378	0.17675062	0.17445148	0.17932941	0.17976231	0.18173721	0.17530721	0.1758704	0.17389952	0.18092693	0.18692984	0.17646271	0.17683906	0.17732063	0.17658946	0.17726366	0.17502836	0.17508948
Subfornical_organ	0.00523788	0.00518171	0.0051402	0.00514515	0.00497514	0.00516523	0.00544818	0.00516233	0.00491689	0.00508265	0.00529217	0.0055138	0.0054264	0.00539727	0.00554627	0.00530212	0.00540603	0.00550568	0.00515985
subicular_region	1.76274387	1.76087345	1.77801069	1.74164973	1.77146037	1.76273734	1.76690269	1.7542739	1.76382026	1.75884957	1.76104615	1.75932772	1.76358438	1.75692397	1.76090801	1.75653246	1.75748498	1.75621435	1.7603314
substantia_nigra	0.15951368	0.16008819	0.16007151	0.15702011	0.15996389	0.15503844	0.15577115	0.15902521	0.15226599	0.15591286	0.15397512	0.15269436	0.16110433	0.15834932	0.16280263	0.15751757	0.16278063	0.16376947	0.15815916
Superior_Colliculus	1.12233479	1.1259534	1.13363189	1.10341754	1.127697	1.12802579	1.13046123	1.11458625	1.12830671	1.12586878	1.12821663	1.12390439	1.12420105	1.12034647	1.12344913	1.12229843	1.12175157	1.11551358	1.12394389
Temporal_Association	0.78459125	0.78529879	0.79602771	0.77825348	0.7957064	0.77663922	0.77119227	0.7852031	0.77881607	0.78104324	0.77268225	0.77102813	0.78405452	0.77656079	0.78254193	0.77841676	0.78287146	0.77976869	0.78139836
Thalamus	3.37400999	3.40915772	3.38539916	3.36162227	3.41743938	3.41550255	3.43978953	3.35426413	3.36030831	3.40549892	3.41341276	3.44448931	3.39404215	3.36791395	3.40357267	3.38055719	3.40648354	3.36073536	3.39597458
Third_ventricle	0.31489512	0.31533821	0.31426587	0.31322865	0.31468365	0.32440396	0.32833354	0.30947878	0.31805994	0.31921573	0.32421301	0.32580071	0.31727818	0.31629119	0.31677825	0.31804641	0.31819267	0.31341531	0.31824543
trochlear_nerve	0.00554516	0.00581923	0.00588024	0.00531359	0.00594903	0.00563477	0.00561129	0.00574577	0.00540122	0.00548129	0.0053753	0.0053524	0.00561597	0.00577757	0.00581639	0.00569499	0.00584603	0.00575271	0.00539521
ventral_pallidum	0.17513771	0.17891136	0.17885646	0.17465934	0.17815031	0.17843362	0.1783086	0.17566008	0.17248916	0.17162155	0.17697169	0.18050901	0.17646278	0.17686375	0.17804856	0.1774175	0.17865239	0.17644876	0.17387164

	69	75	85	111	112	115	3	5	58	66	67	76	78	79	83	84	104	106	110
	Het	Het	Het	Het	Het	Het	WT	WT	WT	WT	WT	WT	WT	WT	WT	WT	WT	WT	WT
Relative Volumes	M	M	M	M	M	M	F	F	F	F	F	F	F	F	F	F	F	F	F
	Mat	Mat	Mat	Mat	Mat	Mat	Mat	Mat	Mat	Mat	Mat	Mat	Mat	Mat	Mat	Mat	Mat	Mat	Mat
amygdaloid_area	2.07050057	2.09612263	2.09449988	2.10025148	2.07718851	2.09362366	2.07339652	2.06967176	2.10153152	2.07995472	2.0869251	2.08454163	2.07475124	2.06392629	2.09656494	2.09504238	2.07972123	2.09315525	2.05406257
Anterior_part_of_anterior_commissure	0.09237748	0.09426406	0.09429592	0.0946151	0.092689	0.0934243	0.09485581	0.09279933	0.09574654	0.09155143	0.09120059	0.0953078	0.08971431	0.08956365	0.09533734	0.0943885	0.09341175	0.09377454	0.09411013
Aqueduct	0.11557791	0.11330569	0.11296241	0.11228692	0.11538541	0.11361389	0.11309313	0.11135155	0.11260071	0.11548571	0.11668358	0.11401866	0.11851694	0.1208301	0.11374133	0.11545081	0.11601943	0.11559111	0.11150749
auditory_cortex	1.44628974	1.44884849	1.45161012	1.45742201	1.44936917	1.45729268	1.44147245	1.43943495	1.45088007	1.46488808	1.46303143	1.44849951	1.4714743	1.46178251	1.45225457	1.45325729	1.44521384	1.45522773	1.43022238
basal_forebrain	1.18207407	1.19124762	1.18638674	1.19350056	1.19043602	1.19026759	1.1995196	1.18311374	1.20316314	1.16701011	1.20228506	1.19340413	1.20417421	1.20416118	1.18459673	1.1964746	1.19702768	1.20314245	1.15949943
Bed_nucleus_of_stria_terminalis	0.20174482	0.20329438	0.20347388	0.20371909	0.20112777	0.20454191	0.20435457	0.20594683	0.21082349	0.20576088	0.20178297	0.20668532	0.19141788	0.18574063	0.20416785	0.2059796	0.20226755	0.20424836	0.19854506
caudaputamen	3.19279567	3.22657182	3.20709758	3.23213627	3.21004393	3.22243289	3.23889513	3.20050029	3.24649181	3.15915946	3.24180954	3.22705927	3.24348884	3.24027733	3.20831315	3.23569854	3.23357082	3.24887532	3.14387983
cerebellar_lobule_1_2	0.56659776	0.56537139	0.57042922	0.57154961	0.57293464	0.57195253	0.55903964	0.56341763	0.56766958	0.56690778	0.56994273	0.57218362	0.5622255	0.56654915	0.57059276	0.5736673	0.57339209	0.57531151	0.56674688
cerebellar_lobule_10	0.2464144	0.23803775	0.23870715	0.24183767	0.24015237	0.23821398	0.2336824	0.23657461	0.24255651	0.23854535	0.24067533	0.24183443	0.23450813	0.24007447	0.2393287	0.23948439	0.24243329	0.24345621	0.23452908
cerebellar_lobule_3	0.49473015	0.49325273	0.49434192	0.50174805	0.49499805	0.49564258	0.4826003	0.49065841	0.49468584	0.49371478	0.49106963	0.50017517	0.47775748	0.4844479	0.49602346	0.49777646	0.49954245	0.50036613	0.49389579
cerebellar_lobule_4_5	1.53499575	1.50277282	1.50542317	1.52642894	1.52809741	1.51053394	1.48999219	1.50300782	1.52132937	1.50175034	1.531947	1.52723328	1.52404806	1.53578194	1.5133887	1.52302725	1.53436611	1.54174738	1.49739606
cerebellar_lobule_6	0.6199542	0.59816429	0.59897453	0.6097813	0.59869456	0.60703133	0.59557033	0.60566187	0.61787036	0.59828716	0.60808768	0.60569137	0.60736309	0.61199272	0.59840112	0.60303936	0.61236965	0.61001736	0.59086899
cerebellar_lobule_7	0.23736915	0.22727155	0.22782865	0.23055048	0.22653582	0.23187599	0.23216123	0.23462209	0.23733397	0.23074878	0.2358283	0.22930648	0.23592051	0.23804523	0.22727918	0.22977503	0.23521718	0.23096088	0.22224076
cerebellar_lobule_8	0.26903575	0.25836498	0.25951347	0.26525911	0.25730287	0.26313306	0.25699679	0.26167703	0.26824697	0.25818784	0.26294695	0.26211065	0.26345603	0.26676443	0.25782233	0.25975999	0.26462255	0.26473557	0.25808974
cerebellar_lobule_9	0.62336874	0.60024119	0.60152161	0.61320222	0.59909567	0.61120817	0.60033873	0.61079743	0.62214491	0.59817478	0.61155638	0.60928096	0.61589379	0.62136411	0.59998681	0.60538002	0.6165263	0.61276113	0.59630868
Cerebellar_White_Matter_Arbor_vita_of_cerebellum	1.93109716	1.89441976	1.89997754	1.92423831	1.90709054	1.9070209	1.88095371	1.89518956	1.9314938	1.8886421	1.90810905	1.91804001	1.87892618	1.89827371	1.90654318	1.91951874	1.93078629	1.92790583	1.88093487
cerebral_peduncle	0.20451758	0.20528317	0.20416795	0.20496903	0.20307849	0.206208	0.2033937	0.20331804	0.20429183	0.2083322	0.20533897	0.20417404	0.20309416	0.20205108	0.20472818	0.20497286	0.20393571	0.20429576	0.19926821
Cingulate_Cortex_area_1	1.06059969	1.07611087	1.05990627	1.07456764	1.05803116	1.06712279	1.08145514	1.050979	1.06867502	1.04721909	1.07899961	1.07032254	1.09381038	1.09612467	1.06130631	1.07306649	1.0727004	1.08074413	1.05088946
Cingulate_Cortex_area_2	0.65878373	0.66136046	0.65584539	0.66190612	0.65722979	0.65819876	0.66836208	0.65613475	0.66451918	0.64631554	0.67183479	0.66296162	0.68016374	0.68017524	0.65427549	0.66353939	0.66311328	0.66781778	0.64486979
cingulum	0.23018379	0.23296085	0.23357785	0.234593	0.23055397	0.23319485	0.23202267	0.23192934	0.23384994	0.23167243	0.23119317	0.23416366	0.22845039	0.22752188	0.23383746	0.23349134	0.23139778	0.23350229	0.23082917
Cochlear_nucleus	0.07589258	0.07734012	0.07706907	0.07760738	0.07514176	0.07618348	0.07422796	0.07522874	0.07676789	0.07446039	0.07303829	0.07787988	0.06888575	0.07110492	0.0772654	0.07714273	0.07676688	0.07597614	0.07658176
Commisure_inferior_Colliculus	0.02196727	0.02044137	0.02047339	0.02021182	0.02243672	0.02063201	0.0219162	0.02076892	0.02078489	0.02142887	0.02319164	0.02082899	0.0255635	0.02547323	0.02088935	0.02143178	0.02179758	0.02192023	0.02047969
commisure_superior_collicuus	0.01306633	0.0129511	0.01320339	0.01295144	0.01278996	0.01310583	0.01329468	0.01309961	0.01321093	0.01334555	0.01311289	0.01315604	0.01281247	0.01274587	0.01305145	0.01312311	0.01295035	0.0129555	0.01281667
copula	0.19821182	0.19383657	0.19458898	0.19853569	0.19263763	0.1989938	0.19556737	0.1986068	0.20114364	0.19402799	0.19632483	0.19480322	0.19556226	0.19439787	0.19371974	0.19580837	0.1984271	0.19585735	0.19168289
Corpus_Callosum_associated_White_Matter	2.91846406	2.93168422	2.91581991	2.9344133	2.92008821	2.93558395	2.92753238	2.90772031	2.92723259	2.91581109	2.95883316	2.92549222	2.96109164	2.95208523	2.91747524	2.93557367	2.93145075	2.94747977	2.86050131
Crus_1_ansiform_lobule	1.19540662	1.17007445	1.17093656	1.19224853	1.17893906	1.18230145	1.16751733	1.1767672	1.19935902	1.16780828	1.18325373	1.18164307	1.17110496	1.17221703	1.1739448	1.18402375	1.19234828	1.19089909	1.15982922
Crus_2_ansiform_lobule	0.70358708	0.68621081	0.68678416	0.69976673	0.67820601	0.69847991	0.68713641	0.69430657	0.7107559	0.67939876	0.68478122	0.69512333	0.67721883	0.68777176	0.68729578	0.69382469	0.70158466	0.6921438	0.68346877
dentate_gyrus	1.13714007	1.14518126	1.14717775	1.15421646	1.14221023	1.15394294	1.13358386	1.13337158	1.14492092	1.15084919	1.14528698	1.14583622	1.14818302	1.13949122	1.14880858	1.14897778	1.13893092	1.14614812	1.14060016
Dentate_nucleus	0.0602125	0.06101829	0.06103292	0.06165865	0.05951566	0.06034637	0.05856849	0.0597546	0.0604735	0.06030404	0.05812079	0.06142887	0.05416991	0.0555236	0.06128711	0.06070371	0.06086263	0.06008834	0.06032863
Dorsal_Peduncular_Cortex	0.10656848	0.10846213	0.10604104	0.10824011	0.10415006	0.10803409	0.10641013	0.10633273	0.10651912	0.10473284	0.10580361	0.10753106	0.10494301	0.10416571	0.10600874	0.10718541	0.10657483	0.10733723	0.10491133
Dorsal_Tenia_Tecta	0.07407252	0.07457146	0.07450189	0.07475988	0.07243913	0.07344267	0.07459332	0.07424863	0.07522918	0.07344051	0.07294794	0.07571291	0.07098437	0.07113859	0.07409252	0.07460229	0.07342338	0.07419656	0.07329157
Endopiriform_Nucleus	0.61293495	0.61332161	0.60991377	0.61410188	0.6177068	0.61231488	0.62299062	0.61159524	0.6196792	0.6033766	0.63059116	0.61366031	0.64325058	0.64326289	0.61072852	0.61799824	0.62056065	0.62442162	0.59996758
entopeduncular_nucleus	0.01595198	0.01519197	0.01531995	0.01538888	0.01537565	0.01526751	0.01511331	0.01562179	0.01522084	0.01559826	0.01628611	0.0155552	0.01699116	0.01719003	0.01533708	0.01500259	0.01546001	0.01590104	0.01542707
external_medullary_lamina	0.04556633	0.04581328	0.04506711	0.04539185	0.04523211	0.04569323	0.04560734	0.04512427	0.04554299	0.04694285	0.04566894	0.04529102	0.04429831	0.0444801	0.04527329	0.0459438	0.04556244	0.04536786	0.04364981
Fasciculus_retroflexus	0.0163267	0.01577892	0.0156705	0.01581381	0.01635527	0.01561393	0.0158565	0.01550036	0.01560962	0.01563736	0.01736995	0.0155547	0.01927005	0.01962586	0.01562182	0.01550611	0.01607544	0.0164049	0.01522638
fastigial_nucleus	0.07417435	0.07167898	0.07223926	0.07194322	0.07291373	0.07088941	0.07110738	0.07110807	0.07250349	0.06952067	0.07310837	0.07245835	0.07362796	0.0747533	0.0723396	0.07233647	0.07305639	0.07311919	0.07032434
Fimbria	0.32752814	0.32982552	0.33033413	0.33124473	0.32888956	0.32753781	0.32637147	0.32590751	0.33118572	0.32437228	0.33080278	0.32835777	0.33175072	0.33324316	0.33007437	0.32868825	0.32884161	0.33136542	0.32221369
flocculus	0.74922743	0.7346366	0.7393945	0.74586646	0.74852614	0.73896868	0.72646436	0.73429994	0.73894523	0.73794161	0.75256935	0.74697483	0.74868234	0.76032856	0.74182388	0.74502168	0.75099772	0.75579762	0.73325524
Fornix	0.0393053	0.04053916	0.03960627	0.03975327	0.0397455	0.04083176	0.04085439	0.03855355	0.04001166	0.03821927	0.03974379	0.0398061	0.03958774	0.039929	0.04017755	0.04110338	0.04057513	0.04030848	0.03979018
Fourth_ventricle	0.19910164	0.19925265	0.20056515	0.20411246	0.19806944	0.20143337	0.19644142	0.19955819	0.20292065	0.19765691	0.19693812	0.20084486	0.19162319	0.19090262	0.20014055	0.20148948	0.20097942	0.20069172	0.20044609
Frontal_Association_Cortex	7.81736468	8.01871739	7.73906901	8.02608522	7.76255935	7.95888557	7.92110496	7.72898235	7.89870536	7.86162827	8.02536241	7.92134976	8.09346349	8.16540275	7.84844748	7.9434223	7.97183412	8.11139248	7.75831332
Globus_pallidus	0.30699647	0.31046887	0.30919696	0.31060642	0.3082408	0.31199106	0.31032431	0.30897748	0.31211226	0.3068008	0.3107383	0.31191225	0.30682336	0.30554946	0.30977149	0.31120453	0.31061056	0.31224116	0.30313665
hindbrain_medulla_pons	6.70091055	6.54920863	6.5721704	6.64377463	6.57242844	6.61856864	6.51569904	6.57954222	6.67997675	6.57289225	6.62356153	6.64986457	6.58858682	6.6622648	6.58246088	6.62737156	6.67731818	6.6541071	6.52056487
Hippocampal_layer_CA1	1.43407194	1.43598462	1.44206996	1.44789037	1.44015982	1.44769699	1.42545543	1.42509507	1.43598721	1.45352442	1.44940529	1.43853561	1.45915661	1.44966612	1.4399273	1.44141947	1.43246326	1.44260359	1.42689422
Hippocampal_layer_CA2	0.1565426	0.1555391	0.15605811	0.15571801	0.1571445	0.15562773	0.15709885	0.1553624	0.15592705	0.15788791	0.16162996	0.15490554	0.16514636	0.16549348	0.15601895	0.15659136	0.15701533	0.15831233	0.15093774
Hippocampal_layer_CA3	1.42280248	1.4383749	1.44211813	1.44879898	1.4252882	1.44215904	1.41869838	1.42099955	1.43964253	1.44213901	1.42898406	1.43289212	1.41552293	1.40924794	1.44161016	1.43717216	1.42348963	1.43310287	1.41617897
hypothalamus	1.90692596	1.92832841	1.92635006	1.93047512	1.91689804	1.92915183	1.91716635	1.90495597	1.93353165	1.90645873	1.9309984	1.92003483	1.92505323	1.91750975	1.92889241	1.93130508	1.9206165	1.93218555	1.89111428
Inferior_Colliculus	1.07950951	1.07626611	1.08153313	1.08076664	1.08182192	1.08170473	1.05473187	1.06512395	1.07288752	1.08511815	1.08074422	1.08850342	1.08080472	1.0876521	1.08002952	1.0852503	1.08353808	1.08747425	1.07292245
Infralimbic_Cortex	0.10202685	0.10609923	0.10407194	0.10566089	0.10291323	0.10476441	0.10661856	0.10244129	0.10473703	0.1013362	0.101781	0.10532583	0.10311704	0.10285246	0.10551673	0.10557724	0.10424902	0.10457588	0.10618426
Insular_Cortex	1.66217078	1.68995586	1.67309124	1.69151414	1.66470072	1.6869718	1.68457017	1.66312586	1.69395411	1.64361803	1.673627	1.6808681	1.65994742	1.65388282	1.67210377	1.69062949	1.68303623	1.68816178	1.64224606
Internal_capsule	0.54522647	0.54849044	0.54632592	0.54819257	0.54669421	0.54727587	0.54501325	0.54265019	0.54955833	0.54422442	0.55367859	0.54405637	0.55529416	0.55301095	0.54680036	0.54659697	0.54796529	0.55053082	0.53023293
interposed_nucleus	0.08819615	0.08859821	0.08842532	0.08861678	0.0881809	0.08733566	0.08753804	0.0876417	0.08907074	0.08805728	0.08674295	0.0889629	0.08094043	0.08193294	0.08980148	0.0893737	0.08854594	0.08704508	0.08640052
intrabulbar_part_of_anterior_commisure	0.17932175	0.18567839	0.17583393	0.18772669	0.18158109	0.19216459	0.18481136	0.17453353	0.18099461	0.18137738	0.19217161	0.18137037	0.20221485	0.20309002	0.18087935	0.18626946	0.18849669	0.19289443	0.17642414
Lateral_olfactory_tract	0.16382696	0.1649781	0.16315759	0.16536087	0.16345715	0.16253284	0.1672328	0.16432961	0.16753379	0.16381149	0.16690546	0.16658659	0.16689172	0.16766582	0.16410062	0.16530559	0.16467249	0.16716533	0.16122659
lateral_septum	0.66427977	0.6732842	0.66992459	0.67638606	0.66635285	0.67634777	0.67324384	0.66891585	0.67732381	0.66064202	0.67086948	0.67454086	0.66008538	0.65713224	0.67021751	0.67475951	0.67437434	0.6760419	0.65880663
Lateral_ventricle	0.9457433	0.95288359	0.95129969	0.95587352	0.95265619	0.9543434	0.95570262	0.95148497	0.9625173	0.95045046	0.96192677	0.95317921	0.95767565	0.9496358	0.95455679	0.95899188	0.95197329	0.95894826	0.93843418
mamillary_bodies	0.11412282	0.11215687	0.1113853	0.11223191	0.1141214	0.1119225	0.11283486	0.112265	0.1116784	0.11405782	0.11792758	0.11147512	0.12248085	0.12314607	0.11161525	0.11168961	0.11305495	0.1146702	0.10777915
mammilothalamic_tract	0.02403267	0.02428718	0.02458634	0.02443554	0.02386087	0.02421126	0.02402998	0.02404431	0.02439001	0.02483699	0.02437006	0.02438917	0.0238964	0.024045	0.02479926	0.02421274	0.02401731	0.0243849	0.02480239
medial_septum	0.09116811	0.09331751	0.09147404	0.09328468	0.09174948	0.09469774	0.09294791	0.09055512	0.09160765	0.08904371	0.09154993	0.09257687	0.09196226	0.09184791	0.09252035	0.09341465	0.09393575	0.09316397	0.0917787
median_preoptic_area	0.00331554	0.00348286	0.00358293	0.00359818	0.00350204	0.00341774	0.00351507	0.00334553	0.00359358	0.0031121	0.00337294	0.00339716	0.00346424	0.00347575	0.00355489	0.0035701	0.00347463	0.00346121	0.00358091
midbrain	2.35688147	2.38006828	2.38788236	2.39547103	2.37679562	2.3979389	2.35068393	2.35085885	2.37441597	2.40170202	2.36560483	2.38691354	2.36839216	2.34219283	2.38050404	2.3951446	2.36721635	2.37746655	2.36860807
Navicular_nuclear_basin_forebrain	0.12090494	0.12305106	0.12141842	0.12264136	0.11970931	0.12212817	0.12355106	0.12047713	0.12174174	0.11787482	0.1213527	0.12247452	0.12212339	0.12192924	0.1207097	0.12401971	0.12137616	0.12204817	0.11923128
Nucleus_accumbens	0.49017718	0.49731017	0.48786866	0.49709205	0.48619151	0.4950511	0.49502104	0.48734376	0.48992792	0.48115956	0.4963134	0.4935448	0.49428617	0.49735698	0.48732257	0.4946725	0.49516858	0.49680056	0.48002572
Occipital_Cortex	0.935272	0.9317851	0.94201737	0.94018383	0.94183473	0.94358911	0.91657555	0.92735163	0.93241997	0.94354022	0.93889356	0.94372064	0.9321336	0.93572087	0.93819081	0.94502319	0.942307	0.94697917	0.93591559
Olfactory_Bulb	9.77698698	9.44347643	9.83160862	8.95494033	9.9369842	9.2317857	10.0241822	10.3595029	9.18136334	9.92413253	9.15532448	9.29959329	9.28047738	9.27226386	9.71569126	9.17036398	9.28283222	8.82821352	10.9135154
Olfactory_tubercle	0.83167097	0.84093955	0.82835302	0.84108608	0.82829772	0.83661275	0.84548644	0.82652295	0.83398926	0.81542247	0.84417978	0.83792678	0.85182785	0.856488	0.82838715	0.84019422	0.84063595	0.84580103	0.82139019
Optic_Chiasm	0.01694769	0.01750807	0.017904	0.01771183	0.017665	0.01747986	0.01793142	0.01731147	0.0183952	0.01719387	0.01707276	0.0179626	0.01704389	0.01689485	0.01825787	0.01794247	0.01754902	0.01764743	0.01871211
Optic_tract	0.20224437	0.20449541	0.20506239	0.20554892	0.20481584	0.20429667	0.20514201	0.20262886	0.20689239	0.20308143	0.20581115	0.20381868	0.20766667	0.20624207	0.20521405	0.20598337	0.20474902	0.20558687	0.20123985
Orbitofrontal_Cortex	0.03087032	0.03062277	0.03039571	0.03078568	0.03057348	0.03047308	0.03151856	0.03074932	0.03153183	0.0306952	0.03194924	0.03087595	0.03250822	0.03203065	0.03056147	0.0310484	0.03059102	0.03098291	0.03036891
paraflocculus	0.85499112	0.84061923	0.84444984	0.85765351	0.84670506	0.84480563	0.82674063	0.83947685	0.85020732	0.84257971	0.84631718	0.85229462	0.82987052	0.83658792	0.84591056	0.84733989	0.85219519	0.85553408	0.8403435
paramedian_lobe	0.56770968	0.55209085	0.55227787	0.56168066	0.54937194	0.55600417	0.54322485	0.55305978	0.56760212	0.5490044	0.54956149	0.5601017	0.53859537	0.54742576	0.55189975	0.55408114	0.56018568	0.55818805	0.54510382
Parietal_Association_Cortex	0.75110199	0.76067895	0.76231967	0.76366765	0.7525152	0.75977699	0.75082531	0.75219954	0.76313513	0.75837904	0.75587473	0.75724885	0.75105905	0.74546256	0.76199032	0.75759357	0.7525235	0.7581302	0.74555931
Periaqueductal_grey	0.70794171	0.71378683	0.7182247	0.72220167	0.70914087	0.72024812	0.69595565	0.70922721	0.71313393	0.72465734	0.7036299	0.72032641	0.69893168	0.68754011	0.71238835	0.71337597	0.70691676	0.71127698	0.71312111
Piriform_Cortex	1.87957762	1.89197577	1.88385629	1.89618463	1.88681351	1.89013322	1.89354315	1.8747827	1.89722268	1.86139493	1.9130749	1.88904624	1.92745173	1.92591729	1.8843183	1.89374107	1.89542143	1.90915336	1.85049463
pons	1.53044651	1.54429576	1.54890217	1.54527737	1.54458682	1.54946104	1.52080229	1.52365123	1.53625625	1.56062756	1.53546866	1.55358836	1.53378692	1.52261871	1.54313142	1.55225934	1.54199156	1.54487679	1.53789349
posterior_commisure	0.01466548	0.01495865	0.01525226	0.01551498	0.0146837	0.01539896	0.01382686	0.01466255	0.01496183	0.01536816	0.01425102	0.01527484	0.01336799	0.01312654	0.01511236	0.01488386	0.01467394	0.01468961	0.01554562
Posterior_part_of_anterior_commissure	0.02178618	0.0219945	0.02217246	0.02215814	0.02169032	0.021986	0.02178271	0.02228505	0.02255141	0.02196841	0.02167358	0.02228935	0.02079663	0.02046567	0.02222549	0.0218355	0.02167893	0.02205032	0.02167717
Prelimbic_Cortex	0.27637383	0.28151784	0.27337419	0.28024126	0.27267132	0.27634669	0.27980092	0.27189024	0.27354011	0.27130878	0.2795354	0.27538993	0.28430094	0.28647662	0.27273312	0.27607221	0.27772043	0.28070532	0.26903871
Primary_Motor_Cortex	1.34518755	1.37438573	1.35310215	1.37257038	1.33753723	1.36329427	1.36280186	1.34101822	1.35904601	1.32772478	1.34874263	1.36477359	1.345392	1.34196418	1.35284251	1.36405007	1.35758652	1.36587889	1.33941576
Primary_Somatosensory_Cortex	5.59229421	5.65795931	5.61792723	5.66461356	5.60741104	5.64722319	5.65790408	5.58920943	5.67075505	5.54129922	5.65871391	5.64136503	5.65365931	5.64622332	5.6202045	5.66367998	5.65003412	5.6803619	5.51845434
Primary_Visual_Cortex	1.79573956	1.80394104	1.80770392	1.8094118	1.80453038	1.81450133	1.78447185	1.78457436	1.79954265	1.82697362	1.80717067	1.81337159	1.80574425	1.7976169	1.80272003	1.81272023	1.80142123	1.80830541	1.78633547
Retrosplenial_Cortex	2.15458682	2.1645668	2.16795577	2.17126971	2.16311663	2.17371901	2.14441292	2.15107584	2.16334565	2.19069842	2.17135034	2.17255263	2.16162826	2.14843059	2.1643854	2.17115551	2.16030708	2.17110948	2.13474735
rhinal_cortex	3.25437121	3.27280719	3.28094634	3.28506032	3.26971559	3.28872004	3.23609787	3.23730936	3.26556113	3.30847461	3.27489787	3.28595967	3.27493012	3.25653651	3.27369165	3.28680423	3.26384907	3.27783614	3.24841521
Secondary_Motor_Cortex	0.82431053	0.83711668	0.81858283	0.83618321	0.82164988	0.83477664	0.83662033	0.81883691	0.82757277	0.81269117	0.83743758	0.82298365	0.8480867	0.8404436	0.81746533	0.83372543	0.83289701	0.83814494	0.80616199
Secondary_Somatosensory_Cortex	1.48239107	1.50103236	1.49525604	1.50103117	1.48511455	1.49745777	1.49201302	1.48489914	1.51175801	1.47421164	1.49127519	1.49818721	1.46848993	1.46402082	1.49706235	1.50192801	1.49211523	1.50083744	1.46151814
Secondary_Visual_Cortex	2.15548722	2.16965719	2.17683775	2.18186057	2.16761381	2.18449348	2.14902703	2.15320545	2.17093988	2.20002081	2.16924891	2.17910286	2.16688875	2.14572767	2.17315291	2.18228075	2.16232935	2.17293546	2.15740254
Simple_Lobule	1.17942222	1.1569977	1.16131361	1.17635847	1.16869943	1.16083862	1.14136085	1.15241812	1.17071701	1.15280406	1.17049073	1.17262531	1.15776907	1.17415948	1.16385997	1.16908711	1.17740347	1.18238559	1.15577937
stria_medullaris_thalamus	0.04351924	0.04470412	0.04353028	0.04406673	0.04347817	0.04435205	0.04401652	0.04325206	0.04413785	0.04253886	0.04372364	0.04322052	0.04334431	0.04416321	0.04357746	0.04418668	0.04397548	0.04388019	0.04231439
Stria_terminalis	0.17583733	0.17632697	0.17576201	0.17633181	0.17710244	0.17575811	0.17466562	0.17365276	0.17525974	0.17439197	0.17980302	0.17502391	0.18547347	0.18579702	0.17618785	0.17609946	0.1762016	0.17788733	0.17284448
Subfornical_organ	0.00526772	0.00552528	0.00540639	0.00558858	0.00536385	0.00528406	0.00511064	0.00542743	0.00546086	0.00539172	0.0052819	0.00546617	0.00529449	0.00524348	0.00548353	0.0053483	0.00548119	0.00539578	0.00497232
subicular_region	1.7525972	1.76244168	1.76738485	1.76965701	1.76377056	1.77500032	1.75012193	1.74911659	1.76140002	1.78886239	1.7615873	1.77326471	1.7638153	1.74317786	1.76006177	1.77423015	1.75722512	1.76387596	1.74404265
substantia_nigra	0.16034368	0.16227694	0.16331555	0.16527946	0.15844207	0.16437669	0.15631784	0.16030429	0.16122312	0.16505359	0.15692206	0.16362561	0.14954079	0.14828894	0.16296191	0.16200584	0.15866368	0.15915097	0.16389406
Superior_Colliculus	1.11550014	1.12560641	1.12459755	1.12377594	1.12549589	1.12964016	1.11842162	1.11302646	1.12016244	1.140922	1.12278195	1.12908981	1.11813508	1.11110835	1.12276567	1.13166384	1.12325631	1.1241178	1.10425357
Temporal_Association	0.77435763	0.78564682	0.78653432	0.78847299	0.78196709	0.79178613	0.77818327	0.77590578	0.78439817	0.79079587	0.77580797	0.78844548	0.77229227	0.76187419	0.78489128	0.79259656	0.78239929	0.7820367	0.7825683
Thalamus	3.35633926	3.38054974	3.37737054	3.3898385	3.36543987	3.38126787	3.35242172	3.34778999	3.38237319	3.37563507	3.39896748	3.3618571	3.40369045	3.38735281	3.38138612	3.37488836	3.36130982	3.38878193	3.31170167
Third_ventricle	0.31265045	0.31275467	0.31304614	0.31527118	0.31517183	0.31349709	0.31400423	0.31588104	0.31452392	0.31605577	0.32064188	0.31452222	0.32529844	0.32455838	0.31431403	0.31231569	0.31449324	0.3181447	0.30845861
trochlear_nerve	0.00579713	0.00589629	0.00571163	0.00576503	0.00574135	0.00575401	0.00577287	0.00550812	0.0057059	0.00584676	0.00547511	0.00597147	0.00512556	0.00544184	0.00585286	0.00603858	0.00601899	0.00578102	0.00550881
ventral_pallidum	0.17519161	0.17746944	0.17639623	0.17778049	0.17584304	0.17684081	0.17802149	0.17494385	0.17717761	0.17131759	0.17839957	0.17652861	0.17948641	0.18135532	0.17509759	0.17724226	0.17775626	0.17852399	0.17199633

	113	114	1	4	59	60	63	68	71	73	74	77	80	81	82	15	20	25	26
	WT	WT	WT	WT	WT	WT	WT	WT	WT	WT	WT	WT	WT	WT	WT	Het	Het	Het	Het
Relative Volumes	F	F	M	M	M	M	M	M	M	M	M	M	M	M	M	F	F	F	F
	Mat	Mat	Mat	Mat	Mat	Mat	Mat	Mat	Mat	Mat	Mat	Mat	Mat	Mat	Mat	Pat	Pat	Pat	Pat
amygdaloid_area	2.08110629	2.0869716	2.10599552	2.09583797	2.10972376	2.09667619	2.08178478	2.0967413	2.11296502	2.0913479	2.08227783	2.0914491	2.09968724	2.00198111	2.10236342	2.06509042	2.09218012	2.09303775	2.11212768
Anterior_part_of_anterior_commissure	0.09321537	0.09488885	0.09591504	0.09511313	0.09506253	0.09486134	0.09234279	0.09356203	0.09220078	0.09449816	0.094946	0.09659993	0.09370961	0.0912489	0.09640937	0.09322048	0.09372288	0.09298771	0.09486354
Aqueduct	0.11231048	0.11449715	0.11349928	0.11484106	0.11310917	0.11255994	0.11622087	0.11213191	0.11491462	0.11328233	0.11268555	0.11206431	0.11669399	0.11335017	0.11331216	0.11349518	0.11367241	0.1157831	0.11521988
auditory_cortex	1.44648188	1.44788828	1.44959984	1.4550854	1.46519252	1.45339137	1.45616352	1.45212875	1.47452602	1.45315921	1.44373874	1.45119064	1.4677986	1.39756723	1.45590031	1.44262294	1.45870056	1.46303833	1.47359981
basal_forebrain	1.18023217	1.20107765	1.19968248	1.1899712	1.20476278	1.21215142	1.20063413	1.19069977	1.20770546	1.18978396	1.18309371	1.19273833	1.20342863	1.13177901	1.19786342	1.18217518	1.2026355	1.20490165	1.20716491
Bed_nucleus_of_stria_terminalis	0.20610108	0.20684687	0.20498754	0.20359942	0.21271299	0.20613311	0.20124651	0.20918527	0.20652082	0.20396544	0.20219602	0.20621044	0.20544287	0.19593346	0.20621916	0.20858045	0.20551778	0.21581263	0.2069645
caudaputamen	3.197001	3.24616659	3.24132785	3.21192464	3.25801383	3.26934869	3.2395426	3.22140505	3.26751144	3.22194811	3.20054469	3.22626924	3.25067633	3.06611054	3.23825006	3.20047876	3.24950814	3.25410524	3.25891902
cerebellar_lobule_1_2	0.57473754	0.57069261	0.56851958	0.57838304	0.56042454	0.55445417	0.5615424	0.56842826	0.55501145	0.57250301	0.5684265	0.55997273	0.56151733	0.5944671	0.5684213	0.565426	0.56275101	0.56704848	0.56770382
cerebellar_lobule_10	0.24396031	0.24209653	0.23636628	0.24209594	0.23510764	0.23510913	0.24191601	0.23627371	0.23703224	0.24188108	0.23992398	0.23167449	0.23858058	0.2730739	0.23772004	0.24079827	0.23347418	0.23873603	0.23817815
cerebellar_lobule_3	0.50411492	0.49625085	0.49267994	0.50227195	0.48330415	0.47881985	0.48705544	0.49214123	0.47935255	0.49914501	0.49430917	0.48446101	0.48342616	0.52974351	0.49335435	0.49266205	0.48481254	0.48877271	0.48862363
cerebellar_lobule_4_5	1.53310345	1.5223927	1.50438174	1.5299955	1.49459001	1.4946087	1.51924677	1.51044099	1.49807816	1.52524186	1.51851837	1.48171814	1.51233886	1.65771853	1.50569303	1.51750507	1.49870523	1.52240845	1.51788017
cerebellar_lobule_6	0.61525589	0.60470581	0.59492786	0.61024585	0.59732392	0.59524767	0.61112764	0.60449077	0.60485141	0.60426637	0.60552889	0.58106739	0.60372596	0.69665913	0.59417097	0.60274103	0.59281637	0.60672515	0.60451277
cerebellar_lobule_7	0.23517798	0.23169902	0.22643864	0.23266873	0.23174396	0.22855147	0.23691216	0.23279885	0.23714265	0.2294461	0.23011922	0.22099044	0.23546822	0.26659997	0.22503332	0.23339668	0.22827572	0.23836793	0.2342776
cerebellar_lobule_8	0.26646825	0.26155033	0.25742879	0.26371666	0.2551047	0.25688308	0.2628614	0.25985937	0.26083167	0.26086397	0.26137529	0.24981719	0.25939073	0.30260451	0.25655302	0.25778149	0.25302407	0.25937933	0.25879216
cerebellar_lobule_9	0.61851472	0.6066554	0.5981426	0.61402456	0.59891588	0.59714418	0.61386143	0.60760212	0.60936513	0.60570156	0.60852356	0.58138538	0.60644323	0.70231699	0.59609904	0.60236811	0.59337584	0.60853148	0.60619371
Cerebellar_White_Matter_Arbor_vita_of_cerebellum	1.93373322	1.91053524	1.8982551	1.93643474	1.88058939	1.86768743	1.90214295	1.89906667	1.87954981	1.91688365	1.92039472	1.85874913	1.89308753	2.12916579	1.89296388	1.90328225	1.87000958	1.91020219	1.90293515
cerebral_peduncle	0.20464549	0.20466882	0.20420887	0.20450823	0.20857855	0.20393329	0.20525315	0.20565743	0.20896123	0.20493645	0.20195151	0.20363162	0.20762019	0.19534942	0.20351854	0.20540571	0.20545091	0.20916181	0.20758639
Cingulate_Cortex_area_1	1.05896427	1.07452954	1.07713679	1.05986452	1.07652848	1.08325628	1.07753475	1.05596496	1.08506269	1.06956533	1.06253387	1.0690373	1.09034586	1.03067624	1.07428293	1.06286876	1.07846324	1.07699787	1.08282246
Cingulate_Cortex_area_2	0.65332787	0.66799109	0.66156743	0.65493133	0.66854943	0.67212922	0.67082331	0.65788355	0.67507824	0.66121824	0.65481058	0.66054156	0.67607293	0.63020909	0.66277451	0.66052175	0.67122277	0.67375094	0.67282378
cingulum	0.23267591	0.23343446	0.23379858	0.23354225	0.23455133	0.2341831	0.23181901	0.23337356	0.23346306	0.23434984	0.23218942	0.23459519	0.2328871	0.22393485	0.23524197	0.23106813	0.23382235	0.23200418	0.23432608
Cochlear_nucleus	0.07804802	0.07576728	0.07681047	0.07790154	0.07340606	0.07223681	0.07314169	0.07502474	0.07203485	0.07775499	0.07735423	0.07476515	0.073077	0.08344543	0.07697682	0.07455832	0.07269583	0.073126	0.07417443
Commisure_inferior_Colliculus	0.02043138	0.02162518	0.02103238	0.02105474	0.0220902	0.02211904	0.02298179	0.02084358	0.02280897	0.02049102	0.02081722	0.02082358	0.02368849	0.02062637	0.02070491	0.02192852	0.02254095	0.02368741	0.02305328
commisure_superior_collicuus	0.01305048	0.01278693	0.01319261	0.01327885	0.01321636	0.01310719	0.01306241	0.01308882	0.01318002	0.01316815	0.01312878	0.01350131	0.01314935	0.01279782	0.01321809	0.01293982	0.01318775	0.0130654	0.01342096
copula	0.20010583	0.19472034	0.19356544	0.19802352	0.19574336	0.19304356	0.19620861	0.1987315	0.19780907	0.19580085	0.19688183	0.18928883	0.19425187	0.22662186	0.19169964	0.19534471	0.19322562	0.19853491	0.19584593
Corpus_Callosum_associated_White_Matter	2.91253738	2.93972883	2.92509193	2.91691257	2.9572525	2.94312765	2.95022911	2.93028844	2.98255608	2.93117726	2.90019514	2.91995837	2.96871149	2.81164236	2.92773115	2.92353334	2.94952263	2.97068207	2.96535914
Crus_1_ansiform_lobule	1.1974725	1.1799385	1.1699101	1.19348708	1.17062779	1.16075125	1.17994694	1.17905268	1.17196635	1.18298935	1.18802869	1.14924104	1.17662354	1.33777427	1.16340376	1.18295738	1.16262871	1.19320031	1.17885899
Crus_2_ansiform_lobule	0.70399036	0.68949323	0.68730587	0.70436227	0.68515903	0.67480927	0.69550164	0.69413555	0.68703361	0.69157295	0.69793231	0.66325	0.68542294	0.80579224	0.68249735	0.68457043	0.67318787	0.69309582	0.68993323
dentate_gyrus	1.1437215	1.1409258	1.1458458	1.15305261	1.14935075	1.13849112	1.13797276	1.14344553	1.15326816	1.14924886	1.14260426	1.14857681	1.14812453	1.10730164	1.1525531	1.13074581	1.14524844	1.14093894	1.15467945
Dentate_nucleus	0.06198661	0.06005503	0.06026896	0.06168468	0.05849388	0.05727713	0.05845518	0.0598516	0.05760167	0.06157304	0.06064693	0.05937721	0.05768702	0.06661182	0.06059706	0.05977869	0.0581558	0.05809883	0.0586116
Dorsal_Peduncular_Cortex	0.10735534	0.10681916	0.10642541	0.10536028	0.10776124	0.10624469	0.10548814	0.1063122	0.10772026	0.10856397	0.10566367	0.10592617	0.10582374	0.10256732	0.10677544	0.10628118	0.10623442	0.10597791	0.10600317
Dorsal_Tenia_Tecta	0.07464125	0.0747917	0.07406084	0.07459962	0.07435362	0.07422607	0.07354322	0.07378568	0.07374546	0.07549849	0.07388695	0.07493263	0.07430181	0.07272571	0.07544632	0.07417904	0.07403841	0.07398401	0.07485985
Endopiriform_Nucleus	0.60643852	0.62174998	0.61802857	0.61042787	0.62546521	0.63051175	0.62909864	0.61395097	0.63223298	0.61324306	0.61062173	0.61590891	0.63401293	0.58224455	0.61648818	0.61417361	0.62799902	0.63087837	0.630491
entopeduncular_nucleus	0.01576027	0.01571598	0.01512921	0.01514337	0.01527233	0.01590714	0.01630539	0.01540395	0.01639895	0.01579535	0.01500856	0.01512693	0.0156741	0.01472742	0.01537103	0.01560202	0.01597118	0.01500524	0.01591665
external_medullary_lamina	0.04553082	0.04540158	0.04545459	0.04554794	0.04674295	0.04495593	0.04559389	0.04577717	0.04661271	0.0450229	0.04478192	0.04478908	0.04660589	0.04356784	0.04487685	0.04613577	0.04518713	0.04768449	0.04618755
Fasciculus_retroflexus	0.0152979	0.01602643	0.01578346	0.01573037	0.01590364	0.0167201	0.01714843	0.01564078	0.01708521	0.01557494	0.01559021	0.01553761	0.01712461	0.01521032	0.01565724	0.01569245	0.0165638	0.01602412	0.01678907
fastigial_nucleus	0.07239786	0.07278068	0.07218483	0.0726859	0.07115167	0.07169325	0.07209405	0.07055197	0.07108219	0.07316592	0.07272236	0.07049145	0.07272239	0.07969293	0.07206989	0.07133988	0.07104096	0.07151008	0.07289007
Fimbria	0.32651168	0.32970924	0.33244672	0.33066761	0.3295458	0.33287603	0.33103829	0.32876609	0.33282304	0.33007014	0.32831104	0.32949106	0.33146492	0.31509147	0.33179341	0.3228658	0.33107735	0.32483519	0.33367242
flocculus	0.74895897	0.74493048	0.7380577	0.75116286	0.7254037	0.72871171	0.74204681	0.73536502	0.72895139	0.74637888	0.74080994	0.72642088	0.73745279	0.78871433	0.73835414	0.74082583	0.73363494	0.73849447	0.74384596
Fornix	0.03903886	0.03943486	0.04192607	0.04020759	0.04018729	0.03996894	0.03960448	0.0395839	0.04071152	0.03955049	0.04047929	0.04020519	0.04059836	0.03775901	0.04035468	0.0388601	0.03992276	0.03972688	0.04012878
Fourth_ventricle	0.20408421	0.19835297	0.19902249	0.20292712	0.1962724	0.19361661	0.19437217	0.20054107	0.19461521	0.20178243	0.20193461	0.19607858	0.19394886	0.22201145	0.19885682	0.1980554	0.19500691	0.19775633	0.1968893
Frontal_Association_Cortex	8.02345904	7.95657456	8.02696376	7.91264293	7.89516956	8.01821003	7.86804123	7.8178539	8.11659623	7.89366415	7.87030964	7.79657224	8.10646567	8.0987176	7.9148439	7.90992712	7.94273737	7.84605173	8.01263259
Globus_pallidus	0.31160999	0.31140488	0.31305946	0.31071205	0.31348704	0.31238238	0.30971176	0.31159635	0.31491037	0.31075255	0.30776199	0.30900094	0.30980607	0.29659118	0.31126575	0.30730366	0.31108767	0.31125556	0.31285041
hindbrain_medulla_pons	6.6954492	6.61357329	6.55207025	6.70033492	6.5185454	6.46357851	6.61432306	6.59147229	6.55339413	6.62330864	6.61153051	6.41667844	6.57469564	7.2679547	6.54664099	6.58167518	6.48437472	6.61978194	6.59867569
Hippocampal_layer_CA1	1.43432418	1.43743768	1.43342339	1.44405192	1.44673938	1.43829245	1.44101283	1.43940189	1.45632131	1.44237215	1.43196284	1.44079602	1.45049411	1.38770378	1.44434782	1.42877796	1.44342063	1.44602339	1.45605079
Hippocampal_layer_CA2	0.15407755	0.15732125	0.1561009	0.156235	0.15904129	0.15945985	0.1608022	0.15696466	0.16232123	0.15578577	0.15487943	0.15642489	0.16282111	0.14925284	0.15629726	0.15679579	0.15956247	0.16150107	0.16120804
Hippocampal_layer_CA3	1.43346274	1.42816562	1.43764952	1.44283174	1.44632523	1.4298244	1.42394738	1.43960291	1.44562439	1.43956262	1.43220185	1.43905868	1.43694637	1.38350824	1.44520311	1.41995376	1.43321162	1.43305734	1.44819168
hypothalamus	1.91118787	1.92352924	1.94143977	1.92730126	1.94417996	1.93642163	1.92530371	1.92976776	1.95240566	1.92486051	1.91871691	1.92753465	1.94164336	1.83799208	1.93609439	1.90149992	1.93505286	1.93143004	1.95042407
Inferior_Colliculus	1.0865158	1.07943003	1.07327728	1.09519253	1.05814983	1.05337906	1.07052967	1.06974645	1.05853458	1.08418936	1.07393292	1.06139932	1.06500951	1.1033704	1.07991663	1.06570883	1.06404154	1.06596098	1.07371058
Infralimbic_Cortex	0.10337123	0.10489463	0.10735427	0.10511436	0.10563422	0.10563706	0.10308574	0.10307646	0.10350708	0.10622935	0.10663967	0.10724266	0.10449352	0.10176809	0.10734617	0.10256647	0.10484866	0.10160259	0.10550069
Insular_Cortex	1.67060051	1.6841897	1.69300436	1.67624082	1.69719523	1.68823233	1.66929615	1.67749201	1.69194486	1.68055949	1.67051999	1.67816786	1.68413599	1.60438581	1.68731627	1.66054673	1.67987006	1.69136711	1.68819082
Internal_capsule	0.54214835	0.54868228	0.54966685	0.5456794	0.55551681	0.55317029	0.55391576	0.55009032	0.55958261	0.54600054	0.54195562	0.54402243	0.55844109	0.51995987	0.54639041	0.5448353	0.55204728	0.55690533	0.55721025
interposed_nucleus	0.09035846	0.08866155	0.08864794	0.08976492	0.08909535	0.08515808	0.08670578	0.08796302	0.08642566	0.0898164	0.08952962	0.08698933	0.08732566	0.09849592	0.08887393	0.08997454	0.08693337	0.09037042	0.08856665
intrabulbar_part_of_anterior_commisure	0.18485051	0.18254811	0.18564209	0.18406759	0.18320717	0.18433747	0.18355102	0.18130253	0.19457587	0.18055661	0.181377	0.17576643	0.19141172	0.19393866	0.18133317	0.18252567	0.18500482	0.18525288	0.18596251
Lateral_olfactory_tract	0.16622913	0.16848079	0.16579382	0.16453018	0.16774224	0.16966381	0.16700655	0.16426017	0.16785653	0.16550123	0.16443452	0.16623618	0.16996891	0.16299876	0.16735049	0.16740433	0.16769179	0.16941778	0.16947171
lateral_septum	0.67154179	0.67622981	0.67610413	0.6694886	0.67964346	0.67732442	0.67052723	0.67448751	0.67944659	0.67318341	0.66581744	0.67107225	0.66873113	0.63986379	0.67453979	0.66822623	0.67446214	0.67397869	0.67430133
Lateral_ventricle	0.94927105	0.95878721	0.95808787	0.95218026	0.97444472	0.96579715	0.95806613	0.95953565	0.9716083	0.95146659	0.94994616	0.95737282	0.97177244	0.91058918	0.95921573	0.95465054	0.96573503	0.97835059	0.97157391
mamillary_bodies	0.11106343	0.11312358	0.11172957	0.11193891	0.11406022	0.11529016	0.11698928	0.11222795	0.11796647	0.1116505	0.11057054	0.11102808	0.117954	0.10728702	0.11163078	0.11304224	0.11488482	0.11581151	0.11748776
mammilothalamic_tract	0.02440951	0.02436526	0.02485181	0.02474218	0.02409158	0.02464252	0.02430638	0.02467798	0.02463196	0.02451606	0.02453548	0.0248158	0.02431847	0.0236039	0.02490284	0.02405128	0.02446179	0.02343549	0.02468956
medial_septum	0.09102984	0.09241754	0.09399366	0.09216149	0.09271757	0.09277102	0.09170851	0.0921295	0.09289879	0.09287276	0.09235745	0.09295604	0.09195174	0.08695185	0.0927412	0.09056295	0.09233586	0.0904705	0.09253978
median_preoptic_area	0.00325797	0.00349632	0.00366183	0.00353077	0.00356183	0.0036348	0.00340669	0.00337657	0.00330613	0.00343764	0.00364972	0.00373	0.00359113	0.0033446	0.00365262	0.00336788	0.00344501	0.0034087	0.00358966
midbrain	2.38280325	2.36820775	2.3669837	2.39511644	2.37324599	2.34599342	2.35104979	2.37544932	2.36819354	2.38613934	2.37469937	2.38015633	2.36437635	2.32876804	2.38993833	2.34975857	2.36396766	2.3756806	2.37809988
Navicular_nuclear_basin_forebrain	0.12046673	0.12127375	0.12234368	0.12117735	0.12197004	0.12136107	0.12096228	0.11966514	0.12258026	0.12235211	0.12159981	0.12181686	0.12286696	0.11735934	0.12274785	0.1192028	0.1220652	0.12169464	0.12222326
Nucleus_accumbens	0.4895039	0.49506895	0.49225578	0.48637801	0.49333361	0.49503339	0.49553139	0.48965616	0.49997512	0.49451954	0.48667184	0.49037478	0.49684351	0.46865177	0.49093289	0.49118802	0.49258392	0.49491897	0.49308412
Occipital_Cortex	0.94752332	0.93949438	0.93384188	0.95340628	0.92156682	0.9144757	0.92719971	0.93612909	0.91653496	0.94078944	0.93469649	0.92253496	0.92294306	0.97084585	0.93522478	0.93105688	0.9288685	0.93235484	0.93414162
Olfactory_Bulb	9.29519663	9.34870908	9.44210375	9.16845758	9.42908107	9.72211169	9.57866658	9.68115149	8.9609244	9.35746767	9.83333944	10.2238024	9.12210081	9.3061139	9.44173218	10.0546498	9.68599575	9.21264206	8.9190339
Olfactory_tubercle	0.82708755	0.84265621	0.838903	0.82760426	0.84030699	0.84516394	0.84467335	0.8289105	0.84942886	0.83952844	0.83008839	0.8344013	0.84753303	0.79828156	0.83756679	0.82998603	0.8434991	0.83821779	0.84336682
Optic_Chiasm	0.01761557	0.01785764	0.01854831	0.01826613	0.01785775	0.01823831	0.0172572	0.01778705	0.01717577	0.01788397	0.01832656	0.01869707	0.01748059	0.01725421	0.01868248	0.01712311	0.01810731	0.0172433	0.01802482
Optic_tract	0.20327954	0.20440925	0.20661008	0.20676118	0.20692179	0.20636464	0.2041717	0.20460656	0.20715036	0.20389762	0.20560182	0.20651638	0.20851786	0.19692606	0.20703646	0.20106315	0.2064634	0.20641505	0.20893639
Orbitofrontal_Cortex	0.03076602	0.03133834	0.03077331	0.03034337	0.03213539	0.0316377	0.0313657	0.03079767	0.03186841	0.03065377	0.03036403	0.03092888	0.03268399	0.0296658	0.03093264	0.03169866	0.0317823	0.03293322	0.03205068
paraflocculus	0.8610432	0.84718269	0.83790558	0.85429244	0.82870997	0.82802887	0.83791431	0.84189631	0.83044143	0.85397955	0.84880299	0.82673104	0.83049508	0.93825925	0.83941036	0.84628796	0.82899964	0.83897718	0.83848492
paramedian_lobe	0.56691478	0.55672193	0.54828232	0.56325169	0.54474303	0.54068178	0.55595925	0.55069679	0.54767412	0.55784768	0.55612356	0.53382838	0.5481103	0.64139699	0.54830089	0.5508524	0.53825307	0.54896663	0.54928443
Parietal_Association_Cortex	0.75744878	0.75591955	0.76202213	0.76174778	0.76609348	0.75825205	0.75374437	0.76238939	0.76685757	0.76012627	0.75663234	0.75981564	0.76090072	0.73020792	0.76353772	0.74932708	0.76001711	0.75826664	0.7672552
Periaqueductal_grey	0.72403618	0.70981821	0.70503212	0.72000115	0.70467838	0.70106473	0.69951641	0.71612271	0.70249366	0.71931196	0.71045436	0.71181153	0.6925377	0.7093849	0.71741999	0.70323589	0.70412786	0.70019292	0.70555656
Piriform_Cortex	1.87393873	1.90369494	1.89974543	1.88349299	1.90760651	1.91817797	1.9091654	1.8902003	1.92644573	1.89265079	1.87743846	1.8912758	1.91791044	1.80014046	1.89895497	1.87752731	1.91177454	1.90292453	1.9191437
pons	1.55355508	1.54128292	1.53002657	1.55268974	1.52931617	1.51463587	1.5281979	1.53888204	1.5225268	1.54456006	1.53866022	1.53292011	1.52204357	1.54034059	1.54745467	1.52625431	1.52924247	1.54214125	1.5351488
posterior_commisure	0.0156457	0.01487224	0.01444817	0.01501397	0.014415	0.01434059	0.01425662	0.0150054	0.01430267	0.01534897	0.01470921	0.01494561	0.01384797	0.01469733	0.01508236	0.01466819	0.01446265	0.0138225	0.01400167
Posterior_part_of_anterior_commissure	0.02239234	0.02241492	0.02199568	0.02203602	0.02233093	0.02233182	0.02177715	0.02248384	0.02191261	0.02235887	0.02192054	0.02235486	0.02139396	0.02120024	0.02246162	0.02215729	0.02219512	0.02215451	0.02207103
Prelimbic_Cortex	0.27521305	0.27768726	0.27722861	0.27173901	0.27702731	0.28049307	0.28057253	0.27310671	0.28267424	0.27690094	0.2727647	0.27459778	0.28260173	0.26757614	0.27521938	0.27582264	0.2786491	0.27689275	0.27905644
Primary_Motor_Cortex	1.3541284	1.36304839	1.37060996	1.35243818	1.36558276	1.36499715	1.35220838	1.34911127	1.36669458	1.36681043	1.35114282	1.36007939	1.36039585	1.31090003	1.36623384	1.34554983	1.35858144	1.35056162	1.36196315
Primary_Somatosensory_Cortex	5.59780982	5.6662066	5.67804697	5.62303311	5.69867142	5.69688646	5.65296116	5.63364458	5.71384726	5.64285738	5.60811717	5.64212563	5.69331886	5.38014362	5.66722799	5.59311249	5.67151113	5.68446774	5.7011183
Primary_Visual_Cortex	1.80847859	1.80175463	1.79169451	1.81698075	1.79705718	1.78120983	1.7972829	1.80282163	1.80028553	1.80867858	1.79525977	1.79645029	1.79731556	1.78200814	1.80916164	1.79107114	1.79452894	1.80787805	1.8062232
Retrosplenial_Cortex	2.170309	2.16542962	2.15372334	2.17524217	2.17181353	2.14982838	2.16404703	2.17020097	2.17577302	2.16949329	2.15107004	2.15807622	2.16826413	2.11997888	2.16908656	2.15716426	2.16432467	2.18375129	2.17763109
rhinal_cortex	3.27809965	3.26505401	3.25558679	3.2921358	3.26509206	3.23736162	3.25800434	3.26726613	3.26994115	3.28085774	3.25916209	3.26476109	3.26261223	3.21633762	3.28387003	3.24131826	3.25900101	3.27451437	3.27830989
Secondary_Motor_Cortex	0.82339711	0.82730652	0.83279607	0.81611865	0.83812345	0.83558299	0.83063817	0.82499278	0.84879076	0.82450362	0.81796688	0.81992731	0.84241975	0.7916184	0.82235377	0.82368125	0.83247357	0.84236648	0.83551669
Secondary_Somatosensory_Cortex	1.49008034	1.49977287	1.50944228	1.49900135	1.51186835	1.50561674	1.48730099	1.50171702	1.50945499	1.49573444	1.48861996	1.49785343	1.49904713	1.42988485	1.50587173	1.481728	1.49745535	1.5040241	1.50855144
Secondary_Visual_Cortex	2.17717506	2.16592923	2.15995784	2.1859565	2.17531813	2.14769276	2.15636361	2.17425969	2.16979366	2.17663037	2.16368178	2.17026054	2.16688375	2.13632363	2.17963099	2.15572827	2.16500617	2.18273366	2.1799757
Simple_Lobule	1.17999897	1.1670708	1.15907382	1.17804514	1.13828474	1.14137249	1.15711145	1.15355011	1.14254039	1.1724583	1.16933582	1.13641473	1.15116374	1.27847716	1.15745496	1.15881681	1.13983959	1.15530023	1.1587713
stria_medullaris_thalamus	0.04359326	0.04323153	0.04477249	0.04426785	0.04403073	0.04303479	0.04281613	0.04315504	0.04426038	0.04319776	0.04396488	0.04260377	0.04389668	0.04192741	0.04344756	0.04202503	0.04315268	0.04387998	0.04403622
Stria_terminalis	0.17385672	0.17683179	0.17684968	0.17595741	0.17582148	0.17879459	0.17882637	0.17507151	0.17984226	0.17613951	0.1756698	0.17539752	0.17884105	0.16786851	0.17701282	0.17225243	0.17746807	0.17388795	0.17919021
Subfornical_organ	0.00550441	0.00551283	0.00535015	0.00547626	0.0053499	0.00524164	0.00535673	0.00557095	0.00536845	0.00551847	0.00531422	0.00525243	0.00522757	0.00521525	0.00540279	0.00520762	0.00538657	0.00509789	0.00526382
subicular_region	1.76956582	1.75685967	1.75298919	1.77850661	1.76405394	1.74306138	1.75337448	1.76418179	1.76091316	1.76775543	1.7586345	1.76229532	1.75486621	1.73857162	1.76954231	1.75139973	1.75793247	1.77421111	1.7687619
substantia_nigra	0.16482833	0.16015646	0.16071672	0.1637561	0.16147961	0.15662722	0.15681336	0.16147951	0.15975074	0.1643671	0.16060754	0.16229195	0.15529989	0.1579847	0.16273229	0.1600153	0.15890798	0.15744876	0.15878214
Superior_Colliculus	1.12521576	1.12339276	1.11681633	1.1302241	1.12774087	1.10952784	1.12174132	1.12238068	1.12438503	1.1250723	1.11841014	1.11994445	1.12531186	1.10601169	1.12489957	1.12004628	1.1201971	1.14005672	1.12865115
Temporal_Association	0.78716768	0.77903362	0.78416459	0.79376102	0.78480475	0.76927612	0.77171474	0.78489598	0.77633278	0.78628545	0.78456871	0.78408557	0.77553986	0.77875041	0.78813493	0.7761222	0.77745987	0.78677577	0.7832429
Thalamus	3.35545752	3.3744396	3.39065946	3.37886494	3.41536406	3.39537607	3.38895673	3.38592103	3.44040786	3.37562104	3.35529966	3.37434895	3.41913265	3.2318614	3.38669043	3.35187197	3.39725705	3.40363471	3.43019653
Third_ventricle	0.31368198	0.31704529	0.31547562	0.31388049	0.32062766	0.32087383	0.32237928	0.31638075	0.32409847	0.31545094	0.31111795	0.31410292	0.32225729	0.29929842	0.31424691	0.31632414	0.32098647	0.31891026	0.32215765
trochlear_nerve	0.00580482	0.00571232	0.00592682	0.00609868	0.00564077	0.00533337	0.00568025	0.00553813	0.00548257	0.0057682	0.0057611	0.00567381	0.00582491	0.00574731	0.00577599	0.00565446	0.00554036	0.00567336	0.00559814
ventral_pallidum	0.17474251	0.17799659	0.17738621	0.17647383	0.17608876	0.17921649	0.1783418	0.17592122	0.17866195	0.17777188	0.17530613	0.17583221	0.17642413	0.16831537	0.17713436	0.17381718	0.17748023	0.17489798	0.1771592

	38	40	43	45	53	56	87	88	90	91	103	21	30	31	42	46	49	52	93
	Het	Het	Het	Het	Het	Het	Het	Het	Het	Het	Het	Het	Het	Het	Het	Het	Het	Het	Het
Relative Volumes	F	F	F	F	F	F	F	F	F	F	F	M	M	M	M	M	M	M	M
	Pat	Pat	Pat	Pat	Pat	Pat	Pat	Pat	Pat	Pat	Pat	Pat	Pat	Pat	Pat	Pat	Pat	Pat	Pat
amygdaloid_area	2.08055667	2.07431149	2.10343199	2.11600505	2.10506732	1.99860583	2.10509061	2.09905614	2.10639314	2.07728325	2.09778794	2.09982208	2.08267196	2.1111395	2.08547693	2.07064694	2.11315884	2.10357422	2.07987888
Anterior_part_of_anterior_commissure	0.09349475	0.09332782	0.09388306	0.09198115	0.09540931	0.09203763	0.09481314	0.09389648	0.09476378	0.09188167	0.09527322	0.09448743	0.09307933	0.09431221	0.0950956	0.09182768	0.09546589	0.09427228	0.09236382
Aqueduct	0.11684593	0.11280877	0.11980882	0.11754036	0.11386589	0.10934438	0.11667309	0.11473611	0.11631245	0.11738189	0.11256294	0.11355035	0.1148426	0.11333545	0.11381776	0.11831873	0.11231914	0.1126579	0.11453765
auditory_cortex	1.4685391	1.43737899	1.48358725	1.47447323	1.45723147	1.37935323	1.46748485	1.46132141	1.47128455	1.46314715	1.45961882	1.47181767	1.46418943	1.47308564	1.45357035	1.45980232	1.45996837	1.4507919	1.45757048
basal_forebrain	1.20438943	1.1788676	1.22255406	1.21026576	1.19750916	1.14353165	1.20417076	1.19719478	1.20762605	1.19794095	1.1887933	1.20191921	1.2014589	1.21841761	1.19776954	1.21111359	1.20447779	1.19933364	1.17607566
Bed_nucleus_of_stria_terminalis	0.21219076	0.20352449	0.19521941	0.20382739	0.2079987	0.19674006	0.20241148	0.20458581	0.20893338	0.19590503	0.20906887	0.21625949	0.20469732	0.24525277	0.20826057	0.20522818	0.2100836	0.2086901	0.19860309
caudaputamen	3.23742167	3.18591759	3.28340103	3.26280142	3.24272636	3.10258614	3.24751658	3.23072189	3.25489683	3.23456358	3.21975014	3.25051216	3.24199351	3.29629069	3.2320531	3.26490833	3.25953183	3.24488257	3.17713942
cerebellar_lobule_1_2	0.56492669	0.55990739	0.5603331	0.5604379	0.57381139	0.56698262	0.56341806	0.56271618	0.56600463	0.56396527	0.56725586	0.56367277	0.55763569	0.5650868	0.56183199	0.55993658	0.56680344	0.56510244	0.57106548
cerebellar_lobule_10	0.2348999	0.23136448	0.23609983	0.23566589	0.24124834	0.25952795	0.2393877	0.23797718	0.23782237	0.23662688	0.2387311	0.23749112	0.23897624	0.23065921	0.23653005	0.2300464	0.2409225	0.23781482	0.24378137
cerebellar_lobule_3	0.48113661	0.48417362	0.47555433	0.47944407	0.5023989	0.50873585	0.48720301	0.48497144	0.48466837	0.48729381	0.49165176	0.48762838	0.48485155	0.47603208	0.48703401	0.47468639	0.49528744	0.49284743	0.49751653
cerebellar_lobule_4_5	1.51363061	1.4739968	1.51940436	1.50313093	1.52937356	1.58117921	1.51690145	1.51447401	1.51949472	1.52127625	1.51407126	1.51728501	1.50555992	1.49520003	1.50490625	1.4947918	1.51397714	1.50740019	1.52638143
cerebellar_lobule_6	0.60793849	0.58226845	0.59869698	0.5974041	0.60690874	0.67474878	0.60281671	0.61201858	0.60555301	0.60268261	0.60778985	0.6041565	0.60399845	0.5965146	0.6039694	0.58455308	0.60459314	0.59972012	0.6187522
cerebellar_lobule_7	0.24231519	0.22246136	0.23574528	0.23331109	0.22934339	0.26104692	0.23101292	0.23781452	0.23694535	0.23322583	0.23670785	0.23471535	0.23805477	0.2432378	0.2348437	0.23046828	0.23044444	0.22837422	0.23701293
cerebellar_lobule_8	0.26162456	0.25091775	0.25908402	0.25732924	0.26209285	0.29399266	0.26252811	0.26389019	0.26100297	0.26047304	0.26141447	0.25983721	0.26103908	0.24699373	0.26040903	0.24926094	0.26049204	0.25979644	0.26913689
cerebellar_lobule_9	0.61424709	0.58416541	0.60522854	0.60178021	0.60995251	0.68350901	0.60774946	0.61764294	0.60952816	0.60814557	0.61015813	0.60600943	0.60804797	0.59283613	0.60835813	0.58580352	0.60583033	0.60258286	0.62292534
Cerebellar_White_Matter_Arbor_vita_of_cerebellum	1.8904059	1.85749105	1.87686867	1.88060259	1.92146245	2.03581709	1.89171509	1.90564324	1.89963907	1.88304664	1.90695797	1.89378556	1.88467119	1.87774249	1.89310359	1.85426691	1.90469264	1.89850495	1.935409
cerebral_peduncle	0.20659482	0.20458702	0.20531292	0.2097088	0.20632	0.19423564	0.20432265	0.20509701	0.20737247	0.20264361	0.2066846	0.20797429	0.20672754	0.21708841	0.20457444	0.20642458	0.20697098	0.2052454	0.20386035
Cingulate_Cortex_area_1	1.07965005	1.05810973	1.09837625	1.07904452	1.07500795	1.05802358	1.08092954	1.07951736	1.08612258	1.07598277	1.07336282	1.07785189	1.08613147	1.10386263	1.08009712	1.09056035	1.0790631	1.06842857	1.0535622
Cingulate_Cortex_area_2	0.67551757	0.6519872	0.68579281	0.67129451	0.66124062	0.6387792	0.66995645	0.6652921	0.67325102	0.67157608	0.66112944	0.67211683	0.67329865	0.69167395	0.66864202	0.6803425	0.66642967	0.66181872	0.65136899
cingulum	0.23100505	0.22968033	0.23077126	0.23087114	0.23511442	0.2257869	0.23392371	0.23269661	0.23364977	0.23132086	0.23437436	0.23551401	0.23232905	0.23599452	0.23281051	0.2298393	0.23634443	0.23401584	0.23170035
Cochlear_nucleus	0.07034855	0.0750384	0.06901945	0.07235757	0.07798292	0.07999344	0.07368484	0.07350513	0.07250352	0.07140387	0.074994	0.07255435	0.07260984	0.06874489	0.07356935	0.06975469	0.07635945	0.07636543	0.07713308
Commisure_inferior_Colliculus	0.02469178	0.020616	0.02615343	0.02382616	0.02049573	0.01941477	0.02276325	0.02279267	0.02358493	0.02410151	0.02119889	0.02265747	0.02284109	0.0251628	0.02232796	0.02539753	0.0202679	0.02056507	0.02105829
commisure_superior_collicuus	0.01336765	0.01302191	0.0133334	0.0131436	0.01306778	0.01240658	0.01331233	0.01319436	0.01331181	0.01292323	0.01343013	0.01328732	0.01325895	0.01322923	0.01343538	0.01301951	0.01328814	0.01310703	0.01333703
copula	0.19864784	0.18941288	0.19076762	0.19316651	0.19637268	0.21940638	0.19245147	0.20000287	0.19636074	0.1938588	0.20024007	0.19625795	0.19552722	0.20137104	0.19691015	0.18949637	0.19665687	0.19574508	0.20097141
Corpus_Callosum_associated_White_Matter	2.96606041	2.89896139	2.9823857	2.97574027	2.94244542	2.80806335	2.95169891	2.94319419	2.9684405	2.94953313	2.93702393	2.97012052	2.96026953	3.02793038	2.93842614	2.97227797	2.94941382	2.93588195	2.91035169
Crus_1_ansiform_lobule	1.18059634	1.14746215	1.16229921	1.16653295	1.18494469	1.27549358	1.16728932	1.1880233	1.18305375	1.16702946	1.18967061	1.18134272	1.16866884	1.19457232	1.17519129	1.15305658	1.18112413	1.17485979	1.19680846
Crus_2_ansiform_lobule	0.69276342	0.66987204	0.67302927	0.68144145	0.69584376	0.78392088	0.68121417	0.70181003	0.69059593	0.67522024	0.69738813	0.6835818	0.68452824	0.68832255	0.69148908	0.66304668	0.69030319	0.68588039	0.71036188
dentate_gyrus	1.14087048	1.13239767	1.14951275	1.14683787	1.15117729	1.08910818	1.15170158	1.14836183	1.15063575	1.14576331	1.14667478	1.15103545	1.13845752	1.13550674	1.13818255	1.13296253	1.15127585	1.14437367	1.14960924
Dentate_nucleus	0.05588314	0.05953051	0.05380296	0.05665597	0.06181329	0.06394326	0.05789325	0.05797581	0.05745626	0.05690538	0.05988193	0.0582708	0.05823454	0.05628797	0.05844104	0.05493061	0.0612422	0.06064176	0.0613514
Dorsal_Peduncular_Cortex	0.10332959	0.10591314	0.10150345	0.10500299	0.1086642	0.10705013	0.10522748	0.10560443	0.10437992	0.10500733	0.10624689	0.1062292	0.10640609	0.10594456	0.10616458	0.10493364	0.10901577	0.10780533	0.10532256
Dorsal_Tenia_Tecta	0.07423023	0.07256846	0.0721458	0.07117036	0.07489284	0.07433189	0.07413755	0.07332486	0.07412992	0.07250658	0.07448061	0.07580296	0.07475507	0.07708702	0.07538794	0.0721836	0.07587935	0.07434641	0.07356717
Endopiriform_Nucleus	0.63599185	0.60891932	0.65380183	0.63711219	0.6145323	0.58731595	0.62902134	0.62557496	0.63331056	0.63284927	0.61690443	0.62871645	0.62935465	0.64638607	0.6242698	0.64313283	0.61862983	0.61669902	0.60743071
entopeduncular_nucleus	0.015226	0.01478112	0.01670479	0.01594455	0.01562234	0.01534355	0.01609831	0.01540979	0.01536928	0.01675171	0.01527152	0.01567961	0.01668231	0.01344122	0.01551408	0.01529743	0.01554004	0.01550842	0.01605981
external_medullary_lamina	0.04714894	0.0462997	0.04563128	0.04739047	0.04547936	0.04338956	0.04507566	0.04549989	0.04651468	0.04409757	0.04599984	0.04654007	0.04620809	0.0519072	0.04570306	0.04704819	0.04594555	0.04540216	0.04506304
Fasciculus_retroflexus	0.01731104	0.01541995	0.01951376	0.01746995	0.01551556	0.01500314	0.01734096	0.01666022	0.01691647	0.01846837	0.01562507	0.01629476	0.01708898	0.01459081	0.01632908	0.01739285	0.01560659	0.01552073	0.01615168
fastigial_nucleus	0.07163874	0.07014426	0.07421523	0.07287757	0.07200021	0.0753558	0.07362891	0.0725749	0.07266559	0.07279204	0.07104528	0.0712458	0.07145036	0.06708037	0.07112702	0.0710289	0.07113221	0.07196839	0.07365918
Fimbria	0.32672996	0.3255308	0.33881709	0.33400166	0.33116762	0.31503659	0.33519954	0.33119554	0.33196569	0.3335831	0.3289704	0.32761568	0.32990429	0.31571955	0.3294939	0.32595475	0.33155229	0.3307169	0.32976158
flocculus	0.73911876	0.72251505	0.74878446	0.73486777	0.74834446	0.75589014	0.74591564	0.73583016	0.73989654	0.74790344	0.73498509	0.73973708	0.73781988	0.71646215	0.73445175	0.73300713	0.73805051	0.73588161	0.74813522
Fornix	0.03800819	0.0407719	0.03960795	0.04128325	0.04049425	0.03779051	0.03998903	0.04030559	0.04038874	0.03858274	0.03998869	0.03893556	0.03855583	0.0393946	0.03906433	0.04033414	0.04046855	0.0403399	0.03928668
Fourth_ventricle	0.19461386	0.194519	0.18824422	0.19273391	0.20197911	0.21164401	0.19465226	0.1977778	0.19580732	0.19421342	0.20108864	0.19750031	0.19434904	0.1962849	0.19707798	0.18939352	0.20075876	0.20038675	0.20309508
Frontal_Association_Cortex	7.91771217	7.79182302	8.02054605	7.92342316	8.09250284	8.52246453	8.03832179	8.1077388	8.08185987	7.94107055	8.06569954	7.97688835	8.20401833	8.05342984	7.98573128	7.88139542	7.97029543	7.90564067	7.94739498
Globus_pallidus	0.3051135	0.30711631	0.30810093	0.31310096	0.31404191	0.2999643	0.30977766	0.31083801	0.30994024	0.30655642	0.3091602	0.3103847	0.31014887	0.31305804	0.3084765	0.307965	0.31507352	0.31396228	0.3085854
hindbrain_medulla_pons	6.61033509	6.43014553	6.53868323	6.5231241	6.65398021	7.00248966	6.57422768	6.63041434	6.61359	6.5851938	6.61044356	6.57890558	6.56637943	6.53217728	6.58270578	6.43882426	6.58627303	6.56127594	6.69969416
Hippocampal_layer_CA1	1.45421907	1.42409717	1.46619725	1.45273858	1.44589327	1.36466259	1.45445929	1.44683166	1.45824243	1.45385218	1.4450584	1.45849841	1.44511038	1.44857362	1.43490599	1.44423817	1.44507871	1.43745857	1.44465295
Hippocampal_layer_CA2	0.16464206	0.15479363	0.16968513	0.1637721	0.15569025	0.14602694	0.16105542	0.15965054	0.1631532	0.16202965	0.15803484	0.16194674	0.16211089	0.16598765	0.15885681	0.16399505	0.15664586	0.15550337	0.15570078
Hippocampal_layer_CA3	1.43131663	1.42387229	1.43379078	1.44026256	1.44517826	1.37166635	1.44356302	1.43779515	1.44477815	1.42114216	1.44511738	1.44783469	1.42890896	1.44875894	1.42951264	1.41214181	1.45067434	1.4390352	1.43689772
hypothalamus	1.91997001	1.90924401	1.94936547	1.95892714	1.93815604	1.83918883	1.94265833	1.93795215	1.94551426	1.91844958	1.93078713	1.93679012	1.92203895	1.95044025	1.92308915	1.92129966	1.94435823	1.9365989	1.91402864
Inferior_Colliculus	1.06371946	1.06038786	1.06994441	1.06330893	1.08900178	1.06626494	1.0782039	1.06509196	1.06807205	1.08568035	1.06659516	1.06594424	1.06284607	1.03551637	1.06422137	1.05841017	1.07495225	1.07192677	1.08522195
Infralimbic_Cortex	0.10106732	0.10374081	0.10446189	0.10240854	0.10575001	0.10507954	0.10557673	0.10551778	0.10445761	0.10358501	0.10581475	0.10365792	0.10289406	0.09967901	0.1050314	0.10253229	0.10604576	0.10444634	0.10267167
Insular_Cortex	1.66941536	1.67249584	1.67027372	1.68995791	1.69445904	1.62883877	1.68039592	1.6805599	1.68403464	1.65617244	1.67736822	1.68013569	1.66849835	1.71839915	1.67907774	1.67972207	1.70045007	1.69438056	1.65416039
Internal_capsule	0.55679656	0.54477266	0.56467534	0.56564907	0.54971147	0.52068831	0.55393219	0.55277665	0.5582271	0.55268307	0.54999353	0.55433739	0.55463955	0.57144241	0.54961014	0.55779601	0.55231404	0.54966608	0.54376343
interposed_nucleus	0.08675594	0.08732844	0.08330987	0.08663934	0.08950287	0.09309741	0.08490302	0.08766882	0.08791819	0.0838162	0.08946064	0.08744286	0.08680536	0.09455074	0.08732313	0.08625931	0.08891573	0.0885639	0.08934962
intrabulbar_part_of_anterior_commisure	0.18568288	0.18177234	0.1934525	0.19512482	0.18600097	0.20737464	0.18668546	0.19039768	0.19066845	0.18817336	0.18700159	0.18284934	0.19135959	0.18847414	0.18214186	0.19109238	0.18123516	0.18273979	0.18713981
Lateral_olfactory_tract	0.17152675	0.16165072	0.17216944	0.16445127	0.16703468	0.16602584	0.16902861	0.16860117	0.17124936	0.16754555	0.16812104	0.17144972	0.17123903	0.18159275	0.16964372	0.16922604	0.16678507	0.16561899	0.16281392
lateral_septum	0.66152699	0.66582981	0.66148258	0.67259599	0.68155043	0.65214568	0.67120506	0.66840264	0.66913958	0.66408376	0.67153666	0.67551063	0.67046299	0.68200994	0.66913496	0.66939945	0.68408124	0.68039319	0.66276811
Lateral_ventricle	0.97540271	0.94714974	0.97325292	0.97407832	0.96039448	0.90779733	0.96463678	0.96629876	0.9771362	0.95508684	0.96492169	0.97849414	0.95941776	1.02634717	0.96128802	0.97089924	0.96363069	0.96215157	0.94218749
mamillary_bodies	0.11996333	0.11060725	0.125379	0.11962488	0.11164568	0.10617244	0.11748573	0.11543815	0.11755287	0.11964733	0.11275312	0.11585055	0.11831598	0.11620573	0.1150453	0.11915585	0.11246729	0.111513	0.11379005
mammilothalamic_tract	0.02357367	0.02397713	0.02473897	0.02402683	0.02472885	0.02357943	0.02504262	0.02424059	0.0244298	0.02423428	0.02482198	0.02471249	0.02462235	0.02269961	0.02432103	0.02322069	0.02488248	0.02445409	0.02464953
medial_septum	0.08814479	0.09233283	0.09010864	0.09222716	0.09374073	0.08953979	0.09241092	0.09203561	0.09190114	0.09149152	0.0922073	0.09097324	0.09062993	0.08631221	0.09106063	0.09173249	0.09339461	0.0928728	0.09249934
median_preoptic_area	0.00359225	0.00348952	0.00379684	0.00352318	0.00341312	0.00307901	0.00358669	0.00361345	0.00377829	0.00349954	0.00359767	0.00350773	0.00335054	0.00349384	0.00356344	0.0035892	0.00345508	0.00339348	0.00331545
midbrain	2.36907915	2.35451685	2.35988111	2.36165583	2.39131614	2.2677359	2.37252158	2.37235424	2.37865652	2.3738154	2.37854188	2.38552193	2.34962817	2.36583143	2.35390737	2.3523072	2.37970985	2.37525263	2.38384682
Navicular_nuclear_basin_forebrain	0.12051958	0.12007572	0.12114949	0.12137812	0.12118994	0.12039995	0.1213988	0.1212758	0.12164438	0.11892429	0.12017503	0.12117675	0.12097363	0.1242092	0.12181507	0.12200488	0.12300129	0.12190276	0.11959073
Nucleus_accumbens	0.48787745	0.48916865	0.4924433	0.49510925	0.49648616	0.48168921	0.49296279	0.48896479	0.49169787	0.49253428	0.49021761	0.49331027	0.49521322	0.49957484	0.49092452	0.49882882	0.49889241	0.49347531	0.48395724
Occipital_Cortex	0.93055093	0.92506311	0.92296458	0.91946159	0.94496545	0.92969417	0.93260116	0.92465333	0.93047275	0.93769291	0.93342111	0.92950924	0.92135285	0.92261556	0.92742207	0.92118833	0.93414781	0.92947941	0.94312511
Olfactory_Bulb	9.44828097	10.7642613	9.10049014	9.29265907	8.78047689	9.99008724	9.14769765	9.1464548	8.90918547	9.50625342	9.21469575	9.08490634	9.30591774	8.80792377	9.60432124	9.95105145	9.01815888	9.45144865	9.47062426
Olfactory_tubercle	0.83403025	0.82804602	0.85326899	0.84361648	0.83963925	0.81986293	0.8428787	0.83694073	0.83987816	0.84187334	0.83389414	0.83862256	0.84507807	0.8390995	0.83900474	0.85125656	0.84316719	0.83758817	0.82469129
Optic_Chiasm	0.01715088	0.01723478	0.01806117	0.01698581	0.01808138	0.01706412	0.01816356	0.01804665	0.01806871	0.01749429	0.01816909	0.01807773	0.01716577	0.01667863	0.01774299	0.0169753	0.01797652	0.01785025	0.01751341
Optic_tract	0.20893643	0.20324107	0.21242954	0.20812653	0.20492931	0.19390126	0.20810586	0.20799181	0.2094035	0.20593411	0.2058757	0.20713635	0.20429581	0.21050151	0.20614506	0.2061652	0.20507196	0.20449632	0.2037193
Orbitofrontal_Cortex	0.03336297	0.03034178	0.03293347	0.03171469	0.03090463	0.03019087	0.031739	0.03187868	0.03280602	0.03183117	0.03160574	0.03287343	0.03221022	0.03754138	0.03207985	0.03313622	0.03113687	0.03096114	0.03011089
paraflocculus	0.82767807	0.82123806	0.82238717	0.8236738	0.85775507	0.89581624	0.83779715	0.83805404	0.83545156	0.83844833	0.84617314	0.84165787	0.83516685	0.81946165	0.83436965	0.81355902	0.85031655	0.84549225	0.85599825
paramedian_lobe	0.541707	0.53506588	0.53351852	0.54077221	0.55960311	0.61911683	0.54895377	0.5536159	0.54692923	0.5429565	0.55320765	0.54550582	0.54774939	0.53036892	0.54858656	0.52353328	0.55633273	0.55064587	0.5676334
Parietal_Association_Cortex	0.75719357	0.75086363	0.76086168	0.76496036	0.76353525	0.72780446	0.76454101	0.76184211	0.76411834	0.75323628	0.76321364	0.76471285	0.75661033	0.76982828	0.75859127	0.7463129	0.7673929	0.76266493	0.75767699
Periaqueductal_grey	0.69553763	0.70113164	0.68764533	0.69042191	0.72177823	0.69600124	0.70836159	0.70290145	0.70052298	0.71114651	0.71427004	0.71219685	0.70198859	0.67968173	0.70426829	0.68205566	0.71781803	0.71604761	0.72022385
Piriform_Cortex	1.90246372	1.86787505	1.94927171	1.92709286	1.90098946	1.81696539	1.91903538	1.9043614	1.91690488	1.91704461	1.89369588	1.90909827	1.91062852	1.90803793	1.89652575	1.91642619	1.90835948	1.89906904	1.87569832
pons	1.5329654	1.52422482	1.52615279	1.52789416	1.55168856	1.49043752	1.53708034	1.5315624	1.53450288	1.54359839	1.53889368	1.54178535	1.52279878	1.51779076	1.52570786	1.52591789	1.53773938	1.54005138	1.547094
posterior_commisure	0.01329348	0.01451364	0.01255056	0.01332661	0.01542988	0.01491398	0.01424947	0.01411807	0.0139821	0.01440829	0.01483521	0.01472368	0.01410225	0.01313601	0.01402912	0.01295589	0.01519226	0.01491749	0.01505089
Posterior_part_of_anterior_commissure	0.02190701	0.02152242	0.0212679	0.02147416	0.02245207	0.02164124	0.02189844	0.02185623	0.02189629	0.02205083	0.0224651	0.02269049	0.02193199	0.02277867	0.02208445	0.02119964	0.02269917	0.022469	0.02153858
Prelimbic_Cortex	0.27812884	0.27513914	0.28342707	0.27922787	0.27916198	0.27704666	0.27911237	0.27949666	0.2797122	0.28149943	0.27853592	0.27635201	0.28395851	0.2807821	0.27955664	0.2819798	0.27986851	0.27642789	0.27373196
Primary_Motor_Cortex	1.33582098	1.34726411	1.34020485	1.34947859	1.37465888	1.34578695	1.3565171	1.35522459	1.3553585	1.34146341	1.36130613	1.35646863	1.35919633	1.36689053	1.35964635	1.34526315	1.38051475	1.3664395	1.33992723
Primary_Somatosensory_Cortex	5.64723937	5.59318975	5.71653406	5.71046287	5.67761882	5.4392372	5.68124202	5.66391278	5.6927949	5.63509367	5.64498219	5.67548885	5.65505514	5.75899963	5.65178388	5.6869298	5.70099978	5.67263993	5.57194286
Primary_Visual_Cortex	1.80341713	1.78333733	1.8036146	1.79876395	1.81290187	1.73422173	1.80501434	1.7982541	1.80620008	1.81359069	1.80539365	1.8117053	1.79662981	1.79217338	1.7916547	1.79429	1.80427041	1.79970253	1.81042131
Retrosplenial_Cortex	2.17858258	2.14224123	2.17175149	2.1744215	2.17797242	2.07735596	2.16842588	2.16480545	2.17888754	2.17337935	2.17508036	2.1893294	2.16641174	2.21009467	2.16081567	2.16531325	2.17404695	2.16529994	2.16648566
rhinal_cortex	3.2657072	3.23695092	3.27361988	3.26892704	3.29244185	3.14554462	3.28151732	3.26471964	3.27856308	3.28474835	3.27526565	3.28878962	3.25751642	3.24522808	3.2510574	3.24656313	3.27813408	3.26918733	3.28367157
Secondary_Motor_Cortex	0.83364087	0.82814312	0.83581048	0.84490219	0.83484834	0.81210474	0.83093919	0.83613653	0.83611991	0.8280911	0.82976385	0.8316369	0.83446971	0.86941883	0.83112851	0.85084737	0.83783514	0.83378019	0.81722071
Secondary_Somatosensory_Cortex	1.49057197	1.48384821	1.48995272	1.50700812	1.5104571	1.43874206	1.50156768	1.49786325	1.5051542	1.47677198	1.49864233	1.50538954	1.48789932	1.53422815	1.49554485	1.48652532	1.51713809	1.51074552	1.47908103
Secondary_Visual_Cortex	2.1814354	2.1494747	2.16699434	2.16537865	2.18420762	2.0818571	2.17219618	2.17050624	2.18045767	2.17278379	2.1807029	2.19070518	2.16011187	2.19496541	2.16162881	2.15881774	2.17644231	2.17055536	2.17728647
Simple_Lobule	1.14746748	1.13282959	1.15571233	1.14615525	1.17454079	1.22087016	1.16408871	1.15627244	1.15670912	1.15866232	1.15740527	1.15480236	1.15166397	1.11175991	1.14981589	1.13105221	1.16164351	1.16012637	1.17808041
stria_medullaris_thalamus	0.04248809	0.04411484	0.04311925	0.04516113	0.04378933	0.04261391	0.04317694	0.04397341	0.04311872	0.04232735	0.04240155	0.04153594	0.04242284	0.04277551	0.04298478	0.04367874	0.04377869	0.04405548	0.04325309
Stria_terminalis	0.17574546	0.1732808	0.18685559	0.18134704	0.17628652	0.16777264	0.18111111	0.17834413	0.17843693	0.18270469	0.1749171	0.17557455	0.17794448	0.16508883	0.17552923	0.1776051	0.176374	0.17588686	0.1765243
Subfornical_organ	0.00507618	0.00526174	0.00510264	0.00525401	0.00550768	0.00561161	0.00525539	0.00521946	0.00505421	0.00546805	0.00522616	0.00521654	0.00535714	0.00471757	0.0052755	0.00481385	0.00543454	0.00557798	0.00537527
subicular_region	1.76981172	1.74654961	1.76249726	1.75960271	1.77215247	1.69035774	1.7612111	1.7620654	1.7677222	1.76866918	1.76887597	1.77469326	1.75889	1.77204688	1.75874371	1.7574256	1.76522992	1.76242022	1.77172472
substantia_nigra	0.15296941	0.16004411	0.14689487	0.15466784	0.16493593	0.15757766	0.15762174	0.15728218	0.1568203	0.15503335	0.16218744	0.16012326	0.15721589	0.15724867	0.1576262	0.15158915	0.16436193	0.16229516	0.16341635
Superior_Colliculus	1.13311622	1.11694053	1.1249863	1.13131391	1.12691387	1.0710842	1.11947513	1.12190616	1.1299402	1.12213929	1.12653521	1.13262366	1.12267854	1.14805884	1.12017312	1.132877	1.12398276	1.12061745	1.12481905
Temporal_Association	0.77919884	0.77888031	0.76743176	0.77806644	0.78883458	0.75559989	0.77565877	0.78098515	0.78116987	0.77427416	0.78495468	0.782721	0.77024066	0.79098774	0.77827786	0.77534074	0.78424338	0.78324383	0.78525453
Thalamus	3.40336018	3.3470435	3.45068242	3.44688546	3.39313544	3.21620548	3.41651074	3.40491351	3.42542356	3.39271392	3.3949905	3.41584639	3.39722397	3.45291136	3.38205927	3.38894156	3.40576369	3.38817336	3.37003147
Third_ventricle	0.32014632	0.31000284	0.33072077	0.32393862	0.31587776	0.29935014	0.32044528	0.31844414	0.32140762	0.3239994	0.31691243	0.32154721	0.32409775	0.32475613	0.31727733	0.32280152	0.31853239	0.31637822	0.31436361
trochlear_nerve	0.00540246	0.00607378	0.00530091	0.00574805	0.00587887	0.00565013	0.00557089	0.00557759	0.00558664	0.00532834	0.0055687	0.00531383	0.0054258	0.00568598	0.00570947	0.00559257	0.00576947	0.0056693	0.00562844
ventral_pallidum	0.17378198	0.17345393	0.1796393	0.17752193	0.17733924	0.17145064	0.1778952	0.17546835	0.17501662	0.1781704	0.17426603	0.17471132	0.17773616	0.16678462	0.17573662	0.17751404	0.1781585	0.17749223	0.17519963

	96	18	22	27	28	29	32	33	35	36	37	39	44	47	50	51	94	95	98
	Het	WT	WT	WT	WT	WT	WT	WT	WT	WT	WT	WT	WT	WT	WT	WT	WT	WT	WT
Relative Volumes	M	F	F	F	F	F	F	F	F	F	F	F	F	F	F	F	F	F	F
	Pat	Pat	Pat	Pat	Pat	Pat	Pat	Pat	Pat	Pat	Pat	Pat	Pat	Pat	Pat	Pat	Pat	Pat	Pat
amygdaloid_area	2.11347677	2.09442831	2.07649929	2.10053203	2.10231545	2.0993989	2.07903306	2.08326782	2.08344262	2.068213	2.08668737	2.08753794	2.06540237	2.0728428	2.12882303	2.08502006	2.08799721	2.10954875	2.09114841
Anterior_part_of_anterior_commissure	0.09422163	0.09357176	0.09393324	0.09561207	0.09434666	0.09669104	0.09304681	0.09193058	0.09120687	0.09158519	0.09482777	0.09201754	0.09250945	0.09396643	0.09591436	0.09259129	0.09374777	0.09633126	0.09207423
Aqueduct	0.11197589	0.11455977	0.11352324	0.11450763	0.11517951	0.11205256	0.11572142	0.11962557	0.11789054	0.11332895	0.11231214	0.12022079	0.11800651	0.11216032	0.11133827	0.11358696	0.11798012	0.11297553	0.11750621
auditory_cortex	1.46309048	1.45339082	1.44823677	1.45430117	1.46348144	1.45600884	1.4579782	1.46800182	1.46668775	1.45014736	1.44859433	1.461999	1.44639925	1.44189369	1.46269539	1.44912168	1.46099597	1.45588934	1.46485451
basal_forebrain	1.19374314	1.19353351	1.17796881	1.20502454	1.19918389	1.19260957	1.17010603	1.21513046	1.20485901	1.183669	1.18380812	1.21451184	1.19265302	1.17286598	1.20518596	1.17353792	1.21049285	1.19682236	1.19616075
Bed_nucleus_of_stria_terminalis	0.20785365	0.2051695	0.20831816	0.20815404	0.2085469	0.20206972	0.20001467	0.20132231	0.20450266	0.20918282	0.20203024	0.20294131	0.20363861	0.20202827	0.20791666	0.20153085	0.20246833	0.20360927	0.20216456
caudaputamen	3.23003288	3.23102602	3.19732478	3.25819867	3.24109824	3.21628931	3.1685098	3.26815586	3.24733053	3.19851383	3.19388326	3.27339913	3.21668449	3.18173322	3.2655487	3.1756691	3.25303176	3.23493602	3.2254394
cerebellar_lobule_1_2	0.56082454	0.57049996	0.58230657	0.5735388	0.56831947	0.56068251	0.57995821	0.55710288	0.56638522	0.56044639	0.56766495	0.56180867	0.57208937	0.57559745	0.55990033	0.5729026	0.56487115	0.56316064	0.5576189
cerebellar_lobule_10	0.23724248	0.23989885	0.24657279	0.24246263	0.2398886	0.23134848	0.2408246	0.23200238	0.23830016	0.23805569	0.23837744	0.23701399	0.23661247	0.24763832	0.23608132	0.24591135	0.23700018	0.23644128	0.24049657
cerebellar_lobule_3	0.49045737	0.49544382	0.50989239	0.50010078	0.49025658	0.48246971	0.49858831	0.47139426	0.48381262	0.48658109	0.49423667	0.48079247	0.4903056	0.50595128	0.48968717	0.50245601	0.48214088	0.48833059	0.48365973
cerebellar_lobule_4_5	1.49701508	1.51395713	1.54918395	1.52945624	1.51648462	1.48304995	1.51518758	1.49584831	1.52808737	1.50668721	1.50398154	1.50607351	1.51959469	1.54235783	1.49115615	1.54067156	1.51127305	1.4989194	1.51153735
cerebellar_lobule_6	0.59424173	0.60510476	0.62881062	0.610313	0.60786535	0.58941314	0.6073846	0.59138774	0.60392852	0.60994434	0.60620082	0.5997462	0.60370469	0.62837452	0.59165378	0.6237774	0.59490146	0.59557833	0.60143188
cerebellar_lobule_7	0.22597047	0.23244442	0.24325996	0.23308863	0.23728795	0.22545058	0.23571467	0.23335554	0.23765044	0.24106069	0.23347317	0.23485519	0.23564301	0.24201753	0.22348084	0.23758273	0.23075063	0.22568776	0.23394864
cerebellar_lobule_8	0.25647186	0.26053339	0.27219378	0.26442866	0.26112341	0.25574756	0.26536285	0.25426585	0.2591261	0.26225691	0.2639055	0.2584358	0.25896033	0.27356952	0.25506943	0.27079567	0.25498001	0.25754394	0.25798799
cerebellar_lobule_9	0.59627593	0.60846632	0.63281468	0.6127842	0.6103953	0.59388433	0.61010153	0.59700191	0.60767957	0.61409576	0.6116389	0.60452702	0.60747148	0.63288329	0.59209889	0.62803125	0.59594533	0.59850515	0.60214171
Cerebellar_White_Matter_Arbor_vita_of_cerebellum	1.87994508	1.91035467	1.96137931	1.92605437	1.91609899	1.87301644	1.93386493	1.8601743	1.89808557	1.89072124	1.90731407	1.88718061	1.89943098	1.95982171	1.87040213	1.95226759	1.88168227	1.8922527	1.88566511
cerebral_peduncle	0.20746641	0.20710527	0.20685447	0.20478052	0.20794797	0.20280302	0.20408024	0.20719587	0.20707359	0.20638933	0.20327801	0.20799281	0.20380905	0.2024898	0.20676351	0.20446044	0.20424737	0.20423783	0.20730976
Cingulate_Cortex_area_1	1.06015627	1.06553679	1.05277969	1.07664807	1.0813094	1.06818179	1.05684442	1.09720119	1.09033797	1.05929977	1.06009264	1.09745526	1.06926133	1.05284349	1.08438032	1.05246887	1.08298342	1.07762606	1.06727567
Cingulate_Cortex_area_2	0.65829795	0.66057151	0.65310396	0.66796546	0.66738794	0.65599577	0.64972353	0.68280294	0.6750724	0.66333363	0.65291839	0.68056158	0.66500024	0.64663598	0.66652641	0.64716088	0.67392518	0.66015127	0.66538902
cingulum	0.23555107	0.23310832	0.23316032	0.234941	0.23383014	0.23249987	0.23302929	0.2284845	0.23027054	0.23051608	0.2322022	0.23042329	0.22952518	0.23180409	0.23707968	0.23197147	0.23167807	0.23455607	0.23107617
Cochlear_nucleus	0.07578666	0.07654022	0.07855271	0.07693979	0.07508311	0.07495581	0.07736596	0.0696315	0.07087191	0.07270189	0.07674622	0.07260439	0.07319327	0.07880218	0.07579496	0.07833906	0.07155904	0.07633672	0.07240935
Commisure_inferior_Colliculus	0.02031603	0.0214269	0.02068173	0.02111078	0.02236055	0.0209932	0.02165141	0.02594607	0.02476621	0.02269625	0.020413	0.02463943	0.02394507	0.02000197	0.01997346	0.02043025	0.02453052	0.02080422	0.0235931
commisure_superior_collicuus	0.01320891	0.01296352	0.01294291	0.01313265	0.01321205	0.01345033	0.01290939	0.01305243	0.01297316	0.01305361	0.01304308	0.01302394	0.01306038	0.01295425	0.01318985	0.01326517	0.01320533	0.0132937	0.01299026
copula	0.19287518	0.1975565	0.2057847	0.19695097	0.19847175	0.19353061	0.19964483	0.18996276	0.19554388	0.19941325	0.19843432	0.19184776	0.1958254	0.20428841	0.19171766	0.20311961	0.19000265	0.19366949	0.19262395
Corpus_Callosum_associated_White_Matter	2.93514312	2.93463772	2.91821908	2.94314562	2.95640522	2.91255844	2.91226104	2.9774728	2.96799432	2.93378813	2.90234318	2.98587952	2.93716767	2.90044724	2.95095197	2.90220501	2.9553493	2.92989183	2.95176423
Crus_1_ansiform_lobule	1.16411517	1.18142996	1.21993967	1.18917068	1.18915419	1.16016217	1.19487663	1.15302424	1.18126589	1.17952597	1.18024699	1.16556825	1.1775348	1.21491293	1.15686176	1.21032845	1.16519984	1.17167591	1.16954932
Crus_2_ansiform_lobule	0.67777444	0.69637872	0.72151654	0.69732226	0.69998186	0.68153949	0.70042431	0.67435774	0.68280592	0.6935752	0.69838902	0.68913497	0.68861752	0.72115049	0.67477748	0.71861049	0.67338139	0.68782579	0.68082327
dentate_gyrus	1.15529799	1.14568188	1.14238069	1.14619792	1.14731884	1.153331	1.16563597	1.13980546	1.14020452	1.12905989	1.14625811	1.13864317	1.13331098	1.14508425	1.15276228	1.14726318	1.13874261	1.15212778	1.14167362
Dentate_nucleus	0.06036783	0.0605326	0.06295955	0.06103703	0.05966663	0.05856155	0.06154806	0.05412664	0.05630781	0.05844003	0.060748	0.05688319	0.05800772	0.06302546	0.06031729	0.06228093	0.05628847	0.06002059	0.0576176
Dorsal_Peduncular_Cortex	0.10724156	0.10753033	0.10721681	0.10744182	0.1061949	0.10560924	0.10548292	0.10444771	0.10441294	0.10543339	0.1063994	0.10644855	0.10450491	0.10657377	0.109172	0.10584337	0.1024808	0.1065571	0.10317216
Dorsal_Tenia_Tecta	0.07464594	0.07374725	0.07496191	0.07563698	0.0739395	0.07332389	0.07373054	0.07166289	0.07216344	0.07420209	0.07410765	0.07244936	0.07227667	0.07350484	0.07581225	0.07328184	0.07297951	0.0740911	0.07261711
Endopiriform_Nucleus	0.61427264	0.61619333	0.60523204	0.62143526	0.62470025	0.61557561	0.60391068	0.64774071	0.63905919	0.6193726	0.606901	0.64260801	0.62558866	0.60066018	0.62035877	0.60259299	0.63767461	0.61681388	0.62796251
entopeduncular_nucleus	0.01584734	0.01539678	0.01554804	0.01553029	0.01522358	0.01472529	0.01528116	0.01527508	0.01558656	0.01595166	0.01531532	0.01541481	0.01540693	0.01540484	0.01584992	0.01550766	0.01581812	0.01494594	0.01633547
external_medullary_lamina	0.04592954	0.04601866	0.04624615	0.04561028	0.04720654	0.04512847	0.04466635	0.04747239	0.04670455	0.04628618	0.04512909	0.04773536	0.04573873	0.04511904	0.04584691	0.04511745	0.04553397	0.04536338	0.04616155
Fasciculus_retroflexus	0.01566252	0.01570235	0.01538149	0.01584428	0.015916	0.01604198	0.01521747	0.01804652	0.01746371	0.01638092	0.01587509	0.01714019	0.01681794	0.01539544	0.01558274	0.01565926	0.01774768	0.01590162	0.01752016
fastigial_nucleus	0.07087667	0.07167531	0.0725466	0.07252862	0.07168743	0.0715031	0.0747687	0.0725472	0.07277389	0.07077019	0.07199118	0.07260343	0.07158097	0.07342975	0.07040434	0.07371242	0.07253421	0.07186706	0.07212775
Fimbria	0.33232458	0.32863638	0.32424675	0.33089885	0.32831719	0.33172222	0.32631546	0.32874439	0.32804545	0.32504503	0.329037	0.32927262	0.32673281	0.32665934	0.33534947	0.32790048	0.33314356	0.33342056	0.33177269
flocculus	0.72994056	0.73950062	0.75652426	0.7492148	0.73956403	0.72479443	0.74792125	0.73404686	0.74809879	0.7343114	0.73635467	0.73822876	0.74602732	0.75249266	0.72900679	0.7498739	0.74161285	0.73063953	0.73675474
Fornix	0.03960321	0.04115708	0.03905245	0.0403887	0.04113222	0.04082458	0.04198438	0.04091012	0.04040413	0.03753201	0.03929092	0.04209977	0.03995246	0.03877637	0.0409532	0.03957842	0.04008841	0.04156101	0.0395639
Fourth_ventricle	0.19852946	0.19966432	0.20769976	0.20134949	0.19861729	0.1973891	0.20651416	0.18722674	0.19338122	0.19713352	0.20220246	0.19075437	0.19622342	0.20759289	0.19742433	0.20582578	0.19119462	0.19859582	0.19170096
Frontal_Association_Cortex	7.86641786	7.92158634	7.94394038	7.92438099	8.10661025	7.85304491	7.8691732	7.98053635	8.04833533	7.69644759	7.95560286	8.10467556	7.85496326	7.93223722	8.10530643	7.90330547	7.86760292	8.10629755	7.90170596
Globus_pallidus	0.31377736	0.31236127	0.31035895	0.3135934	0.31191465	0.30774325	0.30721766	0.30811797	0.30853174	0.30731514	0.30798299	0.31175357	0.30639596	0.30674924	0.31671241	0.30944021	0.30876913	0.31156746	0.30892531
hindbrain_medulla_pons	6.50564342	6.62818731	6.81632508	6.66751024	6.62881168	6.48150341	6.66735368	6.47857611	6.59727391	6.59786006	6.6148365	6.55423521	6.62568948	6.77586616	6.48083549	6.73955012	6.52804271	6.53020447	6.5466273
Hippocampal_layer_CA1	1.45183533	1.44184366	1.43777438	1.43891391	1.4465111	1.44403481	1.45436108	1.4490201	1.44934896	1.43370261	1.43570031	1.44558495	1.43453878	1.43815126	1.44571938	1.43759373	1.44745889	1.44451954	1.44872804
Hippocampal_layer_CA2	0.15727899	0.15615959	0.15414912	0.15692906	0.15994423	0.15640642	0.1539725	0.16598479	0.16447429	0.16007192	0.15453994	0.16364548	0.15985718	0.15316214	0.15718578	0.1543312	0.16338738	0.15634527	0.16295399
Hippocampal_layer_CA3	1.45419372	1.43665212	1.42998972	1.43916552	1.44294872	1.44380266	1.44088864	1.42038604	1.42490626	1.42079979	1.43968862	1.42047987	1.41131555	1.4294535	1.45797592	1.43699808	1.42543548	1.44758617	1.43317606
hypothalamus	1.94291227	1.93086486	1.90738023	1.93644012	1.94248242	1.9307478	1.92073788	1.93378111	1.92968675	1.90425263	1.91662248	1.93856845	1.91182459	1.90328	1.95937136	1.91724611	1.93267778	1.94283085	1.93221352
Inferior_Colliculus	1.0664768	1.08092867	1.09791581	1.08528056	1.07013487	1.06065484	1.09506945	1.058521	1.06870786	1.05890489	1.07579845	1.06694086	1.08162517	1.08982005	1.06834917	1.08642187	1.07104341	1.06808791	1.06618826
Infralimbic_Cortex	0.10377256	0.10482575	0.10252266	0.10574481	0.10544921	0.10827637	0.10598207	0.10299274	0.10287823	0.09995326	0.10545773	0.10315296	0.10244895	0.10460631	0.10725409	0.10348295	0.10399312	0.10828499	0.10109363
Insular_Cortex	1.68383343	1.68723982	1.66850726	1.69499789	1.68879568	1.68342696	1.65834048	1.68616909	1.67326133	1.65249663	1.66962965	1.69761275	1.66568568	1.66019482	1.70565292	1.65854225	1.67116695	1.69303489	1.65606921
Internal_capsule	0.55094693	0.54818409	0.54193718	0.54982883	0.55419656	0.54629457	0.53740303	0.56151229	0.55655601	0.55067111	0.54346894	0.56035899	0.54965352	0.5396314	0.55598551	0.5418669	0.55781958	0.54952501	0.55666824
interposed_nucleus	0.087898	0.08923047	0.0914968	0.08865675	0.08971764	0.0871007	0.09076608	0.08458464	0.08670743	0.08798407	0.08869589	0.08662398	0.0872085	0.09118213	0.08728366	0.09070227	0.08624572	0.08832488	0.0870926
intrabulbar_part_of_anterior_commisure	0.17907401	0.18409519	0.18374378	0.18122012	0.19198341	0.18156396	0.18441143	0.19628025	0.19398804	0.17408511	0.18334035	0.20005027	0.18592675	0.18255958	0.1847746	0.184747	0.18323368	0.18703588	0.18580292
Lateral_olfactory_tract	0.1647918	0.16362148	0.16425302	0.16715459	0.16882741	0.16437529	0.16197443	0.1693932	0.16959986	0.16645379	0.16404371	0.16835187	0.16579266	0.16319682	0.16756783	0.16209046	0.16981287	0.16692576	0.16719657
lateral_septum	0.67832704	0.67744653	0.67422562	0.68030109	0.67463092	0.66694331	0.66280791	0.66668962	0.66581955	0.66192531	0.66647773	0.67431635	0.66523023	0.6679654	0.68575128	0.66540982	0.66566113	0.67407572	0.66474591
Lateral_ventricle	0.96325098	0.95723041	0.94990226	0.96090051	0.96891672	0.95528387	0.95023385	0.97351981	0.97211138	0.9586731	0.94711853	0.97026124	0.95704808	0.94170241	0.96818606	0.9443961	0.96692175	0.96000838	0.96388773
mamillary_bodies	0.11245566	0.11204428	0.1109851	0.11306416	0.11457897	0.11223599	0.10806494	0.12195307	0.1194734	0.11595907	0.11183947	0.11884818	0.11539075	0.11005713	0.11251359	0.11108201	0.11876133	0.11206407	0.11933945
mammilothalamic_tract	0.02484048	0.02418979	0.02457911	0.02457996	0.02447062	0.02470883	0.02499482	0.02323262	0.02376637	0.02367253	0.02471871	0.02354012	0.02367771	0.02430486	0.02529526	0.02445191	0.02418736	0.02496509	0.02437933
medial_septum	0.09234523	0.09397334	0.09188675	0.09342442	0.0923679	0.09265398	0.09306601	0.09119317	0.09085416	0.08775326	0.09207171	0.09348319	0.09129994	0.0918681	0.09375405	0.09102825	0.09088246	0.09437604	0.09030495
median_preoptic_area	0.00335326	0.00346371	0.00322252	0.00353888	0.00365338	0.00380148	0.00331978	0.00363396	0.00351229	0.00335573	0.00353026	0.00355552	0.00355003	0.00336062	0.00352721	0.00338347	0.00368356	0.0036868	0.00345493
midbrain	2.38449124	2.37769337	2.38827042	2.37763513	2.3763461	2.38596495	2.42817287	2.34862747	2.36224836	2.34397694	2.37519982	2.36078916	2.36082791	2.39212157	2.37813655	2.38268786	2.35841557	2.3849771	2.35396083
Navicular_nuclear_basin_forebrain	0.12061111	0.12153987	0.12085173	0.12283081	0.12177423	0.12112229	0.12108096	0.1231032	0.12178582	0.11896914	0.11994869	0.1235127	0.11940986	0.11810792	0.12291556	0.11926974	0.12036391	0.12164819	0.11823704
Nucleus_accumbens	0.49058921	0.49357354	0.48977266	0.49570579	0.49430689	0.48485645	0.48380784	0.49836787	0.49345078	0.48790756	0.4860531	0.50455022	0.49096048	0.4877741	0.4997905	0.48315754	0.48946887	0.49196751	0.48820272
Occipital_Cortex	0.92761474	0.940142	0.95991136	0.94273094	0.93244201	0.92043639	0.96458599	0.91469174	0.92960487	0.92413724	0.93898341	0.92500488	0.94588453	0.9479636	0.92737586	0.94420736	0.92984973	0.92607214	0.92229667
Olfactory_Bulb	9.62676391	9.3504628	9.0090803	8.97708053	8.9297801	9.99084589	9.3872413	9.65242454	9.24024483	10.2819954	9.74324066	9.07614504	9.81826806	9.32238357	9.05858292	9.41477968	9.68464458	9.27764861	9.74931604
Olfactory_tubercle	0.83029941	0.83782238	0.82648969	0.84311414	0.84150194	0.83221635	0.82766924	0.85346195	0.8443658	0.82658794	0.82787846	0.85856468	0.83548555	0.82293816	0.84595705	0.82036412	0.84146177	0.83930863	0.83221727
Optic_Chiasm	0.01779598	0.01767362	0.0176276	0.01828179	0.01785801	0.01869846	0.01864043	0.01687115	0.01716361	0.01677231	0.01792197	0.01672576	0.01717837	0.01781915	0.01830004	0.01777109	0.01796037	0.01867192	0.01722849
Optic_tract	0.20608374	0.20409451	0.2022738	0.20578888	0.2068982	0.20866513	0.20481591	0.20924368	0.20794466	0.20290731	0.2047361	0.20634765	0.20436616	0.20162042	0.20682727	0.20328685	0.20829472	0.20792731	0.20571162
Orbitofrontal_Cortex	0.03071266	0.03076233	0.03102602	0.03123742	0.03179727	0.03088155	0.03047543	0.03298496	0.0328961	0.03204777	0.03027014	0.03247133	0.03182941	0.02989062	0.03115822	0.02982331	0.03234983	0.03094382	0.03165463
paraflocculus	0.83901812	0.84206881	0.87108366	0.85290815	0.8389746	0.82573619	0.85606314	0.80668793	0.83591894	0.836904	0.84603782	0.819762	0.83543521	0.87180911	0.83624546	0.86819059	0.82675243	0.83665143	0.83254272
paramedian_lobe	0.54758954	0.55638618	0.57710022	0.5607785	0.55432912	0.53965683	0.55754118	0.52946722	0.54101659	0.55121521	0.55653783	0.54303111	0.54463787	0.5785986	0.5448993	0.5735195	0.53756187	0.5478245	0.54672416
Parietal_Association_Cortex	0.77001911	0.75873332	0.75734529	0.76151002	0.76268554	0.76199585	0.75590038	0.75127585	0.75324844	0.75248853	0.75978144	0.75052645	0.74625646	0.75286446	0.77384506	0.75795523	0.75533407	0.76536373	0.75927045
Periaqueductal_grey	0.71824489	0.71283375	0.72490052	0.71454937	0.70179297	0.71083751	0.72264409	0.67611321	0.68979939	0.70298508	0.71673974	0.68390508	0.69827293	0.72523282	0.71898082	0.71922291	0.69233781	0.71151706	0.69703025
Piriform_Cortex	1.89804476	1.89436398	1.87204908	1.9062447	1.90427639	1.88781454	1.86708488	1.92488526	1.91380848	1.88196076	1.87487605	1.9249278	1.89084102	1.86553375	1.91928316	1.86807031	1.91732758	1.90067064	1.90801817
pons	1.5354926	1.54224298	1.55934795	1.54384972	1.53912959	1.53287	1.5779768	1.51675053	1.52878439	1.52099709	1.53987244	1.53422558	1.53869806	1.55479803	1.53702527	1.54857823	1.5313398	1.53933185	1.52980891
posterior_commisure	0.01544154	0.01489891	0.01539217	0.01477969	0.01414917	0.01444405	0.01582774	0.01241369	0.01341049	0.014324	0.01507047	0.01301887	0.01386944	0.01581178	0.01552583	0.01520509	0.01344209	0.01466254	0.01417935
Posterior_part_of_anterior_commissure	0.02262023	0.02212886	0.02243336	0.02238526	0.02185706	0.02198756	0.02130781	0.02076948	0.02136528	0.02228032	0.02199353	0.02104374	0.02152306	0.02268692	0.02291879	0.02200335	0.02162727	0.02197428	0.02175591
Prelimbic_Cortex	0.27415774	0.27610484	0.27171581	0.27700105	0.27909699	0.27526451	0.27167914	0.28329687	0.28256267	0.27626214	0.2746718	0.28577488	0.27757117	0.27379635	0.28107037	0.27266485	0.27862869	0.27834912	0.27659434
Primary_Motor_Cortex	1.3579824	1.36065561	1.34948523	1.36911845	1.363062	1.35590583	1.34804134	1.34578141	1.34876418	1.33600338	1.35131701	1.36117247	1.33959478	1.35039995	1.38733321	1.34653138	1.3417619	1.37173672	1.33446885
Primary_Somatosensory_Cortex	5.65625497	5.65402317	5.58887874	5.68974944	5.68085816	5.64343316	5.57285456	5.70768402	5.67266578	5.58882365	5.60037615	5.72294489	5.61749584	5.56754428	5.72593293	5.57051768	5.67204994	5.67610503	5.62984478
Primary_Visual_Cortex	1.80137619	1.80721997	1.81692908	1.80866471	1.80602545	1.79730562	1.82598757	1.7908962	1.80147439	1.78850663	1.79734246	1.8027348	1.80300521	1.8110194	1.79913699	1.80741326	1.80008786	1.80106208	1.80093926
Retrosplenial_Cortex	2.17074659	2.16783589	2.18008819	2.17278764	2.17466634	2.15465789	2.17671948	2.15857981	2.17146348	2.16297212	2.15422699	2.17102826	2.16544534	2.16735974	2.17392036	2.16538301	2.16646416	2.16354254	2.1719852
rhinal_cortex	3.27598079	3.27601499	3.28772791	3.27803297	3.27251559	3.26588068	3.31745153	3.2450976	3.26073353	3.24276605	3.26488479	3.26426717	3.25870623	3.28463676	3.27958749	3.28119994	3.26199873	3.27519008	3.26627698
Secondary_Motor_Cortex	0.82671832	0.83270749	0.81972509	0.83168536	0.83833791	0.822461	0.81803165	0.85291211	0.84419784	0.82109838	0.81956873	0.85680786	0.83008811	0.81341857	0.84129709	0.81609089	0.82876998	0.83054838	0.82186886
Secondary_Somatosensory_Cortex	1.50933242	1.50070865	1.4884539	1.51214	1.50449331	1.49764023	1.47854745	1.48923278	1.48759565	1.47973635	1.48926733	1.4991393	1.48079383	1.48143719	1.52431269	1.48442275	1.49230823	1.50799242	1.48879871
Secondary_Visual_Cortex	2.17476537	2.17183322	2.18648954	2.17712552	2.17744273	2.17331226	2.20118587	2.15457625	2.16721346	2.15761278	2.16812486	2.16104845	2.16393947	2.17848218	2.1723555	2.17585657	2.16108572	2.17418948	2.16174998
Simple_Lobule	1.14975168	1.16003148	1.19305301	1.17572904	1.15996291	1.14212017	1.18048639	1.13585175	1.1595917	1.1465872	1.16240914	1.14871464	1.15606132	1.19376987	1.14587921	1.18903456	1.15005553	1.15279493	1.14966893
stria_medullaris_thalamus	0.04388232	0.04444871	0.04307271	0.04391426	0.04410667	0.04450263	0.04331113	0.04503057	0.04328094	0.04184407	0.04414138	0.04521483	0.04285851	0.04293419	0.04424652	0.04377195	0.04300342	0.0442549	0.04249812
Stria_terminalis	0.17689171	0.17592123	0.17297002	0.17656287	0.17626074	0.17716463	0.17442336	0.18084516	0.17928022	0.17361098	0.17538255	0.17880421	0.17549522	0.17405004	0.17815149	0.17527627	0.17991657	0.17755398	0.17991359
Subfornical_organ	0.00567884	0.00536471	0.00558717	0.00537652	0.00516131	0.00529322	0.00492434	0.00492478	0.00502874	0.00527702	0.00534137	0.00506668	0.00517972	0.00559815	0.00555716	0.00546048	0.00509804	0.00533292	0.00532755
subicular_region	1.76083095	1.76597649	1.77777464	1.76863667	1.76812337	1.76765033	1.78472193	1.75184824	1.76170068	1.75271293	1.75907275	1.7624614	1.76290692	1.77130247	1.76099561	1.76809999	1.75980357	1.76573046	1.75556315
substantia_nigra	0.16543552	0.16268679	0.16470481	0.16129556	0.15902415	0.16052674	0.16791692	0.14827986	0.15159678	0.15851487	0.16289347	0.15198968	0.15455454	0.16546268	0.16498591	0.164556	0.15311839	0.16167814	0.15609214
Superior_Colliculus	1.11840735	1.12684973	1.13096367	1.12715837	1.13353329	1.12237732	1.13508838	1.12870227	1.12865325	1.11967084	1.11685095	1.14041457	1.12649417	1.12529692	1.11890498	1.12207547	1.12665036	1.1237912	1.12568087
Temporal_Association	0.78143457	0.78629711	0.7917184	0.78572134	0.78722177	0.78882483	0.79904957	0.77159	0.77550384	0.77003457	0.78345587	0.77828002	0.78047684	0.78711222	0.78204566	0.78699232	0.77392902	0.78700024	0.77031935
Thalamus	3.41193347	3.38370066	3.35096158	3.38767941	3.40747289	3.38233389	3.36072725	3.4117792	3.40456942	3.3704569	3.3637613	3.40418733	3.36075773	3.34272238	3.42848407	3.36528205	3.40243266	3.39904102	3.41484789
Third_ventricle	0.31731212	0.31530969	0.31380189	0.31592934	0.31749328	0.31257971	0.31197325	0.32400218	0.32266207	0.32020121	0.31223115	0.32177567	0.31708406	0.3109842	0.3209923	0.31271529	0.32315078	0.31582268	0.32396712
trochlear_nerve	0.00562258	0.0059825	0.00581875	0.00582632	0.00585182	0.00564027	0.00573441	0.00574607	0.00556711	0.00540586	0.00573631	0.00609644	0.00586686	0.00574314	0.00572913	0.0057261	0.00570185	0.00590113	0.00568915
ventral_pallidum	0.17660198	0.17770118	0.17427185	0.17904326	0.1759432	0.17607656	0.17299916	0.17797439	0.17648625	0.17239742	0.17595367	0.17898614	0.17454044	0.17386136	0.17851322	0.17452571	0.17651218	0.17700005	0.1755999

	100	101	102	14	16	17	19	23	24	34	41	48	54	55	86	89	92	97	99
	WT	WT	WT	WT	WT	WT	WT	WT	WT	WT	WT	WT	WT	WT	WT	WT	WT	WT	WT
Relative Volumes	F	F	F	M	M	M	M	M	M	M	M	M	M	M	M	M	M	M	M
	Pat	Pat	Pat	Pat	Pat	Pat	Pat	Pat	Pat	Pat	Pat	Pat	Pat	Pat	Pat	Pat	Pat	Pat	Pat
amygdaloid_area	2.10195378	2.07465874	2.05682867	2.11664189	2.09268588	2.09762043	2.13089173	2.10619703	2.09994847	2.06982134	2.11860596	2.08768302	2.11631147	2.11581389	2.1018214	2.07363419	2.1065439	2.08531247	2.09635684
Anterior_part_of_anterior_commissure	0.09460222	0.09160413	0.09038352	0.09457199	0.09366053	0.09449742	0.09618926	0.09488309	0.0951686	0.09125312	0.09593698	0.09358563	0.09656303	0.09577129	0.09425238	0.09428442	0.09283988	0.09283524	0.09411309
Aqueduct	0.11430628	0.11838629	0.114088	0.11359542	0.11379575	0.1135535	0.11352017	0.11308203	0.11692444	0.1143116	0.11273035	0.11377644	0.11341107	0.11149712	0.11185579	0.11218113	0.11356581	0.11810548	0.11208682
auditory_cortex	1.46200215	1.46867444	1.43906081	1.47328406	1.45664977	1.45714199	1.46424941	1.45727316	1.46401404	1.43425654	1.46431199	1.44551616	1.46250147	1.45680125	1.45676673	1.44030967	1.46083408	1.46355278	1.45360666
basal_forebrain	1.18875734	1.19960193	1.20468733	1.21673579	1.21065545	1.19686309	1.20744261	1.19689894	1.21908089	1.18747758	1.2057967	1.1855693	1.21073119	1.20208542	1.19066824	1.17634771	1.18505871	1.20386878	1.18240155
Bed_nucleus_of_stria_terminalis	0.20374494	0.19650464	0.19790495	0.21168269	0.21062558	0.21017621	0.2056469	0.21044009	0.20946123	0.20708802	0.2052665	0.20424691	0.2075214	0.20802186	0.21137674	0.20312271	0.20768231	0.19645723	0.20216341
caudaputamen	3.21005996	3.23053853	3.2454049	3.29062414	3.26340846	3.23383706	3.26298263	3.23905076	3.28429105	3.2060964	3.26040486	3.20950559	3.27405916	3.25419685	3.22477365	3.18960103	3.21417225	3.24523435	3.20377161
cerebellar_lobule_1_2	0.56473536	0.56002419	0.5319191	0.55744251	0.5560021	0.56811038	0.56752371	0.56379643	0.56997609	0.56511522	0.5655869	0.57421311	0.56909742	0.56709665	0.55715599	0.56503902	0.56677576	0.57597305	0.56997187
cerebellar_lobule_10	0.23591105	0.23557553	0.22363118	0.23728762	0.2321612	0.23949669	0.23650629	0.23684762	0.2398729	0.23396288	0.23379135	0.24606883	0.23874829	0.23980661	0.23523079	0.24007108	0.23598734	0.24333312	0.24126678
cerebellar_lobule_3	0.48668121	0.47898807	0.45130026	0.48561637	0.47771875	0.49394031	0.48865116	0.49209453	0.49085377	0.4862696	0.49060415	0.50544401	0.49611813	0.49808799	0.48376515	0.49522749	0.48927825	0.49445938	0.49717384
cerebellar_lobule_4_5	1.50132236	1.51765526	1.44093414	1.50211328	1.48485313	1.51502666	1.50286747	1.4981097	1.52819022	1.50340407	1.49483765	1.54810967	1.51835181	1.5127649	1.48321903	1.50826522	1.49855964	1.54974584	1.51742699
cerebellar_lobule_6	0.59260688	0.6037739	0.57928801	0.59944644	0.5849473	0.60590621	0.59852745	0.59103611	0.60264074	0.5951309	0.59340082	0.62140558	0.60091562	0.6040037	0.59052201	0.60243474	0.60139639	0.62329257	0.60963595
cerebellar_lobule_7	0.22828165	0.23616658	0.23148927	0.23252523	0.22554523	0.23417286	0.22813953	0.22469901	0.23040555	0.22886093	0.22640053	0.23539875	0.22810229	0.22961596	0.22729371	0.2304898	0.23591971	0.24246666	0.23469311
cerebellar_lobule_8	0.25450104	0.25902104	0.24688822	0.25712047	0.24953122	0.25956288	0.25836161	0.2543732	0.25925196	0.25549296	0.25690852	0.26898454	0.26023478	0.26107239	0.2529882	0.26191705	0.25797038	0.27040981	0.26449657
cerebellar_lobule_9	0.59298556	0.60880013	0.58281213	0.6000738	0.58451547	0.607372	0.601873	0.59157093	0.60384668	0.59726362	0.59749409	0.62362824	0.60387572	0.60665161	0.58971417	0.60636086	0.60354755	0.63070398	0.61386099
Cerebellar_White_Matter_Arbor_vita_of_cerebellum	1.88621849	1.883093	1.78713621	1.88142119	1.84912138	1.90892221	1.90161159	1.8830025	1.90024664	1.88628601	1.8839302	1.9516609	1.90567099	1.9048613	1.86406693	1.90129305	1.89312031	1.93315966	1.9164329
cerebral_peduncle	0.20676862	0.20471515	0.20263566	0.2092076	0.20612786	0.20667925	0.20578009	0.20693043	0.20551115	0.20467534	0.20606845	0.20349009	0.2047987	0.20574898	0.20715634	0.20285698	0.20995512	0.20290828	0.20464102
Cingulate_Cortex_area_1	1.06089776	1.08247054	1.08500269	1.08989512	1.0768551	1.06364098	1.07765776	1.06714912	1.08452396	1.06029242	1.07532786	1.06718142	1.0813962	1.07858395	1.06480959	1.05297536	1.06465476	1.08458815	1.06178741
Cingulate_Cortex_area_2	0.65586029	0.67227923	0.67605499	0.68007249	0.67434872	0.66205049	0.66474316	0.66287722	0.67817971	0.65650069	0.66624989	0.65611082	0.66913421	0.66226501	0.65939542	0.65023612	0.6568321	0.67305105	0.65552582
cingulum	0.23243503	0.22880029	0.22737248	0.23671341	0.2331685	0.23425253	0.23425773	0.23473363	0.23471529	0.22840195	0.23504236	0.23357859	0.23757598	0.23628584	0.23454568	0.23183008	0.23287457	0.23048662	0.23327669
Cochlear_nucleus	0.07449913	0.0698469	0.06519251	0.07355035	0.0715266	0.07563619	0.0765675	0.07591984	0.07329692	0.07418301	0.07600134	0.0781953	0.07708222	0.07727971	0.07425682	0.07726388	0.07496515	0.07333919	0.07734185
Commisure_inferior_Colliculus	0.02194991	0.02576108	0.02462463	0.02219788	0.02305051	0.02142941	0.02096968	0.0207794	0.02358382	0.02212264	0.02070474	0.02053362	0.02065623	0.01989716	0.02095827	0.0204321	0.02128211	0.02438708	0.02031547
commisure_superior_collicuus	0.01328242	0.01313793	0.012734	0.01338152	0.01316047	0.01323779	0.01327801	0.01315207	0.0130485	0.0129281	0.01324575	0.01315836	0.01316964	0.01292613	0.01334386	0.01298313	0.01317291	0.01287929	0.01310456
copula	0.19285205	0.19459856	0.18934219	0.19516533	0.18940772	0.19821954	0.19522885	0.19129508	0.19316858	0.19383993	0.1941116	0.20083742	0.19548913	0.1960702	0.19263524	0.19629745	0.19887512	0.20096016	0.19977447
Corpus_Callosum_associated_White_Matter	2.92790636	2.95334363	2.9356168	2.98046451	2.95727925	2.93880959	2.94425347	2.94183416	2.9727091	2.91330052	2.94889521	2.91414665	2.94964797	2.94158071	2.93331744	2.9029394	2.94102827	2.95032244	2.91571688
Crus_1_ansiform_lobule	1.17061678	1.17206901	1.12181037	1.17159004	1.14862281	1.18556116	1.17596783	1.16393442	1.17777182	1.17099176	1.16466587	1.20905631	1.17674215	1.17903596	1.15789788	1.1770616	1.17822821	1.19833448	1.18895822
Crus_2_ansiform_lobule	0.67840463	0.68220312	0.65173357	0.68110214	0.66191347	0.69521145	0.69324808	0.6771883	0.68048923	0.68179713	0.68400591	0.70706589	0.6885357	0.69086539	0.67187058	0.69091485	0.6916648	0.70390037	0.69889474
dentate_gyrus	1.14967461	1.14558326	1.11175831	1.15229156	1.13815155	1.14760944	1.15473254	1.1479476	1.14636973	1.12367534	1.15787934	1.14197828	1.1562835	1.14872749	1.14274803	1.14021135	1.146431	1.14565094	1.148208
Dentate_nucleus	0.0589773	0.05493526	0.05215576	0.05882631	0.05674696	0.06043535	0.0596627	0.06049058	0.05828909	0.05835256	0.05972219	0.06224297	0.06100036	0.06148858	0.05955614	0.06116384	0.05991415	0.05766635	0.06131708
Dorsal_Peduncular_Cortex	0.10378537	0.10286079	0.10292063	0.10830269	0.10594137	0.10663704	0.10649867	0.10701796	0.10611972	0.10544979	0.10824772	0.10735045	0.10884558	0.10859105	0.10676194	0.10660081	0.10701427	0.10568902	0.10701791
Dorsal_Tenia_Tecta	0.07296422	0.07084274	0.07046141	0.07570672	0.07427157	0.07424998	0.07383798	0.07500378	0.0749151	0.07091991	0.07458121	0.07474391	0.0756519	0.07501674	0.07449802	0.07353972	0.07286682	0.07266981	0.07451132
Endopiriform_Nucleus	0.61790513	0.63872846	0.64233381	0.63266522	0.63273131	0.61831361	0.62386299	0.61783033	0.63560912	0.61902727	0.6221606	0.60918038	0.62213281	0.61662768	0.61488777	0.60520598	0.61388378	0.63423961	0.60972449
entopeduncular_nucleus	0.0152729	0.0162747	0.01642387	0.01625881	0.01596968	0.01543877	0.01511044	0.01533383	0.01594632	0.01445413	0.01522559	0.01561482	0.01553954	0.01561463	0.01556191	0.01520241	0.01519565	0.01637551	0.01563604
external_medullary_lamina	0.046121	0.04489963	0.04522599	0.04631527	0.04603722	0.04616135	0.04619461	0.04640801	0.04539082	0.04676545	0.04591019	0.04482178	0.04509296	0.0456157	0.04614847	0.04476194	0.04717461	0.04449723	0.04532476
Fasciculus_retroflexus	0.01600761	0.0184671	0.01841628	0.01648991	0.01655364	0.01557245	0.01592969	0.01556166	0.01696525	0.01563874	0.01594822	0.01545842	0.01572352	0.01576393	0.01541539	0.01550353	0.01548302	0.01821364	0.01583577
fastigial_nucleus	0.0716504	0.07291214	0.06828846	0.07032375	0.07014743	0.0710469	0.07241694	0.07047508	0.07266175	0.07144747	0.07091991	0.07397818	0.07253184	0.07106481	0.06985652	0.07158693	0.07020639	0.07522627	0.07228901
Fimbria	0.33140485	0.33107637	0.32960302	0.33285337	0.33006322	0.32872158	0.33594554	0.33051838	0.33289748	0.32290855	0.33369456	0.32916792	0.33373307	0.33355463	0.32905312	0.32670489	0.32749644	0.33408157	0.33105074
flocculus	0.73221869	0.74175223	0.70351913	0.73117126	0.72611885	0.73763966	0.73391052	0.73201179	0.75009618	0.73383906	0.73285479	0.75525048	0.74274543	0.73948534	0.72161601	0.73704209	0.73027341	0.76054021	0.74036779
Fornix	0.0405562	0.0394437	0.03919799	0.04012405	0.04000483	0.04011276	0.04220298	0.04035283	0.03991406	0.04111044	0.04103817	0.04014303	0.04084977	0.04024567	0.03956866	0.03951694	0.04071442	0.03960808	0.03984426
Fourth_ventricle	0.19677658	0.19193588	0.18226343	0.19629214	0.19143573	0.20016167	0.19925725	0.19762323	0.19600327	0.19631379	0.19864845	0.20467487	0.20131149	0.20146886	0.19675486	0.2009512	0.19953967	0.19888023	0.20288141
Frontal_Association_Cortex	7.81099106	7.92138193	7.89980587	8.00176713	7.81023121	7.87994235	8.04373881	7.86920421	7.97286918	7.82387515	7.94420842	8.11686517	8.02342445	8.20356459	7.88624164	7.80347932	7.92094564	8.05855146	7.96017955
Globus_pallidus	0.30906095	0.3063345	0.30658999	0.31651071	0.31315188	0.31260673	0.31529112	0.313361	0.31316851	0.3092494	0.31302707	0.31249452	0.31624429	0.31516412	0.31161998	0.30684143	0.31114434	0.30847607	0.31018395
hindbrain_medulla_pons	6.51375932	6.56500405	6.26132103	6.52987668	6.41918184	6.61783947	6.57034616	6.51600484	6.60192575	6.51396412	6.53043496	6.72806042	6.59533135	6.59094983	6.45642202	6.59933118	6.56785452	6.76209307	6.64055579
Hippocampal_layer_CA1	1.44712191	1.45484458	1.4176743	1.45382758	1.43956147	1.44224857	1.44592907	1.44247106	1.45240598	1.41859695	1.45185072	1.43044677	1.44782408	1.44474006	1.44060152	1.43243117	1.44292105	1.44948092	1.44068391
Hippocampal_layer_CA2	0.15888525	0.16431035	0.16443013	0.16114434	0.16077375	0.15721642	0.15815226	0.1571366	0.16171029	0.15683228	0.15762747	0.15389856	0.15601382	0.15629704	0.15718414	0.15406163	0.15770316	0.16145376	0.15516636
Hippocampal_layer_CA3	1.44373155	1.41829597	1.39346986	1.45084563	1.42899712	1.44014848	1.45529342	1.44582117	1.43367822	1.41236418	1.45425569	1.43257064	1.45076515	1.4502119	1.44436136	1.4258194	1.44797203	1.4235577	1.44389607
hypothalamus	1.93648438	1.92328181	1.91351995	1.95476277	1.93516515	1.93249968	1.96504786	1.93836095	1.94074433	1.91410049	1.94868838	1.92234218	1.95104301	1.94495495	1.93348354	1.90573609	1.93744445	1.92623856	1.9275934
Inferior_Colliculus	1.06627484	1.06882518	1.01580808	1.06050249	1.05644754	1.07268444	1.07188763	1.07121944	1.08459335	1.05766353	1.07368127	1.08708377	1.08258126	1.07579861	1.05880844	1.07563172	1.0671702	1.09828562	1.07964488
Infralimbic_Cortex	0.1041519	0.10342612	0.10167799	0.10543501	0.1033371	0.10412733	0.10702489	0.10475028	0.10437418	0.10154343	0.10708191	0.10489077	0.10809648	0.10683943	0.10459138	0.10496644	0.10398161	0.10518709	0.10577256
Insular_Cortex	1.66858836	1.65404901	1.65594558	1.70246602	1.68649035	1.68297943	1.70917996	1.69128992	1.69513308	1.67788522	1.70584991	1.67658784	1.70740252	1.6976868	1.67914896	1.66277873	1.68161699	1.67147597	1.67342914
Internal_capsule	0.55171991	0.55422846	0.55816524	0.55799593	0.55653741	0.55057635	0.55755572	0.55228526	0.55538061	0.54874003	0.55316144	0.54330876	0.55086411	0.55300098	0.54999208	0.54285153	0.55337483	0.55264393	0.54694835
interposed_nucleus	0.08878914	0.0850545	0.08069426	0.08784718	0.08628081	0.08989822	0.08894604	0.08871626	0.08671998	0.08766871	0.08748123	0.08969342	0.08859768	0.08860492	0.08829822	0.08847579	0.09032565	0.08635593	0.08931735
intrabulbar_part_of_anterior_commisure	0.18215494	0.19093323	0.18968988	0.185133	0.17914657	0.18272928	0.18850542	0.17976876	0.18668954	0.1901336	0.18532974	0.19036339	0.18519313	0.18759657	0.17823124	0.17623315	0.18865613	0.1927639	0.18239407
Lateral_olfactory_tract	0.16469218	0.16816517	0.16778323	0.17037245	0.16826447	0.16609512	0.16610342	0.16603833	0.17048388	0.16222592	0.16555436	0.16549292	0.16721821	0.16839011	0.16693977	0.16305184	0.16328323	0.16769185	0.16486398
lateral_septum	0.66450029	0.65875939	0.66293139	0.68535317	0.67653735	0.67684421	0.67937028	0.67899774	0.68022486	0.66860607	0.68040053	0.673639	0.68466728	0.68365508	0.6767918	0.66812404	0.67303648	0.66485716	0.67025007
Lateral_ventricle	0.96197106	0.96087689	0.95893029	0.97870154	0.97219624	0.96499529	0.96783267	0.96441578	0.97354659	0.95703566	0.96390937	0.94954405	0.96563476	0.96402922	0.96440803	0.94561107	0.96537434	0.95641255	0.95173224
mamillary_bodies	0.11352672	0.12077122	0.12009021	0.11636497	0.115947	0.11245766	0.11294535	0.11252415	0.11659336	0.11231671	0.11272198	0.11087386	0.11205346	0.11175064	0.1120779	0.10992821	0.11282063	0.11924638	0.11170949
mammilothalamic_tract	0.0247062	0.02381184	0.02361885	0.02511295	0.02424928	0.02460075	0.02490119	0.02467692	0.02454828	0.02321248	0.02481441	0.02455802	0.0249244	0.02489578	0.02471148	0.02444456	0.02439668	0.02404	0.02484622
medial_septum	0.0915251	0.0906185	0.09088468	0.09274768	0.09116754	0.09222024	0.09434042	0.09261881	0.09281552	0.09178779	0.09421006	0.09248866	0.09443152	0.0939456	0.09184442	0.09260694	0.09300731	0.09258417	0.09266451
median_preoptic_area	0.00377458	0.00362898	0.00351274	0.00336693	0.00347293	0.00347362	0.00371975	0.00345677	0.00357306	0.00350376	0.00371717	0.00341353	0.00355127	0.00354697	0.00345731	0.00359139	0.00351446	0.00349597	0.00343251
midbrain	2.38130506	2.36134734	2.27709359	2.36861225	2.35482607	2.37991791	2.38265945	2.38105439	2.38035849	2.33926858	2.39712675	2.37325545	2.39501885	2.38212678	2.36795187	2.37478406	2.37808599	2.37222631	2.38148462
Navicular_nuclear_basin_forebrain	0.11954751	0.11964739	0.11928745	0.12290946	0.12188358	0.12031696	0.12283685	0.12157061	0.12166694	0.12041814	0.12250673	0.121916	0.12403765	0.12131442	0.1204907	0.11919613	0.121301	0.12140072	0.12059494
Nucleus_accumbens	0.48427969	0.48690843	0.49432378	0.50269408	0.4943889	0.49066996	0.49309782	0.49358494	0.4983356	0.48882622	0.49666263	0.49091312	0.49854184	0.49759349	0.49118912	0.48849406	0.49204738	0.49230376	0.48896709
Occipital_Cortex	0.92789788	0.92396354	0.88002896	0.92046583	0.91727908	0.93663651	0.9302843	0.93233877	0.94357283	0.92533508	0.931709	0.94483491	0.9372709	0.93540726	0.92151113	0.93135492	0.93277551	0.95046921	0.93903779
Olfactory_Bulb	9.89421131	9.72721392	11.4854558	8.93072491	10.0255802	9.37166008	8.92554005	9.55692979	8.85349767	10.4695471	9.1377982	8.98471618	8.7451326	8.80639478	9.95062868	10.108085	9.49031023	8.72168895	9.38644051
Olfactory_tubercle	0.82606566	0.83916428	0.84472433	0.85290867	0.84170513	0.832145	0.84117923	0.83657769	0.84899625	0.8288901	0.84444196	0.83289139	0.84794855	0.84092617	0.83042438	0.82642191	0.83130673	0.84500428	0.83069194
Optic_Chiasm	0.01824104	0.01754757	0.01686311	0.0178656	0.01767495	0.01796114	0.01858424	0.01785112	0.01817367	0.01672158	0.01834971	0.01794489	0.01865094	0.01830041	0.01781663	0.01777471	0.01730272	0.01764423	0.01801908
Optic_tract	0.20744366	0.20780289	0.20419894	0.20682086	0.20582973	0.2052065	0.20998074	0.20615452	0.20783379	0.20358076	0.20794035	0.20287718	0.20753434	0.20534194	0.20440353	0.20211176	0.20427169	0.20730263	0.20512562
Orbitofrontal_Cortex	0.03095473	0.03214488	0.0322824	0.0321174	0.03230514	0.03119829	0.03084894	0.03129625	0.03271905	0.03121741	0.03076478	0.03040887	0.03104944	0.03085727	0.03138943	0.0302551	0.03082205	0.03198381	0.03038464
paraflocculus	0.83264141	0.82764676	0.78774377	0.83590261	0.81968055	0.84302966	0.83568466	0.83452179	0.84237396	0.82849851	0.83357441	0.86901696	0.84959164	0.85109892	0.83101094	0.84792048	0.83651455	0.85216932	0.85267213
paramedian_lobe	0.5419669	0.54084838	0.51201433	0.54652107	0.53105284	0.55491858	0.54892994	0.54553308	0.54688782	0.53959805	0.54517322	0.57117517	0.55271978	0.55674995	0.54125542	0.55630872	0.54800172	0.56121377	0.56065661
Parietal_Association_Cortex	0.76179592	0.75109569	0.74287858	0.7685189	0.75788789	0.7622806	0.77191326	0.76436668	0.76022912	0.74598629	0.76958619	0.75767085	0.76868614	0.76796203	0.76462959	0.75387622	0.76435737	0.75533178	0.76368248
Periaqueductal_grey	0.70633022	0.69132147	0.66437413	0.70786187	0.6982742	0.71152853	0.70819346	0.71429197	0.70864566	0.68879662	0.71805248	0.72006598	0.72166393	0.72044892	0.71326542	0.71799354	0.70970431	0.7083853	0.72238903
Piriform_Cortex	1.89258716	1.91298172	1.91643914	1.93184894	1.91455921	1.895021	1.91437958	1.89853774	1.92682922	1.87586086	1.9114371	1.88433844	1.91621276	1.90924637	1.89213923	1.87151539	1.88933542	1.91813857	1.88530063
pons	1.53853852	1.52466138	1.46617235	1.52710263	1.52331004	1.53980909	1.53831628	1.54400336	1.54840472	1.51477941	1.54448393	1.54524615	1.55082338	1.54091671	1.53315051	1.53737501	1.54091794	1.54476871	1.5457468
posterior_commisure	0.01448186	0.01322856	0.01263572	0.01459236	0.01411156	0.01491187	0.01437146	0.01503956	0.01434512	0.01382315	0.01501751	0.0153236	0.01519331	0.01552036	0.01499205	0.01520756	0.01480542	0.01378348	0.01530124
Posterior_part_of_anterior_commissure	0.02193242	0.02120628	0.02129454	0.02266006	0.02213636	0.02223127	0.02211095	0.02228701	0.02238251	0.02125619	0.0222921	0.02215931	0.02254003	0.02270439	0.02239553	0.02222491	0.02201967	0.02159474	0.02225595
Prelimbic_Cortex	0.27244921	0.28010086	0.28297422	0.28231079	0.27679172	0.27313083	0.27652379	0.27462906	0.27992209	0.27334493	0.27794073	0.27635089	0.27847094	0.27968845	0.27513066	0.2735381	0.27649777	0.28256353	0.27547668
Primary_Motor_Cortex	1.34033173	1.33376455	1.33771502	1.37855462	1.35481103	1.35245769	1.37160191	1.36152908	1.36226418	1.33811347	1.37200609	1.36578744	1.38200294	1.37958375	1.35880108	1.35046646	1.3568559	1.35210918	1.35650006
Primary_Somatosensory_Cortex	5.62882926	5.63371526	5.63868811	5.74143027	5.68959835	5.65382399	5.72213321	5.67256643	5.71950273	5.61598483	5.70952597	5.62322242	5.72188134	5.69752948	5.64453413	5.5826133	5.64422387	5.66306003	5.62180695
Primary_Visual_Cortex	1.80411917	1.79894912	1.73739431	1.80319816	1.79079185	1.80680002	1.80191643	1.80685787	1.81481993	1.77536134	1.81117398	1.80465758	1.81164079	1.80295424	1.79627936	1.79809503	1.80607057	1.81472497	1.80659346
Retrosplenial_Cortex	2.16937146	2.1633119	2.11209005	2.18110137	2.16580134	2.17578645	2.16975746	2.17583867	2.18397571	2.13957194	2.17564252	2.16384239	2.17744442	2.17277873	2.1690384	2.15704021	2.17764577	2.17099388	2.16754118
rhinal_cortex	3.27491208	3.25905096	3.15678778	3.27477469	3.25111322	3.27542709	3.279307	3.27826665	3.28892232	3.21659374	3.29097336	3.27620328	3.29552649	3.27875803	3.26417827	3.26106918	3.27827942	3.2837244	3.27971529
Secondary_Motor_Cortex	0.81787707	0.83283349	0.83784613	0.84356642	0.83361143	0.82570496	0.83689313	0.82837924	0.83900683	0.83646759	0.83687363	0.82695056	0.8362985	0.83583046	0.82683759	0.81658309	0.83502325	0.83683975	0.82245044
Secondary_Somatosensory_Cortex	1.49393242	1.47179176	1.4710616	1.51927735	1.50467561	1.50424321	1.52255896	1.51102252	1.51108729	1.48714213	1.51448505	1.49648266	1.52002852	1.51585705	1.50344362	1.4843198	1.49948525	1.48488141	1.49320344
Secondary_Visual_Cortex	2.17562916	2.16287095	2.09190054	2.17521301	2.16027282	2.17904538	2.17718095	2.17816933	2.18171744	2.13881135	2.18642373	2.1711968	2.18666093	2.17508368	2.16798829	2.16424136	2.17822419	2.17390134	2.17655627
Simple_Lobule	1.14832327	1.15037606	1.08753498	1.14593334	1.12687966	1.15796874	1.15686065	1.14798636	1.16542933	1.14734413	1.14924005	1.19075963	1.16783586	1.16452818	1.1343923	1.16328184	1.14559855	1.18510516	1.17015445
stria_medullaris_thalamus	0.04331079	0.04293747	0.04221389	0.04341626	0.04331984	0.0436263	0.04562144	0.0438685	0.04309459	0.04466901	0.04496354	0.04351797	0.04442446	0.04370934	0.04272835	0.04258862	0.04391427	0.04373738	0.04379324
Stria_terminalis	0.17747587	0.18223325	0.17964515	0.17867541	0.17689377	0.17479975	0.1790673	0.17530629	0.17869423	0.17279137	0.17799013	0.1754859	0.17813985	0.17734432	0.17455174	0.17420097	0.17484132	0.1828097	0.17626344
Subfornical_organ	0.00511887	0.00512077	0.00518275	0.00530194	0.00539276	0.00533852	0.00545694	0.00545516	0.00522505	0.00504377	0.00546351	0.00545411	0.00550159	0.00567846	0.00539919	0.00550304	0.00524532	0.00534116	0.00549309
subicular_region	1.76595382	1.7624005	1.69940248	1.76351181	1.75547374	1.77002504	1.7651715	1.76766374	1.77301895	1.7380369	1.77484038	1.76400219	1.77507356	1.76304323	1.7601606	1.76184025	1.76757825	1.76946127	1.76634088
substantia_nigra	0.15955321	0.15208965	0.14620766	0.16143664	0.15697661	0.16280459	0.16060426	0.16255731	0.15692472	0.15537738	0.16303902	0.16308844	0.16322589	0.16382259	0.16343033	0.16278353	0.16323116	0.15349157	0.16350652
Superior_Colliculus	1.12769985	1.12204315	1.08703472	1.12519482	1.12188752	1.1301725	1.12681877	1.13001505	1.12953955	1.11550645	1.12958529	1.11989016	1.12664007	1.12109586	1.1216019	1.11870669	1.13327873	1.12453702	1.1217689
Temporal_Association	0.78461682	0.77247313	0.74099905	0.77841907	0.77428627	0.78811336	0.78961774	0.78706814	0.78200132	0.77592555	0.79100455	0.7844819	0.79082276	0.78258036	0.78054774	0.78199955	0.78686945	0.7804823	0.7861805
Thalamus	3.40020044	3.39991266	3.37405493	3.43620337	3.4005202	3.39129695	3.42966247	3.39809603	3.40848208	3.34763582	3.41437588	3.36531327	3.40722653	3.40653968	3.39692347	3.34617636	3.40678197	3.39817603	3.38317011
Third_ventricle	0.31703899	0.32483633	0.32657108	0.3256497	0.3229287	0.31886776	0.31702541	0.31740541	0.32302513	0.31192839	0.31720254	0.31455566	0.31885571	0.31954075	0.31794005	0.31329987	0.31674748	0.32192378	0.31492238
trochlear_nerve	0.00577504	0.0053438	0.00507606	0.00554216	0.00555464	0.00589235	0.00597672	0.00594667	0.00561395	0.00592643	0.0058556	0.00583626	0.00573183	0.00571914	0.00560904	0.00580734	0.00579105	0.00547649	0.00573212
ventral_pallidum	0.17338963	0.17652336	0.17682389	0.17989134	0.17730232	0.17604404	0.1787098	0.17661607	0.17894871	0.17367848	0.17933157	0.17680144	0.18023221	0.17785395	0.17451442	0.17457652	0.17443837	0.1789859	0.17599874

	Mat – Full Group							
Relative Volumes	Het		WT					
	Mean	SD	Mean	SD	%Diff	Effect	P-Value	FDR
amygdaloid_area	2.09262656	0.01479527	2.08536265	0.02130693	0.34832841	0.34091774	0.16034881	0.5087509
Anterior_part_of_anterior_commissure	0.09387845	0.00125638	0.0937977	0.00188303	0.0860939	0.04288515	0.85684203	0.90292405
Aqueduct	0.11453425	0.00212097	0.1142987	0.0021865	0.20608114	0.10772827	0.69297781	0.8084597
auditory_cortex	1.45717308	0.00998059	1.45169469	0.01444799	0.37737908	0.37918024	0.11869286	0.5087509
basal_forebrain	1.19726286	0.01015733	1.19225629	0.01679883	0.41992404	0.29803089	0.20176281	0.52158367
Bed_nucleus_of_stria_terminalis	0.20435617	0.00363504	0.20375079	0.00546913	0.29711924	0.11069094	0.64142928	0.78574874
caudaputamen	3.23184805	0.02354613	3.22228786	0.04185987	0.29668973	0.22838574	0.31831688	0.56717306
cerebellar_lobule_1_2	0.56606449	0.00446037	0.56804099	0.00798611	-0.347951	-0.2474928	0.27918654	0.53775834
cerebellar_lobule_10	0.23747762	0.00361917	0.24001767	0.0072741	-1.0582782	-0.3491915	0.12051217	0.5087509
cerebellar_lobule_3	0.48879938	0.00598533	0.49296943	0.01036254	-0.8459031	-0.4024151	0.08351648	0.5087509
cerebellar_lobule_4_5	1.51068661	0.01368562	1.51975294	0.03123096	-0.5965658	-0.2902993	0.18615073	0.52123923
cerebellar_lobule_6	0.6010517	0.00750956	0.60674345	0.01936585	-0.938082	-0.2939065	0.17399294	0.5087509
cerebellar_lobule_7	0.23089809	0.00475118	0.23286537	0.00797546	-0.8448133	-0.2466664	0.28778824	0.53775834
cerebellar_lobule_8	0.25935449	0.00362655	0.26216878	0.00885162	-1.0734636	-0.3179404	0.14466283	0.5087509
cerebellar_lobule_9	0.60400113	0.00796746	0.61018607	0.02020623	-1.0136139	-0.3060902	0.15795243	0.5087509
Cerebellar_White_Matter_Arbor_vita_of_cerebellum	1.89594758	0.01622193	1.91016272	0.04769031	-0.7441852	-0.298072	0.16236563	0.5087509
cerebral_peduncle	0.2051448	0.00172591	0.20423634	0.00267336	0.4448088	0.3398194	0.15321987	0.5087509
Cingulate_Cortex_area_1	1.07061202	0.00880932	1.07041343	0.014836	0.01855256	0.01338563	0.95370706	0.96351814
Cingulate_Cortex_area_2	0.66364161	0.00653502	0.66257111	0.01106025	0.16156721	0.09678779	0.67456348	0.8084597
cingulum	0.23228192	0.00156704	0.23242504	0.00242023	-0.0615757	-0.0591338	0.80197765	0.88307363
Cochlear_nucleus	0.07446888	0.00218897	0.07546685	0.00282237	-1.3224005	-0.3535937	0.16006516	0.5087509
Commisure_inferior_Colliculus	0.02204384	0.00141252	0.0217362	0.00138416	1.41529612	0.22225224	0.42744551	0.68671342
commisure_superior_collicuus	0.01315849	0.00018426	0.01309294	0.00018091	0.50063453	0.36231327	0.19764544	0.52158367
copula	0.19503496	0.00330264	0.19672948	0.00641097	-0.8613487	-0.2643167	0.24051664	0.53775834
Corpus_Callosum_associated_White_Matter	2.9361754	0.02229958	2.9280507	0.03301014	0.27747803	0.2461273	0.30467459	0.55292448
Crus_1_ansiform_lobule	1.17474341	0.01183725	1.18292606	0.0325723	-0.6917297	-0.251215	0.2407212	0.53775834
Crus_2_ansiform_lobule	0.68656847	0.00925285	0.69368104	0.02403829	-1.0282209	-0.2967171	0.16962401	0.5087509
dentate_gyrus	1.14614007	0.00764735	1.14355256	0.00894431	0.22626924	0.28929097	0.26587565	0.53775834
Dentate_nucleus	0.05888588	0.00166238	0.05977793	0.00228574	-1.4922751	-0.3902676	0.11408478	0.5087509
Dorsal_Peduncular_Cortex	0.10545563	0.00188509	0.10618796	0.00123866	-0.6896525	-0.5912256	0.09742638	0.5087509
Dorsal_Tenia_Tecta	0.07345894	0.00098046	0.07401575	0.00111603	-0.7522948	-0.4989252	0.06056589	0.5087509
Endopiriform_Nucleus	0.62227518	0.0094346	0.61866097	0.01294927	0.58419997	0.27910589	0.2558822	0.53775834
entopeduncular_nucleus	0.01547141	0.00056268	0.01562302	0.00058199	-0.9704165	-0.260502	0.34078676	0.59638015
external_medullary_lamina	0.04568961	0.00055079	0.04535768	0.00080947	0.73179916	0.41005485	0.09078522	0.5087509
Fasciculus_retroflexus	0.0163487	0.00087615	0.01618894	0.00110487	0.98685915	0.14459842	0.56551106	0.71974142
fastigial_nucleus	0.07210149	0.00123497	0.07238753	0.00182332	-0.3951526	-0.1568796	0.51196478	0.68947378
Fimbria	0.33028282	0.00347244	0.32906362	0.00379766	0.37050788	0.32104128	0.23014113	0.53775834
flocculus	0.73901343	0.00709657	0.74267221	0.01289578	-0.4926515	-0.2837196	0.214162	0.53775834
Fornix	0.04014821	0.00102287	0.03993824	0.00085486	0.52574655	0.24562302	0.41953975	0.68524108
Fourth_ventricle	0.19745812	0.00345376	0.19925179	0.0056678	-0.9002059	-0.3164679	0.17650562	0.5087509
Frontal_Association_Cortex	7.89642205	0.09831553	7.94876762	0.1155401	-0.658537	-0.4530512	0.08353947	0.5087509
Globus_pallidus	0.31014864	0.00264657	0.30979483	0.00359935	0.11420532	0.0982961	0.68827336	0.8084597
hindbrain_medulla_pons	6.5654772	0.05622924	6.61706288	0.14441637	-0.7795857	-0.3572011	0.1000855	0.5087509
Hippocampal_layer_CA1	1.4439653	0.00914029	1.43888626	0.01324372	0.35298384	0.38350528	0.11454886	0.5087509
Hippocampal_layer_CA2	0.15860694	0.00318065	0.15750402	0.00367764	0.70025036	0.29989992	0.25108261	0.53775834
Hippocampal_layer_CA3	1.43540871	0.00986737	1.43084268	0.01361555	0.31911493	0.33535427	0.17268756	0.5087509
hypothalamus	1.93059916	0.01446422	1.92279291	0.02098601	0.40598511	0.37197413	0.12544288	0.5087509
Inferior_Colliculus	1.07170891	0.00910999	1.07633407	0.0124277	-0.4297137	-0.3721649	0.13239341	0.5087509
Infralimbic_Cortex	0.10428439	0.00191761	0.1046324	0.00176703	-0.3325984	-0.1969442	0.4948409	0.68947378
Insular_Cortex	1.67891377	0.01427001	1.67439472	0.01976171	0.26989155	0.22867705	0.34954464	0.60095003
Internal_capsule	0.55071866	0.00586433	0.54731554	0.0080428	0.62178322	0.42312571	0.08760993	0.5087509
interposed_nucleus	0.08749777	0.00126883	0.08806662	0.0029841	-0.6459269	-0.1906255	0.38097303	0.63281358
intrabulbar_part_of_anterior_commisure	0.18538294	0.00440648	0.18549978	0.00709112	-0.062983	-0.016476	0.94367152	0.96333514
Lateral_olfactory_tract	0.16571694	0.00250621	0.16612433	0.00199484	-0.2452287	-0.2042195	0.51349152	0.68947378
lateral_septum	0.6708603	0.00618577	0.67017695	0.00846586	0.10196519	0.08071798	0.74124127	0.85199603
Lateral_ventricle	0.95974945	0.00797282	0.95548637	0.01165264	0.44616843	0.36584656	0.13083114	0.5087509
mamillary_bodies	0.1145806	0.00310079	0.11354233	0.003717	0.91443235	0.27932922	0.27795277	0.5377534
mammilothalamic_tract	0.02430876	0.00033034	0.02441537	0.00033587	-0.4366317	-0.3173973	0.2504609	0.53775834
medial_septum	0.09212784	0.00165328	0.09209156	0.00142208	0.03939384	0.02551088	0.93189876	0.96333514
median_preoptic_area	0.00356833	0.00012026	0.00348417	0.00013954	2.41565904	0.60317882	0.02233924	0.5087509
midbrain	2.37359863	0.01406428	2.37074374	0.01714718	0.1204217	0.16649327	0.51359647	0.68947378
Navicular_nuclear_basin_forebrain	0.12111021	0.00140429	0.12140903	0.00149824	-0.2378909	-0.1927737	0.4738914	0.68947378
Nucleus_accumbens	0.49071238	0.00472235	0.49120265	0.00650414	-0.0998107	-0.0753786	0.75731006	0.85199603
Occipital_Cortex	0.93194626	0.00731562	0.93557066	0.01219901	-0.3874005	-0.2971066	0.20225132	0.52158367
Olfactory_Bulb	9.59275498	0.4292816	9.51137197	0.45554954	0.85563904	0.178648	0.50773901	0.68947378
Olfactory_tubercle	0.83584826	0.00714768	0.83644237	0.01212337	-0.071078	-0.0490051	0.83144821	0.90215429
Optic_Chiasm	0.01778774	0.00045476	0.01781584	0.00054526	-0.1577551	-0.0515452	0.84042395	0.90215429
Optic_tract	0.20644296	0.00715989	0.20510099	0.00231338	0.6542998	0.58009303	0.03430278	0.5087509
Orbitofrontal_Cortex	0.03119344	0.00077741	0.03113095	0.00071148	0.20073379	0.08783161	0.76118179	0.85199603
paraflocculus	0.8378837	0.00879888	0.84537468	0.02066494	-0.8861134	-0.3624971	0.09902498	0.5087509
paramedian_lobe	0.54806549	0.00719612	0.55494884	0.01877794	-1.2403562	-0.3665653	0.09113788	0.5087509
Parietal_Association_Cortex	0.75911038	0.00506729	0.75663131	0.00747321	0.32764468	0.33172644	0.1687596	0.5087509
Periaqueductal_grey	0.70642186	0.00826406	0.70907734	0.00921959	-0.374497	-0.288025	0.27701904	0.53775834
Piriform_Cortex	1.89855695	0.0168744	1.89308576	0.02621845	0.28900914	0.20867712	0.37707447	0.63281358
pons	1.53520653	0.00925019	1.53728732	0.01171819	-0.1353543	-0.1775687	0.4800215	0.68947378
posterior_commissure	0.01444578	0.00059803	0.01466704	0.00066024	-1.6448967	-0.3954798	0.15306584	0.5087509
Posterior_part_of_anterior_commissure	0.0218859	0.00024582	0.02195163	0.000508	-0.2994441	-0.1293954	0.55913088	0.71974142
Prelimbic_Cortex	0.27611752	0.00313318	0.2765684	0.00460564	-0.163028	-0.0978983	0.68236244	0.8084597
Primary_Motor_Cortex	1.35181496	0.01383043	1.35448637	0.0133997	-0.1972269	-0.1993636	0.47869992	0.68947378
Primary_Somatosensory_Cortex	5.6516749	0.04015892	5.63524151	0.06657446	0.29161827	0.24684231	0.28889117	0.53775834
Primary_Visual_Cortex	1.80041376	0.00864305	1.80062171	0.01093167	-0.0115487	-0.0190225	0.9395762	0.96333514
Retrosplenial_Cortex	2.16456462	0.00950283	2.16205484	0.01418344	0.11608277	0.17695094	0.45835448	0.68947378
rhinal_cortex	3.2661122	0.01613041	3.26594664	0.01926555	0.00506632	0.00859365	0.97325495	0.9732331
Secondary_Motor_Cortex	0.82966333	0.0085728	0.82748584	0.01267995	0.2631408	0.17172409	0.47281369	0.68947378
Secondary_Somatosensory_Cortex	1.49641463	0.01092608	1.49177081	0.01809469	0.31129631	0.25664032	0.27050809	0.53775834
Secondary_Visual_Cortex	2.16921769	0.00869698	2.16743285	0.01358478	0.08234808	0.13138527	0.57669412	0.72452734
Simple_Lobule	1.15661919	0.01092382	1.16511474	0.02589368	-0.7291605	-0.3280938	0.13400547	0.5087509
stria_medullaris_thalamus	0.04387348	0.0010338	0.04351898	0.00067196	0.81457715	0.52755657	0.1409128	0.5087509
Stria_terminalis	0.17722381	0.00279978	0.17664533	0.00347843	0.32747995	0.16630413	0.51114674	0.68947378
Subfornical_organ	0.00529763	0.00018047	0.00535785	0.00013476	-1.1239455	-0.4468753	0.17183828	0.5087509
subicular_region	1.76178108	0.00744576	1.76021161	0.01139863	0.08910644	0.13760094	0.56098908	0.71974142
substantia_nigra	0.15919432	0.00360316	0.15988729	0.0041746	-0.4334138	-0.1674878	0.52082223	0.68973992
Superior_Colliculus	1.12354098	0.00619392	1.12145641	0.00781415	0.18588057	0.26676859	0.29085128	0.53775834
Temporal_Association	0.78203438	0.0066873	0.78145398	0.00730446	0.07427173	0.07945817	0.76506606	0.85199603
Thalamus	3.38963917	0.02520498	3.37487704	0.0373637	0.4374124	0.39509281	0.10201594	0.5087509
Third_ventricle	0.31690224	0.00455563	0.31621893	0.00537541	0.21608803	0.12711792	0.62200605	0.77160423
trochlear_nerve	0.00566694	0.00018629	0.00570775	0.00022209	-0.7148631	-0.1837173	0.47495834	0.68947378
ventral_pallidum	0.17667984	0.00206347	0.17655215	0.00264928	0.07231999	0.04819524	0.84692487	0.90215429

	Mat – Males							
Relative Volumes	Het		WT					
	Mean	SD	Mean	SD	%Diff	Effect	P-Value	FDR
amygdaloid_area	2.09115749	0.0128709	2.08991009	0.02801983	0.05968708	0.0445187	0.90247556	0.98701117
Anterior_part_of_anterior_commissure	0.09406832	0.00137036	0.09434382	0.00165269	-0.2920142	-0.1666963	0.6854702	0.98701117
Aqueduct	0.11342269	0.00134189	0.11374349	0.00148243	-0.2820352	-0.2163985	0.61006691	0.98701117
auditory_cortex	1.452775	0.00561746	1.45195709	0.01828932	0.0563315	0.0447206	0.89853484	0.98701117
basal_forebrain	1.19130018	0.00629344	1.19263802	0.0200542	-0.1121752	-0.0667114	0.84937169	0.98701117
Bed_nucleus_of_stria_terminalis	0.20417622	0.00268745	0.20495024	0.00398857	-0.377662	-0.1940594	0.61824832	0.98701117
caudaputamen	3.22061284	0.01745974	3.22406716	0.05180435	-0.1071417	-0.0666801	0.85013882	0.98701117
cerebellar_lobule_1_2	0.56730793	0.00470375	0.56708242	0.01070903	0.03976795	0.02105858	0.95352591	0.98701117
cerebellar_lobule_10	0.23864182	0.00387968	0.24051962	0.01025614	-0.7807264	-0.1830904	0.60821241	0.98701117
cerebellar_lobule_3	0.49269619	0.00583241	0.49231264	0.0133903	0.07790837	0.02864407	0.93675852	0.98701117
cerebellar_lobule_4_5	1.50964287	0.01678441	1.51942851	0.04371064	-0.6440344	-0.2238733	0.53199624	0.98701117
cerebellar_lobule_6	0.60133722	0.00919999	0.60797183	0.02783865	-1.0912698	-0.2383238	0.50118546	0.98701117
cerebellar_lobule_7	0.22910697	0.00371606	0.23337798	0.01102593	-1.8300805	-0.3873599	0.27936439	0.98701117
cerebellar_lobule_8	0.26004607	0.00473851	0.26209926	0.01271298	-0.7833622	-0.1615032	0.65048159	0.98701117
cerebellar_lobule_9	0.60393385	0.00981548	0.61073274	0.02890613	-1.1132357	-0.235206	0.50753147	0.98701117
Cerebellar_White_Matter_Arbor_vita_of_cerebellum	1.89976448	0.0201013	1.91345929	0.0682135	-0.7157094	-0.2007639	0.56764693	0.98701117
cerebral_peduncle	0.2049257	0.00132754	0.20446988	0.0034243	0.22292574	0.13311235	0.70954193	0.98701117
Cingulate_Cortex_area_1	1.06727187	0.00672731	1.07013769	0.01551322	-0.267799	-0.1847339	0.60983431	0.98701117
Cingulate_Cortex_area_2	0.65991018	0.00275383	0.66204534	0.01199025	-0.3225091	-0.1780743	0.60803479	0.98701117
cingulum	0.23282055	0.00177553	0.23291763	0.00286703	-0.0416838	-0.0338639	0.92920513	0.98701117
Cochlear_nucleus	0.07601828	0.00156577	0.07568691	0.00316364	0.43781816	0.10474366	0.77546045	0.98701117
Commisure_inferior_Colliculus	0.02105622	0.00100809	0.02154479	0.00106415	-2.2676797	-0.4591137	0.29247846	0.98701117
commisure_superior_collicuus	0.01307642	0.00015196	0.01316075	0.00015501	-0.6407821	-0.5440428	0.22058032	0.98701117
copula	0.19505552	0.00275894	0.19751307	0.00915126	-1.2442501	-0.2685483	0.44663102	0.98701117
Corpus_Callosum_associated_White_Matter	2.92754072	0.01223072	2.92806724	0.04156931	-0.0179817	-0.012666	0.97111492	0.98701117
Crus_1_ansiform_lobule	1.17518244	0.0129512	1.18644637	0.04696305	-0.9493837	-0.2398466	0.49405442	0.98701117
Crus_2_ansiform_lobule	0.68793252	0.01033197	0.69652116	0.03444453	-1.2330764	-0.249347	0.47922834	0.98701117
dentate_gyrus	1.14651825	0.00576011	1.14383353	0.01208957	0.23471231	0.22206901	0.54473964	0.98701117
Dentate_nucleus	0.06014652	0.00122686	0.06000971	0.00247413	0.22798591	0.05529779	0.88024386	0.98701117
Dorsal_Peduncular_Cortex	0.10669325	0.00143774	0.1062025	0.0014619	0.46208513	0.33568979	0.44494683	0.98701117
Dorsal_Tenia_Tecta	0.07408563	0.00096365	0.07423895	0.00076655	-0.206527	-0.2000163	0.68216869	0.98701117
Endopiriform_Nucleus	0.61498632	0.00472076	0.61786426	0.01363242	-0.4657869	-0.2111093	0.55211184	0.98701117
entopeduncular_nucleus	0.01538808	0.00023283	0.01548183	0.00050462	-0.6055406	-0.1857804	0.6104216	0.98701117
external_medullary_lamina	0.04554083	0.00040272	0.04540997	0.00089708	0.28816715	0.14587029	0.68778607	0.98701117
Fasciculus_retroflexus	0.01590637	0.00032192	0.01605438	0.00069539	-0.9219507	-0.2128492	0.55998458	0.98701117
fastigial_nucleus	0.07193925	0.00111389	0.07248529	0.00232862	-0.7533163	-0.2344925	0.52290654	0.98701117
Fimbria	0.32949544	0.00204609	0.32956812	0.0045989	-0.0220541	-0.0158045	0.96516345	0.98701117
flocculus	0.73870747	0.00776391	0.74060232	0.01638065	-0.255853	-0.1156763	0.75140752	0.98701117
Fornix	0.04001396	0.00065457	0.04008745	0.00093564	-0.1833209	-0.0785438	0.84114917	0.98701117
Fourth_ventricle	0.19922673	0.00258073	0.19969076	0.00746441	-0.2323718	-0.062165	0.86042375	0.98701117
Frontal_Association_Cortex	7.88089673	0.11130498	7.94892699	0.11097893	-0.8558419	-0.6130015	0.17332241	0.98701117
Globus_pallidus	0.3100683	0.00218406	0.31007984	0.00449418	-0.0037222	-0.0025682	0.99439995	0.99440484
hindbrain_medulla_pons	6.57198779	0.07232237	6.61804058	0.20811916	-0.6958674	-0.2212808	0.53340861	0.98701117
Hippocampal_layer_CA1	1.44125731	0.00566997	1.43822461	0.01650651	0.21086458	0.18372789	0.60421556	0.98701117
Hippocampal_layer_CA2	0.15635812	0.00145061	0.15741434	0.00356899	-0.6709799	-0.2959429	0.4129048	0.98701117
Hippocampal_layer_CA3	1.43747847	0.00952071	1.43402203	0.01651163	0.24103107	0.20933355	0.57911781	0.98701117
hypothalamus	1.92593919	0.01169757	1.92643551	0.02819187	-0.0257637	-0.0176051	0.96089998	0.98701117
Inferior_Colliculus	1.07522517	0.00837592	1.0728175	0.0147713	0.2244244	0.16299613	0.66439729	0.98701117
Infralimbic_Cortex	0.10465884	0.00195332	0.10516374	0.00184942	-0.4801155	-0.2730091	0.54514582	0.98701117
Insular_Cortex	1.67993668	0.01224108	1.67680701	0.02337979	0.18664465	0.1338622	0.71787616	0.98701117
Internal_capsule	0.54784397	0.00342557	0.54803015	0.01007934	-0.0339736	-0.018472	0.95826396	0.98701117
interposed_nucleus	0.08801867	0.00068177	0.08883012	0.00324103	-0.9134915	-0.25037	0.47108484	0.98701117
intrabulbar_part_of_anterior_commisure	0.1831743	0.00485892	0.18469749	0.00550604	-0.8246961	-0.2766405	0.51163292	0.98701117
Lateral_olfactory_tract	0.16452513	0.00136178	0.16641103	0.00210735	-1.1332795	-0.8949165	0.0287609	0.98701117
lateral_septum	0.67188022	0.00513024	0.6707869	0.0101856	0.16299046	0.10733963	0.77061809	0.98701117
Lateral_ventricle	0.95481403	0.00722148	0.95692946	0.01603288	-0.2210649	-0.1319436	0.71624083	0.98701117
mamillary_bodies	0.11275463	0.00130402	0.11310181	0.00317303	-0.3069577	-0.1094143	0.76064925	0.98701117
mammilothalamic_tract	0.02433022	0.00038259	0.02451054	0.00035988	-0.7356512	-0.5010349	0.27329585	0.98701117
medial_septum	0.09245656	0.0013566	0.09217012	0.00167039	0.31077375	0.1714813	0.67502688	0.98701117
median_preoptic_area	0.00350585	9.53E-05	0.00352956	0.00013972	-0.6717825	-0.1697088	0.66368813	0.98701117
midbrain	2.37848479	0.01362009	2.36923923	0.01854337	0.39023335	0.4985911	0.21760988	0.98701117
Navicular_nuclear_basin_forebrain	0.12167592	0.00111278	0.12144637	0.00150689	0.18901733	0.15233634	0.70182679	0.98701117
Nucleus_accumbens	0.49189768	0.00411105	0.49078137	0.00770298	0.22745535	0.14491914	0.69663963	0.98701117
Occipital_Cortex	0.93457924	0.00799652	0.93309146	0.01559083	0.15944558	0.09542619	0.79596256	0.98701117
Olfactory_Bulb	9.63631726	0.38322541	9.482081	0.33318956	1.62660771	0.46290845	0.32708337	0.98701117
Olfactory_tubercle	0.83493137	0.00534821	0.83556849	0.01320652	-0.0762501	-0.048243	0.89289447	0.98701117
Optic_Chiasm	0.01767054	0.00040059	0.01795811	0.00054772	-1.6013122	-0.5250267	0.19467222	0.98701117
Optic_tract	0.20498394	0.00145507	0.20546788	0.00287889	-0.2353339	-0.1681015	0.64862746	0.98701117
Orbitofrontal_Cortex	0.03078371	0.00046259	0.03108851	0.00082438	-0.9804193	-0.3697316	0.32891467	0.98701117
paraflocculus	0.84266203	0.00995535	0.84591286	0.02932405	-0.3842982	-0.1108588	0.75374107	0.98701117
paramedian_lobe	0.55225607	0.00877141	0.55668437	0.02657388	-0.7954764	-0.1666408	0.63711394	0.98701117
Parietal_Association_Cortex	0.75942737	0.00510107	0.75864057	0.00925319	0.10371272	0.08503083	0.81978007	0.98701117
Periaqueductal_grey	0.71307163	0.00674664	0.70844843	0.00844527	0.65258123	0.54743072	0.18738835	0.98701117
Piriform_Cortex	1.89032627	0.00852041	1.89332348	0.03148243	-0.1583043	-0.0952027	0.78480481	0.98701117
pons	1.5391036	0.00900916	1.53401956	0.01099135	0.33141951	0.4625493	0.26595071	0.98701117
posterior_commissure	0.01494243	0.00043738	0.01464722	0.00042206	2.01703315	0.6999905	0.12731286	0.98701117
Posterior_part_of_anterior_commissure	0.02202154	0.00022901	0.02204293	0.00040511	-0.097041	-0.052802	0.88793116	0.98701117
Prelimbic_Cortex	0.27639611	0.00287601	0.27634632	0.00448676	0.01801703	0.01109695	0.97693852	0.98701117
Primary_Motor_Cortex	1.35796776	0.01355429	1.35670805	0.01550205	0.0928504	0.08126077	0.84589259	0.98701117
Primary_Somatosensory_Cortex	5.6392242	0.03200005	5.64083705	0.08475717	-0.0285924	-0.0190291	0.95736156	0.98701117
Primary_Visual_Cortex	1.80192813	0.0079122	1.79816972	0.01006715	0.20901357	0.37333477	0.36071847	0.98701117
Retrosplenial_Cortex	2.16418897	0.0067951	2.16127673	0.01524494	0.13474584	0.19102938	0.5989305	0.98701117
rhinal_cortex	3.27014484	0.01294456	3.26253759	0.01958725	0.23316972	0.38837754	0.32102907	0.98701117
Secondary_Motor_Cortex	0.8285791	0.00792429	0.82660251	0.01440055	0.23912269	0.1372582	0.71325688	0.98701117
Secondary_Somatosensory_Cortex	1.49654622	0.0099432	1.49549333	0.02112653	0.07040463	0.04983763	0.89122924	0.98701117
Secondary_Visual_Cortex	2.17042769	0.00948967	2.16636563	0.01364518	0.18750571	0.29769189	0.44989486	0.98701117
Simple_Lobule	1.1599005	0.01337499	1.16425253	0.03672504	-0.3738047	-0.1185031	0.73875826	0.98701117
stria_medullaris_thalamus	0.04395208	0.00054573	0.04349042	0.00079658	1.06150923	0.57954946	0.1477379	0.98701117
Stria_terminalis	0.17605557	0.00078391	0.17631481	0.0029805	-0.1470288	-0.0869766	0.80271843	0.98701117
Subfornical_organ	0.00538972	0.0001376	0.00535729	0.00011229	0.6051852	0.28873442	0.55025033	0.98701117
subicular_region	1.76276471	0.00706893	1.7591343	0.01076778	0.20637441	0.33715442	0.38683562	0.98701117
substantia_nigra	0.16208263	0.00255059	0.16030052	0.0028538	1.11172975	0.62446838	0.14877343	0.98701117
Superior_Colliculus	1.12286946	0.00467519	1.12095894	0.0069305	0.17043613	0.27566814	0.48052877	0.98701117
Temporal_Association	0.78364483	0.00514399	0.78171653	0.00693578	0.24667517	0.27802224	0.48710072	0.98701117
Thalamus	3.37933325	0.01658742	3.37988494	0.04962237	-0.0163229	-0.0111178	0.97484287	0.98701117
Third_ventricle	0.31469386	0.00221176	0.3161685	0.00648651	-0.4664093	-0.2273394	0.52180318	0.98701117
trochlear_nerve	0.00573993	0.00014125	0.00571168	0.00019431	0.49456536	0.14537282	0.71366868	0.98701117
ventral_pallidum	0.17649938	0.0014315	0.17637495	0.00269904	0.07054818	0.04610135	0.90102929	0.98701117

	Mat – Females							
Relative Volumes	Het		WT					
	Mean	SD	Mean	SD	%Diff	Effect	P-Value	FDR
amygdaloid_area	2.09345291	0.01612033	2.08142154	0.01291306	0.57803636	0.93172155	0.0299089	0.15475334
Anterior_part_of_anterior_commissure	0.09377165	0.00122075	0.0933244	0.00199504	0.47924932	0.22418383	0.4543083	0.62709006
Aqueduct	0.11515949	0.00225365	0.11477988	0.00260809	0.33073386	0.14555342	0.66717351	0.81727848
auditory_cortex	1.45964701	0.01115417	1.45146728	0.01075851	0.56354874	0.76030267	0.04689831	0.18382825
basal_forebrain	1.20061687	0.01051755	1.19192546	0.01411643	0.72919105	0.61569476	0.06059958	0.21209371
Bed_nucleus_of_stria_terminalis	0.20445739	0.00415444	0.20271126	0.00644643	0.86138734	0.27086768	0.37429456	0.57313683
caudaputamen	3.23816786	0.02462009	3.2207458	0.03276496	0.5409327	0.53172863	0.10354153	0.23932684
cerebellar_lobule_1_2	0.56536505	0.0043107	0.56887175	0.00480702	-0.616432	-0.7294973	0.04079907	0.17384123
cerebellar_lobule_10	0.23682275	0.00341454	0.23958265	0.00338342	-1.1519604	-0.8157134	0.03158223	0.15475334
cerebellar_lobule_3	0.48660742	0.00499401	0.49353864	0.00725678	-1.4043913	-0.9551368	0.00411533	0.06721688
cerebellar_lobule_4_5	1.51127372	0.01218211	1.52003411	0.01559551	-0.5763286	-0.561725	0.09082759	0.2282415
cerebellar_lobule_6	0.60089109	0.00670909	0.60567885	0.00750941	-0.7904779	-0.6375679	0.07096524	0.22032968
cerebellar_lobule_7	0.2319056	0.005074	0.23242111	0.00424419	-0.221801	-0.1214631	0.76199946	0.88900305
cerebellar_lobule_8	0.25896548	0.00293588	0.26222903	0.00354486	-1.2445421	-0.9206419	0.00901912	0.08543
cerebellar_lobule_9	0.60403898	0.00708386	0.60971228	0.00840855	-0.9304871	-0.6747055	0.05093251	0.19197702
Cerebellar_White_Matter_Arbor_vita_of_cerebellum	1.89380057	0.01385221	1.9073057	0.01947008	-0.7080738	-0.6936353	0.03316284	0.15476452
cerebral_peduncle	0.20526805	0.0019445	0.20403394	0.00190737	0.60485528	0.64702347	0.08517943	0.22032968
Cingulate_Cortex_area_1	1.07249085	0.00946416	1.0706524	0.01476753	0.17171285	0.1244926	0.68087454	0.82374789
Cingulate_Cortex_area_2	0.66574053	0.00715768	0.66302678	0.01059308	0.4092982	0.256182	0.40740031	0.5958983
cingulum	0.23197895	0.00140557	0.23199813	0.00195715	-0.0082663	-0.0097988	0.97509287	0.98254429
Cochlear_nucleus	0.07359734	0.00202692	0.07527614	0.00258841	-2.230185	-0.6485822	0.05295717	0.1922144
Commisure_inferior_Colliculus	0.02259937	0.00131754	0.02190209	0.00163119	3.18358499	0.42746289	0.19938282	0.39311244
commisure_superior_collicuus	0.01320465	0.00018893	0.01303417	0.00018589	1.30795757	0.91709505	0.01708266	0.10881793
copula	0.19502339	0.00365949	0.19605037	0.00253359	-0.5238352	-0.4053466	0.37424536	0.57313683
Corpus_Callosum_associated_White_Matter	2.94103241	0.02541563	2.92803637	0.02490694	0.44384814	0.52178362	0.16153924	0.33683069
Crus_1_ansiform_lobule	1.17449645	0.01159975	1.17987512	0.01158418	-0.4558678	-0.4643117	0.2068944	0.39755139
Crus_2_ansiform_lobule	0.68576994	0.00884621	0.6912196	0.00913714	-0.7884134	-0.5964307	0.1023144	0.23932684
dentate_gyrus	1.14592735	0.00870297	1.14330906	0.00537328	0.22900969	0.48727911	0.32576414	0.55040006
Dentate_nucleus	0.05817677	0.0014591	0.05957706	0.00217626	-2.3503835	-0.6434383	0.04296943	0.17545869
Dorsal_Peduncular_Cortex	0.10475947	0.00177405	0.10617535	0.00106148	-1.3335324	-1.3338698	0.01220487	0.08543
Dorsal_Tenia_Tecta	0.07310642	0.00082135	0.07382231	0.00134613	-0.9697498	-0.5318131	0.08216832	0.22032968
Endopiriform_Nucleus	0.62637517	0.00898476	0.61935145	0.01276697	1.134044	0.55014758	0.08543292	0.22032968
entopeduncular_nucleus	0.01551828	0.0006864	0.01574538	0.00063277	-1.4423275	-0.3588966	0.34703169	0.55571808
external_medullary_lamina	0.0457733	0.00061493	0.04531236	0.00075443	1.01723842	0.61097318	0.07160346	0.22032968
Fasciculus_retroflexus	0.01659752	0.00099474	0.01630556	0.00138145	1.79053673	0.21134149	0.50278079	0.66584375
fastigial_nucleus	0.07219275	0.00132433	0.07230281	0.00132179	-0.1522138	-0.0832622	0.81859714	0.91154698
Fimbria	0.33072573	0.00405937	0.32862638	0.00304051	0.63882534	0.69045949	0.11585523	0.24886078
flocculus	0.73918553	0.00695283	0.74446612	0.00912709	-0.7093123	-0.5785621	0.07919708	0.22032968
Fornix	0.04022373	0.00119524	0.03980893	0.00078767	1.04198951	0.52661943	0.26666203	0.49306943
Fourth_ventricle	0.19646327	0.00354978	0.19887136	0.00372311	-1.2108771	-0.6467938	0.0754909	0.22032968
Frontal_Association_Cortex	7.90515504	0.09290952	7.94862951	0.12324203	-0.546943	-0.3527569	0.27455525	0.49827244
Globus_pallidus	0.31019383	0.00294225	0.30954783	0.00274448	0.20869035	0.23537997	0.53297263	0.6964144
hindbrain_medulla_pons	6.56181499	0.04721665	6.61621554	0.05563153	-0.8222306	-0.9778725	0.00635312	0.07782639
Hippocampal_layer_CA1	1.44548854	0.01047145	1.4394597	0.01019626	0.41882679	0.59127991	0.11554001	0.24886078
Hippocampal_layer_CA2	0.1598719	0.00321295	0.15758174	0.00389255	1.45331736	0.58834515	0.08368495	0.22032968
Hippocampal_layer_CA3	1.43424448	0.01016978	1.4280872	0.01031103	0.43115235	0.59714983	0.10501387	0.23932684
hypothalamus	1.9332204	0.01553724	1.91963599	0.01204687	0.70765544	1.12762936	0.01125289	0.08543
Inferior_Colliculus	1.06973102	0.0091531	1.07938176	0.00945557	-0.8940986	-1.0206402	0.00727071	0.07917716
Infralimbic_Cortex	0.10407376	0.00192801	0.10417189	0.00161265	-0.0942	-0.0608501	0.87933524	0.93424427
Insular_Cortex	1.67833839	0.01564977	1.67230407	0.01656932	0.36083834	0.36418597	0.30563573	0.52546968
Internal_capsule	0.55233568	0.0064046	0.54669622	0.0060653	1.03155256	0.92979075	0.0177659	0.10881793
interposed_nucleus	0.08720477	0.00144001	0.08740491	0.00267574	-0.2289862	-0.0747999	0.79541703	0.90961994
intrabulbar_part_of_anterior_commisure	0.18662531	0.00372861	0.1861951	0.00835913	0.2310557	0.05146639	0.85286896	0.92867716
Lateral_olfactory_tract	0.16638734	0.00278011	0.16587585	0.00193016	0.30835498	0.2649965	0.55901268	0.72081903
lateral_septum	0.6702866	0.00679778	0.66964833	0.00697509	0.09531339	0.09150631	0.79824347	0.90961994
Lateral_ventricle	0.96252563	0.00714537	0.9542357	0.00615859	0.86875098	1.34607609	0.00174123	0.05687824
mamillary_bodies	0.11560771	0.00336915	0.11392412	0.00420466	1.47781297	0.40040914	0.227035	0.42787302
mammilothalamic_tract	0.02429669	0.00031001	0.02433289	0.00030142	-0.1487609	-0.1200914	0.74432499	0.87885327
medial_septum	0.09194293	0.00181398	0.09202348	0.00122387	-0.0875239	-0.0658099	0.88656833	0.93424427
median_preoptic_area	0.00360348	0.00012096	0.00344483	0.00013133	4.60556537	1.20808765	0.00151824	0.05687824
midbrain	2.37085016	0.01397022	2.37204765	0.01638267	-0.0504832	-0.0730946	0.82783381	0.91154698
Navicular_nuclear_basin_forebrain	0.12080762	0.00148503	0.12137667	0.00154284	-0.4688308	-0.3688343	0.30404369	0.52546968
Nucleus_accumbens	0.49004565	0.00503489	0.49156776	0.00551535	-0.309645	-0.2759778	0.42834323	0.60837743
Occipital_Cortex	0.93046521	0.00671017	0.9377193	0.00824615	-0.7735892	-0.8796948	0.01160428	0.08543
Olfactory_Bulb	9.5682512	0.46340802	9.53675747	0.55098497	0.33023512	0.05715895	0.86413189	0.93060217
Olfactory_tubercle	0.83636401	0.00810553	0.83719972	0.01151669	-0.0998224	-0.0725654	0.81595481	0.91154698
Optic_Chiasm	0.01785366	0.00048211	0.01769255	0.00053024	0.91062832	0.30384918	0.38286202	0.57723391
Optic_tract	0.20726367	0.00208311	0.20478301	0.00172738	1.21135712	1.43680213	0.00118448	0.05687824
Orbitofrontal_Cortex	0.03142392	0.00083394	0.03116774	0.00062499	0.82194138	0.4098942	0.34368672	0.55571808
paraflocculus	0.83519589	0.00704355	0.84490826	0.00927455	-1.1495172	-1.0472064	0.00258742	0.06339279
paramedian_lobe	0.54570829	0.00503566	0.55344471	0.00833818	-1.3978662	-0.9278305	0.00376308	0.06721688
Parietal_Association_Cortex	0.75893207	0.00520691	0.75488996	0.00522695	0.535456	0.77331928	0.03951617	0.17384123
Periaqueductal_grey	0.70268137	0.00659849	0.70962239	0.010105	-0.9781286	-0.6868894	0.03021361	0.15475334
Piriform_Cortex	1.90318671	0.01879797	1.89287974	0.0218189	0.54451289	0.4723875	0.1686314	0.34427862
pons	1.53301443	0.00899953	1.54011937	0.01194837	-0.4613239	-0.5946366	0.06947483	0.22032968
posterior_commisure	0.01413503	0.00046878	0.01408421	0.00075123	-3.7399115	-0.7316395	0.02013039	0.11604401
Posterior_part_of_anterior_commissure	0.0218096	0.00022686	0.0218725	0.0005853	-0.2875918	-0.1074725	0.69249811	0.82762568
Prelimbic_Cortex	0.27596081	0.00335003	0.27676087	0.00485469	-0.2890808	-0.1648021	0.59533785	0.74799072
Primary_Motor_Cortex	1.34835401	0.01313678	1.35256092	0.0114778	-0.3110327	-0.3665255	0.35158525	0.55571808
Primary_Somatosensory_Cortex	5.65867842	0.04346166	5.63039204	0.04833156	0.50238743	0.58525696	0.09691067	0.23742866
Primary_Visual_Cortex	1.79956192	0.00916436	1.80274677	0.01154021	-0.1766661	-0.275978	0.40023224	0.59432276
Retrosplenial_Cortex	2.16477592	0.01094202	2.16272921	0.01370089	0.09463579	0.14938563	0.64817957	0.80406475
rhinal_cortex	3.26384383	0.01765481	3.26890114	0.01915242	-0.1547097	-0.2640557	0.45042214	0.62709006
Secondary_Motor_Cortex	0.83027316	0.00911022	0.8282514	0.01144441	0.24409913	0.17665864	0.58925577	0.74799072
Secondary_Somatosensory_Cortex	1.49634062	0.01175845	1.48854462	0.01499536	0.52373254	0.5198938	0.1168124	0.24886078
Secondary_Visual_Cortex	2.16853707	0.00846278	2.16835778	0.01394073	0.0082685	0.01286093	0.96551544	0.98254429
Simple_Lobule	1.15477345	0.00924258	1.16586199	0.01165043	-0.9511029	-0.9517717	0.00629577	0.07782639
stria_medullaris_thalamus	0.04382926	0.00124313	0.04354373	0.00057053	0.65573604	0.50046855	0.42320914	0.60837743
Stria_terminalis	0.17788094	0.00330678	0.17693178	0.00394095	0.53645364	0.24084468	0.4723427	0.64291319
Subfornical_organ	0.00524584	0.00018456	0.00535834	0.0001556	-2.0995248	-0.722984	0.07777977	0.22032968
subicular_region	1.76122779	0.00781955	1.76114715	0.01221394	0.00457856	0.00660191	0.98256844	0.98254429
substantia_nigra	0.15756965	0.00307926	0.15952917	0.00507323	-1.2283134	-0.3862468	0.20056887	0.39311244
Superior_Colliculus	1.12391872	0.00702164	1.12188756	0.00872704	0.18104819	0.232743	0.47959882	0.64380435
Temporal_Association	0.78112849	0.00741675	0.78122643	0.00784519	-0.012536	-0.0124834	0.97174263	0.98254429
Thalamus	3.39543625	0.02775156	3.37053686	0.02320115	0.73873675	1.07319673	0.01143904	0.08543
Third_ventricle	0.31814445	0.00510146	0.31626263	0.0044337	0.5950184	0.42443605	0.28341055	0.50499488
trochlear_nerve	0.00562589	0.00019973	0.00570433	0.00025047	-1.3751972	-0.3131886	0.34140393	0.55571808
ventral_pallidum	0.17678134	0.00238521	0.17670573	0.00269025	0.04279011	0.02810616	0.93448034	0.97424164

	Pat – Full Group							
Relative Volumes	Het		WT					
	Mean	SD	Mean	SD	%Diff	Effect	P-Value	FDR
amygdaloid_area	2.09107798	0.02470275	2.09328296	0.01771184	-0.105336	-0.1244918	0.68618446	0.95658946
Anterior_part_of_anterior_commissure	0.09377844	0.00116703	0.09386217	0.0016734	-0.0892041	-0.0500352	0.83169718	0.95658946
Aqueduct	0.11464194	0.00236105	0.11452026	0.00241488	0.10625706	0.05039008	0.84689497	0.95658946
auditory_cortex	1.45896951	0.01978098	1.45652661	0.00902957	0.16772122	0.27054501	0.51479622	0.94940684
basal_forebrain	1.19808458	0.01602383	1.19618519	0.01322971	0.15878669	0.14356947	0.61625607	0.94940684
Bed_nucleus_of_stria_terminalis	0.20759206	0.00971043	0.20499306	0.00404467	1.26784924	0.64257512	0.15222783	0.93735435
caudaputamen	3.23594412	0.03915769	3.23212933	0.03155819	0.11802701	0.12088099	0.67657698	0.95658946
cerebellar_lobule_1_2	0.56436034	0.00373632	0.56568673	0.00860489	-0.2344741	-0.1541437	0.47970914	0.94940684
cerebellar_lobule_10	0.23808344	0.00564491	0.2381212	0.00465137	-0.0158573	-0.008118	0.97739037	0.98622648
cerebellar_lobule_3	0.48785183	0.00807282	0.48968574	0.01051959	-0.3745081	-0.174333	0.47080003	0.94940684
cerebellar_lobule_4_5	1.51358121	0.01898413	1.51052066	0.02128031	0.20261512	0.1438204	0.56951729	0.94940684
cerebellar_lobule_6	0.60483837	0.01686352	0.60269818	0.01151645	0.3551 02	0.18583791	0.55768337	0.94940684
cerebellar_lobule_7	0.2348904	0.00741819	0.23263294	0.00517968	0.97039604	0.4358305	0.16659741	0.93735435
cerebellar_lobule_8	0.26028184	0.00863067	0.25987496	0.00597992	0.15656668	0.06804063	0.82842545	0.95658946
cerebellar_lobule_9	0.60796858	0.01844977	0.60560587	0.01242582	0.39013923	0.19014496	0.55183063	0.94940684
Cerebellar_White_Matter_Arbor_vita_of_cerebellum	1.89825835	0.0346988	1.89802763	0.03275541	0.01215544	0.00704353	0.97914179	0.98622648
cerebral_peduncle	0.20611736	0.00374745	0.20555335	0.00189407	0.27438825	0.29777934	0.44005714	0.94940684
Cingulate_Cortex_area_1	1.07687471	0.0122539	1.07222206	0.01272524	0.43392586	0.36562378	0.16226496	0.93735435
Cingulate_Cortex_area_2	0.66783856	0.01128732	0.66394577	0.0097578	0.58631185	0.39894152	0.15777306	0.93735435
cingulum	0.23268809	0.00245017	0.23271631	0.00248452	-0.0121257	-0.0113577	0.96539575	0.98622648
Cochlear_nucleus	0.07367767	0.0027846	0.07471277	0.00293534	-1.3854423	-0.3526348	0.17510812	0.93735435
Commisure_inferior_Colliculus	0.02256014	0.00181508	0.02204324	0.00176537	2.34495271	0.29280261	0.27367582	0.93735435
commisure_superior_collicuus	0.01317909	0.00022283	0.0131092	0.00015682	0.53314334	0.4456856	0.15555747	0.93735435
copula	0.19664376	0.00588655	0.1958529	0.00412391	0.40380657	0.19177596	0.53933287	0.94940684
Corpus_Callosum_associated_White_Matter	2.94718581	0.03940624	2.93879986	0.02275563	0.28535309	0.36852227	0.29612341	0.93735435
Crus_1_ansiform_lobule	1.17999083	0.02407818	1.17700931	0.01904373	0.25331388	0.15656218	0.59268441	0.94940684
Crus_2_ansiform_lobule	0.68896562	0.01267428	0.68896275	0.0144301	0.14556221	0.00762391	0.83503124	0.95658946
dentate_gyrus	1.14255649	0.01343416	1.14463227	0.00958091	-0.1813495	-0.2166585	0.48386375	0.94940684
Dentate_nucleus	0.05858978	0.00231614	0.05922467	0.00244157	-1.0719915	-0.2600309	0.31563774	0.93735435
Dorsal_Peduncular_Cortex	0.1058954	0.00156855	0.10612365	0.00167574	-0.2150772	-0.1362072	0.59623872	0.94940684
Dorsal_Tenia_Tecta	0.07410983	0.00133064	0.07366869	0.00137243	0.59880686	0.32142391	0.21953274	0.93735435
Endopiriform_Nucleus	0.62532367	0.01420218	0.62766029	0.01237755	0.58928944	0.29596953	0.29102709	0.93735435
entopeduncular_nucleus	0.01560785	0.00068525	0.01553965	0.00044351	0.43885796	0.15376821	0.63820887	0.95647864
external_medullary_lamina	0.04614453	0.00156405	0.04583654	0.00080204	0.67193557	0.38400982	0.31527624	0.93735435
Fasciculus_retroflexus	0.01645633	0.0011222	0.01628602	0.00095314	1.04576853	0.17868654	0.52749764	0.94940684
fastigial_nucleus	0.07188702	0.00160309	0.07189412	0.00138349	-0.0098758	-0.005132	0.98538907	0.98622648
Fimbria	0.32907051	0.00552477	0.32999431	0.00311894	-0.2799446	-0.2961912	0.40729612	0.94940684
flocculus	0.73851411	0.00860757	0.73830866	0.01089607	0.02782624	0.01885482	0.93819406	0.98622648
Fornix	0.03965967	0.00088302	0.04026484	0.00096327	-1.502958	-0.6282395	0.0162049	0.52936513
Fourth_ventricle	0.19718155	0.00472548	0.19793687	0.00548465	-0.3815958	-0.1377151	0.58167193	0.94940684
Frontal_Association_Cortex	8.00023847	0.14602239	7.94667621	0.10890313	0.67402092	0.491834	0.10655582	0.93735435
Globus_pallidus	0.30990164	0.00340973	0.31070192	0.00308789	-0.2575697	-0.2591654	0.34644946	0.94525784
hindbrain_medulla_pons	6.58787557	0.10818524	6.58214987	0.10574414	0.08698819	0.05414667	0.8384826	0.95658946
Hippocampal_layer_CA1	1.44378653	0.01932248	1.44240992	0.0085518	0.09543818	0.16097303	0.70466486	0.95658946
Hippocampal_layer_CA2	0.1598178	0.00476291	0.15847292	0.00357767	0.84865504	0.37591135	0.21356098	0.93735435
Hippocampal_layer_CA3	1.4342023	0.01709599	1.43507309	0.01413294	-0.0606791	-0.0616142	0.82945548	0.95658946
hypothalamus	1.929174	0.02397232	1.9308784	0.01524385	-0.0882707	-0.111809	0.73506125	0.95658946
Inferior_Colliculus	1.06796703	0.01060319	1.0722969	0.01484243	-0.4037943	-0.2917226	0.22084516	0.93735435
Infralimbic_Cortex	0.10386289	0.00166629	0.10458529	0.00220414	-0.6907263	-0.3604531	0.14786381	0.93735435
Insular_Cortex	1.67844183	0.01770736	1.67975157	0.01672413	-0.0779721	-0.0783143	0.77131709	0.95658946
Internal_capsule	0.55272584	0.00943999	0.55110521	0.00597497	0.29406885	0.27123636	0.4141264	0.94940684
interposed_nucleus	0.08805643	0.00251484	0.08803701	0.00204296	0.0220571	0.00950501	0.97371161	0.98622648
intrabulbar_part_of_anterior_commisure	0.18738278	0.00588626	0.18568886	0.00538431	0.91223408	0.3146022	0.25188171	0.93735435
Lateral_olfactory_tract	0.16852296	0.00392047	0.16630654	0.00239715	1.33273025	0.92460606	0.00802888	0.52936513
lateral_septum	0.6709398	0.00752626	0.67210729	0.00744779	-0.1737059	-0.1567565	0.553696	0.94940684
Lateral_ventricle	0.9651722	0.01978721	0.96090432	0.00898823	0.44415295	0.4748305	0.25645106	0.93735435
mamillary_bodies	0.11551231	0.00397332	0.11418851	0.00350383	1.15931456	0.37781592	0.17670858	0.93735435
mammilothalamic_tract	0.02426813	0.00059679	0.0243996	0.00052503	-0.538846	-0.2504164	0.36898928	0.94940684
medial_septum	0.09141125	0.00166769	0.09229057	0.00138716	-0.9527752	-0.6339028	0.02938739	0.57603268
median_preoptic_area	0.00349178	0.00015152	0.00352535	0.00012845	-0.9520557	-0.2612895	0.35687978	0.94525784
midbrain	2.36575325	0.02411868	2.37201502	0.02294344	-0.2639854	-0.2729221	0.31160213	0.93735435
Navicular_nuclear_basin_forebrain	0.12119177	0.00117417	0.12106256	0.00148467	0.10672469	0.08702525	0.72065201	0.95658946
Nucleus_accumbens	0.49232051	0.00425699	0.4920945	0.00516712	0.0459292	0.04374101	0.85899124	0.95658946
Occipital_Cortex	0.92976742	0.00642284	0.93239173	0.01434523	-0.2814606	-0.1829399	0.40357156	0.94940684
Olfactory_Bulb	9.3958252	0.46140263	9.4739384	0.56785287	-0.8270677	-0.1379862	0.57405473	0.94940684
Olfactory_tubercle	0.83824193	0.00776033	0.8372924	0.00923698	0.1134044	0.10279621	0.67830937	0.95658946
Optic_Chiasm	0.01761648	0.00047678	0.01779599	0.00057149	-1.0086818	-0.3141016	0.20680233	0.93735435
Optic_tract	0.20805701	0.00358602	0.20577058	0.00213363	0.13919892	0.13424539	0.69681237	0.95658946
Orbitofrontal_Cortex	0.03202236	0.00150088	0.03133784	0.00083835	2.18431239	0.8165033	0.0259563	0.57603268
paraflocculus	0.83884427	0.01653091	0.83921798	0.01697092	-0.0445304	-0.0220204	0.93265363	0.98622648
paramedian_lobe	0.54919786	0.01768898	0.54979327	0.01320053	-0.108298	-0.0451054	0.88100059	0.966005
Parietal_Association_Cortex	0.75920191	0.00909902	0.7591653	0.00732682	0.00482261	0.00499693	0.98623804	0.98622648
Periaqueductal_grey	0.70397322	0.01154301	0.70733195	0.01420946	-0.4748456	-0.2363731	0.33683112	0.94525784
Piriform_Cortex	1.90203995	0.0248641	1.89942554	0.01901663	0.13764185	0.13747987	0.64417599	0.95647864
pons	1.53192357	0.01214362	1.53686903	0.01683499	-0.3217879	-0.2937607	0.21876691	0.93735435
posterior_commisure	0.01425523	0.00078232	0.01434652	0.00085941	-1.7994495	-0.3040342	0.23466367	0.93735435
Posterior_part_of_anterior_commissure	0.02204258	0.00045363	0.0219926	0.00050753	0.22726252	0.09847838	0.69691737	0.95658946
Prelimbic_Cortex	0.27865518	0.00264352	0.2772957	0.00358251	0.49026263	0.37947578	0.11571384	0.93735435
Primary_Motor_Cortex	1.35466954	0.01110638	1.35584837	0.01405227	-0.0869443	-0.0838892	0.73026222	0.95658946
Primary_Somatosensory_Cortex	5.65760884	0.06221597	5.65422844	0.04950776	0.05978541	0.06828028	0.81478992	0.95658946
Primary_Visual_Cortex	1.79860977	0.0157181	1.8015716	0.01396703	-0.1644025	-0.2120586	0.44432316	0.94940684
Retrosplenial_Cortex	2.16809662	0.02300105	2.16723514	0.01267508	0.03975018	0.06796643	0.85118324	0.95658946
rhinal_cortex	3.2632199	0.02937918	3.26882574	0.02539489	-0.171494	-0.2207468	0.43171264	0.94940684
Secondary_Motor_Cortex	0.83406641	0.01101516	0.83095916	0.01014198	0.37393609	0.30637566	0.2630249	0.93735435
Secondary_Somatosensory_Cortex	1.49659262	0.018142	1.4971892	0.01440923	-0.039847	-0.041403	0.88713575	0.966005
Secondary_Visual_Cortex	2.16894654	0.02158537	2.16985706	0.01708816	-0.0419625	-0.053284	0.85531064	0.95658946
Simple_Lobule	1.15550574	0.019581	1.15695498	0.0203869	-0.1252637	-0.071087	0.7839569	0.95658946
stria_medullaris_thalamus	0.04323941	0.00082784	0.04367272	0.0008537	-0.9921843	-0.5075708	0.05478252	0.89479846
Stria_terminalis	0.17654249	0.00445342	0.1769944	0.00248431	-0.255326	-0.1819071	0.61299349	0.94940684
Subfornical_organ	0.00526834	0.00022847	0.00531394	0.00018935	-0.8581026	-0.2408138	0.40060511	0.94940684
subicular_region	1.76099274	0.01649951	1.7629211	0.01341452	-0.1093842	-0.1437515	0.62000749	0.94940684
substantia_nigra	0.15835421	0.00434314	0.15956834	0.00521623	-0.7608807	-0.232759	0.34777401	0.94525784
Superior_Colliculus	1.12406417	0.01346047	1.12465334	0.00826857	-0.0523871	-0.0712545	0.83277484	0.95658946
Temporal_Association	0.77918331	0.00747078	0.78173142	0.00957181	-0.3259569	-0.2662096	0.27441561	0.93735435
Thalamus	3.39532123	0.04656513	3.39059313	0.02437408	0.13944752	0.19398056	0.6056458	0.94940684
Third_ventricle	0.31902875	0.0059453	0.31818759	0.00437801	0.26435961	0.19213304	0.52731929	0.94940684
trochlear_nerve	0.00560709	0.00017553	0.00572892	0.0001949	-2.1265416	-0.6250773	0.0160977	0.52936513
ventral_pallidum	0.17572055	0.0027147	0.17646072	0.00206857	-0.4194517	-0.3578161	0.23264888	0.93735435

	Pat – Males							
Relative Volumes	Het		WT					
	Mean	SD	Mean	SD	%Diff	Effect	P-Value	FDR
amygdaloid_area	2.09553846	0.01616388	2.10099312	0.01674935	-0.2596229	-0.3256638	0.43696765	0.7513231
Anterior_part_of_anterior_commissure	0.09390287	0.00122302	0.09440037	0.00139281	-0.527009	-0.3571899	0.38080548	0.72711251
Aqueduct	0.11392838	0.0019041	0.11362456	0.00172732	0.26739561	0.17589467	0.6876366	0.92310496
auditory_cortex	1.46154296	0.00748865	1.45694186	0.00982437	0.3158051	0.46833496	0.23628028	0.70137893
basal_forebrain	1.20047879	0.01174447	1.19860512	0.01294609	0.15632048	0.14472832	0.72319309	0.94666405
Bed_nucleus_of_stria_terminalis	0.21165875	0.01345042	0.20693624	0.00404907	2.28211017	1.16632134	0.1995071	0.70137893
caudaputamen	3.24414939	0.03214784	3.24100062	0.03083254	0.09715429	0.10212493	0.81133235	0.96960082
cerebellar_lobule_1_2	0.56355108	0.00403531	0.56617976	0.00562315	-0.4642839	-0.4674752	0.23093685	0.70137893
cerebellar_lobule_10	0.23705158	0.00440167	0.23815246	0.00366604	-0.4622599	-0.3002921	0.50889777	0.81759471
cerebellar_lobule_3	0.48737124	0.00791452	0.49158143	0.00656358	-0.8564579	-0.641447	0.16597731	0.70137893
cerebellar_lobule_4_5	1.50694632	0.010751	1.51036533	0.01920067	-0.2263699	-0.1780674	0.62889864	0.89324956
cerebellar_lobule_6	0.60116658	0.00931065	0.60154016	0.01029156	-0.0621037	-0.0362995	0.92906097	0.98198517
cerebellar_lobule_7	0.23368022	0.00538977	0.23092055	0.00468331	1.19507056	0.58925499	0.19314573	0.70137893
cerebellar_lobule_8	0.25815969	0.00662851	0.25929229	0.00543022	-0.4368015	-0.208572	0.64793339	0.89433988
cerebellar_lobule_9	0.60318552	0.01067929	0.60389705	0.01173461	-0.1178229	-0.0606351	0.88201248	0.98198517
Cerebellar_White_Matter_Arbor_vita_of_cerebellum	1.89134682	0.02212018	1.89780049	0.02464187	-0.3400602	-0.2618984	0.52154616	0.82440096
cerebral_peduncle	0.20737027	0.00388803	0.20578348	0.00198324	0.77109499	0.8000968	0.18652551	0.70137893
Cingulate_Cortex_area_1	1.07774596	0.01543108	1.07195745	0.01051789	0.5399942	0.55034886	0.275959	0.71644074
Cingulate_Cortex_area_2	0.66933214	0.0120086	0.66422331	0.00871768	0.76914409	0.58603112	0.23193117	0.70137893
cingulum	0.23378879	0.00225217	0.23385872	0.00229012	-0.0299023	-0.0305351	0.94188093	0.98198517
Cochlear_nucleus	0.07365308	0.0030194	0.07540037	0.00188933	-2.3173417	-0.924815	0.08691645	0.70137893
Commisure_inferior_Colliculus	0.02228824	0.00196303	0.02145626	0.00127705	3.87756832	0.6514845	0.21060884	0.70137893
commisure_superior_collicuus	0.01324128	0.00012241	0.01313563	0.00014946	0.80428279	0.70684094	0.08453913	0.70137893
copula	0.19620125	0.00365505	0.19571099	0.00335577	0.25050331	0.14609559	0.73709691	0.94666405
Corpus_Callosum_associated_White_Matter	2.95553501	0.03341099	2.94039035	0.0211308	0.51505631	0.71671056	0.17652549	0.70137893
Crus_1_ansiform_lobule	1.1766377	0.01393025	1.17652628	0.01474498	0.00946984	0.00755614	0.98541259	0.99187627
Crus_2_ansiform_lobule	0.68614314	0.01249951	0.68741675	0.01170622	-0.1852752	-0.108798	0.80100816	0.9691349
dentate_gyrus	1.14407795	0.00806343	1.14618098	0.00817139	-0.1834816	-0.2573652	0.5410189	0.82442008
Dentate_nucleus	0.05886313	0.00224442	0.0598047	0.00151875	-1.5744122	-0.619965	0.22306177	0.70137893
Dorsal_Peduncular_Cortex	0.10656259	0.00126938	0.10700537	0.00103057	-0.4137979	-0.429652	0.35233126	0.71681831
Dorsal_Tenia_Tecta	0.07485061	0.00142833	0.07418653	0.00121872	0.89514463	0.54489652	0.23103285	0.70137893
Endopiriform_Nucleus	0.62543244	0.01299533	0.62050518	0.00935909	0.79407217	0.52646783	0.28331128	0.71644074
entopeduncular_nucleus	0.01550781	0.00087643	0.01552988	0.00047127	-0.142129	-0.0468358	0.93494097	0.98198517
external_medullary_lamina	0.04663854	0.00206127	0.04578877	0.00075674	1.85585145	1.12293945	0.1475006	0.70137893
Fasciculus_retroflexus	0.01607089	0.00085022	0.01600355	0.00073934	0.42077743	0.09108068	0.83761656	0.97721327
fastigial_nucleus	0.07106321	0.00171936	0.0716362	0.00148294	-0.7998587	-0.3863857	0.38990546	0.72711251
Fimbria	0.32811595	0.00503342	0.33077782	0.00337738	-0.8047307	-0.7881455	0.12668505	0.70137893
flocculus	0.73483176	0.00856064	0.73781018	0.01031199	-0.403683	-0.2888301	0.47036257	0.78129731
Fornix	0.03955364	0.00068744	0.04033443	0.00070451	-1.9357935	-1.1082756	0.01330225	0.66803557
Fourth_ventricle	0.1974862	0.00400958	0.19888738	0.00318161	-0.704511	-0.4404004	0.34554942	0.71681831
Frontal_Association_Cortex	7.97680135	0.10297872	7.95744302	0.11366928	0.24327328	0.170304	0.67687142	0.92127965
Globus_pallidus	0.31127018	0.00271969	0.31240845	0.00275095	-0.3643501	-0.4137702	0.32915081	0.71681831
hindbrain_medulla_pons	6.56131988	0.07028216	6.57751075	0.08797299	-0.246155	-0.1840437	0.64107515	0.89433988
Hippocampal_layer_CA1	1.44559468	0.00705335	1.4422513	0.0090941	0.23181648	0.36764227	0.35165323	0.71681831
Hippocampal_layer_CA2	0.15978068	0.00384528	0.15764824	0.00247846	1.35265777	0.86038992	0.10415393	0.70137893
Hippocampal_layer_CA3	1.438662	0.01349547	1.44003488	0.01253782	-0.0953368	-0.1094993	0.80035116	0.9691349
hypothalamus	1.93239513	0.01260273	1.93613786	0.01518866	-0.1933091	-0.2464161	0.53728317	0.82442008
Inferior_Colliculus	1.06505733	0.01358746	1.07335526	0.0116234	-0.7730834	-0.7138987	0.12025369	0.70137893
Infralimbic_Cortex	0.10341456	0.00181469	0.10512499	0.001615	-1.6270506	-1.059096	0.02315322	0.66803557
Insular_Cortex	1.68429527	0.01853737	1.68758755	0.01415705	-0.1950879	-0.232554	0.62217318	0.89324956
Internal_capsule	0.55383511	0.00769684	0.55157608	0.00449758	0.40955842	0.50227604	0.36072296	0.71681831
interspersed_nucleus	0.08856763	0.00245526	0.08832671	0.00121252	0.27275413	0.19869011	0.7438137	0.94666405
intrabulbar_part_of_anterior_commisure	0.1851229	0.00448982	0.18492922	0.00480959	0.10473269	0.04026981	0.92208753	0.98198517
Lateral_olfactory_tract	0.16924011	0.00549832	0.16637937	0.00238152	1.7194125	1.20122838	0.08162924	0.70137893
lateral_septum	0.6746764	0.00713311	0.67633469	0.00614753	-0.2451889	-0.2697504	0.54679542	0.82442008
Lateral_ventricle	0.96974079	0.02333584	0.96283621	0.00885839	0.71710769	0.77943853	0.29645209	0.71644074
mamillary_bodies	0.11497771	0.00266817	0.11327074	0.00246026	1.50698898	0.69381909	0.11964647	0.70137893
mammilothalamic_tract	0.02426697	0.00077202	0.02455834	0.0004528	-1.186417	-0.6434685	0.24333171	0.70137893
medial_septum	0.09131339	0.0020937	0.09284257	0.0009495	-1.6470755	-1.6105255	0.01892098	0.66803557
median_preoptic_area	0.00344689	9.8735E-05	0.00351796	9.7951E-05	-2.0202538	-0.7255814	0.09584357	0.70137893
midbrain	2.37005518	0.01486986	2.37554736	0.01395499	-0.2311966	-0.3935642	0.36555589	0.71681831
Navicular_nuclear_basin_forebrain	0.12169838	0.00134967	0.12152255	0.00119363	0.1446865	0.14730386	0.73875944	0.94666405
Nucleus_accumbens	0.49386287	0.0050291	0.49364437	0.00409676	0.04426205	0.05333408	0.90707735	0.98198517
Occipital_Cortex	0.92849501	0.00697212	0.93314269	0.00908348	-0.4980671	-0.5116623	0.1977226	0.70137893
Olfactory_Bulb	9.36901292	0.35360856	9.34154218	0.55048353	0.29407067	0.04990292	0.89436083	0.98198517
Olfactory_tubercle	0.83875639	0.0077989	0.83827871	0.00816054	0.05698281	0.05853473	0.887809	0.98198517
Optic_Chiasm	0.01753073	0.00048522	0.01791473	0.00047425	-2.1434666	-0.8096869	0.06634002	0.70137893
Optic_tract	0.20595725	0.00202552	0.20576975	0.0020815	0.091123	0.090081	0.82918423	0.97721327
Orbitofrontal_Cortex	0.03230696	0.00220832	0.03122612	0.00072104	3.46134658	1.49900044	0.08207081	0.70137893
paraflocculus	0.83722669	0.01370694	0.84145382	0.01198444	-0.5023601	-0.3527181	0.42934008	0.7513231
paramedian_lobe	0.54643839	0.01302032	0.55041848	0.0097149	-0.7231034	-0.4096896	0.39322662	0.72711251
Parietal_Association_Cortex	0.7615344	0.00763187	0.76231034	0.00684932	-0.1017882	-0.1132874	0.79630826	0.9691349
Periaqueductal_grey	0.70583617	0.01547622	0.71184758	0.00896298	-0.8444795	-0.6706931	0.2280237	0.70137893
Piriform_Cortex	1.90243203	0.0120112	1.90216878	0.01815432	0.01383948	0.01450069	0.96938297	0.99187627
pons	1.53270866	0.00995096	1.53869717	0.00972757	-0.3891931	-0.6156218	0.15626926	0.70137893
posterior_commisure	0.01439435	0.00089567	0.01477122	0.00054168	-2.5514221	-0.6957608	0.20021424	0.70137893
Posterior_part_of_anterior_commissure	0.02222358	0.0005692	0.02220319	0.00036305	0.09184204	0.05616782	0.91351709	0.98198517
Prelimbic_Cortex	0.27853502	0.00354591	0.27701943	0.0029514	0.54710307	0.51351365	0.2631188	0.71623864
Primary_Motor_Cortex	1.35914765	0.01194082	1.36209031	0.01211413	-0.2160395	-0.2429108	0.56365674	0.83699453
Primary_Somatosensory_Cortex	5.67001054	0.04945318	5.67021483	0.0464471	-0.0036029	-0.0043984	0.99185571	0.99187627
Primary_Visual_Cortex	1.80024707	0.00741746	1.80324597	0.00985049	-0.1663058	-0.304442	0.43599971	0.7513231
Retrosplenial_Cortex	2.17428265	0.01575876	2.17023753	0.01063345	0.18639089	0.38041521	0.45075478	0.76155763
rhinal_cortex	3.26623649	0.0165555	3.27330203	0.01874631	-0.2158535	-0.3769028	0.35632763	0.71681831
Secondary_Motor_Cortex	0.83700618	0.01508462	0.8323323	0.007075	0.56154026	0.660619	0.2997381	0.71644074
Secondary_Somatosensory_Cortex	1.50287603	0.01734895	1.50451212	0.01268049	-0.1087455	-0.1290241	0.78861974	0.9691349
Secondary_Visual_Cortex	2.17391984	0.01286564	2.17316793	0.01157304	0.03459963	0.06497068	0.88214869	0.98198517
Simple_Lobule	1.14985515	0.01895286	1.15745614	0.0169123	-0.6566981	-0.4494356	0.31205561	0.71681831
stria_medullaris_thalamus	0.04315193	0.00081724	0.04381207	0.00079352	-1.5067469	-0.8319049	0.06029009	0.70137893
Stria_terminalis	0.17526878	0.00390871	0.17674097	0.00247367	-0.8329613	-0.5951422	0.25862856	0.71623864
Subfornical_organ	0.00527191	0.00032091	0.00539335	0.00014561	-2.2516076	-0.834004	0.20378757	0.70137893
subicular_region	1.76466725	0.00657436	1.76470264	0.00886989	-0.0020055	-0.0039901	0.99176944	0.99187627
substantia_nigra	0.15992357	0.00443243	0.16101879	0.0033526	-0.6801789	-0.326677	0.49191394	0.80346227
Superior_Colliculus	1.12713753	0.00937538	1.12476496	0.00496791	0.21093951	0.47757974	0.4131229	0.74965752
Temporal_Association	0.78130492	0.00603039	0.78377504	0.00510504	-0.3151557	-0.4838577	0.28751904	0.71644074
Thalamus	3.40143162	0.0242326	3.39603626	0.02526737	0.15887212	0.21353053	0.60818586	0.88954516
Third_ventricle	0.31967403	0.00371443	0.31823867	0.00374351	0.45103262	0.38342601	0.36573763	0.71681831
trochlear_nerve	0.00560194	0.00014426	0.00575074	0.00015517	-2.5874676	-0.9589186	0.02726624	0.66803557
ventral_pallidum	0.17554834	0.00350023	0.17712024	0.00211733	-0.8874754	-0.7423965	0.1726809	0.70137893

	Pat – Females							
Relative Volumes	Het		WT					
	Mean	SD	Mean	SD	%Diff	Effect	P-Value	FDR
amygdaloid_area	2.08840169	0.02885745	2.08740855	0.01644627	0.04757761	0.06038688	0.89645515	0.98883138
Anterior_part_of_anterior_commissure	0.09370377	0.00116912	0.0934521	0.00178248	0.26930485	0.14119157	0.63613772	0.98883138
Aqueduct	0.11507008	0.00256178	0.1152027	0.0026699	-0.1151162	-0.0496711	0.88212854	0.98883138
auditory_cortex	1.45742545	0.02457583	1.45621023	0.00860975	0.08345087	0.14114466	0.8347239	0.98883138
basal_forebrain	1.19664805	0.01836057	1.19434144	0.01345699	0.19312829	0.17140624	0.66587159	0.98883138
Bed_nucleus_of_stria_terminalis	0.20515205	0.0058753	0.20351254	0.00343923	0.80560479	0.47670712	0.29931632	0.98883138
caudaputamen	3.23102096	0.04311868	3.22537026	0.03112462	0.17519529	0.18155074	0.65029106	0.98883138
cerebellar_lobule_1_2	0.56484589	0.00359942	0.56531108	0.01045093	-0.0822889	-0.0445117	0.86995148	0.98883138
cerebellar_lobule_10	0.23870255	0.00633902	0.23809737	0.00537234	0.25417198	0.11264668	0.75907204	0.98883138
cerebellar_lobule_3	0.48814018	0.00842817	0.4882414	0.01272068	-0.0207328	-0.0079576	0.9787422	0.98883138
cerebellar_lobule_4_5	1.51756214	0.0219261	1.51063901	0.02320776	0.45829137	0.29831098	0.37308875	0.98883138
cerebellar_lobule_6	0.60704144	0.02009451	0.60358047	0.01254608	0.57340623	0.27586041	0.52883231	0.98883138
cerebellar_lobule_7	0.23561651	0.00850292	0.23393761	0.00526395	0.71766821	0.31894236	0.46937944	0.98883138
cerebellar_lobule_8	0.26155513	0.0096247	0.2603189	0.0064632	0.47488746	0.19127083	0.64719848	0.98883138
cerebellar_lobule_9	0.61083841	0.02169142	0.60690783	0.01305871	0.64764043	0.30099311	0.50234315	0.98883138
Cerebellar_White_Matter_Arbor_vita_of_cerebellum	1.90240526	0.04061128	1.8982007	0.03841565	0.2215026	0.10944925	0.75379003	0.98883138
cerebral_peduncle	0.20536562	0.00358029	0.20537801	0.00185281	-0.0060327	-0.006687	0.98925484	0.98926006
Cingulate_Cortex_area_1	1.07635196	0.01048046	1.07242367	0.01443637	0.36630029	0.27211074	0.3760362	0.98883138
Cingulate_Cortex_area_2	0.66694242	0.01116278	0.66373431	0.01069015	0.48334134	0.30009878	0.38952177	0.98883138
cingulum	0.23202768	0.00239124	0.23184591	0.00231043	0.07840062	0.07867297	0.81994708	0.98883138
Cochlear_nucleus	0.07369242	0.00274381	0.07418889	0.00348792	-0.6691946	-0.1423393	0.64946361	0.98883138
Commisure_inferior_Colliculus	0.02272329	0.00177042	0.02249046	0.00197508	1.03520264	0.11787993	0.71832032	0.98883138
commisure_superior_collicuus	0.01314178	0.00026274	0.01308906	0.00016287	0.40274663	0.32367626	0.46249177	0.98883138
copula	0.19690927	0.00700657	0.19596101	0.00470507	0.48389942	0.20153878	0.62970403	0.98883138
Corpus_Callosum_associated_White_Matter	2.94217629	0.04291305	2.93758805	0.02436442	0.15619068	0.18831715	0.68595173	0.98883138
Crus_1_ansiform_lobule	1.18200272	0.02880988	1.17737733	0.0221225	0.39285551	0.20908089	0.58913583	0.98883138
Crus_2_ansiform_lobule	0.69225911	0.02720887	0.69014066	0.01702151	0.30695976	0.12445747	0.77551713	0.98883138
dentate_gyrus	1.14164361	0.01603006	1.1434523	0.0105721	-0.1581782	-0.1710817	0.68548504	0.98883138
Dentate_nucleus	0.05842578	0.00242028	0.05878274	0.00291995	-0.6072528	-0.1222487	0.70084446	0.98883138
Dorsal_Peduncular_Cortex	0.10549508	0.00163198	0.10545185	0.00177826	0.04099626	0.02431105	0.94115262	0.98883138
Dorsal_Tenia_Tecta	0.07366536	0.00108565	0.07327415	0.00137786	0.5338952	0.28392312	0.36702071	0.98883138
Endopiriform_Nucleus	0.6252584	0.01532492	0.62254037	0.01442885	0.43660357	0.18837489	0.59061388	0.98883138
entopeduncular_nucleus	0.01566787	0.00056762	0.01554709	0.00043283	0.77684569	0.27903729	0.47345161	0.98883138
external_medullary_lamina	0.04584813	0.00115756	0.04587294	0.00085158	-0.0540834	-0.0291338	0.94128871	0.98883138
Fasciculus_retroflexus	0.0166876	0.00122598	0.01650123	0.00105491	1.12940677	0.17666466	0.62832686	0.98883138
fastigial_nucleus	0.0723813	0.00135451	0.07209063	0.00130468	0.40320732	0.22279355	0.52087853	0.98883138
Fimbria	0.32964325	0.00589325	0.32939736	0.00284423	0.07464935	0.08645322	0.8686654	0.98883138
flocculus	0.74072351	0.00811763	0.73868846	0.01155858	0.27549522	0.17606411	0.56210556	0.98883138
Fornix	0.03972329	0.00099968	0.04021181	0.00113627	-1.2148637	-0.4299304	0.19061898	0.98883138
Fourth_ventricle	0.19699877	0.00523479	0.19721267	0.00672911	-0.1084655	-0.0317884	0.91876175	0.98883138
Frontal_Association_Cortex	8.01430074	0.16853815	7.93847293	0.1072095	0.95519396	0.70728633	0.1079462	0.98883138
Globus_pallidus	0.30908052	0.00359821	0.3094017	0.00271707	-0.103809	-0.1182109	0.76187333	0.98883138
hindbrain_medulla_pons	6.60380898	0.12522023	6.58568444	0.11955129	0.27521115	0.1516047	0.66290151	0.98883138
Hippocampal_layer_CA1	1.44270164	0.02411604	1.44253078	0.00834132	0.01184507	0.02048463	0.97609689	0.98883138
Hippocampal_layer_CA2	0.15984008	0.00536825	0.15910124	0.00418018	0.46438236	0.176748	0.64530388	0.98883138
Hippocampal_layer_CA3	1.43152648	0.01885821	1.43129267	0.01438515	0.01633523	0.01625322	0.96655944	0.98883138
hypothalamus	1.92724132	0.02902882	1.92687119	0.01436188	0.01920882	0.02577165	0.95994606	0.98883138
Inferior_Colliculus	1.06971285	0.0083963	1.07149053	0.01713563	-0.1659077	-0.1037421	0.713521	0.98883138
Infralimbic_Cortex	0.10413189	0.00157254	0.10417409	0.00220524	-0.0405038	-0.0191337	0.94984042	0.98883138
Insular_Cortex	1.67492977	0.0168379	1.6737813	0.01632755	0.06861526	0.07033937	0.83848519	0.98883138
Internal_capsule	0.55206027	0.01054906	0.55074645	0.00698404	0.23855387	0.18811858	0.65541175	0.98883138
interspersed_nucleus	0.08774972	0.0025839	0.08781629	0.00250833	-0.0758126	-0.0265419	0.93864729	0.98883138
intrabulbar_part_of_anterior_commisure	0.1887387	0.00633637	0.18626764	0.00583275	1.32662268	0.42365396	0.23494939	0.98883138
Lateral_olfactory_tract	0.16809267	0.00272887	0.16625106	0.00246621	1.10772837	0.74673795	0.04198187	0.98883138
lateral_septum	0.66869784	0.00704434	0.6688864	0.00680527	-0.0281913	-0.0277091	0.93608725	0.98883138
Lateral_ventricle	0.96243106	0.0176235	0.9594324	0.00901692	0.31254468	0.33255864	0.50791641	0.98883138
mamillary_bodies	0.11583307	0.0046448	0.11488777	0.00404616	0.82280996	0.23363096	0.52013948	0.98883138
mammilothalamic_tract	0.02426882	0.0004945	0.02427866	0.00055398	-0.0405438	-0.0177687	0.95653339	0.98883138
medial_septum	0.09146997	0.0014333	0.09187	0.00153555	-0.4354311	-0.260513	0.43391977	0.98883138
median_preoptic_area	0.00351872	0.00017342	0.00353097	0.00014976	-0.3470359	-0.0818239	0.82205126	0.98883138
midbrain	2.36317209	0.02846546	2.36932371	0.02799785	-0.2596363	-0.2197178	0.522953	0.98883138
Navicular_nuclear_basin_forebrain	0.1208878	0.00097982	0.1207121	0.00161271	0.14555636	0.10894983	0.71029759	0.98883138
Nucleus_accumbens	0.49139509	0.00358782	0.49091363	0.00566436	0.09807402	0.08499789	0.77383508	0.98883138
Occipital_Cortex	0.93053086	0.00619112	0.93181958	0.01754243	-0.1383009	-0.0734627	0.78747015	0.98883138
Olfactory_Bulb	9.41152428	0.52685368	9.57481171	0.5730978	-1.7053853	-0.2849207	0.38984255	0.98883138
Olfactory_tubercle	0.83793325	0.00799432	0.83654092	0.01011248	0.16643849	0.13768396	0.66063803	0.98883138
Optic_Chiasm	0.01766793	0.000481	0.01770552	0.00063191	-0.2122805	-0.0594787	0.84772478	0.98883138
Optic_tract	0.20611687	0.00433263	0.20577122	0.0022237	0.16797831	0.1554399	0.75583277	0.98883138
Orbitofrontal_Cortex	0.03185159	0.00091146	0.03142296	0.00092605	1.36407013	0.46285741	0.17719002	0.98883138
paraflocculus	0.83981482	0.01840906	0.83751448	0.02009118	0.27466254	0.11449496	0.72815967	0.98883138
paramedian_lobe	0.55085354	0.02023225	0.54931692	0.01556669	0.27973235	0.09871186	0.79818809	0.98883138
Parietal_Association_Cortex	0.75780242	0.00985579	0.75676908	0.00689212	0.13654626	0.14993059	0.71305742	0.98883138
Periaqueductal_grey	0.70285545	0.00885784	0.70389148	0.01656633	-0.1471862	-0.0625384	0.82705402	0.98883138
Piriform_Cortex	1.9018047	0.03054596	1.89733546	0.01982792	0.23555351	0.22540133	0.59757624	0.98883138
pons	1.53145252	0.01360332	1.53547617	0.02084395	-0.2620456	-0.1930367	0.51786667	0.98883138
posterior_commisure	0.01417175	0.00072642	0.01432245	0.00100893	-1.052192	-0.1493651	0.62486057	0.98883138
Posterior_part_of_anterior_commissure	0.02193398	0.0003453	0.02183215	0.00054981	0.46642218	0.18520835	0.53139815	0.98883138
Prelimbic_Cortex	0.27872727	0.00206905	0.27750619	0.00405725	0.44002118	0.30096374	0.293204	0.98883138
Primary_Motor_Cortex	1.35198268	0.0100273	1.35109262	0.01380064	0.06587685	0.06449392	0.83294795	0.98883138
Primary_Somatosensory_Cortex	5.65016782	0.06930746	5.64204832	0.04933161	0.14391041	0.1645901	0.68341184	0.98883138
Primary_Visual_Cortex	1.79762739	0.01927914	1.80029588	0.01656547	-0.1482254	-0.1610878	0.65905003	0.98883138
Retrosplenial_Cortex	2.16438501	0.02622752	2.16494761	0.01384468	-0.0259871	-0.0406371	0.93384081	0.98883138
rhinal_cortex	3.26140994	0.03537858	3.26541523	0.02947898	-0.1226579	-0.1358694	0.71383896	0.98883138
Secondary_Motor_Cortex	0.83230255	0.00777295	0.82991295	0.01203944	0.28793382	0.19848096	0.50516723	0.98883138
Secondary_Somatosensory_Cortex	1.49282257	0.01811396	1.49160984	0.01332459	0.0813036	0.09101461	0.81809827	0.98883138
Secondary_Visual_Cortex	2.16596256	0.02540527	2.1673345	0.02024123	-0.0633009	-0.0677795	0.85800717	0.98883138
Simple_Lobule	1.15889609	0.01979374	1.15657315	0.02309226	0.20084714	0.10059405	0.75447738	0.98883138
stria_medullaris_thalamus	0.0432919	0.00085812	0.04356656	0.00090123	-0.6304363	-0.3047595	0.36439458	0.98883138
Stria_terminalis	0.17730671	0.00470997	0.17718749	0.00253562	0.0672834	0.04701714	0.92241047	0.98883138
Subfornical_organ	0.0052662	0.00016399	0.00525344	0.00019937	0.24289533	0.06400231	0.84007581	0.98883138
subicular_region	1.75878804	0.02041627	1.76156373	0.01613781	-0.15757	-0.1719995	0.65159937	0.98883138
substantia_nigra	0.1574126	0.00415081	0.15846324	0.00613034	-0.6630154	-0.171383	0.5689971	0.98883138
Superior_Colliculus	1.12222015	0.01541808	1.1245683	0.01022433	-0.2088045	-0.229663	0.58578077	0.98883138
Temporal_Association	0.77791035	0.00814137	0.78017438	0.01181027	-0.2901958	-0.1917004	0.52616371	0.98883138
Thalamus	3.391655	0.05646475	3.38644598	0.02342609	0.15381945	0.22235948	0.70557877	0.98883138
Third_ventricle	0.31864159	0.00705387	0.31814868	0.00489759	0.15493017	0.10064304	0.80571644	0.98883138
trochlear_nerve	0.00561018	0.00019672	0.00571229	0.00022281	-1.7875937	-0.4582915	0.1642194	0.98883138
ventral_pallidum	0.17582388	0.00225295	0.17595823	0.00193048	-0.0763529	-0.0695937	0.84884897	0.98883138

Chapter 5

Excessive Laughter-Like Vocalizations, Microcephaly, and Translational Outcomes in the *Ube3a* Deletion Rat Model of Angelman Syndrome

This chapter has been submitted for publication: Elizabeth L. Berg, Shekib A. Jami, Stela P. Petkova, Annuska Berz, Timothy A. Fenton, Jason P. Lerch, David J. Segal, John A. Gray, Jacob Ellegood, Markus Wöhr, and Jill L. Silverman (in review). *Journal of Neuroscience.*

Abstract

Angelman Syndrome (AS) is a rare genetic neurodevelopmental disorder (NDD) characterized by intellectual disabilities, motor and balance deficits, impaired communication, and a happy, excitable demeanor with frequent laughter. We sought to elucidate a preclinical outcome measure in rats that addressed communication abnormalities of AS and other NDDs in which communication is atypical and/or lack of speech is a core feature. We discovered, and herein report for the first time, excessive laughter-like 50-kHz ultrasonic emissions in the *Ube3a*$^{mat-/pat+}$ rat model of AS, which suggests an excitable, playful demeanor and elevated positive affect, similar to the demeanor of individuals with AS. Also in line with the AS phenotype, *Ube3a*$^{mat-/pat+}$ rats demonstrated aberrant social interactions with a novel partner, distinctive gait abnormalities, impaired cognition, an underlying long-term potentiation deficit, and profound reductions in brain volume. These unique, robust phenotypes provide advantages compared to currently available mouse models and will be highly valuable as outcome measures in the evaluation of therapies for AS.

Significance Statement

Angelman Syndrome (AS) is a severe neurogenetic disorder for which there is no cure, despite decades of research using mouse models. This study utilized a recently developed rat model of AS to delineate disease-relevant outcome measures in order to facilitate therapeutic development. We found the rat to be a strong model of AS, offering several advantages over mouse models by exhibiting numerous AS-relevant phenotypes including overabundant laughter-like vocalizations, reduced hippocampal long-term potentiation, and volumetric anomalies across the brain. These findings are unconfounded by detrimental motor abilities and background strain,

issues plaguing mouse models. This rat model represents an important advancement in the field of AS and the outcome metrics reported herein will be central to the therapeutic pipeline.

Introduction

Angelman Syndrome (AS) is a rare neurodevelopmental disorder characterized by developmental delay, impaired communication skills, intellectual disability, ataxia, motor and balance deficits, and seizures. Those with AS very often display a happy disposition with a high degree of excitability, smiling, and easily provoked laughter (1). AS is caused by the loss of expression or function of the maternally inherited allele of the ubiquitin protein ligase E3A (*UBE3A*), which typically results from a *de novo* deletion in the 15q11-q13 region (2). Restoring a functional copy of *UBE3A* is seemingly possible by innovative gene therapy approaches including antisense oligonucleotides (3), viral vector delivery (4), artificial transcription factors (5), stem cell mediated therapies (6), and the cutting edge Cas9 (7). With these methods to target the underlying cause of AS, which has been known for more than two decades, gene replacement therapy is on the horizon. Indeed, two clinical trials using "gene therapy-like" antisense oligonucleotide interventions began recruitment in 2020, highlighting this as a groundbreaking time in AS and gene therapy research (GeneTx NCT04259281; Roche NCT04428281).

Indispensable to such a strategy of therapeutic development are *in vivo* studies utilizing preclinical model systems with rigorous translational outcomes. However, one domain that is critically impaired in AS and many other neurodevelopmental disorders (NDDs) but difficult to study in preclinical models is communication. The utility of non-human animals to model this domain is inherently limited by their lack of human-interpretable language, however animal models are not irrelevant to this pursuit and can be useful for communication studies. In fact, the

increasing availability of rat models of NDDs opens up new opportunities in the development of preclinical outcome measures of social communication. While the mouse has been the preferred model species in recent decades due to the sophisticated genetic technologies available, there are complex behaviors and physiological processes difficult or impossible to investigate in mice without confounds that are easily observable/obtained in rats (8). One prominent example is the greater sophistication and complexity in the rat acoustic communication system. Rats emit uniquely detectable ultrasonic vocalizations (USV) that serve as situation-dependent, evolved signals which accomplish important communicative functions that are not observed as functions of mouse USV (9, 10).

There are two main types of USV in juvenile and adult rats. Low-frequency 22-kHz "alarm calls" are produced in aversive situations and are used as warning calls of threats (11-13). High-frequency 50-kHz "pro-social calls" occur in positive contexts such as social investigation and play. These types of calls help to maintain social proximity through eliciting social approach (14), extend periods of play (15), and coordinate complex social interactions such as social cooperation (16). Additionally, 50-kHz USV are associated with the release of dopamine in the nucleus accumbens (17, 18), are self-administered by rats (19), and can be evoked by tickling (20, 21). These calls are thought to reflect optimism (22) and have been compared to laughter (20, 23, 24).

The rat model of AS provides the unique opportunity to investigate these distinct types of vocalizations as well as other types of social behaviors that are difficult to capture with high signal sensitivity, rigor, and reproducibility in mice (9, 25-28), such as same-sex interactions and structured play (29), (30). To date, studies of communication in AS mouse models have focused on pup and female-induced mating USV while assessments of social behavior have predominantly relied on the metric of sniff/contact time in the three-chambered social approach task or female-

elicited interactions (31-33). Mice do not emit 22-kHz USV like rats and, compared to mice, rats are quicker to approach a same-sex conspecific, show more affiliative behaviors, and have greater consistency in their levels of sociability (34, 35). The broader and more nuanced social behavioral repertoire of rats is particularly obvious during social play, which is a complex process that involves the rapid integration of coordinated physical behaviors with simultaneous bi-directional acoustic communication (36, 37). Therefore, as compared to previous mouse models of AS, the rat model offers a greater diversity of social and communication behaviors to characterize and potentially utilize as preclinical outcome measures (8, 15, 38-42).

Recently, the first reports of a full *Ube3a* deletion rat described the generation and initial characterization of this highly novel genetic model of AS (43, 44). This full deletion model has opened up new avenues of research into the effects of loss of all isoforms of UBE3A and made it possible to investigate the aforementioned complex behaviors that have been difficult to capture with high signal sensitivity in mice. Since the initial studies of this model revealed deficits in motor, cognition, social approach, and pup vocalizations, we sought to explore other social behaviors and further characterize vocalization patterns with the goal of delineating useful metrics for future preclinical studies. Since antisense oligonucleotides and other treatments are being assessed in clinical trials, and novel therapies are being evaluated at the investigational drug discovery level, clinically relevant outcome measures are vital and imperative to demonstrate functional efficacy of the varied intervention approaches.

Our present investigation leveraged the advanced social communication system of the rat to show that the *Ube3a* maternal deletion rat (*Ube3a*$^{mat-/pat+}$) produces excessive signals of positive affect characteristic of AS. We identified several other AS-relevant phenotypes in the *Ube3a*$^{mat-/pat+}$ rat model at various life stages, including atypical interactions with conspecifics and

maladaptive impairments in gait and cognition. We also report, for the first time, reduced hippocampal long-term potentiation, observed in mouse models of AS but not yet in rats, as a putative cellular mechanism underlying the learning and memory deficits apparent in the rat model. Finally, we extended our mesoscopic neuroimaging analysis to adults and discovered decreased brain volume in numerous regions and pronounced increased severity with age.

Results

Overabundant emission of laughter-like 50-kHz calls in juvenile *Ube3a*$^{mat-/pat+}$ rats. Since deficient expressive communication and elevated rates of positive affect are key clinical features of AS, we sought to quantify these characteristics in *Ube3a*$^{mat-/pat+}$ and *Ube3a*$^{mat+/pat+}$ (wildtype) rats. While vocalizations are readily collected during social play, recording USV from multiple interacting animals makes it difficult to determine which animal made each call. We therefore took advantage of the fact that rats emit laughter-like 50-kHz calls when social play is simulated by an experimenter via tickling and other physical maneuverings (19, 21, 45, 46). We implemented a standardized heterospecific play procedure (**Figure 1A**) to elicit USV (**Figure 1B**) while maintaining full confidence in the identity of the caller and controlling for the level of physical interaction across subjects.

We discovered that while both groups increased 50-kHz USV emission across consecutive sessions, *Ube3a*$^{mat-/pat+}$ emitted a substantially elevated level of 50-kHz USV (**Figure 1C**; $F_{Genotype(G)}$ (1, 48) = 7.351, p = 0.009; $F_{Day(D)}$ (3.007, 144.3) = 10.82, $p < 0.0001$; $F_{D\times G}$ (4, 192) = 1.052, $p > 0.05$). In total, *Ube3a*$^{mat-/pat+}$ emitted an average of 33 ± 5 USV per minute (mean ± S.E.M.), more than twice the rate of controls, which produced an average of 15 ± 3 calls per minute (**Figure 1D**; U = 175, $p.$ = 0.007). A closer examination revealed that 50-kHz USV were elevated

during the break and belly tickle phases (**Figure 1E**; F_G (1, 48) = 6.927, p = 0.011; $F_{Phase\ (P)}$ (1.722, 82.64) = 27.83, p < 0.0001; $F_{P\times G}$ (4, 192) = 2.075, p > 0.05; *post hoc*: break, p = 0.023; belly tickle, p = 0.023), although calling during the other phases also trended higher, providing strong evidence of elevated positive affect and a high hedonic impact of the assay (p = 0.057; push and drill, p = 0.057; flip over, p = 0.057). There was no effect of sex, nor an interaction with sex, (p > 0.05) for any parameter.

Additionally, 50-kHz USV were more frequently emitted during the anticipation period immediately prior to the play sessions (**Figure 1F**; U = 146.5, p = 0.001). In total, across all four anticipation timepoints (days 2-5), *Ube3a*$^{mat-/pat+}$ emitted an average of 9 ± 2 USV per minute (mean ± S.E.M.), more than four times the rate of wildtypes, which produced an average of 2 ± 0.4 calls per minute. This indicates that *Ube3a*$^{mat-/pat+}$ predicted the impending onset of play and that the interaction had a high degree of incentive salience.

Excessive vocalization by *Ube3a*$^{mat-/pat+}$ rats was specific to 50-kHz USV. Production of short 22-kHz USV, which are emitted in modest amounts during play, was low and did not differ between genotypes (**Figure 1G**; F_G (1, 48) = 1.771, p > 0.05; F_D (1.825, 87.62) = 3.160, p > 0.05; $F_{D\times G}$ (4, 192) = 1.330, p > 0.05). Elevated 50-kHz calling by *Ube3a*$^{mat-/pat+}$ was also specific to being provoked by heterospecific play, as 50-kHz and short 22-kHz USV production was normal during exploration of an empty cage (albeit a slight trend toward greater 50-kHz USV; **Figure 1H**; 50-kHz, U = 374.5, p > 0.05; 22-kHz, U = 433, p > 0.05) and in response to the acoustic presentation of 50-kHz USV (**Figure 1I**; 50-kHz, U = 53, p > 0.05; 22-kHz, U = 44.50, p > 0.05). No gross abnormalities in call structure were observed. Specifically, 50-kHz calls were of normal duration and peak frequency, suggesting that increased heterospecific play 50-kHz call numbers were not inflated by shorter or broken calls. Since the average duration of the juvenile 22-kHz

USV fell short of the usual durations of adult "typical 22-kHz" USV, we herein refer to them as "short 22-kHz" USV (**Figure S1A-H**).

Intact social interest but deficient expression of key social interaction behaviors in juvenile *Ube3a*$^{mat-/pat+}$ rats. We sought to investigate whether elevated 50-kHz USV emission in *Ube3a*$^{mat-/pat+}$ rats was associated with greater social engagement with a conspecific. Starting around two weeks of age, rats play fight with each other by chasing, pouncing, pinning, and wrestling in a manner similar to cats and dogs. Through developmental experience, they learn how to appropriately initiate, engage in, and terminate play bouts with others. In order to more closely examine social behavior and the nuanced reciprocal interactions of social play (**Table S1**), we gave juvenile subjects the opportunity to freely interact with a conspecific (47). Despite greater 50-kHz calling during heterospecific play, *Ube3a*$^{mat-/pat+}$ rats showed a normal degree of interest in the stimulus animal, demonstrated by the amounts of time spent social sniffing (**Figure 2A**; t (20) = 1.646, $p > 0.05$) and anogenital sniffing (**Figure 2B**; t (20) = 0.4457, $p > 0.05$). Putting forth a similar level of investigative effort suggested that *Ube3a*$^{mat-/pat+}$ are just as motivated for social interaction as controls. Levels of self-grooming (**Figure 2C**; U = 38, $p > 0.05$) and arena exploration (**Figure 2D**; U = 30, $p > 0.05$) were also normal but *Ube3a*$^{mat-/pat+}$ spent markedly less time following or chasing the stimulus rat (**Figure 2E**; U = 29, p = 0.041). The key observation was the reduced time spent rough-and-tumble playing (**Figure 2F**; U = 33.50, p = 0.029) compared to wildtypes. In an attempt to reconcile the near lack of play with intact levels of social interest, we quantified specific components of rough-and-tumble play. While the number of side-to-side social contacts via push pasts were similar across genotypes (**Figure 2G**; t (20) = 0.3852, $p > 0.05$), there was a trending reduction in the number of push under or crawl overs (**Figure 2H**; U = 31.5,

$p = 0.061$) and almost a complete lack of pouncing in *Ube3a*$^{mat-/pat+}$ (**Figure 2I**; $U = 24$, $p = 0.008$). A separate test of olfaction was used to rule out an olfactory deficit as a confounder of social investigation (**Figure S2**).

Abnormal gait in *Ube3a*$^{mat-/pat+}$ rats. In an effort to assess the potential contribution of motor defects to social play behavior, we explored motor dysfunction, which is a core clinical feature of AS prevalent in mouse models (32, 44, 48, 49) and hypothesized by our group to underlie the open field, rotarod, and marble burying phenotypes of AS mouse models. Previously, we discovered lower open field vertical activity in *Ube3a*$^{mat-/pat+}$ rats while other activity indices were typical (44). Using the DigiGait automated treadmill system, we found that juvenile *Ube3a*$^{mat-/pat+}$ rats displayed robust abnormalities in limb propulsion time, indicating reduced limb strength and less force produced per unit time compared to wildtypes (**Figure 3A**; $F_{\text{Genotype(G)}}(1, 44) = 0.0684$, $p > 0.05$; $F_{\text{Limbs(L)}}(1, 44) = 776.8$, $p < 0.0001$; $F_{\text{L×G}}(1, 44) = 12.80$, $p < 0.001$; *post hoc*: forelimbs, $p = 0.030$; hindlimbs, $p = 0.022$; **Figure 3B**; $F_{\text{G}}(1, 44) = 1.012$, $p > 0.05$, $F_{\text{L}}(1, 44) = 687.0$, $p < 0.0001$; $F_{\text{L×G}}(1, 44) = 9.391$, $p = 0.004$; *post hoc*: forelimbs, $p = 0.010$). No abnormalities in swing time (**Figure 3C**; $F_{\text{G}}(1, 44) = 0.1209$, $p > 0.05$, $F_{\text{L}}(1, 44) = 22.62$, $p < 0.0001$; $F_{\text{L×G}}(1, 44) = 0.2552$, $p > 0.05$) or total stride time (**Figure 3D**; $F_{\text{G}}(1, 44) = 0.9166$, $p > 0.05$; $F_{\text{L}}(1, 44) = 13.24$, $p < 0.001$; $F_{\text{L×G}}(1, 44) = 0.7566$, $p > 0.05$) were discovered, suggesting that the opposing effects of propulsion and brake time canceled each other out. Stride length was normal, which was surprising given the published Zeno walkway data in humans (50), but lends to the hypothesis that *Ube3a*$^{mat-/pat+}$ have limb weakness since more time was required to produce force for an equal length step (**Figure 3F**; $F_{\text{G}}(1, 44) = 0.9460$, $p > 0.05$; $F_{\text{L}}(1, 44) = 12.70$, $p < 0.001$; $F_{\text{L×G}}(1, 44) = 0.7719$, $p > 0.05$). Forelimb stance width was reduced (**Figure 3G**; $F_{\text{G}}(1, 44) = 1.605$, $p > 0.05$;

F_{L} (1, 44) = 939.0, $p < 0.0001$; $F_{L\times G}$ (1, 44) = 12.46; *post hoc*: forelimbs, $p = 0.022$) while an elevated forelimb paw angle indicated greater degree of external rotation and splaying (**Figure 3H**; F_{G} (1, 44) = 5.957, $p = 0.019$; F_{L} (1, 44) = 3.726, $p > 0.05$; $F_{L\times G}$ (1, 44) = 3.497, $p > 0.05$; *post hoc*: forelimbs, $p = 0.006$), which has been associated with ataxia, spinal cord injury, and demyelinating disease (51). The observed effects were not attributable to differences in body length (**Figure S3A**) or body width (**Figure S3B**) and, despite abnormalities in some temporal and postural components of gait, the coordination metric of gait symmetry was unaltered (**Figure 3I**; t (44) = 1.023, $p > 0.05$).

Impaired learning and memory in *Ube3a*$^{mat-/pat+}$ rats. Learning and memory impairments, which are characteristic of AS, may hinder the ability of *Ube3a*$^{mat-/pat+}$ rats to learn via developmental experience how to appropriately engage in social interactions. We therefore probed for a juvenile learning and memory deficit using a fear conditioning assay previously used to detect a deficit in adulthood (43). Following successful fear conditioning (**Figure 4A**; $F_{Phase(P)}$ (1, 30) = 48.47, $p < 0.0001$; $F_{Genotype(G)}$ (1, 30) = 0.2203, $p > 0.05$; $F_{P\times G}$ (1, 30) = 0.0613, $p>0.05$; *post hoc*: mat+/pat+, $p < 0.0001$; mat-/pat+, $p < 0.001$), juvenile *Ube3a*$^{mat-/pat+}$ displayed normal levels of freezing in response to the training context (**Figure 4B**; $U = 117.5$, $p > 0.05$) but a robust deficit in cued fear memory 48 hrs after training (**Figure 4C**; F_{G} (1, 30) = 7.395, $p = 0.011$; F_{P} (1, 30) = 42.36, $p < 0.0001$; $F_{P\times G}$ (1, 30) = 8.699, $p = 0.006$; *post hoc*: pre-cue, $p > 0.05$; cue, $p < 0.001$). We assessed the potentially confounding variable of impaired sensorimotor processing by measuring the startle response to an intense acoustic stimulus and quantifying the reduction in startle response following prepulses of varying intensities. Both baseline activity (**Figure S4A**) and the acoustic startle response of *Ube3a*$^{mat-/pat+}$ rats was normal (**Figure S4B**), illustrating intact

hearing abilities. While there was a significant main effect of genotype on prepulse inhibition, indicative of a sensorimotor gating deficit, *post hoc* testing revealed no significant difference between groups at any individual prepulse level (**Figure S4C**).

As an additional assessment of cognitive functioning, we quantified spontaneous alternation during exploration of a Y-maze and found that *Ube3a*$^{mat-/pat+}$ rats displayed reduced spontaneous alternation compared to wildtypes (**Figure 4D**; t (46) = 3.115, $p < 0.01$). *Ube3a*$^{mat-/pat+}$ rats made 40% more errors (**Figure 4E**; t (46) = 3.827, $p < 0.001$) and more arm entries (**Figure 4F**; t (46) = 3.620, $p < 0.001$) despite no difference in the total distance moved (data not shown; Student's t-test: t (46) = 1.721, $p > 0.05$). Taken together, these metrics indicate additional cognitive deficits in the *Ube3a*$^{mat-/pat+}$ rats that were not confounded by a locomotor deficiency.

Reduced hippocampal long-term potentiation (LTP) in *Ube3a*$^{mat-/pat+}$ rats. To elucidate the neurobiology underpinning the learning and memory deficits of *Ube3a*$^{mat-/pat+}$ rats, we quantified long-term potentiation (LTP). Previous studies in mouse models of AS have shown that LTP, a major cellular mechanism underlying learning and memory (52), is impaired (4, 53, 54). Here, we examined the effect of maternal *Ube3a* deletion on hippocampal LTP in adult *Ube3a*$^{mat-/pat+}$ rats compared to wildtype littermate controls. Since we found hippocampal-dependent contextual fear memory intact at the juvenile age, but a previous report detected a clear deficit in adults (43), we measured hippocampal LTP in adulthood. Basal synaptic strength (**Figure 5A**; $F_{Genotype(G)}$ (1, 92) = 0.2013, $p > 0.05$; $F_{Amplitude(A)}$ (5, 111) = 94.04, $p < 0.0001$; $F_{G\times A}$ (5, 92) = 0.4107, $p > 0.05$) and paired-pulse ratio (**Figure 5B**; F_G (1, 56) = 0.065, $p > 0.05$; $F_{Interval(I)}$ (3, 76) = 20.96, $p < 0.0001$; $F_{G\times I}$ (3, 56) = 0.0758, $p > 0.05$) were unaltered in *Ube3a*$^{mat-/pat+}$ rats, suggesting no change in baseline excitatory transmission. However, consistent with the mouse models of AS

(4, 53, 54), we found that the magnitude of LTP was reduced in *Ube3a*$^{mat-/pat+}$ rats (**Figure 5C** and **5D**; t (25) = 4.641, $p < 0.0001$), suggesting a putative mechanism underlying impairment of learning and memory (4, 53-56).

Neuroanatomical pathology in *Ube3a*$^{mat-/pat+}$ rats revealed by high-resolution magnetic resonance imaging (MRI). MRI revealed striking differences in total brain volume at 6.5 months of age, which was decreased by 6.0% in *Ube3a*$^{mat-/pat+}$ rats ($q = 0.04$, **Figure 6**, **Table S2**). The overall brain volume difference was driven by decreases in the hippocampal region (-6.3%, $q = 0.04$), brain stem (-5.6%, $q = 0.04$), thalamus (-7.7%, $q = 0.01$), cerebellum (-9.0%, $q = 0.02$), and deep cerebellar nuclei (-12.3%, $q = 0.0001$). Additional differences were found throughout the white matter fiber tracts (-7.6%, $q = 0.02$), including but not limited to the cerebral peduncle (-7.6%, $q = 0.02$), internal capsule (-8.4%, $q = 0.02$), and arbor vita of the cerebellum (-11.7%, $q = 0.0004$). Moreover, trends were seen in other large white matter structures including the corpus callosum (-6.7%, $q = 0.06$) and fornix system (-6.0%, $q = 0.09$). A complete list of the regional structural differences in both absolute (mm^3) and relative (% total brain) volume is provided in **Table S2**.

As we had previously examined *Ube3a*$^{mat-/pat+}$ rats at a juvenile age (postnatal day (PND) 21) (44), we felt an age by genotype comparison was warranted. Therefore, we combined the data from our previous work to explore a genotype by age interaction model and found significant interactions between genotype and age for the total brain volume ($q = 0.048$), caudoputamen ($q = 0.03$), white matter fiber tracts ($q = 0.03$; **Figure 6A**; $F_{Age(A)}(1, 97) = 546.5$, $p < 0.0001$; $F_{Genotype(G)}(1, 97) = 11.87$, $p <. 0.001$; $F_{A\times G}(1, 97) = 10.68$, $p = 0.002$; *post hoc*: juvenile, $p > 0.05$; adult, $p < 0.0001$), hypothalamus ($q = 0.046$; **Figure 6B**; $F_A(1, 97) = 460.2$, $p < 0.0001$; $F_G(1, 97) = 5.081$,

p = 0.026; $F_{A\times G}$ (1, 97) = 8.760, p = 0.004; *post hoc*: juvenile, $p > 0.05$; adult, p = 0.001), hippocampal region (q = 0.046; **Figure 6C**; F_A (1, 97) = 434.4, $p < 0.0001$; F_G (1, 97) = 10.89, p = 0.001; $F_{A\times G}$ (1, 97) = 8.760, p = 0.004; *post hoc*: juvenile, $p > 0.05$; adult, $p < 0.0001$), and thalamus (q = 0.02; **Figure 6D**; F_A (1, 97) = 430.2, $p < 0.0001$; F_G (1, 97) = 11.14, p = 0.001; $F_{A\times G}$ (1, 97) = 14.96, $p < 0.001$; *post hoc*: juvenile, $p > 0.05$; adult, $p < 0.0001$). A full list of the regional genotype by age interactions is located in **Table S3**. Voxelwise changes were also found throughout the brain of adult *Ube3a*$^{mat-/pat+}$ rats compared to the juvenile age. The changes in the adults were substantially larger, signaling a more severe neuroanatomical phenotype with age (**Figure 6**).

Discussion

While there is currently no effective treatment or cure for AS, the genetic cause of maternal *UBE3A* mutations has been well studied and is targetable by gene therapy approaches. Indispensable to such a strategy of therapeutic development are *in vivo* studies utilizing preclinical model systems with a high degree of genetic conservation and behavioral complexity relative to humans. Therefore, while mouse models (specifically, the exon 2 null mutation model) have prevailed as the animal model of choice for studying AS over the past two decades (53), *Ube3a*$^{mat-/pat+}$ rats offer a unique and suitable system for investigating certain complexities of the human AS phenotype. Rats provide 1) an enhanced sophistication of social play behavior (47, 57, 58) (59, 60) and 2) an acoustic communication system that allow for the collection, observation, and quantification of rigorous, reliable, translatable outcome measures (9, 10, 61). This is particularly advantageous in modeling certain NDDs (29, 62-66), specifically AS, in which there are strong social communication phenotypes characterized by aberrant social behavior but a high level of

interest in engaging with others, and a robust expression of positive affect (i.e., laughing) but deficits in language and speech (67-76). Our discovery of excessive 50-kHz USV is the first report of this affective outcome measure in a model of AS. Moreover, reduced social play, atypical gait, impaired cognition, and anatomical and cellular physiology anomalies were easily detected in this model.

It is important to state that the purpose of this article is not to compare rat and mice acoustic communication but rather to acknowledge that USV and social play are exhibited more vigorously, reliably, quantifiably, and of greater definition (i.e., specific frequency ranges) in rats (35, 39, 41). Specifically, rats emit three subtypes of USV, which are uniquely dependent on age, environmental conditions, and internal affective state (9, 10, 61). Rat pups emit 40-kHz vocalizations when separated from the nest and juvenile and adult rats emit 22-kHz vocalizations in anticipation of inescapable aversive stimuli—these vocalizations reflect a negative affective state. Rats also produce 50-kHz vocalizations, which are understood to reflect a positive affective state, often co-occur with positively valanced appetitive behavior, and have been referred to as rat laughter (20, 23). We leveraged our model species to investigate expression of USV in both sexes across several contexts, beyond neonatal maternal separation.

While a trend suggested that *Ube3a*$^{mat-/pat+}$ rats may produce an abnormally high number of laughter-like 50-kHz USV without provocation, we were able to detect a very clear elevation in 50-kHz calling through a manual heterospecific play method. This behavior, suggestive of an enhanced degree of 'wanting' and 'liking' the interaction (77-80), is a clear and robust phenotype that closely aligns with the AS clinical profile of a happy disposition and easily provoked laughter. This is the first report of this method being used in a genetic rat model and may therefore be encouraging to other groups seeking to study communication in other rat models of NDDs.

Given what is known about the typical functions of rat 50-kHz USV, the increased calling rate could suggest that *Ube3a*$^{mat-/pat+}$ rats put more effort into eliciting social interaction, or it may be unrelated to the social component of heterospecific play. For instance, the phenotype could be a neurobiological consequence of a disinhibited vocal production pathway as AS is typified by laughter that is easily provoked regardless of stimuli valence (both pleasant and unpleasant), or *Ube3a*$^{mat-/pat+}$ rats may be more sensitive to tactile stimulation. Deriving greater reward from physical interactions could help explain why *Ube3a*$^{mat-/pat+}$ rats exhibit typical social investigation in the reciprocal interaction test but reduced social approach in the three-chambered and USV playback assays. Previously, we found that *Ube3a*$^{mat-/pat+}$ rats showed a reduced approach toward the acoustic playback of 50-kHz USV (44). In light of the new evidence here from physical encounters, our previous Berg et al. (44) finding is most likely due to a social-cognitive impairment associated with acoustic stimuli as opposed to reduced social motivation. Regardless of etiology or intended communicative function, if there is indeed one at all, the aberrant call quantity elicited by heterospecific play provides a clear AS-relevant phenotype for use in future preclinical work with this model. This is a particularly valuable outcome measure to the field as it is detectable in both sexes and mouse models of AS have shown inconsistent phenotypes with regards to USV emission. In the presence of a female conspecific, male AS mice displayed a call deficit whereas female AS mice emitted a greater number of calls in one study and a reduced number in another study (31, 81, 82).

One limitation of our USV analysis was the lack of acoustic feature quantification for the calls specifically evoked by heterospecific play. We did, however, subsequently carry out this analysis on all other assays involving USV and found no genotype effect on the acoustic features of 50-kHz and 22-kHz calls across social and non-social contexts. Interestingly, the low frequency

calls emitted in response to 50-kHz USV playback resembled the "short 22-kHz" USV described by Brudzynski et al. (19, 83-86), likely driven by the young age of the animals, which have reduced body size and therefore altered vocal capacity compared to adults. The low frequency calls produced during exploration of an empty cage resembled the "low-shorts" described by Schwarting et al. in the "cage test" (12, 87-90). While a few long "typical 22-kHz" USV known to function as "alarm calls" were observed, they were very low in number and not emitted reliably enough to suggest that our paradigms were aversive or find an effect of genotype. Rather than serving an alarming function, the rare "typical 22-kHz" calls were more likely related to frustration, as subjects never encountered a live "partner" rat during the assay, as previously documented (29).

Juvenile social play is a critical way that rats develop social competence and learn how to appropriately engage and communicate with others. This has been well described by many laboratories and is analogous to play in young children (10, 19, 30, 41, 42, 47, 85, 86, 89, 91-93). In our fine-grained analysis of juvenile reciprocal social interaction, we discovered that *Ube3a*$^{mat-/pat+}$ rats were socially interested in a novel partner but did not engage in the type of rough-and-tumble play behaviors that are characteristic of the species, albeit specific to sex and strain. The low levels of play in *Ube3a*$^{mat-/pat+}$ rats are likely attributable to underlying motor and/or cognitive deficits. For instance, hindlimb weakness may be prohibitive for actions such as chasing and pouncing chasing, which are key components of rough-and-tumble play, and/or cognitive impairment(s) may inhibit the learning of play behaviors or sequences over development. It is also possible that excessive, and therefore inappropriately timed, vocal expression may inhibit the natural progression of play from taking place.

In contrast with previous studies on mouse models of AS which have reported both social deficits and "hypersociability," we found the rat model of AS to exhibit a typical level of social investigation (31, 82, 94). Important factors contributing to this difference likely include the analysis of additional social interaction metrics beyond sniff/contact time and the profound motor deficits that affect gross locomotion in AS mice but not rats, which is a key advantage for the interpretation of behavior in the rat model. Of note, the level of play observed in our wildtypes was lower than that typically found in Sprague Dawley rats (15, 95, 96). This may have been due to mixed genotype housing, which was used to better parse out the effect of the gene deletion from that of the developmental social environment. While our wildtypes were reared by *Ube3a* deletion dams, we do not suspect that this significantly contributed to differences in their behavior since paternal deletions of *Ube3a* have not been shown to have robust effects on behavior (44).

Movement disorders (74) are a hallmark feature of AS, with gait ataxia being one of the most common issues. While the deficits we discovered in *Ube3a*$^{mat-/pat+}$ rats were not gross or obvious to the eye, subtle aberrations in stance and paw placement, paired with abnormal braking and propelling, reflect impaired motor coordination and may be an advanced way to define gait outcome measures for clinical trials. This impairment is likely linked to limb weakness, with aberrations reflecting greater compensatory mechanisms for *Ube3a*$^{mat-/pat+}$ rats than in mice, for which the deficits are gross and confound numerous other assays. All of this evidence suggests that altered postures may affect motor dynamics which in turn results in the gait patterns exhibited by AS individuals and *Ube3a*$^{mat-/pat+}$ rats. The limb weakness indicated by our gait analysis aligns with the reduced rearing previously observed (44) and is likely a main contributing factor to the lack of rough-and-tumble play and associated behaviors such as pouncing.

We discovered and report for the first time, to our knowledge, of long-term potentiation (LTP) deficits in this rat model (53, 54, 97-99). Our finding of reduced LTP provides a putative cellular signaling mechanism underlying the learning and memory impairments that have been reported herein and previously (e.g., delayed touchscreen learning) (43, 44). Juvenile *Ube3a*$^{mat-/pat+}$ rats exhibited deficits in cued fear memory 48 hours after tone-shock training, which extends the previous finding by Dodge et al. of deficient contextual and cued fear conditioning 72 hours post-training at 3-4 months of age (43). We ruled out impaired sensorimotor abilities as a confounding variable since only prepulse inhibition, and not acoustic startle, was affected and not robustly. While reduced hippocampal LTP was discovered, we did not find a deficit in hippocampus-dependent contextual fear memory. One likely explanation for this is that we tested fear memory in juveniles (around 6 weeks of age) but collected electrophysiological readings in adulthood (around 12 weeks of age), suggesting our results become detectable in *Ube3a*$^{mat-/pat+}$ in early adulthood. Another limitation was our failure to collect 22-kHz calls during the fear assay. Laser focused on translation, we began this investigation with a focus on 50-kHz, positive, "happy" calls. Fear conditioning deficits have been detected in mouse models of AS, but not in a consistent fashion. While some models have shown a deficit in contextual memory, others have not (32, 100), and the same is true for cued fear memory (32, 100). This is likely the result of varying training protocols, background strain, and the confounding influence of the severe motor deficit in the AS mouse model.

Pronounced deficits in adulthood are supported by magnetic resonance imaging (MRI). Previously, we reported a variety of trending volumetric abnormalities at PND 21 (44), however, not previously illustrated anywhere is that in adults (6.5 months) we found substantial decreases in brain volume throughout the brain highlighting a more severe neuroanatomical phenotype with

age. Overall, the total brain volume was decreased in adult *Ube3a*$^{mat-/pat+}$ rats, which could indicate a loss of cellular volume or dendritic complexity over time. Additionally, the drastic volume loss in fiber tracts throughout the brain could indicate a loss in axonal numbers, axonal volume, or myelination. Previous research in a mouse model of AS revealed white matter loss to play a large role in the overall microcephaly observed (101), with an 11% loss in the corpus callosum making it the most affected white matter structure. However, this was not the case in our study: we found only a trend towards reduced corpus callosum volume (-6.7%) and the largest white matter deficits were found in the cerebellum, in which overall cerebellar white matter was decreased by 11%. Our rat data reproduces the previous findings by Judson et al. in the mouse and extends on earlier report on younger rats, as the volume loss seen here in the fiber tracts was also disproportionate to the overall brain volume loss, confirming that white matter development plays the major role in the impaired brain growth in the disorder. Another noteworthy discovery was the 9% decrease in the size of the cerebellum. The overall cerebellar loss was consistent with the cortical loss (-9%), however there was a disproportionate loss in the size of the arbor vitae and deep cerebellar nuclei, indicating that the outputs of the cerebellum are impaired.

In conclusion, we discovered that *Ube3a*$^{mat-/pat+}$ rats exhibit interest in a social partner, but express aberrant social behavior and emit an atypically high level of laughter-like vocalizations. Deficits in other AS-relevant domains were also discovered, including gait and cognition, and reduced hippocampal LTP. Future lines of investigation will assess the circuitry and mechanisms underlying the excessive laughter-like USV and social-cognitive anomalies in USV reception, in addition to pursuing other neurobiological endpoints and biomarkers. The larger size of our rat model compared to mice will facilitate procedures such as accessing the intrathecal space and collecting cerebrospinal fluid without blood contamination, crucial for studying *Ube3a* which is

only imprinted in neurons. Overall, our results indicate that the deletion of maternal *Ube3a* in the rat creates a sophisticated rodent model with high face validity to the human AS phenotype. In the pursuit of effective therapeutics, it is essential to be equipped with a diverse set of behavioral outcome measures and neurological biomarkers by which to assess efficacy. Taken together, we demonstrate that the *Ube3a*$^{mat-/pat+}$ rat offers numerous potential outcome measures that are detectable at juvenile and adulthood timepoints.

Materials and Methods

Subjects. Subjects were male and female Sprague Dawley *Ube3a*$^{mat-/pat+}$ rats and their wildtype littermates (*Ube3a*$^{mat+/pat+}$) generated from breeding pairs of paternal *Ube3a* deletion females and wildtype males purchased from Envigo (Indianapolis, IN). The initial generation of *Ube3a* deletion rats using CRISPR/Cas9 was described previously (44). Genotyping was performed using a small sample of tail tissue collected at postnatal day (PND) 2, REDExtract-N-Amp (Sigma Aldrich, St. Louis, MO, USA), and primers Rube1123 TAGTGCTGAGGCACTGGTTCAGAGC, Rube1606r TGCAAGGGGTAGCTTACTCATAGC, Ub3aDelSpcfcF6 ACCTAGCCCAAAGCCATCTC, and Ub3aDelR2 GGGAACAGCAAAAGACATGG. All animals were housed in a temperature-controlled vivarium maintained on a 12:12 light-dark cycle. All procedures were conducted in compliance with the NIH Guidelines for the Care and Use of Laboratory Animals and approved by the Institutional Animal Care and Use Committee of the University of California Davis.

To minimize the carry-over effects from repeated testing and handling, six mixed-sex cohorts of rats were tested and behavioral tests were carried out in order of least to most stressful with at least 48 hrs break between tests. Each cohort was comprised of four to nine litters and subjects were

sampled as followed: subjects for 50-kHz ultrasonic (USV) playback were sampled from Cohort 1; contextual and cued fear conditioning from Cohort 2; gait analysis, heterospecific play, and social play from Cohort 3; acoustic startle and long-term potentiation from Cohort 4; spontaneous exploratory USV from Cohort 5; spontaneous alternation from Cohort 6; and olfactory discrimination from Cohort 7. Following behavioral testing, rats from Cohort 3 were perfused for magnetic resonance imaging.

Juvenile USV in response to heterospecific play. At postnatal day (PND) 30 through 34, rats were provided daily heterospecific play sessions involving manual stimulation using a slightly abbreviated procedure from those described previously (46, 90, 102). For 5 min on 5 consecutive days, rats were individually manipulated by a familiar experimenter using a single clean hand within a clean, empty version of the home cage with fresh bedding (37.2 cm l x 30.8 cm w x 18.7 cm h; illuminated to ~30 lux) while vocalizations were recorded with an overhead ultrasonic microphone (Avisoft Bioacoustics, Glienicke, Germany) for later scoring by a trained observer blinded to genotype. All rats were handled by the experimenter in a standardized fashion (5 min on 3 days) prior to the first heterospecific play session.

The physical manipulations performed were tickling the subject's neck (2x), tickling the subject's belly (1x), pushing into their shoulders ("push and drill"; 1x), and flipping the subject onto their back and momentarily pinning them down ("flip over"; 3x). Each manipulation lasted 30 sec with three 30-sec breaks interspersed at 0, 60, and 150 sec, during which the experimenter did not initiate touching the subject but moved their hand around the cage to encourage following or chasing. In an effort to provide a standardized experience, a single experimenter carried out the procedure for all subjects and the experimenter remained unaware of USV being emitted during

the test, performing the manipulations in an equivalent manner for all rats. To mitigate any potential effect of order, the sequence of manipulations was re-ordered each day but remained consistent across all animals. The testing order of the subjects was also changed from day to day. The number of calls emitted during each 30-sec interval were counted by a trained observer blinded to genotype and classified as either high (50-kHz) or low (short 22-kHz) frequency using a threshold of 33 kHz. Calls emitted during the minute immediately preceding the heterospecific play sessions on days 2-4 ("anticipation") were also counted and classified.

Juvenile spontaneous exploratory USV. At PND 30, rats were individually placed in a clean, empty version of the home cage (illuminated to ~30 lux) with clean bedding for 5 min while vocalizations were recorded with an overhead ultrasonic microphone (Avisoft Bioacoustics). Recording began immediately following the subject being placed into the cage and no other animals or any experimenter were present in the room during recording. Calls were classified by a trained observer blinded to genotype as either high (50-kHz) or low (short 22-kHz) frequency using a threshold of 33 kHz.

Juvenile USV in response to playback of 50-kHz USV. At PND 30 ± 4, subjects were individually presented with 1-min of natural pro-social 50-kHz USV while on a radial maze illuminated to ~8 lux as described previously (30, 44). Response vocalizations were recorded with an overhead ultrasonic microphone (Avisoft Bioacoustics) and the number of calls emitted during the minute of playback were counted by a trained observer blinded to genotype and classified as high (50-kHz) or low (short 22-kHz) frequency using a threshold of 33 kHz.

Juvenile social play. At PND 38 ± 1, social play behavior was assessed following a protocol described previously (29, 103, 104). Each subject rat was placed with a freely moving, unfamiliar, strain-, sex-, and age-matched wildtype stimulus rat for 10 min in a clean, empty test arena (illuminated to ~30 lux) containing a thin layer of clean bedding. In order to facilitate social play, each subject and stimulus animal was socially isolated in a separate holding room for 30 min prior to the test. Stimulus animals were generated from wildtype Sprague-Dawley breeders (Envigo, Indianapolis, IN) and handled in a standardized manner (5 min on 3 days) prior to the assay. The interaction was video-recorded, and behaviors were later scored by a trained observer blinded to genotype as described in **Table S1**. Blind scoring was possible since *Ube3a*$^{mat-/pat+}$ rats have normal body weight and are physically indistinguishable from their wildtype littermates [41].

Olfactory discrimination. At 42 ± 3, the ability of rats to discriminate between a social and non-social odors was tested by measuring the time spent investigating odor-saturated cotton swabs. Subjects were individually tested in clean chambers (40.6 cm l x 40.6 cm w x 28 cm h) dimly illuminated to ~30 lux. On the day before the test, rats were habituated to the test chamber containing a clean dry cotton swab (15.2 cm l) for 20 min. The tip of the swab was secured 3 cm above the floor in the center of the arena by being attached to the top of a clean weighted glass dome (7.6 cm d x 10 cm h) and angled downward. On the day of the test, rats were again habituated to the arena containing a clean dry cotton swab for 10 min, followed by a swab soaked in water, then vanilla (1:100 dilution; McCormick, Hunt Valley, MD), and then a social scent. The social scent was collected by wiping a cotton swab in a zig zag pattern along the bottom of a cage of same sex but unfamiliar Sprague Dawley rats (Envigo, Indianapolis, IN). Each saturated swab was presented for 2 min and the order of odor presentation was consistent across all animals. Time

spent investigating the scents (defined as the nose within 2 cm of the cotton swab tip) was measured using videotracking software (EthoVision XT, Noldus Information Technology, Leesburg, VA), which was subsequently validated manually.

Juvenile gait. At PND 25, gait metrics were collected using the DigiGait automated treadmill system and analysis software (Mouse Specifics, Inc., Framingham, MA). Subjects were placed individually into the enclosed treadmill chamber and allowed to acclimate before the belt was turned on. The belt speed was slowly increased to a constant speed of 20 cm/sec, at which each rat was recorded making clearly visible consecutive strides for 3-6 sec.

Juvenile contextual and cued fear conditioning. At PND 43 ± 1, learning and memory were assessed using an automated fear conditioning chamber (Med Associates, Inc., Fairfax, VT) following methods previously described (104-106). On day one, rats were trained via exposure to a series of three noise-shock (conditioned stimulus-unconditioned stimulus; CS-US; 80 dB white noise, 0.7 mA foot shock) pairings inside a sound-attenuated chamber with specific visual, tactile, and odor cues. On day two (24 hrs post-training), contextual memory was tested by placing each subject back inside the training environment for 5 min. The chamber contained the identical visual, tactile, and odor cues as the training session, but no noise or foot shock occurred. On day three (48 hours post-training), cued memory was evaluated by placing subjects into a novel context with altered visual, tactile, and odor cues. Following a 3-min period of exploration, the white noise CS was presented for 3 min. Time spent freezing during each test phase was measured using VideoFreeze software (Med Associates, Inc.).

Spontaneous alternation. At 10 weeks of age, spontaneous alternation was measured by allowing rats to freely explore a novel Y-maze (black, opaque; arms: 21" l x 4.5" w x 11" h; illuminated to ~30 lux) for 8 min. An overhead camera connected to videotracking software (EthoVision XT; Noldus Information Technology, Wageningen, Netherlands) was used to quantify the number of arm entries, the number of errors (defined as the sum of direct and indirect revisits to an arm), the number of spontaneous alternations, and the maximum number of possible alternations for the entire session.

Prepulse inhibition of an acoustic startle response. At 9-10 weeks of age, prepulse inhibition was measured using an SR-Lab System (San Diego Instruments, San Diego, CA). Subjects were placed in a clear plastic cylinder, which was mounted onto a platform connected to piezoelectric transducers inside a sound-attenuating chamber with internal speakers. The background noise level in the chamber was 70 decibel (dB) white noise. Each session consisted of a 5-min acclimation period followed by a pseudo-randomized presentation of 50 trials of five different trial types: one trial type was a 40-ms 120-dB startle stimulus, three trial types involved an acoustic prepulse (74, 82, or 90 dB) presented 120 ms prior to the 120-dB startle stimulus, and there were also trials with no startle stimulus in order to measure baseline movement inside the cylinder. Each trial type was presented in 10 blocks and was randomized within blocks. The intertrial interval varied randomly between 10 sec and 20 sec. Percent PPI was calculated using the equation: % PPI = [1 – (Prepulse/Max Startle)] x 100.

Long-term potentiation (LTP). *Acute slice preparation.* At 12-13 weeks of age, subjects were deeply anesthetized with isoflurane and, following decapitation, the brain was

rapidly removed and submerged in ice-cold, oxygenated (95% O_2/5% CO_2) ACSF containing (in mM) as follows: 124 NaCl, 4 KCl, 25 $NaHCO_3$, 1 NaH_2PO_4, 2 $CaCl_2$, 1.2 $MgSO_4$, and 10 glucose. On an ice-cold plate, the brain hemispheres were separated, blocked, and the hippocampi removed. The 400-μmat-thick slices were then cut using a McIlwain tissue chopper (Brinkman, Westbury, NY). Slices from the dorsal thirds of the hippocampus were used. Slices were incubated (at 33°C) for 20 min and then maintained in submerged-type chambers that were continuously perfused (2-3 mL/min) with ACSF and allowed to recover for at least 1.5-2 hr before recordings. Just prior to start of experiments slices were transferred to a submersion chamber on an upright Olympus microscope, perfused with 30.4°C normal ACSF saturated with 95% O_2/5% CO_2.

Electrophysiological recordings. A bipolar, nichrome wire stimulating electrode (MicroProbes) was placed in stratum radiatum of the CA1 region and used to activate Schaffer collateral/commissural fiber synapses. Evoked fEPSPs (basal stimulation rate = 0.033 Hz) were recorded in *stratum radiatum* using borosilicate pipettes (Sutter Instruments, Novato, CA) filled with ACSF (resistance 5-10 mΩ). Submerged-type recording chambers were used for all recordings. All recordings were obtained with a MultiClamp 700B amplifier (Molecular Devices, San Jose, CA), filtered at 2 kHz, digitized at 10 Hz. To determine response parameters of excitatory synapses, basal synaptic strength was determined by comparing the amplitudes of presynaptic fiber volleys and postsynaptic fEPSP slopes for responses elicited by different intensities of SC fiber stimulation. Presynaptic neurotransmitter release probability was compared by paired pulse facilitation (PPF) experiments, performed at 25, 50, 100 and 250 msec stimulation intervals. LTP was induced by high frequency stimulation (HFS) using a 2x tetanus (1-s-long train of 100 Hz stimulation) with a 10 sec inter-tetanus interval. At the start of each experiment, the maximal fEPSP amplitude was determined and the intensity of presynaptic fiber stimulation was adjusted

to evoke fEPSPs with an amplitude ~40-50% of the maximal amplitude. The average slope of EPSPs elicited 55-60 min after HFS (normalized to baseline) was used for statistical comparisons.

Magnetic resonance imaging (MRI). At 6.5 months of age, *ex vivo* neuroimaging was carried out by following a previously described protocol (30, 44). Brains were flushed and fixed via transcardial perfusion with 50 mL phosphate-buffered saline (PBS) containing 10 U/mL heparin and 2 mM ProHance (gadolinium contrast agent; Bracco Diagnostics Inc., Monroe Township, NJ) followed by 50 mL 4% paraformaldehyde in PBS containing 2 mM ProHance. Brains were incubated in the 4% PFA solution at 4°C for 24 hrs, transferred to a 0.02% sodium azide PBS solution, and then incubated at 4°C for at least one month before being scanned. Magnetic resonance imaging (MRI) of the brains within their skulls was carried out using a multi-channel 7.0 Tesla scanner (Agilent Inc., Palo Alto, CA). Seven custom millipede coils were used to image the brains in parallel (107, 108). Parameters used in the anatomical MRI scans: T2 weighted 3D fast spin echo sequence, with a cylindrical acquisition of k-space, and with a TR of 350 ms, and TEs of 10.5 ms per echo for 12 echoes, field of view 36 x 36 x 40 mm^3 and a matrix size of 456 x 456 x 504 giving an image with 0.079 mm isotropic voxels (109). The current scan time for this sequence is ~ 3 hours.

To visualize and compare any changes in the rat brains the images were linearly and non-linearly registered together using the pydpiper framework. Registrations were performed using a combination of mni_autoreg tools (110) and ANTS (advanced normalization tools) (111). Following registration, a population atlas was created representing the average anatomy of the study sample. At the end of the registration process all the scans were deformed into alignment with one another in an unbiased fashion. This allows for analysis of the deformations required to

register the brains together, which can be used to assess the volume of the individual brains and compared them to one another (112-117). For comparisons to the juvenile brains, a separate registration pipeline was used that included all the brains from this study as well as the previous Berg et al. study. Volumetric differences were calculated on a regional and a voxelwise basis. An in-house manually segmented hierarchical rat brain atlas was used to calculate the volumes of 52 different segmented structures. These structures were derived from multiple atlases (118, 119) and then modified for use in the rat brain.

Statistical analysis. Statistical analyses were performed using GraphPad Prism 8 statistical software (GraphPad Software, San Diego, CA). Clampex 10.6 software suite (Molecular Devices, San Jose, CA) was used for analyzing electrophysiological data. Sample sizes and statistical tests are detailed throughout the text and in figure legends. Congruent with previous studies, no significant sex differences were detected so the results herein include both males and females.

Analysis of behavior and LTP. For single comparisons between two groups, either a Student's *t*-test or Mann-Whitney *U* test was used. Data that passed distribution normality tests, were collected using continuous variables, and had similar variances across groups were analyzed via Student's *t*-test. Alternatively, a Mann-Whitney *U* test was used. To analyze the effects of genotype and a second factor, either two-way or two-way repeated measures (RM) two-way ANOVA was used. In RM ANOVA, genotype was the between-group factor and time, limb set, test phase, scent, or prepulse intensity was the within-group factor. *Post hoc* comparisons were performed following a significant main effect or interaction and were carried out using Holm-Sidak's multiple comparisons test controlling for multiple comparisons. Data points within two

standard deviations of the mean were included, all significance tests were two-tailed, and a *p*-value of < 0.05 was considered significant.

Analysis of MRI. Statistical analyses were used to compare both the absolute and relative volumes voxelwise as well as across the 52 different hierarchical structures in the rat brains. Absolute volume was calculated as mm^3 and relative volume was assessed as a measure of % total brain volume. Voxelwise and regional differences were assessed using linear models. All image analysis tools and software is available on Github (https://github.com/Mouse-Imaging-Centre). Multiple comparisons were controlled for using the False Discovery Rate (120).

References

1. C. Williams, L. Franco, Angelman syndrome at the synapse: meeting report of the Angelman Syndrome Foundation's 2009 scientific symposium. *J Child Neurol* **25**, 254-261 (2010).
2. U. Albrecht *et al.*, Imprinted expression of the murine Angelman syndrome gene, Ube3a, in hippocampal and Purkinje neurons. *Nat Genet* **17**, 75-78 (1997).
3. L. Meng *et al.*, Towards a therapy for Angelman syndrome by targeting a long non-coding RNA. *Nature* **518**, 409-412 (2015).
4. J. L. Daily *et al.*, Adeno-associated virus-mediated rescue of the cognitive defects in a mouse model for Angelman syndrome. *PLoS One* **6**, e27221 (2011).
5. B. J. Bailus *et al.*, Protein Delivery of an Artificial Transcription Factor Restores Widespread Ube3a Expression in an Angelman Syndrome Mouse Brain. *Mol Ther* **24**, 548-555 (2016).
6. Adhikari *et al.*, Functional rescue in an Angelman syndrome model following treatment with lentivector transduced hematopoietic stem cells. *Human Molecular Genetics* **In press** (2021).
7. J. M. Wolter *et al.*, Cas9 gene therapy for Angelman syndrome traps Ube3a-ATS long non-coding RNA. *Nature* **587**, 281-284 (2020).
8. B. Ellenbroek, J. Youn, Rodent models in neuroscience research: is it a rat race? *Dis Model Mech* **9**, 1079-1087 (2016).
9. M. Wohr, R. K. Schwarting, Affective communication in rodents: ultrasonic vocalizations as a tool for research on emotion and motivation. *Cell and tissue research* **354**, 81-97 (2013).
10. S. M. Brudzynski, Ethotransmission: communication of emotional states through ultrasonic vocalization in rats. *Curr Opin Neurobiol* **23**, 310-317 (2013).
11. R. J. Blanchard, D. C. Blanchard, R. Agullana, S. M. Weiss, Twenty-two kHz alarm cries to presentation of a predator, by laboratory rats living in visible burrow systems. *Physiology & behavior* **50**, 967-972 (1991).
12. M. Sadananda, M. Wohr, R. K. Schwarting, Playback of 22-kHz and 50-kHz ultrasonic vocalizations induces differential c-fos expression in rat brain. *Neurosci Lett* **435**, 17-23 (2008).
13. M. Fendt, M. Brosch, K. E. A. Wernecke, M. Willadsen, M. Wohr, Predator odour but not TMT induces 22-kHz ultrasonic vocalizations in rats that lead to defensive behaviours in conspecifics upon replay. *Scientific reports* **8**, 11041 (2018).
14. M. Wohr, R. K. Schwarting, Ultrasonic communication in rats: can playback of 50-kHz calls induce approach behavior? *PloS one* **2**, e1365 (2007).
15. T. M. Kisko, M. Wohr, V. C. Pellis, S. M. Pellis, From Play to Aggression: High-Frequency 50-kHz Ultrasonic Vocalizations as Play and Appeasement Signals in Rats. *Curr Top Behav Neurosci* **30**, 91-108 (2017).
16. S. Lopuch, P. Popik, Cooperative behavior of laboratory rats (Rattus norvegicus) in an instrumental task. *J Comp Psychol* **125**, 250-253 (2011).
17. I. Willuhn *et al.*, Phasic dopamine release in the nucleus accumbens in response to pro-social 50 kHz ultrasonic vocalizations in rats. *J Neurosci* **34**, 10616-10623 (2014).

18. R. Bredewold *et al.*, Involvement of dopamine, but not norepinephrine, in the sex-specific regulation of juvenile socially rewarding behavior by vasopressin. *Neuropsychopharmacology* **43**, 2109-2117 (2018).
19. J. Burgdorf *et al.*, Ultrasonic vocalizations of rats (Rattus norvegicus) during mating, play, and aggression: Behavioral concomitants, relationship to reward, and self-administration of playback. *J Comp Psychol* **122**, 357-367 (2008).
20. J. Panksepp, J. Burgdorf, 50-kHz chirping (laughter?) in response to conditioned and unconditioned tickle-induced reward in rats: effects of social housing and genetic variables. *Behav Brain Res* **115**, 25-38 (2000).
21. S. Ishiyama, M. Brecht, Neural correlates of ticklishness in the rat somatosensory cortex. *Science* **354**, 757-760 (2016).
22. R. Rygula, H. Pluta, P. Popik, Laughing rats are optimistic. *PloS one* **7**, e51959 (2012).
23. J. Panksepp, Psychology. Beyond a joke: from animal laughter to human joy? *Science* **308**, 62-63 (2005).
24. J. Panksepp, J. Burgdorf, "Laughing" rats and the evolutionary antecedents of human joy? *Physiol Behav* **79**, 533-547 (2003).
25. K. Hammerschmidt *et al.*, Mice do not require auditory input for the normal development of their ultrasonic vocalizations. *BMC Neurosci* **13**, 40 (2012).
26. M. A. Hofer, H. N. Shair, S. A. Brunelli, Ultrasonic vocalizations in rat and mouse pups. *Current protocols in neuroscience / editorial board, Jacqueline N. Crawley ... [et al.]* **Chapter 8**, Unit 8 14 (2002).
27. C. V. Portfors, Types and functions of ultrasonic vocalizations in laboratory rats and mice. *J Am Assoc Lab Anim Sci* **46**, 28-34 (2007).
28. C. V. Portfors, D. J. Perkel, The role of ultrasonic vocalizations in mouse communication. *Curr Opin Neurobiol* **28**, 115-120 (2014).
29. E. L. Berg *et al.*, Developmental social communication deficits in the Shank3 rat model of phelan-mcdermid syndrome and autism spectrum disorder. *Autism research : official journal of the International Society for Autism Research* **11**, 587-601 (2018).
30. E. L. Berg *et al.*, Developmental social communication deficits in the Shank3 rat model of phelan-mcdermid syndrome and autism spectrum disorder. *Autism Res* 10.1002/aur.1925 (2018).
31. R. Dutta, J. N. Crawley, Behavioral Evaluation of Angelman Syndrome Mice at Older Ages. *Neuroscience* **445**, 163-171 (2020).
32. H. S. Huang *et al.*, Behavioral deficits in an Angelman syndrome model: effects of genetic background and age. *Behav Brain Res* **243**, 79-90 (2013).
33. Y. H. Jiang *et al.*, Altered ultrasonic vocalization and impaired learning and memory in Angelman syndrome mouse model with a large maternal deletion from Ube3a to Gabrb3. *PLoS One* **5**, e12278 (2010).
34. K. Kondrakiewicz, M. Kostecki, W. Szadzinska, E. Knapska, Ecological validity of social interaction tests in rats and mice. *Genes Brain Behav* **18**, e12525 (2019).
35. S. Netser *et al.*, Distinct dynamics of social motivation drive differential social behavior in laboratory rat and mouse strains. *Nat Commun* **11**, 5908 (2020).
36. C. S. Ku, E. Y. Loy, Y. Pawitan, K. S. Chia, The pursuit of genome-wide association studies: where are we now? *J Hum Genet* **55**, 195-206 (2010).
37. H. Harony-Nicolas *et al.*, Oxytocin improves behavioral and electrophysiological deficits in a novel Shank3-deficient rat. *Elife* **6** (2017).

38. C. C. Parker *et al.*, Rats are the smart choice: Rationale for a renewed focus on rats in behavioral genetics. *Neuropharmacology* **76 Pt B**, 250-258 (2014).
39. J. R. Homberg, M. Wohr, N. Alenina, Comeback of the Rat in Biomedical Research. *ACS Chem Neurosci* **8**, 900-903 (2017).
40. C. J. Reppucci, L. A. Brown, A. Q. Chambers, A. H. Veenema, Wistar rats and C57BL/6 mice differ in their motivation to seek social interaction versus food in the Social versus Food Preference Test. *Physiol Behav* **227**, 113162 (2020).
41. C. J. Burke, T. M. Kisko, H. Swiftwolfe, S. M. Pellis, D. R. Euston, Specific 50-kHz vocalizations are tightly linked to particular types of behavior in juvenile rats anticipating play. *PloS one* **12**, e0175841 (2017).
42. T. M. Kisko, D. R. Euston, S. M. Pellis, Are 50-khz calls used as play signals in the playful interactions of rats? III. The effects of devocalization on play with unfamiliar partners as juveniles and as adults. *Behav Processes* **113**, 113-121 (2015).
43. A. Dodge *et al.*, Generation of a Novel Rat Model of Angelman Syndrome with a Complete Ube3a Gene Deletion. *Autism Res* **13**, 397-409 (2020).
44. E. L. Berg *et al.*, Translational outcomes in a full gene deletion of ubiquitin protein ligase E3A rat model of Angelman syndrome. *Transl Psychiatry* **10**, 39 (2020).
45. J. Burgdorf, J. Panksepp, S. M. Brudzynski, R. Kroes, J. R. Moskal, Breeding for 50-kHz positive affective vocalization in rats. *Behav Genet* **35**, 67-72 (2005).
46. J. Burgdorf, J. Panksepp, Tickling induces reward in adolescent rats. *Physiol Behav* **72**, 167-173 (2001).
47. J. Panksepp, The ontogeny of play in rats. *Dev Psychobiol* **14**, 327-332 (1981).
48. Copping, Silverman, Abnormal electrophysiological phenotypes and sleep deficits in a mouse model of Angelman Syndrome. *Molecular Autism* **In press** (2020).
49. P. T. Leach, J. N. Crawley, Touchscreen learning deficits in Ube3a, Ts65Dn and Mecp2 mouse models of neurodevelopmental disorders with intellectual disabilities. *Genes Brain Behav* **17**, e12452 (2018).
50. J. C. Grieco, A. Gouelle, E. J. Weeber, Identification of spatiotemporal gait parameters and pressure-related characteristics in children with Angelman syndrome: A pilot study. *J Appl Res Intellect Disabil* **31**, 1219-1224 (2018).
51. E. Powell, A. M. Anch, J. Dyche, C. Bloom, R. R. Richtert, The splay angle: A new measure for assessing neuromuscular dysfunction in rats. *Physiol Behav* **67**, 819-821 (1999).
52. G. L. Collingridge, J. T. Isaac, Functional roles of protein interactions with AMPA and kainate receptors. *Neurosci Res* **47**, 3-15 (2003).
53. Y. H. Jiang *et al.*, Mutation of the Angelman ubiquitin ligase in mice causes increased cytoplasmic p53 and deficits of contextual learning and long-term potentiation. *Neuron* **21**, 799-811 (1998).
54. G. M. van Woerden *et al.*, Rescue of neurological deficits in a mouse model for Angelman syndrome by reduction of alphaCaMKII inhibitory phosphorylation. *Nat Neurosci* **10**, 280-282 (2007).
55. R. S. Zucker, W. G. Regehr, Short-term synaptic plasticity. *Annu Rev Physiol* **64**, 355-405 (2002).
56. R. S. Zucker, Short-term synaptic plasticity. *Annu Rev Neurosci* **12**, 13-31 (1989).
57. D. H. Thor, W. R. Holloway, Jr., Social play in juvenile rats: a decade of methodological and experimental research. *Neuroscience and biobehavioral reviews* **8**, 455-464 (1984).

58. M. J. Meaney, J. Stewart, Neonatal-androgens influence the social play of prepubescent rats. *Hormones and behavior* **15**, 197-213 (1981).
59. S. M. Pellis, V. C. Pellis, Play fighting of rats in comparative perspective: a schema for neurobehavioral analyses. *Neuroscience and biobehavioral reviews* **23**, 87-101 (1998).
60. S. M. Pellis, V. C. Pellis, What is play fighting and what is it good for? *Learn Behav* **45**, 355-366 (2017).
61. J. S. Burgdorf, S. M. Brudzynski, J. R. Moskal, Using rat ultrasonic vocalization to study the neurobiology of emotion: from basic science to the development of novel therapeutics for affective disorders. *Curr Opin Neurobiol* **60**, 192-200 (2020).
62. M. D. Braun *et al.*, Sex-specific effects of Cacna1c haploinsufficiency on object recognition, spatial memory, and reversal learning capabilities in rats. *Neurobiology of learning and memory* **155**, 543-555 (2018).
63. T. M. Kisko *et al.*, Sex-dependent effects of Cacna1c haploinsufficiency on juvenile social play behavior and pro-social 50-kHz ultrasonic communication in rats. *Genes Brain Behav* 10.1111/gbb.12552, e12552 (2018).
64. T. M. Kisko *et al.*, Cacna1c haploinsufficiency leads to pro-social 50-kHz ultrasonic communication deficits in rats. *Disease models & mechanisms* **11** (2018).
65. T. M. Redecker, T. M. Kisko, R. K. W. Schwarting, M. Wohr, Effects of Cacna1c haploinsufficiency on social interaction behavior and 50-kHz ultrasonic vocalizations in adult female rats. *Behavioural brain research* **367**, 35-52 (2019).
66. M. Fernandez, I. Mollinedo-Gajate, O. Penagarikano, Neural Circuits for Social Cognition: Implications for Autism. *Neuroscience* **370**, 148-162 (2018).
67. H. Angelman, 'Puppet' children. A report on three cases. *Dev Med Child Neurol* **7**, 681-688 (1965).
68. L. M. Bird, Angelman syndrome: review of clinical and molecular aspects. *Appl Clin Genet* **7**, 93-104 (2014).
69. S. B. Cassidy, E. Dykens, C. A. Williams, Prader-Willi and Angelman syndromes: sister imprinted disorders. *Am J Med Genet* **97**, 136-146 (2000).
70. Finucane BM *et al.*, *15q Duplication Syndrome and Related Disorders.* A. M. Pagon RA, Ardinger HH, et al., editors. , Ed., GeneReviews® [Internet]. (Seattle (WA): University of Washington, Seattle; 1993-2016. , 2016).
71. J. K. Gentile *et al.*, A neurodevelopmental survey of Angelman syndrome with genotype-phenotype correlations. *J Dev Behav Pediatr* **31**, 592-601 (2010).
72. W. H. Tan *et al.*, Angelman syndrome: Mutations influence features in early childhood. *Am J Med Genet A* **155A**, 81-90 (2011).
73. W. H. Tan, L. M. Bird, Angelman syndrome: Current and emerging therapies in 2016. *Am J Med Genet C Semin Med Genet* **172**, 384-401 (2016).
74. A. C. Wheeler, P. Sacco, R. Cabo, Unmet clinical needs and burden in Angelman syndrome: a review of the literature. *Orphanet J Rare Dis* **12**, 164 (2017).
75. C. A. Williams, Neurological aspects of the Angelman syndrome. *Brain Dev* **27**, 88-94 (2005).
76. C. A. Williams, The behavioral phenotype of the Angelman syndrome. *Am J Med Genet C Semin Med Genet* **154C**, 432-437 (2010).
77. K. C. Berridge, 'Liking' and 'wanting' food rewards: brain substrates and roles in eating disorders. *Physiol Behav* **97**, 537-550 (2009).

78. K. C. Berridge, J. W. Aldridge, Decision Utility, Incentive Salience, and Cue-Triggered "Wanting". *Oxf Ser Soc Cogn Soc Neurosci* **2009**, 509-533 (2009).
79. K. C. Berridge, T. E. Robinson, J. W. Aldridge, Dissecting components of reward: 'liking', 'wanting', and learning. *Curr Opin Pharmacol* **9**, 65-73 (2009).
80. S. Okabe, Y. Takayanagi, M. Yoshida, T. Onaka, Post-weaning stroking stimuli induce affiliative behavior toward humans and influence brain activity in female rats. *Sci Rep* **11**, 3805 (2021).
81. P. A. Perrino, S. J. Chamberlain, I. M. Eigsti, R. H. Fitch, Communication-related assessments in an Angelman syndrome mouse model. *Brain Behav* **11**, e01937 (2021).
82. D. C. Stoppel, M. P. Anderson, Hypersociability in the Angelman syndrome mouse model. *Exp Neurol* **293**, 137-143 (2017).
83. S. M. Brudzynski, Ultrasonic calls of rats as indicator variables of negative or positive states: acetylcholine-dopamine interaction and acoustic coding. *Behavioural brain research* **182**, 261-273 (2007).
84. S. Brudzynski, *Handbook of Mammalian Vocalization: An Integrative Neuroscience Approach* (ed. 1st Edition, 2009).
85. S. M. Brudzynski, Communication of adult rats by ultrasonic vocalization: biological, sociobiological, and neuroscience approaches. *ILAR J* **50**, 43-50 (2009).
86. S. M. Brudzynski, Pharmacology of Ultrasonic Vocalizations in adult Rats: Significance, Call Classification and Neural Substrate. *Curr Neuropharmacol* **13**, 180-192 (2015).
87. R. K. W. Schwarting, Ultrasonic vocalization in juvenile and adult male rats: A comparison among stocks. *Physiol Behav* **191**, 1-11 (2018).
88. R. K. W. Schwarting, Ultrasonic vocalization in female rats: A comparison among three outbred stocks from pups to adults. *Physiol Behav* **196**, 59-66 (2018).
89. M. Wohr, D. Seffer, R. K. Schwarting, Studying Socio-Affective Communication in Rats through Playback of Ultrasonic Vocalizations. *Curr Protoc Neurosci* **75**, 8 35 31-38 35 17 (2016).
90. R. K. Schwarting, N. Jegan, M. Wohr, Situational factors, conditions and individual variables which can determine ultrasonic vocalizations in male adult Wistar rats. *Behav Brain Res* **182**, 208-222 (2007).
91. M. A. Hofer, H. Shair, Ultrasonic vocalization during social interaction and isolation in 2-weeek-old rats. *Dev Psychobiol* **11**, 495-504 (1978).
92. J. Panksepp, W. W. Beatty, Social deprivation and play in rats. *Behav Neural Biol* **30**, 197-206 (1980).
93. K. J. Argue, M. M. McCarthy, Utilization of same- vs. mixed-sex dyads impacts the observation of sex differences in juvenile social play behavior. *Curr Neurobiol* **6**, 17-23 (2015).
94. I. Jamal *et al.*, Rescue of altered HDAC activity recovers behavioural abnormalities in a mouse model of Angelman syndrome. *Neurobiol Dis* **105**, 99-108 (2017).
95. K. M. Ku, R. K. Weir, J. L. Silverman, R. F. Berman, M. D. Bauman, Behavioral Phenotyping of Juvenile Long-Evans and Sprague-Dawley Rats: Implications for Preclinical Models of Autism Spectrum Disorders. *PLoS One* **11**, e0158150 (2016).
96. E. I. Varlinskaya, L. P. Spear, Social interactions in adolescent and adult Sprague-Dawley rats: impact of social deprivation and test context familiarity. *Behav Brain Res* **188**, 398-405 (2008).

97. S. L. Ciarlone, J. C. Grieco, D. P. D'Agostino, E. J. Weeber, Ketone ester supplementation attenuates seizure activity, and improves behavior and hippocampal synaptic plasticity in an Angelman syndrome mouse model. *Neurobiol Dis* **96**, 38-46 (2016).
98. I. Filonova, J. H. Trotter, J. L. Banko, E. J. Weeber, Activity-dependent changes in MAPK activation in the Angelman Syndrome mouse model. *Learn Mem* **21**, 98-104 (2014).
99. E. J. Weeber *et al.*, Derangements of hippocampal calcium/calmodulin-dependent protein kinase II in a mouse model for Angelman mental retardation syndrome. *J Neurosci* **23**, 2634-2644 (2003).
100. H. A. Born *et al.*, Strain-dependence of the Angelman Syndrome phenotypes in Ube3a maternal deficiency mice. *Sci Rep* **7**, 8451 (2017).
101. M. C. Judson *et al.*, Decreased Axon Caliber Underlies Loss of Fiber Tract Integrity, Disproportional Reductions in White Matter Volume, and Microcephaly in Angelman Syndrome Model Mice. *J Neurosci* **37**, 7347-7361 (2017).
102. M. Wohr *et al.*, New insights into the relationship of neurogenesis and affect: tickling induces hippocampal cell proliferation in rats emitting appetitive 50-kHz ultrasonic vocalizations. *Neuroscience* **163**, 1024-1030 (2009).
103. E. L. Berg *et al.*, Translational outcomes relevant to neurodevelopmental disorders following early life exposure of rats to chlorpyrifos. *J Neurodev Disord* **12**, 40 (2020).
104. E. L. Berg *et al.*, Developmental exposure to near roadway pollution produces behavioral phenotypes relevant to neurodevelopmental disorders in juvenile rats. *Transl Psychiatry* **10**, 289 (2020).
105. A. Adhikari *et al.*, Cognitive Deficits in the Snord116 Deletion Mouse Model for Prader-Willi Syndrome. *Neurobiol Learn Mem* 10.1016/j.nlm.2018.05.011 (2018).
106. N. A. Copping *et al.*, Neuronal overexpression of Ube3a isoform 2 causes behavioral impairments and neuroanatomical pathology relevant to 15q11.2-q13.3 duplication syndrome. *Human molecular genetics* **26**, 3995-4010 (2017).
107. J. P. Lerch, J. G. Sled, R. M. Henkelman, MRI phenotyping of genetically altered mice. *Methods in molecular biology* **711**, 349-361 (2011).
108. N. A. Bock, B. J. Nieman, J. B. Bishop, R. Mark Henkelman, In vivo multiple-mouse MRI at 7 Tesla. *Magn Reson Med* **54**, 1311-1316 (2005).
109. T. L. Spencer Noakes, R. M. Henkelman, B. J. Nieman, Partitioning k-space for cylindrical three-dimensional rapid acquisition with relaxation enhancement imaging in the mouse brain. *NMR Biomed* **30** (2017).
110. D. L. Collins, P. Neelin, T. M. Peters, A. C. Evans, Automatic 3D intersubject registration of MR volumetric data in standardized Talairach space. *J Comput Assist Tomogr* **18**, 192-205 (1994).
111. B. B. Avants *et al.*, A reproducible evaluation of ANTs similarity metric performance in brain image registration. *Neuroimage* **54**, 2033-2044 (2011).
112. B. J. Nieman *et al.*, MRI to Assess Neurological Function. *Curr Protoc Mouse Biol* **8**, e44 (2018).
113. B. J. Nieman *et al.*, In vivo MRI of neural cell migration dynamics in the mouse brain. *NeuroImage* **50**, 456-464 (2010).
114. J. Bishop *et al.*, Retrospective gating for mouse cardiac MRI. *Magn Reson Med* **55**, 472-477 (2006).

115. J. P. Lerch *et al.*, Automated cortical thickness measurements from MRI can accurately separate Alzheimer's patients from normal elderly controls. *Neurobiol Aging* **29**, 23-30 (2008).
116. J. P. Lerch *et al.*, Automated deformation analysis in the YAC128 Huntington disease mouse model. *NeuroImage* **39**, 32-39 (2008).
117. J. P. Lerch *et al.*, Cortical thickness measured from MRI in the YAC128 mouse model of Huntington's disease. *NeuroImage* **41**, 243-251 (2008).
118. A. E. Dorr, J. P. Lerch, S. Spring, N. Kabani, R. M. Henkelman, High resolution three-dimensional brain atlas using an average magnetic resonance image of 40 adult C57Bl/6J mice. *NeuroImage* **42**, 60-69 (2008).
119. P. E. Steadman *et al.*, Genetic effects on cerebellar structure across mouse models of autism using a magnetic resonance imaging atlas. *Autism research : official journal of the International Society for Autism Research* **7**, 124-137 (2014).
120. C. R. Genovese, N. A. Lazar, T. Nichols, Thresholding of statistical maps in functional neuroimaging using the false discovery rate. *NeuroImage* **15**, 870-878 (2002).

Figures

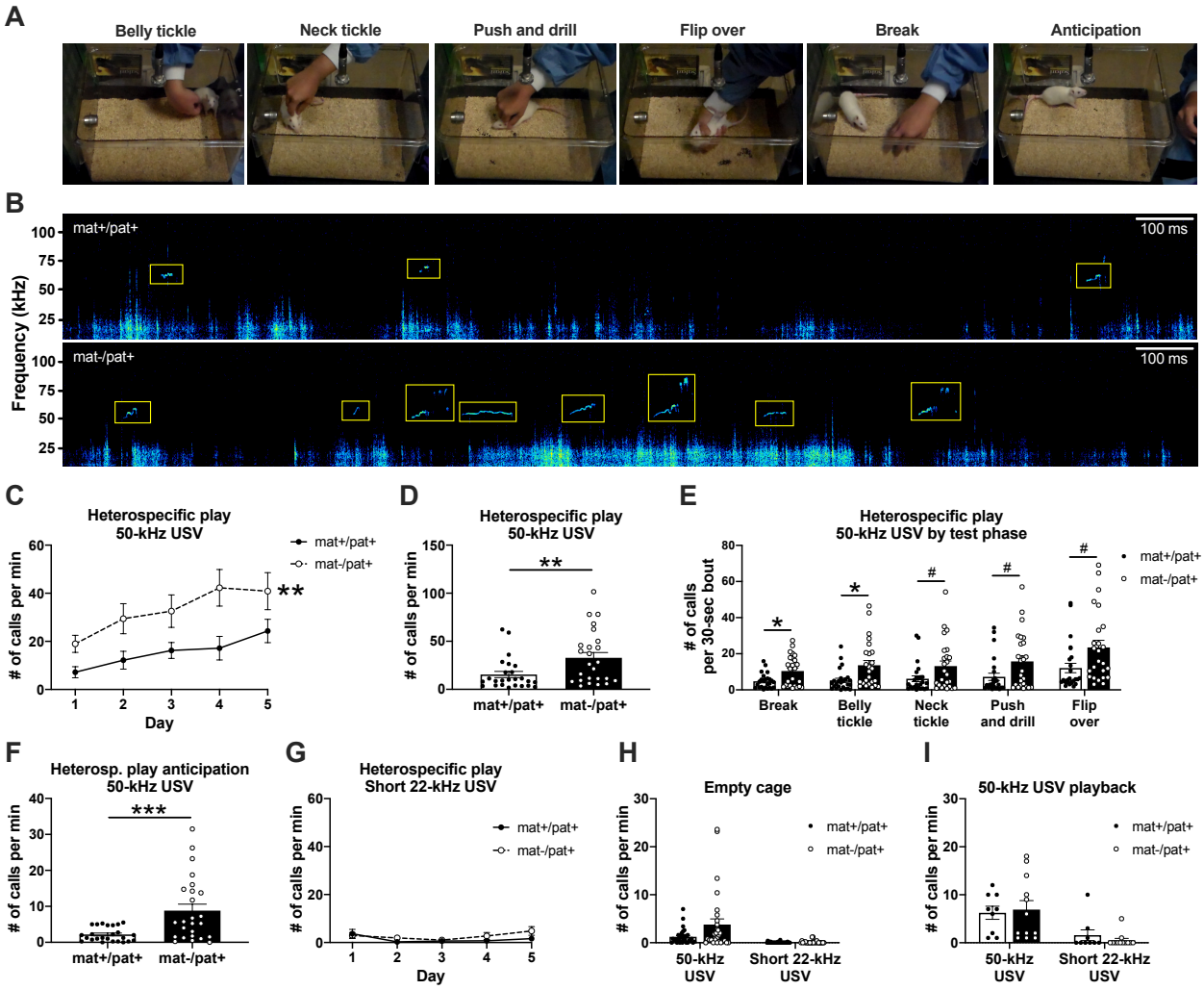

Figure 1. Overabundant emission of laughter-like 50-kHz calls in juvenile *Ube3a*$^{mat-/pat+}$ rats. **(A)** Example images of the manipulations used to mimic social play and elicit ultrasonic vocalizations (USV). **(B)** Example spectrograms of USV from a wildtype littermate control (*Ube3a*$^{mat+/pat+}$; mat+/pat+; upper) and *Ube3a*$^{mat-/pat+}$ rat (mat-/pat+; lower). **(C)** Across five days of heterospecific play sessions, 50-kHz USV emission increased with repeated testing in both mat-/pat+ (n = 25) and controls (n = 25), but the emission rate was substantially elevated in mat-/pat+. **(D)** On average, mat-/pat+ rats produced 50-kHz USV at more than twice the rate of controls. **(E)** Specifically, 50-kHz calling was abnormally high during the break and belly tickle phases, with trending increases during neck tickle, push and drill, and flip over. **(F)** Prior to the onset of play, mat-/pat+ rats emitted anticipatory 50-kHz USV at more than three times the rate of controls. **(G)** Production of short 22-kHz USV was low, did not differ between genotypes, and did not change over subsequent play sessions. **(H)** The rates of 50-kHz and short 22-kHz calling during empty cage exploration were comparable between genotypes (mat+/pat+, n = 32; mat-/pat+, n = 29), as were the **(I)** 50-kHz and short 22-kHz calling rates in response to hearing playback of conspecific 50-kHz USV (mat+/pat+, n = 9; mat-/pat+, n = 12). Of note, long 22-kHz USV known to function

as “alarm calls” were very rarely observed, indicating that our paradigms were not aversive. Data are depicted as mean ± S.E.M. C: $^{**}p < 0.01$, repeated measures ANOVA. D, F: $^{***}p < 0.001$, $^{**}p < 0.01$, Mann-Whitney *U* test. E: $^{*}p < 0.05$, $^{\#}p < 0.06$, repeated measures ANOVA, Holm-Sidak’s *post hoc*.

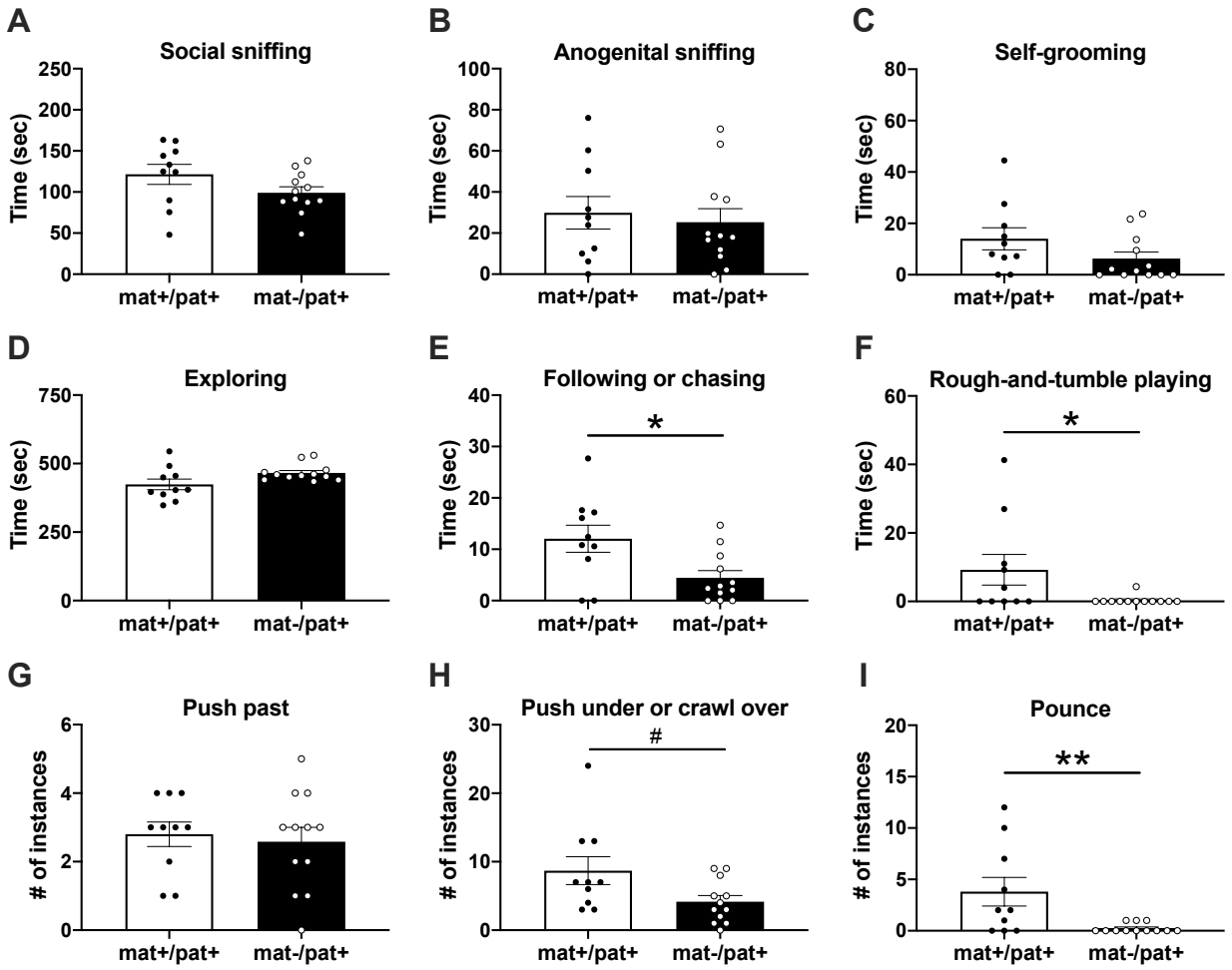

Figure 2. Intact social interest but deficient expression of key social interaction behaviors in juvenile *Ube3a*$^{mat-/pat+}$ rats. **(A)** During a 10-min interaction session with a novel same-sex wildtype conspecific, *Ube3a*$^{mat-/pat+}$ rats (mat-/pat+; n = 12) spent similar amounts of time social sniffing, **(B)** anogenital sniffing, **(C)** self-grooming, and **(D)** exploring the arena compared to wildtype littermate controls (*Ube3a*$^{mat+/pat+}$; mat+/pat+; n = 10). **(E)** Robust deficits, however, were discovered in the time spent following or chasing and **(F)** rough-and-tumble playing. **(G)** The number of push pasts were similar across genotypes but **(H)** there was a trend for mat-/pat+ to less frequently push under or crawl over and **(I)** mat-/pat+ rats did not perform nearly as many pounces as wildtype littermates. Data are depicted as mean ± S.E.M. $^{**}p < 0.01$, $^{*}p < 0.05$, $^{\#}p < 0.065$, Mann-Whitney U test.

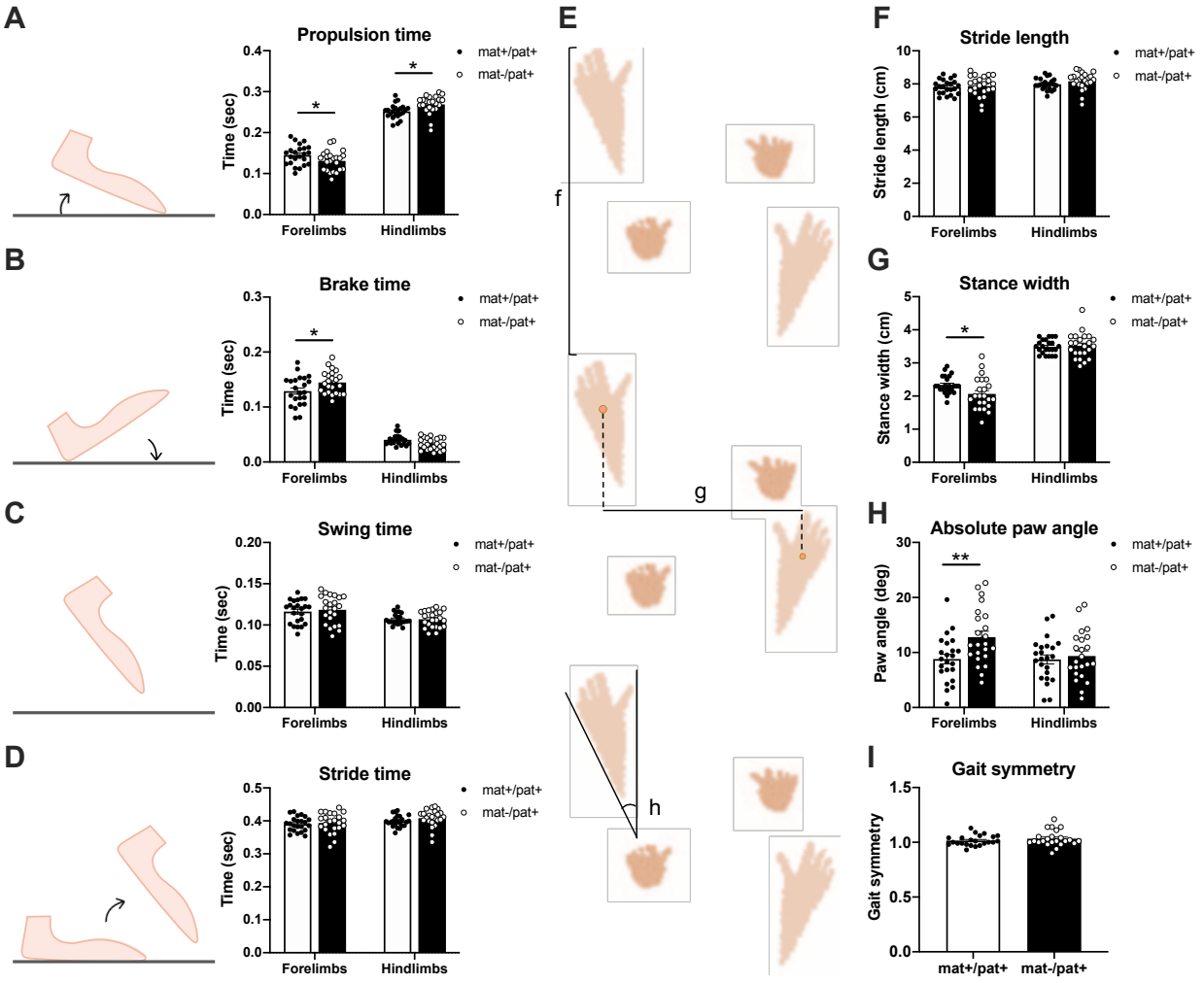

Figure 3. Abnormal gait in *Ube3a*$^{mat-/pat+}$ rats. **(A)** While treadmill walking, *Ube3a*$^{mat-/pat+}$ rats (mat-/pat+; n = 23) displayed aberrant propulsion time (time from maximal paw contact with belt to just before liftoff) in both sets of limbs. Compared to wildtype littermates (*Ube3a*$^{mat+/pat+}$; mat+/pat+; n = 23), propulsion time was decreased in the forelimbs and increased in hindlimbs. **(B)** Brake time (time from initial to maximal paw contact with belt) was significantly elevated in the forelimbs of mat-/pat+ while a trending reduction in hindlimb brake time was found (p=0.150). **(C)** Swing time (no paw contact with the belt) and **(D)** stride time (sum of swing and stance time) were similar across genotypes. **(E)** Example paw prints illustrating the spatial gait parameters depicted in panels F, G, and H. **(F)** Stride length did not differ between groups, but **(G)** forelimb stance width was narrower and **(H)** absolute paw angle for the forelimbs was greater, indicating more external rotation in mat-/pat+ rats. **(I)** No significant difference in gait symmetry (ratio of forelimb to hindlimb stepping frequency) was detected. Data are depicted as mean ± S.E.M. ** $p < 0.01$, * $p < 0.05$, repeated measures ANOVA, Holm-Sidak's *post hoc*.

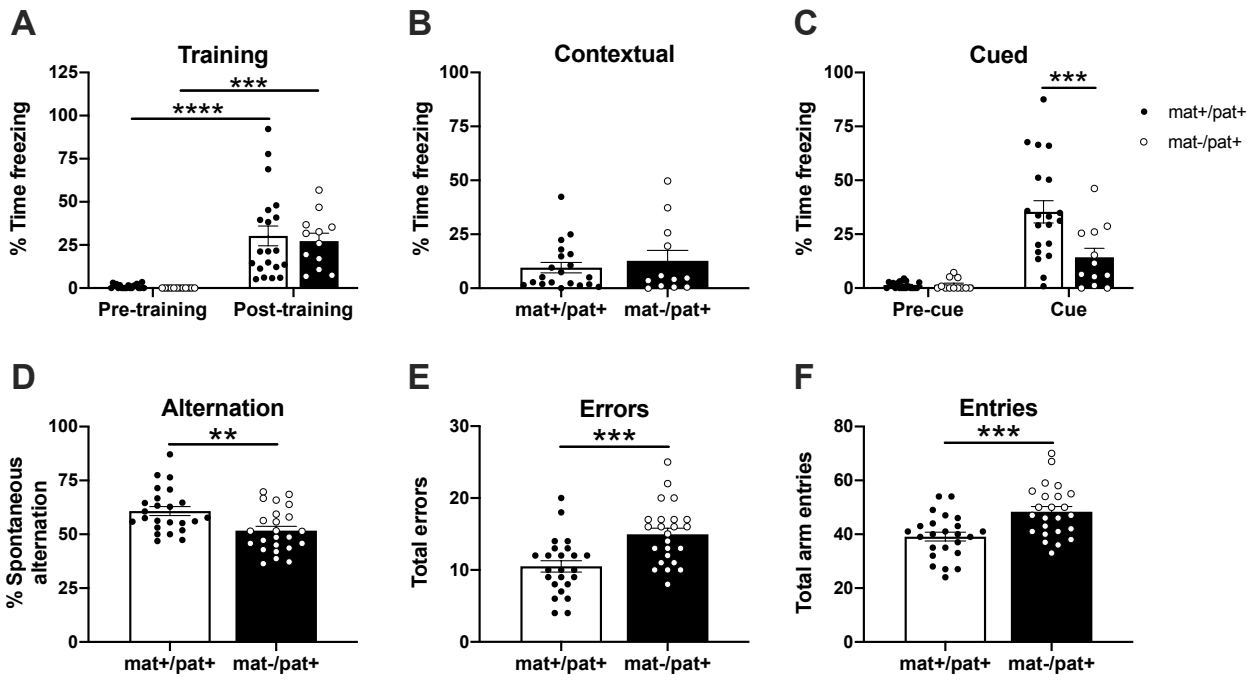

Figure 4. Impaired learning and memory in *Ube3a*$^{mat-/pat+}$ rats. **(A)** During fear conditioning training, juvenile *Ube3a*$^{mat-/pat+}$ (mat-/pat+; $n = 12$) and wildtype littermate controls (*Ube3a*$^{mat+/pat+}$; mat+/pat+; $n = 20$) showed similar increases in freezing post-training. **(B)** When returned to the training context 24 hrs following training, mat-/pat+ rats exhibited a similar level of freezing to wildtypes. **(C)** When introduced to a novel context 48 hrs after training, no difference in freezing pre-cue was found but mat-/pat+ rats froze for less than half the time of wildtypes during presentation of the auditory cue. **(D)** Spontaneous arm alternation during Y-maze exploration was significantly reduced in adult mat-/pat+ rats ($n = 24$) compared to wildtype littermates ($n = 24$). **(E)** Mat-/pat+ rats made 40% more errors and **(F)** made more entries into the maze arms. Bars indicate mean ± S.E.M. A, C: ****$p < 0.0001$, ***$p < 0.001$, repeated measures ANOVA, Holm-Sidak's *post hoc*. D-F: ***$p < 0.001$, **$p < 0.01$, Student's *t*-test.

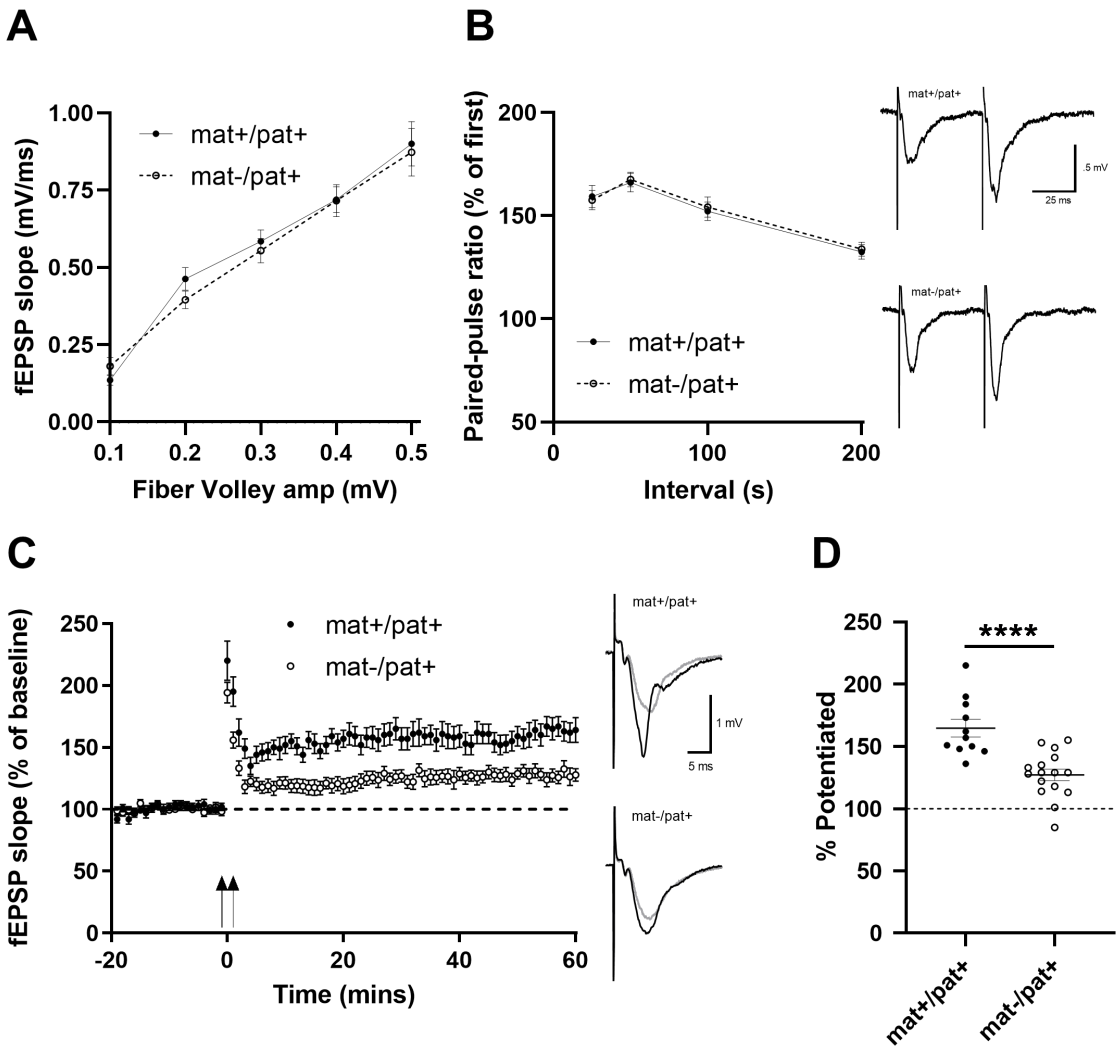

Figure 5. Reduced hippocampal long-term potentiation (LTP) in *Ube3a*$^{mat-/pat+}$ rats. **(A)** Normal basal synaptic transmission as measured by presynaptic fiber volley amplitudes and postsynaptic fEPSP slopes for responses elicited by different intensities of SC fiber stimulation in *Ube3a*$^{mat-/pat+}$ (mat-/pat+; n = 16) and wildtype littermate (*Ube3a*$^{mat+/pat+}$; mat+/pat+; n = 11) hippocampal slices. **(B)** Paired-pulse facilitation was unchanged at mat-/pat+ SC-CA1 synapses compared to mat+/pat+ (n = 15 mat+/pat+ and n = 20 mat-/pat+ slices). (Right) Traces represent fEPSPs evoked by stimulation pulses delivered with a 50 msec interpulse interval. Scale bars: 0.5 mV, 25 msec. **(C)** High frequency stimulation (HFS)-induced LTP in mat+/pat+ (n = 11) was significantly greater compared to mat-/pat+ (n = 16). Traces at right represent superimposed fEPSPs recorded during baseline and 60 min after HFS. Scale bars: 1 mV, 5 msec. **(D)** Summary graph of average percentage potentiation relative to baseline demonstrating that mat+/pat+ exhibited significantly enhanced SC-CA1 LTP at 60 min after HFS (delivered at time = 0), fEPSPs were potentiated to 160 ± 7% of baseline in mat+/pat+ (n = 11) and were 127 ± 5% of baseline in mat-/pat+ slices (n = 16). Data were collected from two rats per genotype. ****$p < 0.0001$, Student's t-test.

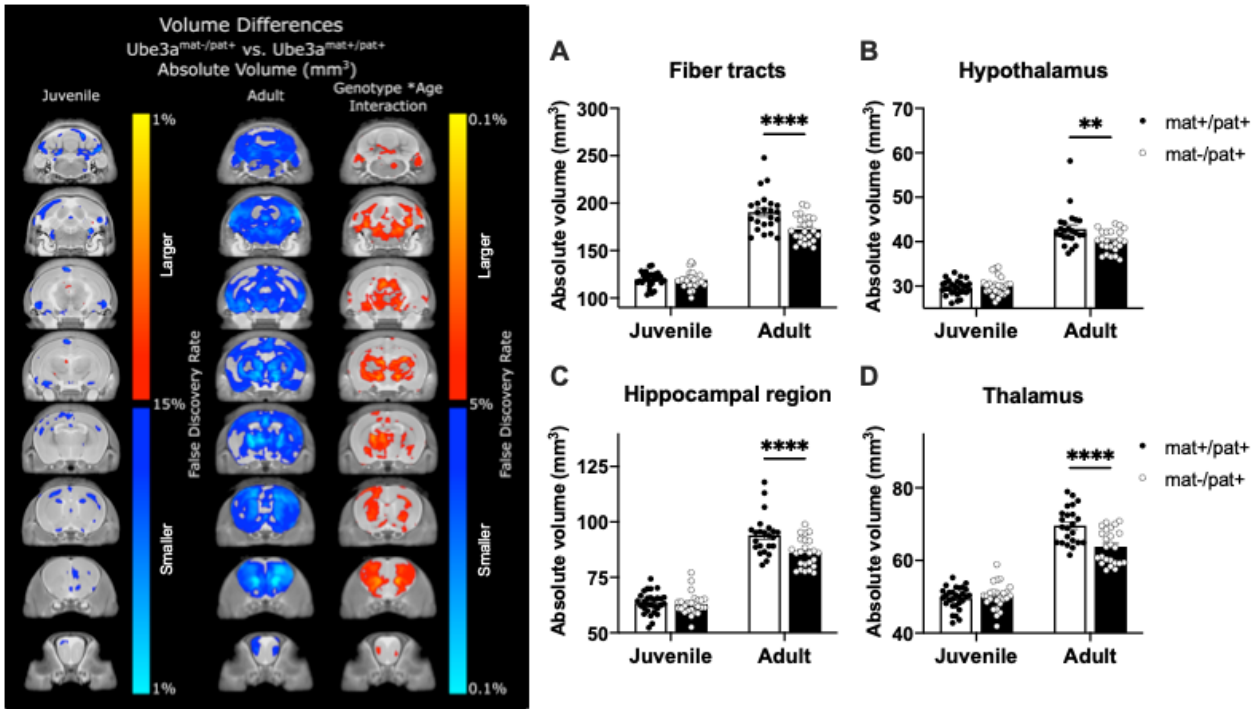

Figure 6. Neuroanatomical pathology in *Ube3a*$^{mat-/pat+}$ rats revealed by high-resolution magnetic resonance imaging (MRI). (Left) Slice series comparing absolute volume (mm^3) of juvenile and adult populations of *Ube3a*$^{mat-/pat+}$ (mat-/pat+) rats and wildtype littermates (*Ube3a*$^{mat+/pat+}$; mat+/pat+). Red to yellow coloration indicates increased volume compared to wildtype whereas dark blue to light blue indicates decreased volume. The leftmost column is data on juvenile mat-/pat+ rats from Berg et al. (2020) and the center column illustrates the same slices on the adult dataset presented here. Most notably, total brain volume was 6.0% smaller in mat-/pat+ rats compared to wildtype. Additionally, the third column shows the genotype by age interaction highlighting several regions of interest, (right) four of which are shown in panels A-D. Namely, **(A)** fiber tracts, **(B)** the hypothalamus, **(C)** the hippocampal region, and **(D)** the thalamus. Full detail of regional findings for adult animals and the interaction effect are described in Tables S2 and S3. Group sizes: juvenile mat+/pat, $n = 29$; juvenile mat-/pat+, $n = 25$; adult mat+/pat+, $n = 23$; adult mat-/pat+, $n = 24$. Bars indicate mean ± S.E.M. ****$p < 0.0001$, **$p < 0.01$, two-way ANOVA, Holm-Sidak's *post hoc*.

Supplementary Information

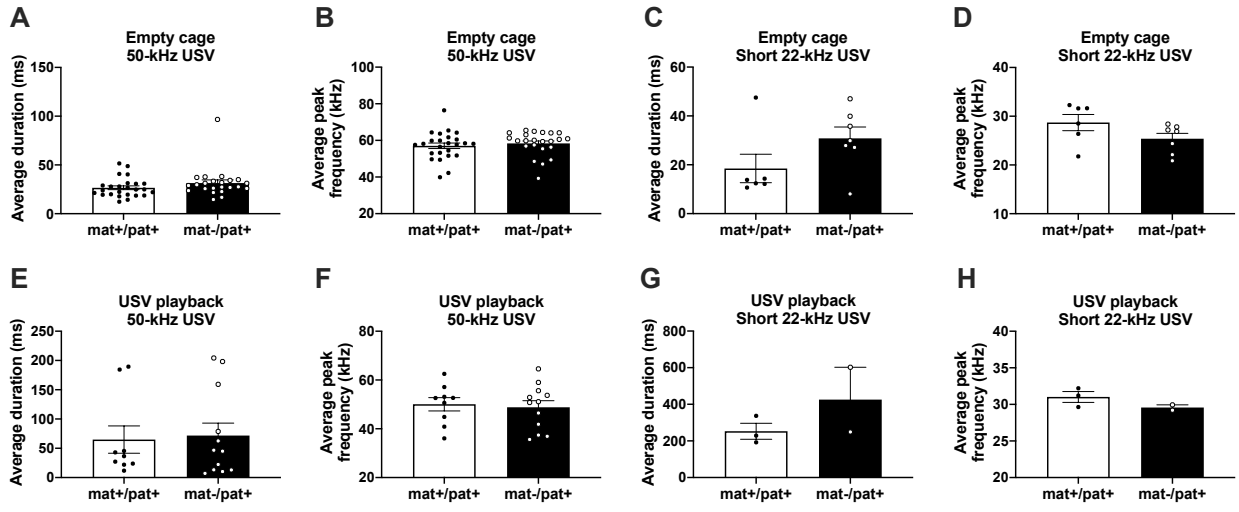

Figure S1. No effect of genotype on call durations and peak frequencies of 50-kHz and short 22-kHz USV in juvenile *Ube3a*$^{mat-/pat+}$ rats. **(A)** The average duration and **(B)** peak frequency of spontaneous 50-kHz calls made during exploration of an empty cage was comparable between *Ube3a*$^{mat-/pat+}$ rats (mat-/pat+; $n = 23$) and wildtype littermate controls (*Ube3a*$^{mat+/pat+}$; mat+/pat+; $n = 25$). **(C)** The average duration and **(D)** average peak frequency of short 22-kHz calls made within an empty cage were also similar between genotypes (mat+/pat+, $n = 6$; mat-/pat+, $n = 7$). **(E)** For 50-kHz USV emitted in response to hearing playback of natural pre-recorded 50-kHz rat USV, average duration and **(F)** average peak frequency were comparable between mat-/pat+ rats ($n = 12$) and wildtype littermates ($n = 9$). **(G)** There was no genotype effect on the average duration or **(H)** average peak frequency of short 22-kHz calls made during USV playback (mat+/pat+, $n = 3$; mat-/pat+, $n = 2$). Data are depicted as mean ± S.E.M. A: Mann-Whitney (MW) *U* test: $U = 205$, $p > 0.05$. B: MW: $U = 240$, $p > 0.05$. C: MW: $U = 12$, $p > 0.05$. D: Student's *t*-test: $t(11) = 1.699$, $p > 0.05$. E: MW: $U = 52$, $p > 0.05$. F: Student's *t*-test: $t(19) = 0.3179$, $p > 0.05$. G: MW: $U = 1$, $p > 0.05$. H: MW: $U = 1$, $p > 0.05$.

Table S1. Ethogram used to score subject behaviors during the juvenile social play assay.

Category	Behavior	Definition	Metric
Mutually exclusive state events	Social sniffing	Sniffing the stimulus rat's face, body, or tail.	Time (sec)
	Anogenital sniffing	Sniffing the stimulus rat's anogenital region.	
	Self-grooming	Subject grooming itself.	
	Exploring	Sitting, walking, rearing, or sniffing the ground or wall.	
	Rough-and-tumble playing	Accelerated movement involving chasing and pouncing; often pinning, tumbling, and push past; and sometimes boxing; requires the stimulus rat's participation (reciprocity).	
Non-mutually exclusive state	Following or chasing	Following (walking pace) or chasing (running pace) the stimulus rat.	
Point events	Push past	Directed movement towards the stimulus rat to get next to, or move closely past, without sniffing or otherwise engaging.	Number (#)
	Push under or crawl over	Head dip under the stimulus rat's belly or completely stepping over stimulus rat.	
	Pounce	Both paws placed (via a leap or directed movement) onto the stimulus rat's back.	

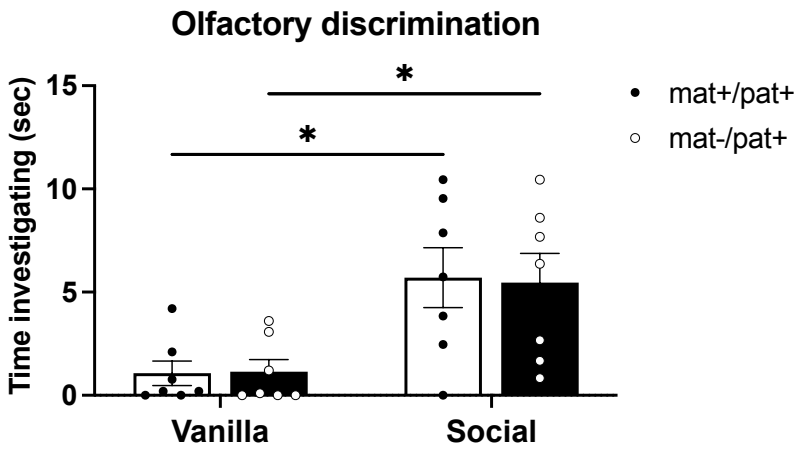

Figure S2. Typical olfactory discrimination in *Ube3a*$^{mat-/pat+}$ rats. Time spent investigating novel odors was similar for *Ube3a*$^{mat-/pat+}$ rats (mat-/pat+; n = 7) and wildtype littermate controls (*Ube3a*$^{mat+/pat+}$; mat+/pat+; n = 7) and both groups spent more time investigating a social scent compared to a non-social vanilla odor. Data are depicted as mean ± S.E.M. Repeated measures ANOVA: $F_{Genotype(G)}(1, 12) = 0.0066$, $p = 0.937$; $F_{Scent(S)}(1, 12) = 14.20$, $p = 0.003$; $F_{S\times G}(1, 12) = 0.0165$, $p = 0.900$; Holm-Sidak's multiple comparisons test, vanilla vs. social: mat+/pat+, *$p = 0.035$; mat-/pat+, *$p = 0.035$.

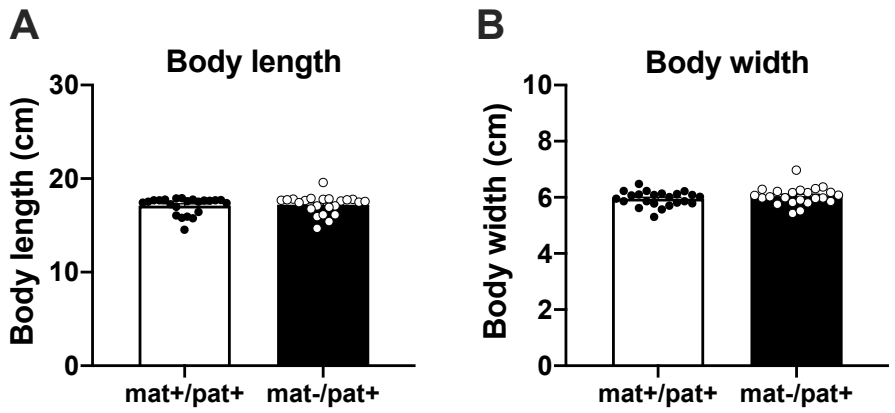

Figure S3. Normal body length and body width in juvenile *Ube3a*$^{mat-/pat+}$ rats. **(A)** At PND 25, both body metrics of length and **(B)** width were similar between *Ube3a*$^{mat-/pat+}$ rats (mat-/pat+; n = 23) and wildtype littermate controls (*Ube3a*$^{mat+/pat+}$; mat+/pat+; n = 23). Data are depicted as mean ± S.E.M. A: Mann-Whitney U test: U = 244.5, $p > 0.05$. B: Student's t-test: t (44) = 0.2719, $p > 0.05$.

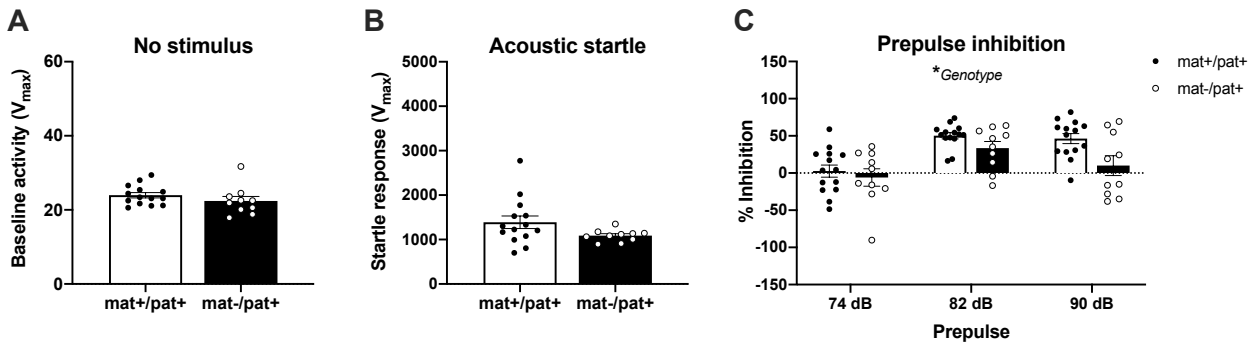

Figure S4. Intact startle response but impaired sensorimotor gating in *Ube3a*$^{mat-/pat+}$ rats. **(A)** Baseline activity within the testing apparatus was comparable between *Ube3a*$^{mat-/pat+}$ rats (mat-/pat+; $n = 10$) and wildtype littermates (*Ube3a*$^{mat+/pat+}$; mat+/pat+; $n = 14$). **(B)** There was no effect of genotype on the startle response to a 120 decibel (dB) startle stimulus. **(C)** Prepulse inhibition of the startle response was generally reduced in adult mat-/pat+ rats. Data are depicted as mean ± S.E.M. A: Students *t*-test: $t\ (22) = 1.735$, $p > 0.05$. B: Students *t*-test: $t\ (22) = 1.157$, $p > 0.05$. C: Repeated measures ANOVA: $F_{Genotype(G)}\ (1, 22) = 4.740$, $^*p = 0.041$; $F_{Prepulse(P)}\ (1.898, 41.75) = 20.64$, $p < 0.0001$; $F_{P\times G}\ (2, 44) = 2.127$, $p = 0.1312$; Holm-Sidak's multiple comparisons test: 74 dB, $p > 0.05$; 82 dB, $p > 0.05$; 90 dB, $p > 0.05$.

Table S2. Brain volumes for adult *Ube3a*$^{mat-/pat+}$ rats and wildtype littermates.

	V1	V2	V9	V11	V15	V18	V21	V22	V24	V31	V32	V37	V39	V43
	/hpf/largep	/hpf/largep	/hpf/largep	/hpf/largep	/hpf/largep	/hpf/largep	/hpf/largep	/hpf/largep	/hpf/largep	/hpf/largep	/hpf/largep	/hpf/largep	/hpf/largep	/hpf/largep
Absolute Volume (mm^3)	mat-/pat+	mat-/pat+	mat-/pat+	mat-/pat+	mat-/pat+	mat-/pat+	mat-/pat+	mat-/pat+	mat-/pat+	mat-/pat+	mat-/pat+	mat-/pat+	mat-/pat+	mat-/pat+
	F	F	F	F	F	F	F	F	F	F	F	F	F	F
Total Brain Volume	1740.83	1714.357	1813.514	1636.148	1667.251	1605.67	1714.136	1684.664	1658.48	1626.099	1802.941	1621.621	1885.971	1670.505
¦–Basic cell groups and regions	1525.011	1499.889	1589.113	1435.062	1459.763	1404.872	1500.348	1473.63	1451.972	1422.72	1576.227	1418.886	1643.692	1462.347
¦ ¦–Cerebrum	949.2186	914.1725	1002.0429	896.1187	897.5961	879.9964	939.5508	929.8604	894.2608	883.6589	992.1677	895.3248	1017.0963	922.8515
¦ ¦ ¦–Cerebral cortex	799.5972	772.117	847.4397	752.3138	755.6047	744.2828	790.51	783.6498	752.5305	749.0111	831.2005	758.2783	858.2855	781.3392
¦ ¦ ¦ °–Cortical plate	754.5214	730.5476	801.1251	709.8023	713.5592	704.6209	745.1878	739.2216	710.9324	709.2354	783.114	716.108	811.1245	738.9033
¦ ¦ ¦ ¦–Olfactory areas	128.2734	122.8375	130.1791	117.1892	118.9261	119.6606	129.588	123.3438	119.4186	118.4445	138.4278	123.0547	134.917	124.6806
¦ ¦ ¦ ¦ °–Main olfactory bulb	43.84406	43.58355	44.65006	37.46402	40.17385	44.50213	45.5029	40.48076	41.28867	40.56169	47.39891	44.46805	46.73507	44.11575
¦ ¦ ¦ ¦–Hippocampal formation	158.1287	156.6423	168.9933	146.4759	148.2462	149.349	155.061	153.9706	150.5451	149.0951	164.4328	150.6687	171.5817	154.2393
¦ ¦ ¦ ¦ ¦–Retrohippocampal region	67.60161	68.50156	75.13266	65.24793	66.38342	66.96511	69.58645	69.05708	65.0839	64.45255	73.4163	68.49114	76.58603	68.67258
¦ ¦ ¦ ¦ ¦ ¦–Subiculum	23.21156	23.05519	26.37443	22.09067	22.39123	22.69608	22.98885	23.36869	22.84866	22.71635	25.19179	23.50444	26.8423	24.25561
¦ ¦ ¦ ¦ ¦ °–Entorhinal area	44.39005	45.44638	48.75823	43.15726	43.99219	44.26903	46.59761	45.68839	42.23524	41.7362	48.2245	44.98669	49.74373	44.41697
¦ ¦ ¦ ¦ °–Hippocampal region	90.52712	88.14073	93.86059	81.22798	81.86276	82.38393	85.47456	84.91355	85.46124	84.64257	91.01654	82.1776	94.9957	85.56667
¦ ¦ ¦ ¦ ¦–Ammon's horn	66.02625	63.88394	68.14126	59.05162	59.48096	59.82481	61.88738	61.6578	62.70793	61.96023	66.08129	59.42546	69.45098	61.82961
¦ ¦ ¦ ¦ °–Dentate gyrus	24.50087	24.25679	25.71934	22.17636	22.38179	22.55912	23.58718	23.25575	22.75331	22.68235	24.93526	22.75214	25.54472	23.73706
¦ ¦ ¦ °–Isocortex	468.1194	451.0678	501.9527	446.1372	446.387	435.6112	460.5388	461.9071	440.9686	441.6958	480.2533	442.3846	504.6258	459.9834
¦ ¦ °–Cerebral nuclei	149.6214	142.0554	154.6032	143.8048	141.9914	135.7136	149.0408	146.2106	141.7304	134.6478	160.9672	137.0465	158.8108	141.5123
¦ ¦ ¦–Pallidum	41.98206	39.36366	43.91583	40.33585	39.26324	37.23803	42.04594	42.21434	39.84602	37.59879	46.41056	38.7553	44.44058	39.72215
¦ ¦ °–Striatum	107.63932	102.69176	110.68742	103.469	102.72812	98.4756	106.99488	103.99625	101.88435	97.04897	114.55663	98.29122	114.37019	101.79014
¦ ¦ ¦–Striatum ventral region	25.7801	24.69151	26.43442	24.99587	24.1892	23.40738	25.65453	25.13839	24.74767	22.63859	29.07862	24.03199	26.86896	24.74419
¦ ¦ ¦ °–Nucleus accumbens	14.15327	12.99695	14.69743	13.47087	13.49886	12.6243	14.00871	13.79239	13.52697	12.51889	15.64867	12.67783	14.53826	13.50503
¦ ¦ ¦–Lateral septal complex	9.846204	9.322234	9.717074	9.527267	9.509443	9.340541	9.603954	9.221856	8.808838	8.936404	10.356478	9.564255	11.220886	10.45373
¦ ¦ °–Striatum dorsal region	68.00577	64.7285	70.40962	65.0867	65.41446	62.08038	67.82657	65.62226	64.4579	62.14778	70.89757	60.86726	72.1838	62.81469
¦ ¦ °–Caudoputamen	68.00577	64.7285	70.40962	65.0867	65.41446	62.08038	67.82657	65.62226	64.4579	62.14778	70.89757	60.86726	72.1838	62.81469
¦ ¦–Brain stem	378.4739	376.4923	385.3843	351.129	363.8156	347.8852	363.9377	360.0541	361.9034	348.3068	398.97	345.414	407.5291	352.8204
¦ ¦ ¦–Midbrain	126.0267	119.9976	127.3781	114.9375	116.8	112.2446	114.3982	117.4109	116.2074	111.4942	122.5125	113.6397	133.9614	113.1126
¦ ¦ ¦–Hindbrain	150.1126	158.0977	152.1073	142.0595	153.8639	143.9493	152.7919	144.5447	147.6227	142.0291	170.5996	138.1535	163.285	143.4794
¦ ¦ °–Interbrain	102.33455	98.39704	105.89893	94.13198	93.15175	91.69129	96.74761	98.09854	98.07328	94.78358	105.85797	93.62083	110.28267	96.22845
¦ ¦ ¦–Hypothalamus	38.16398	37.56824	39.33033	36.89158	34.17877	34.18899	37.65651	38.73649	36.96464	33.957	42.43162	35.70458	40.25493	36.57401
¦ ¦ °–Thalamus	64.17056	60.82879	66.5686	57.2404	58.97298	57.5023	59.0911	59.36205	61.10864	60.82659	63.42636	57.91626	70.02774	59.65444
¦ °–Cerebellum	197.3188	209.2245	201.6861	187.8144	198.3511	176.9906	196.8596	183.7152	195.8078	190.7546	185.089	178.1467	219.0664	186.6752
¦ ¦–Cerebellar cortex	192.3058	204.334	196.1708	183.4313	193.899	172.5784	192.0461	178.9169	191.1997	186.2409	180.2923	173.7536	213.8171	182.596
¦ °–Cerebellar nuclei	5.012992	4.890508	5.515254	4.383114	4.452037	4.412243	4.813454	4.798334	4.608057	4.513664	4.796687	4.393155	5.249253	4.079235
¦ ¦–Dentate nucleus	1.227655	1.217978	1.369005	1.0858	1.081475	1.073783	1.16249	1.189673	1.141043	1.114257	1.131814	1.088868	1.272965	1.030607
¦ ¦–Interposed nucleus	1.867035	1.810442	2.067861	1.609995	1.653068	1.625434	1.806258	1.774738	1.680633	1.718334	1.832708	1.623705	1.975629	1.497782
¦ °–Fastigial nucleus	1.918302	1.862087	2.078389	1.687319	1.717493	1.713026	1.844706	1.833923	1.78638	1.681073	1.832165	1.680582	2.000659	1.550846
¦–fiber tracts	193.119	192.2166	202.5877	179.7796	185.8947	179.805	192.2647	190.0443	185.5235	183.2298	203.8946	180.8494	217.1109	184.5295
¦ ¦–medial forebrain bundle system	27.90885	26.74095	28.37289	25.44822	25.99336	25.22655	26.26172	26.4654	26.47408	25.83558	28.59683	25.75378	31.26883	27.27222
¦ ¦ °–cerebrum related	23.06352	22.12687	23.4281	20.9977	21.51487	20.86337	21.75099	21.79818	21.87977	21.32213	23.7665	21.38148	25.96107	22.62904
¦ ¦ ¦–anterior commissure, temporal limb	0.7459581	0.6860217	0.7237771	0.6948145	0.6979416	0.6351913	0.741033	0.7228808	0.7064441	0.6823922	0.7838577	0.6747447	0.7945819	0.6969668
¦ ¦ °–fornix system	13.79046	13.35561	13.48871	12.38521	12.67996	12.3954	12.89702	12.72831	13.11929	12.69853	14.12814	12.72873	15.66915	13.72787
¦ ¦ ¦–fimbria	11.42164	11.11339	11.11463	10.19414	10.50914	10.28637	10.63738	10.51561	10.88334	10.54857	11.65726	10.53776	13.05057	11.33771
¦ ¦ °–dorsal fornix	2.368821	2.24222	2.374083	2.191072	2.17082	2.109026	2.259635	2.212695	2.235955	2.149958	2.470884	2.190972	2.618573	2.390158
¦ ¦–cerebellum related fiber tracts	53.68128	55.21427	57.28629	50.27351	53.15555	48.49623	54.15665	52.78377	52.25585	51.78476	51.92961	48.28005	60.04475	48.45118
¦ ¦ ¦–cerebellar peduncles	15.47179	15.46379	15.48222	14.28741	15.0485	13.66868	15.38988	14.87005	14.37436	14.25647	15.58836	13.41172	16.70154	13.75456
¦ ¦ °–arbor vitae	38.20949	39.75048	41.80407	35.9861	38.10705	34.82755	38.76677	37.91372	37.88149	37.52829	36.34124	34.86834	43.34321	34.69661
¦ °–lateral forebrain bundle system	83.11352	81.97145	87.91101	77.01784	79.14311	79.22142	82.91053	82.40278	78.95075	78.50235	92.04651	79.40283	94.03326	80.67706
¦ ¦–corticospinal tract	29.32136	30.10552	31.50033	27.62411	28.39081	29.35891	31.29339	30.03842	28.91534	28.31814	35.60683	30.0796	33.35992	29.04591
¦ ¦ ¦–cerebal peduncle	10.425233	10.384673	10.70019	9.735008	9.835975	9.708116	10.334682	10.327684	10.021743	9.627572	11.025448	10.054076	11.754213	9.732993
¦ ¦ ¦–corticospinal tract-other	6.391196	7.986987	6.912638	5.651951	6.442668	7.819621	8.265125	6.744454	6.700797	6.9953	11.212659	7.837896	7.342612	7.032149
¦ ¦ °–internal capsule	12.50493	11.73386	13.8875	12.23715	12.11217	11.83117	12.69358	12.96629	12.1928	11.69527	13.36873	12.18763	14.26309	12.28076
¦ °–corpus callosum	53.79216	51.86593	56.41068	49.39373	50.7523	49.86252	51.61714	52.36436	50.03541	50.18421	56.43968	49.32323	60.67334	51.63115
°–ventricular systems	22.70008	22.25077	21.81343	21.30652	21.59364	20.99238	21.52286	20.99046	20.98495	20.14853	22.81963	21.88646	25.1688	23.62793

	V5	V6	V17	V19	V25	V30	V34	V36	V38	V40
	/hpf/largep	/hpf/largep	/hpf/largep	/hpf/largep	/hpf/largep	/hpf/largep	/hpf/largep	/hpf/largep	/hpf/largep	/hpf/largep
Absolute Volume (mm^3)	mat-/pat+	mat-/pat+	mat-/pat+	mat-/pat+	mat-/pat+	mat-/pat+	mat-/pat+	mat-/pat+	mat-/pat+	mat-/pat+
	M	M	M	M	M	M	M	M	M	M
Total Brain Volume	1782.253	1758.684	2036.1	1865.115	1975.984	1921.458	1960.694	1987.515	1863.185	1853.808
¦--Basic cell groups and regions	1555.958	1536.364	1780.493	1627.642	1728.936	1673.292	1718.474	1732.031	1621.91	1620.07
¦ ¦--Cerebrum	967.7388	959.0664	1158.1023	1018.7596	1079.768	1031.5895	1073.5236	1069.629	1033.2942	999.7338
¦ ¦ ¦--Cerebral cortex	821.5213	812.7577	970.9495	864.9922	917.855	865.0402	908.8268	903.3448	866.4495	842.6581
¦ ¦ ¦ °--Cortical plate	776.4509	767.8963	914.1791	816.6383	867.1613	816.2471	857.7902	855.6527	817.3048	796.0957
¦ ¦ ¦ ¦--Olfactory areas	129.384	126.7833	155.7732	131.2205	145.9876	131.5453	141.4306	137.4158	135.3973	135.8156
¦ ¦ ¦ ¦ °--Main olfactory bulb	44.84457	43.24504	53.0853	42.80169	51.59829	42.19544	45.82877	47.75968	45.78603	47.33609
¦ ¦ ¦ ¦--Hippocampal formation	166.8429	166.0424	184.1498	171.4945	184.7277	177.652	182.8594	183.9702	175.342	166.0187
¦ ¦ ¦ ¦ ¦--Retrohippocampal region	73.94056	73.87342	87.147	79.22956	81.96543	76.32197	81.76515	81.3421	78.73903	72.75868
¦ ¦ ¦ ¦ ¦ ¦--Subiculum	24.43359	25.21265	28.06848	26.61531	28.52182	26.99731	28.0292	28.60637	27.2522	25.61452
¦ ¦ ¦ ¦ ¦ °--Entorhinal area	49.50697	48.66077	59.07852	52.61424	53.44361	49.32467	53.73595	52.73574	51.48683	47.14416
¦ ¦ ¦ ¦ °--Hippocampal region	92.90236	92.16894	97.00281	92.2649	102.76231	101.33006	101.09421	102.6281	96.60296	93.25998
¦ ¦ ¦ ¦ ¦--Ammon's horn	67.57684	66.64357	70.38878	66.96877	74.08712	73.67482	72.90284	73.72363	70.05017	68.54613
¦ ¦ ¦ ¦ °--Dentate gyrus	25.32552	25.52537	26.61403	25.29613	28.67518	27.65524	28.19137	28.90447	26.55279	24.71385
¦ ¦ ¦ °--Isocortex	480.224	475.0706	574.2561	513.9233	536.4459	507.0497	533.5002	534.2667	506.5655	494.2615
¦ ¦ °--Cerebral nuclei	146.2175	146.3087	187.1527	153.7674	161.913	166.5493	164.6969	166.2842	166.8447	157.0757
¦ ¦ ¦--Pallidum	40.50981	42.25044	52.73007	43.76104	45.24807	46.50483	46.04376	45.37301	47.598	43.60469
¦ ¦ °--Striatum	105.70765	104.05825	134.42266	110.00635	116.66492	120.04444	118.65312	120.91122	119.24671	113.47103
¦ ¦ ¦--Striatum ventral region	25.47954	25.61206	32.65048	27.17652	27.60787	28.10305	28.6103	27.57721	28.30237	26.89191
¦ ¦ ¦ °--Nucleus accumbens	13.85863	13.76804	17.95618	14.72021	14.9468	15.53847	15.49581	15.11071	15.49342	14.74974
¦ ¦ ¦--Lateral septal complex	10.491045	9.827998	11.210959	9.990782	11.338411	11.69458	11.165597	11.67541	11.983029	10.591302
¦ ¦ °--Striatum dorsal region	65.62628	64.60427	85.69454	68.29527	73.09095	75.8015	74.14261	77.10224	74.64008	71.64048
¦ ¦ °--Caudoputamen	65.62628	64.60427	85.69454	68.29527	73.09095	75.8015	74.14261	77.10224	74.64008	71.64048
¦ ¦--Brain stem	377.082	379.5436	421.6849	396.7856	415.3291	414.403	418.689	429.8358	396.5638	399.5027
¦ ¦ ¦--Midbrain	118.828	124.0205	137.7092	125.2528	132.6069	134.5145	132.1132	136.837	130.2385	127.791
¦ ¦ ¦--Hindbrain	160.0926	153.8306	172.8335	165.9836	172.2146	171.329	174.4844	178.9198	156.0217	164.3612
¦ ¦ °--Interbrain	98.16135	101.69257	111.14217	105.54913	110.50763	108.5595	112.09139	114.07892	110.3036	107.35049
¦ ¦ ¦--Hypothalamus	36.98296	38.853	42.33183	38.47126	40.47232	39.47884	42.04636	42.59006	40.13071	40.17299
¦ ¦ °--Thalamus	61.17839	62.83958	68.81034	67.07787	70.03531	69.08067	70.04502	71.48886	70.17289	67.1775
¦ °--Cerebellum	211.1375	197.7542	200.7062	212.0964	233.8386	227.2995	226.2618	232.5666	192.0522	220.8337
¦ ¦--Cerebellar cortex	206.0694	192.7005	194.8137	206.4682	228.2523	221.8221	220.6705	227.076	186.8131	215.6891
¦ °--Cerebellar nuclei	5.068108	5.053756	5.89254	5.628186	5.586286	5.477476	5.591267	5.490681	5.239119	5.14455
¦ ¦--Dentate nucleus	1.319922	1.27179	1.426174	1.354868	1.387548	1.337333	1.397542	1.348894	1.235955	1.289796
¦ ¦--Interposed nucleus	1.859897	1.803871	2.238538	2.104694	2.094477	2.07815	2.080241	2.045812	1.940138	1.929218
¦ °--Fastigial nucleus	1.888289	1.978095	2.227827	2.168624	2.104261	2.061992	2.113484	2.095974	2.063025	1.925535
¦--fiber tracts	200.9901	199.5516	230.2371	214.4503	220.6995	221.1428	216.5986	228.4099	215.8817	208.999
¦ ¦--medial forebrain bundle system	28.25585	28.3378	30.94435	29.48185	31.06648	32.67571	30.15528	32.07899	31.49111	29.91266
¦ ¦ °--cerebrum related	23.4656	23.49851	25.76874	24.36552	25.77915	27.32731	24.96206	26.68763	26.24997	24.71055
¦ ¦ ¦--anterior commissure, temporal limb	0.7185716	0.7204414	0.8836955	0.7676659	0.825283	0.8100611	0.8197921	0.8189962	0.800123	0.7957897
¦ ¦ °--fomix system	14.11629	13.85515	14.33651	14.06296	15.55341	16.67057	14.89482	15.95654	15.75124	14.93167
¦ ¦ ¦--fimbria	11.77721	11.43415	11.77451	11.62406	12.97162	14.06845	12.31947	13.26724	13.06154	12.41469
¦ ¦ °--dorsal fornix	2.339074	2.420996	2.561999	2.438898	2.581793	2.602118	2.57535	2.689301	2.689698	2.516976
¦ ¦--cerebellum related fiber tracts	57.8661	55.19806	61.38939	61.61713	63.13162	61.70813	61.64943	63.33138	55.68557	58.97212
¦ ¦ ¦--cerebellar peduncles	15.80021	15.38296	17.72976	16.93668	17.53087	17.12669	17.21381	17.85888	15.47877	16.42136
¦ ¦ °--arbor vitae	42.06589	39.8151	43.65963	44.68045	45.60074	44.58144	44.43561	45.4725	40.2068	42.55077
¦ °--lateral forebrain bundle system	85.40589	86.59464	104.07875	92.49135	93.63165	95.21144	91.90117	99.94075	98.00137	88.38179
¦ ¦--corticospinal tract	30.25827	30.24936	39.22101	33.21439	32.62851	33.28186	32.16828	36.71986	36.05784	31.27146
¦ ¦ ¦--cerebal peduncle	10.59013	10.762888	12.691452	11.628738	11.264035	11.566506	11.123814	11.962062	11.287905	11.280635
¦ ¦ ¦--corticospinal tract-other	7.006125	6.524413	10.027367	7.498735	6.942481	7.240065	7.142086	10.186865	9.945577	6.601984
¦ ¦ °--internal capsule	12.66202	12.96206	16.50219	14.08692	14.42199	14.47529	13.90238	14.57093	14.82436	13.38884
¦ °--corpus callosum	55.14762	56.34528	64.85774	59.27696	61.00314	61.92958	59.73289	63.22089	61.94352	57.11033
°--ventricular systems	25.30485	22.76814	25.36927	23.02338	26.34855	27.02308	25.62129	27.0738	25.3926	24.73916

	V3	V4	V12	V13	V14	V20	V23	V26	V28	V29	V33	V47
	/hpf/largep	/hpf/largep	/hpf/largep	/hpf/largep	/hpf/largep	/hpf/largep	/hpf/largep	/hpf/largep	/hpf/largep	/hpf/largep	/hpf/largep	/hpf/largep
Absolute Volume (mm^3)	mat+/pat+	mat+/pat+	mat+/pat+	mat+/pat+	mat+/pat+	mat+/pat+	mat+/pat+	mat+/pat+	mat+/pat+	mat+/pat+	mat+/pat+	mat+/pat+
	F	F	F	F	F	F	F	F	F	F	F	F
Total Brain Volume	1739.477	1746.058	1845.778	1818.484	1810.639	1699.629	1831.272	1845.172	2094.088	1853.859	1702.359	1972.144
¦--Basic cell groups and regions	1518.073	1529.402	1612.678	1594.264	1582.755	1486.197	1597.414	1605.219	1826.333	1619.264	1483.31	1720.861
¦ ¦--Cerebrum	946.3864	953.7757	1000.6654	1009.5961	989.4075	907.9523	990.3879	989.5147	1120.6514	1002.4636	909.5261	1079.0936
¦ ¦ ¦--Cerebral cortex	798.9224	808.21	844.2639	852.9981	839.4897	771.3174	832.8959	833.4619	949.1319	847.3741	766.4107	911.8684
¦ ¦ ¦ °--Cortical plate	753.6588	763.8574	798.0646	805.1133	794.0317	729.6455	788.2234	787.5947	898.4683	801.7016	725.874	861.2637
¦ ¦ ¦ ¦--Olfactory areas	124.8048	122.2111	129.8724	133.6472	131.4707	118.81	128.9884	130.884	149.9162	135.0631	120.875	141.1191
¦ ¦ ¦ ¦ °--Main olfactory bulb	42.68016	39.38781	42.39206	47.09345	45.31509	39.2852	44.97157	44.77868	53.26957	47.88688	42.49275	50.18242
¦ ¦ ¦ ¦--Hippocampal formation	158.1469	161.2811	165.1954	170.8998	164.9342	155.1093	168.4184	165.8354	194.7418	175.0932	158.1714	180.7289
¦ ¦ ¦ ¦ ¦--Retrohippocampal region	68.11548	71.64295	74.98624	79.36495	73.60851	69.18205	72.4404	73.98348	84.33156	77.03546	67.47823	79.74749
¦ ¦ ¦ ¦ ¦ ¦--Subiculum	23.6189	24.4369	25.28838	26.10031	24.4457	23.99182	25.92174	25.12963	30.80201	27.01925	23.64247	28.61904
¦ ¦ ¦ ¦ ¦ ¦ °--Entorhinal area	44.49658	47.20605	49.69787	53.26464	49.16281	45.19023	46.51866	48.85385	53.52955	50.01621	43.83576	51.12844
¦ ¦ ¦ ¦ ¦ °--Hippocampal region	90.0314	89.63812	90.20918	91.5348	91.3257	85.92724	95.97803	91.85191	110.41028	98.0577	90.69319	100.98146
¦ ¦ ¦ ¦ ¦ ¦--Ammon's horn	66.05179	65.17572	65.08754	66.54655	66.70759	62.58079	69.84546	66.96752	79.92471	70.96052	65.75927	73.38413
¦ ¦ ¦ ¦ ¦ °--Dentate gyrus	23.97961	24.4624	25.12164	24.98825	24.61811	23.34645	26.13257	24.88439	30.48557	27.09717	24.93392	27.59733
¦ ¦ ¦ °--Isocortex	470.7071	480.3652	502.9967	500.5664	497.6268	455.7263	490.8165	490.8753	553.8103	491.5454	446.8276	539.4157
¦ ¦ °--Cerebral nuclei	147.464	145.5657	156.4015	156.5979	149.9178	136.6349	157.4921	156.0529	171.5195	155.0895	143.1153	167.2253
¦ ¦ ¦--Pallidum	41.5484	40.39576	43.55661	44.4375	41.55548	38.74649	43.83169	43.63912	48.02675	43.49488	39.84415	47.03712
¦ ¦ °--Striatum	105.91561	105.16993	112.8449	112.16044	108.36231	97.88845	113.66038	112.41374	123.49273	111.59459	103.27118	120.18816
¦ ¦ ¦--Striatum ventral region	24.99912	24.89807	26.82987	27.44485	26.01968	24.52389	26.34236	26.24952	29.14949	26.61531	24.92252	28.27218
¦ ¦ ¦ °--Nucleus accumbens	13.68563	13.58402	14.67971	15.35711	14.23232	13.19166	14.91168	14.19957	15.95862	14.60827	13.72991	15.40327
¦ ¦ ¦--Lateral septal complex	9.559779	9.145534	9.709752	10.092889	9.684985	9.011397	9.69251	10.123485	10.741645	9.947654	9.041438	11.328808
¦ ¦ °--Striatum dorsal region	67.30795	67.33546	72.24626	70.51454	68.64116	60.78469	73.79683	72.00003	79.22831	71.03884	65.79564	76.25695
¦ ¦ °--Caudoputamen	67.30795	67.33546	72.24626	70.51454	68.64116	60.78469	73.79683	72.00003	79.22831	71.03884	65.79564	76.25695
¦ ¦--Brain stem	379.1191	366.2683	400.6788	388.431	381.8522	374.2044	393.8799	404.9197	449.2308	400.9895	376.3893	414.4231
¦ ¦ ¦--Midbrain	120.5854	116.5954	126.5738	126.6727	119.3367	116.087	126.7506	127.6033	141.1262	128.1701	119.0179	132.9101
¦ ¦ ¦--Hindbrain	156.1664	150.0942	168.4594	156.3141	162.3286	161.9208	158.5921	172.017	185.5923	164.9468	156.9775	166.7672
¦ ¦ °--Interbrain	102.3673	99.57873	105.64559	105.44412	100.18685	96.19659	108.53724	105.29939	122.51235	107.87256	100.3939	114.74581
¦ ¦ ¦--Hypothalamus	37.29711	35.87743	38.2949	39.2735	36.67148	34.64786	39.25579	39.84217	44.32169	38.68499	36.62479	41.90761
¦ ¦ °--Thalamus	65.07019	63.7013	67.35069	66.17062	63.51537	61.54873	69.28145	65.45722	78.19065	69.18756	63.76911	72.8382
¦ °--Cerebellum	192.5677	209.3579	211.3339	196.2369	211.4954	204.0404	213.1461	210.7843	256.4507	215.8113	197.3952	227.3442
¦ ¦--Cerebellar cortex	187.1094	204.2619	205.7268	190.9458	205.9804	198.6534	207.5603	205.1708	250.212	210.1446	191.9406	221.4636
¦ °--Cerebellar nuclei	5.458332	5.095951	5.607117	5.291057	5.515039	5.387011	5.585829	5.61343	6.238703	5.666712	5.454528	5.880622
¦ ¦--Dentate nucleus	1.360104	1.300848	1.39359	1.317051	1.380764	1.346703	1.334798	1.398792	1.54154	1.383419	1.332575	1.445673
¦ ¦--Interposed nucleus	2.042622	1.874394	2.081957	1.957618	2.111475	2.023822	2.095038	2.080926	2.380298	2.140484	2.081969	2.189155
¦ °--Fastigial nucleus	2.055606	1.920709	2.13157	2.016388	2.022799	2.016486	2.155994	2.133712	2.316866	2.142809	2.039984	2.245794
¦--fiber tracts	198.9109	195.2233	210.9215	201.2473	205.3561	192.8493	211.268	215.8289	242.6374	212.0226	198.1488	225.8833
¦ ¦--medial forebrain bundle system	28.44517	27.12563	28.86563	28.56088	28.04046	26.22155	29.7624	29.6629	33.55171	29.41016	27.53626	32.20842
¦ ¦ °--cerebrum related	23.58555	22.45189	23.82782	23.50467	23.17679	21.59833	24.64092	24.71082	27.76555	24.27446	22.66942	26.81261
¦ ¦ ¦--anterior commissure, temporal limb	0.7237175	0.6771212	0.754658	0.7514968	0.7384301	0.6862869	0.7421411	0.7996073	0.8476385	0.7352132	0.6753755	0.7901969
¦ ¦ °--fornix system	13.74039	13.00332	13.89495	13.72456	13.52758	12.84293	14.43472	14.66322	16.51969	14.50263	13.52067	15.72601
¦ ¦ ¦--fimbria	11.43383	10.77479	11.57564	11.38126	11.26845	10.7025	11.97036	12.10316	13.77375	12.0713	11.247	13.04197
¦ ¦ °--dorsal fornix	2.306553	2.228536	2.319311	2.343295	2.259126	2.140428	2.464358	2.560066	2.745944	2.431338	2.27367	2.684036
¦ ¦--cerebellum related fiber tracts	54.74186	56.45801	60.7879	56.15978	60.21059	58.93863	59.16482	62.28137	71.31216	61.62231	58.41605	62.84638
¦ ¦ ¦--cerebellar peduncles	15.42664	15.40537	16.59636	15.84908	16.78474	16.31333	16.32955	17.4022	19.92865	17.3859	16.67413	17.34926
¦ ¦ °--arbor vitae	39.31522	41.05265	44.19155	40.3107	43.42586	42.62529	42.83527	44.87917	51.38351	44.2364	41.74192	45.49712
¦ °--lateral forebrain bundle system	87.32326	84.2535	90.76969	86.83014	87.31218	79.49568	92.22654	92.51654	102.91328	90.06962	83.84823	98.75294
¦ ¦--corticospinal tract	31.06048	29.37262	33.80919	31.36261	31.12376	29.05441	32.59805	35.87164	37.08667	32.7179	30.97399	35.19319
¦ ¦ ¦--cerebal peduncle	10.76861	9.989739	11.214945	10.59511	11.052775	10.199219	11.372811	11.86919	13.281651	11.226457	10.838329	12.250068
¦ ¦ ¦--corticospinal tract-other	6.611733	6.460819	8.363102	6.809561	6.806121	6.626533	7.077063	9.583495	8.246259	7.333146	7.432064	6.994302
¦ ¦ °--internal capsule	13.68013	12.92206	14.23114	13.95794	13.26487	12.22866	14.14818	14.41895	15.55876	14.1583	12.70359	15.94882
¦ °--corpus callosum	56.26279	54.88088	56.9605	55.46754	56.18842	50.44126	59.62849	56.6449	65.82661	57.35172	52.87425	63.55976
°--ventricular systems	22.49294	21.43281	22.17843	22.97245	22.52766	20.5826	22.58987	24.12468	25.11755	22.57201	20.89986	25.39937

	V7	V8	V10	V16	V27	V35	V41	V42	V44	V45	V46
	/hpf/largep	/hpf/largep	/hpf/largep	/hpf/largep	/hpf/largep	/hpf/largep	/hpf/largep	/hpf/largep	/hpf/largep	/hpf/largep	/hpf/largep
Absolute Volume (mm^3)	mat+/pat+	mat+/pat+	mat+/pat+	mat+/pat+	mat+/pat+	mat+/pat+	mat+/pat+	mat+/pat+	mat+/pat+	mat+/pat+	mat+/pat+
	M	M	M	M	M	M	M	M	M	M	M
Total Brain Volume	2069.789	1945.582	1865.632	1838.135	2053.215	1990.733	1970.301	1929.756	2029.1	1945.026	2067.992
¦–Basic cell groups and regions	1808.317	1695.61	1632.848	1605.569	1790.941	1734.805	1719.158	1678.818	1769.169	1696.17	1805.697
¦ ¦–Cerebrum	1136.9193	1043.0579	1031.4883	1003.3254	1104.5926	1072.9514	1075.1366	1035.1905	1095.998	1050.6632	1113.5216
¦ ¦ ¦–Cerebral cortex	959.0691	883.2293	870.6107	850.7813	929.3491	906.5082	910.6626	870.4221	924.3445	888.925	948.194
¦ ¦ ¦ °–Cortical plate	905.1227	835.081	822.2339	806.3124	879.541	858.8702	861.7922	819.9582	873.988	841.6652	896.9095
¦ ¦ ¦ ¦–Olfactory areas	147.6889	136.5756	131.8158	130.8649	137.7297	140.1322	143.9076	136.6556	143.0314	142.2353	153.0946
¦ ¦ ¦ ¦ °–Main olfactory bulb	48.57714	45.80702	41.99215	44.52285	42.75805	48.97324	51.08007	46.83728	47.89701	50.59658	54.94274
¦ ¦ ¦ ¦–Hippocampal formation	193.7245	182.2465	173.508	167.9992	190.1395	185.6817	183.0894	179.5829	187.9039	175.0664	184.8962
¦ ¦ ¦ ¦ ¦–Retrohippocampal region	87.03464	80.61859	80.20691	76.3271	86.11309	81.35973	82.34048	77.41545	83.72117	77.94804	83.12718
¦ ¦ ¦ ¦ ¦ ¦–Subiculum	29.22139	27.17816	26.74314	24.98738	28.66746	29.20197	28.0925	27.12973	28.98293	26.69821	28.17561
¦ ¦ ¦ ¦ ¦ ¦ °–Entorhinal area	57.81325	53.44043	53.46377	51.33972	57.44563	52.15775	54.24798	50.28572	54.73824	51.24983	54.95158
¦ ¦ ¦ ¦ °–Hippocampal region	106.68986	101.62792	93.3011	91.67207	104.02643	104.32202	100.74894	102.16748	104.18274	97.11836	101.76899
¦ ¦ ¦ ¦ ¦–Ammon's horn	76.98036	73.82746	67.69141	66.82113	75.87518	75.71131	73.5479	73.96218	75.57631	70.25836	73.97714
¦ ¦ ¦ ¦ °–Dentate gyrus	29.7095	27.80045	25.60969	24.85094	28.15124	28.6107	27.20105	28.2053	28.60643	26.86	27.79184
¦ ¦ ¦ °–Isocortex	563.7092	516.2589	516.9101	507.4482	551.6718	533.0563	534.7952	503.7197	543.0527	524.3635	558.9187
¦ ¦ °–Cerebral nuclei	177.8502	159.8286	160.8776	152.5441	175.2435	166.4431	164.4739	164.7684	171.6535	161.7382	165.3275
¦ ¦ ¦–Pallidum	49.97658	44.70391	45.20988	42.9349	48.13678	46.80819	45.38686	45.61436	48.32177	44.6624	46.14273
¦ ¦ °–Striatum	127.8736	115.12471	115.66768	109.6092	127.10672	119.63493	119.08706	119.15406	123.33174	117.07581	119.18482
¦ ¦ ¦–Striatum ventral region	29.88863	27.63725	28.07732	27.09299	30.8011	28.63326	28.14297	27.15445	29.73517	27.88936	28.84235
¦ ¦ ¦ °–Nucleus accumbens	16.20895	14.83314	15.41718	14.69244	16.63569	15.84669	15.34759	14.90176	16.01926	15.03008	15.50856
¦ ¦ ¦–Lateral septal complex	10.84416	10.706953	10.647227	9.835437	10.998601	10.2172	10.677638	11.522025	10.990831	10.719092	10.708772
¦ ¦ °–Striatum dorsal region	82.22022	72.44335	72.64276	68.63499	80.56781	76.27448	75.91991	76.05731	78.04039	74.2878	75.1818
¦ ¦ °–Caudoputamen	82.22022	72.44335	72.64276	68.63499	80.56781	76.27448	75.91991	76.05731	78.04039	74.2878	75.1818
¦ ¦–Brain stem	429.673	417.5117	398.594	393.1869	435.3961	429.7668	414.0977	411.0362	433.8351	410.7977	426.7206
¦ ¦ ¦–Midbrain	139.5023	131.998	131.7601	124.8112	141.5521	136.4384	133.809	131.2038	140.3564	129.8642	133.7853
¦ ¦ ¦–Hindbrain	170.5959	174.0655	158.5522	164.613	175.8852	178.756	168.2672	168.7404	176.6103	172.5163	179.8541
¦ ¦ °–Interbrain	119.57474	111.44827	108.28175	103.76262	117.95875	114.57242	112.0216	111.09202	116.86842	108.41722	113.08126
¦ ¦ ¦–Hypothalamus	43.48907	40.23791	40.5353	38.52417	42.29571	40.96109	39.50854	40.55099	43.02616	38.82217	41.10449
¦ ¦ °–Thalamus	76.08567	71.21036	67.74646	65.23845	75.66304	73.61132	72.51306	70.54103	73.84225	69.59505	71.97676
¦ °–Cerebellum	241.7247	235.0399	202.7653	209.0562	250.9528	232.0864	229.9238	232.5909	239.3362	234.7088	265.4553
¦ ¦–Cerebellar cortex	235.5042	229.0981	197.3658	203.5431	244.6679	226.1462	224.1998	226.9094	233.2171	228.9209	259.5573
¦ °–Cerebellar nuclei	6.220478	5.941823	5.399536	5.513091	6.284814	5.94017	5.724037	5.68155	6.119068	5.787906	5.897993
¦ ¦–Dentate nucleus	1.528681	1.489947	1.27712	1.34943	1.605655	1.416429	1.363087	1.358942	1.472181	1.396838	1.425109
¦ ¦–Interposed nucleus	2.317803	2.184944	2.019391	2.087012	2.318885	2.232351	2.126277	2.139791	2.302495	2.171634	2.245855
¦ °–Fastigial nucleus	2.373994	2.266932	2.103026	2.076649	2.360275	2.29139	2.234673	2.182817	2.344392	2.219434	2.227029
¦–fiber tracts	235.8865	224.2949	209.2857	209.6705	236.7119	232.0216	226.8764	225.6447	234.3949	224.2922	237.001
¦ ¦–medial forebrain bundle system	32.93138	31.60612	30.11828	29.37808	33.05851	32.38682	32.17473	33.29054	33.06431	31.42173	32.29723
¦ ¦ °–cerebrum related	27.3125	26.23506	24.91817	24.25551	27.22128	26.8171	26.66744	27.8497	27.28709	25.99287	26.78392
¦ ¦ ¦–anterior commissure, temporal limb	0.8203488	0.7877274	0.7370627	0.7434619	0.8421406	0.7834493	0.7880374	0.8115855	0.8364574	0.7713425	0.7863776
¦ ¦ °–fornix system	15.93133	15.71596	14.59871	14.22373	16.41059	15.85728	15.53741	17.10346	16.02849	15.34498	15.78214
¦ ¦ ¦–fimbria	13.14045	13.08447	12.03416	11.83	13.69826	13.17942	12.88234	14.38774	13.21857	12.73349	13.06494
¦ ¦ °–dorsal fornix	2.790874	2.631499	2.564544	2.393727	2.712327	2.67786	2.655066	2.715714	2.809924	2.611493	2.717205
¦ ¦–cerebellum related fiber tracts	66.75087	65.78748	58.0917	61.48202	70.10075	65.60805	62.97548	63.20406	67.17011	65.0796	71.52702
¦ ¦ ¦–cerebellar peduncles	17.49623	17.64874	16.11545	17.27387	18.1967	18.17887	16.88728	17.20731	18.26163	17.96548	18.90906
¦ ¦ °–arbor vitae	49.25463	48.13874	41.97626	44.20815	51.90406	47.42918	46.0882	45.99675	48.90848	47.11412	52.61796
¦ °–lateral forebrain bundle system	102.81167	94.71904	90.90467	88.21529	99.91503	100.00442	98.41917	97.95546	100.22007	95.23525	98.94682
¦ ¦–corticospinal tract	36.66379	34.06576	33.03131	31.72147	35.04121	35.71832	34.85963	36.39285	35.14004	34.31323	35.35011
¦ ¦ ¦–cerebal peduncle	12.537287	12.098853	11.63359	11.497172	12.579549	12.485631	11.811001	11.679131	12.368573	11.732492	12.176066
¦ ¦ ¦–corticospinal tract-other	7.502594	7.436105	7.003108	6.991743	7.701018	7.703287	7.59663	10.374957	7.316095	7.248629	7.66717
¦ ¦ °–internal capsule	16.62391	14.5308	14.39461	13.23255	14.76064	15.5294	15.452	14.33876	15.45538	15.3321	15.50688
¦ °–corpus callosum	66.14789	60.65328	57.87336	56.49383	64.87382	64.2861	63.55954	61.56261	65.08003	60.92202	63.59671
°–ventricular systems	25.58595	25.6779	23.49878	22.89622	25.56155	23.90701	24.26687	25.29367	25.53579	24.5638	25.29316

Absolute Volume	mat-/pat+		mat+/pat+						
	Mean	SD	Mean	SD	%Diff	Effect	P-value	FDR	
Total Brain Volume	1785.29	130.32	1898.44	120.47	-5.96	-0.94	0.00	0.04	*
¦--Basic cell groups and regions	1560.78	112.47	1657.08	104.21	-5.81	-0.92	0.00	0.04	*
¦ ¦--Cerebrum	975.21	74.67	1028.79	65.10	-5.21	-0.82	0.01	0.09	-
¦ ¦ ¦--Cerebral cortex	822.94	62.68	869.50	55.13	-5.35	-0.84	0.01	0.07	-
¦ ¦ ¦ °--Cortical plate	777.23	58.84	822.13	52.17	-5.46	-0.86	0.01	0.07	-
¦ ¦ ¦ ¦--Olfactory areas	129.99	9.54	135.28	9.12	-3.91	-0.58	0.06	0.31	
¦ ¦ ¦ ¦ °--Main olfactory bulb	44.55	3.50	46.25	4.14	-3.67	-0.41	0.14	0.67	
¦ ¦ ¦ ¦--Hippocampal formation	164.02	12.81	174.89	11.80	-6.21	-0.92	0.00	0.04	*
¦ ¦ ¦ ¦ ¦--Retrohippocampal region	73.01	6.33	77.74	5.63	-6.09	-0.84	0.01	0.07	-
¦ ¦ ¦ ¦ ¦ ¦--Subiculum	25.04	2.17	26.70	2.04	-6.23	-0.81	0.01	0.07	-
¦ ¦ ¦ ¦ ¦ °--Entorhinal area	47.97	4.30	51.04	3.85	-6.02	-0.80	0.01	0.09	-
¦ ¦ ¦ ¦ °--Hippocampal region	91.01	6.89	97.14	6.65	-6.31	-0.92	0.00	0.04	*
¦ ¦ ¦ ¦ ¦--Ammon's horn	66.08	4.89	70.57	4.73	-6.37	-0.95	0.00	0.04	*
¦ ¦ ¦ ¦ °--Dentate gyrus	24.93	2.04	26.57	1.94	-6.17	-0.84	0.01	0.06	-
¦ ¦ ¦ °--Isocortex	483.22	37.46	511.96	32.34	-5.62	-0.89	0.01	0.06	-
¦ ¦ °--Cerebral nuclei	152.27	12.64	159.30	10.45	-4.41	-0.67	0.04	0.25	
¦ ¦ ¦--Pallidum	42.78	3.65	44.52	2.88	-3.91	-0.61	0.08	0.40	
¦ ¦ °--Striatum	109.49	9.07	114.77	7.61	-4.60	-0.69	0.04	0.21	
¦ ¦ ¦--Striatum ventral region	26.27	2.18	27.40	1.70	-4.13	-0.66	0.05	0.29	
¦ ¦ ¦ °--Nucleus accumbens	14.30	1.23	14.96	0.90	-4.36	-0.72	0.05	0.25	
¦ ¦ ¦--Lateral septal complex	10.22	0.94	10.26	0.72	-0.33	-0.05	0.89	1.00	
¦ ¦ °--Striatum dorsal region	68.88	5.89	72.92	5.08	-5.54	-0.79	0.02	0.09	-
¦ ¦ °--Caudoputamen	68.88	5.89	72.92	5.08	-5.54	-0.79	0.02	0.09	-
¦ ¦--Brain stem	382.98	26.45	405.70	22.24	-5.60	-1.02	0.00	0.04	*
¦ ¦ ¦--Midbrain	123.33	8.49	129.41	7.69	-4.70	-0.79	0.01	0.09	-
¦ ¦ ¦--Hindbrain	157.20	12.07	167.33	8.95	-6.06	-1.13	0.00	0.04	*
¦ ¦ °--Interbrain	102.45	7.04	108.95	6.92	-5.97	-0.94	0.00	0.04	*
¦ ¦ ¦--Hypothalamus	38.51	2.57	39.64	2.47	-2.87	-0.46	0.13	0.65	
¦ ¦ °--Thalamus	63.94	4.81	69.31	4.58	-7.74	-1.17	0.00	0.01	**
¦ °--Cerebellum	202.59	17.00	222.59	20.06	-8.99	-1.00	0.00	0.02	*
¦ ¦--Cerebellar cortex	197.58	16.65	216.88	19.79	-8.90	-0.98	0.00	0.02	*
¦ °--Cerebellar nuclei	5.00	0.49	5.71	0.32	-12.35	-2.22	0.00	0.00	**
¦ ¦--Dentate nucleus	1.23	0.12	1.40	0.08	-12.08	-2.07	0.00	0.00	**
¦ ¦--Interposed nucleus	1.86	0.19	2.14	0.12	-12.91	-2.25	0.00	0.00	**
¦ °--Fastigial nucleus	1.91	0.18	2.17	0.13	-11.98	-2.07	0.00	0.00	**
¦--fiber tracts	201.16	16.26	217.67	15.09	-7.58	-1.09	0.00	0.02	*
¦ ¦--medial forebrain bundle system	28.42	2.32	30.48	2.23	-6.78	-0.93	0.00	0.04	*
¦ ¦ °--cerebrum related	23.55	1.99	25.23	1.89	-6.65	-0.89	0.00	0.05	*
¦ ¦ ¦--anterior commissure, temporal limb	0.75	0.06	0.77	0.05	-2.44	-0.38	0.26	1.00	
¦ ¦ °--fornix system	14.00	1.25	14.90	1.21	-6.04	-0.75	0.02	0.09	-
¦ ¦ ¦--fimbria	11.61	1.08	12.37	1.01	-6.21	-0.76	0.02	0.09	-
¦ ¦ °--dorsal fornix	2.39	0.18	2.52	0.20	-5.22	-0.64	0.02	0.14	
¦ ¦--cerebellum related fiber tracts	55.76	4.85	62.64	4.72	-10.98	-1.46	0.00	0.00	**
¦ ¦ ¦--cerebellar peduncles	15.64	1.32	17.20	1.09	-9.09	-1.43	0.00	0.00	**
¦ ¦ °--arbor vitae	40.13	3.59	45.44	3.71	-11.69	-1.43	0.00	0.00	**
¦ °--lateral forebrain bundle system	87.21	7.69	93.20	6.61	-6.43	-0.91	0.01	0.06	-
¦ ¦--corticospinal tract	31.58	2.96	33.59	2.34	-5.96	-0.86	0.01	0.09	-
¦ ¦ ¦--cerebal peduncle	10.74	0.82	11.62	0.82	-7.55	-1.07	0.00	0.02	*
¦ ¦ ¦--corticospinal tract-other	7.60	1.39	7.52	0.92	1.14	0.09	0.81	1.00	
¦ ¦ °--internal capsule	13.24	1.21	14.45	1.12	-8.38	-1.08	0.00	0.02	*
¦ °--corpus callosum	55.62	4.97	59.61	4.47	-6.70	-0.89	0.01	0.06	-
°--ventricular systems	23.35	2.12	23.69	1.61	-1.44	-0.21	0.54	1.00	

	V1	V2	V9	V11	V15	V18	V21	V22	V24	V31	V32	V37	V39	V43
	/hpf/largep	/hpf/largep	/hpf/largep	/hpf/largep	/hpf/largep	/hpf/largep	/hpf/largep	/hpf/largep	/hpf/largep	/hpf/largep	/hpf/largep	/hpf/largep	/hpf/largep	/hpf/largep
Relative Volume (% of total brain volume)	mat-/pat+	mat-/pat+	mat-/pat+	mat-/pat+	mat-/pat+	mat-/pat+	mat-/pat+	mat-/pat+	mat-/pat+	mat-/pat+	mat-/pat+	mat-/pat+	mat-/pat+	mat-/pat+
	F	F	F	F	F	F	F	F	F	F	F	F	F	F
Total Brain Volume	100	100	100	100	100	100	100	100	100	100	100	100	100	100
¦--Basic cell groups and regions	87.602523	87.489887	87.626178	87.709792	87.555083	87.494442	87.527944	87.473229	87.548358	87.492828	87.425323	87.498004	87.15362	87.539217
¦ ¦--Cerebrum	54.526783	53.324512	55.254214	54.770027	53.836891	54.805558	54.811917	55.1956	53.920506	54.342257	55.030514	55.211717	53.929583	55.243863
¦ ¦ ¦--Cerebral cortex	45.931952	45.038285	46.729151	45.980791	45.320393	46.35341	46.117111	46.516682	45.374711	46.061839	46.102479	46.760513	45.508945	46.772635
¦ ¦ ¦ °--Cortical plate	43.342624	42.613505	44.175292	43.382524	42.798547	43.883295	43.473085	43.879468	42.866504	43.615758	43.435365	44.16001	43.008323	44.232331
¦ ¦ ¦ ¦--Olfactory areas	7.3685196	7.1652229	7.1782793	7.1625061	7.1330651	7.4523781	7.5599602	7.3215668	7.2004848	7.2839661	7.6778885	7.5883761	7.1537155	7.4636472
¦ ¦ ¦ ¦ °--Main olfactory bulb	2.5185722	2.542268	2.4620742	2.2897696	2.4095862	2.7715614	2.6545677	2.4028981	2.4895489	2.494417	2.6289773	2.7421975	2.4780376	2.6408631
¦ ¦ ¦ ¦--Hippocampal formation	9.0835234	9.1370875	9.318555	8.9524847	8.8916546	9.3013508	9.046015	9.1395436	9.0772937	9.1688821	9.1202541	9.2912401	9.097791	9.2330942
¦ ¦ ¦ ¦ ¦--Retrohippocampal region	3.8832976	3.9957582	4.1429325	3.987899	3.9816092	4.17054	4.0595641	4.0991604	3.9243102	3.9636301	4.0720301	4.2236219	4.0608276	4.1108874
¦ ¦ ¦ ¦ ¦ ¦--Subiculum	1.3333617	1.3448302	1.4543273	1.3501633	1.3430029	1.4134959	1.3411334	1.3871425	1.3776868	1.3969844	1.3972609	1.449441	1.4232615	1.4519927
¦ ¦ ¦ ¦ ¦ ¦ °--Entorhinal area	2.549936	2.6509286	2.6886051	2.6377357	2.6386063	2.7570441	2.7184313	2.7120179	2.5466234	2.5666457	2.6747686	2.7741803	2.637566	2.6588948
¦ ¦ ¦ ¦ ¦ °--Hippocampal region	5.2002275	5.1413288	5.1756198	4.9645863	4.9100441	5.1308133	4.9864515	5.0403849	5.1529859	5.2052532	5.0482262	5.0676206	5.036965	5.1222038
¦ ¦ ¦ ¦ ¦--Ammon's horn	3.7928029	3.7264082	3.7574157	3.6091857	3.5676068	3.7258472	3.6104125	3.6599464	3.7810483	3.8103603	3.6651943	3.6645714	3.6825052	3.7012526
¦ ¦ ¦ ¦ °--Dentate gyrus	1.4074246	1.4149206	1.4182047	1.3554006	1.3424367	1.4049662	1.376039	1.3804385	1.3719376	1.3948935	1.3830325	1.4030492	1.3544599	1.4209511
¦ ¦ ¦ °--Isocortex	26.890587	26.311194	27.678457	27.267533	26.773833	27.12956	26.86711	27.418352	26.58872	27.16291	26.637217	27.280394	26.756817	27.53559
¦ ¦ °--Cerebral nuclei	8.5948312	8.2862204	8.5250624	8.7892293	8.5164981	8.4521477	8.694806	8.6789176	8.545801	8.2804184	8.9280348	8.4512041	8.4206385	8.4712288
¦ ¦ ¦--Pallidum	2.4116117	2.296118	2.4215876	2.4652935	2.3549687	2.3191584	2.4528941	2.5058018	2.4025626	2.3122079	2.5741586	2.3899111	2.3563766	2.3778528
¦ ¦ °--Striatum	6.1832183	5.9901036	6.1034776	6.3239389	6.161527	6.1329912	6.2419131	6.1731152	6.1432366	5.968208	6.3538757	6.0612942	6.0642603	6.0933754
¦ ¦ ¦--Striatum ventral region	1.4809085	1.4402782	1.4576353	1.5277267	1.4508433	1.4577952	1.496645	1.4921901	1.4921898	1.3922024	1.6128437	1.4819733	1.4246751	1.4812401
¦ ¦ ¦ °--Nucleus accumbens	0.8130185	0.7581239	0.8104393	0.8233283	0.8096477	0.7862325	0.8172461	0.8187027	0.8156245	0.7698726	0.8679524	0.7817998	0.7708634	0.80844
¦ ¦ ¦--Lateral septal complex	0.565604	0.5437744	0.5358147	0.5822986	0.5703666	0.5817223	0.5602796	0.5474003	0.5311392	0.5495609	0.5744213	0.589796	0.594966	0.6257826
¦ ¦ °--Striatum dorsal region	3.9065141	3.7756722	3.8824966	3.9780448	3.923492	3.8663225	3.9568955	3.8952729	3.8865648	3.821894	3.9323289	3.7534825	3.8274077	3.7602216
¦ ¦ °--Caudoputamen	3.9065141	3.7756722	3.8824966	3.9780448	3.923492	3.8663225	3.9568955	3.8952729	3.8865648	3.821894	3.9323289	3.7534825	3.8274077	3.7602216
¦ ¦--Brain stem	21.741003	21.961138	21.250693	21.460711	21.821285	21.666046	21.231553	21.372458	21.821391	21.419778	22.128844	21.300538	21.60845	21.120583
¦ ¦ ¦--Midbrain	7.2394605	6.9995689	7.0238278	7.0248841	7.0055439	6.9905149	6.6738112	6.9693957	7.0068617	6.8565444	6.7951475	7.0077842	7.1030467	6.771162
¦ ¦ ¦--Hindbrain	8.6230476	9.2219824	8.3874346	8.6825581	9.2285985	8.9650613	8.9136393	8.5800314	8.9010841	8.7343452	9.4622952	8.5194691	8.6578744	8.5889836
¦ ¦ °--Interbrain	5.8784919	5.7395887	5.8394327	5.753268	5.5871461	5.7104691	5.6441035	5.823033	5.9134436	5.8288936	5.8714051	5.7732867	5.8475273	5.7604407
¦ ¦ ¦--Hypothalamus	2.1922864	2.1913895	2.1687359	2.2547826	2.0500075	2.1292663	2.1968216	2.29936	2.2288264	2.0882492	2.3534669	2.2017833	2.1344406	2.1893984
¦ ¦ °--Thalamus	3.6862049	3.5481985	3.6706968	3.4984855	3.5371387	3.5812029	3.4472819	3.523673	3.6846172	3.7406449	3.5179387	3.5715041	3.7130868	3.5710423
¦ °--Cerebellum	11.334754	12.204255	11.121287	11.479059	11.896895	11.02285	11.48448	10.905154	11.806461	11.730811	10.265949	10.985717	11.615576	11.174776
¦ ¦--Cerebellar cortex	11.046788	11.918988	10.817165	11.211168	11.629863	10.748062	11.203668	10.620331	11.528611	11.453233	9.9999002	10.714809	11.337242	10.930587
¦ °--Cerebellar nuclei	0.2879656	0.2852678	0.3041197	0.2678923	0.2670286	0.2747914	0.2808093	0.2848244	0.2778482	0.2775762	0.2660479	0.2709113	0.2783316	0.2441917
¦ ¦--Dentate nucleus	0.0705212	0.0710458	0.0754891	0.0663632	0.0648658	0.0668745	0.0678178	0.0706178	0.0688005	0.0685233	0.062776	0.0671469	0.0674965	0.0616943
¦ ¦--Interposed nucleus	0.1072497	0.1056047	0.1140251	0.0984016	0.0991493	0.1012309	0.1053743	0.1053467	0.1013357	0.1056722	0.101651	0.1001285	0.1047539	0.0896604
¦ °--Fastigial nucleus	0.1101947	0.1086172	0.1146056	0.1031275	0.1030135	0.1066861	0.1076172	0.1088599	0.1077119	0.1033807	0.1016209	0.1036359	0.1060811	0.092837
¦--fiber tracts	11.093501	11.212169	11.171003	10.987979	11.149773	11.198129	11.21642	11.280843	11.186357	11.268059	11.309	11.152384	11.51189	11.04633
¦ ¦--medial forebrain bundle system	1.6031922	1.5598239	1.5645256	1.555374	1.559055	1.5710918	1.5320675	1.5709601	1.5962858	1.5888073	1.5861212	1.5881504	1.6579698	1.6325734
¦ ¦ °--cerebrum related	1.3248577	1.2906804	1.2918621	1.2833619	1.2904398	1.299356	1.2689186	1.2939185	1.3192664	1.3112443	1.3182073	1.3185251	1.376536	1.3546227
¦ ¦ ¦--anterior commissure, temporal limb	0.0428507	0.0400163	0.0399102	0.0424665	0.0418618	0.0395593	0.0432307	0.0429095	0.0425959	0.041965	0.0434766	0.0416093	0.0421312	0.0417219
¦ ¦ °--fornix system	0.7921773	0.7790449	0.7437886	0.7569737	0.760531	0.7719768	0.7523919	0.75554	0.791043	0.7809199	0.7836163	0.7849387	0.8308267	0.8217796
¦ ¦ ¦--fimbria	0.6561031	0.6482541	0.6128781	0.6230573	0.6303274	0.6406279	0.620568	0.6241963	0.6562238	0.648704	0.6465691	0.6498288	0.6919815	0.6786996
¦ ¦ °--dorsal fornix	0.1360742	0.1307907	0.1309107	0.1339165	0.1302036	0.1313487	0.1318236	0.1313434	0.1348195	0.1322157	0.1370474	0.13511	0.1388448	0.14308
¦ ¦--cerebellum related fiber tracts	3.0836601	3.2206985	3.1588557	3.072675	3.1882152	3.0203111	3.1594138	3.1331927	3.1508279	3.1846007	2.8802723	2.9772709	3.1837579	2.9003912
¦ ¦ ¦--cerebellar peduncles	0.8887594	0.9020169	0.8537138	0.8732346	0.9025936	0.8512758	0.8978214	0.8826716	0.8667189	0.8767283	0.8646073	0.8270564	0.8855672	0.8233774
¦ ¦ °--arbor vitae	2.1949007	2.3186816	2.3051418	2.1994404	2.2856217	2.1690354	2.2615924	2.2505212	2.2841089	2.3078724	2.0156644	2.1502151	2.2981907	2.0770132
¦ °--lateral forebrain bundle system	4.7743617	4.7814691	4.8475507	4.7072661	4.7469223	4.9338544	4.83687	4.8913481	4.7604282	4.8276489	5.1053534	4.8965097	4.9859335	4.8295013
¦ ¦--corticospinal tract	1.6843322	1.7560823	1.7369775	1.6883625	1.7028516	1.8284523	1.8256072	1.7830511	1.7434844	1.741477	1.9749304	1.8549094	1.7688459	1.7387503
¦ ¦ ¦--cerebal peduncle	0.5988657	0.6057474	0.5900252	0.5949956	0.5899517	0.6046146	0.6029091	0.6130412	0.6042728	0.5920656	0.6115257	0.6200016	0.6232446	0.5826378
¦ ¦ ¦--corticospinal tract-other	0.367135	0.4658882	0.3811737	0.3454425	0.3864246	0.4870005	0.4821744	0.4003442	0.4040324	0.4301891	0.6219094	0.4833371	0.3893279	0.4209595
¦ ¦ °--internal capsule	0.7183315	0.6844467	0.7657785	0.7479244	0.7264755	0.736837	0.7405235	0.7696662	0.7351792	0.7192225	0.7414957	0.7515708	0.756273	0.7351525
¦ °--corpus callosum	3.0900295	3.0253868	3.1105732	3.0189035	3.0440707	3.1054027	3.0112628	3.108297	3.0169438	3.0861719	3.130423	3.0416003	3.2170876	3.090751
°--ventricular systems	1.3039803	1.2979076	1.2028267	1.3022367	1.2951643	1.3073907	1.2556098	1.2459731	1.2653122	1.2390715	1.2656892	1.3496656	1.3345274	1.4144184

	V5	V6	V17	V19	V25	V30	V34	V36	V38	V40
	/hpf/largep	/hpf/largep	/hpf/largep	/hpf/largep	/hpf/largep	/hpf/largep	/hpf/largep	/hpf/largep	/hpf/largep	/hpf/largep
Relative Volume (% of total brain volume)	mat-/pat+	mat-/pat+	mat-/pat+	mat-/pat+	mat-/pat+	mat-/pat+	mat-/pat+	mat-/pat+	mat-/pat+	mat-/pat+
	M	M	M	M	M	M	M	M	M	M
Total Brain Volume	100	100	100	100	100	100	100	100	100	100
¦--Basic cell groups and regions	87.302869	87.35873	87.446245	87.267648	87.49747	87.084495	87.646211	87.145556	87.0504	87.391467
¦ ¦--Cerebrum	54.298621	54.533185	56.878459	54.621812	54.644572	53.687851	54.752225	53.817405	55.458486	53.928659
¦ ¦ ¦--Cerebral cortex	46.094539	46.21397	47.68673	46.377419	46.450528	45.01999	46.352302	45.450968	46.503675	45.455522
¦ ¦ ¦ °--Cortical plate	43.565695	43.66312	44.898536	43.784877	43.885037	42.480611	43.749315	43.051383	43.866004	42.943805
¦ ¦ ¦ ¦--Olfactory areas	7.2595754	7.2089869	7.6505673	7.0355179	7.3880963	6.8461189	7.2132928	6.9139503	7.266981	7.3263035
¦ ¦ ¦ ¦ °--Main olfactory bulb	2.5161731	2.4589432	2.607205	2.2948553	2.6112706	2.1960116	2.3373749	2.4029846	2.4574065	2.5534516
¦ ¦ ¦ ¦--Hippocampal formation	9.3613477	9.4412868	9.0442414	9.1948486	9.3486435	9.2456874	9.326259	9.2562924	9.4108744	8.9555499
¦ ¦ ¦ ¦ ¦--Retrohippocampal region	4.1487129	4.2004942	4.2800943	4.2479718	4.1480817	3.9720863	4.1702147	4.0926534	4.2260446	3.9248229
¦ ¦ ¦ ¦ ¦ ¦--Subiculum	1.3709384	1.4336089	1.3785413	1.4270064	1.4434236	1.4050429	1.429555	1.4393034	1.4626674	1.3817245
¦ ¦ ¦ ¦ ¦ °--Entorhinal area	2.7777745	2.7668854	2.901553	2.8209649	2.704658	2.5670439	2.7406597	2.6533505	2.7633772	2.5430983
¦ ¦ ¦ ¦ °--Hippocampal region	5.2126359	5.2407903	4.7641476	4.9468746	5.2005639	5.2736026	5.1560422	5.163639	5.1848292	5.0307249
¦ ¦ ¦ ¦ ¦--Ammon's horn	3.7916525	3.7893999	3.4570394	3.5905974	3.7493785	3.8343185	3.7182161	3.709337	3.7597002	3.6975852
¦ ¦ ¦ ¦ °--Dentate gyrus	1.4209834	1.4513904	1.3071082	1.3562772	1.4511848	1.4392841	1.4378261	1.454302	1.425129	1.3331397
¦ ¦ ¦ °--Isocortex	26.944772	27.012846	28.203728	27.55451	27.148292	26.3888	27.209763	26.881141	27.188148	26.661957
¦ ¦ °--Cerebral nuclei	8.2040821	8.3192148	9.1917244	8.2443924	8.1940441	8.6678606	8.3999288	8.3664375	8.9548113	8.4731375
¦ ¦ ¦--Pallidum	2.2729551	2.4023895	2.5897584	2.3462918	2.2899006	2.4202887	2.3483399	2.2829015	2.5546578	2.3521686
¦ ¦ °--Striatum	5.9311248	5.9168247	6.6019675	5.8981001	5.9041429	6.2475703	6.0515879	6.0835375	6.400154	6.1209699
¦ ¦ ¦--Striatum ventral region	1.4296253	1.4563196	1.6035794	1.4570962	1.3971707	1.4625899	1.4591925	1.3875221	1.5190317	1.4506308
¦ ¦ ¦ °--Nucleus accumbens	0.7775905	0.7828604	0.8818909	0.7892387	0.7564231	0.8086812	0.7903227	0.7602816	0.8315556	0.7956455
¦ ¦ ¦--Lateral septal complex	0.5886395	0.5588268	0.5506094	0.5356657	0.5738109	0.6086305	0.5694717	0.5874376	0.6431476	0.5713268
¦ ¦ °--Striatum dorsal region	3.682209	3.6734439	4.2087589	3.661719	3.6989647	3.9449991	3.7814473	3.8793287	4.0060477	3.8645038
¦ ¦ °--Caudoputamen	3.682209	3.6734439	4.2087589	3.661719	3.6989647	3.9449991	3.7814473	3.8793287	4.0060477	3.8645038
¦ ¦--Brain stem	21.157602	21.581114	20.710422	21.274055	21.018849	21.567112	21.354123	21.626795	21.284188	21.550382
¦ ¦ ¦--Midbrain	6.6672913	7.0518922	6.763381	6.7155537	6.7109298	7.0006474	6.7380836	6.8848285	6.9901003	6.8934323
¦ ¦ ¦--Hindbrain	8.9825967	8.7469153	8.4884583	8.8993762	8.7153843	8.9166144	8.8991143	9.0021861	8.3739242	8.8661393
¦ ¦ °--Interbrain	5.5077113	5.7823105	5.4585811	5.6591218	5.5925367	5.6498503	5.7169242	5.7397766	5.9201636	5.7908095
¦ ¦ ¦--Hypothalamus	2.0750679	2.2092087	2.0790644	2.062675	2.0482109	2.0546293	2.1444631	2.1428799	2.1538768	2.1670524
¦ ¦ °--Thalamus	3.4326434	3.5731024	3.3795167	3.5964469	3.5443258	3.5952214	3.5724606	3.5968966	3.7662868	3.6237572
¦ °--Cerebellum	11.846663	11.244442	9.8573842	11.37176	11.834033	11.829533	11.539883	11.701376	10.307736	11.912436
¦ ¦--Cerebellar cortex	11.562298	10.957085	9.5679829	11.069998	11.551323	11.544468	11.254714	11.425121	10.026546	11.634921
¦ °--Cerebellar nuclei	0.2843652	0.2873601	0.2894033	0.3017608	0.2827091	0.2850687	0.2851678	0.2762586	0.2811916	0.2775126
¦ ¦--Dentate nucleus	0.0740592	0.0723149	0.0700444	0.0726426	0.0702206	0.0695999	0.0712779	0.0678684	0.0663356	0.0695755
¦ ¦--Interposed nucleus	0.1043565	0.1025694	0.1099424	0.1128453	0.1059967	0.1081548	0.1060972	0.1029332	0.1041302	0.1040678
¦ °--Fastigial nucleus	0.1059495	0.1124759	0.1094164	0.1162729	0.1064918	0.1073139	0.1077926	0.105457	0.1107257	0.1038692
¦--fiber tracts	11.277305	11.346643	11.30775	11.497967	11.169093	11.509114	11.047037	11.492235	11.586702	11.274037
¦ ¦--medial forebrain bundle system	1.5854006	1.6113071	1.5197854	1.5806988	1.572203	1.7005685	1.5379901	1.6140251	1.6901762	1.6135792
¦ ¦ °--cerebrum related	1.3166256	1.3361417	1.265593	1.3063816	1.3046234	1.4222174	1.2731237	1.3427637	1.4088762	1.3329617
¦ ¦ ¦--anterior commissure, temporal limb	0.0403182	0.0409648	0.0434014	0.0411592	0.0417657	0.0421587	0.0418113	0.041207	0.0429438	0.0429273
¦ ¦ °--fornix system	0.7920475	0.7878135	0.7041162	0.7539996	0.7871223	0.8676	0.7596708	0.8028387	0.8453932	0.8054594
¦ ¦ ¦--fimbria	0.6608046	0.6501538	0.5782874	0.6232356	0.6564638	0.7321758	0.6283219	0.6675291	0.7010329	0.6696859
¦ ¦ °--dorsal fornix	0.1312425	0.1376595	0.1258287	0.1307639	0.1306586	0.1354241	0.1313489	0.1353097	0.1443602	0.1357733
¦ ¦--cerebellum related fiber tracts	3.2467949	3.1386002	3.0150479	3.3036638	3.1949459	3.2115264	3.1442658	3.1864605	2.9887301	3.1811342
¦ ¦ ¦--cerebellar peduncles	0.8865301	0.8746858	0.8707706	0.908077	0.887197	0.8913382	0.8779447	0.8985532	0.8307694	0.8858177
¦ ¦ °--arbor vitae	2.3602648	2.2639144	2.1442773	2.3955869	2.3077484	2.3201881	2.2663205	2.2879073	2.1579607	2.295317
¦ °--lateral forebrain bundle system	4.7920183	4.9238317	5.1116718	4.9590159	4.7384822	4.9551663	4.6871756	5.0284275	5.259884	4.7675806
¦ ¦--corticospinal tract	1.6977539	1.7199997	1.9262811	1.7808226	1.6512538	1.7321149	1.6406578	1.8475262	1.9352796	1.686877
¦ ¦ ¦--cerebal peduncle	0.594199	0.6119853	0.6233216	0.6234864	0.5700469	0.6019651	0.5673406	0.6018602	0.6058392	0.6085115
¦ ¦ ¦--corticospinal tract-other	0.393105	0.3709827	0.4924791	0.4020522	0.351343	0.3768006	0.3642632	0.5125428	0.5337944	0.3561309
¦ ¦ °--internal capsule	0.7104502	0.7370318	0.8104803	0.7552843	0.7298637	0.7533493	0.709054	0.733123	0.7956462	0.7222344
¦ °--corpus callosum	3.0942644	3.203832	3.1853907	3.1781933	3.0872284	3.2230515	3.0465177	3.1809013	3.3246038	3.0807036
°--ventricular systems	1.4198237	1.2946123	1.2459737	1.2344215	1.3334394	1.4063841	1.306746	1.3621935	1.3628598	1.334505

	V3	V4	V12	V13	V14	V20	V23	V26	V28	V29	V33	V47
	/hpf/largep	/hpf/largep	/hpf/largep	/hpf/largep	/hpf/largep	/hpf/largep	/hpf/largep	/hpf/largep	/hpf/largep	/hpf/largep	/hpf/largep	/hpf/largep
Relative Volume (% of total brain volume)	mat+/pat+	mat+/pat+	mat+/pat+	mat+/pat+	mat+/pat+	mat+/pat+	mat+/pat+	mat+/pat+	mat+/pat+	mat+/pat+	mat+/pat+	mat+/pat+
	F	F	F	F	F	F	F	F	F	F	F	F
Total Brain Volume	100	100	100	100	100	100	100	100	100	100	100	100
¦--Basic cell groups and regions	87.271806	87.591707	87.371179	87.669949	87.414167	87.442436	87.229751	86.99563	87.213766	87.345586	87.13262	87.258385
¦ ¦--Cerebrum	54.406376	54.624514	54.213746	55.518558	54.644106	53.420617	54.081966	53.627234	53.51501	54.074425	53.427397	54.716775
¦ ¦ ¦--Cerebral cortex	45.928886	46.287695	45.740273	46.9071	46.364278	45.381516	45.481824	45.169876	45.324356	45.70866	45.02051	46.237415
¦ ¦ ¦ °--Cortical plate	43.326747	43.747539	43.237302	44.273873	43.853673	42.929692	43.042399	42.68408	42.904993	43.245015	42.639302	43.671441
¦ ¦ ¦ ¦--Olfactory areas	7.1748462	6.9992578	7.0361875	7.3493745	7.2610112	6.9903491	7.0436505	7.0933225	7.159021	7.2855109	7.1004412	7.1556185
¦ ¦ ¦ ¦ °--Main olfactory bulb	2.4536203	2.2558134	2.2967042	2.5897093	2.5027126	2.3113985	2.4557559	2.4268025	2.5438076	2.5830918	2.4961098	2.5445617
¦ ¦ ¦ ¦--Hippocampal formation	9.091635	9.2368696	8.9499062	9.3979271	9.1091709	9.1260681	9.1967987	8.9875307	9.2995996	9.444796	9.2913069	9.1640823
¦ ¦ ¦ ¦ ¦--Retrohippocampal region	3.9158598	4.1031254	4.0625817	4.3643469	4.0653333	4.0704207	3.9557422	4.0095709	4.0271259	4.155411	3.9638073	4.0436951
¦ ¦ ¦ ¦ ¦ ¦--Subiculum	1.3578162	1.3995469	1.3700662	1.4352785	1.3501145	1.4115916	1.4155046	1.3619126	1.4709033	1.4574598	1.3888064	1.4511638
¦ ¦ ¦ ¦ ¦ ¦ °--Entorhinal area	2.5580436	2.7035786	2.6925161	2.9290684	2.7152188	2.6588291	2.5402376	2.6476583	2.5562226	2.6979511	2.5750009	2.5925308
¦ ¦ ¦ ¦ °--Hippocampal region	5.1757741	5.1337424	4.8873256	5.0335774	5.0438381	5.0556468	5.2410581	4.9779592	5.2724757	5.2893828	5.3275008	5.1203898
¦ ¦ ¦ ¦ ¦--Ammon's horn	3.7972212	3.7327351	3.526293	3.659452	3.6842015	3.6820265	3.8140407	3.6293375	3.8166834	3.8277194	3.8628321	3.721033
¦ ¦ ¦ ¦ °--Dentate gyrus	1.3785529	1.4010073	1.3610326	1.3741254	1.3596366	1.3736204	1.4270174	1.3486217	1.4557922	1.4616629	1.4646687	1.3993567
¦ ¦ ¦ °--Isocortex	27.060266	27.511411	27.251202	27.526577	27.483491	26.813281	26.801944	26.603227	26.446372	26.514713	26.247554	27.35174
¦ ¦ °--Cerebral nuclei	8.4774906	8.3368193	8.473473	8.6114533	8.2798283	8.0391015	8.6001479	8.4573633	8.1906539	8.3657657	8.4068813	8.4793656
¦ ¦ ¦--Pallidum	2.388557	2.3135406	2.3597968	2.4436564	2.2950726	2.2797028	2.3935106	2.3650435	2.2934447	2.3461806	2.3405257	2.3850753
¦ ¦ °--Striatum	6.0889342	6.0232781	6.1136767	6.1677991	5.9847551	5.759401	6.2066356	6.0923177	5.8972082	6.0195835	6.0663573	6.0942893
¦ ¦ ¦--Striatum ventral region	1.437163	1.4259589	1.4535805	1.5092159	1.437044	1.4428967	1.4384734	1.4226056	1.3919897	1.4356707	1.4639991	1.4335758
¦ ¦ ¦ °--Nucleus accumbens	0.7867669	0.7779822	0.7953129	0.8445007	0.7860385	0.7761494	0.8142799	0.7695526	0.7620797	0.7879925	0.8065226	0.7810419
¦ ¦ ¦--Lateral septal complex	0.5495778	0.5237818	0.526052	0.5550167	0.5348932	0.5301979	0.5292775	0.5486472	0.512951	0.5365917	0.5311123	0.5744412
¦ ¦ °--Striatum dorsal region	3.869436	3.8564274	3.9141359	3.8776552	3.7909909	3.5763505	4.0298126	3.9020769	3.7834279	3.8319441	3.8649686	3.8667029
¦ ¦ °--Caudoputamen	3.869436	3.8564274	3.9141359	3.8776552	3.7909909	3.5763505	4.0298126	3.9020769	3.7834279	3.8319441	3.8649686	3.8667029
¦ ¦--Brain stem	21.795005	20.976869	21.707854	21.360155	21.089361	22.016828	21.508542	21.944821	21.452336	21.629989	22.109866	21.013836
¦ ¦ ¦--Midbrain	6.9322791	6.6776361	6.8574769	6.9658408	6.590861	6.8301376	6.9214513	6.9155233	6.7392679	6.9136919	6.9913514	6.739371
¦ ¦ ¦--Hindbrain	8.977779	8.5961749	9.1267422	8.5958469	8.9652659	9.526832	8.6602154	9.3225455	8.8626791	8.8974836	9.2211749	8.4561371
¦ ¦ °--Interbrain	5.884947	5.7030597	5.7236347	5.7984629	5.5332316	5.6598581	5.9268771	5.706752	5.8503917	5.8188115	5.8973401	5.8183282
¦ ¦ ¦--Hypothalamus	2.1441565	2.0547674	2.0747295	2.1596836	2.0253336	2.0385543	2.1436351	2.1592659	2.1165152	2.0867277	2.151414	2.1249772
¦ ¦ °--Thalamus	3.7407905	3.6482923	3.6489052	3.6387793	3.507898	3.6213038	3.7832419	3.5474861	3.733876	3.7320832	3.7459261	3.693351
¦ °--Cerebellum	11.070437	11.990318	11.449584	10.791236	11.680705	12.004996	11.639238	11.423558	12.246415	11.641193	11.595392	11.527769
¦ ¦--Cerebellar cortex	10.756647	11.69846	11.145804	10.500274	11.376116	11.688045	11.334215	11.119332	11.948495	11.335522	11.274978	11.229586
¦ °--Cerebellar nuclei	0.3137916	0.2918546	0.3037807	0.2909598	0.3045908	0.3169522	0.3050245	0.3042226	0.2979198	0.3056711	0.32041	0.2981842
¦ ¦--Dentate nucleus	0.0781904	0.074502	0.0755015	0.0724258	0.0762584	0.0792351	0.0728891	0.0758082	0.0736139	0.0746237	0.0782781	0.0733046
¦ ¦--Interposed nucleus	0.1174274	0.10735	0.1127956	0.1076511	0.1166149	0.1190743	0.1144034	0.1127768	0.1136675	0.115461	0.1222991	0.1110038
¦ °--Fastigial nucleus	0.1181738	0.1100026	0.1154836	0.1108829	0.1117174	0.1186427	0.117732	0.1156376	0.1106384	0.1155864	0.1198328	0.1138758
¦--fiber tracts	11.435098	11.180803	11.427241	11.066762	11.341637	11.346553	11.536681	11.696953	11.586781	11.436824	11.63966	11.453692
¦ ¦--medial forebrain bundle system	1.6352714	1.5535354	1.5638733	1.5705874	1.54865	1.5427808	1.625231	1.6075954	1.6022111	1.5864292	1.6175354	1.6331678
¦ ¦ °--cerebrum related	1.3558989	1.2858616	1.2909364	1.292542	1.2800337	1.2707673	1.3455631	1.339215	1.3259018	1.3094016	1.3316474	1.3595665
¦ ¦ ¦--anterior commissure, temporal limb	0.0416055	0.03878	0.0408856	0.0413255	0.0407828	0.0403786	0.040526	0.0433351	0.0404777	0.0396585	0.0396729	0.0400679
¦ ¦ °--fornix system	0.789915	0.7447244	0.7527964	0.7547254	0.7471163	0.7556314	0.7882346	0.7946804	0.7888728	0.7822941	0.7942314	0.7974068
¦ ¦ ¦--fimbria	0.6573142	0.6170923	0.6271415	0.6258653	0.6223466	0.6296962	0.6536637	0.6559367	0.6577446	0.6511445	0.6606715	0.6613092
¦ ¦ °--dorsal fornix	0.1326004	0.1276324	0.1256549	0.1288598	0.1247695	0.125935	0.1345708	0.138744	0.1311284	0.1311501	0.13356	0.1360974
¦ ¦--cerebellum related fiber tracts	3.1470298	3.2334556	3.2933484	3.0882746	3.3253779	3.467735	3.2308046	3.3753693	3.4054042	3.324002	3.4314766	3.1867034
¦ ¦ ¦--cerebellar peduncles	0.8868551	0.8822943	0.8991526	0.8715545	0.9270064	0.9598171	0.8917053	0.9431207	0.9516625	0.9378221	0.979472	0.8797157
¦ ¦ °--arbor vitae	2.2601748	2.3511619	2.3941964	2.2167201	2.3983721	2.5079173	2.3390993	2.4322486	2.4537417	2.3861793	2.4520045	2.3069877
¦ °--lateral forebrain bundle system	5.0200871	4.8253552	4.9176927	4.7748641	4.8221749	4.6772372	5.0362011	5.0139792	4.9144678	4.8584936	4.9254141	5.0073899
¦ ¦--corticospinal tract	1.7856218	1.6822248	1.831704	1.7246569	1.7189379	1.709456	1.7800769	1.9440811	1.7710177	1.7648537	1.8194746	1.7845142
¦ ¦ ¦--cerebal peduncle	0.6190717	0.572131	0.6075999	0.5826342	0.610435	0.600085	0.6210334	0.6432566	0.6342451	0.6055723	0.6366653	0.6211548
¦ ¦ ¦--corticospinal tract-other	0.3800989	0.3700232	0.4530936	0.3744636	0.3758961	0.3898811	0.3864561	0.5193822	0.3937876	0.3955612	0.4365744	0.3546547
¦ ¦ °--internal capsule	0.7864508	0.7400705	0.7710104	0.7675591	0.7326071	0.71949	0.7725876	0.7814421	0.742985	0.7637204	0.7462345	0.8087046
¦ °--corpus callosum	3.2344659	3.1431304	3.0859887	3.0502078	3.103237	2.9677806	3.2561242	3.0698981	3.14345	3.0936398	3.1059401	3.2228762
°--ventricular systems	1.2930864	1.227497	1.2015762	1.2632748	1.2441829	1.2110055	1.2335617	1.3074488	1.1994505	1.2175689	1.2276999	1.2879065

	V7	V8	V10	V16	V27	V35	V41	V42	V44	V45	V46
	/hpf/largep	/hpf/largep	/hpf/largep	/hpf/largep	/hpf/largep	/hpf/largep	/hpf/largep	/hpf/largep	/hpf/largep	/hpf/largep	/hpf/largep
Relative Volume (% of total brain volume)	mat+/pat+	mat+/pat+	mat+/pat+	mat+/pat+	mat+/pat+	mat+/pat+	mat+/pat+	mat+/pat+	mat+/pat+	mat+/pat+	mat+/pat+
	M	M	M	M	M	M	M	M	M	M	M
Total Brain Volume	100	100	100	100	100	100	100	100	100	100	100
¦--Basic cell groups and regions	87.367215	87.151814	87.522512	87.347719	87.226179	87.144032	87.253572	86.996387	87.189838	87.205518	87.31644
¦ ¦--Cerebrum	54.929237	53.611613	55.288948	54.58388	53.798195	53.897303	54.567125	53.643595	54.013996	54.017951	53.845547
¦ ¦ ¦--Cerebral cortex	46.336564	45.396663	46.665725	46.285028	45.263117	45.536403	46.219466	45.105293	45.554408	45.702474	45.850951
¦ ¦ ¦ °--Cortical plate	43.730192	42.921912	44.072673	43.865788	42.837258	43.143415	43.739114	42.490253	43.072692	43.272697	43.371033
¦ ¦ ¦ ¦--Olfactory areas	7.1354568	7.0197812	7.065477	7.119439	6.7080018	7.0392263	7.3038383	7.0814963	7.0490069	7.3127711	7.4030557
¦ ¦ ¦ ¦ °--Main olfactory bulb	2.346961	2.3544122	2.2508271	2.4221752	2.0824926	2.4600607	2.5925008	2.4271089	2.3605052	2.6013318	2.6568159
¦ ¦ ¦ ¦--Hippocampal formation	9.3596255	9.3671971	9.3002264	9.1396551	9.2605743	9.3273031	9.2924584	9.30599	9.2604554	9.0007229	8.9408566
¦ ¦ ¦ ¦ ¦--Retrohippocampal region	4.2050006	4.1436747	4.2991817	4.1524208	4.194061	4.0869233	4.1790813	4.0116704	4.1260248	4.0075577	4.0197051
¦ ¦ ¦ ¦ ¦ ¦--Subiculum	1.4118053	1.3969167	1.4334628	1.3593876	1.396223	1.4668954	1.4257974	1.4058632	1.4283638	1.3726403	1.3624622
¦ ¦ ¦ ¦ ¦ °--Entorhinal area	2.7931953	2.746758	2.865719	2.7930332	2.797838	2.6200274	2.7532839	2.6058072	2.697661	2.6349175	2.6572434
¦ ¦ ¦ ¦ °--Hippocampal region	5.1546249	5.2235228	5.0010452	4.9872327	5.0665142	5.2403823	5.1133781	5.2943211	5.134431	4.9931651	4.9211501
¦ ¦ ¦ ¦ ¦--Ammon's horn	3.7192371	3.7946208	3.6283367	3.6352678	3.6954328	3.8031876	3.7328256	3.8327219	3.7246222	3.6122067	3.577245
¦ ¦ ¦ ¦ °--Dentate gyrus	1.4353879	1.4289015	1.3727086	1.3519649	1.371081	1.4371942	1.380553	1.4615993	1.4098088	1.3809584	1.3439046
¦ ¦ ¦ °--Isocortex	27.235105	26.534934	27.70697	27.606688	26.868682	26.776886	27.142817	26.102766	26.76323	26.959203	27.027121
¦ ¦ °--Cerebral nuclei	8.592673	8.2149506	8.6232226	8.2988518	8.5350779	8.3608952	8.3476535	8.5383023	8.459588	8.3154775	7.9945909
¦ ¦ ¦--Pallidum	2.4145737	2.297714	2.4233011	2.335786	2.3444588	2.3513043	2.3035496	2.3637372	2.3814386	2.2962367	2.2312818
¦ ¦ °--Striatum	6.1780983	5.9172376	6.1999194	5.9630658	6.1906191	6.0095919	6.0441049	6.1745661	6.0781499	6.0192414	5.7633115
¦ ¦ ¦--Striatum ventral region	1.4440424	1.4205132	1.5049763	1.4739391	1.50014	1.4383275	1.4283589	1.4071442	1.4654364	1.4338811	1.3947032
¦ ¦ ¦ °--Nucleus accumbens	0.7831209	0.7624012	0.8263784	0.7993123	0.8102264	0.7960229	0.7789465	0.7722095	0.7894761	0.7727444	0.7499333
¦ ¦ ¦--Lateral septal complex	0.5239259	0.5503213	0.5707035	0.535077	0.535677	0.5132381	0.5419293	0.5970716	0.5416604	0.5511028	0.5178343
¦ ¦ °--Striatum dorsal region	3.9723962	3.7234797	3.8937347	3.7339472	3.9239831	3.8314771	3.8532138	3.9412915	3.8460593	3.8193731	3.6354976
¦ ¦ °--Caudoputamen	3.9723962	3.7234797	3.8937347	3.7339472	3.9239831	3.8314771	3.8532138	3.9412915	3.8460593	3.8193731	3.6354976
¦ ¦--Brain stem	20.759266	21.459476	21.365092	21.390534	21.205578	21.58837	21.016977	21.299905	21.380666	21.120422	20.634538
¦ ¦ ¦--Midbrain	6.7399286	6.7844994	7.0624914	6.7900997	6.8941684	6.8536765	6.7912974	6.7989839	6.9171751	6.6767334	6.4693335
¦ ¦ ¦--Hindbrain	8.242188	8.9467059	8.4985785	8.9554358	8.5663313	8.9794061	8.5401774	8.7441314	8.7038736	8.8696141	8.6970404
¦ ¦ °--Interbrain	5.7771464	5.7282741	5.8040251	5.6449945	5.7450754	5.7552881	5.6855069	5.756791	5.7596186	5.5740756	5.4681672
¦ ¦ ¦--Hypothalamus	2.1011354	2.0681683	2.1727382	2.0958292	2.0599747	2.0575883	2.0052033	2.1013532	2.1204554	1.9959718	1.9876523
¦ ¦ °--Thalamus	3.6760109	3.6601058	3.6312874	3.5491653	3.6851007	3.6976993	3.6803037	3.6554378	3.6391627	3.5781038	3.4805144
¦ °--Cerebellum	11.678712	12.080699	10.868451	11.373278	12.222432	11.658339	11.669476	12.052866	11.79519	12.067129	12.836379
¦ ¦--Cerebellar cortex	11.378174	11.775299	10.579032	11.073349	11.916331	11.359946	11.378962	11.75845	11.493623	11.769555	12.551175
¦ °--Cerebellar nuclei	0.3005368	0.3054008	0.2894213	0.2999285	0.3060962	0.2983911	0.2905159	0.2944181	0.3015656	0.2975747	0.2852039
¦ ¦--Dentate nucleus	0.0738569	0.076581	0.0684551	0.073413	0.078202	0.0711511	0.0691817	0.0704204	0.0725534	0.0718159	0.0689127
¦ ¦--Interposed nucleus	0.1119826	0.1123028	0.1082417	0.1135396	0.1129392	0.1121371	0.1079164	0.110884	0.1134737	0.1116506	0.1086008
¦ °--Fastigial nucleus	0.1146974	0.1165169	0.1127246	0.1129759	0.1149551	0.1151028	0.1134178	0.1131136	0.1155385	0.1141082	0.1076904
¦--fiber tracts	11.396645	11.528422	11.217952	11.406698	11.528841	11.655084	11.514809	11.692914	11.551668	11.531578	11.460441
¦ ¦--medial forebrain bundle system	1.5910501	1.6245072	1.6143741	1.5982548	1.6100852	1.6268791	1.6329855	1.7251165	1.6295062	1.6154915	1.5617676
¦ ¦ °--cerebrum related	1.319579	1.3484428	1.3356423	1.3195717	1.3257881	1.3470968	1.3534704	1.4431721	1.3447878	1.3363765	1.2951656
¦ ¦ ¦--anterior commissure, temporal limb	0.0396344	0.040488	0.0395074	0.0404465	0.0410157	0.0393548	0.0399958	0.0420564	0.0412231	0.0396572	0.0380261
¦ ¦ °--fornix system	0.7697079	0.8077768	0.7825075	0.7738131	0.7992631	0.7965548	0.7885805	0.8863017	0.789931	0.7889344	0.7631625
¦ ¦ ¦--fimbria	0.6348691	0.6725222	0.6450447	0.6435871	0.6671615	0.6620386	0.653826	0.745573	0.6514499	0.6546694	0.6317694
¦ ¦ °--dorsal fornix	0.1348386	0.1352551	0.1374625	0.1302259	0.1321015	0.1345163	0.1347543	0.1407284	0.1384813	0.1342652	0.1313934
¦ ¦--cerebellum related fiber tracts	3.2250084	3.3813779	3.1137813	3.3448044	3.4141943	3.295673	3.1962365	3.2752358	3.3103401	3.3459501	3.4587668
¦ ¦ ¦--cerebellar peduncles	0.8453147	0.9071188	0.8638065	0.9397498	0.886254	0.9131747	0.8570914	0.8916832	0.8999867	0.9236627	0.9143681
¦ ¦ °--arbor vitae	2.3796933	2.4742591	2.2499753	2.4050546	2.5279408	2.3824983	2.3391451	2.3835526	2.4103534	2.4222874	2.5443986
¦ °--lateral forebrain bundle system	4.9672537	4.8684168	4.8725938	4.7991736	4.8662722	5.0234974	4.9951337	5.0760542	4.939139	4.8963484	4.784681
¦ ¦--corticospinal tract	1.7713781	1.750929	1.7705158	1.7257421	1.7066508	1.7942296	1.769254	1.8858783	1.7318042	1.7641528	1.709393
¦ ¦ ¦--cerebal peduncle	0.6057278	0.6218629	0.6235737	0.6254803	0.6126757	0.6271876	0.5994516	0.6052128	0.6095596	0.6032049	0.5887869
¦ ¦ ¦--corticospinal tract-other	0.3624811	0.3822047	0.3753746	0.3803716	0.3750712	0.3869573	0.3855568	0.5376305	0.3605586	0.3726752	0.3707543
¦ ¦ °--internal capsule	0.8031693	0.7468614	0.7715675	0.71989	0.7189038	0.7800845	0.7842457	0.7430349	0.7616865	0.7882722	0.749852
¦ °--corpus callosum	3.195876	3.1174877	3.102078	3.073432	3.1596214	3.2292678	3.2258797	3.1901759	3.2073348	3.1321957	3.075288
°--ventricular systems	1.2361622	1.3198056	1.2595614	1.2456223	1.2449524	1.2009149	1.2316326	1.3107186	1.2584786	1.2629034	1.2230782

Relative Volume	mat-/pat+		mat+/pat+						
	Mean	SD	Mean	SD	%Diff	Effect	P-Value		
Total Brain Volume	100.00	0.00	100.00	0.00	0.00				
¦--Basic cell groups and regions	87.43	0.18	87.29	0.17	0.16	0.84	0.01	0.03	*
¦ ¦--Cerebrum	54.62	0.75	54.19	0.59	0.78	0.72	0.04	0.08	-
¦ ¦ ¦--Cerebral cortex	46.09	0.63	45.80	0.52	0.63	0.55	0.10	0.19	
¦ ¦ ¦ °--Cortical plate	43.53	0.58	43.31	0.48	0.52	0.46	0.16	0.27	
¦ ¦ ¦ ¦--Olfactory areas	7.28	0.21	7.13	0.15	2.23	1.05	0.01	0.02	*
¦ ¦ ¦ ¦ °--Main olfactory bulb	2.50	0.14	2.44	0.14	2.58	0.45	0.13	0.24	
¦ ¦ ¦ ¦--Hippocampal formation	9.19	0.15	9.21	0.15	-0.28	-0.18	0.55	0.72	
¦ ¦ ¦ ¦ ¦--Retrohippocampal region	4.09	0.11	4.09	0.11	-0.17	-0.06	0.83	0.92	
¦ ¦ ¦ ¦ ¦ ¦--Subiculum	1.40	0.04	1.41	0.04	-0.30	-0.11	0.71	0.84	
¦ ¦ ¦ ¦ ¦ °--Entorhinal area	2.69	0.09	2.69	0.10	-0.11	-0.03	0.92	0.97	
¦ ¦ ¦ ¦ °--Hippocampal region	5.10	0.12	5.12	0.13	-0.37	-0.15	0.61	0.76	
¦ ¦ ¦ ¦ ¦--Ammon's horn	3.70	0.09	3.72	0.09	-0.42	-0.17	0.55	0.72	
¦ ¦ ¦ ¦ °--Dentate gyrus	1.40	0.04	1.40	0.04	-0.22	-0.08	0.79	0.92	
¦ ¦ ¦ °--Isocortex	27.06	0.43	26.97	0.45	0.34	0.20	0.48	0.66	
¦ ¦ °--Cerebral nuclei	8.53	0.25	8.39	0.17	1.62	0.79	0.04	0.08	-
¦ ¦ ¦--Pallidum	2.40	0.09	2.35	0.05	2.14	0.97	0.02	0.07	-
¦ ¦ °--Striatum	6.13	0.17	6.05	0.13	1.41	0.68	0.06	0.12	
¦ ¦ ¦--Striatum ventral region	1.47	0.06	1.44	0.03	1.92	0.89	0.04	0.09	-
¦ ¦ ¦ °--Nucleus accumbens	0.80	0.03	0.79	0.02	1.63	0.59	0.11	0.21	
¦ ¦ ¦--Lateral septal complex	0.57	0.03	0.54	0.02	5.93	1.58	0.00	0.00	**
¦ ¦ °--Striatum dorsal region	3.86	0.12	3.84	0.10	0.42	0.16	0.63	0.76	
¦ ¦ °--Caudoputamen	3.86	0.12	3.84	0.10	0.42	0.16	0.63	0.76	
¦ ¦--Brain stem	21.46	0.32	21.38	0.38	0.35	0.20	0.46	0.65	
¦ ¦ ¦--Midbrain	6.91	0.15	6.82	0.14	1.35	0.68	0.03	0.08	-
¦ ¦ ¦--Hindbrain	8.81	0.27	8.82	0.30	-0.20	-0.06	0.83	0.92	
¦ ¦ °--Interbrain	5.74	0.12	5.74	0.11	0.02	0.01	0.97	0.97	
¦ ¦ ¦--Hypothalamus	2.16	0.08	2.09	0.05	3.35	1.27	0.00	0.00	**
¦ ¦ °--Thalamus	3.58	0.10	3.65	0.08	-1.89	-0.89	0.01	0.03	*
¦ °--Cerebellum	11.35	0.58	11.71	0.46	-3.06	-0.78	0.02	0.07	-
¦ ¦--Cerebellar cortex	11.07	0.58	11.41	0.46	-2.96	-0.73	0.03	0.08	-
¦ °--Cerebellar nuclei	0.28	0.01	0.30	0.01	-6.99	-2.42	0.00	0.00	**
¦ ¦--Dentate nucleus	0.07	0.00	0.07	0.00	-6.72	-1.60	0.00	0.00	**
¦ ¦--Interposed nucleus	0.10	0.00	0.11	0.00	-7.62	-2.31	0.00	0.00	**
¦ °--Fastigial nucleus	0.11	0.00	0.11	0.00	-6.55	-2.55	0.00	0.00	**
¦--fiber tracts	11.26	0.16	11.46	0.16	-1.75	-1.26	0.00	0.00	**
¦ ¦--medial forebrain bundle system	1.59	0.04	1.61	0.04	-0.86	-0.35	0.27	0.44	
¦ ¦ °--cerebrum related	1.32	0.04	1.33	0.04	-0.73	-0.27	0.39	0.58	
¦ ¦ ¦--anterior commissure, temporal limb	0.04	0.00	0.04	0.00	3.68	1.32	0.00	0.00	**
¦ ¦ °--fornix system	0.78	0.03	0.78	0.03	-0.05	-0.01	0.97	0.97	
¦ ¦ ¦--fimbria	0.65	0.03	0.65	0.03	-0.24	-0.06	0.85	0.92	
¦ ¦ °--dorsal fornix	0.13	0.00	0.13	0.00	0.89	0.28	0.35	0.53	
¦ ¦--cerebellum related fiber tracts	3.12	0.11	3.30	0.11	-5.36	-1.64	0.00	0.00	**
¦ ¦ ¦--cerebellar peduncles	0.88	0.02	0.91	0.03	-3.45	-0.90	0.00	0.00	**
¦ ¦ °--arbor vitae	2.25	0.09	2.39	0.08	-6.08	-1.73	0.00	0.00	**
¦ °--lateral forebrain bundle system	4.88	0.14	4.91	0.10	-0.54	-0.27	0.46	0.65	
¦ ¦--corticospinal tract	1.77	0.09	1.77	0.06	-0.05	-0.01	0.97	0.97	
¦ ¦ ¦--cerebal peduncle	0.60	0.02	0.61	0.02	-1.68	-0.60	0.03	0.08	-
¦ ¦ ¦--corticospinal tract-other	0.43	0.07	0.40	0.05	7.39	0.62	0.10	0.19	
¦ ¦ °--internal capsule	0.74	0.03	0.76	0.03	-2.61	-0.76	0.01	0.05	*
¦ °--corpus callosum	3.11	0.08	3.14	0.07	-0.83	-0.36	0.25	0.42	
°--ventricular systems	1.31	0.06	1.25	0.04	4.76	1.66	0.00	0.00	**

Table S3. Age by genotype interaction for absolute brain volumes of juvenile and adult *Ube3a*$^{mat-/pat+}$ rats and wildtype littermates.

	Age * Genotype Interaction
	FDR
Total Brain Volume	0.048160816
¦--Basic cell groups and regions	0.048328625
¦ ¦--Cerebrum	0.060273407
¦ ¦ ¦--Cerebral cortex	0.06162697
¦ ¦ ¦ °--Cortical plate	0.06162697
¦ ¦ ¦ ¦--Olfactory areas	0.162112068
¦ ¦ ¦ ¦ °--Main olfactory bulb	0.818146498
¦ ¦ ¦ ¦--Hippocampal formation	0.050207275
¦ ¦ ¦ ¦ ¦--Retrohippocampal region	0.06162697
¦ ¦ ¦ ¦ ¦ ¦--Subiculum	0.137297219
¦ ¦ ¦ ¦ ¦ ¦ °--Entorhinal area	0.060273407
¦ ¦ ¦ ¦ °--Hippocampal region	0.045652624
¦ ¦ ¦ ¦ ¦--Ammon's horn	0.043450029
¦ ¦ ¦ ¦ °--Dentate gyrus	0.060273407
¦ ¦ ¦ °--Isocortex	0.06162697
¦ ¦ °--Cerebral nuclei	0.045652624
¦ ¦ ¦--Pallidum	0.049445369
¦ ¦ °--Striatum	0.045652624
¦ ¦ ¦--Striatum ventral region	0.060273407
¦ ¦ ¦ °--Nucleus accumbens	0.06162697
¦ ¦ ¦--Lateral septal complex	0.26465486
¦ ¦ °--Striatum dorsal region	0.02888415
¦ ¦ °--Caudoputamen	0.02888415
¦ ¦--Brain stem	0.026628963
¦ ¦ ¦--Midbrain	0.026628963
¦ ¦ ¦--Hindbrain	0.060273407
¦ ¦ °--Interbrain	0.020181397
¦ ¦ ¦--Hypothalamus	0.045652624
¦ ¦ °--Thalamus	0.020181397
¦ °--Cerebellum	0.06162697
¦ ¦--Cerebellar cortex	0.06162697
¦ °--Cerebellar nuclei	0.135651527
¦ ¦--Dentate nucleus	0.105732771
¦ ¦--Interposed nucleus	0.261336982
¦ °--Fastigial nucleus	0.109005783
¦--fiber tracts	0.02888415
¦ ¦--medial forebrain bundle system	0.026628963
¦ ¦ °--cerebrum related	0.026628963
¦ ¦ ¦--anterior commissure, temporal limb	0.048328625
¦ ¦ °--fornix system	0.026628963
¦ ¦ ¦--fimbria	0.026628963
¦ ¦ °--dorsal fornix	0.048328625
¦ ¦--cerebellum related fiber tracts	0.055278686
¦ ¦ ¦--cerebellar peduncles	0.060273407
¦ ¦ °--arbor vitae	0.060273407
¦ °--lateral forebrain bundle system	0.02888415
¦ ¦--corticospinal tract	0.020181397
¦ ¦ ¦--cerebal peduncle	0.020181397
¦ ¦ ¦--corticospinal tract-other	0.071509727
¦ ¦ °--internal capsule	0.020181397
¦ °--corpus callosum	0.050793185
°--ventricular systems	0.137297219

Chapter 6

Insulin-Like Growth Factor-2 Does Not Improve Behavioral Deficits in Mouse and Rat Models of Angelman Syndrome

This chapter has been submitted for publication: Elizabeth L. Berg[*], Stela P. Petkova[*], Heather A. Born, Anna Adhikari, Anne E. Anderson, and Jill L. Silverman (in review). *Molecular Autism.*

Abstract

Angelman Syndrome (AS) is a rare neurodevelopmental disorder for which there is currently no cure or effective therapeutic. Since the genetic cause of AS is known to be dysfunctional expression of the maternal allele of ubiquitin protein ligase E3A (*UBE3A*), several genetic animal models of AS have been developed. Both the *Ube3a* maternal deletion mouse and rat models of AS reliably demonstrate behavioral phenotypes of relevance to AS and therefore offer suitable *in vivo* systems in which to test potential therapeutics. One promising candidate treatment is insulin-like growth factor-2 (IGF-2), which has recently been shown to ameliorate behavioral deficits in the mouse model of AS and improve cognitive abilities across model systems. We used both the *Ube3a* maternal deletion mouse and rat models of AS to evaluate the ability of IGF-2 to improve electrophysiological and behavioral outcomes. Acute systemic administration of IGF-2 had an effect on electrophysiological activity in the brain and on a metric of motor ability, however the effects were not enduring or extensive. Additional metrics of motor behavior, learning, ambulation, and coordination were unaffected and IGF-2 did not improve social communication, seizure threshold, or cognition. The generalizability of these results to humans is difficult to predict and it remains possible that dosing schemes (e.g., chronic or subchronic dosing), routes, and/or post-treatment intervals other than those used herein may show more efficacy. Despite a few observed effects of IGF-2, our results taken together indicate that IGF-2 treatment does not profoundly improve behavioral deficits in the mouse or rat model of AS. These findings shed cautionary light on the potential utility of acute systemic IGF-2 administration in the treatment of AS.

Background

Angelman Syndrome (AS) is a rare neurodevelopmental disorder caused by the loss of functional ubiquitin protein ligase E3A [1]. Specifically, AS results from deficient expression of the maternal allele, which leaves the entire brain deficient of UBE3A due to neuron-specific imprinting that silences the paternal allele [2-6]. AS is characterized by developmental delay, intellectual disability, impaired communication, gross and fine motor deficits, as well as seizures [7-12]. Since these symptoms are severe and persistent, and there is currently no effective therapeutic or cure for the disorder, those with AS require lifelong supportive care. It is therefore imperative that novel strategies to treat AS are developed.

Several *in vivo* models have been generated to aid in the pursuit of effective treatments, including a conventional germline mouse [13] with a deletion of *Ube3a* in exon 2, a conditional mouse with tamoxifen reactivation [14], a larger deletion mouse [15], and rat model with a full *Ube3a* gene deletion [16]. Various models recapitulate phenotypes of AS and therefore provide useful systems in which to test candidate treatments. Lacking a functional level of UBE3A protein in the brain, models show hypo-locomotion, poor balance, impaired coordination, atypical gait, complex cognitive deficits, alongside communication deficits and aberrant social behavior. Since many of these behavioral deficits are not unique to AS, therapies that are effective for other disorders with shared symptomology, such as autism or other syndromic NDDs, may also be effective in treating AS [17-21].

Insulin-like growth factors (IGFs), a family of proteins with similar structure to insulin, have recently emerged as potential treatments for the social deficits, communication impairments, and repetitive behaviors of genetic syndromes associated with autism spectrum disorder (ASD) [18, 22-30]. IGF-1 is being evaluated as a novel treatment for core symptoms of syndromic autisms

in one of the first clinical trials of its kind (NCT01970345) [17-21, 28-33]. IGF-1 is an FDA approved, commercially available compound that crosses the blood-brain barrier and has beneficial effects on synaptic development by promoting neuronal cell survival, synaptic maturation, and synaptic plasticity. Since IGF-1 has shown efficacy in reversing deficits in mouse and neuronal models of three single gene causes of ASD (namely Rett syndrome [22, 23, 26], Phelan McDermid syndrome [27, 34], and Fragile X syndrome [28]), it may therefore be effective in treating autism spectrum disorders more broadly.

IGF-2, which is important for normal growth and development, tissue repair, and regeneration, has also shown promising effects on ASD-relevant behavioral domains in preclinical studies [35-40]. Injections into the hippocampus have demonstrated that IGF-2 is crucial to the consolidation and enhancement of memories and may be effective in ameliorating memory impairments [30, 41-43]. Since the chemical properties of IGF-2 allow it to exert action within the central nervous system after crossing the blood-brain barrier [44, 45], systemic delivery of IGF-2 represents a highly translational route of treatment. A study in mice by Stern et al. (2014) found that following systemic administration of IGF-2 via subcutaneous injection, adult male C57BL/6J mice showed enhanced novel object recognition, social recognition, contextual fear memory, and working memory [42]. Moreover, in the BTBR mouse model of ASD, Steinmetz et al. (2018) found that IGF-2 treatment normalized behavior in the marble burying task, improved social interaction and social memory deficits, and enhanced novel object recognition along with other types of memory [30].

Despite substantial biological and behavioral differences between the inbred strain BTBR, previously used as an idiopathic ASD model, and the *Ube3a* maternal deletion model of AS, the *Ube3a*$^{mat-/pat+}$ mouse model of AS was recently reported by Cruz et al. (2020) to exhibit behavioral

rescue following acute systemic IGF-2 treatment [46]. These encouraging results prompted us to i) investigate if the effects of IGF-2 would be rigorous, reproducible, and inter-laboratory reliable, ii) examine both the mouse and rat model of AS to determine whether IGF-2 could ameliorate or reduce the severity of communication deficits unique to the rat model of AS [16] and evaluate phenotypes observed across species (i.e., motor impairment), and iii) extend the standard, albeit non-translational, rescue of performance in the cerebellar dependent rotarod assay to a rescue of nuanced impairments in gait, which are being utilized as outcome measures in both AS models and AS individuals.

Following a dose range investigation using intra-cranial electroencephalography (EEG) recordings, we employed a battery of behavioral assays to evaluate the effect of systemic IGF-2 on social communication and several motor and learning outcomes in the mouse and rat models of AS. A subcutaneous injection was used to deliver IGF-2 to mice and rats 20 minutes prior to the start of testing. We utilized the standard behavioral protocol of our laboratory and IDDRC behavioral core [16, 47-54] as well as the protocols utilized by Cruz et al. [46] to compare data directly, fairly, and congruently. A comprehensive battery of tests confirmed that IGF-2 did not change basic functions including physical characteristics, general behavioral responses, and sensory reflexes, which indicated safety. Disappointingly, however, our data did not provide strong support for reproducibility or inter-laboratory reliability of IGF-2's improvement on outcomes since we observed a general lack of effect of IGF-2 in several behavioral domains across two AS rodent models.

Methods

Subjects. All animals were housed in a temperature-controlled vivarium and provided food and water *ad libitum*. Animals were maintained on a 12:12 light-dark cycle with the exception of those used for EEG, which were maintained on a 14:10 light-dark cycle. All procedures were approved by the Institutional Animal Care and Use Committee of the University of California, Davis or the Baylor College of Medicine and conducted in accordance with the National Institutes of Health Guide for the Care and Use of Laboratory Animals. Mouse colonies were maintained by breeding *Ube3a* deletion males (B6.129S7-*Ube3a*^{tm1Alb}/J; Jackson Laboratory, Bar Harbor, ME; Stock No. 016590) with congenic C57BL/6J (B6J) female mice, and rat colonies were maintained by breeding *Ube3a* deletion males with wildtype Sprague Dawley females (Envigo, Indianapolis, IN). Subject animals were generated by breeding *Ube3a* deletion females with wildtype males, producing maternally inherited *Ube3a* deletion animals (*Ube3a*$^{mat-/pat+}$; mat-/pat+; Angelman Syndrome model) and wildtype littermate controls (*Ube3a*$^{mat+/pat+}$; mat+/pat+). Additionally, a mixed-sex cohort of congenic B6J mice was generated from B6J breeder pairs and tested following methods previously described by Cruz et al. (2020) [46] and outlined again in **Supplementary File 1**.

Pups were marked for identification and genotyped as previously described [16, 55]. In order to minimize carry-over effects from repeated testing and handling, at least 24 hours were allowed to elapse between the end of one task and the start of another, and assays were performed in order of least to most stressful. All behavioral testing included both sexes, was conducted blinded to genotype and treatment group, and was carried out between 08:00 and 18:00 h (ZT1-ZT11) during the light phase. Between subjects, all surfaces of the testing apparatus were cleaned using 70% ethanol and allowed to dry. For assays involving bedding, the bedding was replaced between subjects. At least 1 hour prior to the start of behavioral testing, mice were habituated in

their home cages to a dimly lit empty holding room adjacent to the testing area. Two cohorts of mice were tested as follows: Cohort 1 was sampled from 22 litters and, beginning at 8 weeks of age (PND 55), was tested in i) open field, ii) beam walking, iii) DigiGait, iv) novel object recognition, and v) pentylenetetrazol-induced seizures; Cohort 2 was sampled from 15 litters and beginning at 8 weeks of age were tested in i) accelerating rotarod and ii) marble burying. Two cohorts of rats were tested as follows: Cohort 1 was sampled from 6 litters and was tested in i) accelerating rotarod at PND 38 ± 4; Cohort 2 was sampled from 7 litters and was tested in i) pup ultrasonic vocalizations at PND 10 and ii) pro-social USV playback at 9 weeks of age. One mixed-sex cohort of 7 rats was used for recording EEG at 1-2 months of age.

Systemic treatment with insulin-like growth factor-2 (IGF-2). IGF-2 (catalog #792-MG, R&D Systems, Inc., Minneapolis, MN) was dissolved in 0.1% bovine serum albumin (BSA) in phosphate-buffered saline (PBS). Prior to testing, a random number generator was used to randomly assign subjects of each genotype to receive either IGF-2 or vehicle (0.1% BSA-PBS). IGF-2 solutions were made fresh prior to every task and, for multi-day tests, injections were carried out only on the first training day. The acute systemic dosing paradigm used herein was based on previous studies showing IGF-2 enhancing cognition [42, 43] and improving behavioral phenotypes of *Ube3a*$^{mat-/pat+}$ mice when administered 20 min prior to testing [46]. Therefore, for all behavioral tests, IGF-2 was delivered 20 min prior to the task. For optimal post-injection data quality while maintaining relevance to the timescale of behavioral tests, IGF-2 was administered 60 min prior to EEG collection. A minimum of two days was allowed to elapse between injections. The 30 μg/kg IGF-2 dose administered to rats was selected based on a dose response analysis of

EEG activity following administration of 10, 30, and 60 μg/kg IGF-2, while mice were administered 30 μg/kg IGF-2 to match the dose previously found effective by Cruz et al. [46].

Electroencephalography (EEG). To acquire EEG recordings, rats were implanted with two subdural electrodes over the somatosensory cortex and one hippocampal depth electrode as previously described [67]. Rats were anesthetized with isoflurane and positioned within a stereotaxic frame. The cortical recording electrodes were placed at -1.0 mm posterior and ± 3.0 mm lateral relative to bregma, while the hippocampal depth electrode was placed -4.0 mm posterior, +2.8 mm lateral, and -2.8 mm ventral. Metabond (Parkell, Edgewood, NY) and dental cement (Co-Oral-Ite Dental Mfg; Diamond Springs, CA) were used to secure all electrodes, except for the ground electrode which was sutured in the cervical paraspinous region. Electrodes were connected to the commutator via 6-channel pedestal and rats were given minimum 1 week recovery prior to data collection. For pain management, rats were provided with slow release buprenorphine and lidocaine/bupivacaine on the day of surgery, as well as Rimadyl tablets on the day prior to, the day of, and the day after surgery. Video synchronized EEG data was acquired using the Nicolet system (Natus, Pleasanton, CA) and Labchart V8 software (AD Instruments, Colorado Springs, CO) and then inspected and analyzed by a trained experimenter blinded to genotype and treatment group. Pre-injection baseline data (60 min in duration) were recorded from rats 24 hrs prior to administration of vehicle and post-injection data (60 min in duration) were collected 60 min following injection. Data were analyzed using repeated measures ANOVA with group as the between-group factor and frequency as the within-group factor or using two-way ANOVA with genotype and IGF-2 treatment as between-group factors.

Behavioral Assays.

Accelerating rotarod. To test motor coordination, balance, and motor learning, subjects were placed on an Ugo-Basile accelerating rotarod (Stoelting Co., Wood Dale, IL) as described previously in mice and rats [16, 47, 56]. Animals were placed on the cylinder while it rotated at 5 revolutions per minute, and then it slowly accelerated to 40 revolutions per min over the course of the 5 min trial. On three consecutive days, subjects were given three trials per day with a 45-60 min inter-trial rest period. The latency for each subject to fall off the cylinder was recorded with the maximum achievable latency being 300 seconds. Data were analyzed using repeated measures ANOVA with group as the between-group factor and day as the within-group factor.

Isolation-induced pup ultrasonic vocalizations (USV). On PND 10, neonatal rats were assessed by collecting 40 kHz vocalizations made when isolated from dam and littermates following a previously described protocol [16, 47, 56, 57]. Rat pups were selected from the nest at random and placed in a small plastic container with clean bedding. The container was placed inside a sound attenuating chamber for three min while calls were recorded with an ultrasonic microphone and Avisoft-RECORDER software (Avisoft Bioacoustics, Glienicke, Germany). Using spectrograms generated with Avisoft-SASLab Pro software, calls were manually counted by a trained investigator blinded to genotype and treatment group. Data were analyzed using two-way ANOVA with genotype and IGF-2 treatment as between-group factors.

Pro-social USV playback. To evaluate social behavior, the behavioral response to hearing playback of natural conspecific 50-kHz USV social contact calls was quantified following an established protocol [16, 47, 58]. Prior to the test, all subjects were handled in a standardized

manner for 5 min on three consecutive days. Subjects were individually placed on an eight-arm radial maze (arms: 40 cm l x 10 cm w) elevated 48 cm above the floor, surrounded by a black curtain, and illuminated to ~8 lux with indirect white light. An active ultrasonic speaker (ScanSpeak, Avisoft Bioacoustics) was placed 20 cm away from the end of one arm while a second inactive speaker was placed symmetrically at the opposite arm to serve as a visual control. After a 15-min habituation period, an Ultra SoundGate 116 Player (Avisoft Bioacoustics) was used to present one of two 1-min acoustic stimuli: (1) pro-social 50-kHz USV or (2) a time- and amplitude-matched white noise control stimulus. Following a 10-min inter-stimulus interval, the second stimulus was presented, and the test session ended after an additional 10-min post-stimulus period. The order of the stimuli was counterbalanced in order to account for possible sequence effects. An overhead camera and EthoVision XT videotracking software (Noldus Information Technology, Wageningen, Netherlands) were used to measure stimulus-induced changes in locomotion and location on the maze. Intact behavioral inhibition was defined as moving significantly less during the minute of white noise compared to the minute prior by paired *t*-test. Intact social approach was defined as spending significantly more time on the arms proximal to the active speaker compared to the distal arms during the minute of pro-social 50-kHz USV playback and subsequent two min by paired *t*-test. As a control metric for motor behavior, distance traveled during this timeframe (i.e., the minute of USV playback and subsequent two min) was also analyzed using two-way ANOVA with genotype and IGF-2 treatment as between-group factors.

Open field locomotion. General exploratory locomotion was assayed as previously described [55, 59, 60]. Subjects were individually placed within a novel open field (40 cm l x 40 cm w x 30.5 cm h), which was dimly illuminated to ~30 lux, and allowing them to explore for 30

min. Photocell beam breaks were detected automatically by the VersaMax Animal Activity Monitoring System (AccuScan Instruments, Columbus, OH) to measure horizontal activity, vertical activity, and center time. Data were analyzed using two-way ANOVA with genotype and IGF-2 treatment as between-group factors.

Beam walking. A beam walking motor task was carried out by individually placing subjects at one end of a 59 cm long beam as described previously [59]. The beam was elevated 68 cm above a cushion and the time taken to cross the beam was measured. A darkened goal box (12 cm d cylinder) was placed on the far end of the beam in order to provide motivation to walk across. On the first day, three training trials on a large diameter (35 mm) beam were conducted to allow animals to become accustomed to the task. Animals that had scores of 60 seconds on all three trials were excluded from analysis. On the following day, subjects were placed back on the large diameter beam and then on a beam of intermediate width (18 mm d) before being placed onto the test beam, which was the narrowest and therefore most challenging (13 mm d). Two trials per beam were carried out with an inter-trial rest interval of at least 30 minutes and trial duration was capped at a maximum of 60 seconds. The two-trial average latency to traverse the test beam was recorded and data were analyzed via two-way ANOVA with genotype and IGF-2 treatment as between-group factors.

Marble burying. To evaluate marble burying, twenty black glass marbles (15 mm d) were arranged in a 4 x 5 grid on top of 4 cm of clean bedding within a standard mouse cage (27 cm l x 16.5 cm w x 12.5 cm h) following a protocol similar to those described previously [49, 61]. Subjects were individually placed in the center of the cage and allowed to explore for 20 min. The

testing room was dimly illuminated to ~15 lux. The number of marbles buried (defined as at least 50% covered by the bedding) at the end of the test session was recorded. Data were analyzed using two-way ANOVA with genotype and IGF-2 treatment as between-group factors.

Pentylenetetrazol-induced seizures. Susceptibility to primary generalized seizures was behaviorally assessed by systemically administering 80 mg/kg pentelenetetrazol (PTZ; a $GABA_A$ receptor antagonist) via intraperitoneal injection and observing the timing and progression of the subsequent convulsions following a protocol described previously [55, 62, 63]. Immediately following injection of PTZ, animals were individually placed in a clean empty standard mouse cage (27 cm l x 16.5 cm w x 12.5 cm h) and watched carefully by a trained observer blinded to genotype and treatment condition. The latency to generalized clonus was recorded and analyzed using two-way ANOVA with genotype and IGF-2 treatment as between-group factors.

Novel object recognition (NOR). Learning and memory were tested by individually presenting subjects with two identical objects and later testing their ability to recognize the familiar object over a novel one using an established protocol previously described [49, 53, 59, 64]. The NOR assay was carried out within an opaque matte white arena (41 cm l x 41 cm w x 30 cm h) in a 30-lux room and consisted of five phases: a 30-min habituation to the arena on the day prior to the test, a 10-min habituation to the arena on the test day, a 10-min object familiarization session, a 60-min isolation period, and a 5-min object recognition test. Following the 10-min habituation on the day of the test, each animal was removed from the arena and placed in an individual clean holding cage while two clean identical objects were placed inside the arena. Each subject was then returned to its arena and allowed to explore and familiarize with the objects for 10 min. Subjects

were then returned to their holding cages and placed in a nearby low light holding area outside of the testing room. The arenas were cleaned, let dry, and one clean familiar object and one clean novel object were placed inside the arena where the two identical objects had previously been located. After a 60 min interval, subjects were returned to their arenas and allowed to explore the objects for 5 min. Time spent investigating each object was measured using EthoVision XT videotracking software (Noldus Information Technology) and validated by manual scoring by a trained observer blinded to genotype and treatment group. Object investigation was defined as time spent sniffing the object when the nose was within 2 cm of the object and oriented toward the object. Animals who did not spend at least 5 sec sniffing the objects during the familiarization phase were removed from analysis and recognition memory was defined as spending significantly more time investigating the novel object compared to the familiar object by paired *t*-test within group. Object preference was calculated as time spent sniffing the novel object compared to total time sniffing both objects. Fifty percent represents equal time investigating the novel and familiar object (a lack of preference) whereas >50% demonstrates intact recognition memory.

DigiGait. Gait metrics were collected using the DigiGait automated treadmill system and analysis software (Mouse Specifics, Inc., Framingham, MA). Subjects were placed individually into the enclosed treadmill chamber and allowed to acclimate before the belt was turned on and the speed was slowly increased from 5 cm/sec to a constant speed of 20 cm/sec. For each subject, 3-6 sec of clearly visible consecutive strides at the belt speed of 20 cm/sec was recorded. Gait analysis was conducted using the DigiGait software package and was carried out by an experimenter blinded to genotype and treatment condition. Right and left fore- and hindlimbs were

averaged together. Data were analyzed per limb set using two-way ANOVA with genotype and IGF-2 treatment as between-group factors.

Statistical Analysis. All statistical analyses were carried out using Prism 9 software (GraphPad Software, San Diego, CA). All significance levels were set at $p < 0.05$ and all *t*-tests were two-tailed. Outliers were identified and excluded using Grubb's test and D'Agostino & Pearson tests were used to check assumptions of normality. Two-way ANOVAs were used to analyze the effects of both genotype and IGF-2 treatment and two-way repeated measures ANOVAs were used for comparisons across time points (e.g., rotarod). Paired *t*-tests were used for comparisons within a single group. Subsequent to ANOVAs, *post hoc* testing controlling for multiple comparisons was carried out using Sidak's or Tukey's multiple comparisons test. In the case of rotarod, Dunnett's multiple comparisons test was used to test for specific differences between days or groups. Since the overall goal of the study was to evaluate the potential for IGF-2 to ameliorate behavioral deficits, emphasis was placed on i) the comparison between wildtype *Ube3a*$^{mat+/pat+}$ vehicle and *Ube3a*$^{mat-/pat+}$ vehicle to confirm the genotype deficit and ii) the comparison between *Ube3a*$^{mat-/pat+}$ vehicle and *Ube3a*$^{mat-/pat+}$ IGF-2 to identify any effect of IGF-2 treatment on the deficit. Data are presented as mean ± standard error of the mean (S.E.M.) unless otherwise noted and detailed statistics are described in **Supplementary File 2**.

Results

IGF-2 reduced cortical and hippocampal delta power in in *Ube3a*$^{mat-/pat+}$ rats. Since *Ube3a*$^{mat-/pat+}$ rats display the elevation in EEG delta power that is characteristic of AS, we sought to examine whether this core phenotype could be normalized by IGF-2. Prior to treatment, we

confirmed via cortical electrodes that *Ube3a*$^{mat-/pat+}$ rats recapitulated the human phenotype of elevated delta power (**Fig. 1A**; *Ube3a*$^{mat-/pat+}$ vehicle vs. *Ube3a*$^{mat+/pat+}$ vehicle, 1 Hz, $p<0.001$; 2 Hz, $p<0.001$) and, while not statistically significant, hippocampal delta power also appeared elevated (**Fig. 1B**). Specifically, we found that cortical power was elevated at 1 and 2 Hz, frequencies within the 0.5-4 Hz delta band, and that power at these frequencies ("delta power") was still elevated compared to wildtype following treatment with vehicle (**Fig. 1C and 1D**; *Ube3a*$^{mat-/pat+}$ vehicle vs. *Ube3a*$^{mat+/pat+}$ vehicle, cortex, $p < 0.0001$; hippocampus, $p = 0.034$). Treatment with 10, 30, or 60 µg/kg IGF-2, however, significantly reduced cortical delta power in *Ube3a*$^{mat-/pat+}$ compared to vehicle (10 µg/kg IGF-2, $p < 0.0001$; 30 µg/kg IGF-2, $p < 0.0001$; 60 µg/kg IGF-2, $p < 0.0001$). Hippocampal delta power was also reduced in *Ube3a*$^{mat-/pat+}$ by treatment with 10 or 30 µg/kg IGF-2, but not 60 µg/kg IGF-2 (IGF-2 vs. vehicle, 10 µg/kg, $p = 0.001$; 30 µg/kg, $p < 0.001$; 60 µg/kg, $p > 0.05$). To more closely examine dose differences on the EEG phenotype of *Ube3a*$^{mat-/pat+}$ rats, we analyzed each dose's effect on summed power at 1 and 2 Hz ("delta power"). We found no effect of IGF-2 on delta power in wildtype but cortical delta power in *Ube3a*$^{mat-/pat+}$ rats was reduced following treatment with 10 or 30 µg/kg IGF-2 (**Fig. 1E**; IGF-2 vs. vehicle, 10 µg/kg, $p = 0.008$; 30 µg/kg, $p = 0.015$) and hippocampal delta power was reduced by treatment with 30 µg/kg IGF-2 (**Fig. 1F**; 30 µg/kg IGF-2 vs. vehicle, $p = 0.043$). The promising effect of 30 µg/kg IGF-2, specifically, to reduce the elevated delta power of *Ube3a*$^{mat-/pat+}$ rats in both the cortex and hippocampus prompted our investigation of this dose in subsequent behavioral testing.

IGF-2 did not improve motor learning or social communication in *Ube3a*$^{mat-/pat+}$ rats.

In order to assess whether IGF-2 could ameliorate the robust motor learning deficit of *Ube3a*$^{mat-}$

/pat+ rats, we tested *Ube3a*$^{mat-/pat+}$ and wildtype littermate controls (*Ube3a*$^{mat+/pat+}$) with IGF-2 or vehicle treatment on an accelerating rotarod (**Fig. 2A**). The rotarod deficit of *Ube3a*$^{mat-/pat+}$ rats was apparent across the three day task, and statistically significant by stringent posthoc by the third day of testing, when the *Ube3a*$^{mat-/pat+}$ vehicle group was only able to stay on the rotarod for two thirds the time of the wildtype vehicle group ($p = 0.046$). *Ube3a*$^{mat-/pat+}$ rats also exhibited a motor learning deficit, which was unaffected by IGF-2 treatment. While the wildtype vehicle and wildtype IGF-2 groups significantly improved their performance from session 1 to 3 (by 142% and 118%, respectively), both the *Ube3a*$^{mat-/pat+}$ vehicle and *Ube3a*$^{mat-/pat+}$ IGF-2 groups failed to improve over the course of the test (*Ube3a*$^{mat+/pat+}$ vehicle, $p < 0.001$; *Ube3a*$^{mat+/pat+}$ IGF-2, $p < 0.001$; *Ube3a*$^{mat-/pat+}$ vehicle, $p > 0.05$; *Ube3a*$^{mat-/pat+}$ IGF-2, $p > 0.05$), contrasting the recent report by Cruz et al. [46].

We also evaluated the effect of IGF-2 on social communication outcomes, both at an early postnatal timepoint and during adulthood. The *Ube3a*$^{mat-/pat+}$ vehicle group emitted 30% fewer isolation-induced pup USV at PND 10 compared to wildtype vehicle (**Fig. 2B**; $p = 0.024$), reproducing our earlier publication [16], but IGF-2 had no effect on the calling rate of *Ube3a*$^{mat-/pat+}$ rats (*Ube3a*$^{mat-/pat+}$ vehicle vs. *Ube3a*$^{mat-/pat+}$ IGF-2, $p > 0.05$). Then in adulthood, we used a USV playback paradigm to present subjects with pro-social 50-kHz USV and a time- and amplitude-matched white noise acoustic control (**Fig. 2C**). All groups, regardless of genotype or treatment, exhibited the expected behavioral inhibition in response to the noise control wherein they moved less during playback of the noise compared to pre-noise baseline exploration, indicating intact hearing abilities (*Ube3a*$^{mat+/pat+}$ vehicle, $p < 0.001$; *Ube3a*$^{mat+/pat+}$ IGF-2, $p < 0.001$; *Ube3a*$^{mat-/pat+}$ vehicle, $p < 0.0001$; *Ube3a*$^{mat-/pat+}$ IGF-2, $p < 0.0001$). This is further supported by the observation of equivalent levels of locomotion in all groups following initiation of 50-kHz

USV playback (data not shown; two-way ANOVA: F_{Genotype}, $p > 0.05$; $F_{\text{Treatment}}$, $p > 0.05$; $F_{\text{G×T}}$, $p > 0.05$). In response to the pro-social 50-kHz USV, only the wildtype vehicle and wildtype IGF-2 groups showed the typical social approach response by spending more time on the arms proximal to the speaker compared to the distal arms (**Fig. 2D**; *Ube3a*$^{\text{mat+/pat+}}$ vehicle, $p = 0.004$; *Ube3a*$^{\text{mat+/pat+}}$ IGF-2, $p = 0.045$). Both the *Ube3a*$^{\text{mat-/pat+}}$ vehicle and *Ube3a*$^{\text{mat-/pat+}}$ IGF-2 groups failed to show a preference for the proximal arms in response to the USV (*Ube3a*$^{\text{mat-/pat+}}$ vehicle, $p > 0.05$; *Ube3a*$^{\text{mat-/pat+}}$ IGF-2, $p > 0.05$), reproducing our earlier publication [16]. Given no differences in the response to a non-social stimulus and the absence of a motor impairment, the reduced social approach response in both groups of *Ube3a*$^{\text{mat-/pat+}}$ rats reveals a social communication deficit that is not ameliorated by treatment with IGF-2.

IGF-2 did not markedly improve motor deficits, seizure threshold, or object recognition in *Ube3a*$^{\text{mat-/pat+}}$ mice. Next, we examined the ability of IGF-2 to improve the known behavioral deficits of *Ube3a*$^{\text{mat-/pat+}}$ mice. While *Ube3a*$^{\text{mat-/pat+}}$ mice showed strong motoric deficits, performance was not affected by treatment with IGF-2. First, exploration of a novel open arena was used to assess overall locomotive activity. Horizontal activity, which was 40% lower in *Ube3a*$^{\text{mat-/pat+}}$ mice than wildtype littermates (**Fig. 3A**; *Ube3a*$^{\text{mat+/pat+}}$ vehicle vs. *Ube3a*$^{\text{mat-/pat+}}$ vehicle, $p < 0.0001$), was not affected by IGF-2 (*Ube3a*$^{\text{mat-/pat+}}$ vehicle vs. *Ube3a*$^{\text{mat-/pat+}}$ IGF-2, $p > 0.05$). A similar pattern was observed for vertical activity wherein *Ube3a*$^{\text{mat-/pat+}}$ mice showed 54% less rearing and vertical movement compared to wildtype (**Fig. 3B**; *Ube3a*$^{\text{mat+/pat+}}$ vehicle vs. *Ube3a*$^{\text{mat-/pat+}}$ vehicle, $p < 0.0001$), but this was unaffected by IGF-2 (*Ube3a*$^{\text{mat-/pat+}}$ vehicle vs. *Ube3a*$^{\text{mat-/pat+}}$ IGF-2, $p > 0.05$). There was no genotype difference or effect of IGF-2 on time spent

in the center of the open field (**Fig. 3C**). These data were similar to the recent Cruz et al. report [46].

We also assessed balance and motor coordination using a beam walking task but found that IGF-2 did not have an enhancing effect in wildtypes nor ameliorated motor coordination deficits observed in the *Ube3a*$^{mat-/pat+}$ group. *Ube3a*$^{mat-/pat+}$ mice took longer to cross compared to wildtype littermates regardless of treatment with IGF-2 (**Fig. 3D**; $F_{Genotype}$, $p = 0.016$; $F_{Treatment}$, $p > 0.05$; $F_{G\times T}$, $p > 0.05$). However, in the accelerating rotarod task of motor coordination, we were able to detect a moderate effect of IGF-2 in *Ube3a*$^{mat-/pat+}$ mice (**Fig. 3E**). While *Ube3a*$^{mat-/pat+}$ mice had consistently poorer performance, falling off earlier compared to wildtypes on all three test days (*Ube3a*$^{mat+/pat+}$ vehicle vs. *Ube3a*$^{mat-/pat+}$ vehicle, day 1, $p < 0.0001$; day 2, $p = 0.001$; day 3, $p = 0.019$), *Ube3a*$^{mat-/pat+}$ mice treated with IGF-2 only showed a deficit on the first day of testing (*Ube3a*$^{mat+/pat+}$ vehicle vs. *Ube3a*$^{mat-/pat+}$ IGF-2, day 1, $p = 0.007$; day 2, $p > 0.05$; day 3, $p > 0.05$). The effect, however, was only moderate in that the *Ube3a*$^{mat-/pat+}$ IGF-2 group was not significantly better than the *Ube3a*$^{mat-/pat+}$ vehicle group on any day (*Ube3a*$^{mat-/pat+}$ vehicle vs. *Ube3a*$^{mat-/pat+}$ IGF-2, day 1, $p > 0.05$; day 2, $p > 0.05$; day 3, $p > 0.05$).

In the marble burying assay, *Ube3a*$^{mat-/pat+}$ mice covered 88% fewer marbles compared to wildtype littermates but there was no effect of IGF-2 treatment in either group (**Fig. 3F**). Marble burying was lower in the *Ube3a*$^{mat-/pat+}$ vehicle group compared to wildtype vehicle ($p = 0.002$) and lower in the *Ube3a*$^{mat-/pat+}$ IGF-2 group relative to wildtype IGF-2 ($p = 0.004$). As described in previous reports, our laboratory interprets the lack of marble burying as a function of the low motor activity of AS mice, as opposed to traditional interpretations of anxiety-like or repetitive behavior, contrasting other AS laboratories [65]. In a fully capable, typically active mouse, marble burying may hold more meaning, however, after more five years of focused study on these mice, we cannot

delineate the motor impairments related to marble burying. We also investigated IGF-2's influence on seizure threshold in *Ube3a*$^{mat-/pat+}$ mice using the chemo-convulsant pentelenetetrazol. While *Ube3a*$^{mat-/pat+}$ mice exhibited a reduced latency to generalized clonus seizure, latency to seize was unaffected by IGF-2 treatment (**Fig. 3G**). The *Ube3a*$^{mat-/pat+}$ vehicle group was 44% quicker to seize than wildtype vehicle ($p = 0.026$), and the *Ube3a*$^{mat-/pat+}$ IGF-2 group was 64% faster to seize compared to wildtype IGF-2 ($p = 0.002$).

To test the cognition enhancing capabilities of IGF-2 treatment, we evaluated novel object recognition with a standard protocol and found that all groups, regardless of genotype or treatment, demonstrated intact novel object recognition (**Fig. 3H**). Within each group, more time was spent more time investigating the novel object compared to the familiar one (*Ube3a*$^{mat+/pat+}$ vehicle, $p. < 0.001$; *Ube3a*$^{mat+/pat+}$ IGF-2, $p = 0.001$; *Ube3a*$^{mat-/pat+}$ vehicle, $p = 0.006$; *Ube3a*$^{mat-/pat+}$ IGF-2, $p = 0.006$). In addition to the dichotomous yes/no analysis of object recognition, we also explored whether IGF-2 influenced the continuous metric of object preference. There were no differences, however, in percent preference for the novel object across genotypes or treatment (**Fig. 3I**). To facilitate more direct comparisons with the results of Cruz et al. (2020), we also attempted to validate their novel object recognition protocol within our own laboratory. We found, however, that the task failed to elicit recognition memory in congenic C57BL/6J mice, the background strain of the *Ube3a*$^{mat-/pat+}$ mouse model, suggesting it would not be fruitful to apply to *Ube3a*$^{mat-/pat+}$ mice (**Fig. S1**). Concomitantly, using the methods of Cruz et al. [46], we observed that IGF-2 treatment did not affect the cognitive performance of C57BL/6J mice in either the novel object recognition or a contextual fear conditioning task.

As an innovative and unique investigation of nuanced motor phenotypes, we probed for any effect of IGF-2 on several metrics of gait using the automated DigiGait system. While walking

on a treadmill, *Ube3a*$^{mat-/pat+}$ mice took wider, longer, and fewer steps compared to wildtype littermates. The elevated forelimb and hindlimb stance widths exhibited by *Ube3a*$^{mat-/pat+}$ mice (**Fig. 4A**; *Ube3a*$^{mat+/pat+}$ vehicle vs. *Ube3a*$^{mat-/pat+}$ vehicle, fore, $p = 0.005$; hind, $p = 0.039$) were not affected by IGF-2 treatment (*Ube3a*$^{mat-/pat+}$ vehicle vs. *Ube3a*$^{mat-/pat+}$ IGF-2, $p > 0.05$) and the longer forelimb and hindlimb stride lengths (*Ube3a*$^{mat+/pat+}$ vehicle vs. *Ube3a*$^{mat-/pat+}$ vehicle*,* fore, $p < 0.001$; hind, $p < 0.0001$) were further increased by IGF-2 (**Fig. 4B**; *Ube3a*$^{mat-/pat+}$ vehicle vs. *Ube3a*$^{mat-/pat+}$ IGF-2, fore, $p = 0.021$; hind, $p = 0.031$). IGF-2 also led to further reduction of forelimb stride frequency and did not have an effect on the reduced hindlimb stride frequency displayed by *Ube3a*$^{mat-/pat+}$ mice (**Fig. 4C**; *Ube3a*$^{mat+/pat+}$ vehicle vs. *Ube3a*$^{mat-/pat+}$ vehicle*,* fore, $p < 0.0001$; hind, $p < 0.0001$; *Ube3a*$^{mat-/pat+}$ vehicle vs. *Ube3a*$^{mat-/pat+}$ IGF-2, fore, $p = 0.021$; hind, $p > 0.05$) and, interestingly, IGF-2 had varying effects on the time taken to propel each step (**Fig. 4D**). The elevated propulsion time required by *Ube3a*$^{mat-/pat+}$ mice (*Ube3a*$^{mat+/pat+}$ vehicle vs. *Ube3a*$^{mat-/pat+}$ vehicle*,* $p = 0.005$), indicative of limb weakness, was unaffected by IGF-2 in the forelimbs and further elevated by IGF-2 in the hindlimbs, whose function is largely force generation and propulsion (*Ube3a*$^{mat-/pat+}$ vehicle vs. *Ube3a*$^{mat-/pat+}$ IGF-2, fore, $p > 0.05$; hind, $p = 0.032$). In alignment with taking longer steps, *Ube3a*$^{mat-/pat+}$ mice held their paws in a swing state off the ground longer than wildtypes, in both forelimbs and hindlimbs (**Fig. 4E**; *Ube3a*$^{mat+/pat+}$ vehicle vs. *Ube3a*$^{mat-/pat+}$ vehicle*,* fore, $p < 0.001$; hind, $p < 0.0001$). Neither metric differed between *Ube3a*$^{mat-/pat+}$ vehicle and *Ube3a*$^{mat-/pat+}$ IGF-2 groups (fore, $p > 0.05$; hind, $p > 0.05$). Finally, despite increased propulsion and swing times, *Ube3a*$^{mat-/pat+}$ mice spent a normal amount of time braking, which was unchanged by IGF-2 treatment (**Fig. 4F**).

Discussion

Novel data uncovered by this work illustrated that acute systemic administration of IGF-2 reduced delta spectral power in EEG, a theorized biomarker in AS. This was a very promising initial finding. However, disappointingly, the overwhelming majority of metrics for motor behavior, learning, and coordination were unaffected and IGF-2 did not improve social communication, seizure threshold, cognition, or gait. Although our study returned mostly negative results with regard to the potential for IGF-2 to improve behavioral deficits in AS, our findings are nevertheless important to disseminate, in particular as they contrast other reports [46]. While overall inter-laboratory replication was a goal of ours, we did establish strong reproducibility within and between our labs (Anderson and Silverman), as shown previously [16, 67].

We observed a moderate effect of IGF-2 on day 1 of rotarod testing in *Ube3a*$^{mat-/pat+}$ mice, but this did not extend across the rotarod time course that addresses motor learning and it was non-existent in *Ube3a*$^{mat-/pat+}$ rats. However, we were able to replicate all of the *Ube3a*$^{mat-/pat+}$ mouse and rat model deficits previously reported by our groups [16, 66-68] and discover significant reduction of the elevated delta power in *Ube3a*$^{mat-/pat+}$ EEG by IGF-2 treatment. This the first report of detection of alterations in EEG power spectral density (PSD) without any behavioral phenotypic change. One potential explanation as to why we observed effects on EEG activity but no changes in behavioral performance is that the increase in delta power may not have substantial behavioral significance. To our knowledge, it has yet to be shown that delta power is strongly tied to behavioral outcomes, despite many laboratories' working hypothesis that PSDs are effective biomarkers [69-74]. However, we find this explanation unlikely in light of recent evidence from our laboratory illustrating reductions delta power with concomitant behavioral improvements [75].

Given that we were unable to reproduce, nor extend, the broad phenotypic rescue shown in earlier work, it is critical to highlight that our study employed standardized experimental

protocols for behavioral testing [51, 76, 77], which differed from those used by Cruz et al. (2020) [46]. We had aimed to leverage these protocol differences to show that the effects of IGF-2 treatment were robust enough to carry across laboratories and therefore bode well for translation to the clinic. Inter-laboratory methodological discrepancies included rotarod intertrial interval duration, open field lighting and duration, marble quantity and burying criterion, as well as object exploration times and post-training delays. When observing latencies, we did not record scores that exceeded the duration of the test (e.g., Figure 4, Cruz et al., 2020). Additionally, while our washout period was shorter compared to previous work, we do not suspect that this hindered our ability to detect effects of IGF-2 since we did not find evidence of IGF-2 having an effect greater than one day in duration. Moreover, if our washout period had been inadequate, the compounding effects of IGF-2 would have been revealed in subsequent testing. However, this was not the case and for each cohort of animals tested, the final assay of the test battery revealed no effect of IGF-2. Arguably, one of the most crucial methodological details that sets our behavioral experiments apart from those conducted previously is our large sample sizes, which were upwards of 25 animals per group. Since pooling data from small subgroups (i.e., n=3-4/group) can artificially inflate error rates and requires that all groups be subjected to the same exact conditions, it is recommended practice in rodent behavioral testing to use group sizes of 10 to 20 animals within a given experiment. Therefore, we only used small groups in the collection of initial pilot data and for collection of the behavioral data described herein, we used large cohorts with enough subjects per group to achieve ample statistical power. Moreover, the novel object recognition findings in the prior report utilized a protocol i) not validated in congenic B6J mice (i.e., there was not recognition as defined by greater time spent with novel vs. familiar object) and ii) not congruent with many of the best recommended practices disseminated by the IDDRC behavioral working group [78].

Our study was thorough and unique, as we used two different model species and large sample sizes, and we investigated the strongest reported phenotypes in each established model. Our dual species approach allowed us to measure social communication in the rat, which exhibits more nuanced social behavior and employs a more sophisticated communication system as compared to the mouse, and we leveraged the mouse model for its strong motor phenotypes. Because our rotarod paradigm consisted of three consecutive days, we were able to assess motor learning and not solely motor function. Having both of these metrics available in both species was key as wildtype mice exhibited a ceiling effect that impeded interpretation of a motor learning deficit, but we were able to evaluate this outcome in rats since their performance changed significantly across test days. By comparing results across species, and across tests within the same behavioral domain, we were able to provide a more thorough and convincing assessment of this IGF-2 treatment paradigm.

While we did see a few promising trends in EEG and rotarod, we also detected effects on gait in the opposite direction than desired (i.e., worsening the phenotype), and the overwhelming majority of our findings indicate that any effect of IGF-2 is minor and does not lead to robust, reliable, or reproducible behavioral changes in either genotype. We did not observe alterations in wildtype mice, which suggests that IGF-2 does not have motor, communication, or cognition enhancing properties in the time windows we assessed. Furthermore, we did not observe alteration in seizure threshold or susceptibility. An obvious difference from previous work was Cruz et al.'s utilization of 129 background mice for their audiogenic seizure procedure. AS model mice on the traditional B6J background do not exhibit susceptibility to audiogenic seizures [66]. We utilized the B6J background with a chemo-convulsant instead, as 129s have a 70% reduced corpus

callosum which adds to their seizure susceptibility [79, 80], and sensory-dependent audiogenic seizures are triggered by divergent neural circuitry compared to chemo-induction [81].

Therapeutic mimetics of the IGF pathway are being evaluated as small molecule therapy for AS. They activate PI3K-Akt-mTOR and Ras-MAPK-ERK pathways and have been shown to increase synapse number and synaptic plasticity [82, 83]. Spine numbers have been shown to be reduced in AS mouse models [84] and activity dependent ERK phosphorylation and synaptic plasticity are impaired [85-88]. The therapeutic hypothesis is that through upregulating synaptic plasticity and synapse number, these compounds may have benefit in AS. We wanted to disseminate our mostly negative data as some caution should be taken in interpreting IGF-2 data, as this ligand shows some non-specificity in binding both the IGF-1 and IGF-2 receptors. Clinically, IGF-2 mimetics have shown some level of benefit in phase 2 studies in Rett syndrome [89] and Fragile X syndrome [90].

Limitations

The major limitation of the present study is that the results are confined to the three doses (10, 30, and 60 μg/kg) and one route of administration (acute subcutaneous injection) used. Particularly, our behavioral results are limited to a 30 μg/kg injection of IGF-2 delivered 20 min prior to behavioral testing. It remains possible that different doses, injection timing and/or frequency, post-administration interval, and/or routes of administration may show greater efficacy in improving the endpoints measured herein. For instance, our negative results using an acute systemic treatment of IGF-2 do not preclude the possibility that chronic delivery of IGF-2 could ameliorate behavioral deficits over longer periods of time.

Conclusions

IGF-2 did not show robust effects on key behavioral domains of relevance to AS in two genetic rodent models of AS, in contrast to a recently published report. Our findings are cautionary and emphasize that it is important for independent labs to try to replicate each other's experiments – after all, we are in pursuit of therapeutics with broad and reliable efficacy that stand up to the test of minor cross-lab methodological variations. Minimally two cohorts with standardized methods from the literature should be evaluated. Future studies that examine EEG activity during behavioral tasks may be the most informative to confirm that subtle alterations in spectral power have functional meaning before its confirmation as a robust biomarker.

References

1. Albrecht U, Sutcliffe JS, Cattanach BM, Beechey CV, Armstrong D, Eichele G, Beaudet AL: Imprinted expression of the murine Angelman syndrome gene, Ube3a, in hippocampal and Purkinje neurons. *Nat Genet* 1997, 17:75-78.
2. Chamberlain SJ, Chen PF, Ng KY, Bourgois-Rocha F, Lemtiri-Chlieh F, Levine ES, Lalande M: Induced pluripotent stem cell models of the genomic imprinting disorders Angelman and Prader-Willi syndromes. *Proc Natl Acad Sci U S A* 2010, 107:17668-17673.
3. Chamberlain SJ, Lalande M: Neurodevelopmental disorders involving genomic imprinting at human chromosome 15q11-q13. *Neurobiol Dis* 2010, 39:13-20.
4. Chamberlain SJ, Lalande M: Angelman syndrome, a genomic imprinting disorder of the brain. *J Neurosci* 2010, 30:9958-9963.
5. Kishino T, Lalande M, Wagstaff J: UBE3A/E6-AP mutations cause Angelman syndrome. *Nat Genet* 1997, 15:70-73.
6. Matsuura T, Sutcliffe JS, Fang P, Galjaard RJ, Jiang YH, Benton CS, Rommens JM, Beaudet AL: De novo truncating mutations in E6-AP ubiquitin-protein ligase gene (UBE3A) in Angelman syndrome. *Nat Genet* 1997, 15:74-77.
7. Williams CA: Neurological aspects of the Angelman syndrome. *Brain Dev* 2005, 27:88-94.
8. Williams CA: The behavioral phenotype of the Angelman syndrome. *Am J Med Genet C Semin Med Genet* 2010, 154C:432-437.
9. Williams CA, Angelman H, Clayton-Smith J, Driscoll DJ, Hendrickson JE, Knoll JH, Magenis RE, Schinzel A, Wagstaff J, Whidden EM, et al.: Angelman syndrome: consensus for diagnostic criteria. Angelman Syndrome Foundation. *Am J Med Genet* 1995, 56:237-238.
10. Williams CA, Zori RT, Hendrickson J, Stalker H, Marum T, Whidden E, Driscoll DJ: Angelman syndrome. *Curr Probl Pediatr* 1995, 25:216-231.
11. Buiting K, Clayton-Smith J, Driscoll DJ, Gillessen-Kaesbach G, Kanber D, Schwinger E, Williams C, Horsthemke B: Clinical utility gene card for: Angelman Syndrome. *Eur J Hum Genet* 2015, 23.
12. Buiting K, Williams C, Horsthemke B: Angelman syndrome - insights into a rare neurogenetic disorder. *Nat Rev Neurol* 2016, 12:584-593.
13. Jiang YH, Armstrong D, Albrecht U, Atkins CM, Noebels JL, Eichele G, Sweatt JD, Beaudet AL: Mutation of the Angelman ubiquitin ligase in mice causes increased cytoplasmic p53 and deficits of contextual learning and long-term potentiation. *Neuron* 1998, 21:799-811.
14. Silva-Santos S, van Woerden GM, Bruinsma CF, Mientjes E, Jolfaei MA, Distel B, Kushner SA, Elgersma Y: Ube3a reinstatement identifies distinct developmental windows in a murine Angelman syndrome model. *J Clin Invest* 2015, 125:2069-2076.
15. Jiang YH, Pan Y, Zhu L, Landa L, Yoo J, Spencer C, Lorenzo I, Brilliant M, Noebels J, Beaudet AL: Altered ultrasonic vocalization and impaired learning and memory in Angelman syndrome mouse model with a large maternal deletion from Ube3a to Gabrb3. *PLoS One* 2010, 5:e12278.
16. Berg EL, Pride MC, Petkova SP, Lee RD, Copping NA, Shen Y, Adhikari A, Fenton TA, Pedersen LR, Noakes LS, et al: Translational outcomes in a full gene deletion of ubiquitin protein ligase E3A rat model of Angelman syndrome. *Transl Psychiatry* 2020, 10:39.

17. Bou Khalil R: Is insulin growth factor-1 the future for treating autism spectrum disorder and/or schizophrenia? *Med Hypotheses* 2017, 99:23-25.
18. Bozdagi O, Tavassoli T, Buxbaum JD: Insulin-like growth factor-1 rescues synaptic and motor deficits in a mouse model of autism and developmental delay. *Mol Autism* 2013, 4:9.
19. Cioana M, Michalski B, Fahnestock M: Insulin-Like Growth Factor and Insulin-Like Growth Factor Receptor Expression in Human Idiopathic Autism Fusiform Gyrus Tissue. *Autism Res* 2020, 13:897-907.
20. Steinman G: IGF - Autism prevention/amelioration. *Med Hypotheses* 2019, 122:45-47.
21. Vanhala R, Turpeinen U, Riikonen R: Low levels of insulin-like growth factor-I in cerebrospinal fluid in children with autism. *Dev Med Child Neurol* 2001, 43:614-616.
22. Bray N: Neurodevelopmental disorders: righting Rett syndrome with IGF1. *Nat Rev Drug Discov* 2014, 13:653.
23. Castro J, Garcia RI, Kwok S, Banerjee A, Petravicz J, Woodson J, Mellios N, Tropea D, Sur M: Functional recovery with recombinant human IGF1 treatment in a mouse model of Rett Syndrome. *Proc Natl Acad Sci U S A* 2014, 111:9941-9946.
24. Pini G, Scusa MF, Benincasa A, Bottiglioni I, Congiu L, Vadhatpour C, Romanelli AM, Gemo I, Puccetti C, McNamara R, et al: Repeated insulin-like growth factor 1 treatment in a patient with rett syndrome: a single case study. *Front Pediatr* 2014, 2:52.
25. Pini G, Scusa MF, Congiu L, Benincasa A, Morescalchi P, Bottiglioni I, Di Marco P, Borelli P, Bonuccelli U, Della-Chiesa A, et al: IGF1 as a Potential Treatment for Rett Syndrome: Safety Assessment in Six Rett Patients. *Autism Res Treat* 2012, 2012:679801.
26. Yuan ZF, Mao SS, Shen J, Jiang LH, Xu L, Xu JL, Gao F: Insulin-Like Growth Factor-1 Down-Regulates the Phosphorylation of FXYD1 and Rescues Behavioral Deficits in a Mouse Model of Rett Syndrome. *Front Neurosci* 2020, 14:20.
27. Kolevzon A, Bush L, Wang AT, Halpern D, Frank Y, Grodberg D, Rapaport R, Tavassoli T, Chaplin W, Soorya L, Buxbaum JD: A pilot controlled trial of insulin-like growth factor-1 in children with Phelan-McDermid syndrome. *Mol Autism* 2014, 5:54.
28. Wise TL: Changes in insulin-like growth factor signaling alter phenotypes in Fragile X Mice. *Genes Brain Behav* 2017, 16:241-249.
29. Steinman G, Mankuta D: Insulin-like growth factor and the etiology of autism. *Med Hypotheses* 2013, 80:475-480.
30. Steinmetz AB, Stern SA, Kohtz AS, Descalzi G, Alberini CM: Insulin-Like Growth Factor II Targets the mTOR Pathway to Reverse Autism-Like Phenotypes in Mice. *J Neurosci* 2018, 38:1015-1029.
31. Bou Khalil R: Insulin-growth-factor-1 (IGF-1): just a few steps behind the evidence in treating schizophrenia and/or autism. *CNS Spectr* 2019, 24:277-278.
32. Costales J, Kolevzon A: The therapeutic potential of insulin-like growth factor-1 in central nervous system disorders. *Neurosci Biobehav Rev* 2016, 63:207-222.
33. Linker SB, Mendes APD, Marchetto MC: IGF-1 treatment causes unique transcriptional response in neurons from individuals with idiopathic autism. *Mol Autism* 2020, 11:55.
34. Kolevzon A, Bush L, Wang AT, Halpern D, Frank Y, Grodberg D, Rapaport R, Tavassoli T, Chaplin W, Soorya L, Buxbaum JD: Erratum: A pilot controlled trial of insulin-like growth factor-1 in children with Phelan-McDermid syndrome. *Mol Autism* 2015, 6:31.
35. Jones JI, Clemmons DR: Insulin-like growth factors and their binding proteins: biological actions. *Endocr Rev* 1995, 16:3-34.

36. Roth RA: Structure of the receptor for insulin-like growth factor II: the puzzle amplified. *Science* 1988, 239:1269-1271.
37. Roth RA, Steele-Perkins G, Hari J, Stover C, Pierce S, Turner J, Edman JC, Rutter WJ: Insulin and insulin-like growth factor receptors and responses. *Cold Spring Harb Symp Quant Biol* 1988, 53 Pt 1:537-543.
38. Russo VC, Gluckman PD, Feldman EL, Werther GA: The insulin-like growth factor system and its pleiotropic functions in brain. *Endocr Rev* 2005, 26:916-943.
39. Russo VC, Schutt BS, Andaloro E, Ymer SI, Hoeflich A, Ranke MB, Bach LA, Werther GA: Insulin-like growth factor binding protein-2 binding to extracellular matrix plays a critical role in neuroblastoma cell proliferation, migration, and invasion. *Endocrinology* 2005, 146:4445-4455.
40. Werther GA, Russo V, Baker N, Butler G: The role of the insulin-like growth factor system in the developing brain. *Horm Res* 1998, 49 Suppl 1:37-40.
41. Chen ST, Jeng YM, Chang CC, Chang HH, Huang MC, Juan HF, Hsu CH, Lee H, Liao YF, Lee YL, et al: Insulin-like growth factor II mRNA-binding protein 3 expression predicts unfavorable prognosis in patients with neuroblastoma. *Cancer Sci* 2011, 102:2191-2198.
42. Stern SA, Kohtz AS, Pollonini G, Alberini CM: Enhancement of memories by systemic administration of insulin-like growth factor II. *Neuropsychopharmacology* 2014, 39:2179-2190.
43. Stern SA, Chen DY, Alberini CM: The effect of insulin and insulin-like growth factors on hippocampus- and amygdala-dependent long-term memory formation. *Learn Mem* 2014, 21:556-563.
44. Duffy KR, Pardridge WM, Rosenfeld RG: Human blood-brain barrier insulin-like growth factor receptor. *Metabolism* 1988, 37:136-140.
45. Reinhardt RR, Bondy CA: Insulin-like growth factors cross the blood-brain barrier. *Endocrinology* 1994, 135:1753-1761.
46. Cruz E, Descalzi G, Steinmetz A, Scharfman HE, Katzman A, Alberini CM: CIM6P/IGF-2 Receptor Ligands Reverse Deficits in Angelman Syndrome Model Mice. *Autism Res* 2020.
47. Berg EL, Copping NA, Rivera JK, Pride MC, Careaga M, Bauman MD, Berman RF, Lein PJ, Harony-Nicolas H, Buxbaum JD, et al: Developmental social communication deficits in the Shank3 rat model of phelan-mcdermid syndrome and autism spectrum disorder. *Autism Res* 2018.
48. Dhamne SC, Silverman JL, Super CE, Lammers SHT, Hameed MQ, Modi ME, Copping NA, Pride MC, Smith DG, Rotenberg A, et al: Replicable in vivo physiological and behavioral phenotypes of the Shank3B null mutant mouse model of autism. *Mol Autism* 2017, 8:26.
49. Gompers AL, Su-Feher L, Ellegood J, Copping NA, Riyadh MA, Stradleigh TW, Pride MC, Schaffler MD, Wade AA, Catta-Preta R, et al: Germline Chd8 haploinsufficiency alters brain development in mouse. *Nat Neurosci* 2017, 20:1062-1073.
50. Silverman JL, Yang M, Lord C, Crawley JN: Behavioural phenotyping assays for mouse models of autism. *Nat Rev Neurosci* 2010, 11:490-502.
51. Sukoff Rizzo SJ, Silverman JL: Methodological Considerations for Optimizing and Validating Behavioral Assays. *Curr Protoc Mouse Biol* 2016, 6:364-379.

52. Wohr M, Silverman JL, Scattoni ML, Turner SM, Harris MJ, Saxena R, Crawley JN: Developmental delays and reduced pup ultrasonic vocalizations but normal sociability in mice lacking the postsynaptic cell adhesion protein neuroligin2. *Behav Brain Res* 2013, 251:50-64.
53. Yang M, Bozdagi O, Scattoni ML, Wohr M, Roullet FI, Katz AM, Abrams DN, Kalikhman D, Simon H, Woldeyohannes L, et al: Reduced excitatory neurotransmission and mild autism-relevant phenotypes in adolescent Shank3 null mutant mice. *J Neurosci* 2012, 32:6525-6541.
54. Gulinello M, Mitchell HA, Chang Q, Timothy O'Brien W, Zhou Z, Abel T, Wang L, Corbin JG, Veeraragavan S, Samaco RC, et al: Rigor and reproducibility in rodent behavioral research. *Neurobiol Learn Mem* 2018.
55. Copping NA, Adhikari A, Petkova SP, Silverman JL: Genetic backgrounds have unique seizure response profiles and behavioral outcomes following convulsant administration. *Epilepsy Behav* 2019, 101:106547.
56. Berg EL, Pedersen LR, Pride MC, Petkova SP, Patten KT, Valenzuela AE, Wallis C, Bein KJ, Wexler A, Lein PJ, Silverman JL: Developmental exposure to near roadway pollution produces behavioral phenotypes relevant to neurodevelopmental disorders in juvenile rats. *Transl Psychiatry* 2020, 10:289.
57. Berg EL, Ching TM, Bruun DA, Rivera JK, Careaga M, Ellegood J, Lerch JP, Wohr M, Lein PJ, Silverman JL: Translational outcomes relevant to neurodevelopmental disorders following early life exposure of rats to chlorpyrifos. *J Neurodev Disord* 2020, 12:40.
58. Wohr M, Engelhardt KA, Seffer D, Sungur AO, Schwarting RK: Acoustic Communication in Rats: Effects of Social Experiences on Ultrasonic Vocalizations as Socio-affective Signals. *Curr Top Behav Neurosci* 2017, 30:67-89.
59. Adhikari A, Copping NA, Onaga B, Pride MC, Coulson RL, Yang M, Yasui DH, LaSalle JM, Silverman JL: Cognitive Deficits in the Snord116 Deletion Mouse Model for Prader-Willi Syndrome. *Neurobiol Learn Mem* 2018.
60. Copping NA, Berg EL, Foley GM, Schaffler MD, Onaga BL, Buscher N, Silverman JL, Yang M: Touchscreen learning deficits and normal social approach behavior in the Shank3B model of Phelan-McDermid Syndrome and autism. *Neuroscience* 2016.
61. Silverman JL, Pride MC, Hayes JE, Puhger KR, Butler-Struben HM, Baker S, Crawley JN: GABAB Receptor Agonist R-Baclofen Reverses Social Deficits and Reduces Repetitive Behavior in Two Mouse Models of Autism. *Neuropsychopharmacology* 2015, 40:2228-2239.
62. Ellegood J, Petkova SP, Kinman A, Qiu LR, Adhikari A, Wade AA, Fernandes D, Lindenmaier Z, Creighton A, Nutter LMJ, et al: Neuroanatomy and behavior in mice with a haploinsufficiency of AT-rich interactive domain 1B (ARID1B) throughout development. *Mol Autism* 2021, 12:25.
63. Copping NA, Christian SGB, Ritter DJ, Islam MS, Buscher N, Zolkowska D, Pride MC, Berg EL, LaSalle JM, Ellegood J, et al: Neuronal overexpression of Ube3a isoform 2 causes behavioral impairments and neuroanatomical pathology relevant to 15q11.2-q13.3 duplication syndrome. *Hum Mol Genet* 2017, 26:3995-4010.
64. Bevins RA, Besheer J: Object recognition in rats and mice: a one-trial non-matching-to-sample learning task to study 'recognition memory'. *Nat Protoc* 2006, 1:1306-1311.

65. Sonzogni M, Wallaard I, Santos SS, Kingma J, du Mee D, van Woerden GM, Elgersma Y: A behavioral test battery for mouse models of Angelman syndrome: a powerful tool for testing drugs and novel Ube3a mutants. *Mol Autism* 2018, 9:47.
66. Born HA, Dao AT, Levine AT, Lee WL, Mehta NM, Mehra S, Weeber EJ, Anderson AE: Strain-dependence of the Angelman Syndrome phenotypes in Ube3a maternal deficiency mice. *Sci Rep* 2017, 7:8451.
67. Born HA, Martinez LA, Levine AT, Harris SE, Mehra S, Lee WL, Dindot SV, Nash KR, Silverman JL, Segal DJ, et al: Early Developmental EEG and Seizure Phenotypes in a Full Gene Deletion of Ubiquitin Protein Ligase E3A Rat Model of Angelman Syndrome. *eNeuro* 2021, 8.
68. SP P, JD D, JL S: Gait as Translational Outcome for Angelman Syndrome *Autism Research* 2021.
69. Frohlich J, Miller MT, Bird LM, Garces P, Purtell H, Hoener MC, Philpot BD, Sidorov MS, Tan WH, Hernandez MC, et al: Electrophysiological Phenotype in Angelman Syndrome Differs Between Genotypes. *Biol Psychiatry* 2019, 85:752-759.
70. Frohlich J, Senturk D, Saravanapandian V, Golshani P, Reiter LT, Sankar R, Thibert RL, DiStefano C, Huberty S, Cook EH, Jeste SS: A Quantitative Electrophysiological Biomarker of Duplication 15q11.2-q13.1 Syndrome. *PLoS One* 2016, 11:e0167179.
71. den Bakker H, Sidorov MS, Fan Z, Lee DJ, Bird LM, Chu CJ, Philpot BD: Abnormal coherence and sleep composition in children with Angelman syndrome: a retrospective EEG study. *Mol Autism* 2018, 9:32.
72. Judson MC, Wallace ML, Sidorov MS, Burette AC, Gu B, van Woerden GM, King IF, Han JE, Zylka MJ, Elgersma Y, et al: GABAergic Neuron-Specific Loss of Ube3a Causes Angelman Syndrome-Like EEG Abnormalities and Enhances Seizure Susceptibility. *Neuron* 2016, 90:56-69.
73. Sidorov MS, Deck GM, Dolatshahi M, Thibert RL, Bird LM, Chu CJ, Philpot BD: Erratum to: Delta rhythmicity is a reliable EEG biomarker in Angelman syndrome: a parallel mouse and human analysis. *J Neurodev Disord* 2017, 9:30.
74. Sidorov MS, Deck GM, Dolatshahi M, Thibert RL, Bird LM, Chu CJ, Philpot BD: Delta rhythmicity is a reliable EEG biomarker in Angelman syndrome: a parallel mouse and human analysis. *J Neurodev Disord* 2017, 9:17.
75. Adhikari A, Copping NA, Fink KD, Silverman JL, Anderson JD: Functional rescue in an Angelman syndrome model following treatment with lentivector transduced hematopoietic stem cells. *Human Molecular Genetics* 2021, ddab104.
76. Silverman JL, Nithianantharajah J, Der-Avakian A, Young JW, Sukoff Rizzo SJ: Lost in translation: At the crossroads of face validity and translational utility of behavioral assays in animal models for the development of therapeutics. *Neurosci Biobehav Rev* 2020, 116:452-453.
77. Sukoff Rizzo SJ, Anderson LC, Green TL, McGarr T, Wells G, Winter SS: Assessing Healthspan and Lifespan Measures in Aging Mice: Optimization of Testing Protocols, Replicability, and Rater Reliability. *Curr Protoc Mouse Biol* 2018, 8:e45.
78. Gulinello M, Mitchell HA, Chang Q, Timothy O'Brien W, Zhou Z, Abel T, Wang L, Corbin JG, Veeraragavan S, Samaco RC, et al: Rigor and reproducibility in rodent behavioral research. *Neurobiol Learn Mem* 2019, 165:106780.

79. Balogh SA, McDowell CS, Stavnezer AJ, Denenberg VH: A behavioral and neuroanatomical assessment of an inbred substrain of 129 mice with behavioral comparisons to C57BL/6J mice. *Brain Research* 1999, 836:38-48.
80. Wahlsten D, Metten P, Crabbe JC: Survey of 21 inbred mouse strains in two laboratories reveals that BTBR T/+ tf/tf has severely reduced hippocampal commissure and absent corpus callosum. *Brain Research* 2003, 971:47-54.
81. Kandratavicius L, Balista PA, Lopes-Aguiar C, Ruggiero RN, Umeoka EH, Garcia-Cairasco N, Bueno-Junior LS, Leite JP: Animal models of epilepsy: use and limitations. *Neuropsychiatric Disease and Treatment* 2014, 10:1693-1705.
82. Guan J, Harris P, Brimble M, Lei Y, Lu J, Yang Y, Gunn AJ: The role for IGF-1-derived small neuropeptides as a therapeutic target for neurological disorders. *Expert Opin Ther Targets* 2015, 19:785-793.
83. Dyer AH, Vahdatpour C, Sanfeliu A, Tropea D: The role of Insulin-Like Growth Factor 1 (IGF-1) in brain development, maturation and neuroplasticity. *Neuroscience* 2016, 325:89-99.
84. Dindot SV, Antalffy BA, Bhattacharjee MB, Beaudet AL: The Angelman syndrome ubiquitin ligase localizes to the synapse and nucleus, and maternal deficiency results in abnormal dendritic spine morphology. *Hum Mol Genet* 2008, 17:111-118.
85. Filonova I, Trotter JH, Banko JL, Weeber EJ: Activity-dependent changes in MAPK activation in the Angelman Syndrome mouse model. *Learn Mem* 2014, 21:98-104.
86. Greer PL, Hanayama R, Bloodgood BL, Mardinly AR, Lipton DM, Flavell SW, Kim TK, Griffith EC, Waldon Z, Maehr R, et al: The Angelman Syndrome protein Ube3A regulates synapse development by ubiquitinating arc. *Cell* 2010, 140:704-716.
87. Sato M, Stryker MP: Genomic imprinting of experience-dependent cortical plasticity by the ubiquitin ligase gene Ube3a. *Proc Natl Acad Sci U S A* 2010, 107:5611-5616.
88. Yashiro K, Riday TT, Condon KH, Roberts AC, Bernardo DR, Prakash R, Weinberg RJ, Ehlers MD, Philpot BD: Ube3a is required for experience-dependent maturation of the neocortex. *Nat Neurosci* 2009, 12:777-783.
89. Glaze DG, Neul JL, Kaufmann WE, Berry-Kravis E, Condon S, Stoms G, Oosterholt S, Della Pasqua O, Glass L, Jones NE, et al: Double-blind, randomized, placebo-controlled study of trofinetide in pediatric Rett syndrome. *Neurology* 2019, 92:e1912-e1925.
90. Berry-Kravis E, Horrigan JP, Tartaglia N, Hagerman R, Kolevzon A, Erickson CA, Hatti S, Snape M, Yaroshinsky A, Stoms G, et al: A Double-Blind, Randomized, Placebo-Controlled Clinical Study of Trofinetide in the Treatment of Fragile X Syndrome. *Pediatr Neurol* 2020, 110:30-41.

Figures

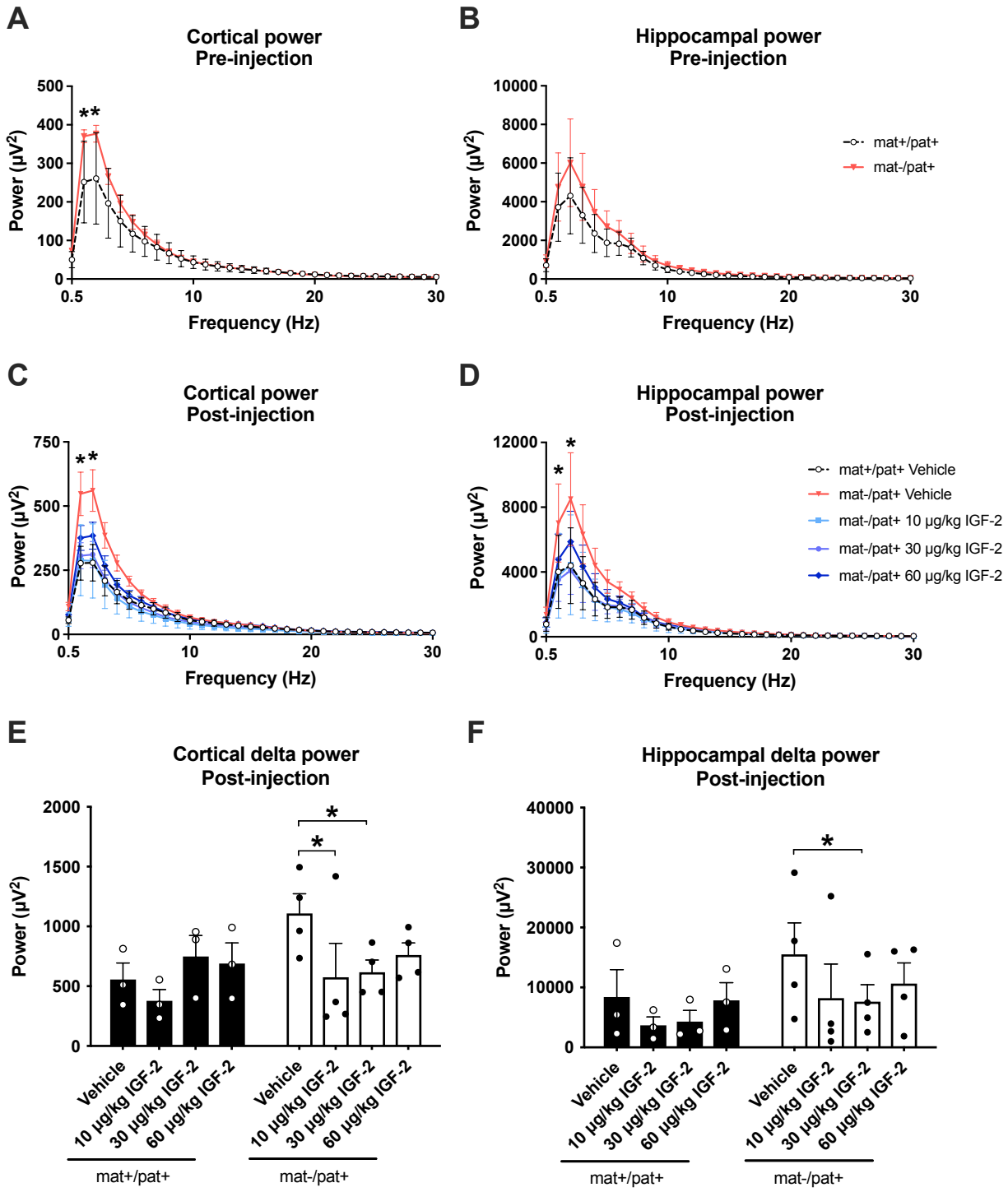

Fig. 1 IGF-2 reduced cortical and hippocampal delta power in *Ube3a*$^{mat-/pat+}$ rats. (A) Baseline cortical power pre-injection was elevated in *Ube3a*$^{mat-/pat+}$ (mat-/pat+) rats at 1 and 2 Hz compared to wildtype (*Ube3a*$^{mat+/pat+}$; mat+/pat+) rats. **(B)** Pre-injection hippocampal power trended higher in mat-/pat+ rats. **(C)** Following injection of vehicle, cortical power was higher in mat-/pat+ than

wildtype rats at 1 and 2 Hz. Compared to vehicle, treatment with 10, 30, or 60 μg/kg IGF-2 led to reduced 1 and 2 Hz power in mat-/pat+ rats. **(D)** Post-injection hippocampal power was higher in mat-/pat+ rats at 1 and 2 Hz, which was reduced by treatment with 10 and 30 μg/kg IGF-2. **(E)** Cortical power at 1 and 2 Hz ("delta power") was lower in mat-/pat+ rats following treatment with 10 or 30 μg/kg IGF-2 compared to vehicle while **(F)** hippocampal delta power (at 1 and 2 Hz) was reduced by 30 μg/kg IGF-2. Delta power in wildtype rats was not affected by IGF-2. Data are expressed as mean ± S.E.M. n = 3-4 rats/genotype. A-D: *$p < 0.05$, mat-/pat+ vs. mat+/pat+, Sidak's multiple comparisons following repeated measures ANOVA. E, F: *$p < 0.05$, Tukey's multiple comparisons following repeated measures ANOVA.

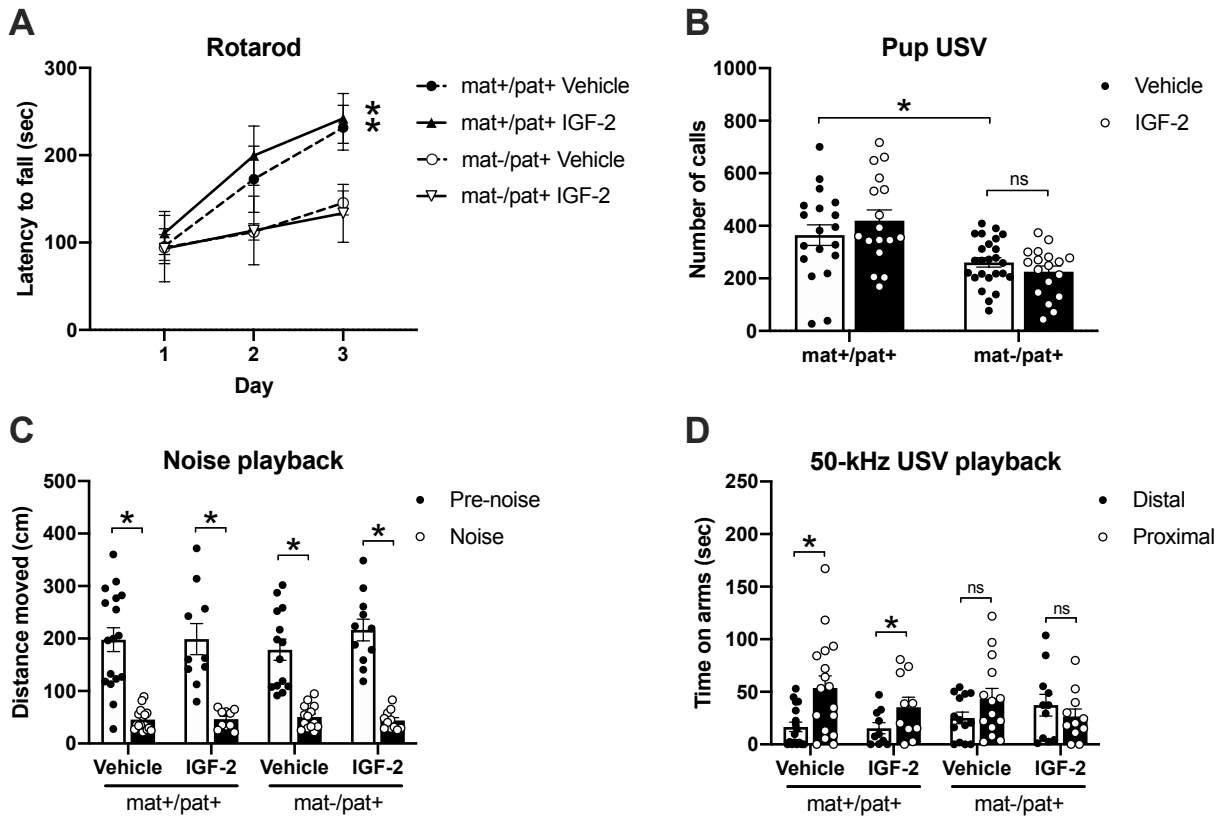

Fig. 2 IGF-2 did not rescue or improve motor learning or social communication in *Ube3a*$^{mat-/pat+}$ rats. (A) Latency to fall off an accelerating rotarod significantly improved from session 1 to 3 for both wildtype groups (*Ube3a*$^{mat+/pat+}$; mat+/pat+), but not for either *Ube3a*$^{mat-/pat+}$ group (mat-/pat+). **(B)** At PND 10, mat-/pat+ pups emitted fewer isolation-induced ultrasonic vocalizations (USV) than wildtype littermates, but IGF-2 had no effect on vocalization rates in mat-/pat+ rats. **(C)** All groups showed behavioral inhibition (i.e., reduced locomotion) during playback of white noise compared to baseline. **(D)** During playback of pro-social 50-kHz USV, only the wildtype groups, and not mat-/pat+ rats, spent significantly more time on the arms proximal to the speaker compared to the distal arms (i.e., social approach). Data are expressed as mean ± S.E.M. n = 6-25 rats/group. A: *$p < 0.05$, Day 1 vs. 3, Dunnett's multiple comparisons following repeated measures ANOVA. B: *$p < 0.05$, Sidak's multiple comparisons test following two-way ANOVA. C, D: *$p < 0.05$, paired t-test. ns, not significantly different, $p > 0.05$.

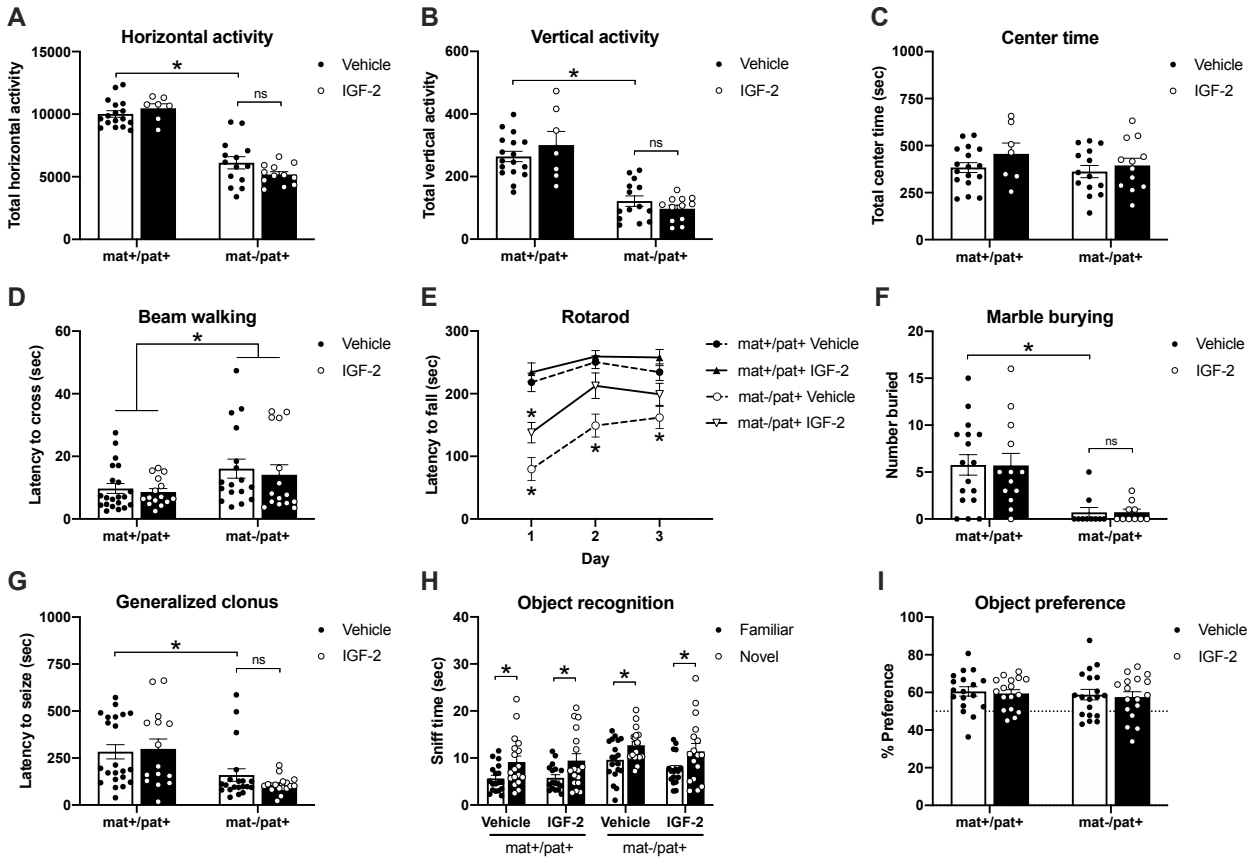

Fig. 3 IGF-2 did not markedly improve motor deficits, seizure threshold, or object recognition in *Ube3a*$^{mat-/pat+}$ mice. (A) Horizontal and **(B)** vertical activity in an open field assay were reduced in *Ube3a*$^{mat-/pat+}$ mice (mat-/pat+) compared to wildtype littermates (*Ube3a*$^{mat+/pat+}$; mat+/pat+), but unaffected by IGF-2. **(C)** Center time did not differ among groups. **(D)** Latency to cross a thin beam was elevated in mat-/pat+ mice, but unchanged by IGF-2. **(E)** Accelerating rotarod performance was moderately improved by IGF-2 treatment in mat-/pat+ mice, only on first day of testing. **(F)** Regardless of IGF-2 treatment, mat-/pat+ mice demonstrated a marble burying deficit and **(G)** mat-/pat+ mice were quicker to exhibit generalized clonus following pentylenetetrazol administration, which was unaffected by IGF-2. **(H)** All groups demonstrated intact novel object recognition as measured by more time spent investigating the novel object compared to the familiar object and by **(I)** novel object percent preference. Data are expressed as mean ± S.E.M. n = 10-22 mice/group. A-C, F, G, I: *$p < 0.05$, Sidak's multiple comparisons following two-way ANOVA. D: *$p < 0.05$, main effect of genotype, two-way ANOVA. E: *$p < 0.05$ vs. mat+/pat+ vehicle, Dunnett's multiple comparisons test following repeated measures ANOVA. H: *$p < 0.05$, paired t-test. ns, not significantly different, $p > 0.05$.

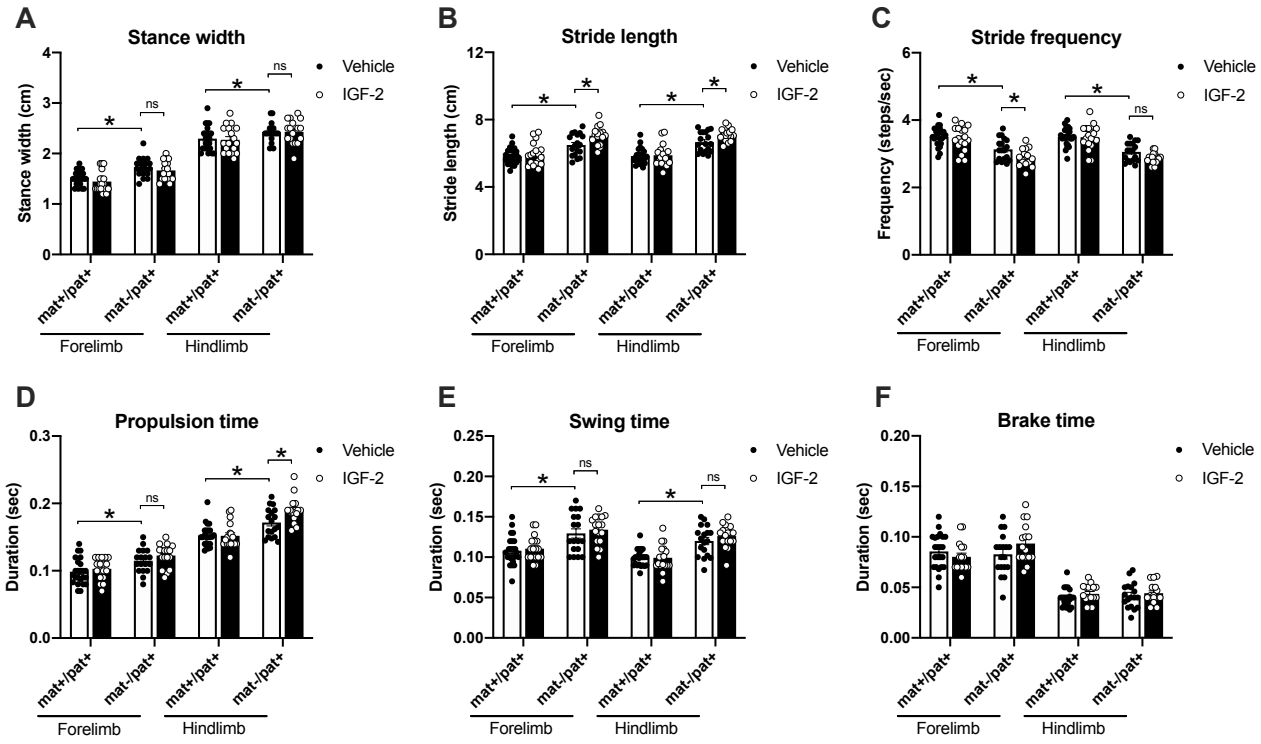

Fig. 4 IGF-2 did not rescue or improve gait deficits in *Ube3a*$^{mat-/pat+}$ mice. (A) Compared to wildtype littermates (*Ube3a*$^{mat+/pat+}$; mat+/pat+), *Ube3a*$^{mat-/pat+}$ (mat-/pat+) mice exhibited wider stances while treadmill walking, which were unaffected by IGF-2 treatment. **(B)** Stride lengths were increased in mat-/pat+ mice and were further increased by IGF-2 while **(C)** the reduced stride frequency of mat-/pat+ mice was further decreased in forelimbs by IGF-2. **(D)** IGF-2 had no effect on the elevated forelimb propulsion time of mat-/pat+ mice and led to further elevation of the increased hindlimb propulsion time. **(E)** Swing time was elevated in mat-/pat+ mice, regardless of IGF-2 treatment and **(F)** brake time was normal in mat-/pat+ mice and unchanged by IGF-2. Data are expressed as mean ± S.E.M. n = 17-24 mice/group. A-F: *$p < 0.05$, Sidak's or Tukey's multiple comparisons test following two-way ANOVA (per limb set). ns, not significantly different, $p > 0.05$.

Supplementary Information

Methods

Novel object recognition (NOR) in C57BL/6J mice. Learning and memory were tested by individually presenting subjects with two identical objects and later testing their ability to recognize the familiar object over a novel one following a protocol previously described by Cruz et al. (2020) [1]. The NOR assay was carried out within an opaque matte white arena (41 cm l x 41 cm w x 30 cm h) in a 30-lux room and consisted of four phases: a 5-min habituation to the arena on the day prior to the test, a 3-min object familiarization session, a 24-hr isolation period, and a 5-min object recognition test. Twenty min prior to the familiarization phase, mice were administered 30 µg/kg IGF-2 or vehicle via subcutaneous injection. Following the 5-min habituation period, each animal was removed from the arena and placed in an individual clean holding cage while two clean identical objects were placed inside the arena. Each subject was then returned to its arena and allowed to freely explore and familiarize with the objects for 3 min. After 24 hrs, subjects were returned to their arenas and allowed to freely explore one familiar and one novel object for 5 min. Time spent investigating each object was measured manually by a trained observer blinded to treatment group. Recognition memory was defined as spending significantly more time investigating the novel object compared to the familiar object by paired *t*-test within group. Object preference was calculated as time spent sniffing the novel object compared to total time sniffing both objects. Fifty percent represents equal time investigating the novel and familiar object (a lack of preference) whereas >50% demonstrates intact recognition memory. The effect of IGF-2 on percent preference was analyzed using unpaired *t*-test (**Supplementary File 2**).

Contextual fear conditioning in C57BL/6J mice. Contextual fear conditioning was carried out using an automated fear conditioning chamber (Med Associates, Inc., Fairfax, VT, USA) following the training protocol previously described by Cruz et al. (2020) [1]. On the training day, mice were administered 30 μg/kg IGF-2 or vehicle via subcutaneous injection and, after a 20 min delay, exposed to a noise-shock (CS-US) pairing within a testing chamber with specific visual, odor, and tactile cues. After 2 min, a 2-sec foot shock (0.7 mA) was delivered. A 1 min exploration period followed the noise-shock pairing before the mouse was placed back in the home cage. Twenty four hours later, the subject was placed back inside the training environment for 5 min. The chamber contained identical contextual cues as the training session, but no foot shock occurred, and the percent time spent freezing was automatically measured by VideoFreeze software (Med Associates). The effect of IGF-2 on percent time freezing was analyzed using unpaired *t*-test (**Supplementary File 2**).

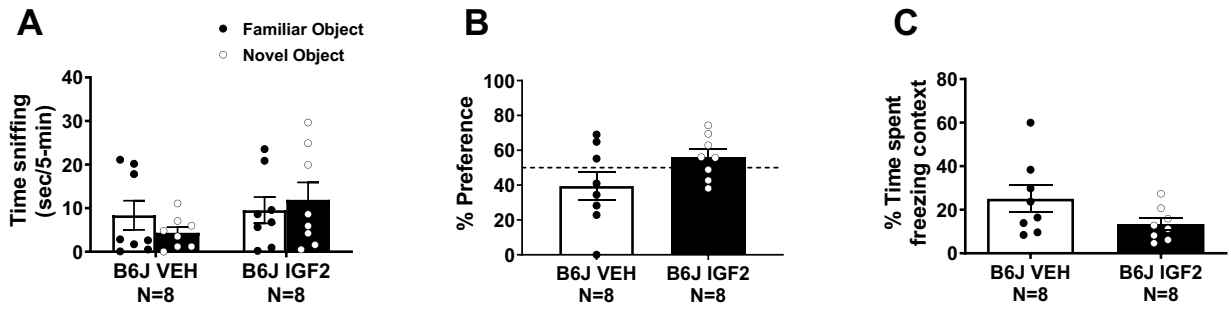

Fig S1. IGF-2 did not enhance cognition in novel object recognition or contextual fear conditioning tasks in pure congenic C57BL/6J mice. The cognitive enhancing capabilities of IGF-2 were assessed in congenic C57BL/6J (B6J) mice. **(A)** Novel object recognition was tested using the protocol of Cruz et al. (2020) with administration of 30 µg/kg IGF-2 20 minutes before the familiarization phase and the recognition memory test 24 hours after familiarization. Neither vehicle (VEH) nor IGF-2-treated mice met the criteria for recognition memory as they did not spend more time sniffing the novel object compared to the familiar object. **(B)** There was no difference between vehicle and IGF-2 groups in percent preference for the novel object. **(C)** Contextual fear conditioning was evaluated using the training protocol of Cruz et al. (2020) with administration of 30 µg/kg IGF-2 20 minutes before the training session and the contextual memory test 24 hours after training. There was no difference in percent time freezing between the vehicle and IGF-2 group. Data are expressed as mean ± S.E.M. *n* = 8 mice/group.

References

1. Cruz E, Descalzi G, Steinmetz A, Scharfman HE, Katzman A, Alberini CM: CIM6P/IGF-2 Receptor Ligands Reverse Deficits in Angelman Syndrome Model Mice. *Autism Res* 2020.

Supplementary File 2

Figure 1 Statistics

Panel A	Cortical power pre-injection	Two-way RM ANOVA	**ANOVA table**	**SS**	**DF**	**MS**	**F (DFn, DFd)**	**P-value**
			Genotype	5545	1	5545	F (1, 5) = 0.4673	P=0.5246
			Frequency	1807711	50	36154	F (50, 250) = 37.00	P<0.0001
			Interaction	56918	50	1138	F (50, 250) = 1.165	P=0.2248
			Subject	59329	5	11866	F (5, 250) = 12.14	P<0.0001
		Sidak's multiple comparisons test (mat+/pat+ Vehicle vs. mat-/pat+ Vehicle)	**Frequency (Hz)**	**Adjusted p-value**				
			0.5	>0.9999				
			1	0.0005				
			2	0.0008				
			3	0.3485				
Panel B	Hippocampal power pre-injection	Two-way RM ANOVA	**ANOVA table**	**SS**	**DF**	**MS**	**F (DFn, DFd)**	**P-value**
			Genotype	2464318	1	2464318	F (1, 5) = 0.3025	P=0.6060
			Frequency	474082389	50	9481648	F (50, 250) = 11.72	P<0.0001
			Interaction	12471481	50	249430	F (50, 250) = 0.3082	P>0.9999
			Subject	40736376	5	8147275	F (5, 250) = 10.07	P<0.0001
		Sidak's multiple comparisons test (mat+/pat+ Vehicle vs. mat-/pat+ Vehicle)	**Frequency (Hz)**	**Adjusted p-value**				
			0.5	>0.9999				
			1	0.9999				
			2	0.6884				
			3	0.9266				
Panel C	Cortical power post-injection	Two-way RM ANOVA	**ANOVA table**	**SS**	**DF**	**MS**	**F (DFn, DFd)**	**P-value**
			Genotype	125432	7	17919	F (7, 20) = 1.048	P=0.4303
			Frequency	8039513	50	160790	F (50, 1000) = 122.4	P<0.0001
			Interaction	757746	350	2165	F (350, 1000) = 1.649	P<0.0001
			Subject	341859	20	17093	F (20, 1000) = 13.02	P<0.0001
		Sidak's multiple comparisons test	**Frequency (Hz)**	**Comparison**	**Adjusted p-value**			
			1	mat+/pat+ Vehicle vs. mat-/pat+ Vehicle	<0.0001			
				mat-/pat+ Vehicle vs. mat-/pat+ 10 µg/kg IGF-2	<0.0001			
				mat-/pat+ Vehicle vs. mat-/pat+ 30 µg/kg IGF-2	<0.0001			
				mat-/pat+ Vehicle vs. mat-/pat+ 60 µg/kg IGF-2	<0.0001			
			2	mat+/pat+ Vehicle vs. mat-/pat+ Vehicle	<0.0001			
				mat-/pat+ Vehicle vs. mat-/pat+ 10 µg/kg IGF-2	<0.0001			
				mat-/pat+ Vehicle vs. mat-/pat+ 30 µg/kg IGF-2	<0.0001			
				mat-/pat+ Vehicle vs. mat-/pat+ 60 µg/kg IGF-2	<0.0001			
Panel D	Hippocampal power post-injection	Two-way RM ANOVA	**ANOVA table**	**SS**	**DF**	**MS**	**F (DFn, DFd)**	**P-value**
			Genotype	45888149	7	6555450	F (7, 20) = 0.9609	P=0.4848
			Frequency	1386484435	50	27729689	F (50, 1000) = 37.08	P<0.0001
			Interaction	250201546	350	714862	F (350, 1000) = 0.956	P=0.6901
			Subject	136442974	20	6822149	F (20, 1000) = 9.123	P<0.0001
		Sidak's multiple comparisons test	**Frequency (Hz)**	**Comparison**	**Adjusted p-value**			
			1	mat+/pat+ Vehicle vs. mat-/pat+ Vehicle	0.0343			
				mat-/pat+ Vehicle vs. mat-/pat+ 10 µg/kg IGF-2	0.0014			
				mat-/pat+ Vehicle vs. mat-/pat+ 30 µg/kg IGF-2	0.0002			
				mat-/pat+ Vehicle vs. mat-/pat+ 60 µg/kg IGF-2	0.6278			
			2	mat+/pat+ Vehicle vs. mat-/pat+ Vehicle	<0.0001			
				mat-/pat+ Vehicle vs. mat-/pat+ 10 µg/kg IGF-2	<0.0001			
				mat-/pat+ Vehicle vs. mat-/pat+ 30 µg/kg IGF-2	<0.0001			
				mat-/pat+ Vehicle vs. mat-/pat+ 60 µg/kg IGF-2	0.0933			
Panel E	Cortical delta power post-injection	Two-way RM ANOVA	**ANOVA table**	**SS**	**DF**	**MS**	**F (DFn, DFd)**	**P-value**
			Genotype	202284	1	202284	F (1, 5) = 0.6891	P=0.4443
			Treatment	456776	3	152259	F (3, 15) = 3.885	P=0.0308
			Interaction	423496	3	141165	F (3, 15) = 3.602	P=0.0386
			Subject	1467817	5	293563	F (5, 15) = 7.491	P=0.0011
		Tukey's multiple comparisons test	**Genotype**	**Comparison**	**Adjusted p-value**			
			mat+/pat+	Vehicle vs. 10 µg/kg IGF-2	0.6917			
				Vehicle vs. 30 µg/kg IGF-2	0.642			
				Vehicle vs. 60 µg/kg IGF-2	0.8416			
				10 µg/kg IGF-2 vs. 30 µg/kg IGF-2	0.1432			
				10 µg/kg IGF-2 vs. 60 µg/kg IGF-2	0.257			
				30 µg/kg IGF-2 vs. 60 µg/kg IGF-2	0.9828			
			mat-/pat+	Vehicle vs. 10 µg/kg IGF-2	0.0084			
				Vehicle vs. 30 µg/kg IGF-2	0.0151			
				Vehicle vs. 60 µg/kg IGF-2	0.1039			
				10 µg/kg IGF-2 vs. 30 µg/kg IGF-2	0.9902			
				10 µg/kg IGF-2 vs. 60 µg/kg IGF-2	0.563			
				30 µg/kg IGF-2 vs. 60 µg/kg IGF-2	0.7387			
Panel F	Hippocampal delta power post-injection	Two-way RM ANOVA	**ANOVA table**	**SS**	**DF**	**MS**	**F (DFn, DFd)**	**P-value**
			Genotype	135138612	1	135138612	F (1, 5) = 0.7055	P=0.4393
			Treatment	172835342	3	57611781	F (3, 15) = 4.044	P=0.0272
			Interaction	19257328	3	6419109	F (3, 15) = 0.4505	P=0.7206
			Subject	957798152	5	191559630	F (5, 15) = 13.45	P<0.0001
		Tukey's multiple comparisons test	**Genotype**	**Comparison**	**Adjusted p-value**			
			mat+/pat+	Vehicle vs. 10 µg/kg IGF-2	0.4476			
				Vehicle vs. 30 µg/kg IGF-2	0.5637			
				Vehicle vs. 60 µg/kg IGF-2	0.998			
				10 µg/kg IGF-2 vs. 30 µg/kg IGF-2	0.9969			
				10 µg/kg IGF-2 vs. 60 µg/kg IGF-2	0.5469			
				30 µg/kg IGF-2 vs. 60 µg/kg IGF-2	0.6672			
			mat-/pat+	Vehicle vs. 10 µg/kg IGF-2	0.0657			
				Vehicle vs. 30 µg/kg IGF-2	0.0432			
				Vehicle vs. 60 µg/kg IGF-2	0.3002			
				10 µg/kg IGF-2 vs. 30 µg/kg IGF-2	0.9958			
				10 µg/kg IGF-2 vs. 60 µg/kg IGF-2	0.8			
				30 µg/kg IGF-2 vs. 60 µg/kg IGF-2	0.6749			

Figure 2 Statistics

Panel A	Rotarod	Repeated measures ANOVA	**ANOVA table**	**SS**	**DF**	**MS**	**F (DFn, DFd)**	**P-value**
			Time	100473	2	50237	F (1.985, 41.69) = 69.07	P<0.0001
			Group	72136	3	24045	F (3, 21) = 1.744	P=0.1887
			Time x Group	26350	6	4392	F (6, 42) = 6.038	P=0.0001
		Dunnett's multiple comparisons test (day 1 vs. day 3)	**Group**	**Adjusted p-value**				
			mat+/pat+ Vehicle	0.0004				
			mat+/pat+ IGF-2	0.0002				
			mat-/pat+ Vehicle	0.055				
			mat-/pat+ IGF-2	0.1301				
		Dunnett's multiple comparisons test (mat+/pat+ Vehicle vs. mat-/pat+ Vehicle)	**Day**	**Adjusted p-value**				
			Day 1	0.9999				
			Day 2	0.3598				
			Day 3	0.0458				
Panel B	Pup USV	Two-way ANOVA	**ANOVA table**	**SS**	**DF**	**MS**	**F (DFn, DFd)**	**P-value**
			Genotype	430577	1	430577	F (1, 75) = 24.55	P<0.0001
			Treatment	1858	1	1858	F (1, 75) = 0.1059	P=0.7457
			Interaction	40091	1	40091	F (1, 75) = 2.286	P=0.1347
		Sidak's multiple comparisons test	**Comparison**	**Adjusted p-value**				
			mat+/pat+ Vehicle vs. mat-/pat+ Vehicle	0.0239				
			mat-/pat+ Vehicle vs. mat-/pat+ IGF-2	0.6222				
Panel C	Noise playback	Paired t-test (pre-noise vs. noise)	**Group**	**t and df**	**P-value**			
			mat+/pat+ Vehicle	t=7.297, df=16	<0.0001			
			mat+/pat+ IGF-2	t=5.164, df=9	0.0006			
			mat-/pat+ Vehicle	t=6.157, df=13	<0.0001			
			mat-/pat+ IGF-2	t=8.434, df=10	<0.0001			
Panel D	50-kHz USV playback	Paired t-test (distal vs. proximal)	**Group**	**t and df**	**P-value**			
			mat+/pat+ Vehicle	t=3.348, df=16	0.0041			
			mat+/pat+ IGF-2	t=2.321, df=9	0.0454			
			mat-/pat+ Vehicle	t=1.427, df=13	0.1772			
			mat-/pat+ IGF-2	t=0.8548, df=10	0.4127			

Figure 3 Statistics

Panel A	Horizontal activity	Two-way ANOVA	**ANOVA table**	**SS**	**DF**	**MS**	**F (DFn, DFd)**	**P-value**
			Genotype	237447445	1	2.4E+08	F (1, 46) = 146.0	P<0.0001
			Treatment	665621	1	665621	F (1, 46) = 0.4094	P=0.5255
			Interaction	5438585	1	5438585	F (1, 46) = 3.345	P=0.0739
		Sidak's multiple comparisons test	**Comparison**	**Adjusted p-value**				
			mat+/pat+ Vehicle vs. mat-/pat+ Vehicle	<0.0001				
			mat-/pat+ Vehicle vs. mat-/pat+ IGF-2	0.1303				
Panel B	Vertical activity	Two-way ANOVA	**ANOVA table**	**SS**	**DF**	**MS**	**F (DFn, DFd)**	**P-value**
			Genotype	336319	1	336319	F (1, 46) = 70.63	P<0.0001
			Treatment	436.9	1	436.9	F (1, 46) = 0.09176	P=0.7633
			Interaction	10319	1	10319	F (1, 46) = 2.167	P=0.1478
		Sidak's multiple comparisons test	**Comparison**	**Adjusted p-value**				
			mat+/pat+ Vehicle vs. mat-/pat+ Vehicle	<0.0001				
			mat-/pat+ Vehicle vs. mat-/pat+ IGF-2	0.6151				
Panel C	Center time	Two-way ANOVA	**ANOVA table**	**SS**	**DF**	**MS**	**F (DFn, DFd)**	**P-value**
			Genotype	19543	1	19543	F (1, 46) = 1.255	P=0.2684
			Treatment	31079	1	31079	F (1, 46) = 1.996	P=0.1645
			Interaction	4604	1	4604	F (1, 46) = 0.2956	P=0.5893
Panel D	Beam walking	Two-way ANOVA	**ANOVA table**	**SS**	**DF**	**MS**	**F (DFn, DFd)**	**P-value**
			Genotype	582.8	1	582.8	F (1, 64) = 6.170	P=0.0156
			Treatment	40.21	1	40.21	F (1, 64) = 0.4257	P=0.5164
			Interaction	2.874	1	2.874	F (1, 64) = 0.03043	P=0.8621
		Sidak's multiple comparisons test	**Comparison**	**Adjusted p-value**				
			mat+/pat+ Vehicle vs. mat-/pat+ Vehicle	0.0981				
			mat+/pat+ IGF-2 vs. mat-/pat+ IGF-2	0.2369				
Panel E	Rotarod	Repeated measures ANOVA	**ANOVA table**	**SS**	**DF**	**MS**	**F (DFn, DFd)**	**P-value**
			Time	72808	2	36404	F (1.692, 76.12) = 21.11	P<0.0001
			Group	299534	3	99845	F (3, 45) = 20.31	P<0.0001
			Time x Group	21053	6	3509	F (6, 90) = 2.034	P=0.0691
		Dunnett's multiple comparisons test (day 1 vs. day 3)	**Group**	**Adjusted p-value**				
			mat+/pat+ Vehicle	0.5591				
			mat+/pat+ IGF-2	0.1749				
			mat-/pat+ Vehicle	0.0098				
			mat-/pat+ IGF-2	0.0287				
		Dunnett's multiple comparisons test (vs. mat+/pat+ Vehicle)	**Day**	**Group**	**Adjusted p-value**			
			Day 1	mat+/pat+ IGF-2	0.8047			
				mat-/pat+ Vehicle	<0.0001			
				mat-/pat+ IGF-2	0.0039			
			Day 2	mat+/pat+ IGF-2	0.8689			
				mat-/pat+ Vehicle	0.0006			
				mat-/pat+ IGF-2	0.2883			
			Day 3	mat+/pat+ IGF-2	0.4784			
				mat-/pat+ Vehicle	0.0111			
				mat-/pat+ IGF-2	0.2981			
Panel F	Marble burying	Two-way ANOVA	**ANOVA table**	**SS**	**DF**	**MS**	**F (DFn, DFd)**	**P-value**
			Genotype	301.2	1	301.2	F (1, 46) = 22.49	P<0.0001
			Treatment	0.01561	1	0.01561	F (1, 46) = 0.001166	P=0.9729
			Interaction	0.01561	1	0.01561	F (1, 46) = 0.001166	P=0.9729
		Sidak's multiple comparisons test	**Comparison**	**Adjusted p-value**				
			mat+/pat+ Vehicle vs. mat-/pat+ Vehicle	0.0023				
			mat-/pat+ Vehicle vs. mat-/pat+ IGF-2	>0.9999				
Panel G	Generalized clonus	Two-way ANOVA	**ANOVA table**	**SS**	**DF**	**MS**	**F (DFn, DFd)**	**P-value**
			Genotype	442915	1	442915	F (1, 69) = 17.92	P<0.0001
			Treatment	6311	1	6311	F (1, 69) = 0.2554	P=0.6149
			Interaction	20525	1	20525	F (1, 69) = 0.8305	P=0.3653
		Sidak's multiple comparisons test	**Comparison**	**Adjusted p-value**				
			mat+/pat+ Vehicle vs. mat-/pat+ Vehicle	0.026				
			mat-/pat+ Vehicle vs. mat-/pat+ IGF-2	0.5381				
Panel H	Object recognition	Paired t-test (familiar vs. novel)	**Group**	**t and df**	**P-value**			
			mat+/pat+ Vehicle	t=4.089, df=17	0.0008			
			mat+/pat+ IGF-2	t=3.982, df=16	0.0011			
			mat-/pat+ Vehicle	t=3.122, df=18	0.0059			
			mat-/pat+ IGF-2	t=3.192, df=16	0.0057			
Panel I	Object preference	Two-way ANOVA	**ANOVA table**	**SS**	**DF**	**MS**	**F (DFn, DFd)**	**P-value**
			Genotype	57.51	1	57.51	F (1, 67) = 0.4963	P=0.4836
			Treatment	24.79	1	24.79	F (1, 67) = 0.2140	P=0.6452
			Interaction	0.1372	1	0.1372	F (1, 67) = 0.001184	P=0.9727

Figure 4 Statistics

Panel A	Stance width	Forelimb	Two-way ANOVA	**ANOVA table**	**SS**	**DF**	**MS**	**F (DFn, DFd)**	**P-value**
				Genotype	0.9009	1	0.9009	F (1, 69) = 29.28	P<0.0001
				Treatment	0.1272	1	0.1272	F (1, 69) = 4.135	P=0.0459
				Interaction	0.01786	1	0.01786	F (1, 69) = 0.5806	P=0.4487
			Tukey's multiple comparisons test	**Comparison**	**Adjusted p-value**				
				mat+/pat+ Vehicle vs. mat-/pat+ Vehicle	0.0045				
				mat-/pat+ Vehicle vs. mat-/pat+ IGF-2	0.8174				
		Hindlimb	Two-way ANOVA	**ANOVA table**	**SS**	**DF**	**MS**	**F (DFn, DFd)**	**P-value**
				Genotype	0.5551	1	0.5551	F (1, 69) = 13.42	P=0.0005
				Treatment	0.004924	1	0.004924	F (1, 69) = 0.1190	P=0.7312
				Interaction	0.01	1	0.01	F (1, 69) = 0.2418	P=0.6245
			Sidak's multiple comparisons test	**Comparison**	**Adjusted p-value**				
				mat+/pat+ Vehicle vs. mat-/pat+ Vehicle	0.0393				
				mat-/pat+ Vehicle vs. mat-/pat+ IGF-2	0.8119				
Panel B	Stride length	Forelimb	Two-way ANOVA	**ANOVA table**	**SS**	**DF**	**MS**	**F (DFn, DFd)**	**P-value**
				Genotype	17.43	1	17.43	F (1, 69) = 60.00	P<0.0001
				Treatment	1.397	1	1.397	F (1, 69) = 4.811	P=0.0317
				Interaction	1.297	1	1.297	F (1, 69) = 4.467	P=0.0382
			Tukey's multiple comparisons test	**Comparison**	**Adjusted p-value**				
				mat+/pat+ Vehicle vs. mat-/pat+ Vehicle	0.0004				
				mat-/pat+ Vehicle vs. mat-/pat+ IGF-2	0.021				
		Hindlimb	Two-way ANOVA	**ANOVA table**	**SS**	**DF**	**MS**	**F (DFn, DFd)**	**P-value**
				Genotype	22.85	1	22.85	F (1, 69) = 116.0	P<0.0001
				Treatment	0.6194	1	0.6194	F (1, 69) = 3.143	P=0.0806
				Interaction	1.059	1	1.059	F (1, 69) = 5.376	P=0.0234
			Tukey's multiple comparisons test	**Comparison**	**Adjusted p-value**				
				mat+/pat+ Vehicle vs. mat-/pat+ Vehicle	<0.0001				
				mat-/pat+ Vehicle vs. mat-/pat+ IGF-2	0.0312				
Panel C	Stride frequency	Forelimb	Two-way ANOVA	**ANOVA table**	**SS**	**DF**	**MS**	**F (DFn, DFd)**	**P-value**
				Genotype	4.824	1	4.824	F (1, 69) = 58.72	P<0.0001
				Treatment	0.3077	1	0.3077	F (1, 69) = 3.745	P=0.0571
				Interaction	0.2882	1	0.2882	F (1, 69) = 3.508	P=0.0653
			Sidak's multiple comparisons test	**Comparison**	**Adjusted p-value**				
				mat+/pat+ Vehicle vs. mat-/pat+ Vehicle	<0.0001				
				mat-/pat+ Vehicle vs. mat-/pat+ IGF-2	0.0213				
		Hindlimb	Two-way ANOVA	**ANOVA table**	**SS**	**DF**	**MS**	**F (DFn, DFd)**	**P-value**
				Genotype	6.329	1	6.329	F (1, 69) = 107.4	P<0.0001
				Treatment	0.09467	1	0.09467	F (1, 69) = 1.607	P=0.2092
				Interaction	0.232	1	0.232	F (1, 69) = 3.938	P=0.0512
			Sidak's multiple comparisons test	**Comparison**	**Adjusted p-value**				
				mat+/pat+ Vehicle vs. mat-/pat+ Vehicle	<0.0001				
				mat-/pat+ Vehicle vs. mat-/pat+ IGF-2	0.0558				
Panel D	Propulsion time	Forelimb	Two-way ANOVA	**ANOVA table**	**SS**	**DF**	**MS**	**F (DFn, DFd)**	**P-value**
				Genotype	0.006743	1	0.006743	F (1, 69) = 21.65	P<0.0001
				Treatment	0.0005767	1	0.0005767	F (1, 69) = 1.852	P=0.1780
				Interaction	0.00008093	1	0.00008093	F (1, 69) = 0.2599	P=0.6118
			Sidak's multiple comparisons test	**Comparison**	**Adjusted p-value**				
				mat+/pat+ Vehicle vs. mat-/pat+ Vehicle	0.0053				
				mat-/pat+ Vehicle vs. mat-/pat+ IGF-2	0.363				
		Hindlimb	Two-way ANOVA	**ANOVA table**	**SS**	**DF**	**MS**	**F (DFn, DFd)**	**P-value**
				Genotype	0.01701	1	0.01701	F (1, 69) = 53.35	P<0.0001
				Treatment	0.0007698	1	0.0007698	F (1, 69) = 2.414	P=0.1248
				Interaction	0.002031	1	0.002031	F (1, 69) = 6.372	P=0.0139
			Tukey's multiple comparisons test	**Comparison**	**Adjusted p-value**				
				mat+/pat+ Vehicle vs. mat-/pat+ Vehicle	0.0033				
				mat-/pat+ Vehicle vs. mat-/pat+ IGF-2	0.032				
Panel E	Swing time	Forelimb	Two-way ANOVA	**ANOVA table**	**SS**	**DF**	**MS**	**F (DFn, DFd)**	**P-value**
				Genotype	0.01091	1	0.01091	F (1, 69) = 32.78	P<0.0001
				Treatment	0.0002719	1	0.0002719	F (1, 69) = 0.8167	P=0.3693
				Interaction	0.00004343	1	0.00004343	F (1, 69) = 0.1305	P=0.7190
			Sidak's multiple comparisons test	**Comparison**	**Adjusted p-value**				
				mat+/pat+ Vehicle vs. mat-/pat+ Vehicle	0.0003				
				mat-/pat+ Vehicle vs. mat-/pat+ IGF-2	0.6238				
		Hindlimb	Two-way ANOVA	**ANOVA table**	**SS**	**DF**	**MS**	**F (DFn, DFd)**	**P-value**
				Genotype	0.01186	1	0.01186	F (1, 69) = 64.58	P<0.0001
				Treatment	0.00003816	1	0.00003816	F (1, 69) = 0.2078	P=0.6500
				Interaction	0.0002315	1	0.0002315	F (1, 69) = 1.260	P=0.2655
			Sidak's multiple comparisons test	**Comparison**	**Adjusted p-value**				
				mat+/pat+ Vehicle vs. mat-/pat+ Vehicle	<0.0001				
				mat-/pat+ Vehicle vs. mat-/pat+ IGF-2	0.4827				
Panel F	Brake time	Forelimb	Two-way ANOVA	**ANOVA table**	**SS**	**DF**	**MS**	**F (DFn, DFd)**	**P-value**
				Genotype	0.0004719	1	0.0004719	F (1, 69) = 1.460	P=0.2311
				Treatment	0.0001162	1	0.0001162	F (1, 69) = 0.3593	P=0.5508
				Interaction	0.001147	1	0.001147	F (1, 69) = 3.549	P=0.0638
		Hindlimb	Two-way ANOVA	**ANOVA table**	**SS**	**DF**	**MS**	**F (DFn, DFd)**	**P-value**
				Genotype	0.00004612	1	0.00004612	F (1, 69) = 0.4559	P=0.5018
				Treatment	0.000167	1	0.000167	F (1, 69) = 1.651	P=0.2031
				Interaction	0.00001722	1	0.00001722	F (1, 69) = 0.1703	P=0.6812

Figure S1 Statistics

Panel A	Object recognition	Paired t-test (familiar vs. novel)	**Group**	**t and df**	**P-value**
			B6J Vehicle	t=1.746, df=7	0.1243
			B6J IGF-2	t=1.075, df=7	0.3182
Panel B	Object preference	Unpaired t-test (B6J Vehicle vs. B6J IGF-2)	**t and df**	**P-value**	
			t=1.776, df=14	0.0975	
Panel C	Context freezing	Unpaired t-test (B6J Vehicle vs. B6J IGF-2)	**t and df**	**P-value**	
			t=1.730, df=14	0.1056	

Chapter 7

Investigation of an Antisense Oligonucleotide Therapy in the *Ube3a* Deletion Rat Model of Angelman Syndrome

Elizabeth L. Berg, Nycole Copping, Anna Adhikari, Henriette O'Geen, Peter Deng, Matthew Matson, Sarah G. B. Christian, Kyle D. Fink, David J. Segal, Scott V. Dindot, and Jill L. Silverman.

Abstract

Angelman Syndrome (AS) is a neurodevelopmental disorder caused by disrupted functioning of maternal *UBE3A*, the gene encoding ubiquitin protein ligase E3A. Those with AS exhibit developmental delay, intellectual disability, impaired communication, motor deficits, and seizures. Since UBE3A in neurons is solely expressed from the maternal allele, it is believed that the AS phenotype is predominantly driven by neuronal deficiency of active UBE3A. While the paternal allele of *UBE3A* is intact, it is epigenetically silenced by a long non-coding RNA, termed *UBE3A* antisense transcript (*UBE3A-ATS*). Therefore, a putative therapeutic approach for AS is to restore levels of UBE3A in neurons by targeting and knocking down *UBE3A-ATS* to unsilence the paternal allele. Antisense oligonucleotides (ASOs) offer a mechanism by which *UBE3A-ATS* can be bound and degraded, facilitating paternal UBE3A expression. Here, we examined ASO tolerability and ASO-mediated changes in expression of *UBE3A-ATS*, *Ube3a* RNA, and UBE3A protein in the *Ube3a* deletion rat model of AS. This study therefore represents the first gene reactivation effort in the rat model of AS. Through an investigation of two different ASO compounds, a wide dose range, and three routes of administration, we identified an ASO treatment that successfully achieved reduction of *UBE3A-ATS* expression in the brain. Although further molecular and behavioral characterization following ASO delivery is warranted, we found that the rat model of AS generally exhibited normal susceptibility to ASO-related adverse effects. The model of ASO treatment established here in rats, which can be delivered via the same route of administration as used in human clinical trials, offers a powerful tool for the continuing pursuit for a safe and effective therapy for those with AS.

Abbreviations

AS: Angelman Syndrome; Ube3a: ubiquitin protein ligase E3A; Ube3a-ATS: Ube3a antisense transcript; ASO: antisense oligonucleotide; CNS: central nervous system; CSF: cerebrospinal fluid; SAE: serious adverse event; EEG: electroencephalographic; aCSF: artificial CSF; ICM: intracisterna magna; ICV: intracerebroventricular; IT: intrathecal.

Introduction

Angelman Syndrome (AS) is a rare neurodevelopmental disorder that occurs in about one in 15,000 live births and is characterized by developmental delay, intellectual disabilities, communication deficits, motor impairments, and frequent seizures. AS is caused by the loss of function of the chromosome 15 gene *UBE3A* (ubiquitin protein ligase E3A), and specifically results from dysfunction of the maternal allele. This can occur for a variety of reasons, with the most common being deletion or mutation of the gene. Within neurons, the maternal allele of *UBE3A* is solely responsible for producing active UBE3A protein and the paternal allele is kept epigenetically silenced[1]. Therefore, the maternal allele disruption that occurs in AS leaves the brain severely lacking active UBE3A thus impeding normal cellular functioning and resulting in AS phenotypes[2–5].

UBE3A has several important biological roles, including acting as a ligase within the ubiquitin proteasome pathway, which is responsible for the appropriate marking and degradation of surplus cellular products. Without functional UBE3A to aid in protein clearance, levels of UBE3A substrates are likely to be dysregulated, disrupt intracellular homeostasis and synaptic functioning, interfere with neurodevelopment, and lead to the numerous phenotypic deficits observed in AS[6–9]. Since the symptoms are pervasive and severe, those with AS require lifelong caretaking and there remains a great unmet need for an effective therapeutic. Over the last few

decades, mouse models of AS have greatly facilitated the investigation of various treatment strategies, yet there is still no gene-specific treatment available to the AS population to date[10–18].

Fortunately, since the genetic cause of AS has been identified and well-studied, it is presumably targetable by various molecular and gene therapy approaches. The most direct and seemingly promising approach for treating AS would be to restore functional levels of UBE3A in neurons. One mechanism for achieving this is through the use of antisense oligonucleotides (ASOs) to reduce or knock down the long non-coding RNA, called *Ube3a* antisense transcript (*Ube3a-ATS)*, that is responsible for silencing the paternal allele of *UBE3A* in neurons. ASOs are short synthetic DNA strands that can be created to specifically bind the sequence of *Ube3a-ATS*. ASO binding to *Ube3a-ATS* RNA initiates RNase H1-mediated degradation of the transcript, thereby removing the brake off the paternal allele and facilitating expression *UBE3A* (**Figure 1**). While ASOs are not technically considered gene therapy since they target RNA, they can be classified as a "gene therapy-like" treatment.

ASOs are currently being evaluated in humans with AS through two separate clinical trials, and a third trial is set to begin soon. While various ASO therapies have been tested in non-human primates and human clinical trials for a range of diseases without the occurrence of serious adverse events (SAEs)[19–27], a unique situation recently arose in one of the currently active clinical trials for AS. In said trial, all patients administered the ASO exhibited mild to moderate lower extremity weakness[28,29]. For two of the five patients, the weakness progressed into an inability to walk. Onset of the first SAE prompted a pause in ASO administration, during which time the other cases manifested but all eventually resolved within a few months. Encouragingly, clinical efficacy persisted for months and patients continued to demonstrate improvements across several

behavioral domains such as motor, communication, and sleep, and none of the participants dropped out of the study.

The SAE, however, sparked a few key questions including whether a dose is possible that can achieve behavioral improvements but avoid the SAE, and whether AS individuals are more susceptible to SAE development compared to controls. This cannot be carried out in neurotypical volunteer subjects due to the risks associated with UBE3A overexpression[30]. Studies of the ASO in non-human primates had not indicated any risk of the lower extremity weakness observed in humans, despite delivery of doses much higher than what was provided in the clinical trial (accounting for cross-species equivalencies).

Importantly, all of the non-human primate research was carried out in non-AS model animals since a genetic non-human primate model of AS has yet to be developed. Therefore, in order to shed light on the question of differential ASO tolerability in the AS population, as well as help elucidate the pathophysiology of the clinical trial SAE, the present study sought to establish a paradigm of ASO administration in AS model animals and to compare outcomes between AS model animals and wildtype controls. An auxiliary goal was to compare ASO tolerance across different routes of entry into the central nervous system (CNS). Namely, we tested intracisterna magna injection, intracerebroventricular delivery as was previously used in a mouse model of AS[31], and intrathecal lumbar puncture, which is the mode of administration used to deliver ASOs to AS patients.

To achieve these aims, we took advantage of the rat model of AS, which offers several crucial advantages compared to currently available mouse models. In addition to greater physiologic and metabolic similarity to humans, the larger size of the rat facilitates access to cerebrospinal fluid (CSF) spaces, thereby enabling both injections and CSF withdrawals[32].

Additionally, the rat model does not display the elevated weight or severe gross motor deficit exhibited by the mouse model of AS. The lack of these potentially confounding phenotypes in the rat greatly benefits the clear evaluation of specific effects due to ASO treatment. As reported previously, the rat model of AS recapitulates several key AS phenotypes including learning and memory impairments, aberrant social behavior, communication deficits, poor motor coordination, altered EEG activity, and microcephaly[33–37]. This makes it a strong model of the disorder with high construct and face validity and offers the long-term opportunity to harness these phenotypes in the assessment of ASO efficacy.

Although our study is the first to utilize ASO technology in the rat model of AS, candidate ASOs for application in rats have already been identified. Following *in vitro* screening on a set of custom-designed ASOs targeted to various sites along the rat *Ube3a-ATS*, two candidate compounds were identified: ASO 1.1 and 3.1. We initially pursued both ASO 1.1 and 3.1 to determine the more tolerable and effective molecule *in vivo*. Mortality rates and weight change were used to assess tolerability, and expression of *Ube3a-ATS* RNA, *Ube3a* RNA, and UBE3A protein were measured as indications of molecular efficacy. Our study revealed that ASO 3.1 was capable of downregulating expression of rat *Ube3a-ATS* and that this dose could feasibly be delivered by intrathecal lumbar puncture, therefore mirroring the delivery route used in humans.

Methods

Subjects. All animals were housed in a temperature-controlled vivarium maintained on a 12:12 light-dark cycle and provided food and water *ad libitum*. All procedures were approved by the Institutional Animal Care and Use Committee of the University of California Davis and conducted in compliance with the National Institutes of Health Guide for the Care and Use of

Laboratory Animals. *Ube3a* subject rats were generated by breeding *Ube3a* deletion females with wildtype Sprague Dawley males (Envigo, Indianapolis, IN). The resulting maternally inherited *Ube3a* deletion animals (*Ube3a*$^{mat-/pat+}$) were tested alongside wildtype littermate controls (*Ube3a*$^{mat+/pat+}$).

Animals were given identifying marks as pups and again at weaning as previously described[34]. A small tissue sample collected on postnatal day 2 was used to genotype each subject following a previously reported protocol[34]. As multiple independent labs have found sex differences in the rat model to be not significant[33,34], and this aligns with the equal incidence rates of AS across sex in humans, mixed-sex cohorts were utilized for the present study. Three independently generated cohorts of rats were used: Cohort 1 was sampled from 6 litters and tested at 3 months of age; Cohort 2 was sampled from 7 litters and tested at 4-5 weeks of age; and Cohort 3 was sampled from 9 litters and tested at 6-8 weeks of age.

Rat *Ube3a-ATS* antisense oligonucleotides (ASOs). Single strand oligonucleotides were used to bind the RNA transcript antisense to *Ube3a* (*Ube3a-ATS*) that is responsible for the silencing of paternal *UBE3A*. The efficacy of two rat-specific oligonucleotides, termed ASO 1.1 and 3.1, were compared. The sequences of the ASOs were designed to be complementary to, and therefore target, different sites along *Ube3a-ATS*. Based on the results from Cohort 1, subsequent cohorts focused solely on ASO 3.1. Lyophilized ASO (ChemGenes, Wilmington, MA) was resuspended in sterile endotoxin-free saline. Saline solely constituted the vehicle for Cohorts 1 and 2 whereas artificial cerebrospinal fluid (aCSF; Harvard Apparatus, Holliston, MA) was used as the vehicle for Cohort 3. Therefore, for Cohort 3, 25 μL saline per mg ASO was used for resuspension

and the remainder of the solution consisted of aCSF. Initial doses of ASO were selected based on previous dosing regimens used in non-human primates and mice (data unpublished).

Routes of ASO administration. *Intracisterna magna (ICM) injection*. Cohort 1 was administered ASO (50 or 75 μg of ASO 1.1 or 3.1) or vehicle (saline) via ICM injection. Rats were anesthetized and placed into a stereotaxic frame with the head angled downward. A small incision at the base of the head was made and 10 μL of ASO or vehicle was injected into the cisterna magna using a 100 μL syringe (Hamilton Company, Reno, NV) at a rate of 30 μL per 30 sec. The needle was left in place for 30 sec before being slowly removed and the incision was sutured. Carprofen (Rimadyl; Zoetis, Parsippany-Troy Hills, NJ) was used for management of post-operative pain.

Intracerebroventricular (ICV) injection. Cohort 2 was administered ASO (75, 120, 180, or 300 μg of ASO 3.1) or vehicle (saline) via bilateral ICV injection. Rats were anesthetized and placed into a stereotaxic frame with the head positioned lateral to the base of the frame. The skull was exposed, and a surgical drill was used to create two burr holes at 1.0 mm posterior and ±1.5 mm lateral to bregma. Through each burr hole, a 10 μL Neuros syringe (Hamilton) was lowered to a depth of 3.5 mm and delivered 2.5 μL of ASO or vehicle at a rate of 1 μL per 30 sec. For each injection, the needle was left in place for 1 min before being slowly withdrawn. Burr holes were filled with bone wax (CP Medical Inc., Norcross, GA) before the incision was sutured. Carprofen (Zoetis) was administered to manage post-operative pain.

Intrathecal (IT) injection. Cohort 3 was administered ASO (300 or 400 μg of ASO 3.1) or vehicle (aCSF) via IT injection. Rats were anesthetized and positioned in the prone position over a 50 mL Falcon tube in order to arch the lumbosacral area. A small incision was made and 40 μL of ASO or vehicle was injected into the intrathecal space between the sixth lumbar (L6) and first

sacral (S1) vertebrae using a 100 μL syringe (Hamilton) at a rate of 30 μL per 30 sec. The needle remained in place for 30 sec before being withdrawn slowly and the incision was sutured. Carprofen (Rimadyl; Bio-Serv, Flemington, NJ) was provided for post-operative pain management.

Molecular analyses. *Tissue extraction.* Two weeks following ASO administration, rats were anesthetized, CSF was collected from the cisterna magna, and rats were cervically dislocated. For fresh tissue collection, brains were rapidly extracted and the CSF, brain tissue, and a sample of liver as a peripheral tissue control were placed into individual tubes and flash frozen over dry ice. Brain tissue was later homogenized and separated for genomic DNA, RNA, or protein. For eventual histological evaluation, a subset of tissue was fixed using 4% paraformaldehyde (PFA). For Cohort 1, one brain hemisphere per rat was fixed in 4% PFA. For a subset of Cohort 2, CSF was collected from the cisterna magna, a liver sample was retrieved, and rats were immediately transcardially perfused with cold 1X phosphate-buffered saline containing 10 U/mL heparin followed by 4% PFA. The CSF and liver sample were flash frozen over dry ice, while the fixed brain was cryopreserved via 30% sucrose soak.

Quantitative polymerase chain reaction (qPCR). For Cohort 1, total RNA was isolated using the Direct-zol RNA Miniprep Kit (ZymoResearch, Irvine, CA). RNA was reverse transcribed using the SuperScript VILO MasterMix (Invitrogen, Carlsbad, CA). *Ube3a-ATS* expression was measured by RT-qPCR and *Ube3a* expression was determined by Taqman. All reactions were performed in triplicate. RT-qPCR was performed using 2× iQ SYBR mix (Bio-Rad, Hercules, CA) with the CFX384 Real-Time System C1000 Touch system (Bio-Rad). Gene expression analysis was performed with *Pgk1* as a reference gene using at least three biological

replicates and the following primer sequences: rat *Ube3a-ATS* primers (rUbe3a-AS_qF1 5'-AGTTACCACCTGCAAGGAGC -3'; rUbe3a-AS_qR1 5'-ACTGATCCCTGTGTCTCTTAGGT -3'), rat *Pgk1* primers (Pgk1_qF 5'-CTTTGGACAAGCTGGACGTG -3'; Pgk1_qR 5'- ACAACCGACTTGGCTCCATT -3'). Taqman reaction was performed using TaqMan Fast Advanced Master Mix (Applied Biosystems, Foster City, CA) with the following primer/probe mixes: Ube3a Rn01409804_m1 (labeled with FAM) and Pgk1 Rn00821429_g1 (labeled with VIC). RT-qPCR and Taqman reactions were executed with the CFX384 Real-Time System C1000 Touch system (Bio-Rad) and gene expression analysis was performed with *Pgk1* as the reference gene. Relative target gene expression was calculated as the difference between the target gene and the reference gene (dCq = Cq[target]-Cq[Pgk1]). Data are presented as ΔΔCt normalized to *Ube3a*$^{mat-/pat+}$ vehicle.

For Cohort 2, tissue was immersed in 350 µl of Trizol and sonicated using a QSonica (QSonica, Newtown, CT). Sonicated tissue was then centrifuged at 10,000 rcf and supernatant was removed and incubated with an equivalent volume of 100% molecular grade ethanol. Total RNA then was extracted following Direct-zol RNA Extraction (ZymoResearch). cDNA was generated using RevertAid Random Hexamer (ThermoFisher, Waltham, MA). SYBR Green (ThermoFisher) based quantitative real-time PCR was performed using 10 ng of cDNA on a QuantStudio 6 Flex (Applied Biosystems). The *Ube3a-ATS* primers used were: Forward 5'-AGTTACCACCTGCAAGGAGC -3'; Reverse 5'- ACTGATCCCTGTGTCTCTTAGGT-3'. Data are presented as ΔΔCt normalized to wildtype vehicle.

Western blots. Protein was extracted using Pierce RIPA Buffer (ThermoFisher) with Protease & Phosphatase Inhibitor Cocktail (ThermoFisher). Protein concentrations were measured using Pierce Bicinchoninic acid assay kit (ThermoFisher). Forty micrograms of protein lysate were

separated on a 4-20% Stacking TGX Gels (BioRad) and transferred overnight at 30 V onto Immobilon-FL PVDF membrane (Millipore Sigma, Burlington, MA). PVDF membranes were blocked for 1 hr with Intercept Protein-Free Blocking Buffer (LI-COR, Lincoln, NE). Following blocking, PVDF membranes were incubated with ms-Ube3a (1:1000, Millipore Sigma, E8655) and rb-beta actin (1:2000, Millipore Sigma, SAB5600204) in Intercept for 2 hrs at room temperature. Following incubation, membranes were washed with Tris-buffered saline with Tween (TBST) 3X for 5 min. Membranes were then incubated with Goat anti-rabbit LI-COR 680 (1:2000) and goat anti-mouse LI-COR 800 (1:2000) in Intercept TBS for 1 hr at RT. Following incubation, membranes were washed 3X with TBST before storing in 1X TBS. Membranes were imaged on Odyssey CLx imager (LI-COR). Quantitative analysis was performed using Empiria Studio software (LI-COR).

Statistical analyses. All statistical analyses were performed using Prism 9 software (GraphPad Software, San Diego, CA). All significance levels were set at $p < 0.05$ and tests were two-tailed. Repeated measures ANOVAs or mixed-effects models were used for comparisons across time (i.e., weight). One-way ANOVAs were used to analyze the effect of treatment on a single parameter. Two-way ANOVAs were used to analyze the effects of both genotype and ASO treatment. Sidak's multiple comparisons *post hoc* tests were used to detect differences between specific groups. Dunnett's multiple comparisons *post hoc* test was used to detect differences from the vehicle group. Data are presented as mean ± standard error of the mean (S.E.M.) unless otherwise noted and group sizes are depicted by individual data points or provided in figure legends.

Results

We assessed whether CNS administration of two novel ASOs targeted to knock down *Ube3a-ATS* was generally tolerated by rats, as well as differentially tolerated by *Ube3a*$^{mat-/pat+}$ rats compared to wildtype littermate controls, and whether ASO treatment showed molecular efficacy in the brain. In general, we found that the ASO compounds, doses, and routes of administration tested were tolerable by both genotypes, with a few exceptions in which subjects died within 12 hours after receiving ASO. Taking into account all ten iterations of ASO administration, *Ube3a*$^{mat-/pat+}$ rats showed the same susceptibility to post-ASO mortality as wildtype littermates (Wilcoxon matched-pairs signed rank test: $W = -2.000$, $p = 0.875$).

Intracisterna magna administration of *Ube3a-ATS* antisense oligonucleotides. ICM administration of 50 and 75 µg of ASO 1.1 or 3.1 were generally well-tolerated. Out of 31 animals injected, only 1 subject (*Ube3a*$^{mat-/pat+}$ administered 75 µg of ASO 1.1) died (**Table 1**). Overall mortality was therefore 0% for the ICM procedure based on vehicle group survival, 0% for ASO 3.1, but 20% for ASO 1.1. After receiving ASO or vehicle, *Ube3a*$^{mat-/pat+}$ rats and wildtype littermates were monitored and weighed daily to check for major adverse effects on general health. Neither wildtype (**Figure 2B**; $F_{Treatment(T)}$ (4, 6) = 2.220, $p = 0.183$; $F_{Day(D)}$ (1.945, 11.67) = 34.15, $p < 0.0001$; $F_{T\times D}$ (44, 66) = 0.9931, $p = 0.503$) nor *Ube3a*$^{mat-/pat+}$ rats (**Figure 2C**; F_T (4, 14) = 0.7005, $p = 0.604$; F_D (1.423, 19.92) = 16.57, $p < 0.001$; $F_{T\times D}$ (44, 154) = 1.282, $p = 0.138$) displayed any robust changes in body weight as a result of ICM ASO treatment. Across all doses of ASO, *Ube3a*$^{mat-/pat+}$ rats did not show a difference in ICM ASO tolerability compared to wildtype as measured by percent weight change within the acute post-injection period: wildtypes gained an average of 5% body weight from pre-injection baseline to one-week post-injection and

Ube3a$^{mat-/pat+}$ rats gained an average of 2% in the same time frame (Student's *t*-test: t (23) = 1.200, p = 0.242).

Molecular analysis of RNA and protein following intracisterna magna administration of *Ube3a-ATS* antisense oligonucleotides. Two weeks after ICM delivery of ASO, we quantified expression of *Ube3a-ATS* RNA, *Ube3a* RNA, and UBE3A protein in the cortex and cerebellum. In the cortex, treatment with ASO did not change levels of *Ube3a-ATS* (**Figure 3A**; $F_{Treatment(T)}$ (4, 14) = 2.057, p = 0.141) or *Ube3a* RNA expression (**Figure 3B**; F_T (4, 14) = 1.678, p = 0.211) in either *Ube3a*$^{mat-/pat+}$ rats or wildtype littermates. Trends, however, revealed the most promising dose to be 75 µg ASO 3.1, although it did not markedly affect UBE3A protein levels (**Figure 3D**; F_T (1, 5) = 0.08459, p = 0.783; $F_{Genotype(G)}$ (1, 5) = 269.7, p < 0.0001; $F_{T\times G}$ (1, 5) = 2.180, p = 0.200). As expected, Western blot revealed *Ube3a*$^{mat-/pat+}$ rats to exhibit robust reductions in UBE3A protein in the cortex compared to wildtype (Sidak's multiple comparisons: vehicle, p = 0.0001; 75 µg 3.1, p = 0.0002).

In the cerebellum, ASO treatment did not notably influence expression of *Ube3a-ATS* (**Figure 3E**; F_T (4, 14) = 2.232, p = 0.118) or *Ube3a* RNA (**Figure 3F**; F_T (4, 14) = 2.017, p = 0.147). UBE3A protein levels, however, were moderately increased by 75 µg ASO 3.1 in wildtype rats (**Figure 3H**; F_T (1, 5) = 381.7, p < 0.0001; F_G (1, 5) = 24.52, p = 0.004; $F_{T\times G}$ (1, 5) = 20.60, p = 0.006; Sidak's multiple comparisons: *Ube3a*$^{mat+/pat+}$, p = 0.003). Cerebellar UBE3A in *Ube3a*$^{mat-/pat+}$ rats was unaffected by treatment, although the expected protein deficiency was found compared to wildtype (Sidak's multiple comparisons: *Ube3a*$^{mat+/pat+}$ vs. *Ube3a*$^{mat-/pat+}$, vehicle, p < 0.001; 75 µg 3.1, p < 0.0001). The favorable trend of 75 µg ASO 3.1 to both reduce cortical *Ube3a-*

ATS and elevate UBE3A expression in the cortex and cerebellum of *Ube3a*$^{mat-/pat+}$ rats prompted our investigation of this ASO molecule in subsequent testing.

Intracerebroventricular administration of *Ube3a-ATS* antisense oligonucleotides. Given the trend for 75 µg ASO 3.1 to reduce expression of *Ube3a-ATS* and increase *Ube3a* RNA, we focused our efforts on ASO 3.1 at doses of 75 µg and higher. Additionally, we sought out greater efficacy by administering ASO at the juvenile age rather than in adulthood. We found that *Ube3a*$^{mat-/pat+}$ rats showed normal susceptibility to death following ICV ASO administration: out of 40 animals injected, 1 subject (wildtype) administered 180 µg ASO 3.1 and 3 subjects (2 wildtype, 1 *Ube3a*$^{mat-/pat+}$) administered 300 µg of ASO 3.1 died (**Table 2**). Mortality was therefore 0% for the ICV procedure based on vehicle group survival, 0% for 75 µg, 0% for 120 µg, but 12.5% for 180 µg, and 37.5% for 300 µg ASO 3.1. Across modes of delivery for 75 µg ASO 3.1, ICM and ICV both showed full tolerance (i.e., no mortality).

ICV delivery of ASO 3.1 had no major effects on general health or post-injection weight for wildtypes (**Figure 4B**; $F_{Treatment(T)}$ (4, 7) = 0.2664, p = 0.891; $F_{Day(D)}$ (1.118, 7.827) = 70.40, p < 0.0001; $F_{T\times D}$ (52, 91) = 0.08485, p > 0.9999) or *Ube3a*$^{mat-/pat+}$ rats (**Figure 4C**; F_T (1.358, 25.81) = 216.5, p < 0.0001; F_D (4, 19) = 1.830, p = 0.165; $F_{T\times D}$ (52, 247) = 0.8873, p = 0.691). And, in line with normal mortality rates, ICV ASO 3.1 tolerability was comparable across genotypes as measured by percent weight change across the acute post-injection period: wildtypes gained an average of 28% body weight from baseline to one-week post-injection and *Ube3a*$^{mat-/pat+}$ rats gained an average of 26% (Student's *t*-test: t (26) = 0.5946, p = 0.557).

Two weeks following administration of 300 µg ASO 3.1, we detected reduced expression of *Ube3a-ATS* RNA in the cerebrum of *Ube3a*$^{mat-/pat+}$ rats compared to vehicle (**Figure 4D**; F_T (4,

5) = 5.700, $p = 0.042$; F_G (1, 5) = 0.1983, $p = 0.675$; $F_{T\times G}$ (4, 5) = 0.7426, $p = 0.602$; Dunnett's multiple comparisons test: *Ube3a*$^{mat-/pat+}$ vehicle vs. 300 μg 3.1, $p = 0.042$). We did not observe alterations in *Ube3a-ATS* RNA in the cerebellum (**Figure 4E**; F_T (4, 5) = 4.633, $p = 0.062$; F_G (1, 5) = 2.838, $p = 0.153$; $F_{T\times G}$ (4, 5) = 2.988, $p = 0.131$).

Intrathecal administration of *Ube3a-ATS* antisense oligonucleotides. IT administration of ASOs represents the most translational route of delivery, as it mimics the lumbar puncture procedure used to administer ASOs to humans. We therefore sought to investigate the tolerability of this route in rats, which is feasibly higher compared to other modes due to the larger allowable injection volume and therefore less concentrated dosage. Indeed, we found that IT delivery showed improved tolerance and led to lower mortality compared to ICV delivery for the same dose (300 μg ASO 3.1): only 8.3% mortality for IT versus 37.5% mortality following ICV. *Ube3a*$^{mat-/pat+}$ rats appeared to show a greater susceptibility to mortality following the higher (400 μg) ASO dose compared to wildtypes, with 37.5% mortality in *Ube3a*$^{mat-/pat+}$ but 0% in wildtypes (**Table 3**). Of the 36 total animals injected, 1 rat administered 300 μg ASO (wildtype) and 3 rats administered 400 μg ASO (2 wildtype, 1 *Ube3a*$^{mat-/pat+}$) died. Overall mortality was therefore 0% for the IT procedure based on vehicle group survival, 8.3% for 300 μg, and 21.4% for 400 μg ASO 3.1.

IT injection of ASO 3.1 did not affect general health as indicated by body weight changes in wildtype (**Figure 5B**; $F_{Treatment(T)}$ (2, 13) =0.0166, $p = 0.984$; $F_{Day(D)}$ (1.671, 24.55) = 103.8, $p < 0.0001$) or *Ube3a*$^{mat-/pat+}$ rats (**Figure 5C**; F_T (2, 13) = 0.2647, $p = 0.771$; F_D (13, 195) = 111.5, $p < 0.0001$) in the two weeks following the injection. This was unconfounded by baseline pre-injection weights, which did not differ across the ASO treatment groups (Student's *t*-test: t (20) = 0.8771, $p = 0.391$) or by differences in pre-injection weights between those that died after and

those that survived the 400 µg dose (Student's *t*-test: $t\,(12) = 0.5526$, $p = 0.611$). Across both doses of ASO, *Ube3a*$^{mat-/pat+}$ rats did not exhibit differential tolerability to IT ASO 3.1 relative to wildtype as measured by percent weight change across the acute post-injection period: both wildtypes and *Ube3a*$^{mat-/pat+}$ rats gained an average of 10% body weight from baseline to one-week post-injection (Student's *t*-test: $t\,(20) = 0.3669$, $p = 0.718$).

Discussion

Despite the cause of AS being known for decades and various therapeutic strategies being investigated in that time, there is still no gene-specific treatment available to those with AS. The seemingly most targeted and promising treatment approach would be to compensate for the dysfunctional maternal allele of *UBE3A* by providing an alternative source of active UBE3A protein to neurons. This could be achieved via numerous mechanisms, including delivery of UBE3A to the brain using viral vectors[10] or stem cells[38], or by unsilencing the paternal allele of *UBE3A*[30,31,39]. Viral vectors have shown some efficacy in the mouse model of AS[10,39], but their implementation poses several methodological challenges. These include achieving adequate biodistribution, selecting an appropriate promoter and protein isoform(s), providing multiple isoforms, and delivering appropriate amounts of UBE3A to each cell over time[30,40]. Functional levels of UBE3A fall within a relatively narrow range, as overexpression of UBE3A is associated with other neurodevelopmental disorders including Duplication 15q syndrome and autism spectrum disorders[41].

Unsilencing the paternal allele offers a therapeutic approach to restoring UBE3A levels without this risk of overexpression, as it leverages the intact paternal copy of UBE3A already present in the neurons of those with AS[30]. Since the paternal allele is silenced by a long non-coding

RNA transcript that overlaps and is antisense to *UBE3A*[42,43] (*Ube3a-ATS*) numerous strategies are currently being pursued to inactivate or downregulate this transcript. Disruption of *Ube3a-ATS*, either via transcriptional truncation[44] or Cas9 targeting[39], improved behavioral deficits in mouse models of AS and the binding of *Ube3a-ATS* by an artificial transcriptional repressor led to partial unsilencing of the paternal allele in mice[45]. Topoisomerase inhibitors, and topotecan in particular, have also shown efficacy in downregulating *Ube3a-ATS* expression and unsilencing the paternal allele[18]. However, topoisomerase inhibitors, which are widely used as chemotherapeutics, are not targeted compounds and therefore carry high risk of off target effects due to inhibition of other transcripts, among other mechanisms.

On the other hand, ASOs provide a much greater degree of specificity because they are custom designed to the sequence to be targeted. Compared to viral-mediated therapies, ASOs offer several advantages and are not subject to many of the aforementioned limitations (e.g., biodistribution, control of protein level). ASOs are delivered to the CNS via injection into the CSF, as they do not cross the blood brain barrier, and the natural dynamics of CSF flow help to broadly distribute ASOs throughout the CNS[19]. Their small size (typically 18-20 bases; 6-8 kDa) and water solubility aids in their circulation, and ASOs are readily taken up by neurons[19,30]. An additional advantage to ASO therapeutics is their broad applicability across the AS population. Although the specific genetic disruption to maternal *UBE3A* differs between AS individuals, restored expression of neuronal UBE3A would be expected to benefit all patients, across age groups. One of the main limitations to ASO therapies is that they do not result in a permanent change. Over time, ASOs get endogenously degraded and therefore must be administered every few months, which is not ideal for a genetic disorder that lasts a lifetime[19,29,40].

Despite this limitation, however, ASOs have demonstrated profound efficacy in the treatment of other genetic disorders. The resounding success of the ASO nusinersen (Spinraza) for the treatment of spinal muscular atrophy set a promising precedent for the application of ASOs to AS[19,20,30,46]. Using a mouse model of AS, Meng et al. (2014) found that a single intracerebroventricular (ICV) injection of an ASO targeted to the mouse *Ube3a-ATS* showed good biodistribution and moderate unsilencing of the paternal allele[31]. And now, in 2021, there are currently two active clinical trials (NCT04428281: Roche/Genentech, compound RO7248824; NCT04259281: GeneTx/Ultragenyx, compound GTX-102) and one starting soon (Ionis/Biogen) in which ASOs are being administered to patients with AS. Both of the active clinical trials, still in Phase I, are largely focused on evaluating the safety and tolerability of ASOs. The occurrence of a serious adverse event in one of the current trials prompted us to establish an *in vivo* model of ASO administration by which an AS population could be compared to a control population.

The present evaluation of ASO administration in the *Ube3a*$^{mat-/pat+}$ rat represents the first report of ICM- and IT-delivered ASOs in an animal model of AS, and of the first gene reactivation treatment in the rat model of AS. Though ICM administration of two candidate ASOs, we were able to identify the more promising compound and, via ICV delivery, we narrowed in on an effective dose range for rats. The comparable ASO tolerances observed between the AS model and wildtype littermates will be informative for ongoing clinical trials, which are limited by their inability to assess safety and tolerance in neurotypical subjects. Furthermore, we uncovered favorable evidence that our ASO 3.1 is capable of knocking down *Ube3a-ATS* in the brain, highlighting its potential to unsilence the paternal *Ube3a* allele.

Compared to administration of ASO through ICV injection, IT delivery was revealed to have enhanced tolerability, which is encouraging with regard to the general translation of ASO

research in animal models to humans. ICV is a common mode of CNS delivery in animals, as it is performed precisely via a stereotactic frame and can therefore be readily achieved in small animals such as mice. Although IT is the route of administration used in humans, it is much more difficult to perform in small animals. Therefore, for work in animal models that demonstrates ASO efficacy via ICV, lack of full tolerability may not pose a significant issue. Future studies, however, should more deeply elucidate the relationship between modes of delivery by comparing molecular efficacy in addition to tolerability.

While we did not observe significant hindlimb weakness resembling the SAE observed in the clinical trial, future work will seek to elicit this phenotype in the rat by utilizing higher and/or more frequent intrathecal doses. The SAE seen clinically may be the result of accumulated ASO doses and therefore may only manifest with a repeated dosing paradigm. To enhance our ability to detect the phenotype, an extended post-injection observation period can be used, including assays to quantify motor functioning. Since the rat model exhibits deficits in open field rearing activity, gait, and accelerating rotarod, these tests can be leveraged to probe for ASO-related hindlimb weakness and/or behavioral improvements. Modeling the clinical SAE in the rat will allow for detailed inspections into the physiological cause that are not possible in living AS patients and can help determine which factors of the clinical trial ASO administration (e.g., dosage, timing, etc.) should be altered to best avoid the SAE without substantial loss of efficacy.

It is important to note that the generalizability of the present findings to human applications is considerably limited, as we utilized rat specific ASOs and each ASO compound elicits different biochemical responses *in vivo*. Neither the mortality rates nor specific doses used here in rats should be directly translated to humans, thus mortality was not a major deterrence in our pursuit of an effective ASO for rats. However, our development of an *in vivo* AS model of IT ASO-

mediated paternal allele unsilencing is expected to open up numerous avenues for future investigation with important clinical implications. Preeminently, an extremely important and therefore heavily deliberated topic revolves around the timing of treatment[30,39,40,47–50]. The ability to perform precisely timed IT injections of an effective ASO in *Ube3a*$^{mat-/pat+}$ and wildtype controls will help shed light on the necessity to deliver treatment before critical periods of development, as well as how frequently it should be delivered.

Meng et al. (2014) found that, in a mouse model of AS, a single ICV dose of ASO reduced *Ube3a-ATS* for several months, but that levels returned to baseline after 20 weeks[31]. Interestingly, despite a well-tolerated ASO, successful and sustained knockdown of *Ube3a-ATS,* and evidence for unsilencing of the paternal allele, the Meng et al. study did not observe substantial improvement of the model's behavioral deficits. Hypothesized reasons for this included the timing of treatment being late, time allotted for recovery and therefore neural circuitry rewiring being short, and induced UBE3A protein levels being insufficient. Future collection of behavioral metrics in the rat model following ASO administration can help to elucidate the relationships between all of these variables, molecular efficacy, and behavioral rescue.

In addition to behavior, future histological analyses can help to reveal whether AS model rats show increased susceptibility to ASO toxicity on a cellular level. Acutely, ASOs can elicit adverse effects through their affinity for non-RNA molecules. By chelating calcium ions in the CSF and by binding to cell surface receptors, ASOs can disrupt cell signaling and neurotransmission[51]. ASOs can also produce adverse outcomes through liver toxicity, binding off-target RNAs, and activating the immune system either by being recognized as foreign DNA or causing uncontrolled amplification of the complement cascade[51–53]. Local overexpression of UBE3A around the spinal cord may also lead to cellular toxicity and negatively impact the ability

of dorsal root ganglia to transmit sensory information[54,55]. Although the present findings only indicated infrequent acute toxicity, potentially due to liver toxicity or complement cascade activation, the current study's evaluation of ASO tolerance was limited to gross measures of mortality and body weight. Therefore, detailed analyses on the microscopic scale can help to delineate if certain types of toxicities may pose safety concerns to the AS population and elucidate which type(s) contributed to the clinical SAE.

ASO tolerability, distribution, and duration of action are also of interest to many other areas of biomedical research, as ASOs offer a viable therapeutic strategy for numerous CNS diseases. Aside from AS, there are currently eight antisense drugs, all delivered intrathecally, being tested in clinical trials for neurological disorders and many more drug discovery programs seeking potential antisense therapies[19]. As highlighted by the unexpected SAE of the AS clinical trial, ASOs remain a developing technology and implementation strategies are still evolving. Preclinical models with high construct and face validity to the human disorder, such as the rat model of AS, will be invaluable tools in the ongoing characterization of ASO activity *in vivo*, which will ultimately improve our ability to bring any ASO into the clinic safely and effectively.

Figures

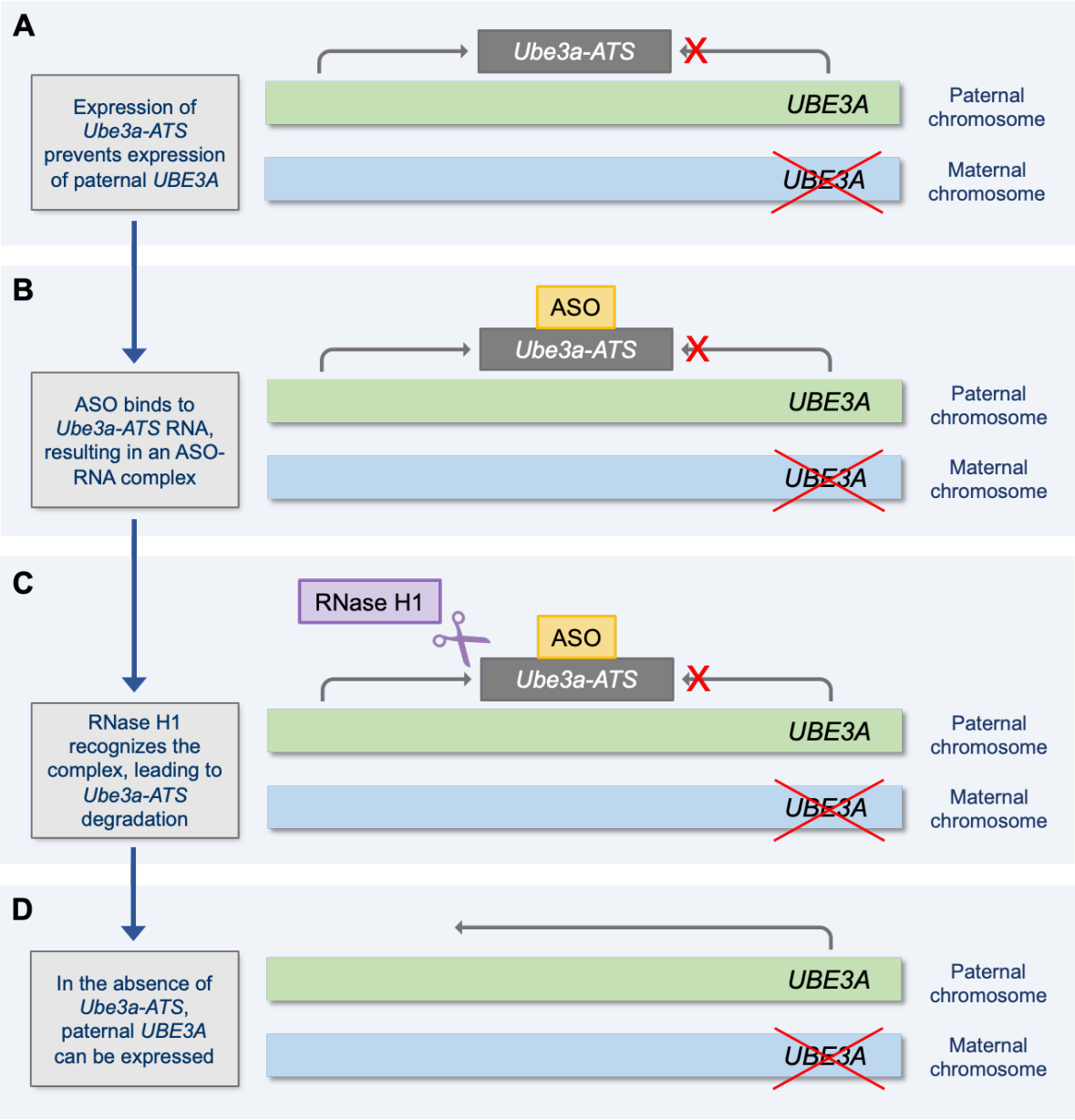

Figure 1. Schematic depicting the mechanism underlying antisense oligonucleotide (ASO) therapy for Angelman Syndrome (AS). **(A)** The normal silencing of paternal *UBE3A* in neurons is maintained by expression of a competing transcript that runs antisense to *UBE3A*, called *Ube3a-ATS*. Dysfunction of maternal *UBE3A*, as occurs in AS, therefore results in the loss of functional UBE3A protein in the brain. **(B)** Injection of an ASO with a sequence complementary to *Ube3a-ATS* RNA results in the ASO binding *Ube3a-ATS*. **(C)** The ASO-RNA complex is recognized by a protein called RNase H1, which leads to the degradation of *Ube3a-ATS* RNA. The DNA-based ASO is left intact and made available to bind additional *Ube3a-ATS* transcripts. **(D)** Without interference by *Ube3a-ATS*, the paternal allele of *UBE3A* can be expressed, providing a source of active UBE3A protein to neurons.

Table 1. Mortality rates for ASO delivered via intracisterna magna injection.

		Vehicle	ASO 1.1		ASO 3.1	
		10 µL	50 µg	75 µg	50 µg	75 µg
Ube3a$^{mat+/pat+}$	Injected	2	3	2	2	2
	Died	0	0	0	0	0
	% Mortality	0	0	0	0	0
Ube3a$^{mat-/pat+}$	Injected	3	5	3	5	4
	Died	0	0	1	0	0
	% Mortality	0	0	**33.3**	0	0
Combined	Injected	5	8	5	7	6
	Died	0	0	1	0	0
	% Mortality	0	0	**20**	0	0

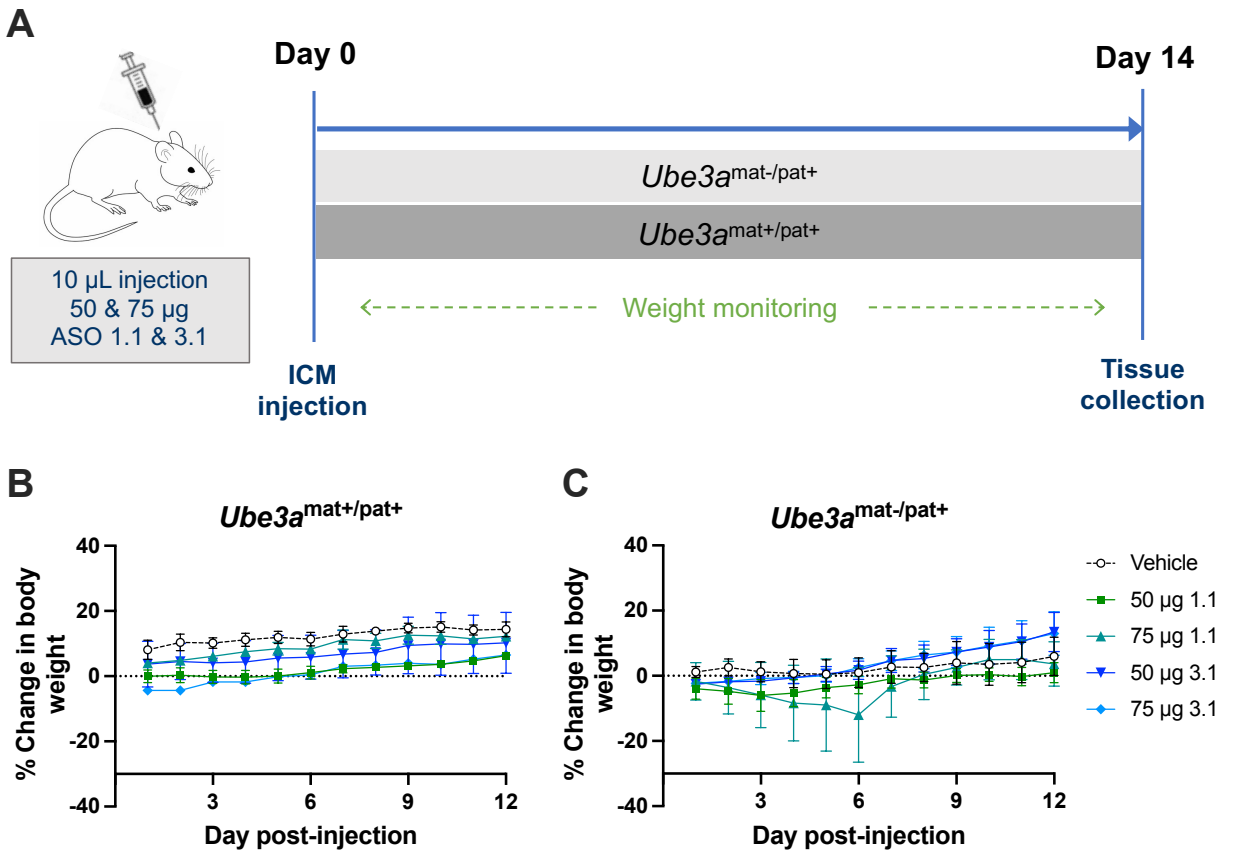

Figure 2. Intracisterna magna administration of *Ube3a-ATS* antisense oligonucleotides (ASOs). **(A)** Experimental design for administration of ASO 1.1 and 3.1 into the cisterna magna of *Ube3a*$^{mat-/pat+}$ rats (n = 19) and wildtype littermates (*Ube3a*$^{mat+/pat+}$; n = 11). **(B)** Changes in body weight following the injection did not differ between treatment groups for either wildtype or **(C)** *Ube3a*$^{mat-/pat+}$ rats. Data are expressed as mean ± S.E.M.

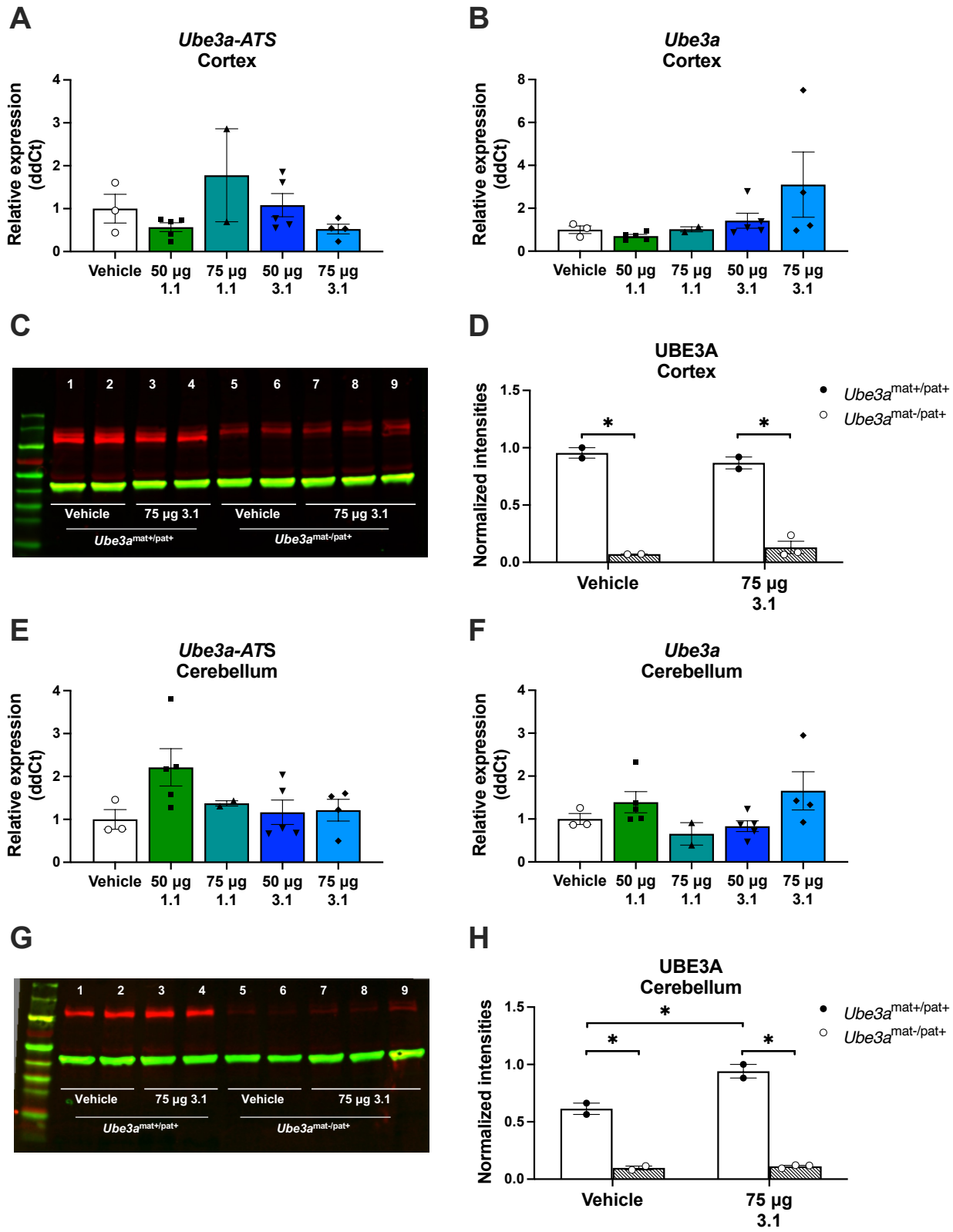

Figure 3. Molecular analysis of RNA and protein following intracisterna magna administration of *Ube3a-ATS* antisense oligonucleotides (ASOs). **(A)** Expression of the *Ube3a* antisense transcript

(*Ube3a-ATS*) RNA and **(B)** expression of *Ube3a* RNA in the cortex were not affected by ASO treatment in *Ube3a*$^{mat-/pat+}$ rats. **(C)** Western blot analysis of cortical UBE3A protein expression in *Ube3a*$^{mat-/pat+}$ rats and wildtype littermates (*Ube3a*$^{mat+/pat+}$) treated with 75 μg ASO 3.1. **(D)** Quantification of the blot revealed *Ube3a*$^{mat-/pat+}$ rats to have deficient UBE3A levels compared to wildtype, but no influence of ASO treatment. **(E)** Expression of *Ube3a-ATS* RNA and **(F)** expression of *Ube3a* RNA in the cerebellum of *Ube3a*$^{mat-/pat+}$ rats were not altered by ASO treatment. **(G)** Western blot analysis of cerebellar UBE3A protein expression in *Ube3a*$^{mat-/pat+}$ and wildtype rats treated with 75 μg ASO 3.1. **(H)** Western blot quantification illustrated deficient UBE3A protein levels in *Ube3a*$^{mat-/pat+}$ rats, and increased UBE3A expression in wildtype treated with 75 μg ASO 3.1 compared to vehicle. Data are expressed as mean ± S.E.M. $*p < 0.05$, Sidak's multiple comparisons test following two-way ANOVA.

Table 2. Mortality rates for ASO 3.1 administered by intracerebroventricular injection.

		Vehicle	ASO 3.1			
		5 µL	75 µg	120 µg	180 µg	300 µg
Ube3a$^{mat+/pat+}$	Injected	3	3	3	3	3
	Died	0	0	0	1	2
	% Mortality	0	0	0	**33.3**	**66.7**
Ube3a$^{mat-/pat+}$	Injected	5	5	5	5	5
	Died	0	0	0	0	1
	% Mortality	0	0	0	0	**20**
Combined	Injected	8	8	8	8	8
	Died	0	0	0	1	3
	% Mortality	0	0	0	**12.5**	**37.5**

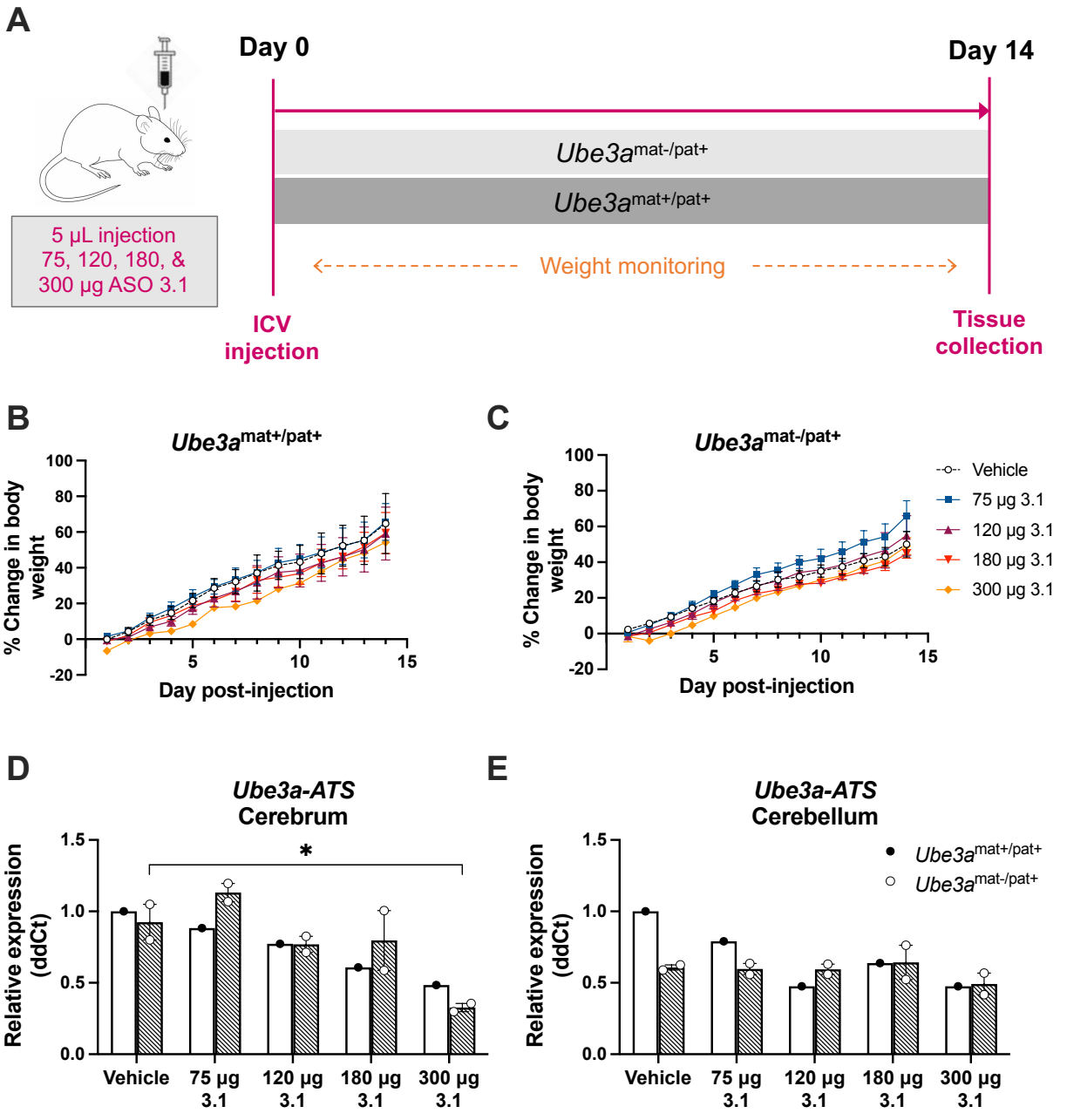

Figure 4. Intracerebroventricular administration of *Ube3a-ATS* antisense oligonucleotides (ASO). **(A)** Experimental design for administration of ASO 3.1 into the lateral ventricles of *Ube3a*$^{mat-/pat+}$ rats (n = 24) and wildtype littermates (*Ube3a*$^{mat+/pat+}$; n = 12). **(B)** Changes in body weight following the injection did not differ across treatment groups in either wildtype or **(C)** *Ube3a*$^{mat-/pat+}$ rats. **(D)** Expression of the *Ube3a* antisense transcript (*Ube3a-ATS*) in the cerebrum was reduced in *Ube3a*$^{mat-/pat+}$ rats treated with 300 µg ASO 3.1 relative to vehicle. **(E)** Cerebellar expression of *Ube3a-ATS* was unaffected by treatment with ASO. Data are expressed as mean ± S.E.M. *$p < 0.05$, Dunnett's multiple comparisons test following two-way ANOVA.

Table 3. Mortality rates for intrathecal injection of ASO 3.1.

		Vehicle	ASO 3.1	
		40 µL	300 µg	400 µg
Ube3a$^{mat+/pat+}$	Injected	5	6	6
	Died	0	1	0
	% Mortality	0	**16.7**	0
Ube3a$^{mat-/pat+}$	Injected	5	6	8
	Died	0	0	3
	% Mortality	0	0	**37.5**
Combined	Injected	10	12	14
	Died	0	1	3
	% Mortality	0	**8.3**	**21.4**

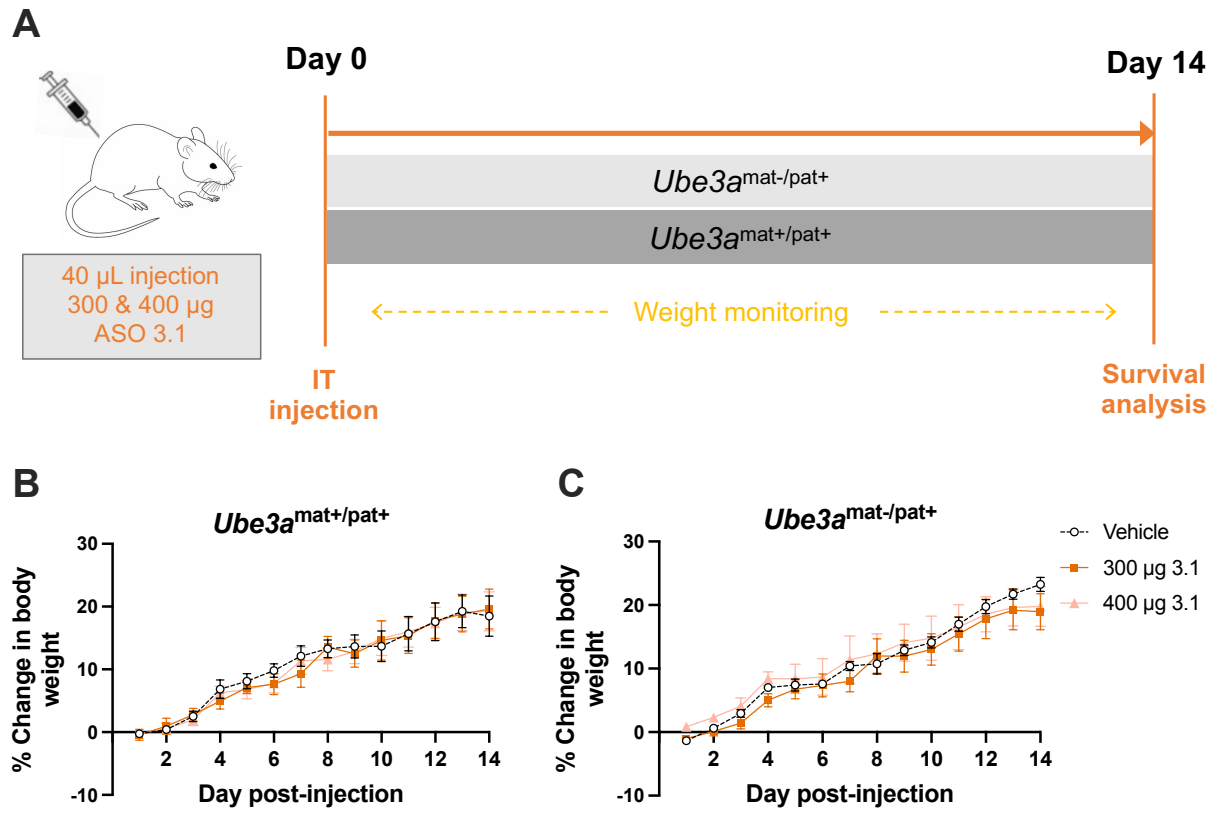

Figure 5. Intrathecal administration of *Ube3a-ATS* antisense oligonucleotides (ASO). **(A)** Experimental design for administration of ASO 3.1 into the intrathecal space of *Ube3a*$^{mat-/pat+}$ rats (n = 16) and wildtype littermates (*Ube3a*$^{mat+/pat+}$; n = 16). **(B)** Changes in body weight following the injection did not differ between treatment groups for wildtype or **(C)** *Ube3a*$^{mat-/pat+}$ rats. Data are expressed as mean ± S.E.M.

References

1. Hillman PR, Christian SGB, Doan R, Cohen ND, Konganti K, Douglas K, Wang X, Samollow PB, Dindot S V. Genomic imprinting does not reduce the dosage of UBE3A in neurons. *Epigenetics and Chromatin*. 2017;10(1):1-14. doi:10.1186/s13072-017-0134-4
2. Kishino T, Lalande M, Wagstaff J. UBE3A/E6-AP mutations cause Angelman syndrome. *Nat Genet*. 1997;15(1):70-73. doi:10.1038/ng0197-70
3. Matsuura T, Sutcliffe J, Fang P, Galjaard RJ, Jiang YH, Benton C, Rommens J, Beaudet A. De novo truncating mutations in the E6-AP ubiquitin-protein ligase gene (UBE3A) in Angelman Syndrome. *Nat Genet*. 1997;15:74-77.
4. Chamberlain SJ, Lalande M. Angelman syndrome, a genomic imprinting disorder of the brain. *J Neurosci*. 2010;30(30):9958-9963. doi:10.1523/JNEUROSCI.1728-10.2010
5. Bossuyt SN V, Punt AM, de Graaf IJ, van den Burg J, Williams MG, Heussler H, Elgersma Y, Distel B. Loss of nuclear UBE3A activity is the predominant cause of Angelman syndrome in individuals carrying UBE3A missense mutations. *Hum Mol Genet*. 2021;00(00):1-13. doi:10.1093/hmg/ddab050
6. Margolis SS, Sell GL, Zbinden MA, Bird LM. Angelman Syndrome. *Neurotherapeutics*. 2015;12(3):641-650. doi:10.1007/s13311-015-0361-y
7. Yi JJ, Ehlers MD. Ubiquitin and protein turnover in synapse function. *Neuron*. 2005;47(5):629-632. doi:10.1016/j.neuron.2005.07.008
8. Greer PL, Hanayama R, Bloodgood BL, Mardinly AR, Lipton DM, Flavell SW, Kim TK, Griffith EC, Waldon Z, Maehr R, Ploegh HL, Chowdhury S, Worley PF, Steen J, Greenberg ME. The Angelman Syndrome Protein Ube3A Regulates Synapse Development by Ubiquitinating Arc. *Cell*. 2010;140(5):704-716. doi:10.1016/j.cell.2010.01.026
9. Khatri N, Man HY. The autism and Angelman syndrome protein Ube3A/E6AP: The gene, E3 ligase ubiquitination targets and neurobiological functions. *Front Mol Neurosci*. 2019;12(April):1-12. doi:10.3389/fnmol.2019.00109
10. Daily JL, Nash K, Jinwal U, Golde T, Rogers J, Peters MM, Burdine RD, Dickey C, Banko JL, Weeber EJ. Adeno-associated virus-mediated rescue of the cognitive defects in a mouse model for Angelman syndrome. *PLoS One*. 2011;6(12). doi:10.1371/journal.pone.0027221
11. Jamal I, Kumar V, Vatsa N, Shekhar S, Singh BK, Sharma A, Jana NR. Rescue of altered HDAC activity recovers behavioural abnormalities in a mouse model of Angelman syndrome. *Neurobiol Dis*. 2017;105:99-108. doi:10.1016/j.nbd.2017.05.010
12. Mandel-Brehm C, Salogiannis J, Dhamne SC, Rotenberg A, Greenberg ME. Seizure-like activity in a juvenile Angelman syndrome mouse model is attenuated by reducing Arc expression. *Proc Natl Acad Sci U S A*. 2015;112(16):5129-5134. doi:10.1073/pnas.1504809112
13. Van Woerden GM, Harris KD, Hojjati MR, Gustin RM, Qiu S, De Avila Freire R, Jiang YH, Elgersma Y, Weeber EJ. Rescue of neurological deficits in a mouse model for Angelman syndrome by reduction of αCaMKII inhibitory phosphorylation. *Nat Neurosci*. 2007;10(3):280-282. doi:10.1038/nn1845
14. Ciarlone SL, Wang X, Rogawski MA, Weeber EJ. Effects of the synthetic neurosteroid ganaxolone on seizure activity and behavioral deficits in an Angelman syndrome mouse model. *Neuropharmacology*. 2017;116:142-150. doi:10.1016/j.neuropharm.2016.12.009
15. Kaphzan H, Hernandez P, Jung JI, Cowansage KK, Deinhardt K, Chao M V., Abel T, Klann E. Reversal of impaired hippocampal long-term potentiation and contextual fear memory

deficits in angelman syndrome model mice by ErbB inhibitors. *Biol Psychiatry*. 2012;72(3):182-190. doi:10.1016/j.biopsych.2012.01.021
16. Cruz E, Descalzi G, Steinmetz A, Scharfman HE, Katzman A, Alberini CM. CIM6P/IGF-2 Receptor Ligands Reverse Deficits in Angelman Syndrome Model Mice. *Autism Res*. Published online 2020:1-17. doi:10.1002/aur.2418
17. Schultz MN, Crawley JN. Evaluation of a TrkB agonist on spatial and motor learning in the Ube3a mouse model of Angelman syndrome. *Learn Mem*. 2020;27(9):346-354. doi:10.1101/lm.051201.119
18. Huang HS, Allen JA, Mabb AM, King IF, Miriyala J, Taylor-Blake B, Sciaky N, Dutton JW, Lee HM, Chen X, Jin J, Bridges AS, Zylka MJ, Roth BL, Philpot BD. Topoisomerase inhibitors unsilence the dormant allele of Ube3a in neurons. *Nature*. 2012;481(7380):185-191. doi:10.1038/nature10726
19. Frank Bennett C, Kordasiewicz HB, Cleveland DW. Antisense Drugs Make Sense for Neurological Diseases. *Annu Rev Pharmacol Toxicol*. 2021;61:831-852. doi:10.1146/annurev-pharmtox-010919-023738
20. Finkel RS, Chiriboga CA, Vajsar J, Day JW, Montes J, De Vivo DC, Yamashita M, Rigo F, Hung G, Schneider E, Norris DA, Xia S, Bennett CF, Bishop KM. Treatment of infantile-onset spinal muscular atrophy with nusinersen: a phase 2, open-label, dose-escalation study. *Lancet*. 2016;388(10063):3017-3026. doi:10.1016/S0140-6736(16)31408-8
21. Chiriboga CA. Nusinersen for the treatment of spinal muscular atrophy. *Expert Rev Neurother*. 2017;17(10):955-962. doi:10.1080/14737175.2017.1364159
22. Gidaro T, Servais L. Nusinersen treatment of spinal muscular atrophy: current knowledge and existing gaps. *Dev Med Child Neurol*. Published online 2018:1-7.
23. Mercuri E, Darras BT, Chiriboga CA, Day JW, Campbell C, Connolly AM, Iannaccone ST, Kirschner J, Kuntz NL, Saito K, Shieh PB, Tulinius M, Mazzone ES, Montes J, Bishop KM, Yang Q, Foster R, Gheuens S, Bennett CF, Farwell W, Schneider E, De Vivo DC, Finkel RS. Nusinersen versus Sham Control in Later-Onset Spinal Muscular Atrophy. *N Engl J Med*. 2018;378(7):625-635. doi:10.1056/nejmoa1710504
24. Tabrizi S, Leavitt B, Kordasiewicz H, Czech C, Swayze E, Norris DA, Baumann T, Gerlach I, Schobel S, Smith A, Lane R, Bennett CF. Effects of IONIS-HTTRx in Patients with Early Huntington's Disease, Results of the First HTT-Lowering Drug Trial (CT.002). *Neurology*. 2018;90.
25. Tabrizi SJ, Flower MD, Ross CA, Wild EJ. Huntington disease: new insights into molecular pathogenesis and therapeutic opportunities. *Nat Rev Neurol*. 2020;16(10):529-546. doi:10.1038/s41582-020-0389-4
26. Tabrizi SJ, Leavitt BR, Landwehrmeyer GB, Wild EJ, Saft C, Barker RA, Blair NF, Craufurd D, Priller J, Rickards H, Rosser A, Kordasiewicz HB, Czech C, Swayze EE, Norris DA, Baumann T, Gerlach I, Schobel SA, Paz E, Smith A V., Bennett CF, Lane RM. Targeting Huntingtin Expression in Patients with Huntington's Disease. *N Engl J Med*. 2019;380(24):2307-2316. doi:10.1056/nejmoa1900907
27. Smith RA, Miller TM, Yamanaka K, Monia BP, Condon TP, Hung G, Lobsiger CS, Ward CM, McAlonis-Downes M, Wei H, Wancewicz E V., Bennett CF, Cleveland DW. Antisense oligonucleotide therapy for neurodegenerative disease. *J Clin Invest*. 2006;116(8):2290-2296. doi:10.1172/JCI25424
28. Pharmaceutical U. GeneTx and Ultragenyx Announce Positive Interim Phase 1/2 Data on Investigational GTX-102 Demonstrating Improvement in Patients with Angelman

Syndrome. Published 2020. https://ir.ultragenyx.com/news-releases/news-release-details/genetx-and-ultragenyx-announce-positive-interim-phase-12-data
29. Pharmaceutical U. GeneTx and Ultragenyx Announce Presentation of Phase 1/2 Data on Investigational GTX-102 in Patients with Angelman Syndrome.
30. Elgersma Y, Sonzogni M. UBE3A reinstatement as a disease-modifying therapy for Angelman syndrome. *Dev Med Child Neurol*. Published online 2021:1-6.
31. Meng L, Ward AJ, Chun S, Bennett CF, Beaudet AL, Rigo F. Towards a therapy for Angelman syndrome by targeting a long non-coding RNA. *Nature*. 2015;518(7539):409-412. doi:10.1038/nature13975
32. Ellenbroek B, Youn J. Rodent models in neuroscience research: Is it a rat race? *DMM Dis Model Mech*. 2016;9(10):1079-1087. doi:10.1242/dmm.026120
33. Dodge A, Peters MM, Greene HE, Dietrick C, Botelho R, Chung D, Willman J, Nenninger AW, Ciarlone S, Kamath SG, Houdek P, Sumová A, Anderson AE, Dindot S V., Berg EL, O'Geen H, Segal DJ, Silverman JL, Weeber EJ, Nash KR. Generation of a Novel Rat Model of Angelman Syndrome with a Complete Ube3a Gene Deletion. *Autism Res*. Published online 2020:1-13. doi:10.1002/aur.2267
34. Berg EL, Pride MC, Petkova SP, Lee RD, Copping NA, Shen Y, Adhikari A, Fenton TA, Pedersen LR, Noakes LS, Nieman BJ, Lerch JP, Harris S, Born HA, Peters MM, Deng P, Cameron DL, Fink KD, Beitnere U, O'Geen H, Anderson AE, Dindot S V., Nash KR, Weeber EJ, Wöhr M, Ellegood J, Segal DJ, Silverman JL. Translational outcomes in a full gene deletion of ubiquitin protein ligase E3A rat model of Angelman syndrome. *Transl Psychiatry 2020 101*. 2020;10(1):1-16. doi:10.1038/s41398-020-0720-2
35. Born HA, Martinez LA, Levine AT, Harris SE, Mehra S, Lee WL, Dindot S V., Nash KR, Silverman JL, Segal DJ, Weeber EJ, Anderson AE. *Early Developmental Eeg and Seizure Phenotypes in a Full Gene Deletion of Ubiquitin Protein Ligase E3a Rat Model of Angelman Syndrome*. Vol 8.; 2021. doi:10.1523/ENEURO.0345-20.2020
36. Berg EL, Petkova SP, Born HA, Adhikari A, Anderson AE, Silverman JL. Insulin-like growth factor-2 does not improve behavioral deficits in mouse and rat models of Angelman Syndrome. *Mol Autism*.
37. Berg EL, Jami SA, Petkova SP, Berz A, Fenton TA, Lerch JP, Segal DJ, Gray JA, Ellegood J, Wöhr M, Silverman JL. Excessive laughter-like vocalizations, microcephaly, and translational outcomes in the Ube3a deletion rat model of Angelman Syndrome. *Proc Natl Acad Sci*.
38. Adhikari A, Copping NA, Beegle J, Cameron DL, Deng P, O'Geen H, Segal DJ, Fink KD, Silverman JL, Anderson JS. Functional rescue in an Angelman syndrome model following treatment with lentivector transduced hematopoietic stem cells. *Hum Mol Genet*. 2021;ddab104:1-59.
39. Wolter JM, Mao H, Fragola G, Simon JM, Krantz JL, Bazick HO, Oztemiz B, Stein JL, Zylka MJ. Cas9 gene therapy for Angelman syndrome traps Ube3a-ATS long non-coding RNA. *Nature*. 2020;587(7833):281-284. doi:10.1038/s41586-020-2835-2
40. Zylka MJ. Prenatal Treatment Path for Angelman Syndrome and Other Neurodevelopmental Disorders. *Autism Res*. 2020;13:11-17.
41. LaSalle J, Reiter L, Chamberlain S. Epigenetic regulation of UBE3A and roles in human neurodevelopmental disorders. *Epigenomics*. 2015;7(7):1213-1228. doi:10.1016/j.jvoice.2017.05.005
42. Jiang Y hui, Lev-Lehman E, Bressler J, Tsai TF, Beaudet AL. Genetics of Angelman

syndrome. *Am J Hum Genet*. 1999;65(1):1-6. doi:10.1086/302473
43. Meng L, Person RE, Beaudet AL. Ube3a-ATS is an atypical RNA polymerase II transcript that represses the paternal expression of Ube3a. *Hum Mol Genet*. 2012;21(13):3001-3012. doi:10.1093/hmg/dds130
44. Meng L, Person RE, Huang W, Zhu PJ, Costa-Mattioli M, Beaudet AL. Truncation of Ube3a-ATS Unsilences Paternal Ube3a and Ameliorates Behavioral Defects in the Angelman Syndrome Mouse Model. *PLoS Genet*. 2013;9(12). doi:10.1371/journal.pgen.1004039
45. Bailus BJ, Pyles B, Mcalister MM, O'Geen H, Lockwood SH, Adams AN, Nguyen JTT, Yu A, Berman RF, Segal DJ. Protein delivery of an artificial transcription factor restores widespread Ube3a expression in an angelman syndrome mouse brain. *Mol Ther*. 2016;24(3):548-555. doi:10.1038/mt.2015.236
46. Wurster C, Ludolph A. Nusinersen for spinal muscular atrophy. *Ther Adv Neurol Disord*. 2018;11:1-3. doi:10.1177/https
47. Silva-Santos S, Van Woerden GM, Bruinsma CF, Mientjes E, Jolfaei MA, Distel B, Kushner SA, Elgersma Y. Ube3a reinstatement identifies distinct developmental windows in a murine Angelman syndrome model. *J Clin Invest*. 2015;125(5):2069-2076. doi:10.1172/JCI80554
48. Sonzogni M, Zhai P, Mientjes EJ, Van Woerden GM, Elgersma Y. Assessing the requirements of prenatal UBE3A expression for rescue of behavioral phenotypes in a mouse model for Angelman syndrome. *Mol Autism*. 2020;11(1):1-12. doi:10.1186/s13229-020-00376-9
49. Rotaru DC, van Woerden GM, Wallaard I, Elgersma Y. Adult Ube3a gene reinstatement restores the electrophysiological deficits of prefrontal cortex layer 5 neurons in a mouse model of angelman syndrome. *J Neurosci*. 2018;38(37):8011-8030. doi:10.1523/JNEUROSCI.0083-18.2018
50. Rotaru DC, Mientjes EJ, Elgersma Y. Angelman Syndrome: From Mouse Models to Therapy. *Neuroscience*. 2020;445:172-189. doi:10.1016/j.neuroscience.2020.02.017
51. Moazami MP, Rembetsy-brown JM, Wang F, Krishnamurthy PM, Fitzgerald KA, Brown RH, Watts JK. Quantifying and Mitigating Motor Phenotypes Induced by Antisense Oligonucleotides in the Central Nervous System. *bioRxiv*. Published online 2021:1-26.
52. Schoch KM, Miller TM. Antisense Oligonucleotides: Translation from Mouse Models to Human Neurodegenerative Diseases. *Neuron*. 2017;94(6):1056-1070. doi:10.1016/j.neuron.2017.04.010
53. Frazier KS. Antisense Oligonucleotide Therapies:The Promise and the Challenges from a Toxicologic Pathologist's Perspective. *Toxicol Pathol*. 2015;43(1):78-89. doi:10.1177/0192623314551840
54. Branca M. Slivers of the spectrum. *Nat Biotechnol*. Published online 2021. doi:10.1038/s41587-021-00913-8
55. Hinderer C, Katz N, Buza EL, Dyer C, Goode T, Bell P, Richman LK, Wilson JM. Severe Toxicity in Nonhuman Primates and Piglets Following High-Dose Intravenous Administration of an Adeno-Associated Virus Vector Expressing Human SMN. *Hum Gene Ther*. 2018;29(3):285-298. doi:10.1089/hum.2018.015

Acknowledgments

While it is ultimately my name on this dissertation, it truly takes a village to raise a graduate student and many people have influenced this work in one way or another. A few of those people deserve special mention here for their scientific contributions but also for their extraordinary kindness, thoughtfulness, and generosity of time.

First and foremost, all of this research was expertly guided by my incredible mentor, Dr. Jill Silverman. Dr. Silverman never failed to provide advice and encouragement when needed, both professionally and personally, and I am continually learning from her what it means to be a successful scientist and effective leader. She entrusted me with a great deal of independence in the lab and supported my participation in numerous conferences, which has made me a stronger, more capable, and well-rounded researcher. It is thanks to Dr. Silverman, as well as the Foundation for Angelman Syndrome Therapeutics and their Chief Scientific Officer Dr. Allyson Berent, that I was afforded the opportunity to devote the bulk of my graduate time to carrying out research. The depth of my gratitude to Dr. Silverman truly transcends words.

I would also like to acknowledge the support and expert guidance of my dissertation committee members, Dr. Brian Trainor and Dr. Karen Bales, who advised my graduate work since its beginning. The insights of Dr. Danielle Stolzenberg and Dr. Markus Wöhr also greatly enriched my studies, with Dr. Wöhr's mentorship, in particular, playing a significant role in the entire direction of this work.

A special acknowledgment goes out to all of my Silverman Lab teammates who are continual sources of inspiration and who all made meaningful contributions to this work. I owe Mike Pride and Dr. Nycole Copping a great deal of gratitude for their training and support since

my first day in the lab, and I have immensely appreciated Nycole passing along advice as she paved the way through our graduate program. Mike, Nycole, Dr. Stela Petkova, Anna Adhikari, and Tim Fenton fostered such a warm and supportive lab environment that, despite spending most of our time on different campuses, it always felt like we were working right alongside each other.

The same can be said about the many fantastic collaborators that I have had the privilege of working with over the years. I especially want to acknowledge Dr. Markus Wöhr, Dr. Jacob Ellegood, Dr. Kyle Fink, Dr. Shekib Jami, as well as Dr. Pamela Lein and her entire lab. It has been a pleasure to work with, learn from, and attend conferences with Dr. Lein, Donald Bruun, Dr. Kelley Patten, Anthony Valenzuela, Eduardo Gonzalez, and Jonas Calsbeek.

I must also mention the many colleagues with whom I have worked alongside at the Rat Phenotyping Lab, headed by Dr. Robert Berman and then Dr. Melissa Bauman. These past few years would not have been nearly as fun or productive without all of you: Dr. Milo Careaga, Josef Rivera, Lauren Pedersen, Alex Chiang, Riki Kar, Tianna Ching, Mika Nakamoto, Yutian Shen, Ruona Lin, Matthew Matson, Steven Xiong, Angelica Bachman, and Annuska Berz.

All of the research herein relied upon rodent colonies housed either at the UC Davis campus or at a satellite site in the bay area. It is therefore important to acknowledge the amazing team of animal care staff that helped make all of this work possible, particularly Tish Ashley and Stefanie Archibeque for supervising the care of the campus colonies, Shanie McCarty for supplying me with equipment to take to the bay area facility, and Nicole McCowan for overseeing so many of our animal care protocols and their last-minute updates.

Personally, I would not have been in a position to accomplish this work without my family and friends, many of whom I consider scientific collaborators. I especially want to acknowledge the enduring support of my parents, Ellen and Lee, whose love for inquiry and analysis make them

invaluable consultants on any topic. Throughout my pursuit of higher education, the steadfast encouragement of my grandmother, Rose, has been a significant source of comfort and strength to me. My partner, Jeff, not only taught me Excel functions that have changed my life, but he also helped ease my struggle through the toughest days of this research. And, by their intangible yet profound effect on me as a person, I am sure that this work has also been shaped by my friendships with Beth Onaga, Julia Schleimer, Danny Kassenbrock, Jason Ford, Grant Anderson, Dillon Miles, Aakash Lakhotia, and Greg Disse, among many others.

Finally, I would like to acknowledge for whom all of this work has been conducted, because while so much of the past few years has been incredibly joyous, rewarding, and scientifically fruitful, the process and effort of research is not without its downsides and disappointments. By its nature, animal work can be highly inconvenient and data collection rife with complications. Each and every difficulty, however, has been worth enduring and worth overcoming in the hopes of helping the parents, families, caregivers, and advocates out there who are working relentlessly, and facing their own incredible challenges, to provide for their children and meet every unique need that arises. All of this work is dedicated to them.